

Atmospheric Secondary Organic Aerosol: Kinetic and Chemical Studies of in-Cloud Reactions of Selected Plant Volatiles



IChF

Institute of Physical Chemistry PAS

**Ph.D. thesis
Kumar Sarang**



*Atmospheric Secondary Organic Aerosol: Kinetic
and Chemical Studies of in-Cloud Reactions of
Selected Plant Volatiles*

Ph.D. thesis

Kumar Sarang

(Year 2022)



*A thesis submitted for the degree of
Doctor of Philosophy in the field of Chemical Sciences*

Atmospheric Secondary Organic Aerosol: Kinetic and Chemical Studies of in-Cloud Reactions of Selected Plant Volatiles

**Ph.D. thesis
Kumar Sarang**

A-21-7, K-g-181, K-g-170

Supervisor: Dr. Rafal W. Szmigielski, Ph.D., D.Sc., Associate Professor, IPC PAS, Warsaw, Poland

Co-supervisor: Dr. Irena Grgić, Ph.D., Associate Professor, NIC, Ljubljana, Slovenia

Biblioteka Instytutu Chemii Fizycznej PAN

F-B-549/22



80000000345657

The present thesis was prepared within the International Doctoral Studies in Chemistry at the Institute of Physical Chemistry of the Polish Academy of Sciences at Warsaw, Poland, in collaboration with the Assoc. Prof. Irena Grgić at National Institute of Chemistry at Ljubljana, Slovenia.

Warsaw, January 2022



B. 54 B / 22

Dedicated to

My Late Grandmother Shanti Gambhir, Late Grandfather Satpal Malik and Late Mother Vanita Gambhir for their immense blessings and keeping an eye on me from their heavenly abode.

My father Rajnish Gambhir, and brother Sahir Gagan, to let the world know that we sailed through despite all the hurdles we faced in our lives. And it wasn't possible without the love and care of these three amazing women in my life, motherly figure Aruna, my wife Anukrati, and my sister Priyanka. They have been a constant pillar of support for me at all times.

Acknowledgments

For the first 24 years of my life, I never thought of pursuing a doctorate in Science. This was a career path never explored by anyone in my family. But here I am, writing the first few pages of my thesis and advancing towards being the first one in my family to be a Ph.D. holder in Science. There is always one person you admire the most while growing up. For me, it was my first cousin, elder brother, Dr. Pankaj Gambhir (Ph.D. Commerce). He enlightened me towards the path of hunger for knowledge and advised me not to be complacent in my career. Chemistry was never a love at first sight for me until school, but then I came across atmospheric chemistry and was left in awe of its occurrence. My good academic performances acted as a booster to pursue my goal and enlightened me on the path to achieve scientific knowledge. I would also like to acknowledge the contribution of the following people who made it possible for me to achieve this goal and thank them for their continued support.

First, I would like to thank my research advisors:

Professor Rafal Szmigielski, for believing in my capabilities, beginning from the process of accepting my Ph.D. application, designing a Ph.D. project, accepting my research ideas, and always encouraging me to pursue each task with excellence. I am grateful to have you as a supervisor and a mentor. Thank you for always believing in me and motivating me with your words of wisdom. You adopted me as graphite and saw the potential to polish me with your expertise and advice, eventually turning me into the scientist I am today. Apart from inspiring me with your passion for science, your life lessons starting with "my boss/teacher once told me," "always look at the bright side of life," and all the fun trips you organized to keep me relaxed made my stay in Poland the most awarding and unforgettable experience in my life. Thank you for being with me as a mentor, a friend, and a sounding board during both good and bad times.

Dr. Krzysztof Rudziński, for being my scientific father in the group, also caring and kind. You made me feel safe and warm from the very first day in Warsaw. Thank you for helping me from the very first day with the medical formalities to shifting in the apartment and offering me breakfast and warm tea in the office. Thank you for all the learnings, teachings, research questions, and knowledge transfer while introducing and taking me deep into the world of atmospheric kinetics. You were really welcoming with all my queries, even the silly ones. I will always be grateful for the valuable guidance, feedback, and support you provided during my Ph.D. studies. The incredibly detailed inputs from you on my kinetics project while preparing the manuscript was a great learning curve, and it taught me how to be sane and patient while working on, with, and in science.

To both of you, dear Rafal and Chris, for always keeping your doors open, with a kind attitude, which created a delightful atmosphere and helped me have open, candid and effective communication, sometimes even involving personal matters. This will always remain a key component of my success, which I would happily like to pass on as a learning to the forthcoming generation. If not pandemic, we could have had more scientific trips like Gothenberg and Slovenia. I have always loved and enjoyed your company.

Dr. Irena Grgić, for your significant inputs and guidance, that shaped me into a better writer, thinker, and scientist. Unfortunately, due to the pandemic, I could not get a chance to work with you. However, I will always appreciate your advice on various scientific duties, ranging from the very basic to the more advanced ones. I am indebted for your prompt replies to my queries and readiness and involvement in the scientific discussions we had while in Ljubljana

and virtually. Thank you for being so welcoming and kind along with other colleagues in the Department of analytical chemistry at NIC during my short stay in Ljubljana, Slovenia.

A special thanks goes to all my mentors and colleagues at Leibniz Institute for Tropospheric Research, Leipzig, Germany (TROPOS).

Professor Hartmut Hermann, for giving me an opportunity and allowing me to work at TROPOS, Leipzig, and providing me with a welcoming and motivating work environment during my stay at TROPOS.

Dr. Thomas Schaefer, and Dr. Tobias Otto, for all your support during my stay at Laser Lab, TROPOS. Thanks, Tobias, for training me on the LFP-LLPA, GC-MS, LC-MS, and other Laser laboratory experimental set-ups. It was a pleasure to work with you two. I am grateful for all the discussions and your efforts, comments, and suggestions during laboratory experiments, especially when I struggled with the COPASI. This enabled me to write and prepare the publications and helped me finish the work as planned.

Dr. Martin Brueggemann, for training and discussions related to the LC-MS experiments at TROPOS, Leipzig.

Dr. Anke Mutzel, for providing me with an opportunity to participate and get trained during the Aerosol particle organic analytical training course (22.01.2018 - 26.01.2018) OGTAC-CC workshop at TROPOS, Leipzig.

Dr. Mohammed Jaoui, for being a mentor and research collaborator from Environmental Protection Agency (EPA), U.S.A.

Dr. Adam Kubas, for being a mentor and research collaborator at IPC PAS. Thank you for teaching me quantum chemistry to help me carry out the density functional theory (DFT) based calculations using a supercomputer facility at ICM, Warsaw.

I would also like to extend my thanks to **Professor Robert Kolos**, who, apart from scientific knowledge, trained me with the soft skill of presenting the scientific work, with his insightful remarks during four years of the doctoral seminars at IPC PAS.

ICM Warsaw, for giving access to its supercomputing facility (Grant: G81-8).

Finally, my colleagues from the Szmigielski group at IPC PAS, Dr. Monika, Dr. Agata, Paulina, Klara, Aleksandra (Ola), and Dr. Faria, for their fantastic company inside and outside the laboratory.

Teachers: Besides my work family, I extend my sincere thanks to all my teachers in school and college, especially Late Mahendra Joshi Sir, Principal Mr. Sudhir Joshi, Vice Principal Labhinder Joshi, Himanshu Tripathi Ma'am, Usha Daga Ma'am, Rozy Punn Ma'am, Anjali Bhatnagar Ma'am, Sube Singh Sir, Rakesh Khanna Sir, Mukesh Tyagi Sir, Noor Mohammed Sir, Late Uma Sharma Ma'am, Mr. Surender Chauhan, Dr. Sharada Pasricha, Dr. Shefali Mishra, and Dr. VC Rao, and all other school and college teachers for their immense support throughout my educational journey.

My wife, Anukrati, you have known me since I was barely 19 years old. We have always acted as a strength for each other since then. You are always the reason I could act decisively when needed, whether it was about moving out of the city, from Delhi to Bangalore or while moving out of the country, from India to Poland, for taking the next big step in my career. Thank you for always being with me as my best friend and my biggest cheerleader.

My father: Thank you, papa, for making me a better human being and inspiring me throughout my life with your noble work. This is an outcome of all your hard work and sleepless nights. It was all worth it.

My foster mothers: No words can ever repay the amount of love, care, and blessings I received from my paternal aunts Aruna, Shashi, and Swarna.

Brother and sister-in-law: Sahir and Priyanka, you were an equal part of this Ph.D. journey by giving me all your support, love, and guidance at all times.

Parents-in-law: Papa (Ajay Chauhan) and Mummy (Rajeshwari Chauhan), for accepting me with your open heart and welcoming me into your family amid this difficult life journey I undertook. It was in itself stress relieving.

Friends and family: Late Om Gambhir (Bade Papa), Ajit Gambhir (Bade Papa), Late Bharti Aunty, Ashok Uncle, Roma aunty, Sahavaniya, Sunil Uncle, Vinod Uncle Eishan, Anuj, Ankit, Monisha, Kakkar, Kandpal, Richa, Ronak, Aanya, Aditya, Aakash, Rameez, Aditya Ahuja and Himanshu. I am forever grateful for the love and support you all have given me in my life.

Lastly, I would like to thank the NaMeS office and administrative staff of the Institute of Physical Chemistry, especially Ola Bernetek, Patrycja, Agnieszka, Joanna, and Eliaz, for their help and cooperation during my stay at IPC and Warsaw.

Declaration of originality

I, ***Kumar Sarang***, hereby declare that the present Ph.D. thesis research was carried out by myself or with support by others included in the acknowledgments.

I state that I have exercised care to ensure that the work is original and contains no previously published material or written by another person, except where citations have been made in the text.

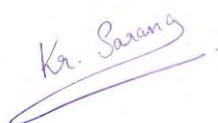
To the best of my knowledge, the content provided here does not violate any copyrights.

I accept that the Polish Academy of Sciences has the right to use plagiarism detection software to ensure the thesis's legitimacy.

I certify that no part of my thesis has been or will be submitted for obtaining a degree or diploma by the Institute of Physical Chemistry Polish Academy of Science, or any other educational institution.

This thesis's copyright rests with the author, and no information derived from it may be published without the author's consent.

Signature.

A handwritten signature in purple ink that reads "Ka. Sarang". The signature is written in a cursive style and is underlined with a single purple stroke.

Date.

25/01/2022

Funding

The present research was financed by

- The European Union Horizon 2020 Research and Innovation Programme under the Marie Skłodowska-Curie grant agreement no. 711859 and the Polish Ministry of Science and Higher Education for implementing an international co-financed project in the years 2017–2021.
- The European Commission Erasmus + program for financing my research visits to TROPOS, Leipzig, and NIC, Slovenia



Horizon 2020
European Union Funding
for Research & Innovation



Ministry of Science
and Higher Education
Republic of Poland



Erasmus+

List of publications

Included in this thesis

1. **Kumar Sarang**, Tobias Otto, Krzysztof Rudzinski, Thomas Schaefer, Irena Grgic, Klara Nestorowicz, Hartmut Herrmann and Rafal Szmigielski, *Reaction Kinetics of Green Leaf Volatiles with Sulfate, Hydroxyl and Nitrate Radicals in Tropospheric Aqueous-Phase*
Open access, **Environ. Sci. Technol.** **2021**, 55, 20, 13666–13676
DOI: 10.1021/acs.est.1c03276
2. **Kumar Sarang**, Krzysztof Rudzinski, Rafal Szmigielski
Green Leaf Volatiles in the atmosphere – properties, transformation, and significance
Open access, **Atmosphere** **2021**, 12(12), 1655
DOI: 10.3390/atmos12121655
3. **Kumar Sarang**, Tobias Otto, Sahir Gagan, Krzysztof Rudzinski, Adam Kubas, Thomas Schaefer, Martin Brüggemann, Irena Grgić, Hartmut Herrmann and Rafal Szmigielski, *Aqueous-Phase Photo-Oxidation of Selected Green Leaf Volatiles: Atmospheric Implications*
Submitted to Chemosphere

Other

4. Krzysztof J. Rudziński, **Kumar Sarang**, Klara Nestorowicz, Monika Asztemborska, Ewa Żyfka-Zagrodzińska, Krzysztof Skotak, Rafał Szmigielski, *Winter sources of PM_{2.5} pollution in Podkowa Leśna, a Central-European garden town*
Under preparation: Expected submission timeline: March 2022
5. Agata Kołodziejczyk, Patryk Pyrcza, Kacper Błaziak, Aneta Pobudkowska, **Kumar Sarang** and Rafał Szmigielski, *Physico-chemical properties of terebic acid, MBTCA, diaterpenylic acid acetate and pinanediol as relevant α pinene oxidation products*,
Open access, **ACS Omega** **2020**, 5, 14, 7919–7927,
DOI: 10.1021/acsomega.9b04231
6. Mohammed Jaoui, Rafal Szmigielski, Klara Nestorowicz, Agata Kolodziejczyk, **Kumar Sarang**, Krzysztof J. Rudzinski, Anna Konopka, Ewa Bulska, Ivan R. Piletic, Michael Lewandowski, Theran P. Riedel, and Tadeusz E. Kleindienst, *Organic Hydroxy Acids as Highly Oxygenated Molecular (HOM) Tracers for Aged Isoprene Aerosol*
Open access, **Environ. Sci. Technol.** **2019**, 53, 24, 14516–14527
DOI: 10.1021/acs.est.9b05075

Presentation at scientific conferences/meetings

Oral

1. American Association for Aerosol Research Conference (AAARC) 2020
Online 38th Annual Conference **Oct 5–9, 2020**
“Atmospheric Significance of the Aqueous-Phase Reactions of Green Leaf Volatiles: 1-Penten-3-ol, (Z)-2-Hexen-1-ol, and (E)-2-Hexen-1-al With Atmospheric Radicals”
 2. **50th General Assembly and 47th World Chemistry Congress of IUPAC 2019**,
Paris, France **July 5–12, 2019**
“Aqueous-Phase Oxidation of 1-Penten-3-ol as a Relevant Green Leaf Volatile with Hydroxyl and Sulfate Radicals”
-

Invited oral talks

3. **Micro symposium** Institute of Physical Chemistry Polish Academy of Sciences,
Jan 25, 2022
Impact Talk: “Chemistry and Atmospheric Significance of Green Leaf Volatiles: Future perspective”
 4. National Institute of Chemistry, Ljubljana, Slovenia **Sept 12, 2019**
“Aqueous-Phase Reaction Kinetics of Green Leaf Volatiles with Hydroxyl, Sulfate and Nitrate Radicals”
 5. Leibniz Institute for Tropospheric Research, Leipzig, Germany **March 18, 2019**
“Aqueous-phase Reactions of Green Leaf Volatiles in the Presence of Atmospheric Radicals as a Source of SOA”
-

Poster

6. European Geosciences Union (EGU) General Assembly 2020 Online **May 4–8, 2020**
“Tropospheric Aqueous-phase Oxidation of Green Leaf Volatiles with Hydroxyl, Sulfate and Nitrate Radicals”
DOI: 10.5194/egusphere-egu2020-4909,
 7. **Micro symposium** Institute of Physical Chemistry Polish Academy of Sciences,
Jan 16, 2020
“Aqueous-Phase Oxidation of 1-Penten-3-ol as a Relevant Green Leaf Volatile with Hydroxyl and Sulfate Radicals”
 8. **EAC 2019** European Aerosol Conference, Gothenburg, Sweden **Aug 25–30, 2019**
“Aqueous-Phase Oxidation of 1-Penten-3-ol as a Relevant Green Leaf Volatile with Hydroxyl and Sulfate Radicals”
-

Others

9. 39th American Association for Aerosol Research Conference (AAARC) 2021 Online
Oct 18–22, 2021
Aerosol Art Competition: “Awarded in the Aerosol Art Competition”
-

Abbreviations

AMS	aerosol mass spectrometry
ACN	acetonitrile
AD	aerodynamic diameter
API-MS	atmospheric pressure ionization-mass spectrometry
ASMS	American society for mass spectrometry
Aq	aqueous
BDEs	bond dissociation energies
BSOA	biogenic secondary organic aerosol
BVOC, BVOCs	biogenic volatile organic compounds
CCN	cloud condensation nuclei
CEAS	cavity-enhanced absorption spectroscopy
CLM	community land model
COPASI	COmplex PAthway Simulator (software)
CPCM	conductor-like polarizable continuum model (in ORCA)
CRAC	smog chamber at the University of Cork
CW laser	continuous wave laser
DAD	diode-array detector (in HPLC)
DCM	dichloromethane
DESI	desorption electrospray ionization source
DFT	density functional theory
DMB	3,4-dimethylbenzaldehyde
DMS	dimethyl sulfide
EI	electron ionization (in mass spectrometry)
EIC	extracted ion chromatogram
EI-MS	electron ionisation quadrupole mass spectrometer
EPA	Environmental Protection Agency
EPI	estimation program interface
EUPHORE	environmental smog chamber in Valencia, Spain
EVK	ethyl vinyl ketone (1-penten-3-one)
FID	flame ionization detector (in gas chromatography)
FTIR	fourier transform infrared spectroscopy

GC	gas chromatography
GCM	group contribution method (for rate constant estimation)
cGC-MS	capillary gas chromatography-mass spectrometry
GLV, GLVs	green leaf volatiles
h, hr	hour
HESI	heated electrospray ionization source
HEXAL	(<i>E</i>)-2-hexen-1-al
HEXOL	(<i>Z</i>)-2-hexen-1-ol
HPLC	high-performance liquid chromatography
HR PTR-TOF-MS	high resolution proton-transfer-reaction mass spectrometry
ICARE-CNRS	Institute of Combustion, Aerothermics, Reactivity and Environment-CNRS
IN	ice nuclei
IPCC	Intergovernmental Panel on Climate Change
JA	jasmonic acid
LC	liquid chromatography
rpLC-MS	reversed phase liquid chromatography-mass spectrometry
LDI	laser desorption ionization (in mass spectrometry)
LFER	linear free energy relation
LFP-LLPA	laser flash photolysis-laser long path absorption
LIP	laser induced photolysis
LISA	smog chamber at the Laboratoire Interuniversitaire des Systèmes Atmosphériques in Paris
LOX	lipoxygenase
LP-FTIR	laser photolysis-fourier transform infrared spectroscopy
LSODA	deterministic ordinary differential equation solver (in COPASI)
LWC	liquid water contents, m ³ (water) m ⁻³ (air)
MBO	2-methyl-3-buten-2-ol
MEGAN	Model of Emission of Gases and Aerosols from Nature
MeJa	methyl jasmonate
MeSa	methyl salicylate
min	minute
MRM	multiple reaction monitoring (in mass spectrometry)
MS	mass spectrometry

MW	molecular weight
NAAQS	National Ambient Air Quality Standards
NIR	near infra-red (spectroscopy)
NMR	nuclear magnetic resonance (spectroscopy)
ODE	ordinary differential equation (in COPASI)
ORCA	ORCA is a quantum chemistry program package
PDA detector	photodiode-array detector (in HPLC)
PDF	probability density function (in COPASI)
PENTOL	1-penten-3-ol
PES	potential energy surface
PI	photoionization detector
PILS-WSOC	Particle-Into-Liquid Sampler used to measure water-soluble organic components
PLP-LIF	pulsed laser photolysis—laser-induced fluorescence
PLP-RF	pulse laser photolysis—resonance fluorescence
PM	particulate matter, ambient aerosol
POA	primary organic aerosol
RH	relative humidity (%)
RRKM	Rice–Ramsperger–Kassel–Marcus theory
s, sec	second
SAR	structure-activity relation
SMPS	scanning mobility particle sizer
SOA	secondary organic aerosol
SPME	solid-phase microextraction
SRR	structure-reactivity relation
SSA	stochastic simulation algorithm (in COPASI)
TAG	Thermal desorption Aerosol GC/MS-FID
TIC	total ion chromatogram
TOF	time of flight analyzer (in mass spectrometry)
TROPOS	Leibniz Institute for Tropospheric Research
TS	transition state
TSP	total suspended particulate matter
TUV	troposphere ultraviolet model

UHPLC+	ultra-high-performance liquid chromatography system
UV	ultraviolet
VOC, VOCs	volatile organic compounds
yr, yrs	year, years

Abstract (in English)

The goal of my Ph.D. research was to assess the role of aqueous-phase reactions of selected green leaf volatiles (GLVs) with atmospheric oxidants leading to the formation of secondary organic aerosol (SOA). The research included: (i) detailed kinetic analysis of 1-penten-3-ol, (*Z*)-2-hexen-1-ol, and (*E*)-2-hexen-1-al reactions with hydroxyl ($\cdot\text{OH}$), sulfate ($\text{SO}_4^{\cdot-}$) and nitrate (NO_3^{\cdot}) radicals in dilute aqueous solutions; (ii) chemical characterization of novel SOA products at the molecular level using high-resolution tandem mass spectrometry in combination with theoretical calculations using quantum-based density functional theory (DFT).

Atmospheric aerosol is a suspension of liquid or solid particles (organic and inorganic) in the air with complex chemical composition and sizes far below 100 μm . It includes primary organic aerosol (POA) emitted directly from various sources (e.g., volcano eruptions) and secondary organic aerosol (SOA), which forms through chemical reactions of organic trace gases combined with physical processes, such as nucleation and condensation. With increasing emissions of anthropogenic pollutants, frequently changing weather patterns, and climate change, the Earth's natural *vegetation*, such as forests, is permanently exposed to extreme stress conditions. The stress profoundly alters the emission patterns of volatile organic compounds (VOCs), which affect the formation of SOA in the Earth's atmosphere. In the presence of various oxidants, such as ozone (O_3), $\cdot\text{OH}$, and NO_3^{\cdot} radicals, VOCs undergo gas-, aqueous-, and multiphase oxidation, which leads to SOA formation and aging. The limited knowledge of the SOA formation processes leads to a significant underestimation of the global SOA budget and its impact on climate change and health.

To reduce discrepancies between hitherto modeling results and field measurement data, I decided to provide experimental evidence on the potential role of actual plant emissions, known as green leaf volatiles (GLVs), in increasing the SOA burden. GLVs actively participate in the gas- and aqueous-phase atmospheric chemistry, like the key plant volatiles isoprene and monoterpenes. In the last decade, the characterization of the aqueous transformation of GLVs has posed a challenge to atmospheric scientists, as it is a potentially relevant source of SOA loads in the atmosphere.

This Ph.D. thesis unveils the potential of GLVs as the missing source of SOA particles in the atmosphere *via* in-cloud reactions with atmospherically relevant radicals. The first part resolves the kinetics of aqueous-phase reactions of three selected GLVs, i.e., 1-penten-3-ol, (*Z*)-

2-hexen-1-ol, and (*E*)-2-hexen-1-al reactions with $\cdot\text{OH}$, $\text{SO}_4^{\cdot-}$ and NO_3^{\cdot} radicals using the technique of laser flash photolysis-laser long path absorption (LFP-LLPA). The rate constants determined for the aqueous-phase reactions of selected GLVs with $\cdot\text{OH}$, $\text{SO}_4^{\cdot-}$, and NO_3^{\cdot} are of the order of 10^9 , 10^8 , and 10^7 L mol⁻¹ s⁻¹, respectively. The $\cdot\text{OH}$ -driven reactions are partially controlled by diffusion of reactants, while those with $\text{SO}_4^{\cdot-}$, and NO_3^{\cdot} radicals are rather chemically-controlled. The activation energies determined from the temperature variation of the second-order rate constants (278 K to 318 K) reveal GLV differ in rate of reactivity towards various radicals. The expected atmospheric lifetimes of GLV vary from a few seconds to a few days. Generally, GLV may effectively contribute to the formation of SOA.

The rate constants for GLV reactions with NO_3^{\cdot} were determined without accounting for a few reactions that could consume the radical. They included the reactions with $\cdot\text{OH}$, HO_2^{\cdot} , H_2O , and $\text{S}_2\text{O}_8^{2-}$, and the autoxidation of alkyl compounds to ROO^{\cdot} radicals. I developed a complete kinetic model of GLV – NO_3^{\cdot} reactions and analyzed it using the COPASI software package to evaluate the bias in the rate constants determined. The analysis showed that the intrinsic experimental uncertainty for the rate constants determined using the LFP-LLPA procedure was significantly higher than the bias due to the “neglected” reactions. Thus the LFP-LLPA experimental method appeared applicable and robust to determine GLV – NO_3^{\cdot} reaction kinetics.

The second part of my Ph.D. research aimed to explain the chemical mechanisms of aqueous-phase reactions of GLV with $\cdot\text{OH}$ radicals. The oxidation of 1-penten-3-ol, (*Z*)-2-hexen-1-ol, and (*E*)-2-hexen-1-al with $\cdot\text{OH}$ radicals was pursued using the aqueous-phase photoreactor under simulated sunlight conditions. The product analysis targeted carbonyls, alcohols, and carboxylic acids as likely abundant oxidation products. It included the advanced hyphenated mass spectrometry (capillary GC-MS, reversed-phase LC with high resolution MS detection, and MS/MS analyses). The analyses confirmed the presence of various carbonyl products, including propanal, butanal, 1-penten-3-one, (*E/Z*)-2-hexen-1-al, and an unknown product of the formula $\text{C}_6\text{H}_{10}\text{O}_2$. The identified carbonyls, chiefly propanal and butanal are highly important because of their high reactivity with OH , O_3 , and other radicals, leading to peroxy acyl nitrates or carboxylic acids. The observed highly reactive primary oxidation products can possibly hydrate and further react with other aldehydes and parent GLVs to produce higher molecular weight oligomers. The latter end products may adversely affect air quality and human health in regions where an increased GLVs mixing ratio occurs. The other carbonyl products detected, including $\text{C}_6\text{H}_{10}\text{O}_2$ (possibly hydroxy-hexenal or hydroxy-

hexenone), and 1-penten-3-one, may indicate SOA aging in the ambient atmosphere via various pathways; e.g., organosulfates formation.

Using the density functional theory (DFT)-based quantum calculations, I provided more insights into mechanistic pathways of the above investigated reactions of GLVs with $\cdot\text{OH}$. An emphasis was given to resolving the addition and hydrogen-abstraction reaction routes and their relative importance. Simple CPCM based continuum solvation model within DFT helped to explain the mechanistic pathways of the formation of experimentally observed reaction products, and identification of all possible mechanistic pathway of unknown product $\text{C}_6\text{H}_{10}\text{O}_2$ formation. Along with suggested activation barrier less fast addition reactions, the results also highlight importance of hydrogen-abstraction route to the formation of experimentally observed products.

The studied aqueous-phase reactions were evaluated for their atmospheric relevance or significance. For this purpose, GLVs atmospheric lifetimes and removal rates were calculated. The results showed that the role of selected GLVs appeared negligible in deliquescent aerosol and haze water. However, it became significant in atmospheric systems of high liquid water contents, such as clouds, rains, and storms. Under such conditions, the atmospheric GLV lifetimes decreased from years or hundred days to a few minutes. The aqueous-phase GLV reactions with $\text{SO}_4^{\cdot-}$ radicals dominated over combined gas- and aqueous-phase reactions with $\cdot\text{OH}$ or NO_3^{\cdot} in a few given conditions. The reaction of GLVs with $\cdot\text{OH}$ radicals dominated over all other oxidants in atmospheric waters, however represents less than 0.1% of the total flux removal by combined gas- and aqueous-phase reactions, indicating required future evaluation of their reaction at the air-water interface than in bulk aqueous phase. In addition, the experimental determination of Henry's constant may further help to improve these results.

A part of my research was an evaluation of the selected physical properties of GLVs. I experimentally obtained the UV spectra of GLV in the aqueous solutions and estimated vapor pressure, solubility, and Henry's constants using the EPI Suite software available from EPA to evaluate their reactivity in the atmospheric waters. The estimated values indicate GLVs as a compound with moderate solubility and fair partitioning into the aqueous phase.

The work of the thesis presented herein, provides a unique inclusive study of the potential of GLVs as a missing SOA source in the atmosphere via complete understanding of their aqueous chemistry involving physical properties, kinetics, and mechanisms.



Abstrakt (in Polish)

Celem przeprowadzonych badań była ocena roli reakcji chemicznych wybranych lotnych substancji pochodzenia roślinnego indukowanych stresem (GLV, ang. *green leaf volatiles*) z utleniaczami atmosferycznymi, przebiegających w fazie wodnej i prowadzących do powstania składników wtórnego aerozolu organicznego (SOA, ang. *secondary organic aerosol*). Badania te obejmowały: (i) szczegółową analizę kinetyczną reakcji 1-penten-3-olu, (Z)-2-heksen-1-olu i (E)-2-heksen-1-olu z rodnikami hydroksylowymi ($\cdot\text{OH}$), siarczanowymi ($\text{SO}_4^{\cdot-}$) i azotanowymi (NO_3^{\cdot}) w rozcieńczonych roztworach wodnych; (ii) charakteryzacja chemiczna tworzących się produktów SOA na poziomie molekularnym z użyciem narzędzi tandemowej spektrometrii masowej o wysokiej rozdzielczości w połączeniu z obliczeniami teoretycznymi wykorzystującymi kwantową teorię funkcjonału gęstości (DFT).

Aerozol atmosferyczny stanowi zawiesinę cząstek ciekłych lub stałych (organicznych i nieorganicznych) w powietrzu o złożonym składzie chemicznym i rozmiarach znacznie poniżej 100 μm . Obejmuje on *pierwotny aerozol organiczny* (POA) emitowany bezpośrednio z różnych źródeł (np. w wyniku erupcji wulkanicznych) oraz *wtórny aerozol organiczny* (SOA), który powstaje w wyniku złożonych procesów chemicznych związków organicznych obecnych w atmosferze ściśle połączonych z procesami fizycznymi, takimi jak kondensacja. Wraz ze wzrostem emisji zanieczyszczeń antropogenicznych, obecnością patogenów oraz często zmieniającymi się warunkami pogodowymi (ocieplenie klimatu), ekosystemy roślinne Ziemi są coraz mocniej narażone na ekstremalne warunki stresowe. Ten stres głęboko zmienia profil emisji lotnych związków organicznych (VOC, ang. *volatile organic compounds*) roślin, który wpływa na bilans powstawania SOA w ziemskiej atmosferze. W obecności dostępnych utleniaczy, takich jak ozon (O_3), rodniki $\cdot\text{OH}$ i NO_3^{\cdot} , lotne substancje roślinne (GLV) ulegają kaskadom reakcji utleniania w fazie gazowej, wodnej i międzyfazowej, co prowadzi do powstawania znanych i nieznanych składników SOA oraz produktów ich dalszego starzenia. Ograniczona wiedza na temat tych procesów prowadzi do znacznego niedoszacowania globalnego budżetu SOA i tym samym – jego wpływu na zachodzące zmiany klimatyczne i zdrowie człowieka.

Niniejsza rozprawa dostarcza dowodów eksperymentalnych weryfikujących potencjalną rolę emisji roślinnych (GLV) w kierunku tworzenia dodatkowych mas pyłu zawieszzonego SOA, co pozwoli zmniejszyć rozbieżności pomiędzy wynikami uzyskiwanymi z modelowania a danymi pochodzącymi z pomiarów terenowych i laboratoryjnych. Wkład emisji roślinnych,

wymuszony stresem biotycznym i abiotycznym, wpływa na procesy chemicznego tworzenia SOA w dolnych warstwach atmosfery (zarówno w fazie gazowej i wodnej), lecz w odróżnieniu od roli izoprenu i monoterpenu, rola GLV to nadal *terra incognita*. W szczególności poznanie szlaków transformacji GLV w fazie wodnej stanowi potężne wyzwanie dla naukowców, zajmujących się atmosferą i jej zanieczyszczeniami, gdyż te procesy są jednym z brakujących i potencjalnie istotnych źródeł nieokreślonych mas aerozolu w atmosferze.

Niniejszy doktorat weryfikuje hipotezę o roli indukowanych stresem emisji związków organicznych z roślin (GLV) – jako brakującego źródła cząstek wtórnego aerozolu SOA w atmosferze poprzez cykl badań reakcji wybranych GLV z rodnikami istotnymi atmosferycznie w fazie wodnej. Pierwsza część opisanych wyników badań dotyczy kinetyki reakcji w fazie wodnej trzech wybranych GLV, tj. 1-penten-3-olu, (*Z*)-2-heksen-1-olu i (*E*)-2-heksen-1-olu reakcje z rodnikami $\cdot\text{OH}$, $\text{SO}_4^{\cdot-}$ i NO_3^{\cdot} z wykorzystaniem techniki laserowej fotolizy połączonej z długą drogą absorpcji światła (LFP-LLPA, ang. *laser flash photolysis-laser long path absorption*).

Wyznaczone stałe szybkości dla reakcji wybranych GLV w fazie wodnej z rodnikami $\cdot\text{OH}$, $\text{SO}_4^{\cdot-}$ i NO_3^{\cdot} były odpowiednio rzędu 10^9 , 10^8 i 10^7 $\text{L mol}^{-1} \text{s}^{-1}$. Reakcje wywołane przez rodniki $\cdot\text{OH}$ były częściowo kontrolowane przez procesy dyfuzji reagentów, podczas gdy te z rodnikami $\text{SO}_4^{\cdot-}$ i NO_3^{\cdot} podlegały większej kontroli chemicznej. Energii aktywacji określone na podstawie zmian temperatury stałych szybkości drugiego rzędu (278 K do 318 K) wykazały, że badane związki organiczne różnią się szybkością reakcji wobec rodników. Obliczone oczekiwane czasy życia tych związków w atmosferze wahały się od kilku sekund do kilku dni. Na tej podstawie postawiono hipotezę, że wszystkie badane GLV mogą skutecznie przyczyniać się do powstania dodatkowych składników SOA.

Stałe szybkości reakcji badanych GLV z rodnikami NO_3^{\cdot} zostały określone bez uwzględnienia kilku ubocznych reakcji, w których ów rodnik mógłby się zużywać. Dotyczy to reakcji z drobinami $\cdot\text{OH}$, HO_2^{\cdot} , H_2O i $\text{S}_2\text{O}_8^{2-}$ oraz samoutlenianie związków alkilowych do rodników ROO^{\cdot} . W swoich badaniach opracowałem pełny model kinetyczny reakcji wybranych GLV z rodnikami NO_3^{\cdot} . W celu oceny błędu systematycznego wyznaczonych stałych szybkości przeanalizowałem zaproponowany model kinetyczny za pomocą modelu COPASI. Analiza ta wykazała, że niepewność eksperymentalna wyznaczonych stałych szybkości za pomocą metody LFP-LLPA była znacznie wyższa, niż błąd systematyczny, wynikający z „pominiętych” reakcji. W ten sposób wykazałem, że eksperymentalna metoda LFP-LLPA okazała się przydatna i solidna do określenia badania kinetyki reakcji GLV z rodnikami azotanowymi.

Celem drugiej części doktoratu była próba wyjaśnienia mechanizmów reakcji utleniania badanych związków GLV z rodnikami hydroksylowymi w fazie wodnej. Reakcje 1-penten-3-olu, (*Z*)-2-heksen-1-olu i (*E*)-2-heksen-1-olu z udziałem tych rodników prowadziłem w specjalnie do tego celu skonstruowanym fotoreaktorze wykorzystującym mimikę światła słonecznego. Analiza chemiczna produktów tych reakcji obejmowała m.in.: związki karbonylowe, alkohole oraz kwasy karboksylowe – jako najbardziej prawdopodobne produkty główne. Analiza próbek reakcji prowadziłem z użyciem zaawansowanych narzędzi spektrometrii mas, w tym: kapilarnej chromatografii gazowej sprzężonej ze spektrometrem mas z jonizacją EI (cGC-EI-MS), wysokosprawnej chromatografii cieczowej o fazach odwróconych z jonizacją typu elektrosprej i detekcją MS o wysokiej rozdzielczości (rpLC-ESI-HR-MS) oraz eksperymentów wymuszonej fragmentacji (MS/MS). Wyniki przeprowadzonych analiz potwierdziły obecność produktów karbonylowych, w tym propanalu, butanal, 1-penten-3-onu, (*E/Z*)-2-heksen-1-olu oraz nieznanego produktu o składzie $C_6H_{10}O_2$. Zidentyfikowane związki karbonylowe (w tym propanal i butanal) są bardzo ważnymi produktami pośrednimi tych reakcji ze względu na ich wysoką reaktywność względem badanych rodników, co umożliwiło wyjaśnienie tworzenia azotanów nadtlenoacylowych, jak również – kwasów karboksylowych. Obserwowane produkty pierwszej generacji badanych przemian mogą też ulegać uwodnieniu i dalej reagować z innymi aldehydami, w tym – wyjściowymi związkami GLV, co prowadzi do tworzenia produktów oligomerycznych o wyższych masach cząsteczkowych. Wszystkie te produkty wchodzą w skład powstającego wtórnego aerozolu i tym samym mogą wpływać na jakość powietrza i zdrowie ludzi w regionach, w których występuje zwiększone stężenie lotnych związków roślinnych typu GLV. Inne wykryte produkty karbonylowe, w tym produkt o składzie $C_6H_{10}O_2$ i niepotwierdzonej strukturze (prawdopodobnie hydroksy-heksenal lub hydroksy-heksenon) i 1-penten-3-on, mogą stanowić nowe markery starzenia się SOA w otaczającej atmosferze.

Korzystając z potencjału metod kwantowo-chemicznych opartych na teorii funkcjonału gęstości (DFT, ang. *density functional theory*), dostarczyłem dodatkowych argumentów potwierdzających zaproponowane mechanizmy badanych reakcji. Szczególny nacisk położyłem na próby wyjaśnienia mechanizmów addycji rodników oraz rodnikowego usuwania atomu wodoru. Prosty model solwatacji opartej na modelu CPCM (ang. *conductor-like polarizable continuum model*) umożliwił wyjaśnienie ścieżek powstawania obserwowanych eksperymentalnie produktów reakcji, w tym – nowego produktu o wzorze sumarycznym $C_6H_{10}O_2$.

Badane reakcje w fazie wodnej zostały ocenione pod kątem ich potencjalnego znaczenia w procesach atmosferycznego tworzenia cząstek SOA. W tym celu obliczyłem czasy życia w związków GLV w atmosferze oraz szybkości ich usuwania. Wyniki pokazały, że rola wybranych GLV jest praktycznie nieistotna dla wilgotnego aerozolu i mgły. Jednakże w układach atmosferycznych o dużej zawartości wody w stanie ciekłym, takich jak chmur i krople deszczu rola ta ma większe znaczenie. W takich warunkach czas atmosferycznego życia GLV zmniejsza się z lat lub setek dni do kilku minut. Badania pokazały, że reakcje wybranych GLV z rodnikami $\cdot\text{OH}$ dominowały nad wszystkimi innymi badanymi czynnikami utleniającymi w kroplach wód atmosferycznych, niemniej stanowił jedynie ok. 0,1% całkowitego strumienia ich usuwania z atmosfery w połączonych procesach w fazie gazowej i wodnej. Ponadto próby wyznaczenia stałych Henry'ego na drodze eksperymentalnej umożliwią dodatkową weryfikację postawionych hipotez.

Niewielki fragment badań poświęciłem ocenie niektórych właściwości fizycznych związków GLV. Zarejestrowałem widma UV tych związków w rozcieńczonych roztworach wodnych, jak również oszacowałem ich prężności pary, rozpuszczalność i stałe Henry'ego. W tym celu wykorzystałem możliwości oprogramowania EPI Suite, który oferuje Amerykańska Agencja Środowiska (EPA U.S.). Oszacowane wartości wskazują badane związki GLV jako układy chemiczne o umiarkowanej rozpuszczalności i dobrym podziale do fazy wodnej.

Pakiet danych wyznaczonych w tym doktoracie, obejmujący właściwości fizyczne, kinetykę i mechanizmy przemian, dostarcza unikalnych wskazówek, pokazujących potencjał indukowanych stresem emisji związków organicznych z roślin (GLV) jako brakujące źródło SOA w atmosferze.

Table of Contents

<i>Acknowledgments</i>	4
<i>Declaration of originality</i>	7
<i>Funding</i>	8
<i>List of publications</i>	9
<i>Presentation at scientific conferences/meetings</i>	10
<i>Abbreviations</i>	11
<i>Abstract (in English)</i>	15
<i>Abstrakt (in Polish)</i>	18
<i>Chapter 1. Introduction to atmospheric aerosol chemistry</i>	26
1.1. <i>Atmospheric aerosol</i>	27
1.1.1. <i>Definition</i>	27
1.1.2. <i>Aerosol particle size distribution</i>	27
1.2. <i>Sources of atmospheric aerosol</i>	29
1.3. <i>Tropospheric aerosol chemistry</i>	30
1.3.1. <i>Biogenic volatile organic compounds (BVOCs) as precursors of secondary organic aerosol (SOA)</i>	31
1.3.2. <i>Atmospheric oxidants and their (photo)chemical reactions with BVOCs</i>	34
1.3.2.1. <i>Kinetics of the atmospheric reactions</i>	35
1.3.2.2. <i>Reactions of BVOCs with oxidants in the troposphere</i>	40
1.4. <i>Impact of atmospheric aerosol on air quality, health and climate</i>	48
<i>Chapter 2. Research background and objectives</i>	50
2.1. <i>Introduction to green leaf volatiles (GLVs)</i>	51
2.2. <i>Gas-phase reactions of GLVs with atmospheric oxidants</i>	55
2.2.1. <i>Products and mechanism</i>	55
2.2.1.1. <i>Reaction with $\cdot\text{OH}$ radicals</i>	55
2.2.1.2. <i>Reactions of GLVs with $\text{NO}_3\cdot$ radicals</i>	59
2.2.1.3. <i>Reactions of GLVs with O_3</i>	61
2.2.1.4. <i>Reactions of GLVs with Cl atoms</i>	64
2.2.1.5. <i>Gas-phase photolysis of GLVs</i>	67
2.2.2. <i>Gas-phase kinetics of GLVs</i>	68
2.2.2.1. <i>Kinetics of reactions with $\cdot\text{OH}$ radicals</i>	69
2.2.2.2. <i>Kinetics of reactions with $\text{NO}_3\cdot$ radicals</i>	71
2.2.2.3. <i>Kinetics of reactions with O_3</i>	71
2.2.2.4. <i>Kinetics of reactions with Cl atoms</i>	73

2.2.2.5.	Gas-phase photolysis.....	75
2.3.	<i>Aqueous-phase kinetics and mechanism patterns for GLVs</i>	75
2.3.1.	Aqueous-phase kinetics.....	76
2.3.2.	Aqueous-phase and multiphase mechanisms	77
2.4.	<i>GLVs multiphase chemistry- novel source of SOA</i>	78
2.4.1.	Smog chamber and ambient aerosol studies	78
2.4.2.	Estimation of atmospheric SOA formation from GLVs	86
2.5.	<i>Selection of green leaf volatiles (GLVs) and aims of the work</i>	88
2.5.1.	Selection of green leaf volatiles (GLVs).....	88
2.5.2.	Key objectives.....	89
	Chapter 3. Instrumentation, techniques, and methods	90
3.1	<i>Chemicals</i>	91
3.2	<i>Experimental techniques – background and working principles</i>	91
3.2.1.	Ultraviolet-Visible (UV-Vis) spectroscopy	92
3.2.1.1.	Background	93
3.2.1.2.	Working principles.....	95
3.2.2.	Laser flash photolysis-laser long path absorption (LFP-LLPA)	97
3.2.2.1.	Kinetic Experiments – operation principles	99
3.2.3.	Photooxidation experiments – operation principles	100
3.2.4.	Hyphenated mass spectrometry	101
3.2.4.1.	Capillary gas chromatography-mass spectrometry (cGC-MS)	101
3.2.4.2.	Liquid chromatography-mass spectrometry (LC-MS).....	103
3.2.4.3.	Mass spectrometry in atmospheric chemistry	108
3.3	<i>Experimental methodology</i>	110
3.3.1.	Kinetic studies.....	110
3.3.1.1.	SO ₄ ⁻ kinetics	113
3.3.1.2.	[•] OH kinetics	113
3.3.1.3.	NO ₃ [•] kinetics	114
3.3.1.4.	Diffusion limitations of rate constants	115
3.3.2.	Product study experiments and analytical protocols	116
3.3.2.1.	Mechanistic investigation	117
3.3.2.2.	UPLC analyses.....	118
3.3.2.3.	Carbonyl-targeted cGC-MS analyses.....	118
3.3.2.4.	Alcohol-targeted cGC-MS analyses.....	119
3.4	<i>Theoretical and simulation methods</i>	120
3.4.1.	COPASI	120

3.4.1.1.	Reaction kinetics modeling.....	121
3.4.2.	Density functional theory calculations.....	121
	Chapter 4. Physical properties of green leaf volatiles (GLVs)	123
	<i>Synopsis</i>	124
4.	<i>Physical properties of GLVs</i>	124
4.1.	EPI-estimated partition coefficients, aqueous solubility and vapor pressure of GLVs.....	124
4.2.	Experimentally-measured UV-Vis spectra of GLVs	132
	Chapter 5. Aqueous-phase reactions of green leaf volatiles with sulfate, hydroxyl and nitrate radicals in troposphere: kinetics and atmospheric implications	138
	<i>Synopsis</i>	139
5.1.	<i>Introduction</i>	139
5.2.	<i>Experimental methods</i>	140
5.3.	<i>Results and Discussion</i>	141
5.3.1.	Reactions of SO ₄ ^{•-} radical with PENTOL, HEXOL, and HEXAL.....	141
5.3.2.	Reactions of [•] OH radicals with PENTOL, HEXOL, and HEXAL.	144
5.3.3.	Reactions of NO ₃ [•] radicals with PENTOL, HEXOL, and HEXAL.	147
5.4.	<i>Activation Parameters</i>	150
5.5.	<i>Atmospheric Implications</i>	152
5.5.1.	Atmospheric lifetimes	152
5.5.1.1.	GLV partitioning between gas- and aqueous phases	155
5.5.1.2.	GLV lifetimes	156
5.5.2.	GLV removal rates.....	159
5.5.2.1.	Gas-phase vs. aqueous-phase reactions.....	159
5.5.2.2.	Relative GLV removal rates.	161
5.5.2.3.	GLV removal rates – aqueous-phase reactions	163
5.5.2.4.	Scaled GLV removal rates	164
5.6.	<i>Conclusions</i>	165
	Chapter 6. Evaluating bias of the experimental rate constants determined for the aqueous-phase reactions of selected GLVs with NO₃[•]: COPASI kinetic modeling.....	168
6.1.	<i>Introduction</i>	169
6.2.	<i>Complete kinetic model of GLV – NO₃[•] reactions</i>	169
6.2.1.	Kinetic parameters for reactions (13), (15), (24), and (25) in Table 6.1	171
6.3.	<i>GLV + NO₃[•] rate constant estimated using Model_1</i>	174
6.4.	<i>Percentage bias of the experimentally determined GLV + NO₃[•] reaction rate constants vs. Model_1 estimations</i>	183

Chapter 7. Product studies on the OH radical-mediated aqueous-phase GLV photooxidation.....	185
Synopsis	186
7.1. Introduction.....	186
7.2. Experimental methods.....	187
7.3. Results and Discussion	187
7.3.1. Group contribution method (GCM) estimation (k_{2nd} GLV-OH)	189
7.3.2. PENTOL with \cdot OH radicals	193
7.3.3. HEXOL with \cdot OH radicals	198
7.3.4. HEXAL with \cdot OH radicals	207
7.3.5. DFT results.....	217
7.3.5.1. Reactivity of PENTOL with \cdot OH radical	218
7.3.5.2. Reactivity of HEXOL with \cdot OH radical.....	220
7.3.5.3. Reactivity of HEXAL with \cdot OH radical.....	222
7.4. Atmospheric Implications	225
7.4.1. GLVs and their oxidation products as a SOA precursor	225
7.4.2. Atmospheric significance and impact of aqueous-phase GLVs conversion pathways ...	227
7.4.3. Flux analysis	229
Chapter 8. Summary and future perspective.....	235
8.1. Kinetic studies of the aqueous-phase reaction of GLVs with sulfate, hydroxyl and nitrate radicals in the troposphere and its atmospheric implications	235
8.2. Product studies on the \cdot OH radical-mediated aqueous-phase GLV photooxidation	236
8.3. Formation of aqueous SOA.....	236
8.4. Future direction	237
Appendix.....	238
1. Molar absorption coefficients for selected GLVs in the aqueous phase	238
2. Density functional theory (DFT).....	274
▪ References	280



Chapter 1

Introduction to atmospheric aerosol chemistry

1.1. Atmospheric aerosol

1.1.1. Definition

Atmospheric aerosol is a suspension of liquid and/or solid particles in the air of complex chemical composition and size far below 100 μm . Although associated with Donnon (1923), the term “aerosol” was first used as an analogy to “hydrosol” by Schmauss in 1920.^{1,2} Aerosols or atmospheric particles are commonly referred to as *particulate matter* (PM). PM is quite irregular in shape or imperfectly spherical. Therefore, particle size is measured in terms of aerodynamic diameter (AD), which is defined as the diameter of a spherical particle with density of 1 g cm^{-3} settling in the air with the velocity equal to that of the particle of interest. The settling velocity of spherical particles larger than approximately 1 μm is defined by Stokes’ Law (equation 1.1),³

$$v = \frac{gd^2(\rho_1 - \rho_2)}{18\eta} \quad (1.1)$$

where, settling velocity, v (cm s^{-1}), gravitational acceleration, g (cm s^{-2}), the density of particle, ρ_1 and density of air, ρ_2 (g cm^{-3}), respectively, and air viscosity, η (poise). Settling velocity of microscopic particles smaller than 1 μm , may deviate from the Stokes’ Law and follow the Brownian motion instead. Atmospheric aerosols are mostly associated to particulate matter (PM) and further classified into subcategories based on their sizes. Such as aerosol particles with AD smaller than 10 μm , 2.5 μm , and 1 μm are defined as PM_{10} , $\text{PM}_{2.5}$, and PM_1 , respectively.⁴

1.1.2. Aerosol particle size distribution

Size or aerodynamic diameters of particles govern their key properties, such as transport, deposition, atmospheric lifetimes, removal efficiency, inhalation by organisms, and chemical composition, which strongly affect air quality, climate, and consequently – human and animal health. Aerosol particles size varies over a wide range from a few nanometres up to 100 μm . Based on the size, the particles are divided into different modes:^{5,6} *the nucleation mode* ($\text{AD} < 0.01 \mu\text{m}$); *the Aitken mode* ($0.01 \mu\text{m} < \text{AD} < 0.1 \mu\text{m}$); *the accumulation mode* ($0.1 \mu\text{m} < \text{AD} < 1 \mu\text{m}$); and *the coarse mode* ($\text{AD} > 1 \mu\text{m}$).⁴ The nucleation and Aitken mode particles are also known as *ultrafine particles* or $\text{PM}_{0.1}$.^{4,7} Their sources are usually anthropogenic, e.g., vehicular or industrial emissions, biomass burning, viruses, tobacco smoking or other combustion processes. Due to their small size, they can easily penetrate human lungs and reach

alveolar regions or blood system to pose a great health risk as reviewed well by Schraufnagel (2020).⁷ The accumulation mode particles are either composed of ultrafine or small particles that are formed *via* coagulation and condensation onto existing smaller particles, or are emitted directly (primary aerosols). They show long lifetimes (typically 7-10 days), during which they can be transported over long distances, and finally removed *via* wet deposition.^{4,5,8} The coarse mode particles are mostly formed from natural but also from anthropogenic processes, such as rock erosion, plant debris, road dust and tyreattrition.⁹ Due to their heavier masses, they have high settling velocities and shorter residence times in the atmosphere and thus, can be removed *via* dry deposition. Figure 1.1 briefly classifies aerosol particles in terms of their sizes and respective roles in the atmosphere.¹⁰

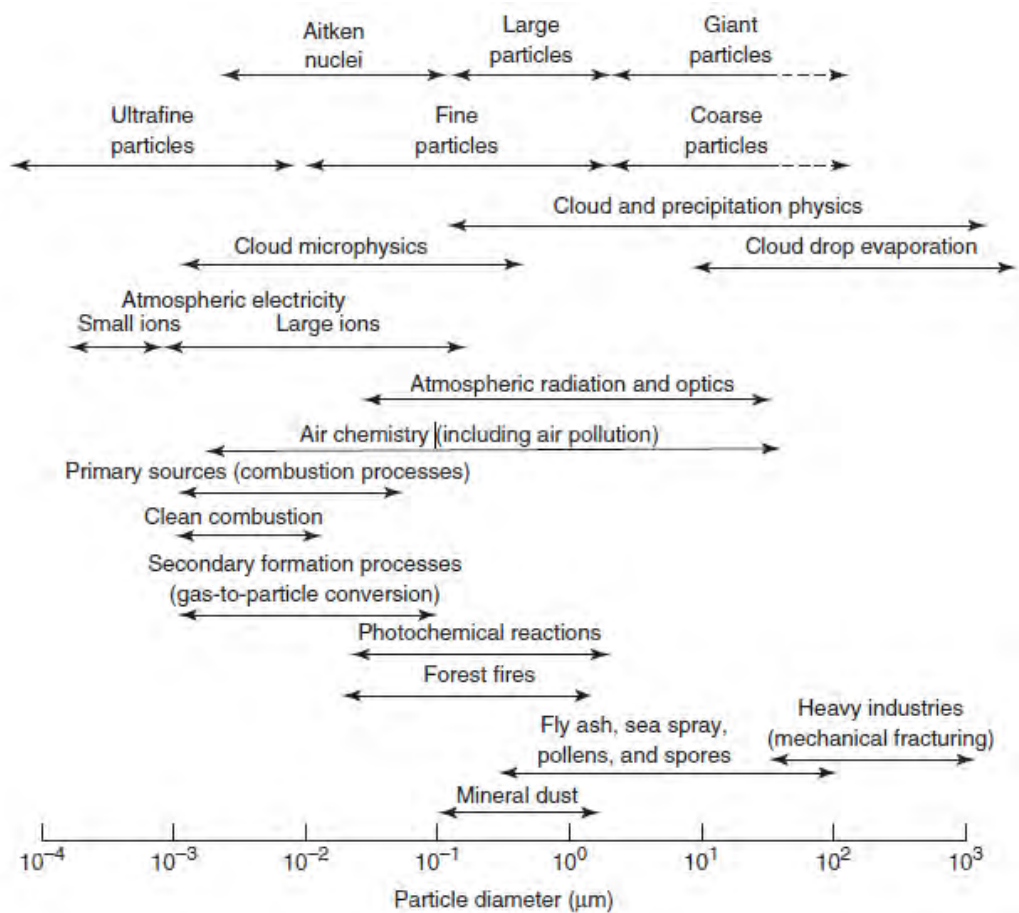


Figure 1.1 Different modes of aerosol particles and their atmospheric roles (by permission from John Wiley and Sons).¹⁰

1.2. Sources of atmospheric aerosol

Atmospheric aerosol originate from either *natural sources* (i.e., biogenic emission, dust, sea-salt spray, volcanic eruption) or *anthropogenic sources* (i.e., industrial emissions, agricultural activities, biomass burning, and fossil fuel combustion)^{11, 12} They are further classified as primary and secondary aerosol.

Primary aerosol include those directly emitted into the atmosphere *via* processes, such as biomass burning, fossil fuel combustion, volcanic eruptions, suspension of mineral dust from mining, soil dust, sea salt spray, carbonaceous materials such as soot. In contrast, secondary particles form in the atmosphere by chemical reactions combined with physical processes (such as nucleation and condensation). These reactions are mainly oxidation processes, which occur in the gas or aqueous phase and are followed by product transfer to the particle phase giving rise to secondary aerosol.¹¹⁻¹⁹ The main physico-chemical processes responsible for the formation of primary and secondary aerosol within the atmosphere include: (a) bulk-to-particle (*b-to-p*) conversion, i.e., physical, chemical, or biological transformation of bulk material into particles and their emission as a primary aerosol into the atmosphere; (b) gas-to-particle (*g-to-p*) conversion of the atmospheric trace gases *via* condensation, nucleation or heterogeneous physico-chemical processes leading to the formation of secondary aerosol; (c) combustion processes, which occur at higher temperatures.¹⁰ The conversion of sulfur dioxide, nitrogen dioxide, and ammonia into particulate phase sulfate, nitrate, and ammonium are simple examples of the formation of secondary particles originating from inorganic sources. Various sources and processes responsible for the formation and transformation of organic aerosol (OA) in the atmosphere is illustrated in Figure 1.2.^{5, 10, 12, 20, 21} Depending on the origin, OA is either primary organic aerosol (POA) or secondary organic aerosol (SOA).

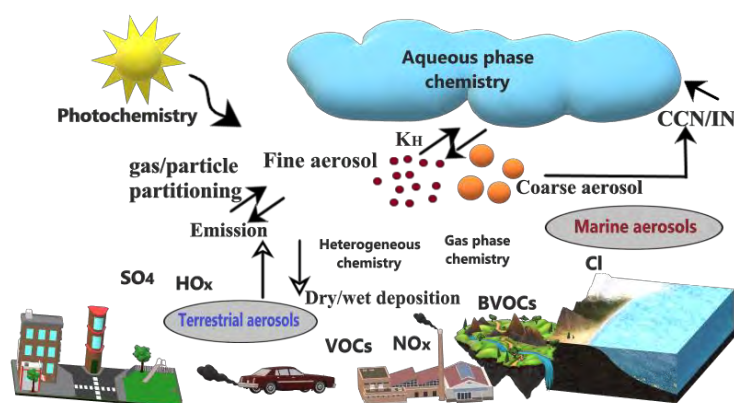


Figure 1.2 Formation and transformation of organic aerosol in the atmosphere^{5, 10, 12, 20, 21}

1.3. Tropospheric aerosol chemistry

The Earth's atmosphere can be divided into several layers, of which the lowest (up to 15 km) is called *the troposphere* and reaches the temperature inversion point, called the tropopause. The troposphere constitutes only a tiny fraction of the whole atmospheric volume, however accounts for 80% of its total mass and contains almost 99% of its water vapor. Due to the temperature inversion in the upper layer (> 15 km) called *the stratosphere*, the mixing between the troposphere and the stratosphere usually is slow, and only trace gases with lifetimes of several years enter the stratosphere. Therefore, it is sufficient to consider only the tropospheric chemistry of all but the halogen containing gases, which do not have any significant removal process in the troposphere.⁴

The bulk composition of the ambient air (99.997% by vol.) consists mainly of N₂ (78 %), O₂ (21%), Ar (0.9%), CO₂ (0.03%). These are stable species with little or no chemistry, except O₂. The remaining components occur in low quantities and are called trace components. About 99% of the atmosphere's mass is allocated below the 50th km, i.e., in the strato- and tropospheres. The atmospheric trace gases vary spatially and temporally, which is significant for the tropospheric chemistry. Table 1.1 lists a few important atmospheric traces gases, their sources, and estimated yearly emissions.²²

Table 1.1. Atmospheric trace gases - sources and emissions ^a (adapted from Wallace and Hobbs)²² given in Tg yr⁻¹ of compound or element (indicated in the parentheses).

Sources		SO ₂ (S)	NH ₃ (N)	N ₂ O (N)	NO _x (N)	CH ₄ (CH ₄)	CO (CO)	VOC ^a (C)
Natural	Biogenic		5.1				100 (60-160)	400 (230-1150)
	Oceans	25 ^b	7.0	3 (1-5)		10 (5-50)	50 (20-200)	50 (20-150)
	Volcanoes	10 (7-10)						
	Others	7.5	2.5	6 (3-10)	13.5 (7-38)	150 ^c		
	Total	42.5	14.6	9 (4-15)	13.5 (7-38)	160 (80-290)	150 (80-360)	450 (250-1300)
Anthropogenic	Fossil fuels	75 ^c			22.5 (20-25)	85 (46-155)	500 (300-900)	70 (60-100)
	Biomass burning	3 ^d	2	0.5 (0.2-1.0)	8 (3-13)	40 (20-80)	500 (400-700)	40 (30-90)
	Agricultural		6.4	3.9 (2-5.8)				
	Industrial			1.3 (0.7-1.8)				
	Others		22			235 (140-380)		
Total	78	30.4	5.7 (3-9)	30.5 (23-38)	360 (206-615)	1000 (700-1600)	110 (90-190)	

^a NO_x, CH₄, CO, and VOC (non-methane volatile organic compounds) are possible O₃ precursors in troposphere. Mean emission values with a range in parenthesis is provided; ^b via oxidation of DMS; ^c major contribution from wetlands (115 Tg yr⁻¹); ^d includes other biospheric source contribution as well.

1.3.1. Biogenic volatile organic compounds (BVOCs) as precursors of secondary organic aerosol (SOA)

It is postulated that up to 90% of OA load present in the Earth's atmosphere is secondary in nature, i.e., exist as SOA, while the rest as POA.¹² The VOCs emission from anthropogenic sources (~150 Tg C yr⁻¹) is far smaller compared to biogenic VOC(BVOCs) emission of 1150 Tg C yr⁻¹ (Table 1.1).²³⁻²⁵ Globally ca. 55% of all emitted BVOCs comes solely from isoprene (35%) and monoterpenes (20%). The remaining mass originates from non-terpenoid compounds, including hexene derivatives (Figure 1.3).²⁶ The estimated contribution of biogenic precursors to SOA is 12–70 Tg yr⁻¹ (bottom-up),^{12, 27} and 140–910 Tg yr⁻¹ (top-down),^{12, 24} much greater than anthropogenic SOA of 0.05–2.5 Tg yr⁻¹ (Table 1.2).²⁸ To address this gap between SOA yields, Hallquist et al.¹² stated that the top-down estimates being two orders of magnitude higher seems highly unrealistic; however, the chamber oxidation

experiments of SOA yields do appear underestimated and warrants further research. Under extreme weather conditions, 90% of the total SOA mass in Europe originates from biogenic sources.²⁹⁻³² Around 30% of PM_{2.5} mass and 20% of PM₁₀ mass comes from organic compounds of mixed volatility that exist both in gas and condensed phases.¹¹ Due to the sparse knowledge on sources, composition, properties, and sink mechanisms of atmospheric aerosols, there are still a significant uncertainties in understanding their impact on climate, human health (e.g., photochemical smog episodes), and in the development of effective inclusive atmospheric models resulting in underestimation of present organic aerosol budget.^{33,34} Prolonged exposure of living organisms to atmospheric aerosols is already known to cause severe health problems, such as asthma, chronic bronchitis, heart, and lung diseases³⁵⁻³⁷ In recent few years, several studies of atmospheric aerosol health effects have been published,^{21, 38-41} including a detailed work of Dr. Faria Khan from Environmental Chemistry Group of the Institute of Physical Chemistry Polish Academy of Sciences.⁴² It is still a big challenge to the scientific community to unveil the uncertainty in the knowledge of sources and precursors of secondary organic aerosol (SOA).^{12, 24, 34, 43, 44}

Table 1.2. Global annual total emissions of BVOCs for the year 2000 using MEGAN 2.1 and respective estimated SOA production from the class of compounds. (Taken from Guenther et al. 2012)⁴⁵

Compound class	Compounds	Emissions (Tg yr ⁻¹)	SOA (Tg yr ⁻¹)	Reference
Isoprene	Isoprene	535	2-6	46, 47
Monoterpenes	α -Pinene	66.1	19.1	27
	<i>t</i> - β -Ocimene	19.4		
	β -Pinene	18.9		
	Limonene	11.4		
	Sabinene	9.0		
	Myrcene	8.7		
	3-Carene	7.1		
Other monoterpenes	Camphene	4.0		
	β -phellandrene	1.5		
	Terpinolene	1.3		
	^a Additional 31 monoterpenes	14.9		
Sesquiterpenes	α -Farnesene	7.1	12.9	48
	β -Carophyllene	7.4		
Other Sesquiterpenes	β -Farnesene	4.0		
	α -Humulene	2.1		
	α -Bergamotene	1.3		

	^b Additional 27 sesquiterpenes	7.1		
232-MBO	232-MBO	2.2	ORVOC:	27
Methanol	Methanol	99.6	15	
Acetone	Acetone	43.7		
Bidirectional VOC	Ethanol	20.7		
	Acetaldehyde	20.7		
	Formaldehyde	5.0		
	Acetic acid	3.7		
	Formic acid	3.7		
Stress VOC	Ethene	26.9		
	Cis-3-hexenal	4.9		
	dimethyl-nonatriene (DMNT)	4.9		
	cis-3-hexenol	2.9		
	^c Additional 11 stress VOC	7.8		
Other VOC	Propene	15.8	-	-
	Butene	8.0		
	Homosalate	2.0		
	Geranyl acetone	0.8		
	^d Additional 45 other VOC	5.5		
Total VOC	Sum of 146 VOC	1007		
CO	CO	81.6		
Total	VOC and CO	1089	Bottom-up: 12-70	12, 24
			Top-down: 140-910	
			Simple models: 20 ± 4.9	49
			Complex models: 59 ± 38	

^a Additional 31 monoterpenes (MT): aromatic MT (*dimethyl styrene, m-cymene, p-cymene, and o-cymene*), MT (*α-phellandrene, α-thujene, α-terpinene, γ-terpinene, bornene, α-fenchene, allo-ocimene, cis-β-ocimene, verbenene, and tricyclene*), oxygenated MT (*camphor, fenchone, piperitone, myrtenal, α-thujone, β-thujone, 1,8-cineole, borneol, linalool, 4-terpineol, α-terpineol, cis-linalool oxide, trans-linalool oxide and bornyl acetate*) and monoterpenoid-related compounds (*β-ionene, ipsenol, and estragole*);

^b Additional 27 sesquiterpenes (ST): sesquiterpenes (*β-bisabolene, acoradiene, aromadendrene, β-bergamotene, α-bisabolene, β-bourbonene, (+)δ-cadinene, (-)δ-cadinene, α-cedrene, α-copaene, α-cubebene, β-cubebene, β-elemene, germacrene B, germacrene D, β-gurjunene, γ-humulene, isolongifolene, longifolene, longipinene, α-muurolene, β-selinene, and δ-selinene*), oxygenated sesquiterpenes (*cis-nerolidol, trans-nerolidol, and cedrol*);

^c Additional 11 stress VOC: *2-hexenal, 3-hexenyl acetate, hydrogen cyanide, hexanal, 1-hexenol, methyl jasmonate, methyl salicylate, toluene, indole, tri-methyl-tridecatetraene (TMTT), jasmine*;

^d Other VOC: leaf surface compounds (*2-ethylhexyl salicylate, oxopentanal, and methyl heptenone*), organic halides (*methyl bromide, methyl chloride, and methyl iodide*), sulfur compounds (*diallyl disulfide, methyl propenyl disulfide, propenylpropydisulfide, carbon disulfide, carbon sulfide, hydrogen sulfide, methyl mercaptan, dimethyl sulfide and dimethyl disulfide*), and alkanes (*methane, ethane, propane, pentane, hexane, heptane*), alkenes (*1-dodecene, 1-tetradecene*), benzenoids (*benzaldehyde, methyl benzoate, 2-phenylacetaldehyde, eugenol, anisole, benzyl acetate, benzyl alcohol, and naphthalene*), oxygenated VOC

(pentanal, hexanal, heptanal, octanal, nonanal, decanal, octanal, octenol, heptanone, 2-butanone, pyruvic acid, 331-methylbutenol, 321-methylbutenol, neryl acetone, α -terpinyl acetate, phenylacetaldehyde and nonenal)

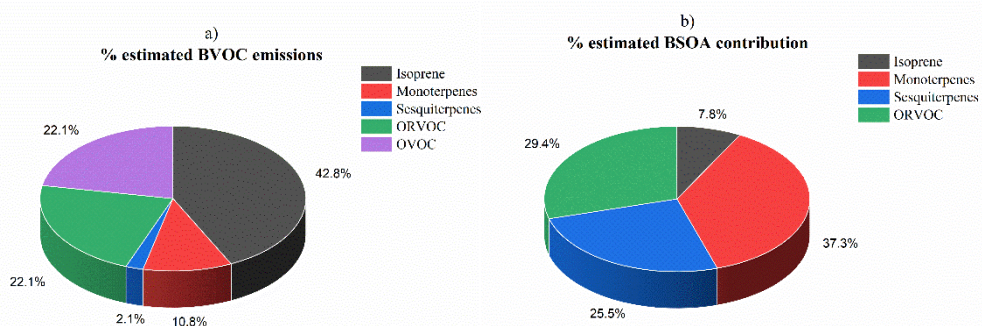


Figure 1.3. a) Estimated annual emission of individual biogenic volatile organic compounds (BVOCs),²⁵ and b) their contribution to the total BSOA budget provided in Table 2.

1.3.2. Atmospheric oxidants and their (photo)chemical reactions with BVOCs

Atmospheric chemical reactions are difficult to simulate in laboratory experiments: *i*) due to very complex system, and *ii*) due to very low concentrations of reactants and products present in natural environment. However, simulation experiments are very useful, including photooxidation in *smog chamber experiments* and/or *aqueous-phase simulation experiments*, where SOA mass forms under strictly controlled conditions from selected organic precursor(s) in the presence of radical species and/or ozone as well as salt seed spray – as condensation nuclei. The most cumbersome part in chamber simulations is a surface of their walls, which can act as a catalyst to reactions or absorb energies, which occurs rarely or very slowly in the actual atmosphere.³

There is a considerable spatial and temporal variation in the emission of natural and anthropogenic VOCs and trace gases, which play an essential role in atmospheric chemistry. A list of gaseous reactive chemical species present in the atmosphere can be categorized as follows:³

- Inorganic oxides (CO, CO₂, NO₂, SO₂)
- Oxidants (O₃, H₂O₂, \cdot OH, HO₂ \cdot , RO₂ \cdot , NO₃)
- Reductants (CO, SO₂, H₂S)
- BVOCs and CH₄

- e. Oxidized organics (carbonyls, organic nitrates, organic sulfates)
- f. Photochemically active species (NO₂, HCHO)
- g. Acids (H₂SO₄), bases (NH₃), and salts (NH₄SO₄)
- h. Unstable reactive or electronically excited species (NO₂, [•]OH)

These species undergo reactions in various phases, such as gas, solid or deliquescent particles, and atmospheric waters, or solid and aqueous surfaces. The key factors of the Earth's tropospheric chemistry include a) UV radiations for photochemical reactions; b) oxidative-capacity radicals, including hydroxy radicals ([•]OH), sulfate radical anions ([•]SO₄⁻), known as atmosphere's detergents, ruling day chemistry, and; c) nitrate radicals (NO₃[•]) governing night chemistry.³ A thorough discussion on radicals is provided in section 1.3.2.2.

1.3.2.1. Kinetics of the atmospheric reactions

It is of the utmost importance to determine the formation and/or decay kinetics of the novel SOA-bound components in order to predict their fate in the atmosphere. Chemical kinetics deals with the reaction rate and the mechanism by defining the importance of each step of the overall reaction. Therefore, I briefly describe the basics of chemical kinetics governing oxidation processes and other chemical reactions in the atmosphere. The determination of kinetics improves the determination of atmospheric lifetimes of atmospheric trace species. Within the scope of the present thesis, basic concepts for understanding the first and second-order reaction kinetics are discussed below.^{50, 51}

1.3.2.1.1. Rate, rate law, and rate constants

Following a general definition, the rate of chemical reaction is a change in the concentration of a reactant or product with time.

Let us consider a reaction $nA + mB \rightarrow pC + qD$, where A, B are reactants and C, D are the reaction products, with n , m , p , q stoichiometric coefficients, respectively.

Then the rate of disappearance of the reactants or appearance of the product is defined by equation 1.2:

$$-\frac{1}{n} \frac{d[A]}{dt} = -\frac{1}{m} \frac{d[B]}{dt} = \frac{1}{p} \frac{d[C]}{dt} = \frac{1}{q} \frac{d[D]}{dt} \quad (1.2)$$

The rate law for non-elementary reactions is defined by equation 1.3:

$$v = k_r A^a B^b \dots \quad (1.3)$$

where: A , and B can be either concentration or partial pressure, p_A , and p_B of the reactants. k is the rate constant and a , and b are the order of reaction with respect to the species. The rate constant shows the probability of the effective collisions between reactants resulting into products and its value dependent on the temperature and pressure.

While dealing with atmospheric chemistry, we present the overall process in terms of elementary reactions, which are usually bimolecular and of order, $(a + b) \leq 3$. Order can be zero, integer, or a fraction. The concentration of the reactants is expressed in M or mol dm⁻³ and time in seconds (s).

Pseudo-first order. If the concentration of one of the reactants in a bimolecular reaction practically remains constant, e.g., in a reaction of O₃ + alkene → products, in the atmosphere. If [O₃] >> [Alkene], then rate law is defined as $-\frac{d[\text{Alkene}]}{dt} = -k_r[\text{O}_3][\text{Alkene}] = -k'_r[\text{Alkene}]$

The first-order rate law is written as $\frac{d[A]}{dt} = -k_r A$, which upon integration results into equation 1.4. The equation describes the exponential decay of the reactant with time during a first order reaction.

$$\ln \frac{[A]}{[A]_0} = -k_r t \quad \text{or} \quad [A] = [A]_0 e^{-k_r t} \quad (1.4)$$

where: $[A]$ and $[A]_0$ are the concentrations of the reactant at time t and 0, respectively. The unit of the first-order rate constant k_{1st} , is s⁻¹.

The second-order rate law is written as $\frac{d[A]}{dt} = -k_r [A]^2$, which upon integration results into equation 1.5. Other types of second-order rate laws are provided in a Table 1.4.

$$\frac{1}{[A]} - \frac{1}{[A]_0} = k_r t \quad (1.5)$$

where: $[A]$ and $[A]_0$ are the concentration of the reactant at time t , and 0, respectively.

Units of the k_{2nd} of the homogeneous reactions of the second order occurring in atmosphere are defined as cm³ molecule⁻¹ s⁻¹ (gas-phase, $[A]$ in molecule cm⁻³), and dm³ mol⁻¹ s⁻¹ (aqueous-phase, $[A]$ in mol dm⁻³).

Heterogeneous reactions are the reactions that occur in more than one phase. Usually, gas or aqueous phase species react on the surface of solid, such as particles or case of rusting of iron, and therefore, its rate is rather governed by the surface area involved. Thus, its k_{2nd} units is defined as $m^2 mol^{-1} s^{-1}$.⁵²

Important conversions factors required, while dealing with kinetics in atmospheric chemistry are provided in Table 1.3.

Table 1.3. Conversion factors for the atmospheric gas-phase reactions. (adapted from Finlayson-Pitts and Pitts, 2000).^{50, 53} The concentration of ppm, ppb, and ppt are relative to air at 1 atm and 298 K.

Conversions Factors for gas-phase reactions	
Concentrations	1 mol L ⁻¹ = 6.02 × 10 ²⁰ molecules cm ⁻³ mg m ⁻³ = 0.0409 × ppm × Mol. Wt.
	1 ppm = 2.46 × 10 ¹³ molecules cm ⁻³ ppm = 24.45 × mg m ⁻³ ÷ Mol. Wt.
	1 ppb = 2.46 × 10 ¹⁰ molecules cm ⁻³ μg m ⁻³ = 0.0409 × ppb × Mol. Wt.
	1 ppt = 2.46 × 10 ⁷ molecules cm ⁻³ ppb = 24.45 × μg m ⁻³ ÷ Mol. Wt.
	1 atm = 760 Torr
Second-order rate constants	cm ³ molecule ⁻¹ s ⁻¹ × 6.02 × 10 ²⁰ = L mol ⁻¹ s ⁻¹
	ppm ⁻¹ min ⁻¹ × 4.08 × 10 ⁵ = L mol ⁻¹ s ⁻¹
	ppm ⁻¹ min ⁻¹ × 6.77 × 10 ⁻¹⁶ = cm ³ molecule ⁻¹ s ⁻¹
	atm ⁻¹ s ⁻¹ × 4.06 × 10 ⁻²⁰ = cm ³ molecule ⁻¹ s ⁻¹

1.3.2.1.2. Half-lives and lifetime or time constant

The integrated rate laws for first-order and second-order reactions are deployed to deduce half-life and time constants, respectively. They are both useful indicators of the order of a reaction. Half-life, $t_{1/2}$ is the time taken for the concentration of the reactant to fall half of its initial concentration, and time constant, τ is the time taken for the reactant concentration to reduce to $1/e$ of its initial concentrations. In atmospheric chemistry, one of the reactant (mosly oxidant) concentration is usually assumed to be constant, while the reactant of interest decreases to $1/e$, which is termed as *a lifetime*. For a first-order reaction, time constant is,

$$\tau = \frac{1}{k_r}.$$
⁵²

Table 1.4. Integrated rate laws and half-life of the zero, first, second, and n^{th} -order reactions (taken from Paula and Atkins, 2014).⁵² Where x is the change in initial concentration of the reactant.

Order, n	Reaction type	Integrated rate laws	$t_{1/2}$	τ
0	$A \rightarrow P$ (Product)	$k_r t = x$ for $0 \leq x \leq [A]_0$	$\frac{[A]_0}{2k_r}$	
1	$A \rightarrow P$	$\ln \frac{[A]_0}{[A]_0 - x} = k_r t$	$\frac{\ln 2}{k_r}$	$\frac{1}{k_r}$
2	$A \rightarrow P$	$\frac{x}{[A]_0([A]_0 - x)} = k_r t$	$\frac{1}{k_r [A]_0}$	
	$A + B \rightarrow P$	$\frac{1}{([B]_0 - [A]_0)} \ln \frac{[A]_0([B]_0 - x)}{([A]_0 - x)[B]_0} = k_r t$		
	$A + 2B \rightarrow P$	$\frac{1}{([B]_0 - 2[A]_0)} \ln \frac{[A]_0([B]_0 - 2x)}{([A]_0 - x)[B]_0} = k_r t$		
	$A \rightarrow P$ with autocatalysis	$\frac{1}{([A]_0 + [P]_0)} \ln \frac{[A]_0([P]_0 + x)}{([A]_0 - x)[P]_0} = k_r t$		
$n \geq 2$	$A \rightarrow P$	$\frac{1}{n-1} \left\{ \frac{1}{([A]_0 - x)^{n-1}} - \frac{1}{([A]_0)^{n-1}} \right\} = k_r t$	$\frac{2^{n-1} - 1}{(n-1)k_r [A]_0^{n-1}}$	

The rate laws, constants, half-lives, and lifetime equation used more in atmospheric chemistry and in some parts of the thesis are provided in Table 1.5. Half-life and lifetimes are calculated with respect to species A of the first-order.

Table 1.5. Rate laws, rate constants, half-lives, and lifetime and their relationship used for atmospheric reactions. (Taken from Finlayson-Pitts and Pitts, 2000)⁵¹

Reaction	Order of reaction	Rate law	Half-life of A, $t_{1/2}^A$	Lifetime of A, τ^A
$A \xrightarrow{k_1} P$	1	$k_1[A]$	$\frac{\ln 2}{k_1}$	$\frac{1}{k_1}$
$A + B \xrightarrow{k_2} P$	2	$k_2[A][B]$	$\frac{\ln 2}{k_2[B]}$	$\frac{1}{k_2[B]}$
$A + B + C \xrightarrow{k_3} P$	3	$k_3[A][B][C]$	$\frac{\ln 2}{k_3[B][C]}$	$\frac{1}{k_3[B][C]}$

In terms of atmospheric chemistry, species A is a VOC emitted into the atmosphere, and B, C are usually oxidants and other molecules present in abundance. The chemical reactions

presented in Table 1.5 are always in competition with the photolysis, other oxidants, and heterogeneous reactions occurring on the surface of other atmospheric particles in the atmosphere, which affect the overall lifetimes of A calculated according to equation 1.6.

$$\frac{1}{\tau_{total}} = \frac{1}{\tau_{OH}} + \frac{1}{\tau_{NO_3}} + \frac{1}{\tau_{hv}} + \dots \quad (1.6)$$

1.3.2.1.3. Temperature-dependence: Arrhenius equation

The Arrhenius expression describes the temperature-dependence of the rate constant for many reactions (equation 1.7).⁵²

$$k = Ae^{-\frac{E_a}{RT}} \quad (1.7)$$

where: k is a rate constant, T is a temperature in K, $R = 8.314 \text{ J K}^{-1} \text{ mol}^{-1}$ is a gas constant, A is a pre-exponential factor, and E_a is the activation energy. Both A and E_a are together known as activation parameters. A plot of $\ln k$ vs. $1/T$ resulting in a straight line is known as the *Arrhenius plot*, for which slope = $-\frac{E_a}{R}$ and $\ln A$ is an intercept at $1/T = 0$ (Figure 1.4a). *The activation energy* is the amount of energy required to overcome the reactants' potential energy barrier and results in the formation of products (Figure 1.4b). The activation energy, i.e., potential energy barrier, can sometimes get negative in value due to the formation of stable intermediate reaction's complexes of lower energies.

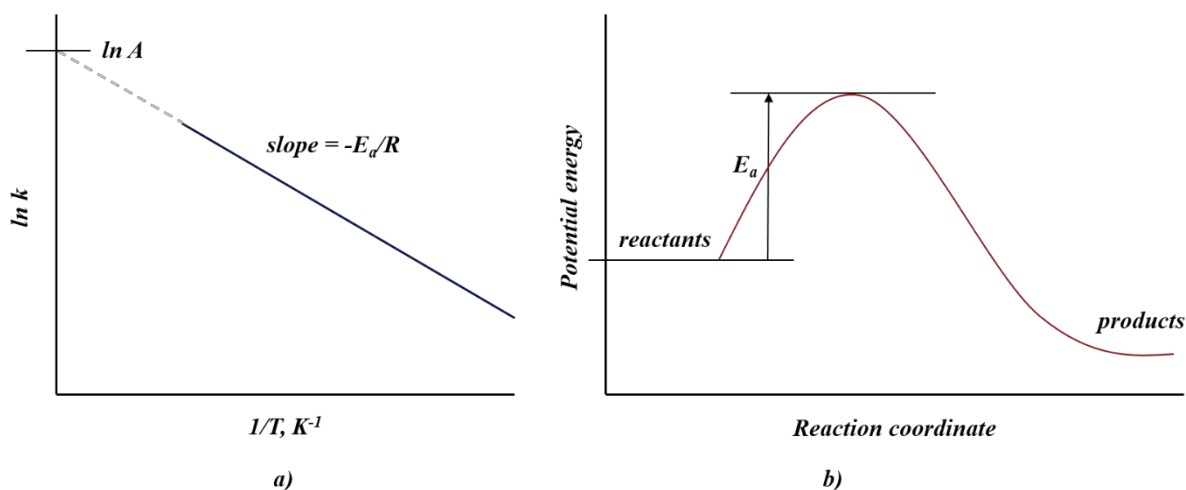
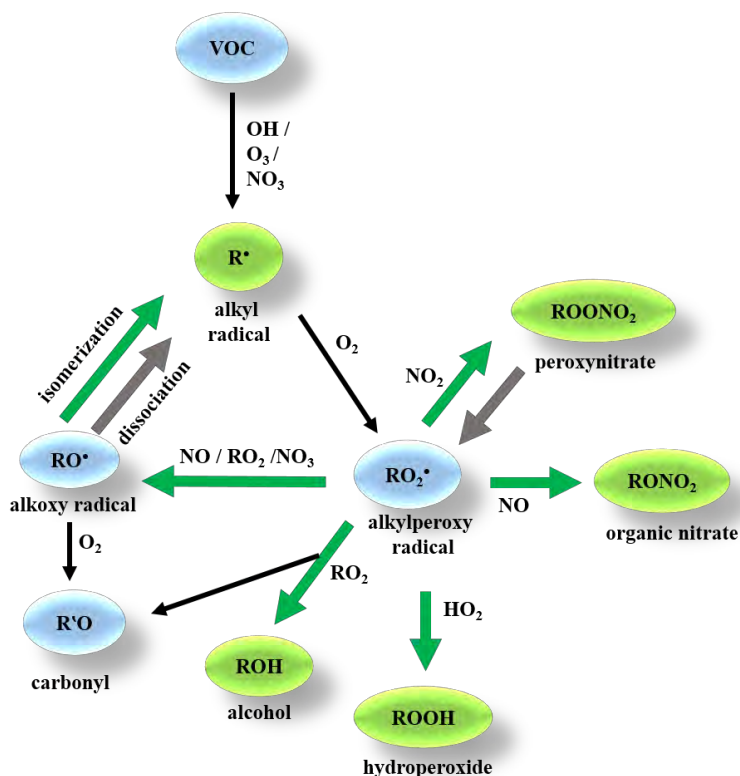


Figure 1.4. a) Arrhenius plot; b) potential energy diagram typical for an exothermic reactions.⁵²

1.3.2.2. Reactions of BVOCs with oxidants in the troposphere

Most of the solar radiation is filtered off by the stratospheric ozone. However, sufficiently energetic light wavelengths enter the troposphere, giving rise to photochemical reactions involving VOCs (biogenic and anthropogenic) with atmospheric oxidants.³ The anthropogenic VOCs mostly include alkanes (paraffins), and alkenes (olefins). While, BVOCs include a broad range of compounds such as alkenes, alkanes, alcohol, aldehydes, ketones, and organic acids. The presence of C=C double bond in the olefin molecules makes them susceptible to photochemical reactions, and hence they have shorter atmospheric lifetimes. The key oxidation pathways of BVOCs are governed by O_x (O_2 , O_3), HO_x ($\cdot OH$, $HO_2\cdot$), and NO_x (NO , NO_2 , and $NO_3\cdot$) chemistry.⁵⁴ Ozone (O_3) mixing ratios range from 20 – 60 ppb, whereas NO_x mixing ratios around 1 – 20 ppb. NO_2 is one of the most photochemically active species within the polluted atmosphere. The criticality remains how the variation in concentration of VOCs and NO_x affect the level of O_3 formation, which has resulted in various photochemical smog episodes in the past (Los Angeles smog 1955, up to 680 ppb).⁴ The most abundant oxidants (O_2 and O_3) are much less reactive under dark conditions due to high bond dissociation energies required. However, the O_3 photodissociation does occur at the wavelengths of 290 – 320 nm, producing excited oxygen atom (O , 1D).⁴

The competitive degradation or oxidation reactions of BVOCs, primarily initiated by $\cdot OH$, O_3 , and $NO_3\cdot$ or $Cl\cdot$ (relevant to marine conditions), depend largely on the structure of VOCs and ambient conditions.^{12, 55, 56} The atmospheric oxidation of VOCs produces species, which are more polar and oxygenated with sufficiently low vapour pressure leading to the formation of SOA.^{12, 56} A general mechanism developed by Kroll and Seinfeld 2008,⁵⁶ is provided in Scheme 1.1 below.



Scheme 1.1 Simplified oxidation mechanism of biogenic VOCs by Kroll and Seinfeld 2008 (permission from Elsevier).⁵⁶ Green color and thick arrow signify transformation to compounds of lower volatility and possible contribution to SOA formation, while grey arrows signify an increase in volatility due to the reaction (Table 1.6).

Pankow and Asher 2007,⁵⁷ developed a group contribution method for the prediction of the volatility change of the oxidation products compared to the parent compounds. Except for aldehydes, ketones and extra carbon (Table 1.6), the addition of oxygen-containing functional group followed by little or no fragmentation of the carbon skeleton leads to the formation of products with at least two order of magnitude lower volatility. Hence, such products most likely lead to the formation of SOA particles in the atmosphere.⁵⁶

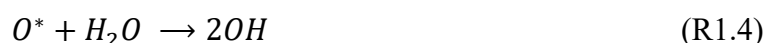
Table 1.6. Change in vapor pressure upon the addition of functional groups to an organic compound, predicted using group contribution method by Pankow and Asher 2007.⁵⁷ (from Kroll and Seinfeld 2008, permission from Elsevier)⁵⁶

Functional Group	Structure	Δ vapour pressure (298 K) ^a
Ketone	-C(O)-	0.10
Aldehyde	-C(O)-H	0.085
Hydroxyl	-OH	5.7×10^{-3}
Hydroperoxyl	-OOH	2.5×10^{-3}
Nitrate	-ONO ₂	6.8×10^{-3}
Carboxylic acid	-C(O)-OH	3.1×10^{-4}
Peroxy acid	-C(O)-OOH	3.2×10^{-3}
Acyl peroxy nitrate	-C(O)-OONO ₂	2.7×10^{-3}
Extra carbon ^b	-CH ₂ -, etc.	0.35

^a Multiplicative factor; ^b for comparison between changes in polarity and changes in the size of a carbon skeleton

1.3.2.2.1. Formation of hydroxyl radicals, $\cdot\text{OH}$

In the atmosphere of unpolluted regions, the photolysis of O₃ at 290 nm < λ > 320 nm produces excited oxygen atom O*, ¹D (R1.1). These O atoms are either deactivated to ground state O, ³P (R1.2, R1.3) or react with water vapor resulting in the formation of hydroxyl radicals ($\cdot\text{OH}$) (R1.4).^{3, 58} According to Levy 1971,⁵⁹ even a small fraction of this atomic oxygen, O produced, reacting with atmospheric water vapor produces sufficient $\cdot\text{OH}$ radicals, making them the most abundant oxidant (1×10^6 $\cdot\text{OH}$ radicals cm⁻³, seasonal and annual average) called a detergent of the atmosphere.^{58, 60} Also, variation in the $\cdot\text{OH}$ concentrations during weekdays, weekends, and under high and low NO_x conditions can certainly occur.⁶¹



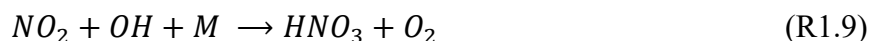
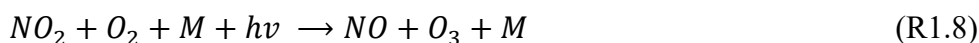
In the presence of organic pollutants, $\cdot\text{OH}$ is produced as an intermediate of the photochemical smog formation (R1.5), while in the higher atmosphere, it is produced via photolysis of H_2O (R1.6).³



1.3.2.2.2. Formation of nitrate radicals, $\text{NO}_3\cdot$

N_2O is the most abundant ($1.3 \times 10^3 \text{ Tg(N)}$) and the only greenhouse gas out of all oxides of nitrogen present in the atmosphere. The other oxides, termed as NO_x (NO and NO_2) are together present in trace amounts (0.75 Tg(N)), but very crucial for the atmospheric chemistry processes. The other nitrogen-containing gas, NH_3 , serves as the neutralizing agent for acids produced from SO_2 and NO_2 , that leads to the formation of salts, such as ammonium sulfates and nitrates, which assist in the aerosol particle formation.¹⁰

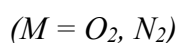
During the daytime, NO and NO_2 undergo interconversion by the NO_x photochemical cycle (R1.7, R1.8). The major NO_2 sink is conversion to HNO_3 (R1.9), which is further removed *via* wet or dry deposition for *ca.* 1 week.^{10, 22}



At night, the chemistry becomes different as no more photolysis of NO_2 occurs, and thus entire NO is converted to NO_2 rapidly upon reaction with O_3 ($k_{\text{NO}_3+\text{O}_3} = 1.9 \times 10^{-14} \text{ cm}^3 \text{ molecule}^{-1} \text{ s}^{-1}$ at 298 K).⁴The formation of nitrate radical ($\text{NO}_3\cdot$) can occur *via* reactions of NO_2 with O_3 (R1.10) and *via* the thermal decomposition of formed N_2O_5 , which is an equilibrium reaction (R1.11):

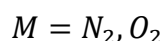
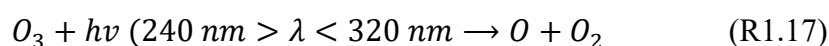
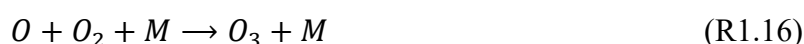
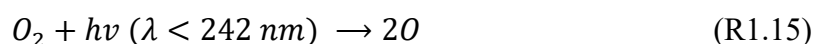


During the day, $\text{NO}_3\cdot$ concentrations are negligible as they are rapidly photolyzed (R1.12, R1.13) and react with NO (R1.14), with a very short lifetime of $\sim 5 \text{ s}$.

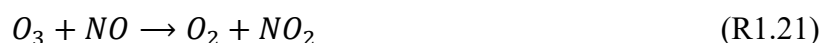
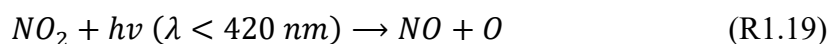


1.3.2.2.3. Formation of Ozone, O₃

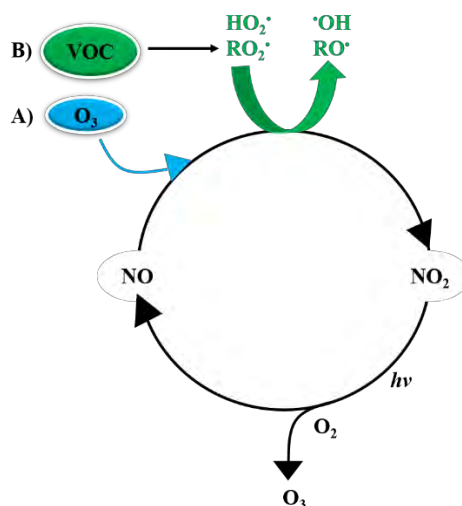
About 90% of the atmospheric O₃ is produced within the stratosphere, where it acts as an ozone layer to absorb and shield human beings from the harmful UV-B solar radiation. In the 1930s, a British scientist, Sydney Chapman, proposed the mechanism of O₃ production in the atmosphere known as *the Chapman cycle* (R1.15 – R1.18).^{4, 5}



The O₃ within the remote troposphere is formed due to the reaction of CO and methane (CH₄) with •OH radicals. Both CO and CH₄ are long-lived species (lifetime with •OH, 2 months - 9 years). The two major precursors for the formation of O₃ within the troposphere are VOCs and NO_x (NO and NO₂).^{4, 22} In the presence of only NO_x, O₃ formation occurs due to the photolysis of NO₂ (R1.19) followed by reaction, R1.20. However, O₃ is immediately removed due to the reaction (R1.21), resulting in its no net loss or formation.^{4, 22, 58}



In the presence of both VOCs and NO_x, net loss and formation of O₃ depends overall on the concentration of NO present in the troposphere (Scheme 1.2).⁵⁸



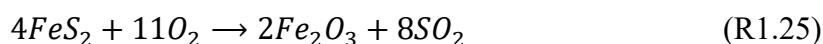
Scheme 1.2. NO-NO₂-O₃ system for the formation of O₃: pathway A) in the absence of VOCs; B) in the presence of VOCs (taken from Roger Atkinson 2000)⁵⁸

1.3.2.2.4. Formation of sulfate radical anions, SO₄⁻

The key sulfur sources in the atmosphere are anthropogenic processes, such as combustion of coal and fossil fuels. However, it is also released in the form of SO₂, H₂S, and dimethyl sulfide (CH₃)₂S by natural sources, such as volcanoes eruptions and oceans. It is worth noting that 99% of the sulfur released into the atmosphere is converted to SO₂, while the remaining mass to SO₃ *via* the following reactions:³

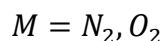


The sulfur originating minerals, such as pyrite is converted to SO₂ by the following equation:

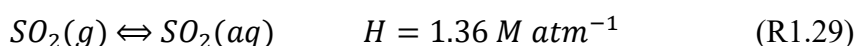


The likely atmospheric chemical reactions of sulfur dioxide (SO₂) include photochemical reactions in the absence and presence of NO_x and alkenes, reactions in water in the presence of metal salts and ions, and on the surface of preexisting aerosol particles. A direct photodissociation is, however, insignificant in the presence of the light of wavelength, $\lambda < 218$ nm, and therefore, the presence of other oxidizing species, such as OH·, HOO·, O₃, NO₃, ROO·, and RO· is a must to oxidize SO₂ in the atmosphere. These conditions required for the oxidation of the SO₂, are also the necessary constituents of the photochemical smog.

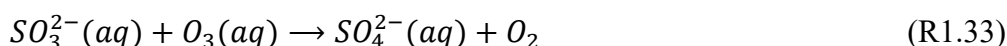
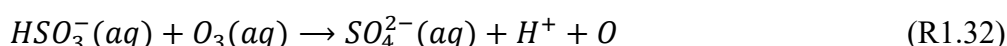
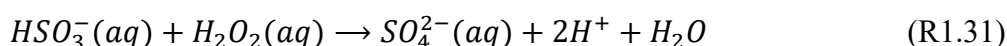
The gas-phase oxidation is believed to be very slow (with an overall contribution of SO₂ to sulfate aerosol conversion of less than 10%).^{3, 62} The most important oxidation reaction is in the presence of ·OH radicals during daytime.^{62, 63}



In the presence of atmospheric waters, such as fog and cloud, the oxidation reaction responsible for SO₂ to particulate sulfate conversion, usually denoted by S(IV) to S(VI) conversion, occurs more rapidly.^{63, 64} After dissolution in water, SO₂ undergoes dissociation forming S(IV) species (i.e., H₂O·SO₂, HSO₃⁻, and SO₃²⁻) which are at pH = 2-7 typical of the atmospheric waters mostly in the form of HSO₃⁻.^{4, 62, 63}

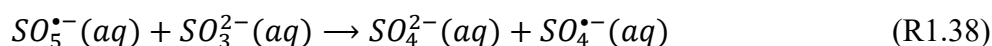
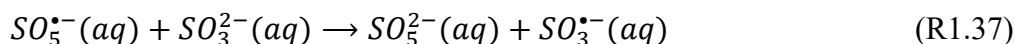
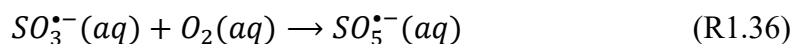
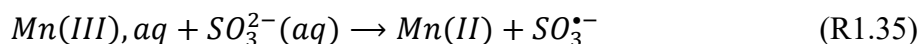
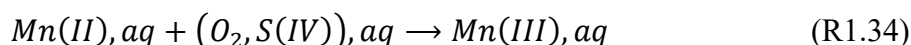


The most likely oxidants responsible for the production of sulfate in the atmospheric aqueous phase are O₃, H₂O₂, and O₂ in presence of transition metal ions as catalysts. However, H₂O₂, which is pH independent (unlike O₃), is considered the leading oxidant.^{3, 62, 63, 65}



Transition metal ions, such as Fe (II)/Fe(III), Mn (II) exist in atmospheric liquid water and surface of the particles (at high humid conditions), and are known to act as catalysts to initiate autoxidation of S(IV) oxides.⁶⁶ Significant contribution to the total oxidation of SO₂ in fog and cloud waters, especially in non-photochemical conditions, such as night time foggy regions, where the concentrations of H₂O₂ and O₃ are low, may come from the autooxidation of S(IV) species in the presence of the transition metal ions.⁶⁷⁻⁶⁹ Also, two or more coexisting transition metal ions can have a significant synergistic effect on the S(IV) autooxidation.⁷⁰⁻⁷² Such catalysis have been extensively investigated in various atmospherically relevant scenarios;^{68, 73-86} a simplified mechanism of the aqueous-phase autoxidation for S(IV) species (as SO₃²⁻) in

presence of Mn(II) as an example is provided below (R1.34 – R1.38) as described by Rudzinski 2004:⁷⁸

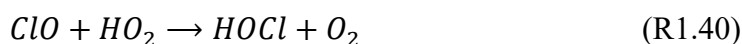


The other pathways of SO₂ oxidation to sulfate include heterogeneous reactions, such as on the surface of soot particles or oxides of metals, which can act as catalysts for the reaction.^{3, 63}

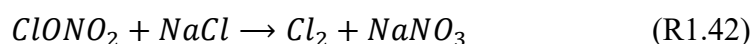
1.3.2.2.5. Formation of Cl atoms

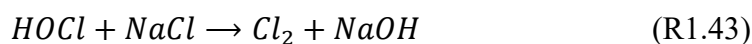
The halogens are known to play an important role in stratospheric chemistry,⁸⁷⁻⁸⁹ but their role in tropospheric chemistry is now continuously growing due to the anthropogenic activities, thereby increasing halogen concentrations within the troposphere.⁹⁰⁻⁹⁴ Despite of the lower concentrations of chlorine (Cl) atoms in the troposphere compared to •OH radicals, their reaction rate is observed to be faster with VOCs and thus cannot be neglected in atmospheric models.^{95, 96} The review articles by Cicerone 1981,⁹⁷ and Simpson *et al.* 2015,⁹⁸ shed the light on the halogen chemistry throughout the troposphere. The oceans inject hygroscopic salts, such as NaCl, KCl, CaSO₄, (NH₄)₂SO₄, which *via* bubble bursting forms sea-salt particles containing Cl⁻(aq). This Cl⁻ ion upon oxidation can lead to the formation of their oxides, such as ClO_x.

Under marine conditions, Cl atoms are readily oxidized by O₃ *via* the following reaction chains:



HOCl and ClONO₂ can be further photolyzed to Cl atoms or can further undergo heterogeneous reaction to generate photochemically active halogen-containing species Cl₂, which upon photolysis produces Cl• radical.²²





1.4. Impact of atmospheric aerosol on air quality, health and climate

Aerosol particles or total suspended particulate matter (TSP) is a highly complex mixture of organic and inorganic compounds. While larger particles usually consist of sand and dust particles, smaller particles are mostly of the secondary origin. In photochemically oxidizing environments, such as smog, they immensely affect air quality and health.^{3, 99}

There are two distinct categories of smogs: *classical smog* (or 1952 London-type smog) and *photochemical smog* (or Los Angeles-type smog). The London-type smog shows the reducing properties, because of the presence of sulfuric acid and SO₂ in a humid atmosphere. London-type smog occurs due to the high levels of uncontrolled combustion of coal for domestic and industrial purposes leading to the extremely high levels of SO₂ and soot particles favourable for classical smog formation.^{3, 100} SO₂ is readily oxidized and has a relatively short lifetime. In contrast, photochemical smog, reveals the oxidative capacity, with hydrocarbons, sunlight and nitrogen oxides acting as essential reactants. Photochemical smog requires the stable atmosphere providing enough time for reactants to react, which is achieved by the phenomenon of temperature inversion.^{3, 100} Such smog conditions lead to reduced visibility, eye irritation, deterioration of materials and loss of lives due to harmful effects on human health. To mitigate and tackle such episodes, various measures have been taken worldwide by various agencies and scientific communities. EUROTRAC-2 project based on “Transport and Chemical Transformation of Environmentally Relevant Trace Constituents in the Troposphere over Europe”, and United States Clean Air Act first formulated in 1963 under which U.S. Environmental Protection Agency (EPA) is required to develop National Ambient Air Quality Standards (NAAQS).

The exposure to toxic aerosol particles of known and unknown composition pays a toll of hundreds of thousands deaths each year around the globe. In Poland, for example, air pollution resulted in nearly 50,000 premature deaths in 2018.¹⁰¹ The EPA also found that most of those (46,300) were caused by PM_{2.5}. In the EU overall, PM_{2.5} caused the premature deaths of 379,000 people, meaning that one in eight were Polish.

In particular, fine and ultrafine particles remain a large concern due to their high surface area and a size range of nanometres leading to very high reactivity and toxicity. They can easily

penetrate down the respiratory system leading to severe cardiovascular, respiratory, and allergic diseases with an adverse effect on human health.^{7, 21, 37, 102-105} For efficient measures to improve air quality, enhanced understanding of the atmospheric reactions *via* investigation of unknown sources, precursors and their toxicological studies are required.²¹

Atmospheric particles have significant climate impacts by either scattering and absorbing light or forming clouds, serving as cloud condensation nuclei (CCN) and ice nuclei (IN). The CCN and IN facilitate the formation of clouds and fogs *via* condensation or nucleation of supersaturated water vapor and can include a variety of species.²⁰ The IPCC 2013 report states that “*Clouds and aerosols continue to contribute the largest uncertainty to estimates and interpretations of the Earth’s changing energy budget*”.¹⁰⁶ To address the issue, aerosol-cloud processes have been the most significant uncertainty source in climate models in the last decade.²² Thus, there is a continuous need to develop our understanding of cloud formation with ambient-like complex particles.

Chapter 2

Research background and objectives



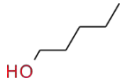
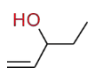

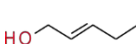
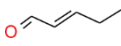
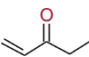
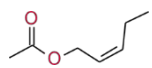
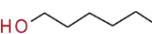
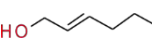
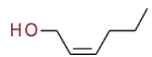
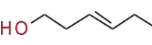
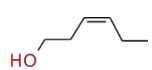
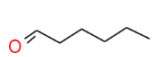
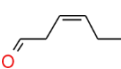
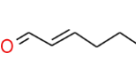

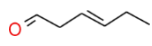
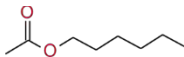
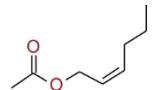
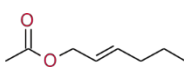
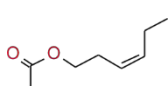
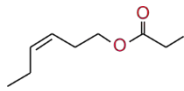
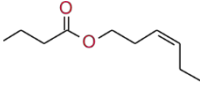
Synopsis

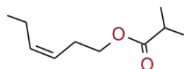
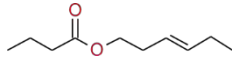
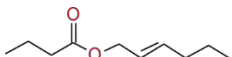
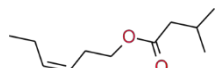
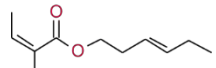
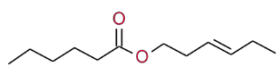
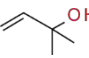
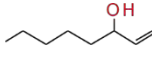
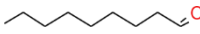
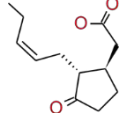
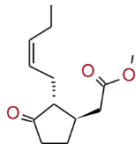
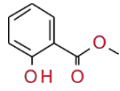
This chapter reviews the current state of atmospheric chemistry and significance of green leaf volatiles (GLVs) as the background for the thesis. I co-authored an extensive review on that topic (“*Green Leaf Volatiles in the Atmosphere—Properties, Transformation, and Significance*”, *Atmosphere* 2021, 12(12), 1655, DOI: 10.3390/atmos12121655), whereas here, I briefly summarize the available scientific data relevant to the present thesis. The chapter summarizes kinetics and oxidation product study data available from the literature for reactions between selected GLVs (1-penten-3-ol, (*Z*)-2-hexen-1-ol, and (*E*)-2-hexen-1-al) and atmospherically relevant radicals, both in gas and aqueous phase. Alongside, multiphase and heterogeneous transformations of GLVs are reviewed to present the smog-chamber and ambient air experiments, products and product yields identified therein, including secondary organic aerosol (SOA) formed. Based on literature review, GLVs were recognized as atmospheric compounds that reside primarily in the gas phase, while their transformation in atmospheric waters should not be excluded.

2.1. Introduction to green leaf volatiles (GLVs)

Green leaf volatiles, commonly abbreviated as GLVs, are C5 and C6 volatile organic compounds (aldehydes, alcohols, ketones, and esters) emitted by plants in response to biotic or abiotic stress conditions, such as mechanical wounding, herbivore attack, drought, high and low temperatures.¹⁰⁷⁻¹¹⁴ These compounds, typically responsible for “green odor” of the green leaves, are synthesized rapidly *via* lipoxygenase (LOX) pathway and are also used for fostering the interplant communication.^{107, 115, 116} The instant emission of GLVs begins with the mechanical damage, such as cutting of plant stem, and continues for hours when the plant material dries.¹¹⁷ The unsaturated C5 and C6 compounds, such as (*Z*)-3-hexenol, (*Z*)-3-hexenyl acetate, (*E*)-2-hexenal, (*Z*)-2-hexen-1-ol, (*Z*)-2-penten-1-ol and 1-penten-3-ol, and plant metabolites and hormones,^{118, 119} such as jasmonic acid (JA), methyl jasmonate (MeJa), methyl salicylate (MeSa), and 2-methyl-3-butene-2-ol (MBO), are all listed as GLVs.¹²⁰⁻¹²⁹ Besides, the wounded plants emit compounds, such as methanol, acetaldehyde, acetone, butanone, and formaldehyde.¹²¹ Conditions, such as the light-dark transition¹²² and high-light exposure¹³⁰ also result in the emission of GLVs from plants. Compounds considered GLVs within the present thesis are listed in Table 2.1.

Table 2.1. Key Green Leaf Volatiles detected in plant emissions.

Name ^a	Chemical formula	MW g mol ⁻¹	Structure	References
pentan-1-ol	C ₅ H ₁₂ O	88.15		115, 131
1-penten-3-ol	C ₅ H ₁₀ O	86.13		115, 123, 125, 131-135
(Z)-2-pentenol	C ₅ H ₁₀ O	86.13		131, 134-136
(E)-2-pentenol	C ₅ H ₁₀ O	86.13		133
(E)-2-pentenal	C ₅ H ₈ O	84.12		133, 135
1-penten-3-one	C ₅ H ₈ O	84.12		115, 123, 132-135
(Z)-2-pentenyl acetate	C ₇ H ₁₂ O ₂	128.17		136
n-hexan-1-ol	C ₆ H ₁₄ O	102.16		123, 131, 133, 137, 138
(E)-2-hexen-1-ol	C ₆ H ₁₂ O	100.16		131, 133, 137
(Z)-2-hexen-1-ol	C ₆ H ₁₂ O	100.16		125
(E)-3-hexen-1-ol	C ₆ H ₁₂ O	100.16		133, 137
(Z)-3-hexen-1-ol (leaf alcohol)	C ₆ H ₁₂ O	100.16		115, 116, 121-123, 125, 131, 133, 136, 137, 139-142
n-hexan-1-al	C ₆ H ₁₂ O	100.16		109, 125, 131, 133, 135, 137-139, 141, 143
(Z)-3-hexenal	C ₆ H ₁₀ O	98.14		115, 121, 122, 125, 131, 133, 137- 139, 142-144
(E)-2-hexenal (leaf aldehyde)	C ₆ H ₁₀ O	98.14		115, 116, 125, 131, 133, 136-138, 140, 141, 143
(Z)-2-hexenal	C ₆ H ₁₀ O	98.14		123, 133
(E)-3-hexenal	C ₆ H ₁₀ O	98.14		133, 137, 142
hexyl acetate	C ₈ H ₁₆ O ₂	144.21		138, 142, 145, 146
(Z)-2-hexenyl acetate	C ₈ H ₁₄ O ₂	142.20		125
(E)-2-hexenyl acetate	C ₈ H ₁₄ O ₂	142.20		133, 142
(Z)-3-hexenyl acetate (leaf acetate)	C ₈ H ₁₄ O ₂	142.20		121-123, 125, 131, 133, 136, 137, 139, 142
(Z)-3-hexenyl propionate	C ₉ H ₁₆ O ₂	156.22		133, 135, 147
(Z)-3-hexenyl butanoate	C ₁₀ H ₁₈ O ₂	170.25		135, 142, 145-148

(Z)-3-hexenyl isobutanoate (isobutyrate)	C ₁₀ H ₁₈ O ₂	170.25		135, 145, 147
(E)-3-hexenyl butanoate	C ₁₀ H ₁₈ O ₂	170.25		146
(E)-2-hexenyl butanoate	C ₁₀ H ₁₈ O ₂	170.25		142, 147
(Z)-3-hexenyl isopentanoate	C ₁₁ H ₂₀ O ₂	184.27		145, 147, 149
(Z)-3-hexenyl 2-methyl-2-butenate	C ₁₁ H ₁₈ O ₂	182.26		145, 147, 149
3-hexenyl hexanoate ^b	C ₁₂ H ₂₂ O ₂	198.3		146
2-methy-3-buten-2-ol	C ₅ H ₁₀ O	86.13		150-152
1-octen-3-ol	C ₈ H ₁₆ O	128.21		125, 133, 153
nonanal	C ₉ H ₁₈ O	142.24		149
jasmonic acid	C ₁₂ H ₁₈ O ₃	210.27		131, 144, 154
methyl jasmonate	C ₁₃ H ₂₀ O ₃	224.30		131, 154
methyl salicylate	C ₈ H ₈ O ₃	152.15		113, 135, 145

^a for convenience of the audience, we used traditional GLV names rather than the latest IUPAC recommendations;
^b unspecified isomer.

The estimated annual global emission of BVOC is 1087 Tg yr⁻¹ (based on Community Land Model (CLM4) integrated with the MEGAN2.1 framework for estimating fluxes of biogenic compounds between terrestrial ecosystems and the atmosphere).⁴⁵ It includes isoprene (535 Tg yr⁻¹), monoterpenes (162 Tg yr⁻¹), and other organics (390 Tg yr⁻¹). The calculations included GLVs within a stress VOC group, which also included: 3-hexenal, 2-hexenal, 3-hexenol, 3-hexenyl acetate, hexanal, 1-hexenol, while MBO was considered individually (see Chapter 1, Table 1.2). The estimated emission of (Z)-3-hexenal, (Z)-3-hexenol, and MBO were 4.9, 2.9, and 2.2 Tg yr⁻¹, respectively. In comparison, the annual emission of MBO averaged throughout 1980 – 2010 was 1.6 ± 0.1 Tg yr⁻¹, including value obtained with MEGAN.¹⁵⁵ Furthermore, approximate 1.5 to 2.6 Tg C yr⁻¹ of GLVs are emitted as a result of plant defence, cutting, and drying yearly in North America, with estimated rates of 0.1 to 0.2 µg C g⁻¹ h⁻¹.¹⁵⁶ In spite of relatively small global emission of GLVs, the local and seasonal emissions of GLVs

may become more significant due to harvesting or grass mowing episodes, impacting local SOA burden, and thus local air quality. The emission budget can increase further, if GLVs based treatments become more popular in the agriculture, horticulture, and forestry practices.¹⁵⁷⁻¹⁶¹

After emission, unsaturated GLV compounds encounter several other reactants or oxidants in the atmosphere, such as $\cdot\text{OH}$ and $\text{NO}_3\cdot$ radicals or O_3 , and immediately react with them forming secondary organic aerosol (SOA).^{162, 163}

Table 2.2. Comparison of different existing model-based SOA production and SOA burden.

S.No.	Model	Emission,	SOA production	SOA Burden	Ref.
1.	STOCHEM	29 Tg yr ⁻¹ (sesquiterpenes (SSTs)) 162 Tg yr ⁻¹ (monoterpenes (MTs))	46.4 Tg yr⁻¹	0.45 Tg Isoprene: 0.010 Tg (2%), MTs: 0.188 Tg (44%), MTs + SSTs: 0.41 Tg (10%)	48
2.	GEOS-CHEM				164
a.	Volatility basis set (VBS)		36.2 Tg yr⁻¹	0.88 Tg	
		biogenic	21.5 Tg yr ⁻¹	0.53 Tg	
		anthropogenic + biomass burning	14.7 Tg yr ⁻¹	0.35 Tg	
b.	Extended VBS Model	Semi-volatile + intermediate-volatile OC + new chamber SOA yields + wet-deposition + dry-deposition + SOA photolysis + heterogenous SOA loss	132. Tg yr⁻¹	0.88 Tg	
		biogenic	97.5 Tg yr ⁻¹	0.59 Tg	
		anthropogenic + biomass burning	8.8 Tg yr ⁻¹	0.08 Tg	
		Semi+intermediate VOC	25.9 Tg yr ⁻¹	0.21 Tg	
3.	CESM model : CAM5.3 and CLM4 components	Isoprene	55.7 Tg yr⁻¹	1.07 Tg	165

All existing model-based estimations of the global SOA production and burden predict mixed results (Table 2.2). The intercomparison based on 31 global chemistry-transport and general circulation models showed that the annual global SOA output ranged from 13 – 121 Tg yr⁻¹, whereas for models considering semi-volatile character of SOA the range was 16 – 121 Tg yr⁻¹.⁴⁹ It was estimated that isoprene alone contributed 6 – 30 Tg yr⁻¹ of SOA (gas-phase reactions)⁴⁷ with additional 2 Tg yr⁻¹ from aqueous-phase reactions.¹⁶⁶ Compared to all predicted SOA from the major biogenic precursors (Table 2.2), 1 – 5 Tg C yr⁻¹ of SOA from GLVs¹⁶⁷ seems less likely or overestimated, and therefore needs re-evaluation.

The present extensive literature review provided a background and framework for designing the research of my thesis as well as for future investigation of GLVs significance and role in the atmospheric processes, especially contribution to the SOA formation. Besides, GLVs based literature review was necessary to make a wise selection of the GLV compounds (i.e., 1-penten-3-ol, (*Z*)-2-hexen-1-ol, and (*E*)-2-hexen-1-al) among 30 of them listed in Table 2.1 for my Ph.D. research work.

2.2. Gas-phase reactions of GLVs with atmospheric oxidants

GLVs are known to react with oxidants, such as hydroxyl ($\cdot\text{OH}$), nitrate ($\text{NO}_3\cdot$) radicals, ozone (O_3) and Cl atoms in the atmospheric gas phase. Here, I briefly outline the detailed chemical mechanisms and oxidation products arising from reactions with selected GLVs or their isomers, as known until 2021. More is discussed in detail within my co-authored review article.¹⁶⁸

2.2.1. Products and mechanism

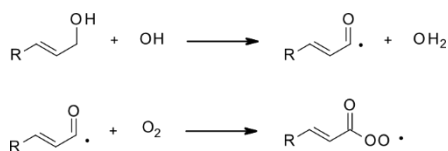
General scheme for the reactions of VOCs with radicals, is provided in Chapter 1 (Section 1.3.2.2, Scheme 1.1).^{169, 170} The reaction between VOC and oxidant/radicals can proceed *via* addition to a double C=C bond or by hydrogen abstraction, which leads to the formation of alkyl radical ($\text{R}\cdot$). The latter reacts with O_2 forming the alkylperoxy radical ($\text{RO}_2\cdot$). $\text{RO}_2\cdot$ has diverse fates based on the availability of the reactants. The possibilities include a self-reaction with another $\text{RO}_2\cdot$, reaction with $\text{HO}_2\cdot$ radicals, reaction with NO_2 , and/or reaction with NO , which lead to variety of product formations, such as carbonyls, alcohols, peroxyxynitrate or alkoxy radicals.

2.2.1.1. Reaction with $\cdot\text{OH}$ radicals

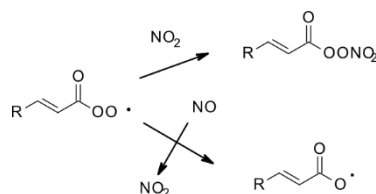
The reactions of unsaturated GLVs with $\cdot\text{OH}$ radicals can proceed *via* addition of $\cdot\text{OH}$ radicals to C=C bond as well as the $\cdot\text{OH}$ radical-driven hydrogen abstraction.

2.2.1.1.1. H-abstraction from GLVs by $\cdot\text{OH}$ radicals

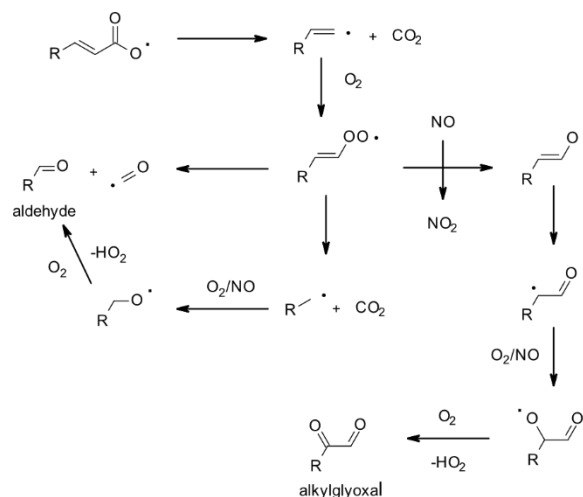
The general scheme based on the experimental findings of Davis et al.¹⁷¹ for the reaction of unsaturated GLV (aldehyde) with $\cdot\text{OH}$ species *via* hydrogen abstraction pathway is provided below in Schemes 2.1 - 2.3, which show the important steps of the process, and thereby the formation of an aldehyde and alkylglyoxal.



Scheme 2.1. Formation of peroxy radicals *via* hydrogen abstraction from an unsaturated GLV compound (aldehyde).¹⁷¹ (Sarang et al. 2021)¹⁷²



Scheme 2.2. Formation of peroxy nitrates and alkoxy radicals *via* reactions of NO₂ and NO with peroxy radicals, respectively.¹⁷¹ (Sarang et al. 2021)¹⁶⁸

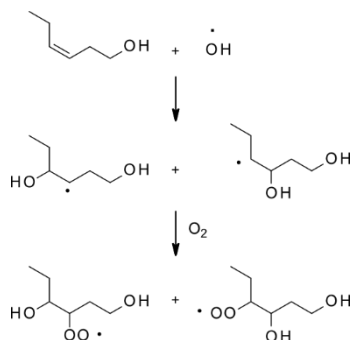


Scheme 2.3. Formation of an aldehyde and an alkylglyoxal *via* reaction of alkoxy radical.¹⁷¹ (Sarang et al. 2021)¹⁶⁸

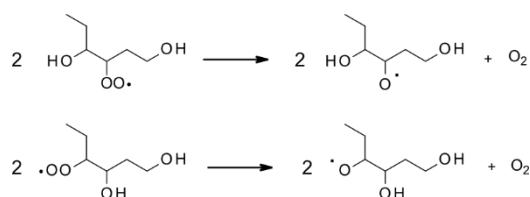
2.2.1.1.2. Addition of ·OH radicals at the C=C bond of GLVs

As a GLV example, (*Z*)-3-hexen-1-ol was used to explain the basic mechanistic concept of ·OH radicals addition at C=C. In Scheme 2.4, the ·OH adds to the C=C bond (either position) producing two alkoxy radical isomers, which further react with O₂ to produce two peroxy radical isomers.¹⁷³ In the absence of NO_x (Scheme 2.5), the self-reaction of peroxy radicals produces two isomeric alkoxy radicals.¹⁷³⁻¹⁷⁶ Whereas, in the presence of NO (Scheme 2.6), it reacts either *via* subtraction of one oxygen atom to produce two alkoxy radicals^{171, 173-182} or *via* addition to produce two organic dihydroxy nitrates.^{177, 180} The alkoxy radicals can either

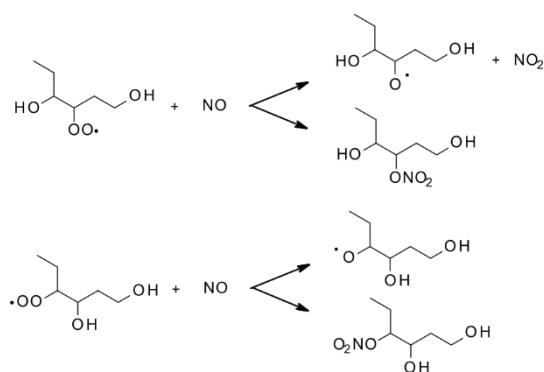
isomerize^{180, 183}, decompose^{173-176, 180} or undergo hydrogen abstraction^{175, 176} (Scheme 2.7). The major products formed include 3,4-dihydroxyhexanal, propanal, 3-hydroxypropanal, and two dihydroxy and one trihydroxy hexanone. Propanal may further react with $\cdot\text{OH}$, O_2 and NO_x to produce peroxy nitrates, formaldehyde (HCHO), and CO_2 .¹⁷³



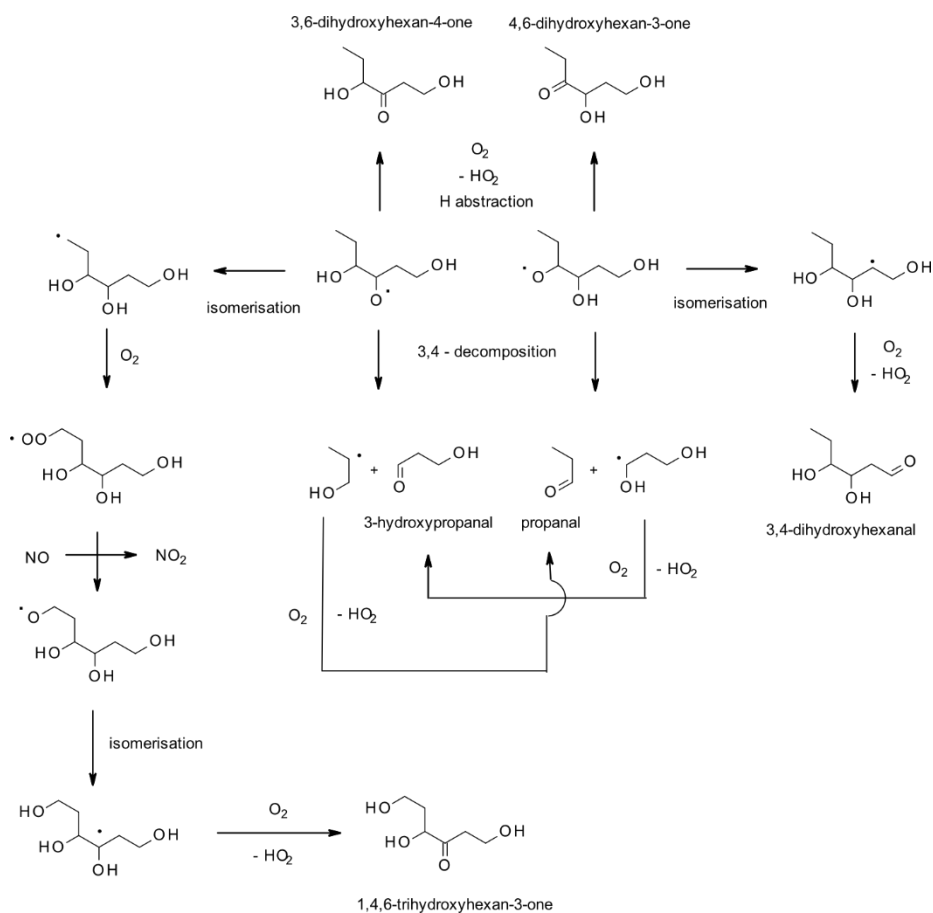
Scheme 2.4. Addition of $\cdot\text{OH}$ radicals to the C=C bond of (Z)-3-hexen-1-ol.¹⁷³ (Sarang et al. 2021)¹⁶⁸



Scheme 2.5. Self-reaction of peroxy radicals.¹⁷³⁻¹⁷⁶ (Sarang et al. 2021)¹⁶⁸

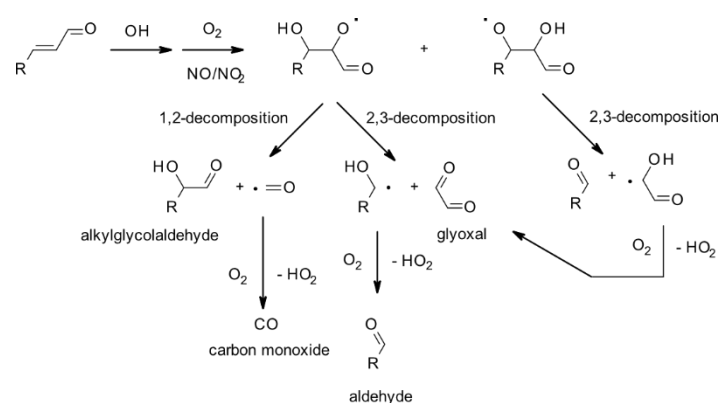


Scheme 2.6. Reactions of peroxy radicals from (Z)-3-hexen-1-ol with NO leading to organic nitrates and alkoxy radicals.^{171, 173-182} (Sarang et al. 2021)¹⁶⁸



Scheme 2.7. Reactions of alkoxy radicals arising from (*Z*)-3-hexen-1-ol^{173-176, 180, 183} (Sarang et al. 2021)¹⁶⁸

Similarly, $\cdot\text{OH}$ radicals may add to GLV aldehydes to form aldehydes, alkylglycolaldehydes, glyoxal, and CO *via* decomposition pathways (Scheme 2.8).¹⁷¹ An alternative decomposition pathway for the alkoxy radical leading to an aldehyde, an alkylglyoxal, and CO₂ is shown in Scheme 2.3.



Scheme 2.8. Mechanistic pathway of $\cdot\text{OH}$ radicals addition to GLV aldehydes unsaturated carbonyl carbon followed by several possible decompositions of an alkoxy radicals.¹⁷¹ (Sarang et al. 2021)¹⁶⁸

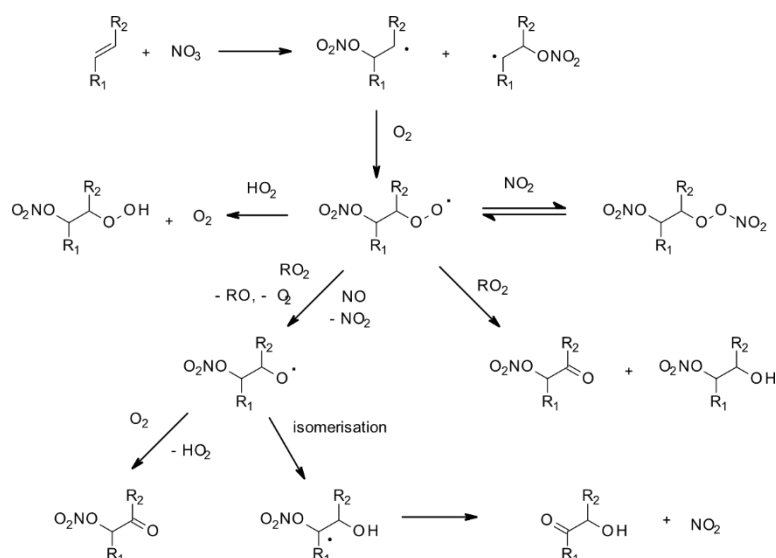
Products and product yields arising from the gas-phase reactions of selected GLVs and their isomers with $\cdot\text{OH}$, observed so far in experiments, are briefly summarized in Table 2.3.

Table 2.3 Observed gas-phase oxidation products of GLV with $\cdot\text{OH}$ radicals.¹⁶⁸

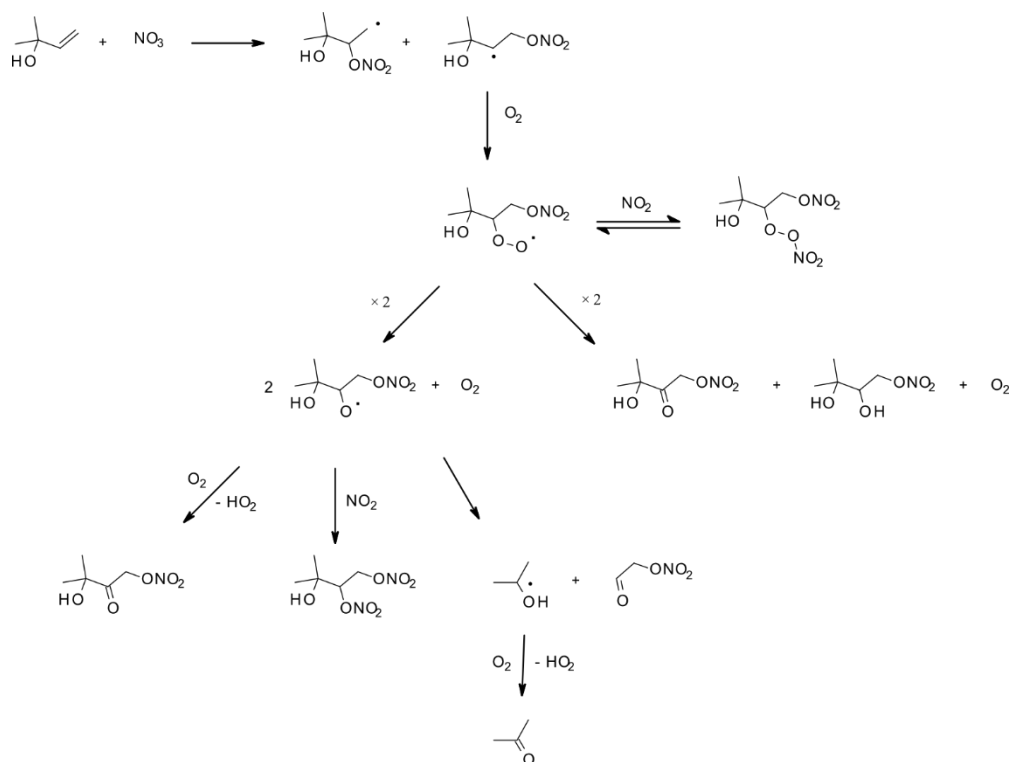
GLV	Product	Yield %	Ref.
1-penten-3-ol	Formaldehyde	35 ± 4	184
	Glycolaldehyde	47 ± 6	
(Z)-2-penten-1-ol	Formaldehyde	11 ± 2	
	Propanal	91 ± 13	
	Glycolaldehyde	87 ± 11	
(E)-2-hexen-1-ol	Butanal	Main	176
(E)-3-hexen-1-ol	Propanal	Main	176
		37 ± 7	175

2.2.1.2. Reactions of GLVs with $\text{NO}_3\cdot$ radicals

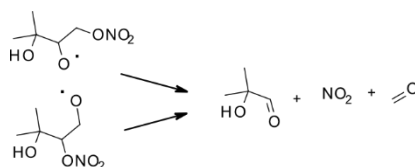
Very few studies were devoted to the reaction mechanism of GLVs with $\text{NO}_3\cdot$ radicals. Therefore, based on the addition reactions to alkenes, a general reaction principle is proposed here.^{169, 170} In Scheme 2.9, the addition of $\text{NO}_3\cdot$ to C=C takes place, resulting in two isomeric alkyl radicals. Further reaction mechanism is the same as for GLV-OH reactions (Section 2.2.1.2). Scheme 2.10 shows the similar mechanism proposed by Fantechi et al. for the reaction of MBO with $\text{NO}_3\cdot$ radicals, which includes the additional decomposition of alkoxy radical leading to the formation of acetone.¹⁸² Other decomposition pathways for MBO-derived alkoxy radicals were also proposed and are shown in Scheme 2.11.¹⁸⁵



Scheme 2.9. Reaction pathways for one of the two possible isomeric alkyl radicals, arising from the reactions between GLV and NO₃ radicals.^{169, 170} (Sarang et al. 2021)¹⁶⁸



Scheme 2.10. Reaction pathways for one of the two possible isomeric alkyl radicals, from the reaction between MBO and NO₃·.¹⁸² (Sarang et al. 2021)¹⁶⁸



Scheme 2.11. Additional MBO-derived nitrate alkoxy radicals decomposition pathways.
¹⁸⁵ (taken from Sarang et al. 2021)¹⁶⁸

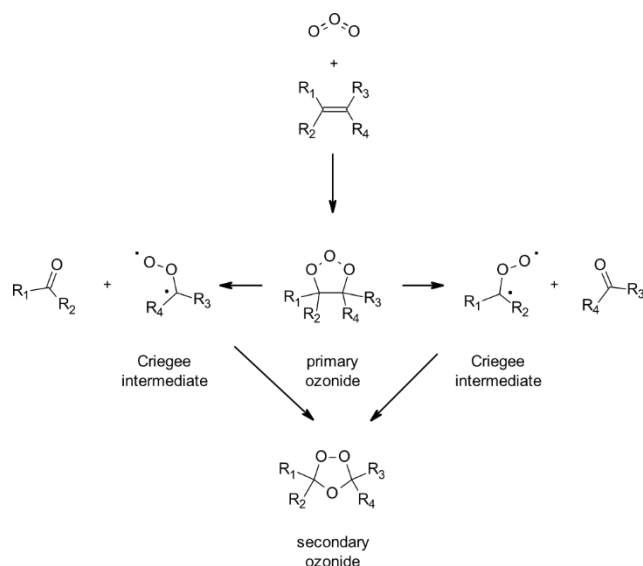
Products and product yields arising from the gas-phase reactions of selected GLVs and their isomers with NO_3^\bullet , observed so far in experiments, are briefly summarized in Table 2.4.¹⁶⁸

Table 2.4. Reaction products observed for GLV with NO_3^\bullet .¹⁶⁸

GLV	Product	Yield, % Molar	Ref.
1-penten-3-ol, (Z)-2-penten-1-ol	2-pentenyl nitrate	observed	¹⁸⁶
	Ethyl vinyl nitrate	observed	
	2-penten-1-ol	observed	
(E)-2-hexenal	PAN analogue	100 ± 2.5	¹⁸⁷
	CO	6.4 ± 4.2	
	Formic acid	observed	

2.2.1.3. Reactions of GLVs with O_3

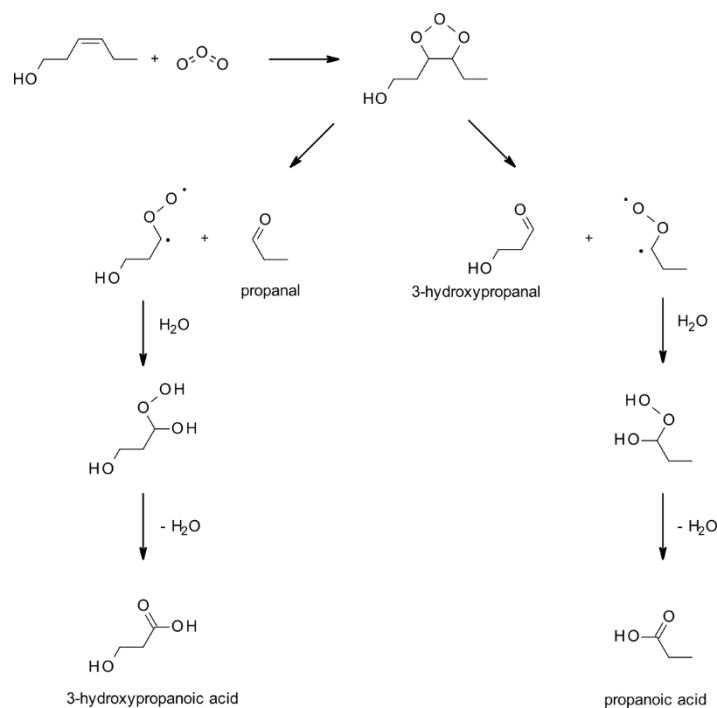
The ozonolysis of unsaturated GLVs follows the pattern known for alkenes. It begins with the addition of O_3 to a double $\text{C}=\text{C}$ bond leading to a primary ozonide, which further decomposes to form carbonyl products and Criegee intermediates. The latter can further recombine to produce a secondary ozonide (Scheme 2.12).¹⁸⁸⁻¹⁹¹



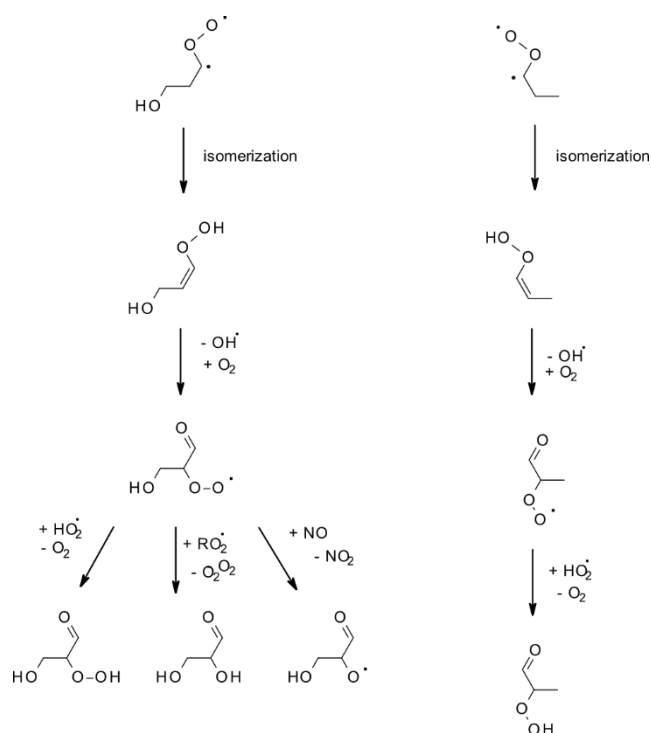
Scheme 2.12. Mechanism of ozonolysis of alkenes, including GLV.^{189, 191} (taken from Sarang et al. 2021)¹⁶⁸

A range of reactions depending upon the R substituents is used to stabilize the above formed Criegee biradicals and are illustrated below for (*Z*)-3-hexenol.

It can be seen that the ozonolysis of (*Z*)-3-hexenol leads to the formation of propanol, 3-hydroxypropanal, and Criegee intermediates, which are stabilized by hydration and dehydration (Scheme 2.13).^{192, 193} Another possibility of the stabilization is the hydroperoxide product channels, which begins with the isomerization steps (Scheme 2.14).¹⁹³



Scheme 2.13. Reaction of O_3 with (Z)-3-hexenol.^{192, 193} (taken from Sarang et al. 2021)¹⁶⁸



Scheme 2.14. Possible hydroperoxide channels in the O_3 reaction with (Z)-3-hexenol.¹⁹³ (taken from Sarang et al. 2021)¹⁶⁸

Products observed in reactions of GLV with O₃ in the experiments are listed in Table 2.5. The SOA formation and its chemical composition during ozonolysis are discussed in Section 2.4.

Table 2.5. Products observed in reactions of GLV with O₃.¹⁶⁸

GLV	Product	Yield, Molar	Ref.
1-penten-3-ol	Formaldehyde	0.49 ± 0.02	194
		0.34 ± 0.04	195, 196
	2-hydroxybutanal	0.46 ± 0.03	194
		0.30 ± 0.05 ^a	195, 196
	Propanal	0.15 ± 0.02	194
0.12 ± 0.01		195, 196	
1-penten-3-one	Formaldehyde	0.37 ± 0.02	194
	2-oxobutanal	0.49 ± 0.03	194
	SOA	0.13–0.17	194
(Z)-3-hexen-1-ol	Propanal	Observed	192
		0.43 ± 0.02	197
		0.59	195, 196
	Propanoic acid	Observed	192
		2-propenal	Observed
	Acetaldehyde	Observed	
	Ethane	0.069 ± 0.005	197
	OH	0.26	174
		0.28 ± 0.06	197
	(E)-2-hexenal	OH	0.62
Butanal		0.53	195, 196
		0.527 ± 0.055	198
Glyoxal		0.56	195, 196
		0.559 ± 0.037	198
2-oxobutanal ^b		0.074 ± 0.006	
acetaldehyde		0.109 ± 0.020	
Propanal		0.067 ± 0.008	
cyclohexanone		0.032 ± 0.003	
(Z)-3-hexenal		Propanal	0.35 ± 0.01
	Ethane	0.079 ± 0.004	
	OH	0.32 ± 0.07	

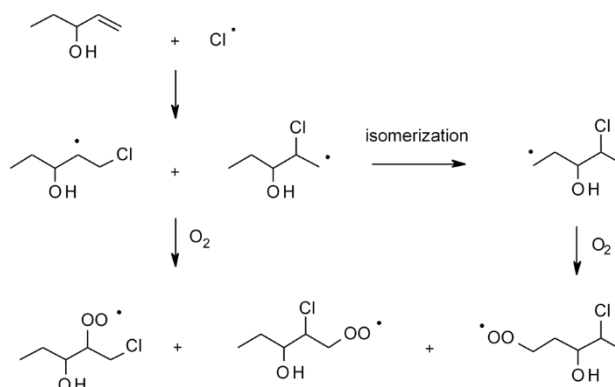
^a measured as 2-oxobutanal; ^b tentative.

2.2.1.4. Reactions of GLVs with Cl atoms

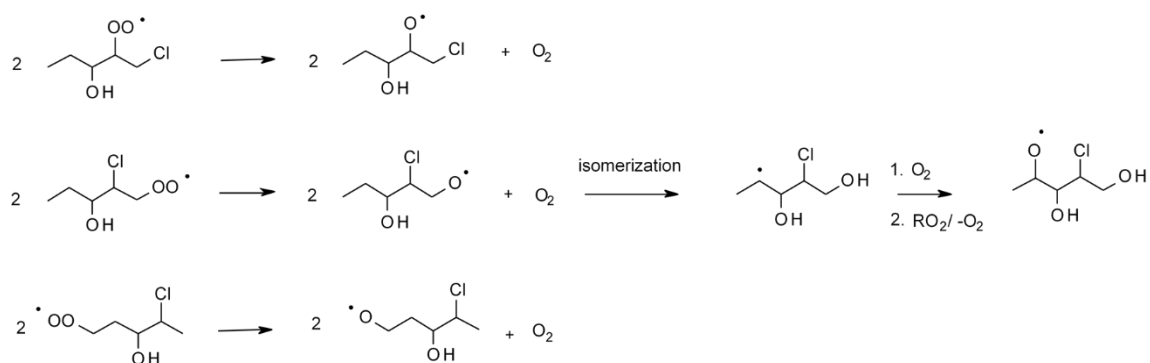
Similarly to ·OH radicals, Cl atoms can either add to a C=C double bond or abstract hydrogen from a given GLV with the formation of HCl, within the gas-phase reaction.^{179, 199, 200} Based on the quantum-mechanical modeling, the addition was proven to be the dominant pathway, however the hydrogen abstraction could not be excluded.^{200, 201} Very few studies have dealt with reaction products from GLV-Cl reactions.¹⁶⁸ For example, both the addition and hydrogen abstraction pathways are feasible for 1-penten-3-ol (see in forthcoming subsections).

2.2.1.4.1. Addition of Cl atoms to C=C bonds of 1-penten-3-ol

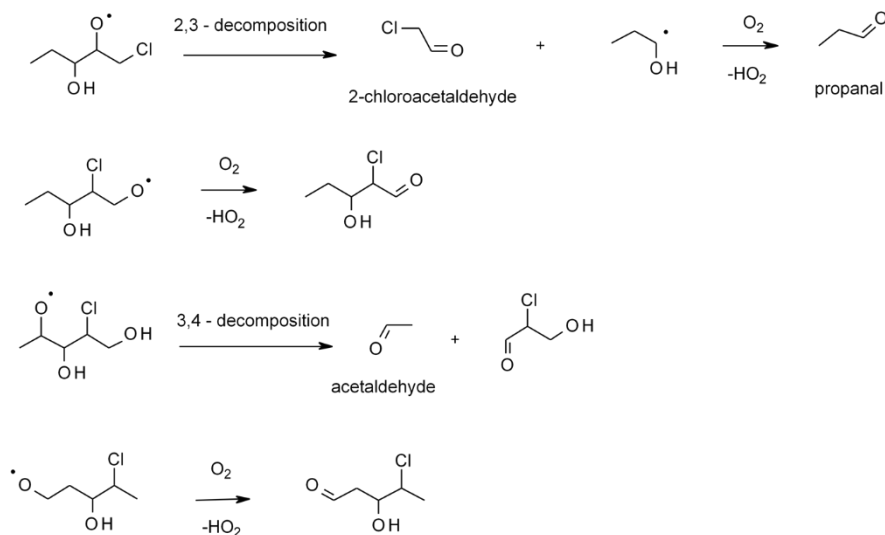
Scheme 2.15 – 2.17 illustrates the likely steps of the addition of Cl atoms for 1-penten-3-ol in the absence of NO: 1) the formation of alkyl radical leading to the production of peroxy radicals; 2) the isomerization and self-reaction of peroxy radicals; 3) decomposition of alkoxy radicals to give stable products.²⁰⁰



Scheme 2.15. Formation of 1-penten-3-ol derived peroxy radicals *via* addition of Cl at C=C bonds.²⁰⁰ (taken from Sarang et al. 2021)¹⁶⁸



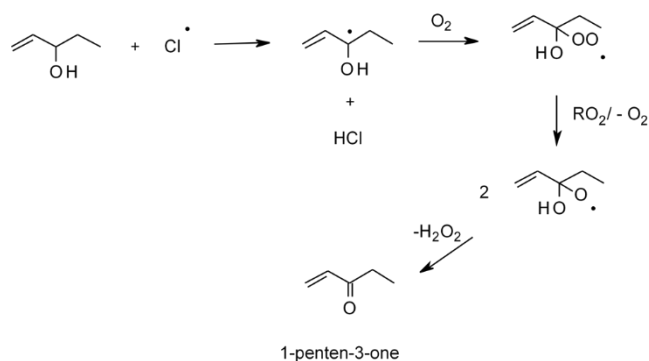
Scheme 2.16. The self-reaction and isomerization of 1-penten-3-ol derived peroxy radicals in the absence of NO.²⁰² (taken from Sarang et al. 2021)¹⁶⁸



Scheme 2.17. Decomposition reactions of 1-penten-3-ol derived alkoxy radicals towards stable products.²⁰⁰ (taken from Sarang et al. 2021)¹⁶⁸

2.2.1.4.2. Hydrogen abstraction for 1-penten-3-ol with Cl atoms

A carbon atom at position 3 in the molecule of 1-penten-3-ol is the most preferable position for hydrogen abstraction with Cl atoms. The alkoxy radicals formed, can lead to the formation of 1-penten-3-one with the release of H₂O₂ (Scheme 2.18).²⁰⁰



Scheme 2.18. Formation of 1-penten-3-one *via* hydrogen abstraction from 1-penten-3-ol by a Cl atom.²⁰⁰ (taken from Sarang et al. 2021)¹⁶⁸

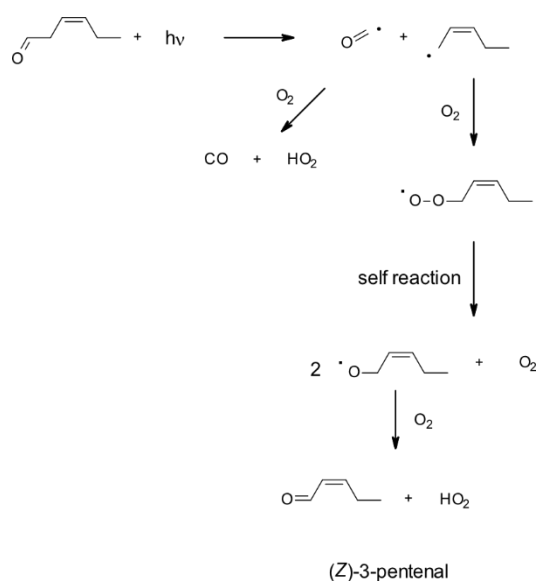
Mechanistic schemes for several other compounds, such as (*E*)-2-hexen-1-al, MBO, (*E*)-2-hexenyl acetate are illustrated in the review article.¹⁶⁸

Table 2.6. Gas-phase reaction products of GLVs and Cl radicals.¹⁶⁸

GLV	Product	Yield %	Ref.
1-penten-3-ol	Chloroacetaldehyde	33 ± 1	200
	Propanal	39 ± 1	
	Acetaldehyde	8 ± 3	
	1-penten-3-one	< 2	
(Z)-2-penten-1-ol	2-chlorobutanal	19 ± 1	200
	Propanal	27 ± 1	
	Acetaldehyde	18 ± 2	
	(Z)-2-pentenal	36 ± 1	
(E)-2-hexenyl acetate	butanal	not quantified	203
	formaldehyde		
	propanal		

2.2.1.5. Gas-phase photolysis of GLVs

Merely a few studies researched the gas-phase photolysis of GLVs. For unsaturated GLVs bearing carbonyl residue, such as (*E*)-2-hexenal, (*Z*)-3-hexenal, the photolytic loss can be significant.

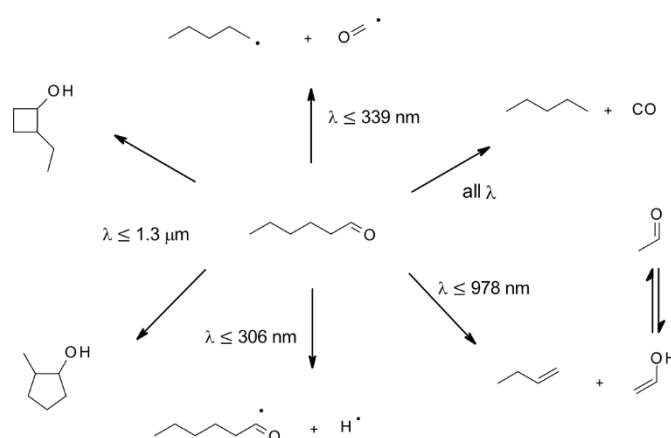


Scheme 2.19. Photolytic decomposition of (*Z*)-3-hexenal.²⁰⁴ (taken from Sarang et al. 2021)¹⁶⁸

O'Connor et al.²⁰⁴ analyzed the sunlight photolysis of (*E*)-2-hexenal, (*Z*)-3-hexenal, and (*E,E*)-2,4-hexadienal in the EUPHORE smog chamber in dry purified air (0.05 – 1.0 % RH and 286 – 294 K). In Scheme 2.19, photolysis of (*Z*)-3-hexenal follows Norrish type 1 mechanism resulting in CO as the major product (34 % yield). The other product, i.e., (*Z*)-2-pentenyl radical, further reacts with O₂ to form pentenyl peroxy radical, which undergoes self-reaction to produce pentenyl oxy radical. The pentenyl oxy radical in reaction with O₂ finally gives (*Z*)-

3-pentenal, observed experimentally. In contrast, (*E*)-2-hexen-1-al undergoes photoisomerization to give (*Z*)-2-hexen-1-al.

Tang and Zhu²⁰⁵ studied the gas-phase photolysis of n-hexanal and n-heptanal for the HCO radicals formation using the cavity ring-down spectroscopy. The radical quantum yields from the thermodynamically feasible dissociation of n-hexanal after UV excitation, ranged from 0.1 to 0.08 for 2 – 8 mmHg partial pressures of hexenal (Scheme 2.20). Besides, several other photolysis products were identified using mass spectrometry, such as acetaldehyde CH_3CHO and butene C_4H_8 (yield 0.28 – 0.31), CO and pentane C_5H_{12} (yield 0.20), C_5H_{11} , 2-methylcyclopentanol (yield 0.12) and 2-ethylcyclobutanol (yield 0.3).



Scheme 2.20. Thermodynamically feasible UV-photolytic dissociation of n-hexanal.²⁰⁵ (taken from Sarang et al. 2021)¹⁶⁸

2.2.2. Gas-phase kinetics of GLVs

The available literature data on the determination of rate constants for reactions of selected GLVs with $\cdot\text{OH}$ and $\text{NO}_3\cdot$ radicals, O_3 , and Cl atoms, as well as the gas-phase photolysis of GLVs were compiled in Tables 2.7 – 2.15. The rate constants were determined either by the relative or absolute approach. For the measurement of the relative rate constants, a decay of a given GLV is measured in reference to the decay of a reactant, for which the rate constant of the reaction with the selected oxidant was reported. In contrast, the absolute rate constants are measured by following the decay of both, a given GLV and oxidant.

2.2.2.1. Kinetics of reactions with $\cdot\text{OH}$ radicals

The experimental rate constants for the gas-phase reactions of selected GLVs with $\cdot\text{OH}$ radicals determined at single temperatures are provided in Table 2.7, while Table 2.8 shows the rate constants determined across the temperature ranges. The $\cdot\text{OH}$ radicals were generated using several different methods such as: photolysis of H_2O_2 (248, 252, or 254 nm); photolysis of H_2O (165 nm); photolysis of methyl nitrite CH_3ONO (300 nm); photolysis of ethyl nitrite $\text{CH}_3\text{CH}_2\text{ONO}$; photolysis of HNO_3 (248 nm); photolysis of HONO (355 nm); reaction of F atoms with H_2O or H atoms with NO_2 . Equations 2.1 show the reaction mechanism for the formation of $\cdot\text{OH}$ radicals *via* photodissociation of CH_3ONO .²⁰⁶



For most of the reactions, their rate decreased with increasing temperature, i.e., showed negative activation energies (Table 2.8). The exception was MeSa – the only aromatic compound studied.¹⁶⁸ Only in some theoretically evaluated cases, the addition reaction between GLV-OH had a positive activation energy.²⁰⁷ Table 2.9 shows the theoretically derived addition and hydrogen abstraction reaction rate constant between GLVs and $\cdot\text{OH}$ radical.²⁰⁸

Table 2.7. Relative and absolute (^a) rate constants for gas-phase reactions of GLV with OH at single temperatures.¹⁶⁸

GLV	k $\text{cm}^3 \text{ molecule}^{-1} \text{ s}^{-1}$	T K	P Atm	Ref.
1-penten-3-ol	$(6.7 \pm 0.9) \times 10^{-11}$	298	1	184
(Z)-2-penten-1-ol	$(1.06 \pm 0.15) \times 10^{-10}$	298	1	209
(E)-2-pentenal	$(2.35 \pm 0.21) \times 10^{-11}$ ^a	298	0.132–0.526	210
1-penten-3-one	3.6×10^{-11} ^b	298	1	211
Hexan-1-ol	$(1.58 \pm 0.35) \times 10^{-11}$	296 ± 2	1	212
(Z)-2-hexen-1-ol	$(1.1 \pm 0.4) \times 10^{-10}$	296 ± 2	1	213
	0.95×10^{-10} ^b	298	1	214
	$(8.53 \pm 1.36) \times 10^{-11}$ ^c	298	1	208
(E)-2-hexen-1-ol	$(1.0 \pm 0.3) \times 10^{-10}$	298	1	174
	$(8.08 \pm 1.33) \times 10^{-11}$ ^c	298	1	209
(E)-2-hexenal	$(0.681 \pm 0.049) \times 10^{-11}$	296 ± 2	0.974	215
	$(2.95 \pm 0.45) \times 10^{-11}$ ^a	298	0.132–0.526	216
	$(3.95 \pm 0.17) \times 10^{-11}$	298 ± 2	1	
(Z)-3-hexenal	$(6.9 \pm 0.9) \times 10^{-11}$	298	1	

^a absolute rate constant; ^b from SAR or LFER; ^c theoretical rate constants for the addition and hydrogen abstraction channels are given in (Table 2.9).

Table 2.8. Absolute (^a) rate constants for gas-phase reactions of GLV with OH radicals – Arrhenius parameters and values at selected temperature T.¹⁶⁸

GLV	A	E _A /R	k _T	T	T range	P	Ref.
	cm ³ molecule ⁻¹ s ⁻¹	K	cm ³ molecule ⁻¹ s ⁻¹	K	K	atm	
1-penten-3-ol	(6.8 ± 0.7) × 10 ⁻¹² ^a	-(690 ± 20)	(7.12 ± 0.73) × 10 ⁻¹¹ ^a	297	243-404	20-100 mmHg	217
	(7.7 ± 1.6) × 10 ⁻¹² ^a	-(606 ± 60) ^a	(5.65 ± 0.76) × 10 ⁻¹¹ ^a	298	263-353		218
(<i>E</i>)-2-penten-1-ol	(6.8 ± 0.8) × 10 ⁻¹² ^a	-(680 ± 20)	(6.76 ± 0.70) × 10 ⁻¹¹ ^a				
1-penten-3-one	(4.4 ± 2.8) × 10 ⁻¹² ^a	-(507 ± 180) ^a	(2.36 ± 0.47) × 10 ⁻¹¹ ^a				
(<i>E</i>)-2-pentenal	(7.9 ± 1.2) × 10 ⁻¹² ^a	-(510 ± 20)	(4.3 ± 0.6) × 10 ⁻¹¹ ^a	297	244-374	0.03 -0.197	171
(<i>E</i>)-2-hexen-1-ol	(5.4 ± 0.6) × 10 ⁻¹² ^a	-(690 ± 20)	(6.15 ± 0.75) × 10 ⁻¹¹ ^a	298	263-353		162
(<i>Z</i>)-3-hexen-1-ol	(1.3 ± 0.1) × 10 ⁻¹¹ ^a	-(580 ± 10)	(1.06 ± 0.12) × 10 ⁻¹⁰ ^a	297	243-404	20-100 mmHg	217
(<i>E</i>)-2-hexenal	(7.5 ± 1.1) × 10 ⁻¹² ^a	-(520 ± 30)	(4.4 ± 0.5) × 10 ⁻¹¹ ^a	297	244-374	0.03-0.197	171
	(9.8 ± 2.4) × 10 ⁻¹² ^a	-(455 ± 80)	(4.68 ± 0.50) × 10 ⁻¹¹ ^a	298	263-353	0.066	219

^a absolute rate constants;**Table 2.9.** Theoretical rate constants (cm³ molecule⁻¹ s⁻¹) for chemical reactions between hexenols and OH radicals proceeding through the OH addition and hydrogen abstraction channels.^{168, 208}

Reactant	KOH addition	KH abstraction	k _{total}	H-Abstraction Branching Ratio	k _{total} Deviation from Experimental Values %
(<i>E</i>)-2-hexen-1-ol	4.97 × 10 ⁻¹¹	9.76 × 10 ⁻¹²	5.95 × 10 ⁻¹¹	0.16	26.4
(<i>Z</i>)-2-hexen-1-ol	5.34 × 10 ⁻¹¹	2.19 × 10 ⁻¹¹	7.53 × 10 ⁻¹¹	0.29	11.7
(<i>E</i>)-3-hexen-1-ol	2.45 × 10 ⁻¹¹	3.50 × 10 ⁻¹¹	5.95 × 10 ⁻¹¹	0.59	34.6
(<i>Z</i>)-3-hexen-1-ol	1.17 × 10 ⁻¹⁰	3.07 × 10 ⁻¹¹	1.48 × 10 ⁻¹⁰	0.21	-46.5
(<i>E</i>)-4-hexen-1-ol	4.74 × 10 ⁻¹¹	1.30 × 10 ⁻¹¹	6.04 × 10 ⁻¹¹	0.22	15.4
(<i>Z</i>)-4-hexen-1-ol	1.10 × 10 ⁻¹⁰	2.73 × 10 ⁻¹¹	1.37 × 10 ⁻¹⁰	0.20	82.6

2.2.2.2. Kinetics of reactions with NO₃[•] radicals

Experimental rate constants for the gas-phase reactions of GLV with NO₃[•] radicals determined at single temperatures are provided in Table 2.10, while Table 2.11 shows rate constants determined across temperature ranges. Methods of generation of NO₃[•] radicals included thermal decomposition of N₂O₅, reaction of F atoms with HNO₃, and reaction of NO₂ with O₃.

Table 2.10. Relative and absolute (^a) rate constants for gas-phase reactions of GLVs with NO₃[•] radicals at single temperatures.¹⁶⁸

GLV	k cm ³ molecule ⁻¹ s ⁻¹	T K	P atm	Ref.
1-penten-3-ol	(1.39 ± 0.19) × 10 ⁻¹⁴ ^a	298 ± 3	1.00 ± 0.03	186
(Z)-2-penten-1-ol	(1.53 ± 0.23) × 10 ⁻¹³ ^a (3.5 ± 1.9) × 10 ⁻¹³			
(E)-2-pentenal	(3.11 ± 0.11) × 10 ⁻¹³ (1.93 ± 0.40) × 10 ⁻¹⁴	295 ± 2	1	220
1-penten-3-one	3.39 × 10 ⁻¹⁴ ^d	298	1	210
(Z)-2-hexen-1-ol	(1.56 ± 0.24) × 10 ⁻¹³ ^a (4.05 ± 0.45) × 10 ⁻¹³ ^b (3.57 ± 0.62) × 10 ⁻¹³ ^c	295 ± 2	1	220
(E)-2-hexen-1-ol	(1.30 ± 0.24) × 10 ⁻¹³ ^a	298 ± 3		221
(Z)-2-hexenal	(1.36 ± 0.29) × 10 ⁻¹⁴	295 ± 2	1	220
(E)-2-hexenal	(1.21 ± 0.10) × 10 ⁻¹⁴	296 ± 2	0.974	174
	(4.7 ± 1.5) × 10 ⁻¹⁵ ^a	294 ± 3	1	187

^a absolute rate constant; ^b (E)-2-butene reference; ^c cyclopentene reference; ^d estimated from SAR or LFER.

Table 2.11. Absolute rate constants for gas-phase reactions of GLV with NO₃[•] radicals – Arrhenius parameters and *k* values at temperature T.¹⁶⁸

GLV	A molecules cm ⁻¹ s ⁻¹	E _A /R K	k _T molecules cm ⁻¹ s ⁻¹	T K	T range K	P mmHg	Ref.
(E)-2-pentenal	(5.40 ± 0.30) × 10 ⁻¹²	1540 ± 200	(2.88 ± 0.29) × 10 ⁻¹⁴	298	298-433	1	222
(E)-2-hexenal	(1.2 ± 0.3) × 10 ⁻¹²	926 ± 85	(5.49 ± 0.95) × 10 ⁻¹⁴	298	298-433	1	222

2.2.2.3. Kinetics of reactions with O₃

Experimentally determined rate constants at single temperatures are provided in Table 2.12, while Table 2.13 shows the temperature-dependent Arrhenius data for the gas-phase reactions of GLVs with O₃. Ozone was generated using an ozone generator in all below-mentioned experiments.

Table 2.12. Relative and absolute (^a) rate constants for gas-phase reactions of GLVs with O₃ at single temperatures. (taken from Sarang et al. 2021)¹⁶⁸

GLV	k cm ³ molecule ⁻¹ s ⁻¹	T K	P atm	References
1-penten-3-ol	(1.64 ± 0.15) × 10 ⁻¹⁷ a	298	1	194
	(1.79 ± 0.18) × 10 ⁻¹⁷ a	289 ± 1	1	223
(Z)-2-penten-1-ol	(11.5 ± 0.66) × 10 ⁻¹⁷ a	298	1	194
	(1.69 ± 0.25) × 10 ⁻¹⁶ a	288 ± 1	1	223
1-penten-3-one	(1.17 ± 0.15) × 10 ⁻¹⁷ a	298	1	194
(Z)-2-hexen-1-ol	(7.44 ± 1.03) × 10 ⁻¹⁷ a	298	1	224
	10.4 × 10 ⁻¹⁷	298		
(E)-2-hexen-1-ol	(5.98 ± 0.73) × 10 ⁻¹⁷	298	1	225
	(1.66 ± 0.22) × 10 ⁻¹⁶ a	298	1	224
	2.86 × 10 ⁻¹⁶	298		
(E)-2-hexenal	(1.28 ± 0.28) × 10 ⁻¹⁸	287.3 ± 1.4	1	198
	(3.0 ± 2.1) × 10 ⁻¹⁸	296 ± 2	0.974	174
(Z)-3-hexenal	(3.45 ± 0.30) × 10 ⁻¹⁷	298	1	216

^a absolute rate constant.**Table 2.13.** Relative rate constants for gas-phase reactions of GLVs with O₃ – Arrhenius parameters and *k* values at selected temperature T (obtained by the relative methods if not marked absolute). (taken from Sarang et al. 2021)¹⁶⁸

GLV	A Molecules cm ⁻¹ s ⁻¹	E _A /R K	k _T Molecules cm ⁻¹ s ⁻¹	T K	T Range K	P Atm	Ref.
1-penten-3-ol	(1.82 ± 2.08) × 10 ⁻¹⁶	730 ± 348	(1.61 ± 0.21) × 10 ⁻¹⁷ a (1.75 ± 0.25) × 10 ⁻¹⁷ b 0.20 × 10 ⁻¹⁷ c	298 ± 2 298 ± 2 298	273–333	1	226
(Z)-2-penten-1-ol	(2.32 ± 1.94) × 10 ⁻¹⁵	902 ± 265	(11.90 ± 1.40) × 10 ⁻¹⁷ a (9.07 ± 1.29) × 10 ⁻¹⁷ b 1.50 × 10 ⁻¹⁷ c	298 ± 2 298 ± 2 298	273–333	1	226
(E)-2-penten-1-al	(1.38 ± 0.73) × 10 ⁻¹⁶ a	1406 ± 163	(1.24 ± 0.06) × 10 ⁻¹⁸ a	298	233–373	0.8-1	227
(E)-3-hexen-1-ol	(1.74 ± 1.65) × 10 ⁻¹⁵	1020 ± 300	(5.97 ± 0.99) × 10 ⁻¹⁷ a (6.50 ± 0.95) × 10 ⁻¹⁷ b 1.48 × 10 ⁻¹⁷ c	298 ± 2 298 ± 2 298	273–333	1	226
(E)-2-hexenal	(1.79 ± 0.54) × 10 ⁻¹⁶ a	1457 ± 90	(1.37 ± 0.03) × 10 ⁻¹⁸ a	298	233–373	0.8-1	227

^a absolute rate constant; ^b practically did not depend on pressure in the range of 0.01–10,000 mmHg; ^c evaluated based on the reference data.

2.2.2.4. Kinetics of reactions with Cl atoms

Values of the experimental rate constants for the gas-phase reactions of GLVs with Cl radicals determined at single temperatures are provided in Table 2.14. Table 2.15 shows the rate constants determined across temperature ranges for three GLVs only till date.

Table 2.14. Relative rate constants for gas-phase reactions of GLVs with Cl at single temperatures. (taken from Sarang et al. 2021)¹⁶⁸

GLV	k cm ³ molecule ⁻¹ s ⁻¹	T K	P atm	Ref.
1-penten-3-ol	(2.96 ± 1.22) × 10 ⁻¹⁰	258 ± 1	1	200
	(2.37 ± 0.38) × 10 ⁻¹⁰	262 ± 1	1	
	(2.40 ± 0.54) × 10 ⁻¹⁰	273 ± 1	1	
	(2.35 ± 0.31) × 10 ⁻¹⁰	298 ± 1	1	
	(2.78 ± 0.30) × 10 ⁻¹⁰	313 ± 1	1	
	(2.57 ± 0.28) × 10 ⁻¹⁰	333 ± 1	1	
(Z)-2-penten-1-ol	(2.99 ± 0.53) × 10 ⁻¹⁰	296 ± 2	1	228
	(3.00 ± 0.49) × 10 ⁻¹⁰	298 ± 1	1	200
	(2.66 ± 0.47) × 10 ⁻¹⁰	313 ± 1	1	
	(3.26 ± 0.48) × 10 ⁻¹⁰	333 ± 1	1	
(E)-2-penten-1-al	(1.31 ± 0.19) × 10 ⁻¹⁰	298	1	229
1-penten-3-one	(2.91 ± 1.10) × 10 ⁻¹⁰	298	1	230
	(1.9 ± 0.4) × 10 ⁻¹⁰	297-400	1	231
(E)-2-hexen-1-ol	(3.41 ± 0.65) × 10 ⁻¹⁰	296 ± 2	1	228
	(3.49 ± 0.82) × 10 ⁻¹⁰	298 ± 3	1	232
(Z)-3-hexen-1-ol	(3.15 ± 0.58) × 10 ⁻¹⁰	296 ± 2	1	228
	(2.94 ± 0.72) × 10 ⁻¹⁰	298 ± 3	1	232
(E)-3-hexen-1-ol	(3.05 ± 0.59) × 10 ⁻¹⁰	296 ± 2	1	228
	(3.42 ± 0.79) × 10 ⁻¹⁰	298 ± 3	1	232
(E)-2-hexen-1-al	(1.92 ± 0.22) × 10 ⁻¹⁰	298	1	229

Table 2.15. Relative and absolute (^a) rate constants for gas-phase reactions of GLV with Cl atoms– Arrhenius parameters and *k* values at selected temperature T.¹⁶⁸

GLV	A	E _A /R	k _T	T	T Range	P	Ref.
	cm ³ Molecule ⁻¹ s ⁻¹	K	cm ³ Molecule ⁻¹ s ⁻¹	K	K	Atm	
hexanal	$(7.91 \pm 0.66) \times 10^{-11}$ ^a	-(349 ± 51)	$(2.56 \pm 0.24) \times 10^{-11}$ ^a	298	265–381	1	233
2-methyl-3-butene-2-ol	$(2.83 \pm 2.50) \times 10^{-14}$	-(2670 ± 249)	$(2.13 \pm 0.19) \times 10^{-10}$	298	256-298	1	234
methyl salicylate	1.2703×10^{-8} ^{a,b,c}	1438.4	1.01×10^{-10} ^{a,b,c,d}	298	278–350	1	235

^a absolute rate constants; ^b determined theoretically; ^c calculated here from the reference data; ^d 100 times higher than experimental values provided in review.¹⁶⁸

2.2.2.5. Gas-phase photolysis

The experimental absolute and relative photolysis rates of GLV, are given in Table 2.16. The relative photolysis rates were obtained against the photolysis of NO₂. All of the GLVs UV spectra deployed to determine the photolysis rates are provided in Sarang et al. 2021 review paper.¹⁶⁸

For 1-penten-3-ol and (*Z*)-3-hexen-1-ol,¹⁶² (*Z*)-3-hexen-1-al,²⁰⁴ MBO,²³⁶ and MeSa²³⁷ tropospheric degradation due to the photolysis was insignificant. In the case of (*Z*)-3-hexenal, photodegradation was observed to be faster than that by the reaction with O₃ (1×10^{12} molecule cm⁻³) and slower than that by the reaction with OH (2×10^6 molecule cm⁻³). (*E*)-2-pentenal, (*E*)-2-hexenal,²³⁸ 1-penten-3-one and hexanal²¹⁸ undergo substantial photodegradation.

Table 2.16. GLVs photolysis rate constants (denoted as *j*), absolute, and relative to the photolysis rate constant of NO₂, determined at given effective quantum yields Φ and the zenith angles θ . (taken from Sarang et al. 2021)¹⁶⁸

GLV	<i>j</i> s ⁻¹	<i>j</i> / <i>j</i> (NO ₂)	Φ	θ °	T K	Ref.
1-penten-3-ol	(1.61-2.36) × 10 ⁻⁶ ^a		1		298	162
1-penten-3-one	(0.36-1.39) × 10 ⁻⁵ ^a		1		298	162
<i>(E)</i> -2-hexenal	1.0 × 10 ⁻⁴	1.8 × 10 ⁻²	0.36		286–294	204
	3.80 × 10 ⁻⁴		1	20	298	238
	4.05 × 10 ⁻⁴			30		
	3.80 × 10 ⁻⁴			40		
	3.42 × 10 ⁻⁴			50		
	2.89 × 10 ⁻⁴			60		
	2.17 × 10 ⁻⁴			70		
<i>(Z)</i> -3-hexen-1-ol	(1.61-2.36) × 10 ⁻⁵ ^a		1		298	162

^a upper limits, 0 – 10 km above the Earth surface.

2.3. Aqueous-phase kinetics and mechanism patterns for GLVs

In comparison to the gas-phase chemistry, the chemistry of the GLVs in the atmospheric aqueous phase and multiphase is far less known. Therefore, all of the aqueous-phase and multiphase chemistry data, involving kinetics and mechanisms, published to date, is compiled and presented in this section. The aqueous-phase chemistry data are summarized in the subsection 2.3.1, where determined rate constants are shown in Tables 2.17 – 2.19, while the reaction mechanisms postulated so far are summarized in subsection 2.3.2.

2.3.1. Aqueous-phase kinetics

Richards-Henderson et al.¹²⁹ studied the aqueous-phase photo-oxidation reaction for the following GLVs: (*Z*)-3-hexen-1-ol, (*Z*)-3-hexenyl acetate, MeSa, MeJa, and MBO, with $\cdot\text{OH}$ radicals (precursor H_2O_2). No photodegradation was observed for GLVs within the control experiments carried out in the absence of H_2O_2 . They applied the technique of competition kinetics to determine the rate constants for reactions against reference sodium benzoate (Table 2.17).

In another study, Richards-Henderson et al.²³⁹ also studied the relative rate constants of several GLVs for a reaction with $^3\text{C}^*$ triplet state and $^1\text{O}_2^*$ singlet molecular oxygen. They used simulated sunlight to generate $^3\text{C}^*$ and $^1\text{O}_2^*$ by irradiating organic chromophores, i.e., 3,4-dimethoxybenzaldehyde (DMB) or methoxyacetophenone (MAP) and Rose Bengal, respectively. For the competition kinetics, involving $^3\text{C}^*$, phenol or syringol was used, while in case of $^1\text{O}_2^*$, furfuryl alcohol was used as a reference compound, respectively. The results are collected in Table 2.18. The SOA product yields were determined gravimetrically as in the above-mentioned experiments with $\cdot\text{OH}$ radicals.¹²⁹ Non-measurable amounts of SOA were reported for (*Z*)-3-hexen-1-ol and MBO in reactions involving $^1\text{O}_2^*$ and $^3\text{DMB}^*$ (Table 2.18).

Table 2.17. Relative rate constants for aqueous-phase reactions of GLV with OH radicals - Arrhenius parameters and k values at 298 K and pH = 5.4, and yields of SOA products.¹⁶⁸

GLV	A	E _A	T range	pH	k _{298 K} ^a	SOA	Ref.
	10 ¹¹ M ⁻¹ s ⁻¹	kJ mol ⁻¹	K		10 ⁸ M ⁻¹ s ⁻¹	%	
1-penten-3-one					7.24 ^b	-	210
(<i>Z</i>)-3-hexen-1-ol	8.1 ± 0.9	12 ± 0.3	278-298	5.4	5.1 ± 0.8	52	129
(<i>Z</i>)-3-hexenyl acetate	190 ± 40	17 ± 1.5	278-298	5.4	8.7 ± 1.1	8	
methyl salicylate	58 ± 40	14 ± 1.4	278-298	5.4	7.8 ± 0.5	87	129
methyl jasmonate	58 ± 9	15 ± 1.5	278-298	5.4	6.8 ± 0.8	67	
2-methyl-3-butene-2-ol	23 ± 5	13 ± 2	278-298	5.4	7.5 ± 1.4	20	

^a experimental values; ^b estimated from SAR or LFER

Table 2.18 Relative rate constants for aqueous-phase reactions of GLVs with singlet molecular oxygen $^1\text{O}_2^*$ and $^3\text{C}^*$ triplet state ($^3\text{DMB}^*$ and $^3\text{MAP}^*$) at pH = 5.1, and yields of some SOA products. ^{168, 239}

GLV	$^1\text{O}_2^*$			$^3\text{DMB}^*$			$^3\text{MAP}^*$
	A	E _A	k _{298 K}	k		SOA	k,
	M ⁻¹ s ⁻¹	kJ mol ⁻¹	10 ⁶ M ⁻¹ s ⁻¹	10 ⁶ M ⁻¹ s ⁻¹		%	10 ⁶ M ⁻¹ s ⁻¹
				pH = 2.1	pH = 5.1		pH = 5.1
				298 K	278-298 K		
(Z)-3-hexen-1-ol	6.1×10 ²⁰	82 ± 7.4	2.5 ± 0.3	0.33 ± 0.04	0.24 ± 0.1	-	1.2 ± 0.8
(Z)-3-hexenyl acetate	2.2×10 ¹⁵	50 ± 7.2	3.9 ± 0.8	14 ± 2	14 ± 7	38	7.3 ± 2
methyl salicylate	-	-	≤ 0.1	29 ± 2	12 ± 4	80	8.0 ± 0.8
methyl jasmonate	3.6×10 ²³	96 ± 4.8	6.0 ± 0.7	3.6 ± 0.5	4.2 ± 3	84	1.2 ± 0.5
2-methyl-3-butene-2-ol	6.7×10 ⁹	22 ± 1.7	7.5 ± 1.4	0.28 ± 0.1	0.13 ± 0.07	-	0.55 ± 0.2

Several other GLVs-based multiphase reactions data were published, mainly concerning the aqueous-phase transformation of MBO. These data were gathered in the review paper by Sarang et al. 2021.¹⁶⁸

Other interesting studies by Heath et al.²⁴⁰ involved the determination of pseudo-first-order rate constants of MeJa with $\cdot\text{OH}$ radicals in the irradiated aqueous solution (bulk) and thin aqueous films. As a precursor of $\cdot\text{OH}$ radicals, H₂O₂ photolysis was selected. The HPLC-UV/DAD was used to follow and measure the extent of reaction by determining the concentration of MeJa. The study concluded that the reaction rate in the films was greater than that in bulk and was inversely proportional to the thickness of the film (Table 2.19).

Table 2.19. Pseudo-first order rate constant for the aqueous-phase reaction of MeJa with OH radicals in bulk solutions and aqueous films, respectively (taken from Sarang et al. 2021)¹⁶⁸

Film thickness, μm	∞ (bulk)	193.1	77.2	38.6
k _{1st} , 10 ⁻⁴ min ⁻¹	2.83 ± 0.02	9.62 ± 0.43	11.0 ± 0.5	12.7 ± 0.6

Liyana-Arachchi et al.²⁴¹ studied the air-water interface reactions using the molecular dynamics approach for MBO and $\cdot\text{OH}$ radicals. It appeared that the possibility of chemical reactions at the interface was relatively high due to sufficient encounters of the species.

2.3.2. Aqueous-phase and multiphase mechanisms

Both GLVs and their gas-phase products (described in Sect. 2.2.1) can partition into aqueous droplets or dequiescent particles in the atmosphere. There, in the presence of other dissolved reactive species, such as trace metal ions, they can either hydrolyze or react *via* various mechanisms. These pathways are briefly reviewed in the paper by Sarang et al. 2021.¹⁶⁸

GLVs can react with both radicals and radical-anions present in the atmospheric aqueous system through: (i) the radical addition to a C=C bond, (ii) electron transfer and (iii) hydrogen abstraction. The addition processes by far lead to atmospherically-relevant products, especially with sulfate radical-anion ($\text{SO}_4^{\cdot-}$). The latter are known to exist only in the aqueous-phases. The reaction mechanisms involving $\text{SO}_4^{\cdot-}$ species with isoprene^{15, 79}, methyl vinyl ketone²⁴², (*Z*)-2-pentenoic acid,²⁴³ and MBO²⁴⁴ were proposed. Hansel et al.^{128, 245} experimentally studied the aqueous-phase oxidation reaction between selected GLVs (i.e., MeJa, and MeSa) and $\cdot\text{OH}$ radicals formed *via* the photodissociation of H_2O_2 .

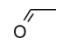
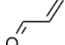
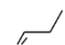
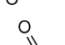
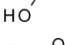
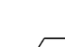
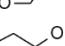
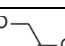
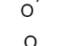
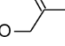
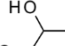
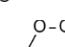
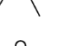
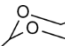

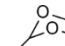




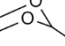
Interestingly, none of hitherto published studies have focused on the ozonolysis of GLVs alone in the aqueous phase in contrast to the multiphase chamber experiments.^{153, 192, 193, 246} In another studies,^{167, 193} primary (*Z*)-3-hexen-1-ol ozonide decomposed to form 3-hydroxypropanal, which can partition to the particle phase and likely form higher molecular weight products *via* several oligomerization reactions. Similarly, the gas-phase ozonolysis of (*Z*)-3-hexenyl acetate produced 3-oxopropyl acetate and propanal, which were proposed to undergo particle-phase oligomerization.¹⁹²

2.4. GLVs multiphase chemistry- novel source of SOA

2.4.1. Smog chamber and ambient aerosol studies

The key findings from GLVs-based smog chamber experiments and ambient aerosol studies have been summarized in details within my review paper.¹⁶⁸ A number of identified ambient aerosol products have been linked to either aqueous-phase or multiphase transformations of atmospheric GLVs. Here, I briefly overview the products identified both, tentatively and firmly (Tables 2.19 – 2.22). Smog chamber experiments involving GLVs and their mixture, as well as field-campaign results presented within this section provided substantial evidence of the GLVs contribution to SOA. However, many compounds identified in ambient aerosol samples may have more than one precursor, so they cannot be linked exclusively to any single GLVs.

Table 2.19. Products of (*Z*)-3-hexen-1-ol photooxidation and ozonolysis in smog chambers. (taken from Sarang et al. 2021)¹⁶⁸

Name	Oxidant	MW	Formula	Structure	Phase	Ref.
acetaldehyde		44	C ₂ H ₄ O			192
2-propenal		56	C ₃ H ₄ O			
propanal		58	C ₃ H ₆ O		gas	
acetic acid		60	C ₂ H ₄ O ₂			
2-propenoic acid		72	C ₃ H ₄ O ₂			
3-hydroxypropanal		74	C ₃ H ₆ O ₂		PM	193
propionic acid		74	C ₃ H ₆ O ₂		Gas, PM	192, 193
2-hydroxyacetic acid	O ₃	76	C ₂ H ₄ O ₃			193
3-hydroxy-2-oxopropanal		88	C ₃ H ₄ O ₃			
2,3-di-hydroxypropanal		90	C ₃ H ₆ O ₃		PM	
2-hydro-peroxypropanal		90	C ₃ H ₆ O ₃			
3-hydroxy-2-oxopropanoic acid		104	C ₃ H ₄ O ₄			
2-hydroperoxy-3-hydroxypropanal		106	C ₃ H ₆ O ₄			
2-ethyl-1,3-dioxan-4-ol		132	C ₆ H ₁₂ O ₃			167, 193
3-(2-hydroxy ethoxy) propanoic acid	OH, O ₃	134	C ₅ H ₁₀ O ₄		PM	167
2-(2-hydroxyethyl)-1,3-dioxan-4-ol		148	C ₆ H ₁₂ O ₄			167, 193
2-(1,3-dioxin-2-yl) ethylformate	O ₃	158	C ₇ H ₁₀ O ₄		PM	193
3-(3-hydroxy propanoyloxy) propanoic acid	OH, O ₃	162	C ₆ H ₁₀ O ₅		PM	167
2-(4-hydroxy-1,3-dioxan-2-yl)ethyl formate		176	C ₇ H ₁₂ O ₅			193
2-(1,3-dioxin-2-yl) ethyl propionate	O ₃	186	C ₉ H ₁₄ O ₄		PM	
1-((2-ethyl-1,3-dioxan-4-yl)oxy)propan-1-ol		190	C ₉ H ₁₈ O ₄			

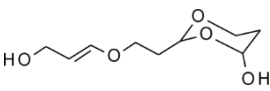
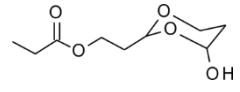
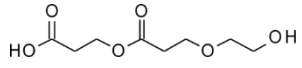
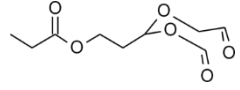
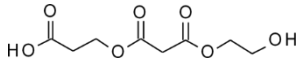
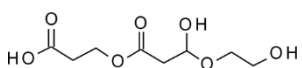
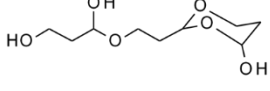
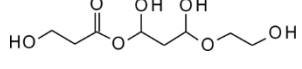
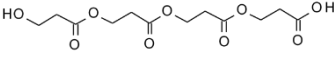
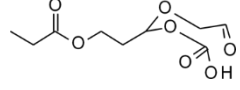
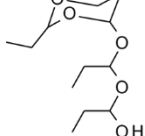
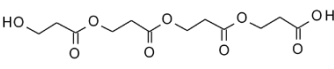
2-(2-((3-hydroxyprop-1-en-1-yl)oxy)ethyl)-1,3-dioxan-4-ol		204	C ₉ H ₁₆ O ₅			
2-(4-hydroxy-1,3-dioxan-2-yl)ethyl propionate		204	C ₉ H ₁₆ O ₅			
3-(3-(2-hydroxyethoxy)propanoyloxy) propanoic acid	OH, O ₃	206	C ₈ H ₁₄ O ₆		PM	167
3-(formyloxy)-3-(2-oxoethoxy) propyl propionate	O ₃	218	C ₉ H ₁₄ O ₆		PM	193
3-(3-(2-hydroxyethoxy)-3-oxopropanoyloxy) propanoic acid		220	C ₈ H ₁₂ O ₇			167
3-(3-(2-hydroxyethoxy)-3-hydroxypropanoyloxy) propanoic acid		222	C ₈ H ₁₄ O ₇			
1-(2-(4-hydroxyl-1,3-dioxan-2-yl)-ethoxy)propane-1,3-diol	OH, O ₃	222	C ₉ H ₁₈ O ₆		PM	
1,3-dihydrox-3-(2-hydroxyethoxy) propyl- 3- hydroxy propanoate		224	C ₈ H ₁₆ O ₇			
3-(3-(3-hydroxy propanoyloxy) Propanoyloxy propanoic acid		234	C ₉ H ₁₄ O ₇			
3-(carboxyoxo)-3-(2-oxoethoxy) propyl propionate		234	C ₉ H ₁₄ O ₇			193
1-(1-((2-ethyl-1,3-dioxan-4-yl)oxy)propoxy) propan-1-ol	O ₃	248	C ₁₂ H ₂₄ O ₅		PM	
3-(3-(3-(3-hydroxy propanoyloxy) propanoyloxy) propanoyloxy)propanoic acid	OH, O ₃	306	C ₁₂ H ₁₈ O ₉		PM	167

Table 2.20. Products of (Z)-3-hexenyl acetate ozonolysis in smog chambers (taken from Sarang et al. 2021)¹⁶⁸

Name	MW	Formula	Structure	Phase	Ref.
2-propenal	56	C ₃ H ₄ O			
Propanal	58	C ₃ H ₆ O		Gas	192
Acetic acid	60	C ₂ H ₄ O ₂			
2-propenoic acid	72	C ₃ H ₄ O ₂			
Propionic acid	74	C ₃ H ₆ O ₂		Gas, PM	192, 193
2-hydroperoxy propanal	90	C ₃ H ₆ O ₃		PM	193
3-oxo-propyl acetate	116	C ₅ H ₈ O ₃		PM	247
2-acetoxyacetic acid	118	C ₄ H ₆ O ₄			
2,3-dioxopropyl acetate	130	C ₅ H ₆ O ₄		PM	193
2-hydroxy-3-oxopropyl acetate	132	C ₅ H ₈ O ₄			
3-acetoxy-propanoic acid	132	C ₅ H ₈ O ₄		PM	193, 247
3-acetoxy-2-oxopropanoic acid	146	C ₅ H ₆ O ₅		PM	193
2-hydroperoxy-3-oxopropyl acetate	146	C ₅ H ₈ O ₅			
3-acetoxypropane peroxoic acid	148	C ₅ H ₈ O ₅		PM	247
3,4-dioxohexyl acetate	172	C ₈ H ₁₂ O ₄		PM	193
2-hydroxyethyl 3-acetoxypropanoate	176	C ₇ H ₁₂ O ₅		PM	247
2-(3-oxopropyl)ethyl 3-acetoxy propanoate	232	C ₁₀ H ₁₆ O ₆		PM	247
3-acetoxypropanoyl 3-acetoxypropanoate	246	C ₁₀ H ₁₄ O ₇		PM	193
2-(2-(3-acetoxypropanoyloxy)ethoxy)propanoic acid	248	C ₁₀ H ₁₆ O ₇		PM	247
5-acetoxy-3-oxopentyl-3-acetoxypropanoate	274	C ₁₂ H ₁₈ O ₇			

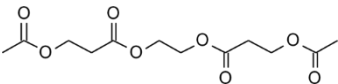
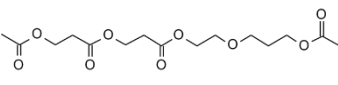
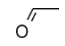
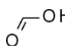
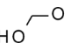
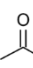
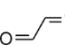
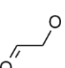
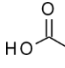
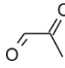
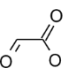
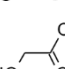
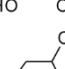
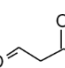
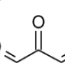
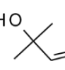
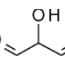
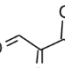
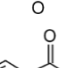
2-(3-acetoxypropoxy)ethyl 3-acetoxypropanoate	290	C ₁₂ H ₁₈ O ₈	
[3-[2-(3-acetoxypropoxy)ethoxy]-3-oxo-propyl] 3-acetoxypropanoate	348	C ₁₅ H ₂₄ O ₉	

Table 2.21. Products of 2-methyl-3-buten-2-ol (MBO) photooxidation in smog chambers and in ambient sample (organosulfates were put separately in Table 2.22). (taken from Sarang et al. 2021).¹⁶⁸

MW	Name	Formula	Structure	Phase	Ref.	Ambient Aerosol
30	formaldehyde	CH ₂ O	=O	Gas	248, 249	
32	methanol	CH ₄ O	-OH	Aqu	244 b	
44	acetaldehyde	C ₂ H ₄ O		Gas	249	
46	formic acid	CH ₂ O ₂			244 b	
48	formaldehyde hydrated (methanediol)	CH ₄ O ₂		Aqu		
58	acetone	C ₃ H ₆ O		Gas, aqu	248, 249, 244 b	
58	glyoxal	C ₂ H ₂ O ₂			249, 250	
60	glycolaldehyde	C ₂ H ₄ O ₂		Gas		
61	acetic acid	C ₂ H ₄ O ₂		Aqu	244 b	
72	methylglyoxal	C ₃ H ₄ O ₂			249	
74	glyoxylic acid	C ₂ H ₂ O ₃		Gas		
76	glycolic acid	C ₂ H ₄ O ₃			244 b	
78	glycolaldehyde hydrated	C ₂ H ₆ O ₃		Aqu		
86	1,3-butanedione	C ₄ H ₆ O ₂			249	
86	2-oxopropanedial	C ₃ H ₂ O ₃		Gas		
88	2-hydroxy-2-methylpropanal	C ₄ H ₈ O ₂		Gas	249, 250	
88	2-hydroxypropaneal	C ₃ H ₄ O ₃			249	
100	2,3-dioxobutanal	C ₄ H ₄ O ₃		Gas		
114	2,3-dioxobutane-1,4-dial	C ₄ H ₂ O ₄				

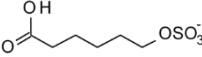
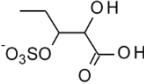
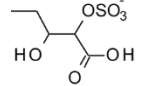
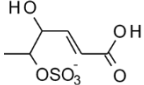
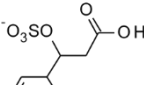
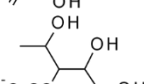
116	2-oxovaleric acid	C ₅ H ₈ O ₃			
118	1,3-dihydroxy-3-methylbutan-2-one	C ₅ H ₁₀ O ₃		Gas, PM	
118	2,3-dihydroxy-3-methylbutanal	C ₅ H ₁₀ O ₃		Gas	
120	2,3-dihydroxyisopentanol	C ₅ H ₁₂ O ₃		PM, aqu	^{249, 251 a, 244 b} PM _{2.5} ^{249, 252}
132	2,3-dihydroxy-2-methylbutane dialdehyde	C ₅ H ₈ O ₄		Gas, PM	²⁴⁹
134	2,3-dihydroxy-3-methylbutanoic acid	C ₅ H ₁₀ O ₄			
134	2-hydroxy-2-methylpropenedioic acid	C ₄ H ₆ O ₅			
136	2-methylerythritol	C ₅ H ₁₂ O ₄		PM	PM _{2.5} ^{249, 252}
136	2-methylthreitol	C ₅ H ₁₂ O ₄			PM _{2.5} ^{249, 252}
164	2,3-dihydroxy-2-methylsuccinic acid ^c	C ₅ H ₈ O ₆			PM _{2.5} ²⁵³

^a aqueous phase reactions of methylbutenol epoxides¹⁶⁸; ^b aqueous-phase addition of sulfate radical anions¹⁶⁸; ^c and isomers

Table 2.22. GLVs-derived organosulfates identified in smog chamber and ambient samples. (taken from Sarang et al. 2021)¹⁶⁸

MW	Name	Product Formula	Structure	Parent Compound	Formation Process	Ref.	Ambient Aerosol
140	Glycolaldehyde sulfate	C ₂ H ₄ O ₅ S		MBO	SO ₄ ⁻ addition	244 b	PM _{2.5} ²⁵⁴ PM ₁₀ ²⁵⁵
154	Hydroxyacetone sulfate	C ₃ H ₆ O ₅ S		(Z)-3-hexen-1-ol	OH photolysis, ozonolysis	246	PM ₁ ^{256, 257} , PM _{2.5} ^{246, 254, 258-261} , PM ₁₀ ²⁵⁵
156	Glycolic acid sulfate	C ₂ H ₄ O ₆ S		MBO	SO ₄ ⁻ addition	244 b	PM ₁ ^{256, 257, 262} , PM _{2.5} ^{254, 258-261, 263, 264}
158	Hydrated glycol sulfate	C ₂ H ₆ O ₆ S		MBO	SO ₄ ⁻ addition	244 b	
170	Lactic acid sulfate	C ₃ H ₆ O ₆ S		(E)-2-pentenal	Ozonolysis	243	PM ₁ ^{256, 262} , PM _{2.5} ^{243, 254, 258-260, 263, 265-267}
170	1-sulfoxy-2-hydroxybutane	C ₄ H ₁₀ O ₅ S		(E)-2-pentenal	Ozonolysis	243	PM _{2.5} ²⁴³
170	2-Sulfoxy-3-hydroxy-propanal	C ₃ H ₆ O ₆ S		(Z)-3-hexen-1-ol	OH photolysis, ozonolysis	246	PM _{2.5} ²⁴⁶
186	3-sulfoxy-2-hydroxy-propanoic acid	C ₃ H ₆ O ₇ S		(Z)-3-hexen-1-ol	OH photolysis, ozonolysis	246	PM _{2.5} ²⁴⁶
198	3-hydroxy-3-methyl-butan-2-one sulfate	C ₅ H ₁₀ O ₆ S		MBO	SO ₄ ⁻ addition	244 b	
198	4-sulfoxy-1-hydroxy-3-methyl-butan-2-one	C ₅ H ₁₀ O ₆ S		MBO	SO ₄ ⁻ addition	244 b	PM _{2.5} ²⁵⁴ , PM _{2.5} ^{264?}
200	2,3-dihydroxy-3-methyl-butane sulfate	C ₅ H ₁₂ O ₆ S		MBO	OH photolysis SO ₄ ⁻ addition	268, ^{251 a} 244 b	PM ₁ ^{257, 256?} , PM _{2.5} ^{254, 259, 268, 264?}
210	(Z)-5-sulfoxy-hex-3-enoic acid	C ₆ H ₁₀ O ₆ S		(Z)-3-hexen-1-ol	OH photolysis, ozonolysis	246	PM ₁ ^{256, 257?} , PM _{2.5} ²⁴⁶ , PM ₁₀ ^{255?}

Chapter 3. Instrumentation, techniques, and methods

212	6-(sulfoxy)hexanoic acid	C ₆ H ₁₂ O ₆ S		(Z)-3-hexen-1-ol	OH photolysis, ozonolysis	246	PM ₁ ^{256, 257?} , PM _{2.5} ²⁴⁶
214	3-sulfoxy-2-hydroxypentanoic acid	C ₅ H ₁₀ O ₇ S		(E)-2-pentenal (E)-2-pentenoic acid	Ozonolysis, SO ₄ ⁻ (aqu)	243	PM ₁ ^{256?} , PM _{2.5} ²⁴³
214	2-sulfoxy-3-hydroxypentanoic acid	C ₅ H ₁₀ O ₇ S		(E)-2-pentenal	Ozonolysis	243	PM ₁ , ^{257I} , ^{256?} , PM _{2.5} ²⁴³
226	(E)-5-sulfoxy-4-hydroxy-hex-2-enoic acid	C ₆ H ₁₀ O ₇ S		(Z)-3-hexen-1-ol	OH photolysis, ozonolysis	246	PM _{2.5} ²⁴⁶
226		C ₆ H ₁₀ O ₇ S		(Z)-3-hexenal	Ozonolysis	269	PM _{2.5} ²⁶⁹
230	3-sulfoxy-2,4-dihydroxypentanoic acid	C ₅ H ₁₀ O ₈ S		(E)-2-pentenal, (Z)-3-hexenal (Z)-2-hexenal	Ozonolysis ozonolysis	243	PM _{2.5} ²⁴³
270		C ₉ H ₁₈ O ₇ S	-	(Z)-3-hexen-1-ol	OH photolysis, ozonolysis	246	PM _{2.5} ²⁴⁶

^a aqueous-phase reactions of methylbutenol epoxides (Section 5); ^b aqueous-phase addition of sulfate radical anions (review paper)¹⁷²; ? unresolved structure.

2.4.2. Estimation of atmospheric SOA formation from GLVs

The literature data (Section 2.4.1) indicate that GLVs contribute to ambient SOA. Several smog-chamber experiments proved the SOA formation from individual GLVs (or their mixtures), and various plant emissions. Compounds identified in ambient aerosol samples are known to originate from reactions of GLVs with oxidants in the lower atmosphere.

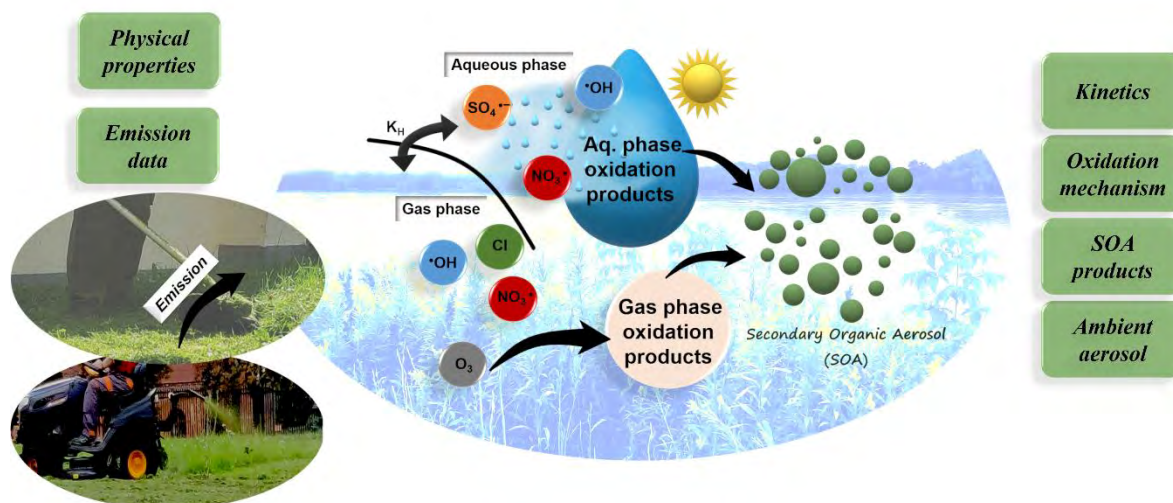
The global estimated SOA production proposed by Hamilton et al.¹⁶⁷ from (*Z*)-3-hexen-1-ol and (*Z*)-3-hexenyl acetate based on the experimental aerosol mass yields for (*Z*)-3-hexen-1-ol (3.1%), (*Z*)-3-hexenylacetate (0.93%) scaled to 7.5% and 2.25 % respectively, was 1 – 5 TgC yr⁻¹. Yearly emissions of hexenol and hexenyl acetate are estimated to be 10 – 50 TgC yr⁻¹.¹⁵⁰ However, it is unclear if Hamilton et al.¹⁶⁷ considered the whole group or each of its member, and thus, their estimation of SOA from GLVs is uncertain and seems overestimated.

Better estimated global annual emissions for the most abundant GLVs, i.e., (*Z*)-3-hexenal (4.9 Tg yr⁻¹), (*Z*)-3-hexenol (2.9 Tg yr⁻¹), and MBO (2.2 Tg yr⁻¹) are also available (see Table 1.2, Chapter 1).⁴⁵ Based on the SOA yields (from 2%²⁴⁶ to 7.5%¹⁶⁷) obtained from the smog chamber photooxidation of (*Z*)-3-hexen-1-ol, the atmospheric SOA formation is estimated to be 0.058 to 0.218 Tg yr⁻¹. In the case of the ozonolysis of (*Z*)-3-hexen-1-ol, the maximum SOA yield of 5.1% gave global estimated SOA load of 0.15 Tg yr⁻¹.²⁴⁶ Smog-chamber SOA yields from MBO were 0.7% (OH)²⁴⁹, and 0.3 – 1.8% (ozonolysis)¹⁷⁸ with global annual SOA production of 0.015 Tg yr⁻¹ and 0.007 – 0.040 Tg yr⁻¹, respectively.¹⁶⁸ Assuming the SOA yield for (*Z*)-3-hexenal to be equal to that from (*Z*)-3-hexen-1-ol, Sarang et al.¹⁶⁸ estimated the overall SOA yield from (*Z*)-3-hexen-1-ol, MBO, and (*Z*)-3-hexenal) to be 0.58 – 1.05 Tg yr⁻¹. Besides, specific emission sources, such grass cutting¹²⁶, grass mowing¹⁹², harvesting and cultivation of switchgrass²⁷⁰ multiplied by respective land use,^{271, 272} can give 0.1 – 0.2 Gg yr⁻¹, 52 Gg yr⁻¹, and 33 Gg yr⁻¹ of SOA, respectively.¹⁶⁸ However, estimation of SOA production based on smog-chamber experiments and estimated GLVs emissions seems rather approximate. An array of factors, such as concentration of reactants, reaction time, meteorological conditions, and last but not least, competition with other reactants, influence and affect the formation and growth of aerosol in the ambient atmosphere in the complicated way that cannot be simulated perfectly within the laboratory experiments.

Based on the calculated Henry's constants, Hansel et al.¹²⁸ concluded that the aqueous-phase reaction products arising from the reactions between MeJa or MeSa with $\cdot\text{OH}$ radicals were more soluble in water than the parent compounds. This should lead to an increase in the global overall aqueous-phase SOA yield. In addition, the partial pressures of the products of MeJa and MeSa oxidation in cloud water were less volatile than their precursors, and most likely remained in the condensed phase as SOA-bound components.

In contrast, Richards-Henderson et al.¹²⁹ estimated that SOA mass produced by (*Z*)-3-hexen-1-ol, (*Z*)-3-hexenyl acetate, MeSa, MeJa, and MBO with $\cdot\text{OH}$ radicals in the aqueous phase was 15-times lower than in the gas phase. This could be explained by low or moderate water solubility of these GLVs. However, if factors, such as ionic strength or presence of other organic compounds could increase the GLVs solubility, one would expect higher SOA yields. In a study of the aqueous-phase reactions of $^1\text{O}_2^*$ and $^3\text{C}^*$ ($^3\text{DMB}^*$, 3,4-dimethoxybenzaldehyde) with (*Z*)-3-hexen-1-ol, (*Z*)-3-hexenyl acetate, MeSa, MeJa, and MBO, it was found that these reactions were a more significant source of aqueous SOA.²³⁹ Only in the case of MeJa, with the $\cdot\text{OH}$ and $^3\text{DMB}^*$, the aqueous-phase reactions seemed a major conversion pathway.

2.5. Selection of green leaf volatiles (GLVs) and aims of the work



2.5.1. Selection of green leaf volatiles (GLVs)

Based on the review in previous chapters, I selected the following GLVs for my Ph.D. research: 1-penten-3-ol, (*Z*)-2-hexen-1-ol, and (*E*)-2-hexen-1-al.

The first argument was that they have never been investigated as potential sources of SOA through the aqueous-phase transformation. Next, the SOA yields from the selected GLVs were unknown (see section 2.4.2 and Sarang et al.¹⁶⁸). Lastly, although the emissions of GLVs are much lower than major BVOCs, like isoprene and monoterpenes, during high emission episodes GLVs may influence the local and regional air quality. In addition, such selection of three compounds consisting of both C5, and C6 unsaturated alcohol as well as aldehyde will better reflect the obtained results for comparison in future studies. In particular, the selected GLVs may become significant under specific scenarios, such as harvesting, switchgrass cultivation, lawn mowing, biotic and abiotic plant stresses, where the GLV emission can attain very high values. The GLVs emissions may further increase if agricultural practices, such as fumigation and plants treatment with GLVs become more widespread in agriculture, horticulture and forestry.

2.5.2. Key objectives

In addition to BVOCs (e.g., isoprene and monoterpenes) abundantly released by Earth's ecosystem into the atmosphere, also GLVs emitted actively participate in the gas-, aqueous- and multiphase atmospheric processes. The aqueous transformations of GLVs pose a challenge to atmospheric scientists as potential novel, but poorly explored precursors of SOA-bound compounds.

The objectives of the my Ph.D. thesis was to verify the hypothesis that three selected GLVs, i.e., 1-penten-3-ol, (*Z*)-2-hexen-1-ol, and (*E*)-2-hexen-1-al. could be a missing source of SOA particles in the atmosphere through in-cloud reactions with ambient radical species.

To predict the fate of any organic compound in the atmosphere, one must determine the kinetics of its chemical reactions with atmospheric oxidants. To address the issue, in the first part of my research, I investigated the kinetics of aqueous-phase reactions of 1-penten-3-ol, (*Z*)-2-hexen-1-ol, and (*E*)-2-hexen-1-al with hydroxyl ($\cdot\text{OH}$), sulfate ($\text{SO}_4^{\cdot-}$) and nitrate (NO_3^{\cdot}) radicals using the technique of laser flash photolysis-laser long path absorption (LFP-LLPA). The experimental studies were supported by computational kinetic investigations carried out using the COPASI software.

In the second part of my thesis, the main goal was to propose chemical mechanisms for the kinetically explored reactions. The aqueous-phase oxidation of the 1-penten-3-ol, (*Z*)-2-hexen-1-ol, and (*E*)-2-hexen-1-al with $\cdot\text{OH}$ radical was carried out in the aqueous-phase photo-reactor under simulated sunlight conditions. The product analyses were focused on targeting carbonyls, alcohols, and carboxylic acids as key oxidation products using advanced hyphenated mass spectrometry (i.e., capillary gas chromatography mass spectrometry (c-GC-MS) and a reversed-phase liquid chromatography high resolution mass spectrometry (rp-LC-HR MS). In order to get more insights into the structures of identified oxidation products and chemical mechanisms of their formation, I deployed a suit of density functional theory (DFT)-based quantum calculations.

Chapter 3. Instrumentation, techniques, and methods



Picture courtesy: taken at Laser Lab, TROPOS, Leipzig

3.1 Chemicals

All chemicals were purchased and used without further purification: 1-penten-3-ol (Sigma Aldrich, 99.0%), (*Z*)-2-hexen-1-ol (Sigma Aldrich, 95.0%), (*E*)-2-hexen-1-al (Sigma Aldrich, 98.0%), sodium persulfate ($\text{Na}_2\text{S}_2\text{O}_8$, Sigma Aldrich and Honeywell, 99.0%), sodium nitrate (NaNO_3 , EMSURE, 99.5%), hydrogen peroxide (H_2O_2 , CHEMSOLUTE, 30.0% wt. in H_2O), potassium thiocyanate (KSCN , CHEMSOLUTE, 99.0%), catalase from bovine liver (Sigma Aldrich, 10000 – 40000 units/mg protein), *O*-(2,3,4,5,6- pentafluorobenzyl) hydroxylamine hydrochloride (Sigma Aldrich, for GC derivatisation, $\geq 99\%$ (AT)), Acetonitrile (Optima, LC-MS grade), fuming Hydrogen Chloride (EMSURE, 37.0%), 2,2,6,6-cyclohexanone- d_4 (ISOTEC, 99 atom % D), 2,2,4-trimethyl pentane or Isooctane (Merck, p.a. $\geq 99.5\%$ GC), Formic acid (LC-MS grade, Merck LiChropur, 98%-100% and fisher Optima). Dichloromethane (Honeywell, $\geq 99.0\%$), 1-penten-3-one (Sigma Aldrich, analytical standard with 0.1% BHT as stabilizer), Propionaldehyde (Merck, $\geq 98\%$), Butyraldehyde (Merck, $\geq 99\%$), *trans*-2-hexenoic acid (Sigma Aldrich, 99%). Aqueous solutions were freshly prepared using Milli-Q water (resistivity of 18.2 M Ω cm, TOC < 5 ppb) for kinetic experiments, while for the photooxidation studies, aqueous solutions were freshly prepared using Milli-Q water (resistivity of 18.2 M Ω cm, TOC < 3 ppb, Elix Miilipore, Milli-Q gradient A10).

3.2 Experimental techniques – background and working principles

In this work, laboratory-based techniques and methods required to study the aqueous-phase chemistry of atmospheric photochemical reactions involving kinetic and mechanistic analyses were used. In order to study the photochemistry of GLVs (i.e., 1-penten-3-ol, (*Z*)-2-hexen-1-ol, and (*E*)-2-hexen-1-al) with $\cdot\text{OH}$, $\text{SO}_4^{\cdot-}$, and NO_3^{\cdot} radicals two different experimental setups for the photodissociation were used. The first was based on laser photolysis combined with UV-vis absorption spectroscopy for the kinetic studies; while the second, which was focused on the photooxidation products in the aqueous-phase, used the Xenon arc lamp as a light source. The hyphenated-mass spectrometry was applied to characterize and quantify organic products of the aqueous-phase reactions. The simulation and theoretical methods, such as kinetic modeling and density functional theory (DFT)-assisted quantum calculations, were used to validate the experimental findings. The present chapter briefly describes the techniques and methods used to

generate and detect the radicals, to analyze the kinetics and photooxidation products, to extract chemical-mechanistic information.

The kinetics of atmospherically relevant aqueous-phase reactions was studied using the technique of laser flash photolysis-laser long path absorption (LFP-LLPA). LFP-LLPA is a combination of laser photolysis technique (to carry out the photodissociation of ions and neutral molecules) and UV-Vis spectrophotometry (fast signal acquisition from the photodiode, which is digitized using a digital oscilloscope).^{273, 274}

There are two types of kinetic measurement techniques: absolute and relative. The absolute approach follows the concentrations of all reactants in a chemical reactor that are necessary to derive the reaction rate constants. The relative approach determines the rate constants by following the concentration of the reactant of interest and a suitable reference compound, for which the rate constant is already known. Both, absolute and relative rate measurement techniques are complementary and help to describe the overall reaction mechanisms. Figure 3.1 taken from Orzel et al.²⁷⁵, provides an overview of time scales of various available kinetic techniques.

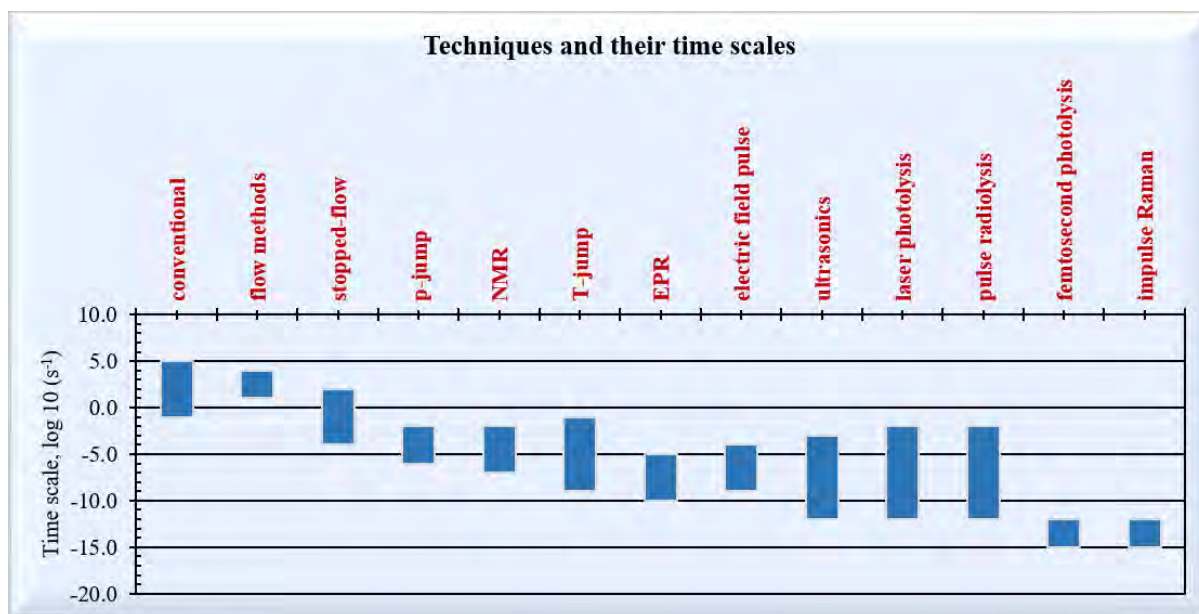


Figure 3.1. Time scales of various kinetic techniques.²⁷⁵

3.2.1. Ultraviolet-Visible (UV-Vis) spectroscopy

UV-Vis absorption spectrophotometers are often coupled with a wide range of reactor systems, such as stopped-flow and flash photolysis for various kinds of chemical analyses. In the

one of the most suitable systems for kinetic experiments, i.e., flash photolysis, UV-Vis is used as the detection system to follow fast reactions with a time scale ranging from milliseconds to picoseconds.²⁷⁶ The system was deployed in the LFP-LLPA method used in this study and described later in this chapter.

3.2.1.1. Background

Spectroscopy is based on electromagnetic radiation (light) interaction with the matter expressed as light absorption, reflection, refraction, transmission, and scattering. Various ranges of electromagnetic radiation deal with the different types of spectroscopy and have different potential applications (Figure 3.2). The wavelength (λ), frequency (ν), and energy (E) of the electromagnetic radiations are related by equations 3.1 – 3.2.

$$\nu = c/\lambda \quad (3.1)$$

$$E = h \nu \quad (3.2)$$

where: ν is the frequency in seconds (s), c is the speed of light ($3 \times 10^8 \text{ ms}^{-1}$), λ is the wavelength (m), E is the energy (J), h is Planck's constant ($6.62 \times 10^{-34} \text{ J s}$).

UV-Vis spectroscopy involves the interaction of light and matter within the UV-Vis range, leading to electronic transitions. Depending upon the type of electronic transitions between ground and higher energy states (Figure 3.3), it gives rise to a distinct spectrum. Only the lowest energy, $\pi \rightarrow \pi^*$ and $n \rightarrow \pi^*$ transitions, achieved between 190 – 800 nm due to the presence of chromophores (Table 3.1), can be observed using UV-Vis spectroscopy. Atmospheric gases, quartz, and special glasses used for measurements absorb below 180 nm. The measurements below 180 nm require special equipment, and the region is known as the vacuum ultraviolet.²⁷⁶ The other part of the UV region extending from 200 – 400 nm divides into far and near UV. UV-Vis spectroscopy is an important analytical tool used for qualitative and quantitative analysis. The superimposed electronic states, including vibrational and rotational states, give rise to multiple transitions, and hence a broad spectrum. They are reported together with the absorption maxima wavelengths (λ_{max}). Types of chromophores and expected electronic transitions along the absorbance wavelengths are described in Table 3.1.

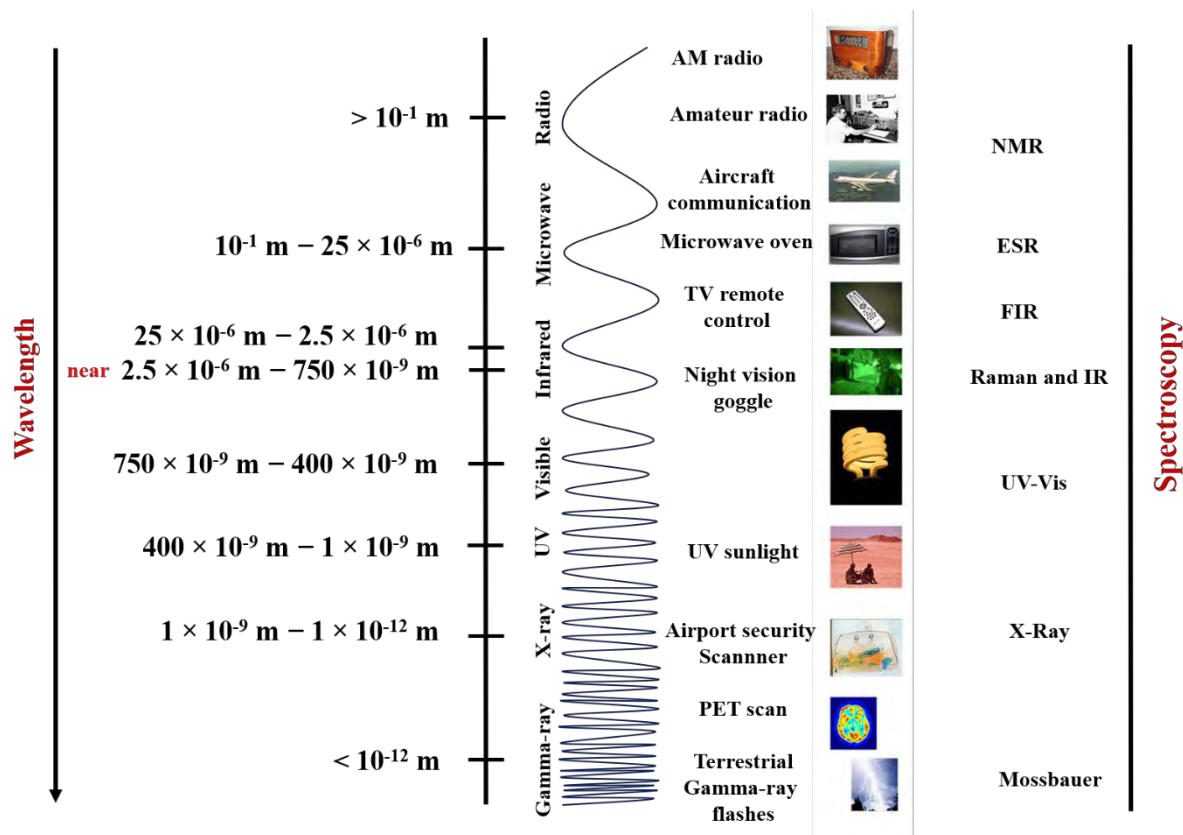


Figure 3.2. The wavelength range of the EM spectrum, associated spectroscopy, and their potential applications (adapted from [NASA's Imagine the Universe](#), and Geiger 2004).²⁷⁷

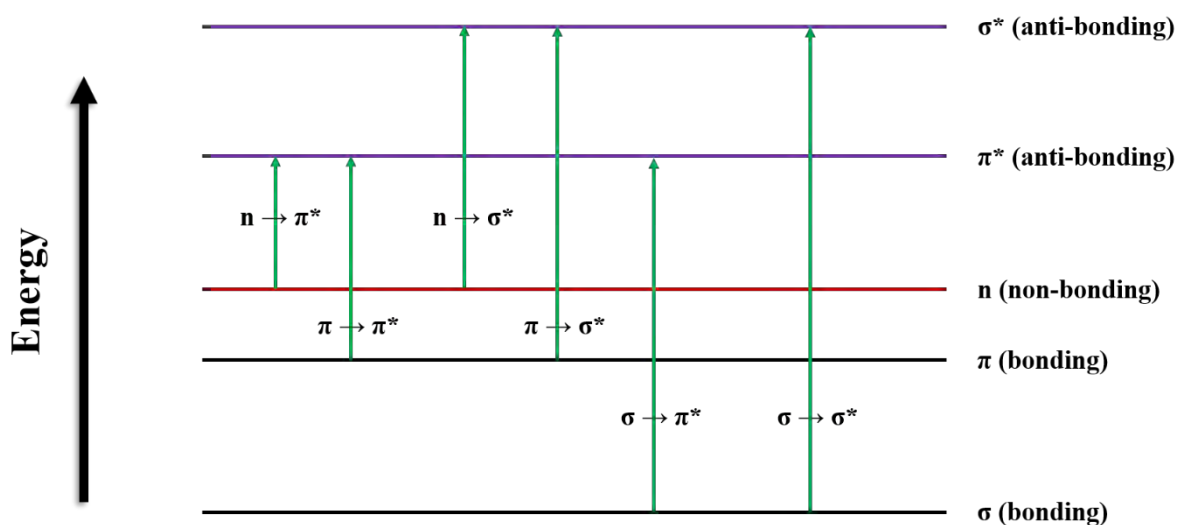


Figure 3.3. Types of possible electronic transitions between energy states relevant to electronic spectroscopy.²⁷⁸

Table 3.1. Electronic transitions, their absorbance maxima, and examples of compounds affected.²⁷⁸

Excitation	Chromophore	Example	λ_{\max}	UV-Vis
$\sigma \rightarrow \sigma^*$	None	Saturated compounds such as CH ₄ , with only C-H groups	125 nm	No
$n \rightarrow \sigma^*$	None	Saturated compounds with non-bonding (lone pair) electron-containing atoms, such as saturated alcohols, amines, ethers, halides, etc.	H ₂ O = 167 nm CH ₃ Cl = 169 nm	No
$\pi \rightarrow \pi^*$	Alkene, alkyne, aldehyde, ketones etc.	Unsaturated compounds	170 – 190 nm	Yes
$n \rightarrow \pi^*$	Ketones, aldehydes, acids, esters etc.	Unsaturated compounds containing atom with non-bonding electron	200 – 350 nm	Yes

3.2.1.2. Working principles

The UV-Vis spectrophotometer is used to acquire UV-Vis spectra. Based on Beer-Lambert law, the concentrations of absorbing compounds can be quantified.^{276, 279} The law states that whenever a beam of monochromatic light passes through a solution containing a light-absorbing substance, the amount of absorbed radiation is proportional to the concentration of that substance and an optical path length (Equation 3.3).

$$A = -\log T = -\log \frac{I}{I_0} = \epsilon lc \quad (3.3)$$

where, ϵ is the molar absorptivity or extinction coefficient, and c is the concentration of the absorbing species, respectively, I_0 and I are the incident and transmitted intensity, and l is the optical path length.

Essential components of a UV-Vis spectrophotometer are:²⁷⁶

1. A light source or sources to cover the entire range of 190 – 800 nm.
2. A light dispersion device, such as a monochromator with a prism or diffraction grating
3. A sample cell or holder
4. A detector to measure light intensity, usually a photomultiplier tube or photodiode detector
5. Other optical components (such as lenses, mirrors, beam splitters)

There are two types of spectrophotometers, single and double beam. In a single-beam spectrophotometer, a single light beam travels through the optical components and sample to the detector (Figure 3.4). Before each measurement, the absorbance scale must be reset to zero. In a double-beam spectrophotometer, one beam passes through a sample and the second one passes through a reference cell, traveling independently to the detector (Figure 3.5). This work used two double-beam spectrophotometers: *i*) Lambda 900 UV/VIS/NIR spectrometer (Perkin Elmer Instruments), and *ii*) Jasco V-570 UV-VIS-NIR spectrophotometer.

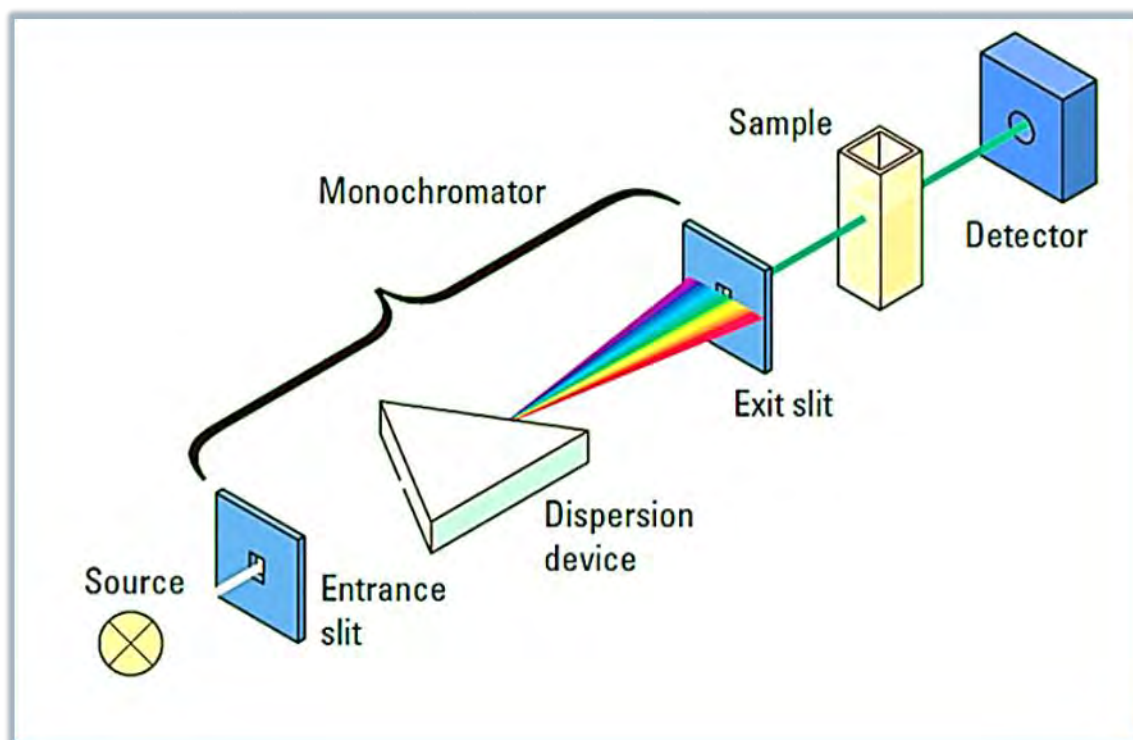


Figure 3.4. Scheme of a single-beam spectrophotometer (taken from Fundamentals of modern UV-visible spectroscopy Primer, Agilent Technologies)²⁷⁹

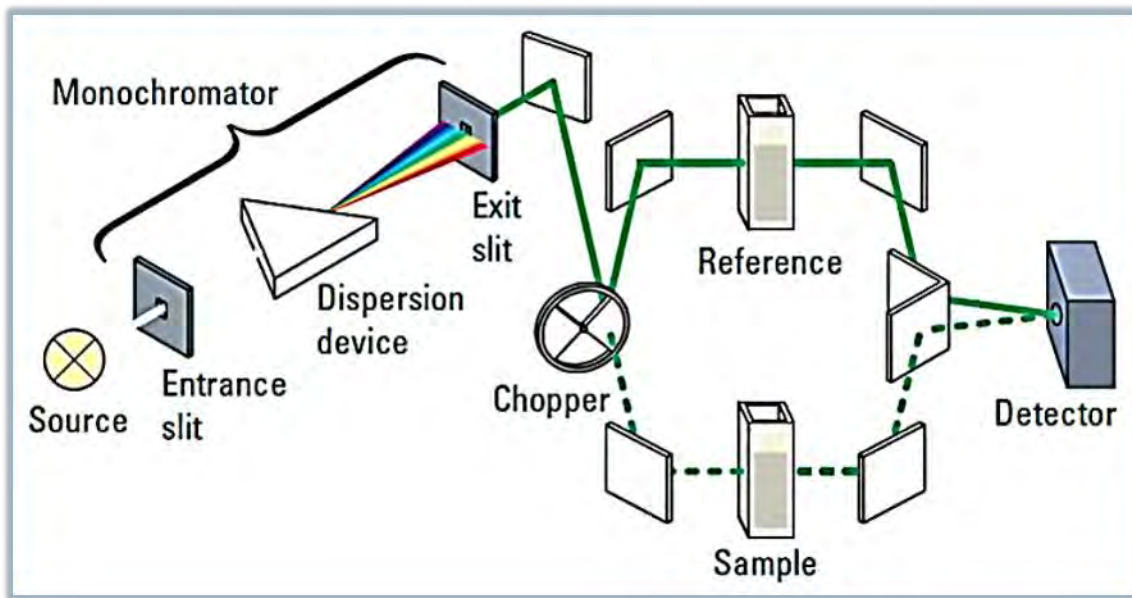


Figure 3.5. Scheme of a dual-beam spectrophotometer (taken from *Fundamentals of modern UV-visible spectroscopy Primer*, Agilent Technologies)²⁷⁹

3.2.2. Laser flash photolysis-laser long path absorption (LFP-LLPA)

Laser is an acronym for "Light Amplification by Stimulated Emission of Radiation"²⁸⁰, which clearly describes it as a device that emits a coherent beam of light through an optical amplification process involving stimulated emission of electromagnetic radiations. The basics of lasers used in chemical kinetics are briefly summarised after Kovalenko and Leone.²⁸¹ Unlike other light sources, lasers emit highly coherent radiations (all photons with the same direction, frequency, and phase), providing unique properties, such as monochromaticity, polarization, and power. Spatial coherence enables the light to be focussed on a narrow region or spot over great distances, while temporal coherence enables lasers to emit light within a narrow region of the spectrum, i.e., single color or monochromatic light. Unlike spontaneous emission, the process of stimulated emission occurs due to the interaction of incoming photon with an excited atomic electron, which causes it to drop to lower quantum energy state releasing a new photon, coherent to the photon of the incident wave. With respect to the absorption and spontaneous emission, stimulated emission is amplified within the lasers. The two common types of laser used in chemistry include pulsed laser and continuous laser, also used in the present study.

Laser flash photolysis coupled with UV-Vis spectrophotometry is a powerful tool used to investigate fast physical and chemical processes involving intermediates (radicals and atoms

usually at very low concentrations in the system), such as kinetics over a wide range of time scales, from milliseconds to femtoseconds.^{275, 282} In 1967, the Noble Prize in Chemistry was awarded to Porter and Norrish for their discovery in 1949,²⁸³ and later another one was awarded to Ahmed Zewail in 1999 for the development of femtosecond spectroscopy.²⁸⁴

The LFP-LLPA (Figure 3.6) applied in the study uses a combination of an *excimer laser* (pulsed) and a *continuous wave laser*.

An excimer laser is a gas laser that produces pulses in the UV region using a combination of a noble gas (Ar, Kr, or Xe) and a reactive gas (F₂ or Cl₂), forming rare gas halides that are chemically inert.²⁸⁵ Under the appropriate conditions of high pressure and the application of intense electric discharge, the formation of a highly excited diatomic molecule known as excimer occurs. Excimer exists only in an energized state for an approximate lifetime in nanoseconds (ns) range and undergoes decay giving rise to the short pulse of the light of a specific wavelength (Table 3.2), with pulse widths below up to 10 ns (reaction R3.1, and R3.2)



The mandatory requirement to study fast or ultrafast reactions is that the pulse width must be much shorter than the half-time of the chemical reaction studied. The most significant disadvantage of UV laser systems is their fixed wavelengths. That precludes studying systems containing the compounds absorbing in different ranges. Therefore, for each chemical system containing inorganic or organic reactant, a particular wavelength laser system is employed as in the present work, where three different radical kinetics ([•]OH, SO₄^{•-}, and NO₃[•]) with GLVs were investigated.

Depending on the orientation of singly occupied *p* orbital of a halogen atom, the interaction between rare gas atom and halogen atom gives rise to the states 1 ²Σ⁺ and 1 ²Π. They are further split into various states due to charge transfer interaction and spin-orbit splitting such as A, B, C and X, of which essential laser transitions are B-X, and C-A described below in Table 3.2. XeCl provides laser emission at 308 nm with a 0.3 nm spectral width and a pulse width of about 10 ns.

Table 3.2. Summary of the different types of rare gas-halide excimer lasers along with their wavelength and transition (*B-X*, and *C-A*) lifetimes (taken from Hutchinson et al. 1987)²⁸⁵. The values in **green bold** correspond to the excimer lasers used in this work.

		F		Cl		Br		I	
		λ , nm	τ , ns	λ , nm	τ , ns	λ , nm	τ , ns	λ , nm	τ , ns
Xe	<i>B-X</i>	351	12 – 19	308	11	282	12	253	12
	<i>C-A</i>	490	93, 113	350	120	302	120	263	110
Kr	<i>B-X</i>	248	6.5 – 9	222		206			
	<i>C-A</i>	275	63						
Ar	<i>B-X</i>	193	4.2	175					
	<i>C-A</i>	203	48	199					
Ne	<i>B-X</i>	108	2.6						
	<i>C-A</i>	117	38						

Continuous-wave (CW) lasers produce a continuous wave with a steady output power over a long time. Different materials, such as gas, semiconductors, or crystals are used to accomplish CW lasers. Stimulated emission and amplifications are achieved with a cavity consisting of an active and gain medium continuously replenished by a steady pump source. The cavity can be made up of doped crystal (solid-state laser), gas (He-Ne laser), or semiconductor P-N junction (diode lasers). In this work, three different CW *diode lasers* were used: 1) LSR 407 nm, Coherent, blue-violet laser; 2) 473 nm CW laser LasNova Series 40 blue, LASOS; 3) 635 nm red CW laser, Radius, Coherent.

More details of the physics behind lasers are beyond the scope of this work and are summarized elsewhere.^{280, 285-289}

3.2.2.1. Kinetic Experiments – operation principles

I deployed the LFP-LLPA (Figure 3.6) to measure the rate constants of the aqueous-phase radical-mediated oxidation of selected GLVs. A detailed description of the setup is provided elsewhere.^{273, 290-295}

The LFP-LLPA method applied is similar to that used by Schöne et al. and Otto et al.^{296, 297} In brief, a freshly prepared aqueous solution containing a given GLV and a radical precursor was transferred into the solution tank. The solution flowed down through the measurement cell (4 cm × 3.5 cm × 2 cm) thermostatted with a water thermostat (Julabo or S LAUDA). The radical precursors' photolysis occurred in the measurement cell by excimer laser (COMPEX 201 series)

pulses of μs width triggered at 4 Hz (DG535 Digital Delay Generator, Stanford Research Systems). A continuous-wave (CW) laser measured the radicals' light absorption after passing the beam several times across the cell by a White mirror setup. The signal's final intensity was measured with a photodiode and recorded with an oscilloscope (Data SYS 944, Gould) and a computer for further data processing to obtain a second-order rate constant k_{2nd} of the reaction. More details of the setup configuration for each set of kinetics observed are provided in Section 3.3.1.

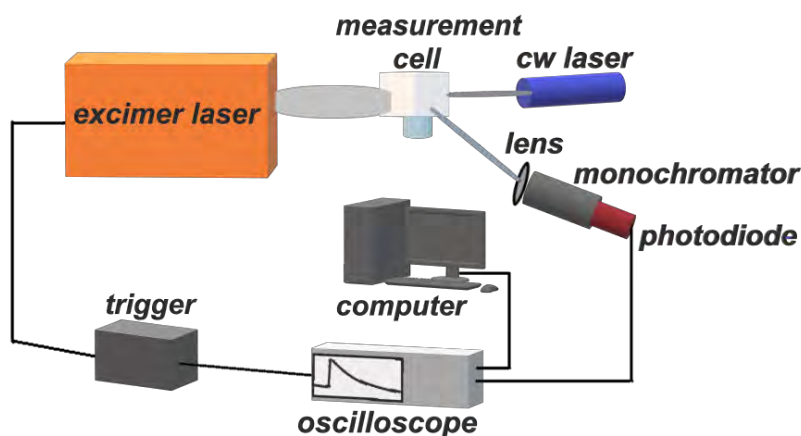


Figure 3.6. The Laser Flash Photolysis-Laser Long Path Absorption (LFP-LLPA) setup used for the kinetic investigations.²⁹⁸

3.2.3. Photooxidation experiments – operation principles

The 300 mL glass photoreactor was used to perform GLVs photooxidation product studies in the presence of $\cdot\text{OH}$ radicals, similar to the study of Otto et al. 2017.²⁹⁰ The reactor was connected to a thermostat unit (Julabo F10 and Julabo HC) to maintain a constant temperature of 298 K and was placed on a magnetic stirrer (IKA[®] RH basic 2). The reactor was sealed and the light was switched on to irradiate the solution through a quartz window. Figure 3.7 shows the reactor setup.

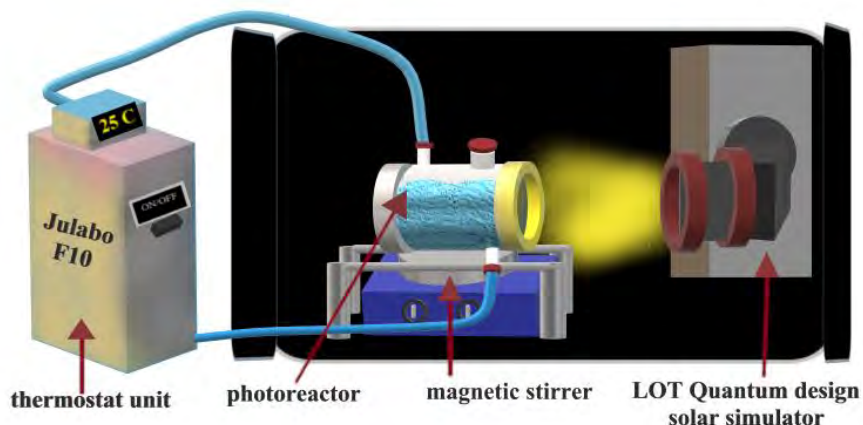


Figure 3.7. The photooxidation reaction setup used for the photooxidation products analysis at TROPOS.

The LOT Quantum Design solar simulator (LSO805) with an arc light source (LSH602) was used to photolyze H_2O_2 and produce $\cdot\text{OH}$ radicals. The lamp housing consisted of a 450 W O_3 free xenon lamp (LSB551), lamp adapter (LSA655), ignitor (LSE641), cable set (LSE662), LSN655 power supply, an optical system including filter holder, electromechanical shutter (LSZ 160), and 90° beam turner with AlMgF2 coated mirror. The light passed through an AM1.5 filter to mimic the daylight conditions, which allowed only light above 290 nm wavelength. That helped to avoid any short-wavelength photolysis of the species in the reactor.

3.2.4. Hyphenated mass spectrometry

3.2.4.1. Capillary gas chromatography-mass spectrometry (cGC-MS)

The capillary gas chromatography-mass spectrometry is a combination of two analytical techniques. The gas chromatography (GC) uses the ability of the inert carrier gas phase to separate volatile mixtures based on their partitioning capabilities between the mobile (gas) and stationary phases as they travel down a capillary column placed within a temperature-controlled oven. When interfaced to a mass spectrometer (MS), the separated volatiles are transferred to a MS, where they are ionized and detected separately in the form of ions based on their mass-to-charge (m/z) ratio (Figure 3.8).²⁹⁹⁻³⁰¹ The cGC-MS technique is perfect for analyzing, detecting, and quantifying hundreds of low molecular weight analytes. The analytes must have sufficiently high

partial pressures and thermal stability. That condition often requires chemical derivatization of analytes prior analysis, particularly regarding SOA-targeted analysis.^{203, 302-304}

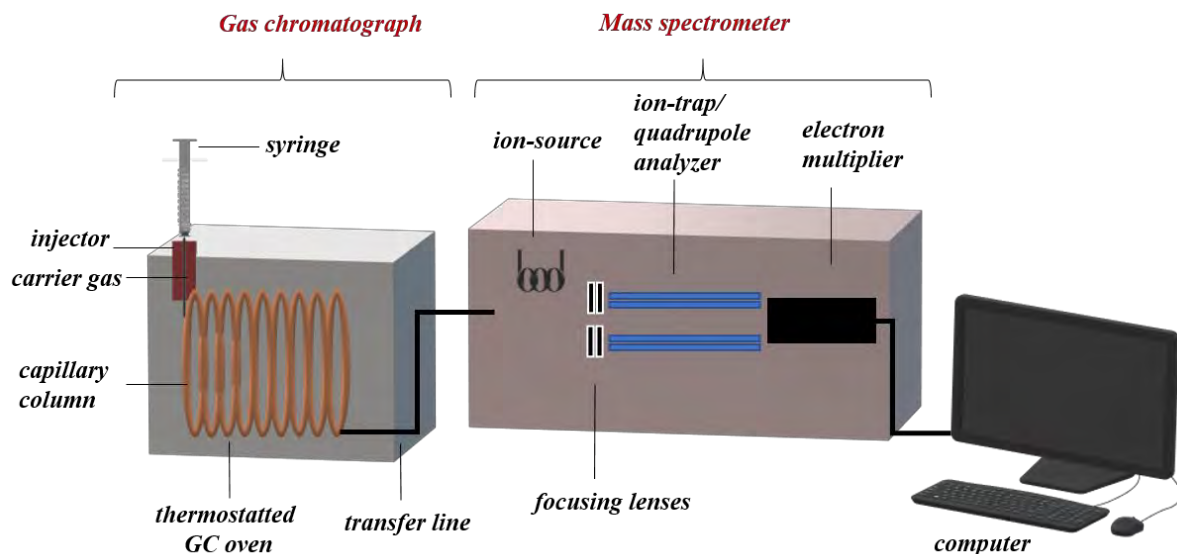


Figure 3.8. Schematic representation of the basic cGC-MS system.

The sample is extracted by a suitable organic solvent and injected into the GC inlet of the GC-MS setup. The inlet is heated to vaporize the sample and transfer it onto the capillary column by a carrier gas, usually He. Based on the interaction of the analyte's mixture with a carrier gas and a coating in the capillary column, the mixture components become separated and elute off the column at different retention times. The outflow of the column is connected *via* a heated transfer line to the ion source of the MS, where the compounds are ionized for detection.^{299, 305} Figure 3.9 shows the cGC-EI-MS used in my Ph.D.

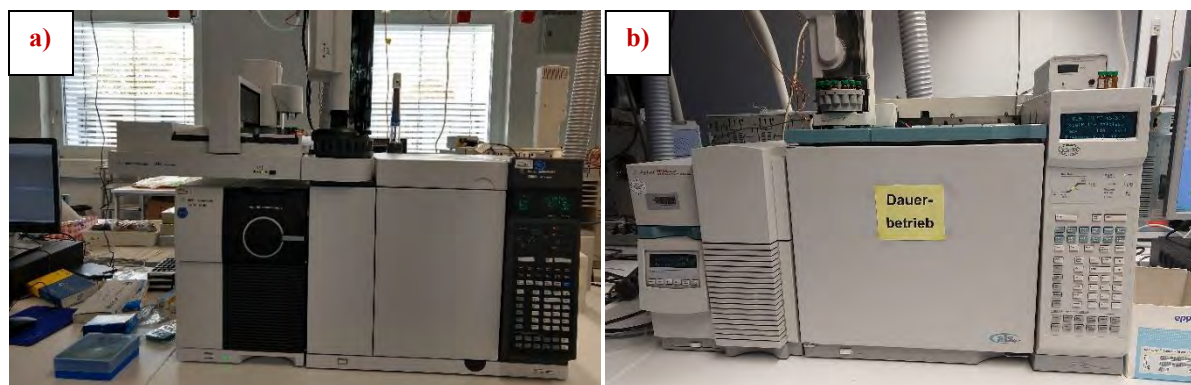


Figure 3.9. Two different Agilent Capillary Gas Chromatography-Electron Ionization Single Quadrupole Mass Spectrometers (cGC-EI/MS) used in my study.

The two most suitable methods for ion formation include electron ionization (EI) and chemical ionization (CI).^{306, 307} In the EI, a high-energy beam of electrons (up to 70 eV) knocks off one electron from the analyte molecule resulting in the formation of the molecular ion (M^+). The latter is identified in a resulting mass spectrum based on the molecular mass equal to that of the parent compound. Besides, a large amount of energy imparted during the ionization breaks the molecule into several charged species (fragments), which depend on the molecule structure, and are identified in the mass spectrum as its fingerprints. In contrast, the CI belongs to soft ionization techniques and produces far fewer fragments, thereby increasing the abundance of the molecular mass-reflecting ions. It uses a suitable reagent gas, such as methane (CH_4), which is first ionized to create primary ions, e.g., CH_5^+ , acting as proton donors to the analyte. These donors are sheer Brønstad acids, and thus can shift a proton to the analyte to afford $[M+H]^+$ adduct ions.³⁰⁸ These two ionization modes often complement each other for better structure elucidation.

The ions formed in the ion source are then transferred into the mass analyzer by an electric field, and are separated based on their m/z values. The most common analyzers used in cGC-MS are quadrupoles and ion traps. The separated ions are transferred to a detector, where their m/z values and abundance are recorded to form a mass spectrum.^{309, 310}

3.2.4.2. Liquid chromatography-mass spectrometry (LC-MS)

LC-MS is alternatively denoted as HPLC-MS or UHPLC-MS. In liquid chromatography (LC), a sample is directly injected onto the column, where it undergoes the separation based on different affinities of its components towards the mobile (solvent) and stationary phases.³¹¹⁻³¹³ In contrast

to GC, LC is perfectly designed and developed for thermally labile and polar analytes.³¹⁴ The LC column is usually made of stainless steel, packed with stationary-phase particles of a size ranging from 2 to 10 μm . In the early instruments, high pressures up to 500 psi were applied to force the samples through columns, so the name high-pressure LC (HPLC) was used.^{315, 316} When columns, which could withstand pressure up to 6000 psi were developed, the name changed to high-performance liquid chromatography but the HPLC acronym remained. In the early XXIst century, technological advancement brought columns made of even smaller particles ($< 1.3 \mu\text{m}$) and withstanding pressure higher than 15000 psi. They provide greater sensitivity and speed of analyses, creating the category of ultra-performance liquid chromatography (UPLC). The LC separation techniques divide into two categories based on the mobile and stationary phases' polarities. Initially, the developed chromatographic technique by Mikhail Tswett used a polar stationary phase column and a non-polar solvent as a mobile phase, hereafter regarded as *normal phase-LC* (NP-LC). The other system is *reversed phase-LC* (RP-LC) and utilizes a non-polar stationary phase and a polar mobile phase. The reversed-phase LC is the most widely used liquid chromatography due to its high reproducibility to many biomolecules and polar analytes of environmental origin. The most commonly used columns in the normal phase chromatography have silica beds, whereas in the case of the reversed-phase chromatography –silica ends up with octadecylsilyl or C-18 residues. The Hydrophilic-Interaction Liquid Chromatography (HILIC) is a normal phase chromatography with the polarity of the mobile non-polar organic phase slightly increased to facilitate the elution of polar molecules that hold firmly to the stationary phase. The Hydrophobic-Interaction Chromatography (HIC), is a reversed-phase chromatography with a moderately hydrophobic stationary phase, such as C-4 groups, used to separate large biomolecules.

The working principle and operation of the mass spectrometer hyphenated to LC remain the same as in the case of GC-MS. Due to the incompatibility of the existing ion sources with the liquid samples flowing out of the column, new ionization sources and transferlines were developed. The electrospray ionization (ESI) developed in the 1980s by Fenn and co-workers and matrix-assisted laser desorption ionization (MALDI) by Tanaka and co-workers were awarded the 2002 Noble Prize in Chemistry.³¹⁷⁻³¹⁹ The main types of ion sources (ESI, APCI, and APPI)³¹³ and analyzers interfaced to LC are briefly discussed below.

3.2.4.1.1. Ion sources

- 1. Electrospray Ionization (ESI).** In ESI, liquid samples are nebulized at the tip of the steel capillary maintained at 3 to 5 kV, and sprayed in the form of charged droplets. These droplets are desolvated with the heat under a dry N₂ curtain and shrink to form ionic plasma. Under such conditions, positive (or negative) charged ions form. These ions pass to a MS for further processing.³²⁰ Unlike the EI, electrospray is a soft ionization technique. Depending on the acidity and structure, the analyte pops up as singly charged ions, i.e., [M+H]⁺ or [M-H]⁻, respectively, depending on the ionization mode. The adduct formation may also occur in presence of salts giving rise to [M+Na]⁺, [M+K]⁺, [M+NH₄]⁺, [M+formate]⁻, or [M+acetate]⁻ ions.
- 2. Atmospheric Pressure Chemical Ionization (APCI).** In the APCI, first in the proximity of a capillary tip, a corona discharge turns solvent molecules into charged plasma, which later reacts with the analyte *via* the charge or electron transfer to form singly charged ions, mainly [M+H]⁺.³²¹⁻³²³ The APCI is more beneficial for more apolar analytes, which are resistant to the ESI ionization.
- 3. Atmospheric Pressure Photoionization (APPI).** The APCI is the youngest of all soft ionization techniques. It is handy for compounds, which are not susceptible to ESI and APCI ionization, e.g., polyaromatic hydrocarbons. Here, light energy turns the solvent into primary ionic plasma, which interacts with the analyte to form adduct ions.³²⁴⁻³²⁶

3.2.4.1.2. Mass analyzers

Despite tremendous efforts, no mass analyzer developed so far is perfect.³²⁷ A detailed overview of the issue is provided elsewhere.^{310, 328-330} The basic mass analyzers, and their principles of operation are summarized in Table 3.3. The following subsections discuss briefly the analyzers relevant to this Ph.D.

Table 3.3. Key mass analyzers used in the modern mass spectrometry.^{327, 328}

Mass analyzer	Acronyms	Principle of action
Time-of-flight	TOF	Ion velocity (flight time of ions)
Magnetic sector	B	Momentum
Quadrupole	Q	Trajectory stability
Ion-trap	IT	Resonance frequency
Fourier transform-ion cyclotron resonance	FT-ICR	Resonance frequency
Orbitrap	Orbitrap	Resonance frequency
Hybrid analyzers	e.g., Q-TOF	

1. **Time-of-flight (TOF) analyzer.** Developed in 1946 by Stephens,³³¹ and commercialized in the 1950s,³³²⁻³³⁴ the TOF analyzer disperses ions of different m/z , after their initial acceleration by a high voltage electrical field. The ions with the same kinetic energies are expelled in pulses. Therefore, the total time-of-flight of ions in the field-free region depends on their m/z , which helps to separate them and record the mass spectrum.^{318, 327, 328} TOF analyzers are more popular with LC-MS technique as they provide highly accurate mass data with high sensitivity, even for ions from small molecules.³³⁵
2. **Quadrupole analyzers.** The discovery of mass-analyzing properties of quadrupoles led Wolfgang Paul to Noble-Prize in the 1960s, and later to the development of quadrupole mass filters.³³⁶⁻³³⁸ They have advantages, such as high transmission, compactness, low voltages for ion acceleration, and fast scanning. Therefore, these instruments are popular in GC-MS technology and low resolution LC-MS.³²⁷ A quadrupole consists of four parallel hyperbolic-shaped metal rods. A pair of opposite rods are held at the same potential combining constant and varying voltages with time. Based on the stability of ion trajectories in the oscillating electric field, ions are transmitted and separated based on their m/z ratios.^{327, 328} In modern MS, Quadrupole filters are often combined into a series of three consecutive units, regarded as a triple-quadrupole mass analyzer. Providing that first (Q1) and third (Q3) quadrupoles scan masses of parent and fragment ions, respectively, and the middle one (Q2) acts as a collision cell to fragment the parent ions, such a technique will be advantageous to conduct thorough fragmentation studies. That technique is often called

a tandem MS and helps to quantify analytes in complex matrices, e.g., atmospheric aerosol.¹¹

3. **Orbitrap analyzers.** The Orbitrap mass analyzer is a relatively novel type of ion trap analyzer developed based on Kingdon trap³³⁹ by Makarov and co-workers and hereafter commercialized by Thermo company under the brand name Orbitrap™. It uses back and forth motion of ions along a central electrode using a static electric field. Orbitrap combines the quadrupole ion trap's quadrupole field with the cylindrical capacitor's logarithmic field.^{327, 328, 340-343} Figure 3.10 presents the Orbitrap analyzer, and Figure 3.11 the Orbitrap MS used in this thesis.

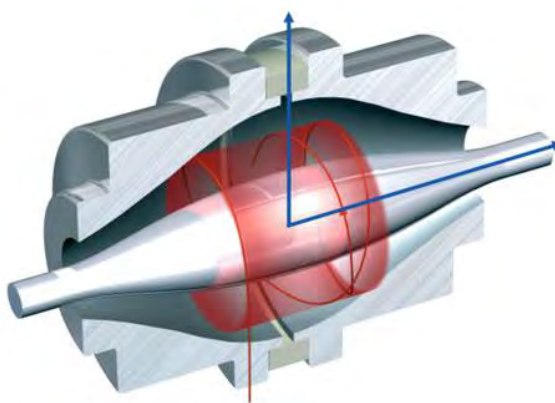


Figure 3.10 Thermo Fisher Orbitrap™ mass analyzer – a cutaway view with ions spiraling around a central spindle-shaped electrode. (taken from)^{327, 342}

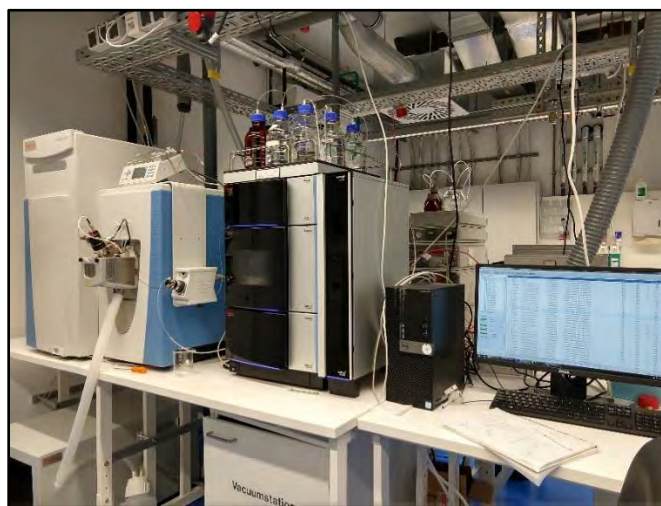


Figure 3.11. Thermo UHPLC⁺-Q-EXCATIVE High Resolution Orbitrap MS used during my laboratory work.

3.2.4.3. Mass spectrometry in atmospheric chemistry

Mass spectrometry is a more than a century-old technique since its invention by Thomson in 1910. Nevertheless, the innovations and applications in MS for extracting more information in science are still in progress and undergoing continuous evolution.^{11, 344} Atmospheric chemistry is one field that relies on a tremendous amount of analytical information from MS. Given the high complexity in the chemical composition of the atmospheric organic aerosol,²⁴ MS (*offline* and *online*), with its high sensitivity and molecular specificity, serves as one of the most reliable and crucial analytical tools to unravel the complex chemistry behind.³⁴⁵ Even with the low atmospheric concentrations of individual compounds (ranging from pg m^{-3} to ng m^{-3}), hyphenated MS, such as cGC-MS and rpLC-MS, can provide the accurate elemental composition with low detection limits, using high-resolution capacity. The tandem MS (i.e., MS/MS) also aids in solidifying structural information of the unknown analytes.³⁴⁵ The MS appeared as an ideal technique for the molecular characterization of atmospheric aerosol and the identification and quantification of intermediates and products arising from the tropospheric aqueous-phase oxidation of GLVs by atmospheric radicals, such as $\cdot\text{OH}$ within the present Ph.D. thesis. The cGC-MS and rpLC-MS are considered state-of-the-art analytical techniques. However, they bear significant limitations in the molecular characterization and quantification of atmospheric aerosol and their sources.³⁴⁵ To circumvent the problem, 2-D GC with TOF-MS and thermal desorption GC-MS (TAG) were also used.³⁴⁶⁻³⁵¹ The rpLC-MS is now often used to complement the findings from cGC-MS in atmospheric chemistry. Polar (e.g., organosulfates), non-volatile, thermally labile compounds and some other compounds are not amenable with cGC-MS even after derivatization. Therefore, they are characterized using rpLC-MS owing to its higher separation efficiency and sensitivity.^{345, 352-357} Other than rpLC-ESI/MS, desorption electrospray ionization (DESI), and nano-DESI have been also employed to improve the chemical characterization of atmospheric aerosol samples.³⁵⁸⁻³⁶¹

Based on the American Society for Mass Spectrometry (ASMS) standards, it was accepted that only accurate mass data corresponding to the single molecular formula are reliable in the structural elucidation of the unknown structure. High-resolution MS can provide the molecular formulas of compounds only up to $300 - 350 \text{ g mol}^{-1}$.²⁴ Therefore, for firm structural identification, additional complementary information is required from other techniques, such as tandem MS and NMR. In general, the problem is still a big challenge in atmospheric analytical chemistry.^{11, 362} Many recent reviews have compared analytical techniques, and their capabilities for the use in

atmospheric chemistry.^{11, 308, 363-366} Seldom, the complete identification of all organic compounds present in the aerosol samples is possible. The partial knowledge of the organic compounds present may resolve numerous problems and save time. Therefore, the separation techniques, such as chromatography along with high-resolution mass spectrometry (HRMS), is often employed as an alternative to the synthesis of authentic standards in atmospheric chemistry.¹¹

Figure 3.12 by Noziere et al.¹¹ summarizes the *I* factor for techniques used in atmospheric chemistry to identify and quantify organic aerosol samples. The *I* factor is the possible number of matching molecules with the requested information or measured by an analytical technique specified. The lower the *I* factor, the more efficient is the analytical approach in structure elucidation of the organic compounds. The coupling of two techniques often decreases the *I* factor, like the hyphenated mass spectrometry techniques used along with chromatography (highlighted in blue).

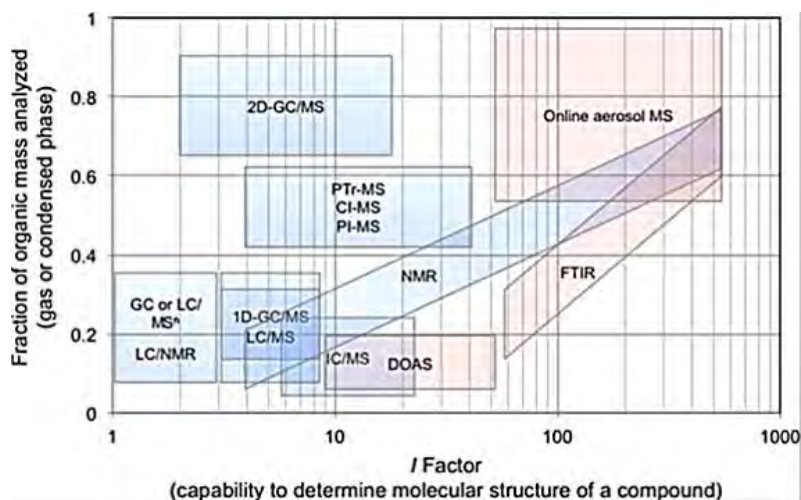


Figure 3.12. Comparison of analytical techniques used for the characterization of atmospheric aerosol samples as a function of *I* factor. (permission taken from Noziere et al.)¹¹

Hallquist et al.¹² classified the SOA quantification and chemical characterization techniques into three major categories: indirect methods, *offline* techniques, and *online* techniques. The indirect methods can only characterize the total SOA mass. *Offline* techniques use highly sophisticated instruments, such as cGC-MS and rpLC-MS, that can provide detailed information on the functional groups and chemical composition of aerosol sample. However, their main drawback is the extensive sampling time. *Online* techniques, such as aerosol mass spectrometry (AMS),

provide only specific information on bulk chemical composition, but the acquisition time corresponds to real-time monitoring mode. Figure 3.13 compares the efficiency of hitherto available techniques regarding the percent of a mass analyzed vs. the chemical and time/size resolution.

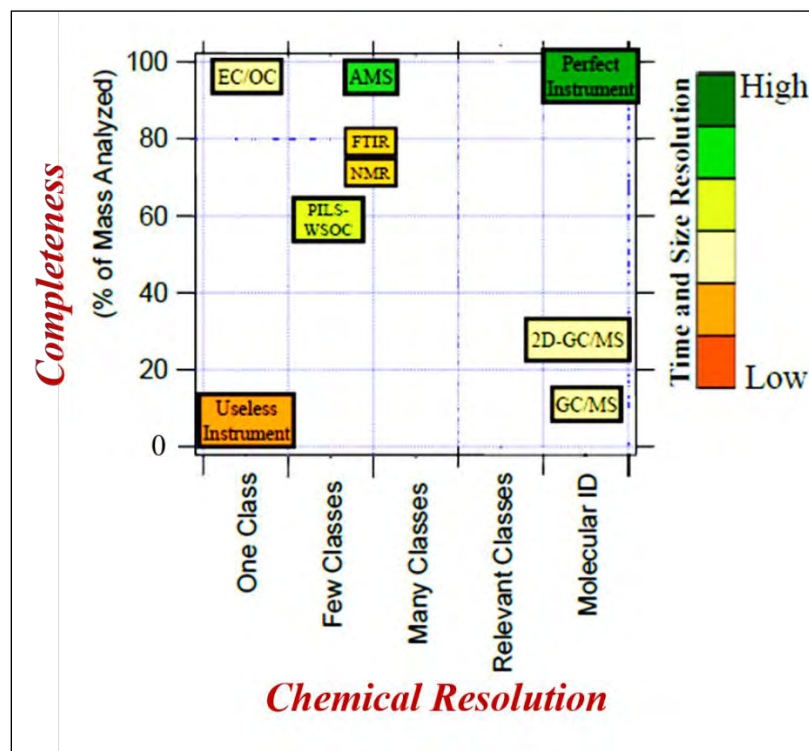


Figure 3.13. 3-D representation of the analytical efficiency of available techniques for organic aerosol analysis. (taken and adapted from Hallquist *et al.* distributed under the Creative Commons Attribution 3.0 License)¹²

3.3 Experimental methodology

3.3.1. Kinetic studies

The basics of the LFP-LLPA setup used to determine the second-order rate constant (k_{2nd}) is provided in Section 3.2.2. Here, only the LFP-LLPA configuration is discussed, required to observe the kinetics of GLVs (1-penten-3-ol, (*Z*)-2-hexen-1-ol, and (*E*)-2-hexen-1-ol) with all three individual radicals. All measurements were carried out at constant temperature (278 K – 318 K), and at pH= 7, as the GLVs (Chapter 5, Scheme 5.1) do not undergo ion speciation. The initial concentrations of the GLVs and radical precursors in the experiments are provided in Table 3.4.

The UV spectra recorded and molar absorption coefficients obtained and used within this study are presented in Chapter 4, respectively.

Table 3.4. Initial concentrations of reactants (mM) in the kinetic experiments with GLVs.

GLV	[GLV]	SO ₄ ^{•-}	•OH		NO ₃ [•]	
		Na ₂ S ₂ O ₈	H ₂ O ₂	KSCN	NaNO ₃	Na ₂ S ₂ O ₈
1-penten-3-ol	0.005 – 0.2	0.5	0.2	0.02	100	30
(Z)-2-hexen-1-ol	0.01 – 0.2	0.5	0.2	0.02	100	30
(E)-2-hexen-1-al	0.0025 – 0.2	5.0	10	0.20	100	30

The determination of rate constants of 1-penten-3-ol (PENTOL), and (Z)-2-hexen-1-ol (HEXOL) reactions with •OH and SO₄^{•-} radicals involved excimer laser of 248 nm to generate radicals *via* photolysis of radical precursors and violet-blue CW laser of 407 nm to follow the radical concentrations. The third GLV, i.e., (E)-2-hexen-1-al (HEXAL) has a strong absorption band at 248 nm ($\epsilon_{248 \text{ nm}} = 1722.1 \text{ L mol}^{-1} \text{ cm}^{-1}$, Chapter 4), and hence, it can easily undergo photolysis at this wavelength. Therefore, another 308 nm excimer laser ($\epsilon_{308 \text{ nm}}(\text{HEXAL}) = 51.8 \text{ L mol}^{-1} \text{ cm}^{-1}$, Chapter 4) and blue 473 nm CW laser were used to determine the rate constants for HEXAL reactions with •OH and SO₄^{•-} radicals. A blue 473 nm CW laser secured sufficient light absorption as the radical concentration obtained with the 308 nm laser was lower than with the 248 nm excimer laser. A typical absorbance vs. time trace obtained in the LFP-LLPA experiments is provided in Figure 3.14. The NO₃[•] radical kinetics was analyzed using a 351 nm excimer laser and red 635 nm CW laser for all GLVs. The setup details and configuration are provided in Table 3.5.

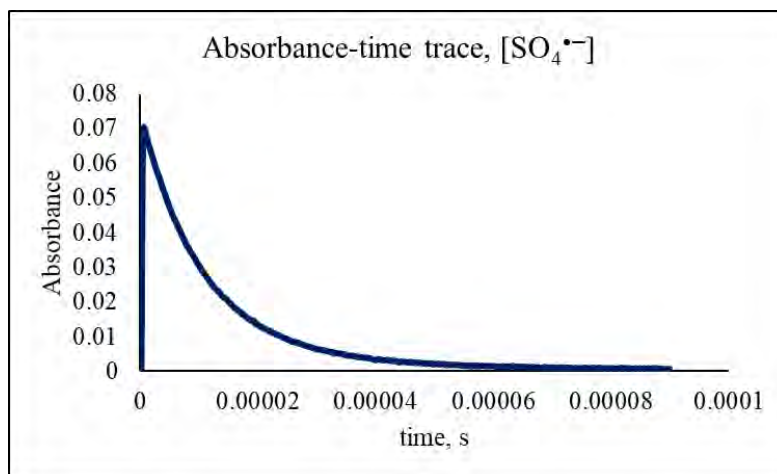


Figure 3.14. Typical absorbance–time trace observed in LFP-LLPA experiments shows the formation and decay of sulfate radicals in the irradiated aqueous solution of $\text{Na}_2\text{S}_2\text{O}_8$ (0.5 mM) and 1-penten-3-ol (0.1 mM) at 298.

Table 3.5. Used LFP-LLPA setup configuration for different radical generation and measurement.

Radical	GLV	Radical precursor	Excimer laser	Continuous-wave laser	Total path length
			λ , nm	λ , nm	
$\text{SO}_4^{\bullet-}$	1-penten-3-ol	$\text{Na}_2\text{S}_2\text{O}_8$	248	407	32
	(Z)-2-hexen-1-ol		248	407	
	(E)-2-hexen-1-al		308	473	
OH^{\bullet}	1-penten-3-ol	H_2O_2	248	407	32
	(Z)-2-hexen-1-ol		248	407	
	(E)-2-hexen-1-al		308	473	
NO_3^{\bullet}	1-penten-3-ol	NaNO_3	351	635	128
	(Z)-2-hexen-1-ol				
	(E)-2-hexen-1-al				

3.3.1.1. $\text{SO}_4^{\bullet-}$ kinetics

The reactions between GLVs and $\text{SO}_4^{\bullet-}$ radical-anions were initiated by photo-dissociating $\text{S}_2\text{O}_8^{2-}$ ions into $\text{SO}_4^{\bullet-}$ radicals in aqueous solutions containing $\text{Na}_2\text{S}_2\text{O}_8$ and GLV. Eight separate irradiations were recorded and averaged to produce one intensity vs. time plot (Figure 5.1). The intensity was then converted to the $\text{SO}_4^{\bullet-}$ concentration, using the molar extinction coefficients ($\epsilon_{407\text{ nm}} = 1260\text{ L mol}^{-1}\text{ cm}^{-1}$ and $\epsilon_{473\text{ nm}} = 1389\text{ L mol}^{-1}\text{ cm}^{-1}$).³⁶⁷ Each concentration vs. time plot had a linear fragment that was used to determine a pseudo-first-order rate constant (k_{1st}) for the reaction. The pseudo-first-order rate constants were obtained for various initial GLV concentrations. The reaction second-order rate constant (k_{2nd}) was determined by plotting the pseudo-first-order rate constants against the GLV initial concentrations.^{296, 297}

3.3.1.2. $\bullet\text{OH}$ kinetics

Direct following of the $\bullet\text{OH}$ radicals concentration is difficult due to the weak light absorption and overlapping spectra of $\bullet\text{OH}$ with other organics and peroxy radicals present in the solution.³⁶⁷⁻³⁶⁹ Therefore, the method of competition kinetics³⁷⁰ was used to analyze the $\bullet\text{OH}$ radical reaction kinetics, where photolysis of H_2O_2 at 248 nm or 308 nm (Table 3.5) produced $\bullet\text{OH}$ radicals and KSCN acted as a reference compound. Reactions (R3.3 – R3.7) explain the chemistry involved that includes the formation of strongly-absorbing dithiocyanate radical-anion ($(\text{SCN})_2^{\bullet-}$) at 400 – 550 nm.³⁶⁷ The reaction (R3.7) is the sink for $(\text{SCN})_2^{\bullet-}$ radical anion:



The absorbance of the radical anion in the solution was measured using a CW laser at 407 nm and 473 nm (Table 3.5). The k_{2nd} of the reaction ($\text{GLV} + \bullet\text{OH}$) was calculated using equations (3.4) and (3.5) from Schaefer and Herrmann²⁹⁵ and Zhu et al.³⁷¹, respectively.

$$\frac{A_{[(SCN)_2^-]_0}}{A_{[(SCN)_2^-]_X}} = \frac{k_{2nd}[GLV]}{k_{ref}[SCN^-]} + 1 \quad (3.4)$$

$$k_{ref}(T) = e^{(28.87) - 1690/T} L mol^{-1} s^{-1} \quad (3.5)$$

where: $A_{[(SCN)_2^-]_0}$ is the absorbance of $(SCN)_2^{\bullet-}$ in the absence of GLV, $A_{[(SCN)_2^-]_X}$ is the absorbance of $(SCN)_2^{\bullet-}$ in the presence of GLV at the concentration X in the reaction solution, k_{ref} is the rate constant for reaction (R3.2). PENTOL, HEXOL, and HEXAL absorb UV light at both excimer laser wavelengths (248 nm and 308 nm, Table 5.3). Thus, they act as an internal filters and reduce the initial concentration of $\bullet OH$ determined in the experiments. Therefore, the internal-filter correction was introduced for $A_{[(SCN)_2^-]_0}$ in equation (3.4) for each GLV and at all temperatures using the procedure described by Schaefer and Herrmann.²⁹⁵ The correction factor for the initial $\bullet OH$ concentrations was $< 0.05\%$ for PENTOL, $0.2 - 0.9\%$ for HEXOL, and $1 - 3\%$ for HEXAL (Table 3.6).

Table 3.6. Change in the initial $\bullet OH$ concentrations due to a GLV as an internal filter of the UV light.

Experiment	[GLV]	[OH] ₀ change, %		
	$10^{-4} L mol^{-1}$	1-penten-3-ol at 248 nm	(Z)-2-hexen-1-ol at 248 nm	(E)-2-hexen-1-al at 308 nm
I	0.5	0.01	0.23	0.87
II	1.0	0.02	0.45	1.74
III	1.5	0.03	0.68	2.59
IV	2.0	0.03	0.90	3.44

3.3.1.3. NO_3^{\bullet} kinetics

The reaction between GLV and NO_3^{\bullet} radicals was initiated with photolysis of an aqueous solution ($NaNO_3$, $Na_2S_2O_8$, and a GLV) to produce NO_3^{\bullet} radicals *via* reactions (R3.8) and (R3.9)^{290, 296, 372} in the measurement cell, using 351 nm excimer laser. A red diode CW laser (635 nm) measured the light absorbance by NO_3^{\bullet} , then converted to the concentrations using the molar extinction coefficient ($\epsilon_{635\text{ nm}} = 1120 M^{-1} cm^{-1}$)³⁷³. The processing of intensity-time traces was done using the same method as described for $SO_4^{\bullet-}$ kinetics to obtain the k_{2nd} (GLV + NO_3^{\bullet}).



The experimental uncertainty of k_{2nd} , was calculated as standard deviation multiplied by the Student's t-factor taken at the 95% confidence level. Each k_{2nd} resulted from at least 40 traces for each GLV concentration, with eight replicates yielding a single trace. At least five different GLV concentrations were considered.

3.3.1.4. Diffusion limitations of rate constants

When the k_{2nd} for the observed radical reactions is of the order $10^9 \text{ L mol}^{-1} \text{ s}^{-1}$ or higher, the reaction kinetics can be partially controlled by diffusion of the reactants in solution. Therefore, the rate constants from LFP-LLPA experiments (k_{obs}) were corrected for diffusional limitations to the true rate constants (k_{reac}) using a simple resistance-in-series approach³⁷⁴ (equation 3.6) with the diffusion rate constant calculated using the Smoluchowski equation (3.7)³⁷⁵:

$$k_{obs}^{-1} = k_{reac}^{-1} + k_{diff}^{-1} \quad (3.6)$$

$$k_{diff} = 4 \times 10^3 \pi N_A (D_A + D_B) (r_A + r_B) \quad (3.7)$$

where: all k are the second-order rate constants ($\text{L mol}^{-1} \text{ s}^{-1}$), D_A and D_B ($\text{m}^2 \text{ s}^{-1}$) are the diffusion coefficients of reactants A and B ($\text{m}^2 \text{ s}^{-1}$), r_A and r_B (m) are reaction radii of the reactants A and B (m), and N_A is the Avogadro number.

The Stoke-Einstein relationship modified by Wilke and Chang³⁷⁶ was used to calculate the diffusion coefficients (equation 3.8):

$$D = 7.4 \times 10^{-12} \frac{(XM)^{0.5} T}{V_m^{0.6} \eta} \quad (3.8)$$

where: X is the solvent association parameter (2.26 for water), M is the molar mass of a diffusing compound, $\text{cm}^3 \text{ mol}^{-1}$, T is the absolute temperature in K, V_m is the molar volume of a diffusing compound⁷, η is the dynamic viscosity of the solvent, mPa or $0.01 \text{ g cm}^{-1} \text{ s}^{-1}$ (0.8891 mPa for water at 298 K). Molar volumes for reactants are given in Table 3.7.

The reaction radii of the reacting compounds were calculated using the procedure of Kojima and Bard 1975 (equation 3.9):³⁷⁷

$$r = \sqrt[3]{\frac{3 \times V_m}{4 \times \pi \times N_A}} \quad (3.9)$$

The radical radii were adopted from Buxton et al., 1988 ($\cdot\text{OH}$),^{9, 378} and Nightingale et al., 1959 ($\text{SO}_4^{\cdot-}$ and NO_3^{\cdot}).³⁷⁹ The radical molar volumes were adopted from Schöne et al. 2014,²⁹⁷ whereas the molar volumes of the organic compounds were calculated using Tyn and Claus method (1975) given in equation (3.10)³⁸⁰ and critical volume described by Joback and Reid, 1987 (equation 3.11)³⁸¹ at the boiling point. The final molar volume at measurement temperatures were obtained using the ideal gas approach ($V_m/T = \text{constant}$).

$$V_m = 0.285 \times V_C^{1.048} \quad (3.10)$$

$$V_C = 17.5 + \sum \Delta V \quad (3.11)$$

Table 3.7. Properties of reacting molecules.

Molecule	V_m cm ³ mol ⁻¹	r nm	D (at 298 K) 10 ⁻⁹ m ² s ⁻¹
$\text{SO}_4^{\cdot-}$	61.5 ^a	0.29 ^a	1.30
$\cdot\text{OH}$	26.9 ^a	0.22 ^a	2.20
NO_3^{\cdot}	46.4 ^a	0.264 ^a	1.54
1-penten-3-ol	89.4 ^b	0.329	1.06
(Z)-2-hexen-1-ol	95.2 ^b	0.335	1.03
(E)-2-hexen-1-al	99.2 ^b	0.340	1.00

^a Schöne et al.²⁹⁷; ^b Estimated using Joback method.³⁸¹

3.3.2. Product study experiments and analytical protocols

This section concerns the experimental methods used to produce the results in Chapter 7. The chemicals used are listed in Section 3.1, while in Section 3.2.3 the basic details of the experimental setup (Figure 3.7) and characterization techniques are provided. This section provides the specific details of the method used during the mechanistic investigation.

3.3.2.1. Mechanistic investigation

For investigating the photooxidation products of the reaction between GLVs and $\cdot\text{OH}$ radicals, an aqueous solution of total volume 300 mL containing a GLV (1×10^{-4} M) and H_2O_2 (5×10^{-3} M) was irradiated using a UV lamp in the reactor (Figure 3.7) for 6 hours. Solution aliquots were taken out from the reactor into two separate vials every 15 min for the first 3 h, and every 30 min for the next 3 h, for GC-MS and LC-MS analyses. Table 3.8 describes the details of the experiments. The sample preparation, analyses, and methods are similar to that used by Otto et al.^{290, 382} The carbonyl targeted GC-MS analysis to identify and quantify carbonyl based oxidation products, and HEXAL substrate decay utilized the method developed by Rodigast et al. 2015³⁸³ (Section 3.3.2.3). Another GC-MS method was developed and used to follow the decay of the other two GLVs (PENTOL, and HEXOL) and screen for other possible alcohol products (Section 3.3.2.4). Besides, the LC-MS analysis was used to quantify GLVs (HEXOL and HEXAL), screen for other possible unsaturated carbonyls, alcohols, and carboxylic acid, and to compare the results with the GC-MS results (Section 3.3.2.2).

Table 3.8. Set-up configuration and reactant concentration details for the GLV-OH photooxidation experiments carried out at 298 K.

S. No.	GLV	Type of experiment	UV light	[GLV], M	[H_2O_2], M	*Repetition sets, <i>n</i>
1		Dark oxidation H_2O_2	No	1×10^{-4}	5×10^{-3}	1
2	PENTOL	Photolysis	Yes	1×10^{-4}	-	1
3		Oxidation $\cdot\text{OH}$	Yes	1×10^{-4}	5×10^{-3}	2
4		Dark oxidation H_2O_2	No	1×10^{-4}	5×10^{-3}	1
5	HEXOL	Photolysis	Yes	1×10^{-4}	-	1
6		Oxidation $\cdot\text{OH}$	Yes	1×10^{-4}	5×10^{-3}	2
7		Dark oxidation H_2O_2	No	1×10^{-4}	5×10^{-3}	1
8	HEXAL	Photolysis	Yes	1×10^{-4}	-	1
9		Oxidation $\cdot\text{OH}$	Yes	1×10^{-4}	5×10^{-3}	2

*Total duration of one experiment set was always 6 hours.

3.3.2.2. UPLC analyses

To quantify HEXOL, and HEXAL and identify other possible oxidation and accretion products, such as carboxylic acids in the reaction samples, an ultra-high performance liquid chromatography system (UHPLC+) coupled to a Q-Exactive PL4US Hybrid Quadrupole-Orbitrap mass spectrometer (UHPLC-UV/PDA-HESI/MS) was used (Figure 3.11). To the 500 μL aliquot taken from the reactor in an LC vial, firstly 25 μL of catalase solution ($\gamma = 5 \text{ mg mL}^{-1}$) was added to avoid dark oxidation by excess H_2O_2 in the sample, followed by the addition of 500 μL acetonitrile (ACN). All these pre-processed samples were stored in LC vials at -25°C until further LC-MS analysis. The calibration standards in the range of 1×10^{-6} to $1 \times 10^{-4} \text{ mol L}^{-1}$ were prepared using the same protocol as described above to quantify HEXOL and HEXAL. The UHPLC+ instrument was equipped with a Vanquish HSS T3 column (1.8 μm , $100 \times 2.1 \text{ mm}$) and was operated with eluent A (0.1 % formic acid in water) and eluent B (0.1 % formic acid in acetonitrile) with a total flow of $300 \mu\text{l min}^{-1}$ at 40°C . 10 μL of the sample were injected, and the elution program was: 1 min 95% eluent A/5% eluent B followed by a linear gradient down to 2 % eluent A/98% eluent B within 18 min followed by flushing to the starting conditions in 3 min at the end. The heated electrospray ionization source (HESI) operated with the following parameters: 2.5 kV spray voltage, sheath gas flow of 50, the auxiliary gas flow of 10, 280°C capillary temperature, and 250°C probe heater temperature. The samples were analyzed in both positive and negative ionization modes. Total ion chromatograms were recorded in the range of m/z 50 – 750 with the resolution of 140,000 at m/z 200. The mass axis calibration was performed using $2 \times 10^{-3} \text{ mol L}^{-1}$ sodium acetate solution. The UV absorbance recorded with PDA detector and MS ion chromatograms were used to quantify GLVs and identify the possible aqueous oxidation products.

3.3.2.3. Carbonyl-targeted cGC-MS analyses

Carbonyl-targeted cGC-MS analysis of reaction samples is based on the method developed by Rodigast et al. 2015.³⁸³ An Agilent 7890 series GC system (G3440 B, Serial # CN17403021) coupled with Agilent 5977B MSD (G7079B, Serial # US1739D006), an Electron Ionisation Quadrupole Mass Spectrometer (EI-MS) (G7079B, Serial # US1739D006) and Agilent Technologies 7693 Autosampler, Made in USA was used (Figure 3.9.a). For separation, HP-5MS

UI Column (Agilent J&W GC columns 19091S-433, 30 m × 0.25 mm × 0.25 μm), was used with a GC inlet in splitless mode at 250 °C. The GC separation was performed with gas flow of 1.2 mL min⁻¹, and inlet temperature program: 70 °C isothermal for 0.41 min, first increased to 325 °C and held for 0 min, followed by achieving 350 °C, where it was held constant for 10 min. The column temperature gradient used was as follows: 50 °C isothermal for first 2 min, followed by the rise at 10 °C min⁻¹ up to 210 °C, where it was held constant for 7 min. At the end, the temperature was held constant for 10 min at 320 °C.

Samples taken from a reactor at specified intervals were stored in 2 ml vials. (ref. Section 3.3.2.1). To each sample in vial, 100 μL of catalase solution ($\gamma = 5 \text{ mg mL}^{-1}$) was added to avoid dark oxidation by excess H₂O₂, followed by the addition of 100 μL of the internal standard 2,2,6,6-cyclohexaone-d₄ ($1.01 \times 10^{-4} \text{ M}$). After taking the last sample at 6th hour of reaction time, 200 μL of the derivatizing agent O-(2,3,4,5,6-pentafluorobenzyl) hydroxylamine hydrochloride (PFBHA, $\gamma = 5 \text{ mg mL}^{-1}$) was added to each sample for derivatization over 18 hours at 20 °C. For quantification, the calibration standards were prepared following the same protocol using (*E*)-2-hexen-1-al, propionaldehyde (propanal), butyraldehyde (butanal), and 1-penten-3-one. The derivatized samples were adjusted to pH = 1.0 ± 0.1 by adding 60 μL hydrochloric acid (37 wt %). The oxime derivatives formed in the samples were extracted by adding 200 μL of 2,2,4-trimethylpentane or isooctane, and shaking with an orbital shaker for 30 min. A 1 μL portion of the isooctane layer containing the derivatized carbonyls was injected and analyzed with a gas chromatography system (Agilent 7890 B) with a multimode inlet coupled to an electron impact mass spectrometer (Agilent 5977B), cGC-MS.

3.3.2.4. Alcohol-targeted cGC-MS analyses

Alcohol-targeted cGC-MS analyses were carried using samples stored in LC vials (Section 3.3.2.2). Unreacted PENTOL and HEXOL substrates in the reaction samples were quantified and screened for any alcohols formed in the reaction. A 500 μL part of each 1 mL sample was moved to an empty vial, 150 μL of dichloromethane (DCM) was added, and the mixture was shaken for 30 min on the orbital shaker. The organic compounds containing alcohol functional groups were extracted with dichloromethane (DCM), using a method developed within the study. The calibration standards for PENTOL and HEXOL were prepared using the same protocol in the concentration range of 1×10^{-4} to $1 \times 10^{-6} \text{ M}$, and the calibration curves were prepared. Due to the

absence of any internal standards, for consistency and reliable results, calibration curve was obtained at the end of each sample run of 0 – 6 h (19 samples each run, Table 7.1, $n=8$). An Agilent 6890 A series GC system (G1530 A) coupled with Agilent 5973 N MSD, an Electron Ionisation Quadrupole Mass Spectrometer, and Agilent Technologies 7683 Autosampler, made in USA was used (Figure 3.9.b). GC separation was carried out using Phenomenex ZB-WAXplus (30 m \times 0.25 mm \times 0.25 μ m) column, and the inlet was operated at 140 °C in the splitless mode. The column temperature gradient was: 40 °C isothermal for 4 minutes and then elevated to 200 °C at 10 °C min^{-1} , where it was held constant for 5 min and ended. The 1 μ L of the organic layer was injected directly to analyze the DCM extracted GLVs compounds on a GC-MS system. The separation was performed on a Phenomenex ZB-WAXplus: flow 1.2 ml min^{-1} , inlet temperature program: 140 °C isothermal, temperature program: 40 °C for 4 min, increased to 200 °C with 10 °C min^{-1} , followed by a 5 min post-run at 230 °C.

3.4 Theoretical and simulation methods

3.4.1. COPASI

Simulation of reaction kinetics and estimation of rate constant based on chemical kinetic models was performed using COPASI software. COPASI (COMplex PATHway SIMulator) is a biochemical modeling and simulation software developed *via* an international collaboration between the Hoops Group at Biocomplexity Institute of Virginia Tech, Computational biology groups at the University of Heidelberg, and Mendes group at the University of Connecticut, UConn Health.³⁸⁴ It is freely available on the Internet (<http://copasi.org/>). It offers both the stochastic simulation algorithms and ordinary differential equation (ODE) solvers. It is easy to use and has a steep learning curve. The usage protocols are provided elsewhere³⁸⁵⁻³⁸⁷. The basic principle and difference behind those two approaches provided by Mendes *et al.* are briefly discussed here.³⁸⁵ The biochemical network is a set of chemical reactions that convert chemical species into each other and change their concentrations with time. Such simulations require prior knowledge of the reaction rates. The ordinary differential equation (ODE) models are considered the most popular means to describe the change in the concentrations of reactants and products. They are used for systems with large number of chemical species involved.

ODE represents the algebraic sum of the rate of reactions affecting the chemical species X, defined by equation 3.12.

$$\frac{dX}{dt} = \sum_{\text{all reactions}} s_i v_i \quad (3.12)$$

where, s_i is defined as a stoichiometry coefficient representing a number of molecules of X consumed (-)/produced (+), and v_i is the velocity defined by rate law of a reaction cycle i . These ODE-based models in COPASI were used in my Ph.D. work to simulate the dynamics of the chemical species concentration with time using their initial concentration values.

The underlying principle of continuous concentrations behind the ODE models fails when the reaction system is governed by complicated rate laws or is diffusionally constrained. Under such conditions, the stochastic approach is recommended. Stochastic models are based on probability density functions (PDF) that describe a system in terms of individual molecules and reaction probability for each molecule. Thus, stochastic simulations are computationally intensive and time-consuming, and used for smaller systems. Gillespie developed the basics of stochastic simulation of chemical reaction systems.^{388, 389} Single simulation runs provide a single probabilistic function, and thus the information provided is constrained.³⁸⁸⁻³⁹⁰

3.4.1.1. Reaction kinetics modeling

Within this work, the reaction rate constants were estimated using COPASI³⁸⁴ evolutionary programming method (number of generations 200, population size 20), while reaction time course simulations were performed using the deterministic ordinary differential equation solver (LSODA).^{384, 391, 392} The chemical-kinetic model applied and simulation results are discussed in Chapter 6.

3.4.2. Density functional theory calculations

The computational investigation with the density functional theory (DFT) was performed using an ORCA 5.0 programs.³⁹³ The calculations utilized hybrid B3LYP functional³⁹⁴⁻³⁹⁷ augmented with the Grimme's dispersion correction (D3BJ).^{398, 399} In all cases, def2-TZVP basis set⁴⁰⁰ was employed. The Coulomb and exchange integrals were efficiently evaluated with resolution-of-identity (RI)^{401, 402}, and chain-of-spheres (COSX)⁴⁰³ approximations, respectively. Matching the Weigend's RI auxiliary basis set⁴⁰⁴ was used throughout my study. All geometric

parameters of the investigated reactants, reaction complexes, transition states, and products were optimized in the vacuum using default thresholds. The character of stationary points was characterized with analytical second-derivative calculations, and all energy minima possessed only positive frequencies. In contrast, the presence of one negative frequency confirmed the transition state (TSs). The latter was always inspected visually to check whether the displacement vector corresponds to the expected movement of atoms in the TS that connects previously localized minimum energy structures. The potential energy scans (PES) were carried out to confirm the most stable conformers in case of addition adducts.

The single-point calculations that included implicit solvation were further performed on the vacuum-optimized structures. The presence of water medium was simulated using the conductor-like polarizable continuum model (CPCM), continuum solvation model and the dielectric constant of 80.4 value.⁴⁰⁵ Within CPCM continuum solvation model the adapted simple approach was simple, where only the single point energies were calculated using the optimized vacuum structures and the relative energies were obtained adding the ZPE correction from the vacuum, because the frequencies calculated in the presence of CPCM model may be questionable.⁴⁰⁶ More physically-sound solution would be to do calculations with micro-solvated model, but this would require proper sampling of the conformation space increasing computational time significantly and therefore is beyond the scope of the present thesis work.

In case of hydrogen-abstraction mechanisms, both in vacuum and in continuum solvation model CPCM, out of all various reaction complex, RC isomers (between substrate and OH radical) examined, the lowest energy state was selected (See appendix for other possible RC and their ΔE value). Activation energy barrier indicated in Scheme 7.5, 7.7, and 7.9 was always calculated using the lowest energy RC state (Activation energy, $dE^\ddagger = dE(\text{TS}) - dE(\text{RC})$).

The bond dissociation energy (BDE) calculations were performed using ORCA version 4.2.1 suite of programs³⁹³ to predict the most favorable site of hydrogen abstraction in the organic compound by $\cdot\text{OH}$ radical. The BDEs were calculated using the equation 3.13 given below, and previously described by He et al. and Otto et al.^{382, 407}

$$\Delta E_{bde}(R-H) = [E(R) + ZPE(R) + E(H)] - [E(\text{GLV}) + ZPE(\text{GLV})] \quad (3.13)$$

where GLV, R, and H denote the GLV compounds, GLV alkyl radicals, and the hydrogen radical, respectively; E and ZPE stand for the electronic energies and zero-point energies, respectively, of the GLV, R, or H.

Chapter 4. *Physical properties of green leaf volatiles (GLVs)*



Part of the data obtained and included in this chapter has been published as a research article in *ACS Environ. Sci. Technol.* 2021, 55, 20, 13666–13676, and a review article in *MDPI Atmosphere* 2021, 12(12), 1655.

Synopsis

The present chapter summarizes the GLVs physical properties obtained experimentally or calculated using correlations to aid the aqueous-phase kinetic and product studies described in Chapters 5 – 7. Aqueous solubility, vapor pressure, Henry's constant, and octanol-water/air partition coefficients of GLV compounds listed in Table 2.1 of Chapter 2 were estimated using EPI suite 2012 by EPA and compared to the available literature data (Section 4.1). UV spectra for a few GLV compounds were determined experimentally and compared to existing literature data (Section 4.2).

4. Physical properties of GLVs

An extensive set of physico-chemical properties data for GLV still needs to be determined experimentally to model better their multiphase processes and completely understand GLVs' atmospheric chemistry. Although reasonable values can be obtained using the available estimation methods, such as the EPI suite, none provides the temperature or pH-dependent data. Experimental measurements of the physical properties are indispensable to verify the estimated values.

4.1. EPI-estimated partition coefficients, aqueous solubility and vapor pressure of GLVs

Henry's constant, H is an equilibrium-partitioning coefficient that links the amount of a gas dissolved in the aqueous phase at a given partial pressure in the gas phase. It quantifies air-water partitioning of the trace species present in the atmosphere when describing systems like cloud droplets or aerosol particles.^{408, 409} The **octanol/water partition coefficient** K_{OW} and **octanol/air partition coefficient** K_{OA} represent equilibria in two-phase three-component systems, solute-water-octanol, and solute-air-octanol, respectively. K_{OW} shows the ratio of the solute concentrations in octanol-rich and water-rich phases and K_{OA} in octanol and air.^{410, 411} K_{OW} shows the balance between the lipophilicity and hydrophilicity of a solute, and K_{OA} estimates the partitioning of a solute between the air and environmental matrices such as soil, vegetation, and aerosol particles.

Along with the experimental values available in the literature, Table 4.1 contains the values of H, K_{OW} , and K_{OA} estimated with the EPI suite within this work. The EPI suite 2012 freely available from the US EPA⁴¹² uses HENRYWIN v3.20 package to estimate Henry's constants

by three different methods, i.e., the bond method, the group method,⁴¹³ and the VaporPressure/WaterSolubility method. The values in Table 4.1 are the means from these methods, with standard deviations as uncertainties. The Log KOW ver. 1.68 (Octanol-Water) and Log KOAWIN ver. 1.1 (Octanol-Air) packages within EPI suite were used to estimate K_{OW} and K_{OA} collected in Table 4.1. Other estimation methods are described elsewhere.^{408, 409, 414}

The aqueous solubilities and equilibrium vapor pressures of GLVs are presented in Table 4.2. The values obtained using MPBPVP and WSKOW packages of the EPI suite⁴¹² are compared to the experimental values from the literature.

In Table 4.1, the experimental Henry's constant assigned to the compilation by Sander and co-workers were presented as the mean values of the values reported by various authors: for pentanol,⁴¹³⁻⁴²¹ for hexanal,⁴²¹⁻⁴²⁵ and for nonanal.⁴²¹⁻⁴²⁴ One value for nonanal seemed to be the outlier and was rejected.⁴²³ 1-penten-3-one (ethyl vinyl ketone), and (*Z*)-2-pentenyl acetate have no experimental H constants, but the EPI-estimates at 298 K are close to the mean H constants of methyl vinyl ketone⁴⁰⁸ ($30.4 \pm 10.1 \text{ M atm}^{-1}$), and amyl acetate or isoamyl acetate⁴⁰⁸ (2.7 ± 0.4 or $2.3 \pm 0.4 \text{ M atm}^{-1}$) that are their respective structural homologues.

More details can be found in my review paper (Sarang et al. 2021),¹⁷² which discusses more experimental data, including the temperature dependency. The experimental determination of the missing GLVs physical properties is highly recommended and beneficial for the scientific community.

Table 4.1. Experimental and EPI-estimated Henry's constants, 1-octanol/water partition coefficients (K_{OW}) and 1-octanol/air partition coefficients (K_{OA}) for GLV in water and aqueous solutions.¹⁷²

GLV	Henry's constant				Octanol/water partition coefficient		Octanol/air partition coefficient	
	H M atm ⁻¹	T K	I M	Ref.	Log (K_{OW})	Ref.	Log (K_{OA})	Ref.
pentanol	87.7 ± 8.9	298	0	408 c	1.5	410	4.7	426
	84.4 ± 7.0	298		427 a	1.34	428	f 4.8	412 i*
	46.1 ± 2.1	306						
	11.9 ± 0.3	323						
	3.8 ± 0.1	343						
	71.9 ± 3.6	298		412 g*	1.3	412 h*	4.6	412 i*
1-penten-3-ol	72.5 ± 40.6	298		412 g*	0.84	429	4.5	412 i*
					0.81	428		
					1.1	412 h*		
(Z/E)-2-pentenol	119.8 ± 34	298	0	412 g*	1.1	412 h*	4.4	412 i*
(E)-2-pentenal	17.3 ± 12.3	298		412 g*	1.1	412 h*	3.6	412 i*
1-penten-3-one	28.5 ± 23.2	298		412 g*	0.9	412 h*	3.8	412 i*
(Z)-2-pentenyl acetate	2.8 ± 0.8	298		412 g*	2.1	412 h*	3.8	412 i*
n-hexanol	61.8 ± 16.3	298	0	408 c	1.84	428	5.2	426
	59.6 ± 2.8	298		427 a	2.03	410	5.0	412 i*
	32.7 ± 1.1	306						
	8.0 ± 0.3	323						
	2.53 ± 0.01	343						
	55.5 ± 3.5	298		412 g*	1.8	412 h*		
n-hexanal	3.2 ± 0.4	295	0	430	1.78	410	4.4	426
	5 ± 1	298		431	1.8	412 h*	f 3.8, 3.9	412 i*
	5.2 ± 0.5		freshwater	425				
	4.4 ± 0.4		25 % seawater					

	3.4 ± 0.3		50 % seawater					
	3.6 ± 0.2		75 % seawater					
	3.2 ± 0.1		100 % seawater					
	4.5 ± 1.0		0	408 c				
	3.9 ± 1.0			412 g*				
hexyl acetate	1.5 ± 0.2	298	0	430	2.59	429	4.6	426
	1.4 ± 0.2			412 g*	2.8	412 h*	4.5 ^f , 4.4	412 i*
hexenol^b	25	298	0	138				
(E/Z)-2-hexenol	94.4 ± 35.2			412 g*	1.6	412 h*	4.8	412 i*
(Z)-3-hexenol	113 ± 7.1	298	0	432	1.6	412 h*	4.8	412 i*
	140 ± 18		0.01					
	132 ± 11		1					
	83.4 ± 8.3	303	0					
	62.7 ± 3.0	308	0					
	129.9 ± 65.6	298		412 g*				
(E)-2-hexenal	14.5 ± 1.7	298	0	430	1.6	412 h*	4.3 ^f , 4.0	412 i*
	20			431, 433				
	13.6 ± 7.3			412 g*				
(Z)-3-hexenal	6			138	1.6	412 h*	3.7	412 i*
	4.1 ± 1.9			412 g*				
hexenyl acetate^b	1			138				
(E/Z)-2-hexenyl acetate	1.8 ± 0.7			412 g*	2.6	412 h*	4.2	412 i*
(Z)-3-hexenyl acetate	3.1 ± 0.4	298	0	430	2.6	412 h*	4.2	412 i*
	3.62 ± 0.22	298	0	432				
	3.29 ± 1.1		0.01					
	2.32 ± 0.17		1					
	3.21 ± 0.17	303	0					
	2.56 ± 0.19	308	0					
	3.3 ± 2.4	298		412 g*				
(E)-3-hexenyl acetate	3.3 ± 0.4	298	0	430				

	3.3 ± 2.4			412 g*				
(Z)-3-hexenyl-propionate	2.4 ± 1.6			412 g*	3.1	412 h*	4.6	412 i*
(E/Z)-3-hexenyl butyrate	1.8 ± 1.1			412 g*	3.6	412 h*	4.9	412 i*
(Z)-3-hexenyl isobutyrate	1.3 ± 0.6			412 g*	3.5	412 h*	4.9	412 i*
(E)-2-hexenyl butanoate	1.2 ± 0.3			412 g*	3.6	412 h*	4.9	412 i*
(Z)-3-hexenyl 3-methylbutanoate	1.1 ± 0.6			412 g*	4.0	412 h*	5.2	412 i*
(Z)-3-hexenyl 2-methyl-2-butenate	1.8 ± 0.6			412 g*	3.9	412 h*	5.4	412 i*
3-hexenyl hexanoate	1.0 ± 0.5			412 g*	4.6	412 h*	5.7	412 i*
2-methyl-3-buten-2-ol	73 ± 3	296 ±	0	434	1.1	412 h*	4.2 ^f , 4.5	412 i*
	38 ± 7	2	40 % wt H ₂ SO ₄					
	48 ± 26		55 % wt H ₂ SO ₄					
	48 ^a	298	0	414				
	52.9 ± 5.1		0					
	38.7 ± 2.2	303	0.01	432				
	21.8 ± 4.4	308	1					
	40.2 ± 5.4		0					
	31.7 ± 2.2		0					
	65 ± 3.5	303	0	431, 435				
62 ± 0.8	303	22.7 mM KNO ₃ + 7.42 mM CaSO ₄	435					
59.8 ± 58.6 ^d			412 g*					
1-octen-3-ol	13.2	>378 K	0	408, 436	2.6	412 h*	5.6	412 i*
	44.5 ± 1.7			412 g*				
nonanal	1.3 ± 0.2	298	0	408 ^c	3.3	412 h*	^f 4.8, 5.0	412 i*
	1.2 ± 0.1	298	Freshwater	425				

	0.51 ± 0.03		50 % seawater					
	0.38 ± 0.03		100 % seawater					
	1.6 ± 0.4			412 g*				
Jasmonic acid^c					2.5	412 h*	9.7	412 i*
methyl jasmonate^c	5081 ± 1003	298	0	437	2.8	412 h*	7.5	412 i*
	8091 ± 1121	298	0	432				
	5454 ± 520	298	0.01					
	3869 ± 261	303	1					
	6716 ± 1272	308	0					
	4837 ± 272							
methyl salicylate^c	33.5 ± 4.0	298	0	437	2.6	412 h*	5.0 ^f , 6.3	412 i*
	37.9 ± 2.1	298	0.01	432				
	26.7 ± 3.4	298	1					
	20.1 ± 1.6	298	0					
	16.4 ± 0.9	303						
	10.0 ± 4.2	308						

^a recalculated from the original data; ^b unspecified structure; ^c mean of experimental values summarized by Sander 2015; ^d EPI suite could not estimate the value using group estimation method, so the difference between bond estimation value and VP/WSol resulted into such large std. deviation; ^e the predicted KH values seem unreasonable and therefore were not included ^f Log KOA (octanol/air): estimated within EPI suite using one of the experimental values; ^g Mean of bond est., group est. and VP/WSol est. values by EPI suite (HENRYWIN v3.20) for which standard deviation is provided as uncertainty; ^h calculated with EPI suite Log KOW (version 1.68 estimate); ⁱ calculated with EPI suite Log Octanol-Air (KOAWIN v1.10), * This work.

Table 4.2. EPI-estimated vapor pressure, and solubility in water (MPBPVP (v1.43), Mean of Antoine & Grain methods, and WSKOW v1.42 method, resp.) of GLVs at 298 K.¹⁷²

GLV	Solubility		Vapor Pressure	
	mmol dm ⁻³	Ref.	Atm	Ref.
1-pentanol	245.5	438	2.9×10^{-3}	439
	307	419	3.7×10^{-3}	419
	257	429	3.49×10^{-3}	412 b*
	236.98	412 a*		
1-penten-3-ol	1047.1	429	1.20×10^{-2}	412 b*
	1035.1	428		
	525.48	412 a*		
(Z/E)-2-penten-1-ol	530.83	412 a*	3.46×10^{-3}	412 b*
(E)-2-pentenal	178.08	412 a*	2.43×10^{-2}	412 b*
1-penten-3-one	260.34	412 a*	5.03×10^{-2}	412 b*
(Z)-2-pentenyl acetate	11.23	412 a*	4.14×10^{-3}	412 b*
n-hexan-1-ol	57.5	438	1.22×10^{-3}	440
	61.3	428	1.16×10^{-3}	412 b*
	67.39	412 a*		
n-hexanal	56.3 ^c	Cited by ⁴¹²	1.49×10^{-2}	440
	49.9	422	1.39×10^{-2}	422
	35.21	412 a*	1.26×10^{-2}	412 b*
hexyl acetate	3.5	441	1.74×10^{-3}	442
	8.9	429	1.91×10^{-3}	412 b*
	2.14	412 a*		
hexenol^f	159.74	412 a*		
(E/Z)-2-hexen-1-ol	159.74	412 a*	1.20×10^{-3}	412 b*
(Z)-3-hexen-1-ol	162 ± 6	432	1.23×10^{-3}	412 b*
	159.74	412 a*		
(E)-2-hexenal	53.61	412 a*	6.21×10^{-3}	412 b*
(Z)-3-hexenal	53.61	412 a*	1.97×10^{-2}	412 b*
(E/Z)-2-hexenyl acetate	3.38	412 a*	2.61×10^{-3}	412 b*
(Z)-3-hexenyl acetate	3.12 ± 0.17	432	1.50×10^{-3}	412 b*
	3.38	412 a*		

(E)-3-hexenyl acetate	3.38	412 a*	1.50×10^{-3}	412 b*
(Z)-3-hexenyl-propionate	1.02	412 a*	5.50×10^{-4}	412 b*
(E/Z)-3-hexenyl butyrate	0.31	412 a*	2.05×10^{-4}	412 b*
(Z)-3-hexenyl isobutyrate	0.35	412 a*	3.71×10^{-4}	412 b*
(E)-2-hexenyl butanoate	0.31	412 a*	2.05×10^{-4}	412 b*
(Z)-3-hexenyl 3-methylbutanoate	0.11	412 a*	1.39×10^{-4}	412 b*
(Z)-3-hexenyl 2-methyl-2-butenoate	0.13	412 a*	7.53×10^{-5}	412 b*
3-hexenyl hexanoate	0.03	412 a*	3.04×10^{-5}	412 b*
2-methyl-3-buten-2-ol	1959 ± 36	432	3.08×10^{-2}	412 b*
	565.89	412 a*		
1-octen-3-ol	14.32	412 a*	3.13×10^{-4}	412 b*
nonanal	0.7	422	4.87×10^{-4}	440
	0.93	412 a*	5.13×10^{-4}	422
			7.42×10^{-4}	412 b*
Jasmonic acid	3.53	412 a*	2.41×10^{-8} d	412 b*
			1.79×10^{-7} e	
methyl jasmonate	4.52 ± 0.09	432	4.43×10^{-7} d	412 b*
			1.24×10^{-6} e	
	0.64	412 a*		
methyl salicylate	5.11 ± 0.06	432	7.03×10^{-5}	412 b*
	4.6 ^c	441		
	12.32	412 a*		

^a estimated with EPI suite (WSKOW v1.42); ^b estimated with EPI suite (MPBPVP (v1.43), mean of Antoine and Grain methods); ^c 308 K; ^d selected VP with modified grain method; ^e subcooled liquid VP with modified grain method; ^f unspecified structure. * This work.

4.2. Experimentally-measured UV-Vis spectra of GLVs

The UV-Vis spectroscopy is often used to follow reactant and product concentrations within the laboratory systems quantitatively. It also allows understanding the photodegradation of compounds in the laboratory mimicking experiments and natural systems. Ozone filters the UV radiation in the 220 – 290 nm range, so the solar flux is considered zero below 290 nm in the troposphere.⁴⁴³ Therefore, the compounds that do not absorb light above 290 nm practically do not undergo photolysis in the troposphere. In the light of experimental work described in Chapters 5 and 7 (performing laser flash photolysis or photooxidation experiments), it was necessary to know the molar extinction coefficients of the selected GLV compounds. The extinction coefficients in the aqueous phase is defined with equation (4.1).

$$\varepsilon(\lambda) = -\frac{\ln[I(\lambda)/I_0(\lambda)]}{Lc} = \frac{A(\lambda)}{Lc} \quad (4.1)$$

where: $\varepsilon(\lambda)$ is extinction coefficient in $\text{cm}^{-1} \text{M}^{-1}$ at wavelength λ , L is the optical path in cm, c is the concentration of absorbing solute in M, $I(\lambda)$ and $I_0(\lambda)$ are the light intensities in the presence and absence of absorbing compound/solute in aqueous solution, respectively, $A(\lambda)$ is the absorbance of a solute at λ , N is the Avogadro's number.

The measured UV spectra for the selected GLVs (1-penten-3-ol, (*Z*)-2-hexen-1-ol, (*E*)-2-hexen-1-ol, (*Z*)-3-hexenyl acetate, methyl salicylate, and 2-methyl-3-buten-2-ol) in the aqueous phase are presented along with the previously published ones. Two different UV-Vis spectrophotometers were used.

At TROPOS, I determined the molar absorption coefficients of GLVs (i.e., 1-penten-3-ol, (*Z*)-2-hexen-1-ol, and (*E*)-2-hexen-1-ol) by measuring the absorption spectra over the wavelength range of 200 – 400 nm using a Lambda 900 UV/VIS/NIR spectrometer (Perkin Elmer Instruments). The UV spectra were recorded for five GLV concentrations in aqueous solutions at 298 K and pH =7, twice for each concentration. Mean $\varepsilon(\lambda)$ values with standard deviations as uncertainties were reported for n=10 recordings. Figures 4.1, 4.2, and 4.3 show the $\varepsilon(\lambda)$ for the following concentration range: 1-penten-3-ol (PENTOL) 31.25 – 500 mM; (*Z*)-2-hexen-1-ol

(HEXOL) 6.25 – 100 mM; (*E*)-2-hexena-1-al (HEXAL) 1.875 – 30 mM). The corresponding numerical values of $\varepsilon(\lambda)$ are provided in Table A4.3, A4.4.a, and A4.5 in the Appendix. Due to the instrumental limitations, the absorbance for (*E*)-2-hexen-1-al could not be recorded below 245 nm wavelength within the selected concentration range. Results published⁴⁴⁴ and discussed in Chapter 5 utilize the molar absorption coefficients determined in this work.

Other UV spectra I recorded at IPC PAS, with a double-beam Jasco V-570 UV-VIS-NIR spectrophotometer using Milli-Q water as a reference medium. Figures 4.2 – 4.6 show the spectra for HEXOL, HEXAL, (*Z*)-3-hexenyl acetate (HexAc), methyl salicylate (MeSa), and 2-methyl-3-buten-2-ol (MBO) in the aqueous solutions at 295 K and pH =7. Tables A4.4.b, A4.5.b, A4.6, A4.7, and A4.8 in the Appendix contain numerical values of $\varepsilon(\lambda)$.

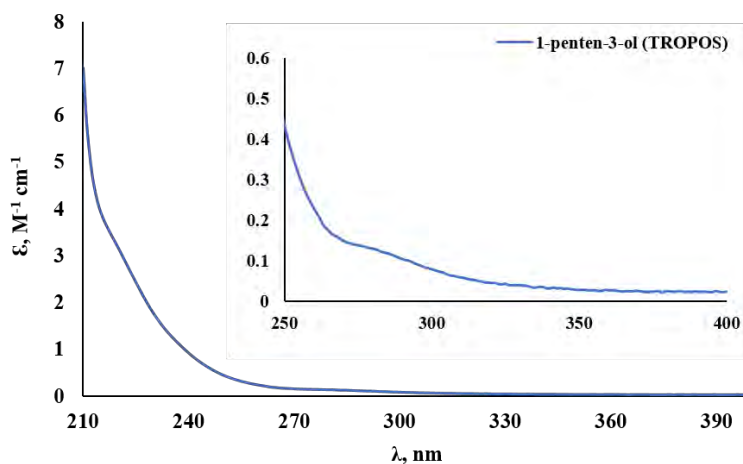


Figure 4.1. Absorption coefficient ε of 1-penten-3-ol in the aqueous phase at 298 K and pH =7.⁴⁴⁴

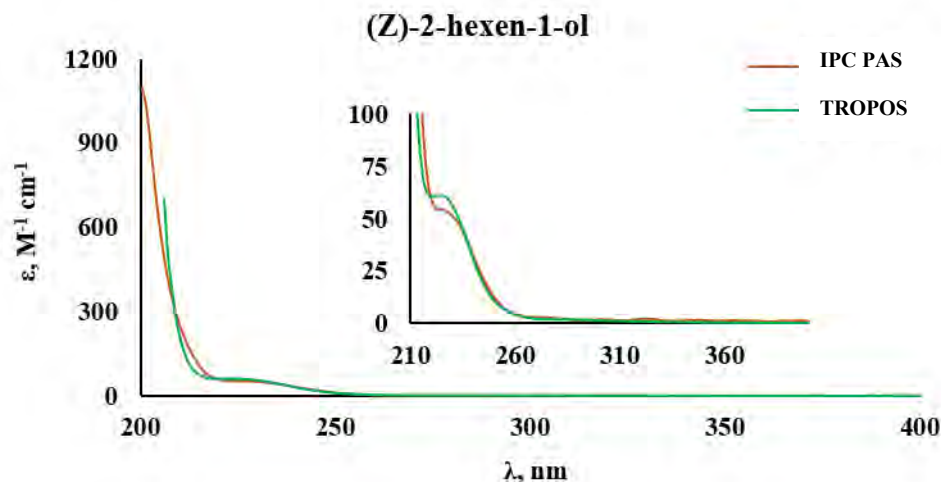


Figure 4.2. Absorption coefficients ε of (*Z*)-2-hexen-1-ol in the aqueous phase at 298 K and pH = 7 measured at TROPOS (green, Table 4.4.a), and at 295 K and pH = 7 at IPC PAS (brown, Table 4.4.b).^{172, 444}

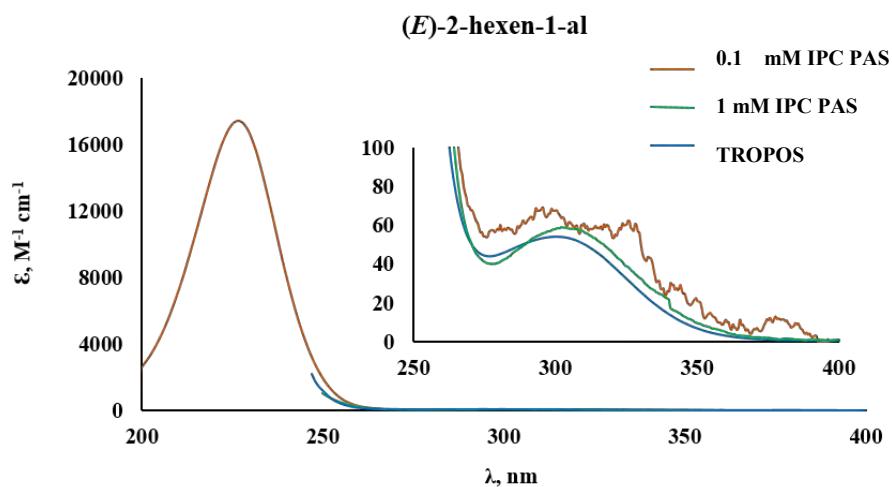


Figure 4.3. Absorption coefficients ε of (*E*)-2-hexen-1-al in the aqueous phase at 298 K and pH = 7 measured at TROPOS (blue, Table 4.5.a), and at 295 K and pH = 7 at IPC PAS (1 mM green and 0.1 mM brown, Table 4.5.b).^{172, 444}

(*E*)-2-hexen-1-al has two absorption maxima. The first one between 225 – 230 nm is so high ($\varepsilon = 17,300 \text{ M}^{-1} \text{ cm}^{-1}$), that even at low concentration of 1 mM it exceeded the limit of detection of the spectrophotometer. However, recording this maximum with the selection of 10 times lower

concentration (0.1 mM) resulted into a compromise of poor spectra recording in the range 260 – 400 nm, where the ϵ of (*E*)-2-hexen-1-al was below $100 \text{ M}^{-1} \text{ cm}^{-1}$, due to the resolution limitations (Figure 4.3 and Table 4.5).

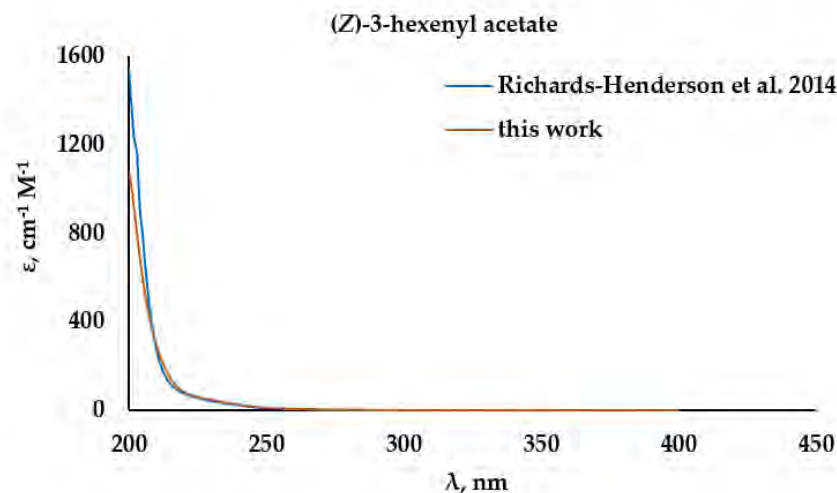


Figure 4.4. Molar absorption coefficients ϵ of (*Z*)-3-hexenyl acetate in the aqueous phase measured at 295 K and pH = 7 at IPC PAS within this study¹⁷² (brown, Table 4.6) compared to that from Richards-Henderson et al.2014.¹²⁹

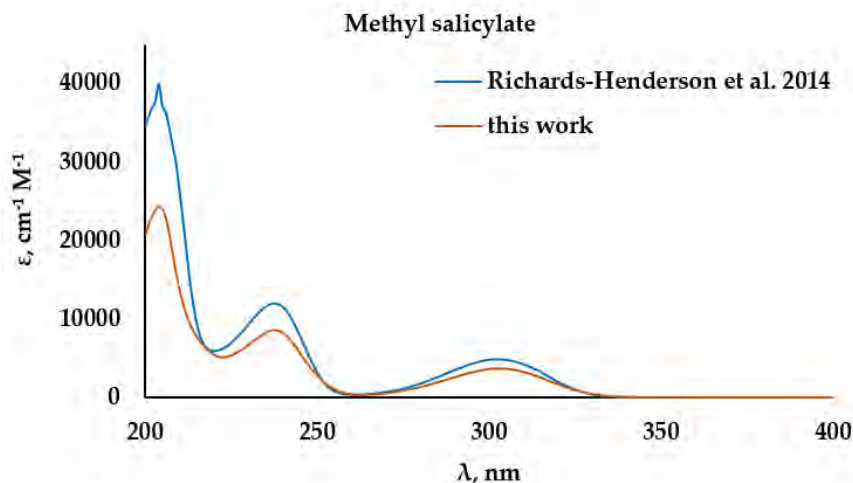


Figure 4.5. Molar absorption coefficients ϵ of MeSa in the aqueous phase measured at 295 K and pH = 7 at IPC PAS within this study¹⁷² (brown, Table 4.7) compared to that from Richards-Henderson et al.2014.¹²⁹

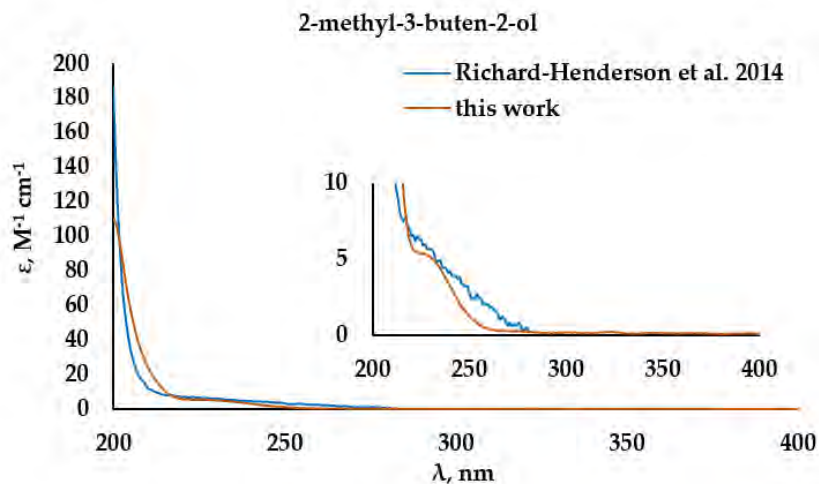


Figure 4.6. Molar absorption coefficients ϵ of MBO in the aqueous phase measured between 200 – 400 nm at 295 K and pH = 7 at IPC PAS within this study¹⁷² (brown, Table 4.7) compared to that from Richards-Henderson et al.2014.¹²⁹

Missing knowledge of organic aerosol sources has led to significant uncertainty in understanding the particle properties including morphology, surface chemistry, hygroscopicity and many more, which are key factors governing CCN/IN activity. Global aq. SOA production is estimated to be 20 to 30 Tg year⁻¹.^{445, 446} GLV derived SOA may significantly influence the CCN/IN activity of the existing aerosols within the atmosphere. McNeill, 2015, highlighted the importance of the atmospheric aqueous-phase as a reaction medium.⁴⁴⁶

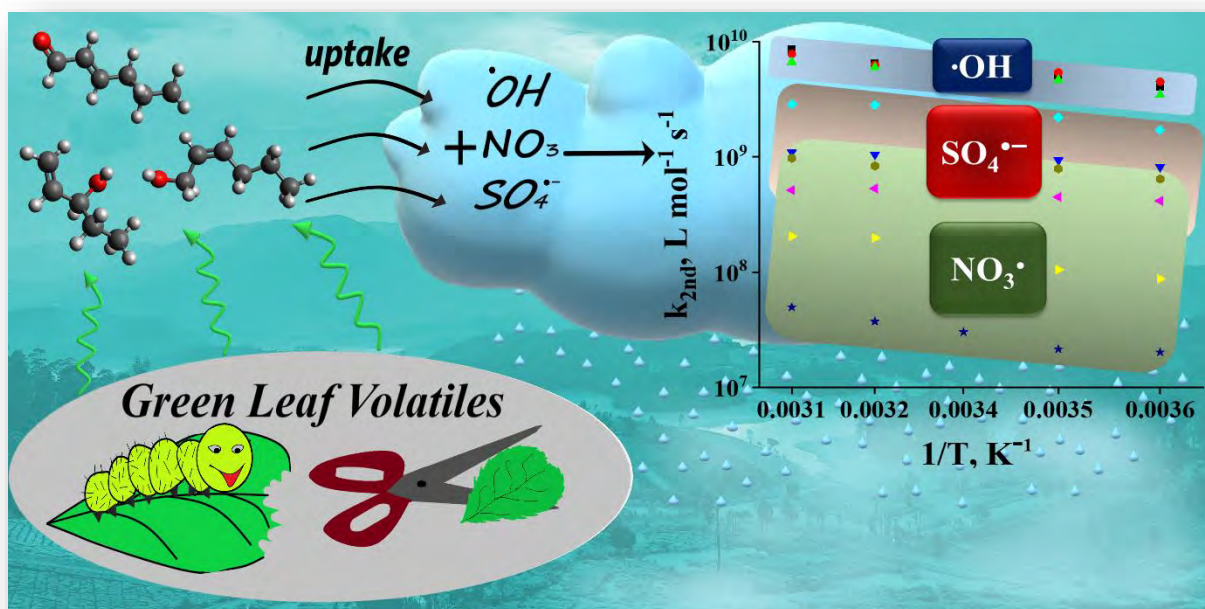
Lack of physio-chemical properties data is the source of large uncertainty in the reaction processes of the organic compounds, where understanding aqueous-phase reactions is one of the most challenging area of research for atmospheric scientist due to vaguely available data.⁴⁴⁷ GLVs as a very broad class including more than 30 compounds can be an important missing source of SOA. For better modelling of the multiphase processes involving GLVs and better understanding GLVs atmospheric chemistry a huge set of physical chemical properties data still needs to be determined experimentally (as can be seen in Table 4.1, 4.2).

Therefore, I decided to collect these data within the work of thesis for GLVs, which are less investigated till date. The estimated and literature based data show (Table 4.1) that GLVs have H

constant $< 100 \text{ M atm}^{-1}$ (exception MeJa), suggesting they reside more in gas phase. But due to their high reactivity (Chapter 5), and resulting lower aldehyde products (Chapter 7), they can possibly undergo oligomerization similar to glyoxal, leading to enhancement in their solubility, and hence aq. SOA.^{446, 448} Sareen et al. identified aqueous phase chemistry as one of the major sink of reactants, such as GLVs (*E*)-2-hexen-1-al, and (*Z*)-3-hexen-1-al, by identifying their products in the ambient aerosol and suggested cloud/fog water processing as one of the source of aq. SOA.⁴⁴⁹ There is still a lot of uncertainties in these processes due to the lack of their fundamental physico-chemical parameters. Thus, their determination in a preliminary work will help to evaluate the importance of chemical processes of GLVs and improve the future models, such as CAPRAM.⁴⁵⁰⁻⁴⁵²

Various existing estimation methods, such as EPI suite used within this paper provide only sometimes very reasonable values, and cannot provide the temperature dependence of the partition coefficients and other parameters such as solubility and vapour pressure. The measurement and building experimental database of these physical properties will help in evaluating the importance of individual phase (gas, aqueous or particle) chemistry of GLVs within the troposphere. Moreover, the present physical property database will ease the understanding and selection for research related to the GLVs as a source of SOA.

Chapter 5. Aqueous-phase reactions of green leaf volatiles with sulfate, hydroxyl and nitrate radicals in troposphere: kinetics and atmospheric implications



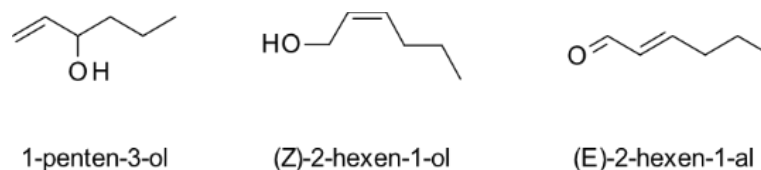
Results of the present chapter have been published in the form of a research article in *Environ. Sci. Technol.* 2021, 55, 20, 13666–13676. Sarang et al., 2021.

Synopsis

Green plants exposed to extreme conditions, such as abiotic stress (drought, high/low temperatures, or wind), wounding by insects or cutting, release C5 and C6 unsaturated oxygenated hydrocarbons termed Green Leaf Volatiles (GLVs). During the events of high emissions, a considerable amount of GLVs partitions into tropospheric waters (i.e., fog, mist, rain, and cloud), leading to the formation of secondary organic aerosol (SOA) *via* aqueous-phase reactions. In the present study, the kinetics of aqueous-phase reactions of selected GLVs, i.e., 1-penten-3-ol (PENTOL), (*Z*)-2-hexen-1-ol (HEXOL) and (*E*)-2-hexen-1-al (HEXAL) with atmospheric radicals $\text{SO}_4^{\cdot-}$, $\cdot\text{OH}$, and NO_3^{\cdot} was explored. The experimental rate constants were determined for a 278 – 318 K temperature range, and the Arrhenius equations were derived. All rate constants increased weakly with temperatures. The rate constants were corrected for diffusional limitations using the resistance-in-series model, which appeared significant only for the GLV- $\cdot\text{OH}$ reactions. Atmospheric lifetimes and removal rates of GLV showed the aqueous-phase reaction were negligible in deliquescent aerosol and haze water, but not in clouds and rain. The atmospheric lifetimes of PENTOL, HEXOL, and HEXAL decreased from several days to a few hours with increasing liquid water content and atmospheric radicals' concentration.

5.1. Introduction

The determination of the kinetics is the first most crucial step required for researching and predicting the fate of atmospheric compounds in the atmosphere.^{453, 454} Even though the selected GLVs are moderately soluble (Table 5.1, and Chapter 4, Table 4.1), they may be effective precursors of SOA formation in the aqueous phase.¹²⁹ A detailed literature review (Chapter 2) clearly shows that comprehensive studies exist for the oxidation of GLVs in the gas phase.^{162, 176, 184, 194, 204, 217, 220, 243, 269, 455} However, very few works have considered the GLV reactions in the aqueous phase as a novel pathway of SOA formation.^{129, 456, 457} The estimated physical properties obtained using the EPI suite⁴¹², used for the kinetic calculations in this thesis are provided in Table 5.1 (the average values obtained using three different estimations within the EPI suite are provided in Chapter 4).



Scheme 5.1. Chemical structures of selected GLVs studied in this work.

The main objective of this work was to determine the rate constants of aqueous-phase reactions of the three selected GLVs – 1-penten-3-ol (PENTOL), (Z)-2-hexen-1-ol (HEXOL), and (E)-2-hexen-1-al (HEXAL) (Scheme 5.1) – with atmospherically relevant radicals $\cdot\text{OH}$, $\text{SO}_4^{\cdot-}$ and NO_3^{\cdot} , and evaluate the atmospheric significance of these reactions. An advanced Laser Flash Photolysis-Laser Long Path Absorption (LFP-LLPA) technique was used at Laser Lab facility, TROPOS (Leipzig, Germany). The results enriched the chemical-kinetic database essential and indispensable for atmospheric models.^{27, 273, 447}

Table 5.1. Values of the physical properties of the selected GLVs at 298 K obtained using EPI suite^{1*}

GLV	Molecular formula	The Henry's Law Constant for water $\text{mol L}^{-1} \text{atm}^{-1}$	Vapor pressure atm	Water solubility mg L^{-1}
PENTOL	$\text{C}_5\text{H}_{10}\text{O}$	101.22	1.20×10^{-2}	4.53×10^4
HEXOL	$\text{C}_6\text{H}_{12}\text{O}$	133.26	1.19×10^{-3}	1.60×10^4
HEXAL	$\text{C}_6\text{H}_{10}\text{O}$	10.12	6.21×10^{-3}	5.26×10^3

* average EPI-estimated values were provided in Chapter 4

5.2. Experimental methods

The explanation of the LFP-LLPA setup used to determine the second-order rate constant ($k_{2\text{nd}}$) is provided in Chapter 3. Section 3.3.1 of Chapter 3 provides all the necessary details of the LFP-LLPA setup configurations required to observe the kinetics of GLVs (PENTOL, HEXOL, and HEXAL) reactions with radicals discussed. All kinetic measurements were carried out at

constant temperature (278 K – 318 K) using a thermostat. The acidity of solutions was pH= 7, as the GLVs studied do not undergo ionic speciation. The initial concentrations of the GLVs and radicals are provided in Table 3.4. The UV spectra recorded and molar absorption coefficients obtained within this study are presented in Figures 4.1, 4.2, and 4.3 (Chapter 4).

5.3. Results and Discussion

5.3.1. Reactions of SO₄^{•-} radical with PENTOL, HEXOL, and HEXAL

Previous studies,⁴⁵⁸ have shown that SO₄^{•-} radicals are strong oxidizing agents, and thus can react with most organic compounds with nearly diffusion-controlled rates. The experimentally observed rate constants for aqueous-phase reactions of PENTOL, HEXOL, and HEXAL with SO₄^{•-} radical determined in this study, k_{obs} , range from $(4.2 \pm 0.2) \times 10^8$ to $(2.9 \pm 0.6) \times 10^9$ L mol⁻¹ s⁻¹ (Table 5.2). The Arrhenius relations for 278 to 318 K show that all rate constants weakly increase with temperature (Figure 5.2, equations 5.1 – 5.3).

$$\text{PENTOL} + \text{SO}_4^{\bullet-}: k_{obs}(T) = (7.9 \pm 0.1) \times 10^9 \exp\left(\frac{-620 \pm 90}{T}\right) \text{L mol}^{-1} \text{s}^{-1} \quad (5.1)$$

$$\text{HEXOL} + \text{SO}_4^{\bullet-}: k_{obs}(T) = (111 \pm 4) \times 10^9 \exp\left(\frac{-1140 \pm 190}{T}\right) \text{L mol}^{-1} \text{s}^{-1} \quad (5.2)$$

$$\text{HEXAL} + \text{SO}_4^{\bullet-}: k_{obs}(T) = (2.9 \pm 0.1) \times 10^9 \exp\left(\frac{-540 \pm 110}{T}\right) \text{L mol}^{-1} \text{s}^{-1} \quad (5.3)$$

The diffusion corrected second-order rate constants (k_{reac}) are slightly higher and range from $(4.4 \pm 0.2) \times 10^8$ to $(3.7 \pm 0.8) \times 10^9$ L mol⁻¹ s⁻¹ (Table 5.2, Figure 5.3). The percentage diffusion contribution (% k_{diff}) to the observed rate constant is about 9% for PENTOL, 19–23% for HEXOL, and 4–5% for HEXAL (Table 5.2). Thus, the GLVs + SO₄^{•-} reactions are mostly chemically controlled.

Table 5.2. Comparison of experimentally observed and diffusion-corrected rate constants for reactions of GLVs with $\text{SO}_4^{\bullet-}$, and rate constants for the diffusion of reactants (k_{obs} , k_{reac} , and k_{diff} , $10^8 \text{ L mol}^{-1} \text{ s}^{-1}$, respectively).

GLV + $\text{SO}_4^{\bullet-}$		278 K	288 K	298 K	308 K	318 K
PENTOL	k_{obs}	8.2 ± 0.7	9.4 ± 0.7	9.4 ± 1.0	10.5 ± 2.1	11.0 ± 2.4
	k_{reac}	9.0 ± 0.8	10.4 ± 0.8	10.2 ± 1.1	11.5 ± 2.3	12.1 ± 2.7
	k_{diff}	88.2	98.8	111	124	126
	% k_{diff}	9	10	9	9	9
HEXOL	k_{obs}	17.1 ± 2.0	22.0 ± 3.3	25.3 ± 3	28.1 ± 6.5	28.7 ± 6.3
	k_{reac}	21.2 ± 2.5	28.4 ± 4.2	32.9 ± 3.9	36.4 ± 8.5	37.3 ± 8.2
	k_{diff}	88.1	98.4	110	123	125
	% k_{diff}	19	22	23	23	23
HEXAL	k_{obs}	4.2 ± 0.2	4.5 ± 0.1	4.8 ± 0.2	5.3 ± 0.3	5.1 ± 0.5
	k_{reac}	4.4 ± 0.2	4.7 ± 0.1	5.0 ± 0.2	5.6 ± 0.3	5.4 ± 0.5
	k_{diff}	88.1	98.3	110	123	124
	% k_{diff}	5	5	4	4	4

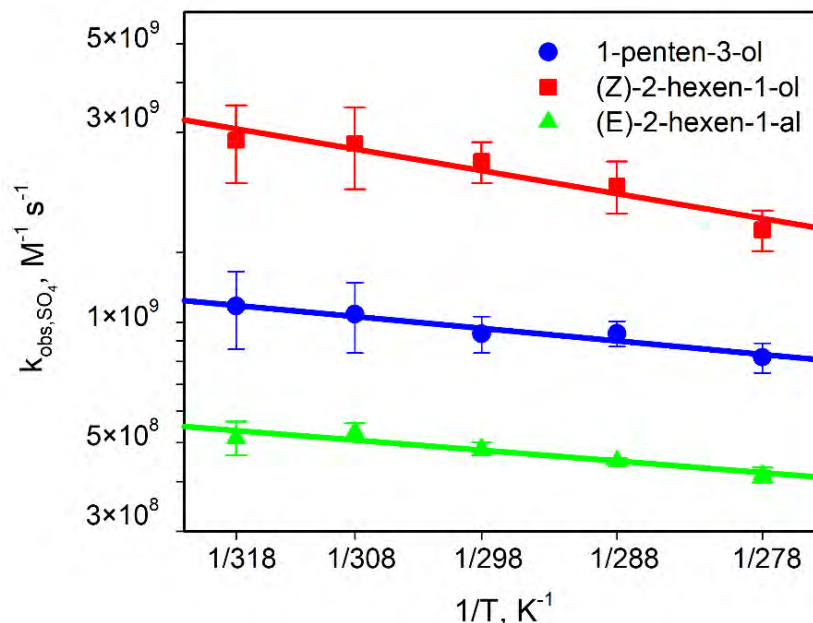


Figure 5.2. Experimental rate constants for reactions of GLVs with $\text{SO}_4^{\bullet-}$ at various temperatures (coefficient of determination R^2 : 0.94 for 1-penten-3-ol; 0.92 for (Z)-2-hexen-1-ol; and 0.90 for (E)-2-hexen-1-al; Table 5.2, equations 5.1 – 5.3).

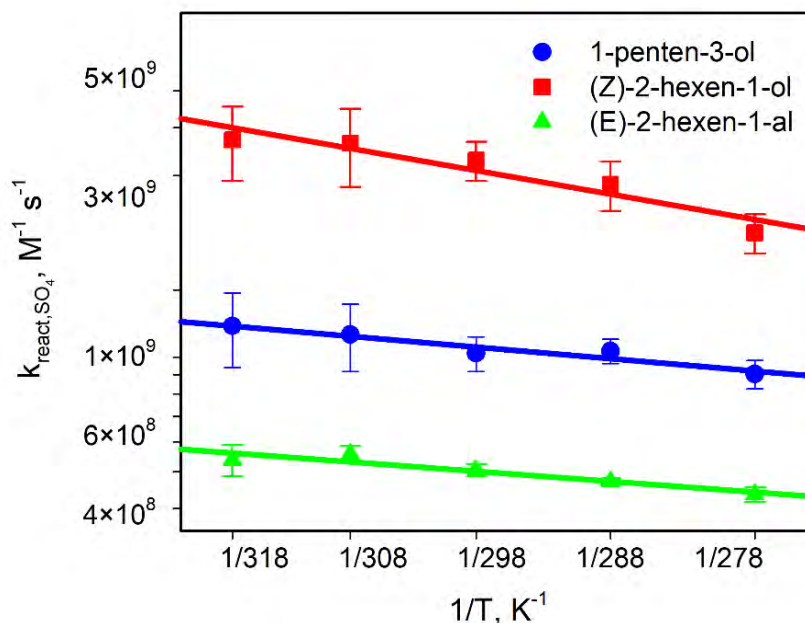


Figure 5.3. Diffusion-corrected rate constants, k_{react} for the reaction of GLVs with $\text{SO}_4^{\bullet-}$ (also Table 5.2).

5.3.2. Reactions of $\cdot\text{OH}$ radicals with PENTOL, HEXOL, and HEXAL.

The experimentally observed rate constants, k_{obs} for the aqueous-phase reactions of GLVs with $\cdot\text{OH}$ studied increase weakly with temperature and range from $(3.5 \pm 0.2) \times 10^9$ to $(8.5 \pm 1.0) \times 10^9 \text{ L mol}^{-1} \text{ s}^{-1}$ (Figure 5.4, equations 5.4 – 5.6, Table 5.3). Figures 5.4 and 5.5 show the temperature dependence of the experimentally observed (k_{obs}) and diffusion-corrected (k_{reac}) rate constants, respectively.

$$\text{PENTOL} + \cdot\text{OH}: \quad k_{obs}(T) = (1040 \pm 29) \times 10^9 \exp\left(\frac{-1540 \pm 190}{T}\right) \text{ L mol}^{-1} \text{ s}^{-1} \quad (5.4)$$

$$\text{HEXOL} + \cdot\text{OH}: \quad k_{obs}(T) = (263 \pm 9) \times 10^9 \exp\left(\frac{-1120 \pm 210}{T}\right) \text{ L mol}^{-1} \text{ s}^{-1} \quad (5.5)$$

$$\text{HEXAL} + \cdot\text{OH}: \quad k_{obs}(T) = (517 \pm 14) \times 10^9 \exp\left(\frac{-1380 \pm 170}{T}\right) \text{ L mol}^{-1} \text{ s}^{-1} \quad (5.6)$$

The rate constants of GLVs reactions with $\cdot\text{OH}$ are larger than these of reactions with $\text{SO}_4\cdot^-$ ($(4.9 \pm 0.2) \times 10^9$ to $(16.4 \pm 0.8) \times 10^9 \text{ L mol}^{-1} \text{ s}^{-1}$, Table 5.3). Besides, they are significantly controlled by the diffusion of reactants. The percentage diffusion contribution ($\% k_{diff}$) is 35–57% for PENTOL, 39–52% for HEXOL, and 30–45% for HEXAL (Table 5.3).

Table 5.3. Comparison of experimentally observed and diffusion-corrected rate constants for reactions of GLVs with $\cdot\text{OH}$, and rate constants for the diffusion of reactants (k_{obs} , k_{reac} , and k_{diff} , respectively, $10^9 \text{ L mol}^{-1} \text{ s}^{-1}$).

GLV + $\cdot\text{OH}$		278 K	288 K	298 K	308 K	318 K
PENTOL	k_{obs}	4.01 ± 0.04	5.1 ± 0.2	6.3 ± 0.1	6.5 ± 0.3	8.5 ± 1.0
	k_{reac}	6.2 ± 0.1	8.7 ± 0.3	11.8 ± 0.3	11.5 ± 0.6	19.8 ± 2.4
	k_{diff}	11.5	12.5	13.6	14.8	14.9
	% k_{diff}	35	41	46	44	57
HEXOL	k_{obs}	4.49 ± 0.04	5.4 ± 0.2	6.7 ± 0.3	6.3 ± 0.3	7.8 ± 0.4
	k_{reac}	7.4 ± 0.1	9.5 ± 0.3	13.1 ± 0.6	11.0 ± 0.4	16.4 ± 0.8
	k_{diff}	11.5	12.5	13.6	14.8	14.9
	% k_{diff}	39	43	49	43	52
HEXAL	k_{obs}	3.5 ± 0.1	4.6 ± 0.1	4.8 ± 0.3	6.0 ± 0.3	6.6 ± 0.4
	k_{reac}	4.9 ± 0.2	7.4 ± 0.2	7.4 ± 0.5	10.1 ± 0.5	12.0 ± 0.7
	k_{diff}	11.6	12.5	13.6	14.7	14.9
	% k_{diff}	30	37	35	41	45

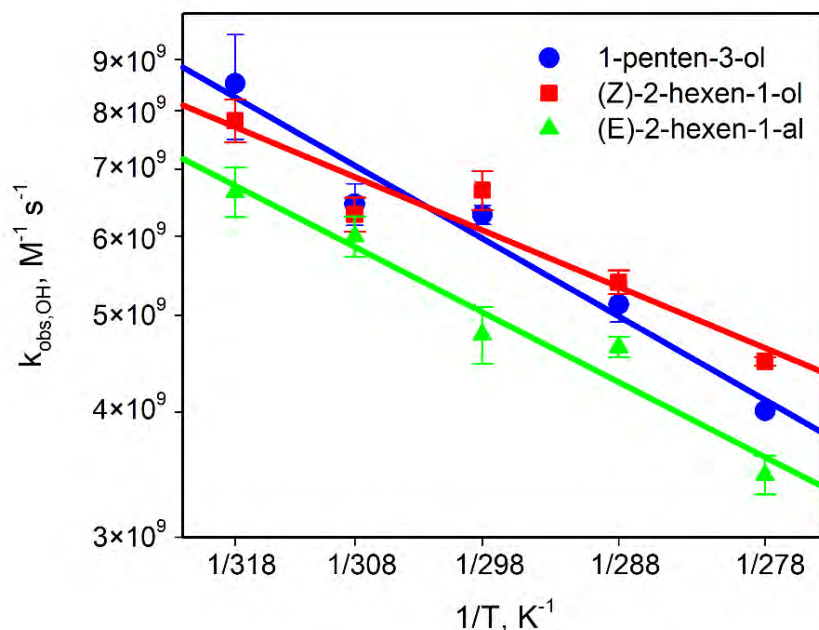


Figure 5.4. Experimental rate constants for reactions of GLVs with $\cdot\text{OH}$ at various temperatures (coefficient of determination R^2 : 0.96 for 1-penten-3-ol, 0.90 for (Z)-2-hexen-1-ol, and 0.96 for (E)-2-hexen-1-al; Table 5.3, equations 5.4 – 5.6).

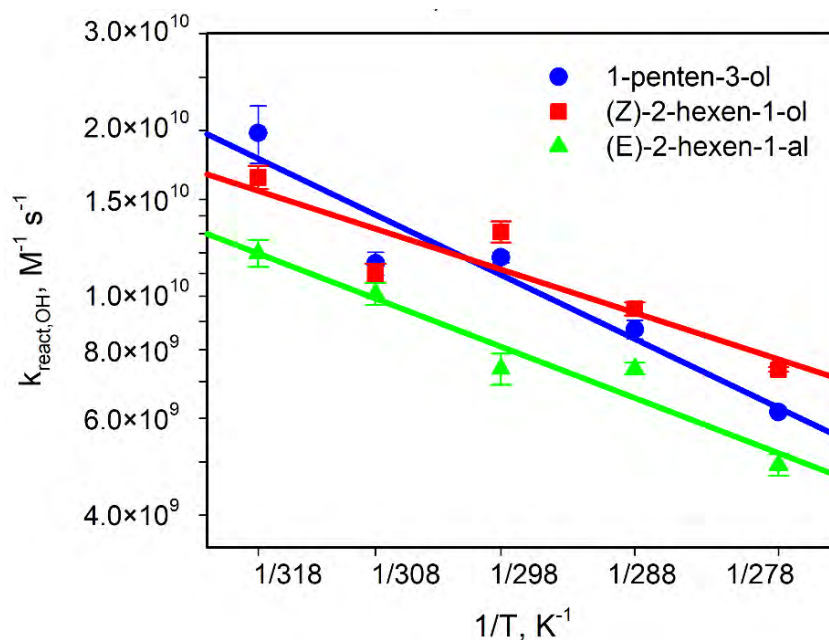


Figure 5.5. Diffusion-corrected rate constants, k_{react} for reactions of GLVs with $\cdot\text{OH}$ (also Table 5.3).

5.3.3. Reactions of NO₃• radicals with PENTOL, HEXOL, and HEXAL.

The rate constants for the aqueous-phase reactions of PENTOL, HEXOL, and HEXAL with NO₃• radicals range from $(2.0 \pm 0.6) \times 10^7$ to $(9.8 \pm 3.9) \times 10^8$ L mol⁻¹ s⁻¹ (Figure 5.6, Table 5.4). The rate constant for HEXOL at 318 K could not be determined, so the fifth value was measured at 293 K. Figure 5.6 and equations 5.7 – 5.9 show the variation in the rate constants with temperature.

$$\text{PENTOL} + \text{NO}_3\cdot: k_{obs}(T) = (250 \pm 14) \times 10^9 \exp\left(\frac{-2080 \pm 240}{T}\right) \text{L mol}^{-1} \text{s}^{-1} \quad (5.7)$$

$$\text{HEXOL} + \text{NO}_3\cdot: k_{obs}(T) = (98.8 \pm 3.3) \times 10^9 \exp\left(\frac{-1130 \pm 140}{T}\right) \text{L mol}^{-1} \text{s}^{-1} \quad (5.8)$$

$$\text{HEXAL} + \text{NO}_3\cdot: k_{obs}(T) = (31.6 \pm 1.3) \times 10^9 \exp\left(\frac{-2070 \pm 240}{T}\right) \text{L mol}^{-1} \text{s}^{-1} \quad (5.9)$$

The GLV + NO₃• reactions are fully chemically controlled, since the diffusion contribution to k_{obs} was minor (1 – 2% for PENTOL, 7 – 8% for HEXOL, and 0.2 – 0.4% for HEXAL (Table 5.4, Figure 5.7). Due to the lower light absorption values in the experiments, the error bars in the case of NO₃• kinetics were comparatively larger, but still fell within the acceptable 95% confidence interval.

The chemical-kinetic model was developed and used to evaluate the bias of the experimental rate constants determined for reactions of GLV with NO₃• radicals, which is discussed in Chapter 6.

Table 5.4. Comparison of experimentally observed and diffusion-corrected rate constants for reactions of GLVs with NO₃, and rate constants for the diffusion of reactants (k_{obs} , k_{reac} , and k_{diff} , respectively, 10⁷ L mol⁻¹ s⁻¹).

GLV + NO ₃ [*]		278 K	288 K	298 K	308 K	318 K
PENTOL	k_{obs}	8.8 ± 1.6	10.5 ± 2.3	15.0 ± 1.5	19.8 ± 4.2	21 ± 9
	k_{reac}	8.9 ± 1.6	10.6 ± 2.3	15.2 ± 1.5	20.1 ± 4.3	20.6 ± 9.2
	k_{diff}	950	1053	1169	1297	1313
	% k_{diff}	1	1	1	2	2
HEXOL	k_{obs}	64.3 ± 14.8	79.1 ± 24.3	83.7 ± 22.8	97.7 ± 39.3	83 ± 19*
	k_{reac}	69 ± 16	85.5 ± 26.2	90.2 ± 24.6	105.7 ± 42.5	-
	k_{diff}	951	1051	1165	1290	-
	% k_{diff}	7	8	7	8	-
HEXAL	k_{obs}	2.0 ± 0.6	2.1 ± 0.2	3.0 ± 0.7	3.7 ± 0.1	5.0 ± 0.8
	k_{reac}	2.0 ± 0.6	2.2 ± 0.2	3.0 ± 0.7	3.7 ± 0.1	5.0 ± 0.8
	k_{diff}	952	1050	1160	1290	1300
	% k_{diff}	0.2	0.2	0.3	0.3	0.4

* at T = 293 K

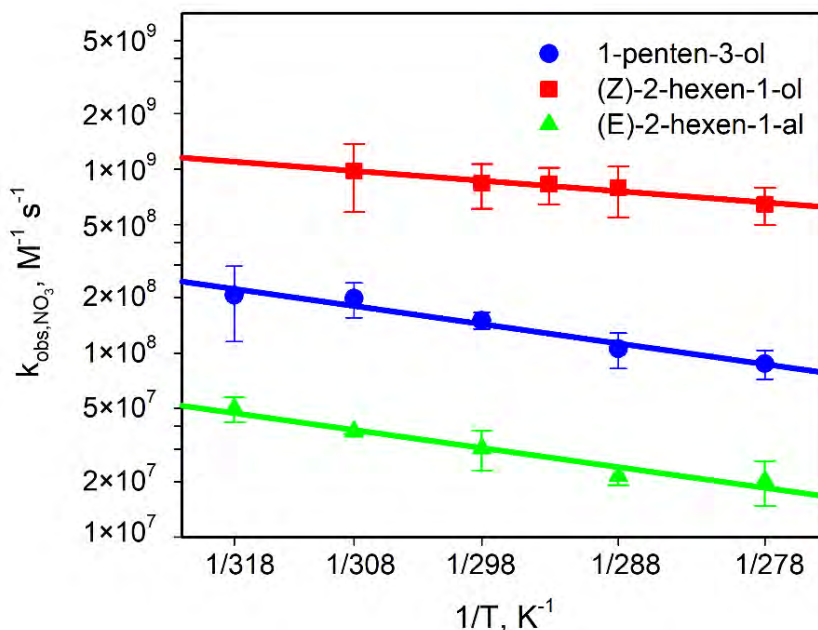


Figure 5.6. Experimental rate constants for reactions of GLVs with NO_3^* at various temperatures (coefficient of determination R^2 : 0.93 for 1-penten-3-ol, 0.94 for (Z)-2-hexen-1-ol, and 0.96 for (E)-2-hexen-1-al; Table 5.4, equations 5.7 – 5.9).

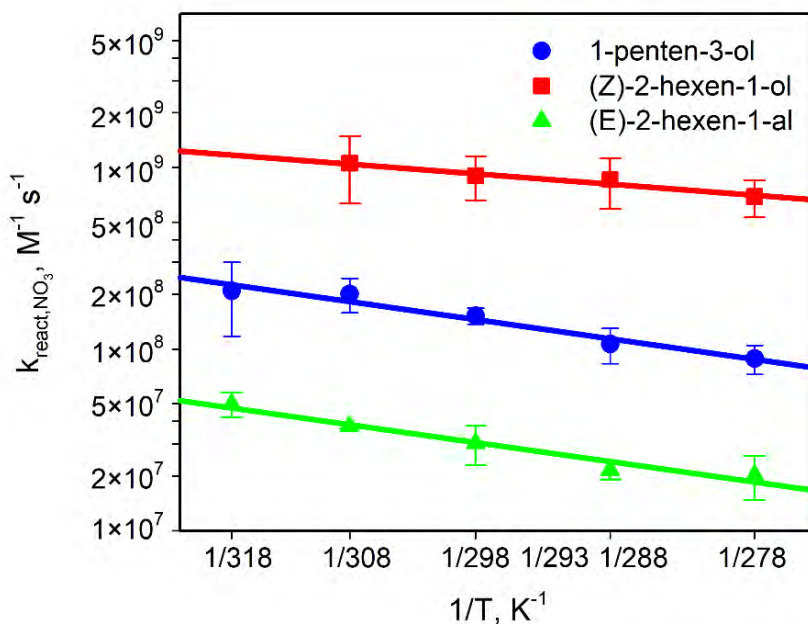


Figure 5.7. Diffusion-corrected rate constants, k_{react} for the reaction of GLVs with NO_3^* (also Table 5.4).

5.4. Activation Parameters

The activation parameters aid to understand and gain more insights into the chemical mechanism of the reaction. The detailed overview of the activation parameters calculated for reactions of GLVs with atmospheric radicals ($\text{SO}_4^{\cdot-}$, $\cdot\text{OH}$, and NO_3^{\cdot}) using experimentally observed and diffusion corrected rate constant is provided in Table 5.5 and 5.6, respectively. Equations (5.19 – 5.21) were used to calculate the activation parameters: activation enthalpy (ΔH^\ddagger), activation entropy (ΔS^\ddagger), Gibb's activation energy (ΔG^\ddagger).^{296, 297, 407} The Arrhenius expressions obtained within this study for the aqueous-phase reactions of 1-penten-3-ol, (*Z*)-2-hexen-1-ol, and (*E*)-2-hexen-1-al with $\text{SO}_4^{\cdot-}$, $\cdot\text{OH}$, and NO_3^{\cdot} (equations 5.1 – 5.9) are provided for the first time. The Arrhenius plots (see Section 5.3) are all linear (Figures 5.2, 5.4, and 5.6):

$$\text{Arrhenius equation:} \quad k(T) = A \exp \frac{-E_A}{RT} \quad (5.10)$$

$$\text{Enthalpy of activation:} \quad \Delta H^\ddagger = E_A - RT \quad (5.11)$$

$$\text{Entropy of activation:} \quad \Delta S^\ddagger = R \left[\ln A - \ln \frac{k_B T}{h} - 1 \right] \quad (5.12)$$

$$\text{Gibb's free energy of activation:} \quad \Delta G^\ddagger = \Delta H^\ddagger - T \Delta S^\ddagger \quad (5.13)$$

where: $k_B = 1.38 \times 10^{23} \text{ JK}^{-1}$ is the Boltzman constant, $h = 6.626 \times 10^{-34} \text{ Js}$ is the Planck constant, k is the rate constant, A is the pre-exponential factor, E_A is the activation energy, R is the gas constant, and T is the absolute temperature.

The reaction rate constant is directly influenced by the ratio of activation energy (E_A) to average kinetic energy expressed by (RT) in equation 5.18. The weak temperature dependence of the rate constants occurs when $E_A < 18 \text{ kJ mol}^{-1}$ (Table 5.5). The low value of activation enthalpies ΔH^\ddagger (2 to 15 kJ mol^{-1}) and negative activation entropies ΔS^\ddagger (from -72 to -23 $\text{J mol}^{-1} \text{ K}^{-1}$) explain that the molecules randomness within the chemical system decreases as the reaction proceeds. Such behavior indicates that the studied aqueous-phase reactions proceed mainly *via* the associative pathway (radical addition to the double bond). Further experimental and theoretical investigation on this problem is required and was carried out for GLV- $\cdot\text{OH}$ reactions, which is discussed in Chapter 7. It shows the dominance of addition or associative pathway, however hydrogen abstraction was also found to be significant in few cases (Chapter 7). The activation

parameters were also calculated for the diffusion-corrected rate constants, and the E_A values were still lower than 20 kJ mol⁻¹ (Table 5.6).

Table 5.5. The experimentally determined activation parameters for the reactions of GLVs with SO₄^{•-}, [•]OH, and NO₃[•] radicals.

Reactants		E_A	A	ΔH^\ddagger	$-\Delta S^\ddagger$	ΔG^\ddagger
		kJ mol ⁻¹	L mol ⁻¹ s ⁻¹	kJ mol ⁻¹	J mol ⁻¹ K ⁻¹	kJ mol ⁻¹
SO ₄ ^{•-}	PENTOL	5 ± 1	(7.9 ± 0.1) × 10 ⁹	3 ± 1	64 ± 1	22 ± 4
	HEXOL	10 ± 2	(1.1 ± 0.1) × 10 ¹¹	7 +12/-7	42 ± 1	20 ± 5
	HEXAL	4 ± 1	(2.9 ± 0.1) × 10 ⁹	2 ± 1	72 ± 2	24 ± 6
[•] OH	PENTOL	13 ± 2	(10.4 ± 0.3) × 10 ¹¹	10 ± 2	23 ± 1	17 ± 3
	HEXOL	9 ± 2	(2.6 ± 0.1) × 10 ¹¹	7 ± 2	35 ± 1	17 ± 4
	HEXAL	12 ± 1	(5.2 ± 0.1) × 10 ¹¹	9 ± 1	29 ± 1	18 ± 3
NO ₃ [•]	PENTOL	17 ± 2	(1.5 ± 0.1) × 10 ¹¹	15 ± 2	39 ± 2	27 ± 5
	HEXOL	9 ± 1	(3.8 ± 0.1) × 10 ¹⁰	7 ± 1	51 ± 1	22 ± 4
	HEXAL	17 ± 2	(3.1 ± 0.1) × 10 ¹⁰	15 ± 2	52 ± 2	30 ± 6

Table 5.6. The diffusion-corrected activation parameters for the reactions of GLVs with SO₄^{•-}, [•]OH and NO₃[•] radicals.

Reactants		E_A	A	ΔH^\ddagger	$-\Delta S^\ddagger$	ΔG^\ddagger
		kJ mol ⁻¹	L mol ⁻¹ s ⁻¹	kJ mol ⁻¹	J mol ⁻¹ K ⁻¹	kJ mol ⁻¹
SO ₄ ^{•-}	PENTOL	5 ± 1	(8.0 ± 0.1) × 10 ⁹	3 ± 1	64 ± 1	22 ± 5
	HEXOL	10 ± 2	(19 ± 1) × 10 ¹⁰	8 ± 2	37 ± 1	19 ± 5
	HEXAL	4 ± 1	(2.9 ± 0.1) × 10 ⁹	2 ± 1	72 ± 2	23 ± 6
[•] OH	PENTOL	19 ± 3	(2.5 ± 0.1) × 10 ¹³	17 ± 4	-3.2 ± 0.2	16 ± 4
	HEXOL	13 ± 3	(2.1 ± 0.1) × 10 ¹²	11 ± 3	17 ± 1	16 ± 6
	HEXAL	15 ± 2	(3.9 ± 0.2) × 10 ¹²	13 ± 2	12 ± 1	17 ± 4
NO ₃ [•]	PENTOL	17 ± 2	(1.6 ± 0.1) × 10 ¹¹	15 ± 2	39 ± 2	26 ± 5
	HEXOL	9 ± 1	(4 ± 1) × 10 ¹⁰	7 ± 1	50 ± 1	22 ± 4
	HEXAL	17 ± 2	(3.2 ± 0.1) × 10 ¹⁰	15 ± 2	52 ± 2	30 ± 6

5.5. Atmospheric Implications

Evaluating the overall atmospheric significance of the reactions responsible for the removal of GLV fluxes from the atmosphere requires extensive modeling involving individual scenarios, aqueous-phase reactions, gas-phase reactions, and land and aquatic depositions, which is far beyond the scope of the presented work. However, Section 5.5.1 provides the atmospheric lifetimes and relative removal rates to evaluate the atmospheric significance of gas-phase and aqueous-phase reactions of GLV with radicals under various liquid water contents and radical concentrations. In Section 5.5.2, the proportion of the aqueous-phase and gas-phase GLV fluxes were estimated by dividing GLV removal rates by the GLV concentrations to get a descriptor comparing GLV fluxes independent of GLV concentrations.

5.5.1. Atmospheric lifetimes

The removal of a GLV from the tropospheric gas phase by the combined action of gas-phase and aqueous-phase reactions with a radical X is approximated by equation 5.14.

$$\frac{d[GLV]_g}{dt} = -(k_g[X]_g[GLV]_g + k_{aq}[X]_{aq}[GLV]_{aq}\omega) \quad (5.14)$$

where, k_g is the gas-phase, and k_{aq} is the aqueous-phase second-order rate constants for reactions of the GLV with X in $L \text{ mol}^{-1} \text{ s}^{-1}$ respectively; ω is the liquid water contents of the atmospheric system in $\text{m}^3 \text{ m}^{-3}$; $[X]_g$ is the gas-phase and $[X]_{aq}$ is the aqueous phase concentration of X in M , respectively.

The gas- and aqueous forms of the reactants GLV and X are assumed to be bound by Henry's Law equilibria defined in equation 5.15 and 5.16.

$$[GLV]_{aq} = H_{d,GLV}[GLV]_g \quad (5.15)$$

$$[X]_g = [X]_{aq}/H_{d,X} \quad (5.16)$$

where: H_d are the dimensionless Henry's constants (equations 5.17).

$$H_d = HRT, \text{ if } H \text{ is in } \text{mol L}^{-1}\text{atm}^{-1} \quad (5.17a)$$

$$H_d = HRT\rho, \text{ if } H \text{ is in } \text{mol kg}^{-1}\text{atm}^{-1} \quad (5.17b)$$

Chapter 5. Aqueous-phase Reactions of Green Leaf Volatiles with Sulfate, Hydroxyl and Nitrate Radicals in Troposphere: Kinetics and Atmospheric Implications

where: R is the gas constant in $\text{atm L mol}^{-1} \text{K}^{-1}$; ρ is the solution density in kg L^{-1} . Equations 5.14 – 5.16 are combined and rearranged to derive equation 5.18.

$$\frac{d[\text{GLV}]_g}{[\text{GLV}]_g} = - \left(\frac{k_g}{H_{d,X}} + k_{aq}H_{d,\text{GLV}}\omega \right) [\text{X}]_{aq} dt \quad (5.18)$$

Integrating equation 5.18 within limits $(t, [\text{GLV}]_0)$ and $(t, [\text{GLV}])$ gives equation 5.19

$$\ln \left(\frac{[\text{GLV}]_g}{[\text{GLV}]_{g,0}} \right) = - \left(\frac{k_g}{H_{d,X}} + k_{aq}H_{d,\text{GLV}}\omega \right) [\text{X}]_{aq} t \quad (5.19a)$$

$$\text{or} \quad \frac{[\text{GLV}]_g}{[\text{GLV}]_{g,0}} = \exp \left(- \left(\frac{k_g}{H_{d,X}} + k_{aq}H_{d,\text{GLV}}\omega \right) [\text{X}]_{aq} t \right) \quad (5.19b)$$

The atmospheric lifetime t_{life} of a GLV removed via gas- and aqueous-phase reaction with radical X is the time required to decrease the initial GLV concentration $[\text{GLV}]_0$ to $[\text{GLV}]_0/e$ (equations 5.20a and 5.20b).

$$\frac{1}{e} = \exp \left(- \left(\frac{k_g}{H_{d,X}} + k_{aq}H_{d,\text{GLV}}\omega \right) [\text{X}]_{aq} t_{life} \right) \quad (5.20a)$$

$$\text{or} \quad t_{life} = \frac{1}{\left(\frac{k_g}{H_{d,X}} + k_{aq}H_{d,\text{GLV}}\omega \right) [\text{X}]_{aq}} \quad (5.20b)$$

Per analogiam, equation 5.21 defines the lifetime of a GLV consumed by reaction with a radical X , e.g., $\text{SO}_4^{\bullet-}$ existing only in the aqueous-phase and does not partition to the gas phase.

$$t_{life,aq} = \frac{1}{k_{aq}H_{d,\text{GLV}}\omega[\text{X}]_{aq}} \quad (5.21)$$

Similarly, equation 5.22 defines the lifetime of a GLV not partitioning to the aqueous phase, and is removed solely by the reaction with an oxidant in the gas phase only.

$$t_{life,g} = \frac{H_{d,X}}{k_g[\text{X}]_{aq}} \quad (5.22)$$

Equations 5.21 and 5.22 help virtually separate the gas-phase and aqueous-phase removal process of a GLV, from the overall combined removal of this GLV within the atmosphere.

Table 5.7 contains all the constants related to the GLVs studied within this work, required for the lifetime and removal calculations.

Table 5.7. Gas-phase rate constants of GLVs with atmospheric radicals at 298 K and dimensionless Henry's constant of GLVs and radicals.

GLV/radical	Gas-phase rate constants		Gas-phase rate constants		H_d
	$\text{cm}^3 \text{ molecule}^{-1} \text{ s}^{-1}$		$\text{L mol}^{-1} \text{ s}^{-1}$		
	k_{OH}	k_{NO_3}	k_{OH}	k_{NO_3}	
PENTOL	$6.7 \times 10^{-11, 12}$ $5.7 \times 10^{-11, 13}$	$13.9 \times 10^{-15, 14}$	3.7×10^{10}	8.4×10^6	2.5×10^3
HEXOL	$6.2 \times 10^{-11, 1}$	$1.6 \times 10^{-13, 15}$	3.7×10^{11}	9.4×10^7	3.3×10^3
HEXAL	$4.4 \times 10^{-11, 16}$	$1.2 \times 10^{-14, 16}$	2.6×10^{11}	6.1×10^6	2.5×10^2
$\cdot OH$					6.1×10^2
$NO_3\cdot$					14.7

*originally, the gas phase rate constants were reported in $\text{cm}^3 \text{ molecule}^{-1} \text{ s}^{-1}$ and were converted to $\text{L mol}^{-1} \text{ s}^{-1}$ for the convenience of present calculations.

The aqueous-phase radical concentrations (Table 5.8) and $LWC^{273, 447}$ used are typical for atmospheric systems.

Table 5.8. Aqueous-phase concentrations of $\cdot OH$, $NO_3\cdot$ and $SO_4\cdot^-$ radicals in various atmospheric systems from CAPRAM modeling.¹⁷

Radical	low		high		extremely high	
	mol L^{-1}		mol L^{-1}		mol L^{-1}	
$\cdot OH$	urban clouds	3.5×10^{-15}	maritime aerosol	1.0×10^{-13}	maritime clouds	2.0×10^{-12}
	remote clouds	2.2×10^{-14}	urban aerosol	4.4×10^{-13}	remote aerosol	3.0×10^{-12}
$NO_3\cdot$	remote clouds	5.1×10^{-15}	remote aerosol	3.5×10^{-13}		
	maritime aerosol	1.9×10^{-15}	urban clouds	1.4×10^{-13}		
	maritime clouds	6.9×10^{-15}	urban aerosol	8.6×10^{-14}		
$SO_4\cdot^-$	maritime clouds	2.3×10^{-15}	remote clouds	2.4×10^{-14}	remote aerosol	3.6×10^{-13}
	urban aerosol	9.3×10^{-15}	maritime aerosol	1.2×10^{-14}		
			urban clouds	1.1×10^{-14}		

5.5.1.1. GLV partitioning between gas- and aqueous phases

The equation 5.23 defines the partitioning of the reactants GLV and X between the gas- and aqueous-phase governed by Henry's Law equilibrium (Figure 5.8).

$$\frac{[GLV]_g}{[GLV]_{aq}} = \frac{[GLV]_g}{[GLV]_{aq}\omega} = \frac{1}{H_d\omega} \quad (5.23)$$

where: $[GLV]_{aq}$, is the aqueous phase GLV concentration per gas phase volume.

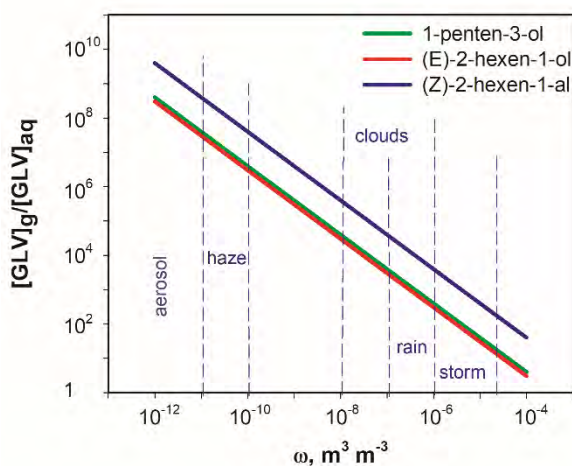


Figure 5.8. Gas-aqueous partitioning of GLV in various atmospheric systems.

Similar partitioning evaluation for the atmospheric radicals shows that the $\cdot\text{OH}$ and $\text{NO}_3\cdot$ predominantly reside in the gas phase, while the $\text{SO}_4\cdot^-$ radicals exclusively in the aqueous phase.

5.5.1.2. GLV lifetimes

The lifetimes of GLVs removed in the atmosphere due to the combined gas- and aqueous-phase reactions with $\cdot\text{OH}$ or $\text{NO}_3\cdot$ radicals (Equation 5.20b), at various liquid water contents (LWC ω) scenarios are shown in Figure 5.9. The apparent lifetimes of GLVs due to the gas-phase reactions with radicals only (Equation 5.22) are presented in Figure 5.10. For all cases with $\omega < 10^{-6}$, the aqueous-phase reaction does not influence much the overall lifetimes of the GLVs studied (Figure 5.9). Only on the extreme right-hand side of (Figure 5.9 at higher LWC, the aqueous-phase reactions significantly reduce the GLV lifetimes. The influence of the ω variable on HEXOL and HEXAL lifetimes due to reactions with $\cdot\text{OH}$ radicals is marginal. The GLV lifetimes due to reactions with $\text{SO}_4\cdot^-$, which occur only in the aqueous phase, decrease from years to hours with increasing ω and $[X]_{aq}$ (Equation 5.21, Figure 5.11).

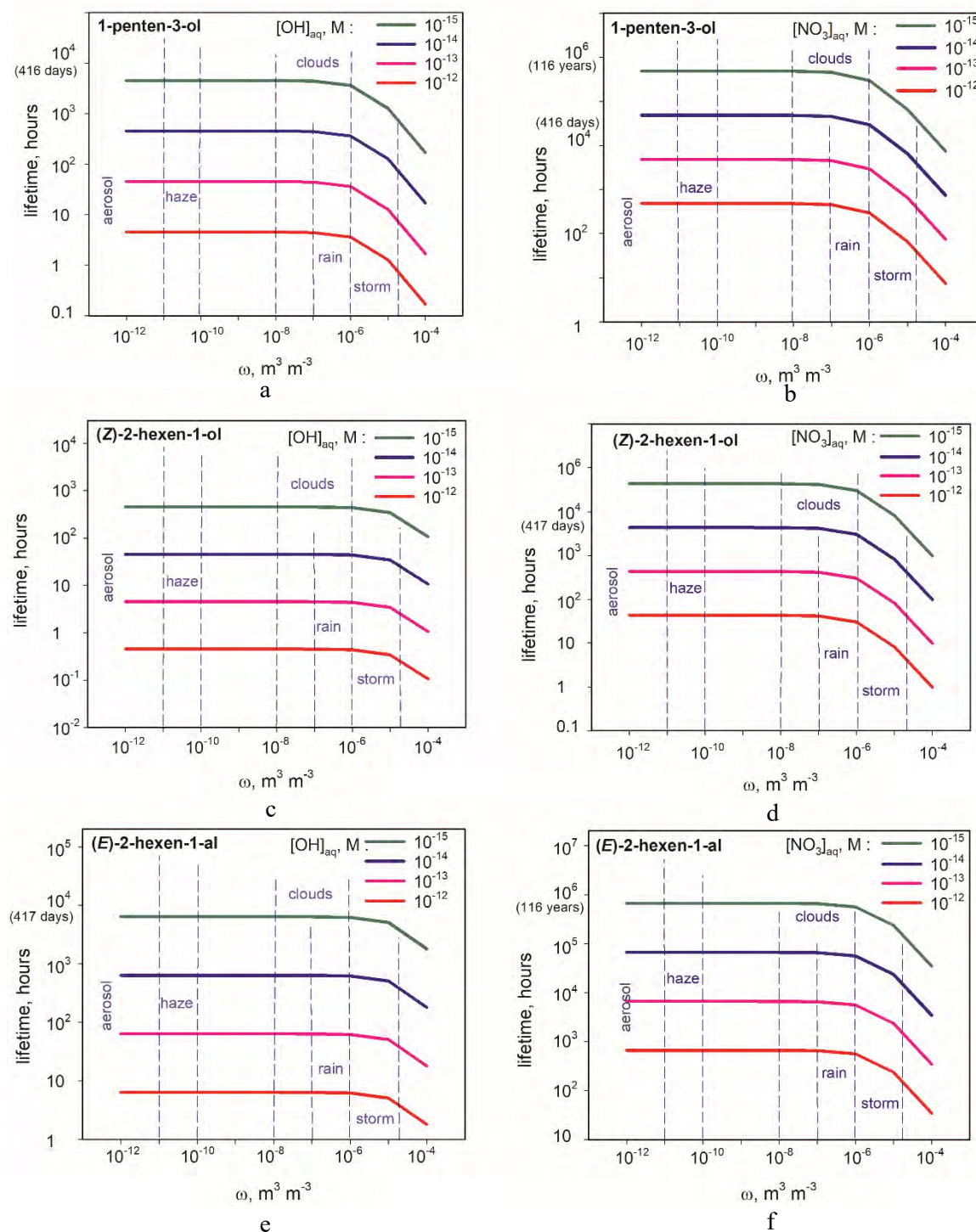


Figure 5.9. Atmospheric lifetimes (t) of GLVs due to combined removal by gas-phase and aqueous-phase reactions with 'OH (a, c, e) and NO_3 ' (b, d, f) radicals at various liquid water contents (ω).

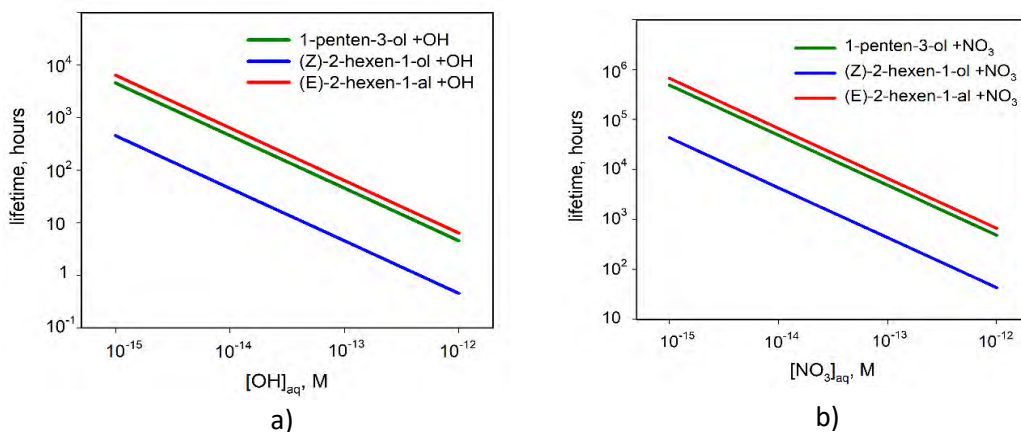


Figure 5.10. Apparent lifetimes of GLVs due to the gas-phase reactions only with (a) $\cdot\text{OH}$ and (b) $\text{NO}_3\cdot$.

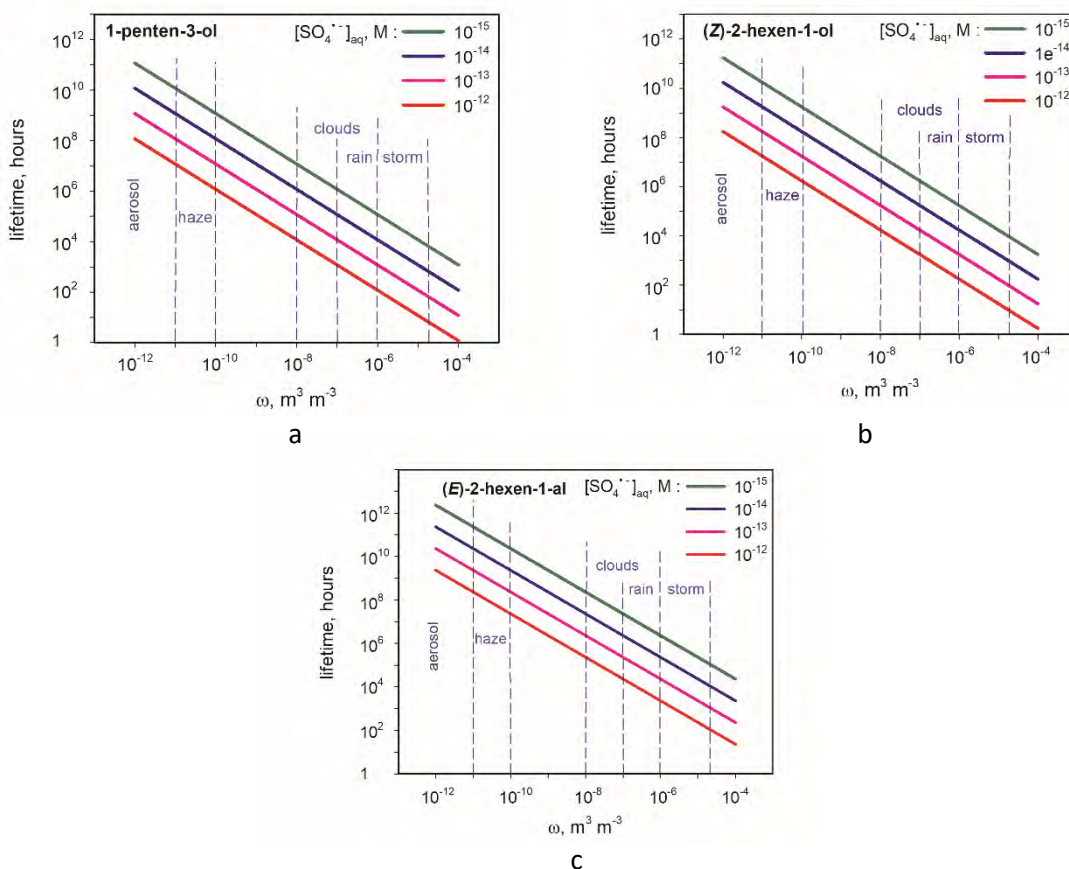


Figure 5.11. Atmospheric lifetimes of GLVs due to the aqueous-phase reactions with $\text{SO}_4\cdot^-$ at various liquid water contents (ω): (a) PENTOL, (b) HEXOL, (c) HEXAL.

5.5.2. GLV removal rates

GLV removal rates by reactions with radicals under various atmospheric conditions were estimated and compared as relative removal by gas- and aqueous-phase reactions, relative removal between the combined gas- and aqueous-phase reaction with radical X and aqueous-phase reaction with $\text{SO}_4^{\cdot-}$ radical, relative removal by two different radicals in the aqueous phase, and overall GLV removal scaled to be independent of the GLV concentrations.

The present Section 5.5.2 compares the GLV removal by gas-phase reactions and the aqueous-phase reactions with $\text{SO}_4^{\cdot-}$; combined gas- and aqueous phase reactions with $\cdot\text{OH}$ or NO_3^{\cdot} and aqueous-phase reactions with $\text{SO}_4^{\cdot-}$; aqueous-phase reactions with $\cdot\text{OH}$ or NO_3^{\cdot} and aqueous-phase reactions with $\text{SO}_4^{\cdot-}$. It also presents scaled GLV removal rates independent of GLV concentration in various atmospheric systems.

5.5.2.1. Gas-phase vs. aqueous-phase reactions

Comparison of atmospheric rate of GLV removal due to the gas-phase reaction with a radical X to the aqueous-phase reaction with $\text{SO}_4^{\cdot-}$ was carried out using equation 5.24.

$$\frac{r_{X,g}}{r_{\text{SO}_4,\text{aq}}\omega} = \frac{k_{X,g}}{k_{\text{SO}_4,\text{aq}}H_{d,X}H_{d,\text{GLV}}\omega} \cdot \frac{[X]_{\text{aq}}}{[\text{SO}_4^{\cdot-}]_{\text{aq}}} \quad (5.24)$$

The ratios calculated for various ω and radical proportions using equation 5.24 are shown in Figure 5.12. The aqueous-phase reactions of GLV with $\text{SO}_4^{\cdot-}$ dominate over the gas-phase reaction with $\cdot\text{OH}$ or NO_3^{\cdot} (the rate ratio below 1) only when $\text{SO}_4^{\cdot-}$ radicals are in excess and ω is high (Figure 5.12). For PENTOL, such conditions occur in storms when $[\cdot\text{OH}]/[\text{SO}_4^{\cdot-}] < 0.2$ and $[\text{NO}_3^{\cdot}]/[\text{SO}_4^{\cdot-}] < 20$, or in rains when $[\cdot\text{OH}]/[\text{SO}_4^{\cdot-}] < 0.01$ and $[\text{NO}_3^{\cdot}]/[\text{SO}_4^{\cdot-}] < 10$, or in rains and clouds when $[\text{NO}_3^{\cdot}]/[\text{SO}_4^{\cdot-}] < 1$. For HEXOL, the conditions are $[\cdot\text{OH}]/[\text{SO}_4^{\cdot-}] < 0.01$ and $[\text{NO}_3^{\cdot}]/[\text{SO}_4^{\cdot-}] < 10$ in storms, and $[\text{NO}_3^{\cdot}]/[\text{SO}_4^{\cdot-}] < 0.01$ in clouds and rains. For HEXAL the conditions are $[\cdot\text{OH}]/[\text{SO}_4^{\cdot-}] < 0.01$ and $[\text{NO}_3^{\cdot}]/[\text{SO}_4^{\cdot-}] < 1$ in storms, or $[\text{NO}_3^{\cdot}]/[\text{SO}_4^{\cdot-}] < 0.01$ in clouds and rains.

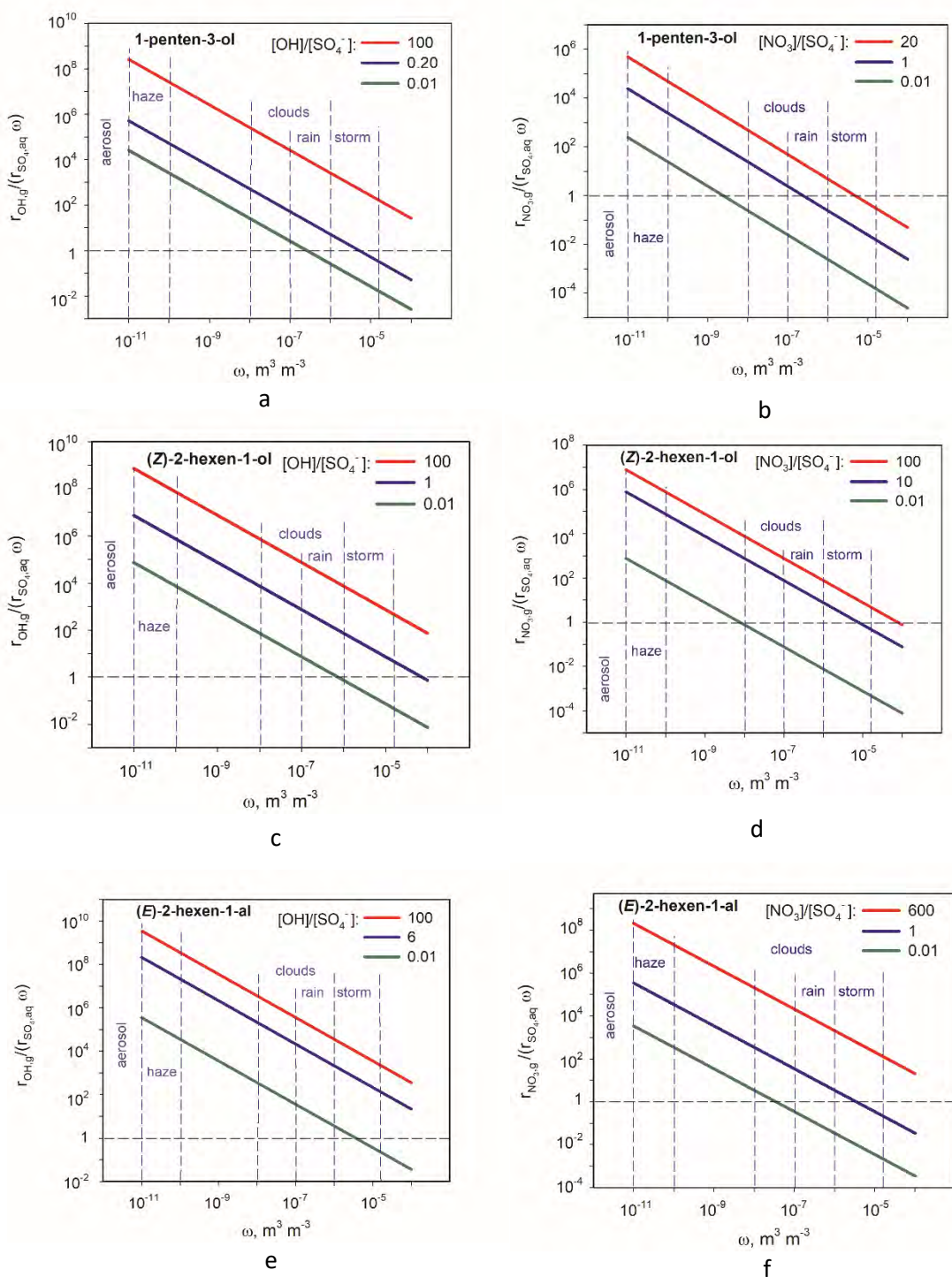


Figure 5.12. Influence of the liquid water contents (ω) and radical ratios on the relative rates of GLV removal from the atmosphere by gas-phase reactions with $\cdot\text{OH}$ (a,c,e) or $\text{NO}_3\cdot$ (b,d,f) and by the aqueous-phase reactions with $\text{SO}_4^{\cdot-}$ defined by Equation (5.24).

5.5.2.2. Relative GLV removal rates.

Equation 5.25 compares the GLV removal by combined gas- and aqueous-phase reaction with radical X ($\cdot\text{OH}$ and $\text{NO}_3\cdot$) to the reaction with $\text{SO}_4^{\cdot-}$ in the aqueous phase.

$$\frac{r_{X,g} + r_{X,aq}\omega}{r_{\text{SO}_4,aq}\omega} = \frac{\frac{k_{X,g}}{H_{d,X}H_{d,GLV}} + k_{X,aq}\omega}{k_{\text{SO}_4,aq}\omega} \cdot \frac{[X]_{aq}}{[\text{SO}_4^{\cdot-}]_{aq}} \quad (5.25)$$

The ratios calculated for various ω and radical proportions using equation 5.25 are shown in Figure 5.13. The aqueous-phase reactions of GLV with $\text{SO}_4^{\cdot-}$ dominate over the combined gas-phase and aqueous-phase reaction with $\cdot\text{OH}$ or $\text{NO}_3\cdot$ (the rate ratio below 1) only when $\text{SO}_4^{\cdot-}$ radicals are in excess and ω is high (Figure 5.13). For PENTOL, such conditions occur in clouds, rains and storms when $[\cdot\text{OH}]/[\text{SO}_4^{\cdot-}] < 0.01$, or $[\text{NO}_3\cdot]/[\text{SO}_4^{\cdot-}] < 1$ (Figures 5.13a,b). For HEXOL the conditions are: $[\cdot\text{OH}]/[\text{SO}_4^{\cdot-}] < 0.01$, or $[\text{NO}_3\cdot]/[\text{SO}_4^{\cdot-}] < 1$ in storms (Figure 5.13c,d), and $[\text{NO}_3\cdot]/[\text{SO}_4^{\cdot-}] < 0.01$ in clouds and rains. For HEXAL the conditions are: $[\cdot\text{OH}]/[\text{SO}_4^{\cdot-}] < 0.01$ and $[\text{NO}_3\cdot]/[\text{SO}_4^{\cdot-}] < 1$ in storms (Figure 5.13e,f), and $[\text{NO}_3\cdot]/[\text{SO}_4^{\cdot-}] < 0.01$ in clouds and rains (Figure 5.13f).

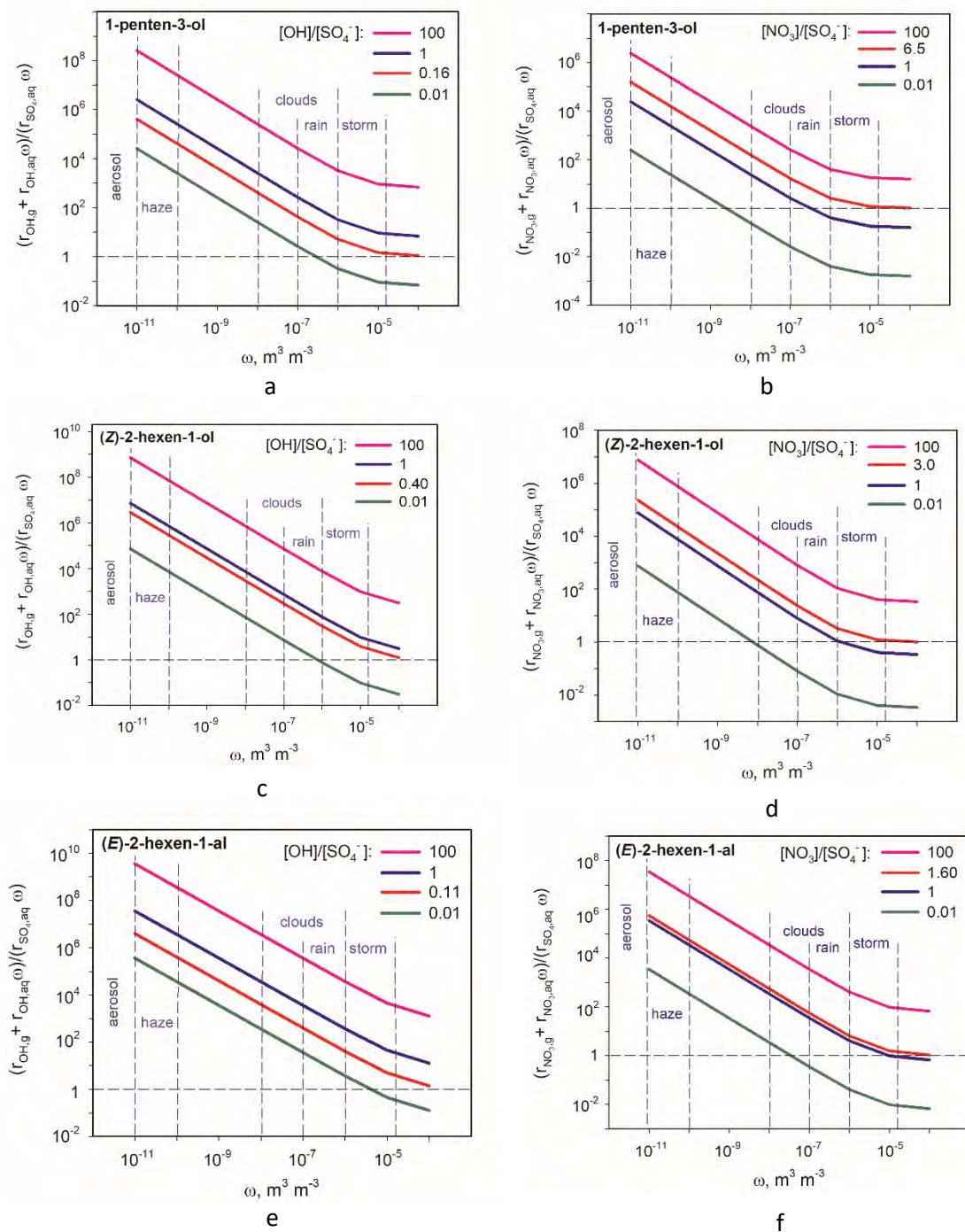


Figure 5.13. Influence of the liquid water contents (ω) and radical ratios on the relative rates of GLV removal from the atmosphere by combined gas-phase and aqueous-phase reactions with $\cdot\text{OH}$ (a,c,e) or $\text{NO}_3\cdot$ (b,d,f) and by the aqueous-phase reactions with $\text{SO}_4^{\cdot-}$.

5.5.2.3. GLV removal rates – aqueous-phase reactions

The atmospheric removal of GLV due to the aqueous-phase reaction by radical X is compared to that reaction with $\text{SO}_4^{\bullet-}$ using equation 5.26.

$$\frac{r_{X,aq}}{r_{\text{SO}_4,aq}} = \frac{k_{X,aq}}{k_{\text{SO}_4,aq}} \cdot \frac{[X]_{aq}}{[\text{SO}_4^{\bullet-}]_{aq}} \quad (5.26)$$

The relative rate ratios calculated using equation 5.26 for various radical ratios are shown in Figure 5.14. For PENTOL, the aqueous-phase reaction with $\text{SO}_4^{\bullet-}$ dominates over that with $\cdot\text{OH}$ radicals if $[\cdot\text{OH}]/[\text{SO}_4^{\bullet-}] < 0.15$, and over the reaction with NO_3^{\bullet} if $[\text{NO}_3^{\bullet}]/[\text{SO}_4^{\bullet-}] < 9$ (Figure 5.14a). For HEXOL, the aqueous-phase reaction with $\text{SO}_4^{\bullet-}$ dominates when $[\cdot\text{OH}]/[\text{SO}_4^{\bullet-}] < 0.8$ and $[\text{NO}_3^{\bullet}]/[\text{SO}_4^{\bullet-}] < 6$ (Figure 5.14b), and for HEXAL, on condition that $[\cdot\text{OH}]/[\text{SO}_4^{\bullet-}] < 0.11$ and $[\text{NO}_3^{\bullet}]/[\text{SO}_4^{\bullet-}] < 16$ (Figure 5.14c).

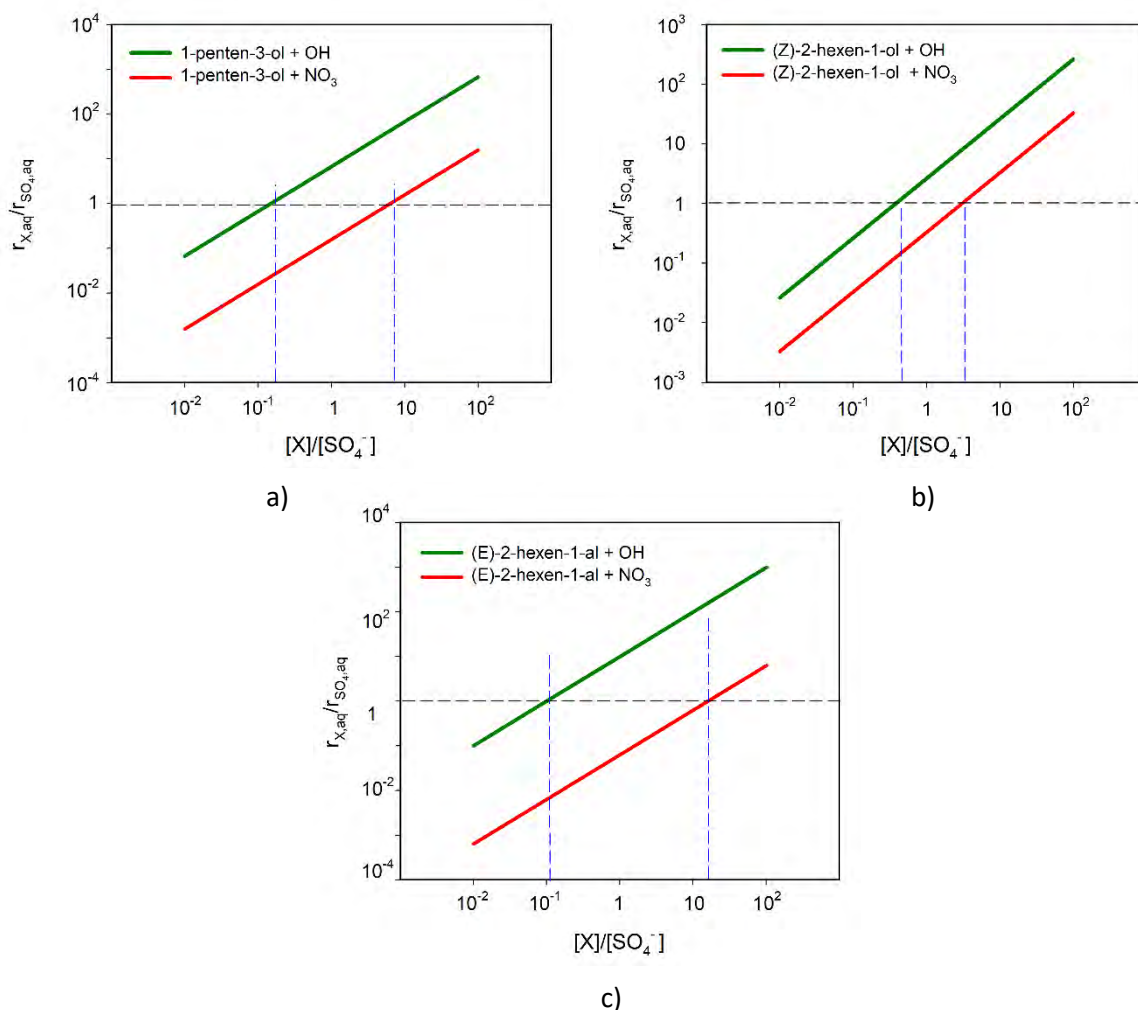


Figure 5.14. Influence of the radical ratio on the relative rates of GLVs removal from the atmosphere by the aqueous-phase reaction with $\cdot\text{OH}$ or $\text{NO}_3\cdot$ radicals and by the aqueous-phase reactions with $\text{SO}_4^{\cdot-}$ radical-anions: (a) PENTOL, (b) HEXOL, (c) HEXAL (Equation 5.34).

5.5.2.4. Scaled GLV removal rates

Equations 5.15 – 5.18 were used to calculate the scaled removal rates of GLVs independent of their concentrations: due to the overall gas- and aqueous-phase reactions of PENTOL, HEXOL, and HEXAL with $\cdot\text{OH}$, $\text{NO}_3\cdot$, and $\text{SO}_4^{\cdot-}$ under various conditions, such as dry air, urban clouds, remote clouds, and urban aerosol (Table 5.9). All data required for the calculations are provided in Tables 5.2 – 5.4, 5.7, and 5.8.

Table 5.9. Scaled removal rates of GLV from the atmosphere due to the gas-phase and aqueous-phase reactions with $\cdot\text{OH}$, $\text{NO}_3\cdot$ and $\text{SO}_4\cdot^-$ at 298 K $\left(\frac{-1}{[\text{GLV}]_g} \frac{d[\text{GLV}]_g}{dt}\right)$.

System	Sink	ω	Scaled removal rates, s^{-1}		
		$\text{m}^3 \text{m}^{-3}$	PENTOL	HEXOL	HEXAL
Urban clouds	Gas-phase reactions	0	3×10^{-7}	3×10^{-6}	2×10^{-6}
	Aqueous-phase reactions	1×10^{-8}	1×10^{-9}	6×10^{-9}	6×10^{-11}
Remote clouds	Gas-phase reactions	0	1×10^{-6}	1×10^{-5}	1×10^{-5}
	Aqueous-phase reactions	1×10^{-8}	4×10^{-9}	7×10^{-9}	3×10^{-10}
Urban aerosol	Gas-phase reactions	0	3×10^{-5}	2×10^{-4}	2×10^{-4}
	Aqueous-phase reactions	1×10^{-12}	7×10^{-12}	1×10^{-11}	5×10^{-13}

Fluxes of PENTOL and HEXOL removed in urban and remote cloud systems of high ω *via* aqueous-phase reactions are comparable to those removed *via* gas-phase reactions. However, fluxes of HEXAL removed *via* gas-phase reactions were higher by orders of magnitude in all clouds and urban aerosol.

5.6. Conclusions

The second-order rate constants, $k_{2\text{nd}}$ determined in the present thesis for the aqueous-phase reactions of GLV with radicals are of the order 10^9 ($\cdot\text{OH}$), 10^8 ($\text{SO}_4\cdot^-$), and 10^7 ($\text{NO}_3\cdot$) $\text{L mol}^{-1} \text{s}^{-1}$ at 298 K. Exceptionally, $k_{2\text{nd}}$ for the reaction of (*Z*)-2-hexen-1-ol with $\text{NO}_3\cdot$ was larger than with $\text{SO}_4\cdot^-$. Of the three GLVs studied, (*Z*)-2-hexen-1-ol appeared to react the fastest. The plausible explanation is two allylic positions available in (*Z*)-2-hexen-1-ol for the hydrogen abstraction versus only one such position in 1-penten-3-ol, and (*E*)-2-hexen-1-ol. More mechanistic details for GLV reactions with $\cdot\text{OH}$ are discussed in Chapter 7. The differences in the rate constants are more prominent for GLV reactions with $\text{SO}_4\cdot^-$ and $\text{NO}_3\cdot$, which are more chemically controlled, than for reactions with $\cdot\text{OH}$, which are partially diffusion-controlled.

Table 5.10 compares the determined rate constants and activation energies for reactions with $\cdot\text{OH}$ against those for other GLVs and structurally similar compounds.^{129, 273, 367} The aqueous-

phase reaction rate constants of the compounds in Table 5.10 range from 2×10^9 to 8.3×10^9 L mol⁻¹ s⁻¹ and the activation energies from 6 to 17 kJ mol⁻¹. Specifically, the present rate constants for 1-penten-3-ol, (Z)-2-hexen-1-ol, and (E)-2-hexen-1-al at 298 K are relatively close to those reported by Richards-Henderson et al. for (Z)-3-hexen-1-ol, (Z)-3-hexenyl acetate, 2-methyl-3-buten-2-ol and methyl jasmonate (Table 5.10).¹²⁹ The activation energies for structurally similar compounds methyl isobutyl ketone and isobutyraldehyde are also close to those determined within this study for GLVs (Table 5.10).

Table 5.10. Rate constants and activation energies for reactions of GLVs and structurally similar organic compounds with $\cdot\text{OH}$.

Compound	$k_{298\text{ K}}$	E_A	Method	Reference
	$10^9 \text{ L mol}^{-1} \text{ s}^{-1}$	kJ mol^{-1}		
(Z)-3-hexen-1-ol	5.3 ± 0.2	12 ± 0.3	a	37
(Z)-3-hexenyl acetate	8.3 ± 0.6	17 ± 2	a	37
2-methyl-3-butene-2-ol	7.3 ± 0.7	13 ± 2	a	37
methyl jasmonate	6.8 ± 0.5	15 ± 2	a	37
methyl salicylate	8.1 ± 0.6	14 ± 1	a	37
methyl isobutyl ketone	2.0 ± 0.2	10 ± 2	b	75
isobutyraldehyde	2.9 ± 1.0	6 ± 3	b	76
1-penten-3-ol	6.3 ± 0.1	13 ± 2	c	this work
(Z)-2-hexen-1-ol	6.7 ± 0.3	9 ± 2	c	this work
(E)-2-hexen-1-al	4.8 ± 0.3	12 ± 1	c	this work

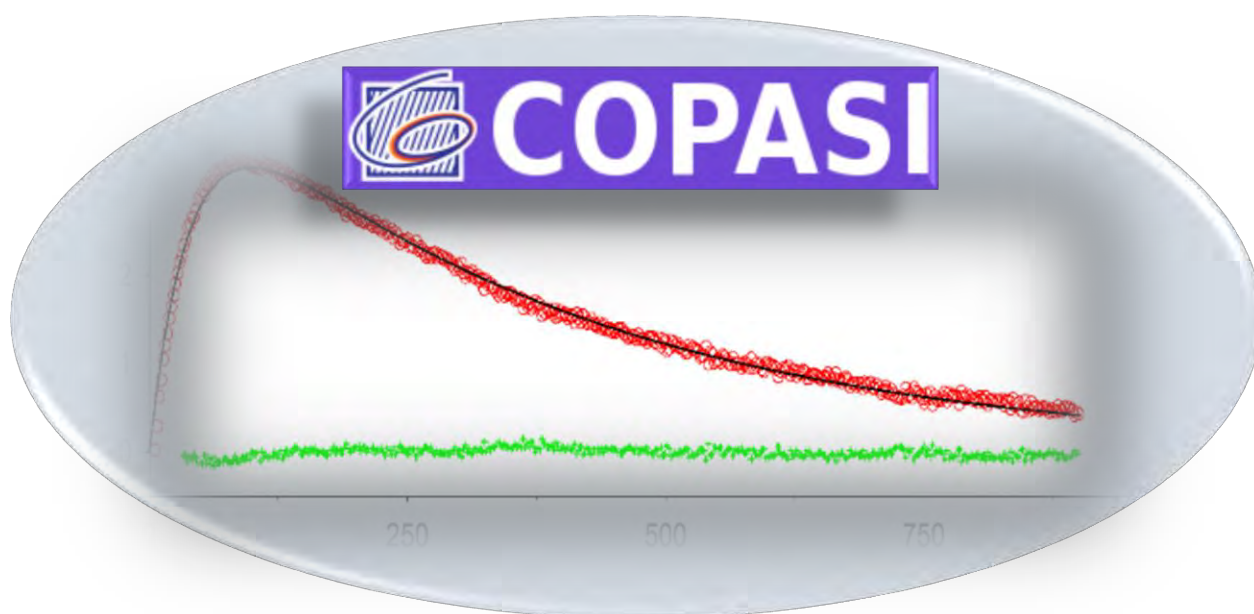
^a Competition kinetics; ^b Static photo reactor/Fenton for OH; ^c LFP-LLPA/photolysis of H₂O₂ (competition kinetic, reference compound SCN⁻)

The present study provided for the first time aqueous-phase rate constants of GLVs reactions with SO₄⁻ and NO₃⁻, so no literature data existed for comparison. However, a detailed review by Herrmann et al.^{273,367} and Neta and Huie⁴⁵⁸ include structurally similar compounds for comparison. For example, Schöne et al. provided the temperature-dependent kinetic data for the aqueous-phase reactions of methacrolein (MAC) and methyl vinyl ketone (MVK) with $\cdot\text{OH}$, SO₄⁻, and NO₃⁻.²⁹⁷

The rate constants for aqueous-phase reactions of MAC and MVK at 298 K were: $(9.4 \pm 0.7) \times 10^9$ L mol⁻¹ s⁻¹ and $(7.3 \pm 0.5) \times 10^9$ L mol⁻¹ s⁻¹ for •OH; $(9.9 \pm 4.9) \times 10^7$ L mol⁻¹ s⁻¹ and $(1.0 \pm 0.2) \times 10^8$ L mol⁻¹ s⁻¹ for SO₄•⁻; $(4.0 \pm 1.0) \times 10^7$ L mol⁻¹ s⁻¹ and $(9.7 \pm 3.4) \times 10^6$ L mol⁻¹ s⁻¹ for NO₃•, respectively. The order of magnitude of these rate constants is similar to the rate constants determined in the present study.

The studied aqueous-phase reactions of GLVs were evaluated for their atmospheric relevance or significance. They appeared negligible in deliquescent aerosol and haze water, and dominate only in systems with high liquid water contents, such as clouds, rains, and storms. With increasing liquid water content and the concentration of radicals in the atmospheric systems, the atmospheric lifetime of GLVs reduced from years or hundred days to a few minutes. The aqueous-phase reaction with SO₄•⁻ dominates over combined gas- and aqueous-phase reactions with •OH or NO₃• only when the system contains a sufficient excess of SO₄•⁻ and high liquid water content, such as in clouds, rains, or storms.

Chapter 6. Evaluating bias of the experimental rate constants determined for the aqueous-phase reactions of selected GLVs with NO_3 : COPASI kinetic modeling



*Results of the present chapter have been published in the form of a research article in **Environ. Sci. Technol.** 2021, 55, 20, 13666–13676. Sarang et al., 2021*

6.1. Introduction

The rate constants for GLV reactions with NO₃[•] were determined without accounting for a few reactions that could consume the radical. They included the reactions with ⁻OH, HO₂[•], H₂O, and S₂O₈²⁻, and autoxidation of alkyl compounds to ROO[•] radicals (Table 6.1). A complete kinetic model of GLV–NO₃[•] reactions was developed and analyzed using the COPASI software package³⁸⁴ to evaluate the bias in the rate constants determined (Section 6.2). Within COPASI, the reaction rate constants were estimated using the evolutionary programming method (number of generations 200, population size 20), while reaction time course simulations were performed using the deterministic ordinary differential equation solver (LSODA).^{384, 391, 392} Chapter 3 (Section 3.4.1) contains more details on COPASI software.

6.2. Complete kinetic model of GLV – NO₃[•] reactions

Table 6.1 contains the reactions and rate constants that constitute a complete kinetic model of GLV–NO₃[•] reactions (Model_1). Model_1 includes reactions 20 – 25 and 30, which are neglected while evaluating the experimental rate constants with the LFP-LLPA method (used in Chapter 5). The bias in the experimental rate constants resulted from additional consumption of NO₃[•] radicals by these reactions. Most of the temperature-dependent kinetic parameters required by Model_1 were available in the literature. A few missing rate constants (reactions (13), (15), (24), and (25)) were estimated within this work using COPASI (Section 6.2.1). The rate constants for reactions (26) and (32) were experimentally determined within this work.

Table 6.1. Model_1 – reactions with temperature-dependent rate constants.

No	Reaction	<i>k</i> (298 K)	References	<i>A</i>	<i>E_A</i>	Ref., <i>E_A</i> (calc./estd.)
				L mol ⁻¹ s ⁻¹	kJ mol ⁻¹	
1	H ₂ O ⇌ H ⁺ + OH ⁻	→ 0.0014 s ⁻¹ ← 1.4×10 ¹¹ L mol ⁻¹ s ⁻¹	⁴⁵⁹	→ 9.9×10 ⁹ ← 5.5×10 ¹³	73 15	⁴⁶⁰
2	H ₂ SO ₄ ⇌ H ⁺ + HSO ₄ ⁻	→ 5.0×10 ¹³ s ⁻¹ ← 5.0×10 ¹⁰ L mol ⁻¹ s ⁻¹	⁴⁶¹	-	-	-

Chapter 6. Evaluating bias of the experimental rate constants determined for the aqueous-phase reactions of selected GLVs with NO_3^-

**table 6.1 continued*

3	$\text{HSO}_4^- \rightleftharpoons \text{H}^+ + \text{SO}_4^{2-}$	$\rightarrow 1.0 \times 10^9 \text{ s}^{-1}$ $\leftarrow 1.0 \times 10^{11} \text{ L mol}^{-1} \text{ s}^{-1}$	461	-	-	-
4	$\text{HNO}_3 \rightleftharpoons \text{H}^+ + \text{NO}_3^-$	$\rightarrow 1.1 \times 10^{12} \text{ s}^{-1}$ $\leftarrow 5.0 \times 10^{10} \text{ L mol}^{-1} \text{ s}^{-1}$	461	-	-	-
5	$\text{HO}_2 \rightleftharpoons \text{H}^+ + \text{O}_2^-$	$\rightarrow 1.4 \times 10^6 \text{ s}^{-1}$ $\leftarrow 5.0 \times 10^{10} \text{ L mol}^{-1} \text{ s}^{-1}$	459	$\rightarrow 1.3 \times 10^9$ $\leftarrow 5.1 \times 10^{12}$	17 12	460
6	$\cdot\text{OH} + \cdot\text{OH} \rightarrow \text{H}_2\text{O}_2$	$3.6 \times 10^9 \text{ L mol}^{-1} \text{ s}^{-1}$	462	7.9×10^{10}	8	460
7	$\cdot\text{OH} + \text{H}_2\text{O}_2 \rightarrow \text{H}_2\text{O} + \text{HO}_2^\cdot$	$2.7 \times 10^7 \text{ L mol}^{-1} \text{ s}^{-1}$	293 K, 463	5.3×10^8	7	463
8	$\cdot\text{OH} + \text{HO}_2^\cdot \rightarrow \text{H}_2\text{O} + \text{O}_2^-$	$6.0 \times 10^9 \text{ L mol}^{-1} \text{ s}^{-1}$	462	8.2×10^{11}	12	462
9	$\cdot\text{OH} + \text{O}_2^- \rightarrow \text{OH}^- + \text{O}_2$	$1.1 \times 10^{10} \text{ L mol}^{-1} \text{ s}^{-1}$	463	2.9×10^{10}	2	460
10	$\cdot\text{OH} + \text{HSO}_4^- \rightarrow \text{SO}_4^{\cdot-} + \text{H}_2\text{O}$	$3.5 \times 10^5 \text{ L mol}^{-1} \text{ s}^{-1}$	464	2.0×10^7	10	c
11	$\text{SO}_4^{\cdot-} + \text{H}_2\text{O} \rightarrow \cdot\text{OH} + \text{HSO}_4^-$	$7.9 \text{ L mol}^{-1} \text{ s}^{-1}$	464	4.1×10^3	16	465
12	$\text{SO}_4^{\cdot-} + \text{HNO}_3 \rightarrow \text{NO}_3^\cdot + \text{HSO}_4^-$	$5.5 \times 10^5 \text{ L mol}^{-1} \text{ s}^{-1}$	466	1.0×10^8	13	373
13	$\text{SO}_4^{\cdot-} + \text{NO}_3^- \rightarrow \text{NO}_3^\cdot + \text{SO}_4^{2-}$	$9.0 \times 10^4 \text{ L mol}^{-1} \text{ s}^{-1}$ $9.2 \times 10^4 \text{ L mol}^{-1} \text{ s}^{-1}$	467 *	4.1×10^8	21	*Table 6.2
14	$\text{SO}_4^{\cdot-} + \text{HO}_2^\cdot \rightarrow \text{HSO}_4^- + \text{O}_2$	$3.5 \times 10^9 \text{ L mol}^{-1} \text{ s}^{-1}$	468	5.2×10^9	1	373
15	$\text{SO}_4^{\cdot-} + \text{S}_2\text{O}_8^{2-} \rightarrow \text{S}_2\text{O}_8^{\cdot-} + \text{SO}_4^{2-}$	$1.0 \times 10^4 \text{ L mol}^{-1} \text{ s}^{-1}$ $1.4 \times 10^4 \text{ L mol}^{-1} \text{ s}^{-1}$	465 *	2.2×10^6	-60	*Table 6.3
16	$\text{SO}_4^{\cdot-} + \cdot\text{OH} \rightarrow \text{HSO}_5^-$	$1.0 \times 10^{10} \text{ L mol}^{-1} \text{ s}^{-1}$	469	1.5×10^{10}	1	373
17	$\text{SO}_4^{\cdot-} + \text{SO}_4^{\cdot-} \rightarrow \text{S}_2\text{O}_8^{2-}$	$2.0 \times 10^8 \text{ L mol}^{-1} \text{ s}^{-1}$	465	4.0×10^8	2	465
18	$\text{SO}_4^{\cdot-} + \text{HSO}_5^- \rightarrow \text{HSO}_4^- + \text{SO}_5^-$	$1.0 \times 10^5 \text{ L mol}^{-1} \text{ s}^{-1}$	470	1.9×10^7	13	373
19	$\text{SO}_4^{\cdot-} + \text{OH}^- \rightarrow \text{SO}_4^{2-} + \cdot\text{OH}$	$1.4 \times 10^7 \text{ L mol}^{-1} \text{ s}^{-1}$	471	1.8×10^9	12	373
20	$\text{NO}_3^\cdot + \text{NO}_3^\cdot \rightarrow \text{N}_2\text{O}_6$	$3.0 \times 10^7 \text{ L mol}^{-1} \text{ s}^{-1}$	472	6.0×10^7	2	d
21	$\text{NO}_3^\cdot + \text{OH}^- \rightarrow \cdot\text{OH} + \text{NO}_3^-$	$8.2 \times 10^7 \text{ L mol}^{-1} \text{ s}^{-1}$	467	1.0×10^{10}	12	d
22	$\text{NO}_3^\cdot + \text{H}_2\text{O} \rightarrow \cdot\text{OH} + \text{HNO}_3$	$0.9 \text{ M}^{-1} \text{ s}^{-1}$	273	4.7×10^2	16	d
23	$\text{NO}_3^\cdot + \text{HO}_2^\cdot \rightarrow \text{NO}_3^- + \text{H}^+ + \text{O}_2$	$3.0 \times 10^9 \text{ L mol}^{-1} \text{ s}^{-1}$	468	4.5×10^9	1	d
24	$\text{NO}_3^\cdot + \text{S}_2\text{O}_8^{2-} \rightarrow \text{NO}_3^- + \text{S}_2\text{O}_8^{\cdot-}$	$1.0 \times 10^4 \text{ L mol}^{-1} \text{ s}^{-1}$ $1.0 \times 10^4 \text{ L mol}^{-1} \text{ s}^{-1}$	465 *	3.6×10^7	27	*Table 6.4

Chapter 6. Evaluating bias of the experimental rate constants determined for the aqueous-phase reactions of selected GLVs with NO₃[•]

**table 6.1 continued*

25	NO ₃ [•] → products	47 ± 19 s ⁻¹	*Table 6.5	-	-	-
26a	SO ₄ ⁻ + PENTOL → PENTOL alkyl	9.4 × 10 ⁸ L mol ⁻¹ s ⁻¹	*Table 5.2	7.9 × 10 ⁹	5	*Table 5.5
26b	SO ₄ ⁻ + HEXOL → HEXOL alkyl	2.5 × 10 ⁹ L mol ⁻¹ s ⁻¹	*Table 5.2	1.1 × 10 ¹¹	10	*Table 5.5
26c	SO ₄ ⁻ + HEXAL → HEXAL alkyl	4.8 × 10 ⁸ L mol ⁻¹ s ⁻¹	*Table 5.2	2.9 × 10 ⁹	5	*Table 5.5
27	GLV alkyl + O ₂ → GLV peroxy	2.0 × 10 ⁹ L mol ⁻¹ s ⁻¹	⁴⁷³	8.5 × 10 ¹¹	15	²⁹¹
28	2 GLV peroxy → GLV p	1.6 × 10 ⁸ L mol ⁻¹ s ⁻¹	⁴⁷⁴	5.9 × 10 ⁸	3	⁴⁷⁵
29	[•] OH + GLV peroxy → GLV p1	9.6 × 10 ¹⁰ L mol ⁻¹ s ⁻¹	b, ⁴⁷⁶	1.4 × 10 ¹¹	1	³⁷³
30	NO ₃ [•] + GLV peroxy → GLV p2	1.2 × 10 ⁹ L mol ⁻¹ s ⁻¹	b, ⁴⁷⁷	1.8 × 10 ⁹	1	³⁷³
31	SO ₄ ⁻ + GLV peroxy → GLV p3	3.5 × 10 ⁹ L mol ⁻¹ s ⁻¹	a, ⁴⁶⁸	5.2 × 10 ⁹	1	³⁷³
32a	NO ₃ [•] + PENTOL → PENTOL alkyl2	1.5 × 10 ⁸ L mol ⁻¹ s ⁻¹	*Table 5.4	1.5 × 10 ¹¹	17	*Table 5.5
32b	NO ₃ [•] + HEXOL → HEXOL alkyl2	8.4 × 10 ⁸ L mol ⁻¹ s ⁻¹	*Table 5.4	3.8 × 10 ¹⁰	9	*Table 5.5
32c	NO ₃ [•] + HEXAL → HEXAL alkyl2	3.0 × 10 ⁷ L mol ⁻¹ s ⁻¹	*Table 5.4	3.2 × 10 ¹⁰	17	*Table 5.5

^a adopted from the reaction of SO₄⁻ with HO₂[•]; ^b adopted from gas-phase reactions of RO₂[•] radicals, *This work; ^c an average of the activation energy of reaction 7 and 8; ^d E_a from corresponding reactions of SO₄⁻ radicals, and A values calculated using the rate constants at 298 K

6.2.1. Kinetic parameters for reactions (13), (15), (24), and (25) in Table 6.1

The temperature-dependent kinetic parameters for reactions (13), (15), (24), and (25), were estimated using the experimental data collected during the background runs without GLV added. The data were processed using an evolutionary algorithm (200 generations and population size 20) in COPASI software.



Chapter 6. Evaluating bias of the experimental rate constants determined for the aqueous-phase reactions of selected GLVs with NO₃[•]

Tables 6.2 – 6.5 show the estimated rate constants at various temperatures, which were used to derive the corresponding Arrhenius Equations 6.1 – 6.3, (also Figures 6.1 – 6.3), respectively. The values calculated from these equations were used in Model_1 for the bias calculations.

Table 6.2. The temperature-dependent rate constants for reaction (13).

SO ₄ ^{•-} + NO ₃ [•] → NO ₃ [•] + SO ₄ ²⁻ (13)				
k (L mol ⁻¹ s ⁻¹)				
278 K	288 K	298 K	308 K	318 K
4.5×10 ⁴	6.4×10 ⁴	9.0×10 ⁴	1.2×10 ⁵	1.7×10 ⁵
6.7×10 ⁴	8.4×10 ⁴	9.1×10 ⁴	8.4×10 ⁴	-
5.4×10 ⁴	7.0×10 ⁴	9.5×10 ⁴	1.5×10 ⁵	1.9×10 ⁵
Average				
(5.5 ± 1.1)×10 ⁴	(7.3 ± 1.0)×10 ⁴	(9.2 ± 0.3)×10 ⁴	(1.2 ± 0.3)×10 ⁵	(1.8 ± 0.1)×10 ⁵

$$k(T) = 4.1 \times 10^8 \exp\left(-\frac{2490 \pm 210}{T}\right) \text{ L mol}^{-1} \text{ s}^{-1} \quad (6.1)$$

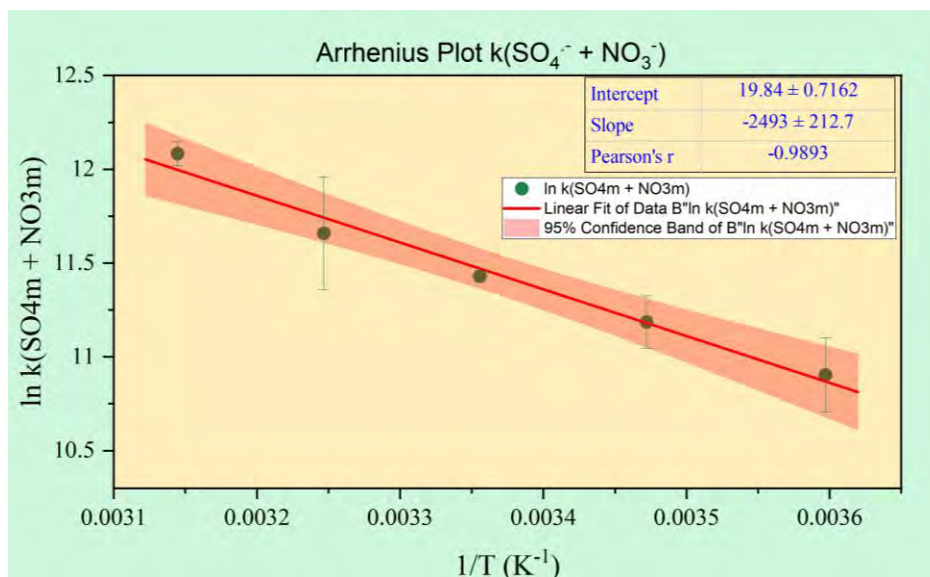


Figure 6.1. Arrhenius plot for reaction SO₄^{•-} + NO₃[•] → NO₃[•] + SO₄²⁻ (13)

Table 6.3. The temperature-dependent rate constants for reaction (15).

$\text{SO}_4^{\cdot-} + \text{S}_2\text{O}_8^{2-} \rightarrow \text{S}_2\text{O}_8^{\cdot-} + \text{SO}_4^{2-}$ (15)				
k ($\text{L mol}^{-1} \text{s}^{-1}$)				
278 K	288 K	298 K	308 K	318 K
5.0×10^4	8.0×10^4	2.2×10^4	1.0×10^4	6.0×10^3
5.0×10^4	5.0×10^4	1.0×10^4	1.0×10^3	-
7.6×10^4	5.0×10^4	1.0×10^4	1.0×10^4	2.0×10^3
Average				
$(5.9 \pm 1.5) \times 10^4$	$(6.0 \pm 1.7) \times 10^4$	$(1.4 \pm 0.7) \times 10^4$	$(7.0 \pm 5.2) \times 10^3$	$(4.0 \pm 2.8) \times 10^3$
$k(T) = 2.2 \times 10^6 \exp\left(-\frac{-7190 \pm 1230}{T}\right) \text{L mol}^{-1} \text{s}^{-1} \quad (6.2)$				

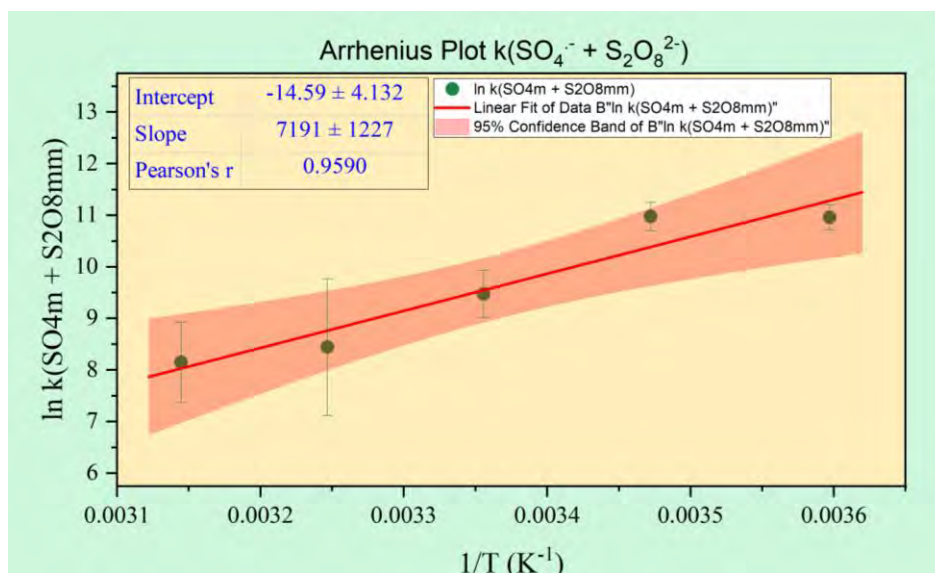


Figure 6.2. Arrhenius plot for reaction $\text{SO}_4^{\cdot-} + \text{S}_2\text{O}_8^{2-} \rightarrow \text{S}_2\text{O}_8^{\cdot-} + \text{SO}_4^{2-}$ (15).

Table 6.4. The temperature-dependent rate constants for reaction (24).

$\text{NO}_3^\bullet + \text{S}_2\text{O}_8^{2-} \rightarrow \text{NO}_3^- + \text{S}_2\text{O}_8^{\cdot-}$ (24)				
k ($\text{L mol}^{-1} \text{s}^{-1}$)				
278 K	288 K	298 K	308 K	318 K
2×10^3	3×10^3	1×10^4	1.6×10^4	4.0×10^4
2×10^3	4.4×10^3	1×10^4	1.8×10^3	-
2×10^3	6×10^3	1×10^4	1.6×10^4	3.0×10^4
Average				
2×10^3	$(4.5 \pm 2.5) \times 10^3$	1.0×10^4	$(1.7 \pm 0.8) \times 10^4$	$(3.5 \pm 2.1) \times 10^4$

$$k(T) = 3.6 \times 10^7 \exp\left(-\frac{3200 \pm 900}{T}\right) \text{L mol}^{-1} \text{s}^{-1} \quad (6.3)$$

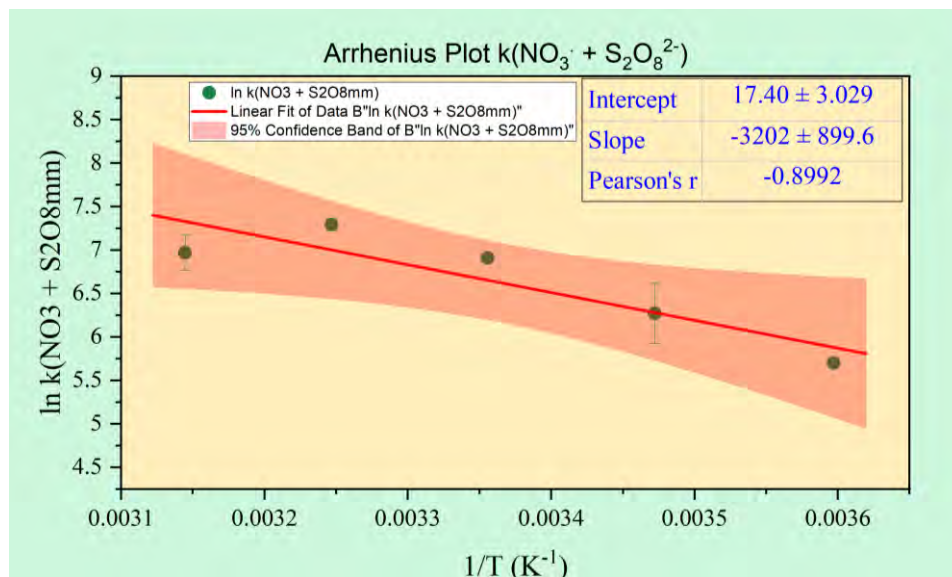


Figure 6.3. Arrhenius plot for reaction $\text{NO}_3^\bullet + \text{S}_2\text{O}_8^{2-} \rightarrow \text{NO}_3^- + \text{S}_2\text{O}_8^{\bullet-}$ (24).

In the case of reaction (25), describing the first-order decay of NO_3^\bullet radicals, no Arrhenius relation of the rate constants was observed. Instead, one rate constant value ($(47 \pm 19) \text{s}^{-1}$) averaged across the temperature range was used. The first-order decay of NO_3^\bullet radicals occurred in all blank experiments and could result from physical processes, such as wall loss. The share of that process was smaller than 10% of the total sink of NO_3^\bullet in background reactions without GLV added.

Table 6.5. The estimation of the rate constants for the first-order sink of NO_3^\bullet radicals.

$\text{NO}_3^\bullet \rightarrow \text{products}$					
Average k (s^{-1})					
278 K	288 K	298 K	308 K	318 K	278-318 K average
49	67	32	64	25	47 ± 19

6.3. GLV + NO_3^\bullet rate constant estimated using Model_1.

The second-order rate constants $k_{2\text{nd}}$, for the aqueous-phase reactions between GLV and NO_3^\bullet were estimated using the original data from LFP-LLPA experiments, Model_1 reaction set (Table 6.1), and the evolutionary programming algorithm in COPASI (number of generations 200, population size 20). Initial concentrations of reactants were 0.03 mol L^{-1} for $\text{S}_2\text{O}_8^{2-}$, 0.1 mol L^{-1} for NO_3^\bullet , (2.3

$\pm 0.1) \times 10^{-7} \text{ mol L}^{-1}$ for $\text{SO}_4^{\bullet-}$, and $(0 - 1) \times 10^{-4} \text{ mol L}^{-1}$ for GLV. The estimated rate constants are presented and analyzed in Section 6.4. The quality of fitting Model_1 with these constants to the original experimental data was good (Figures 6.4 – 6.16).

A) 1-penten-3-ol + NO_3^\bullet

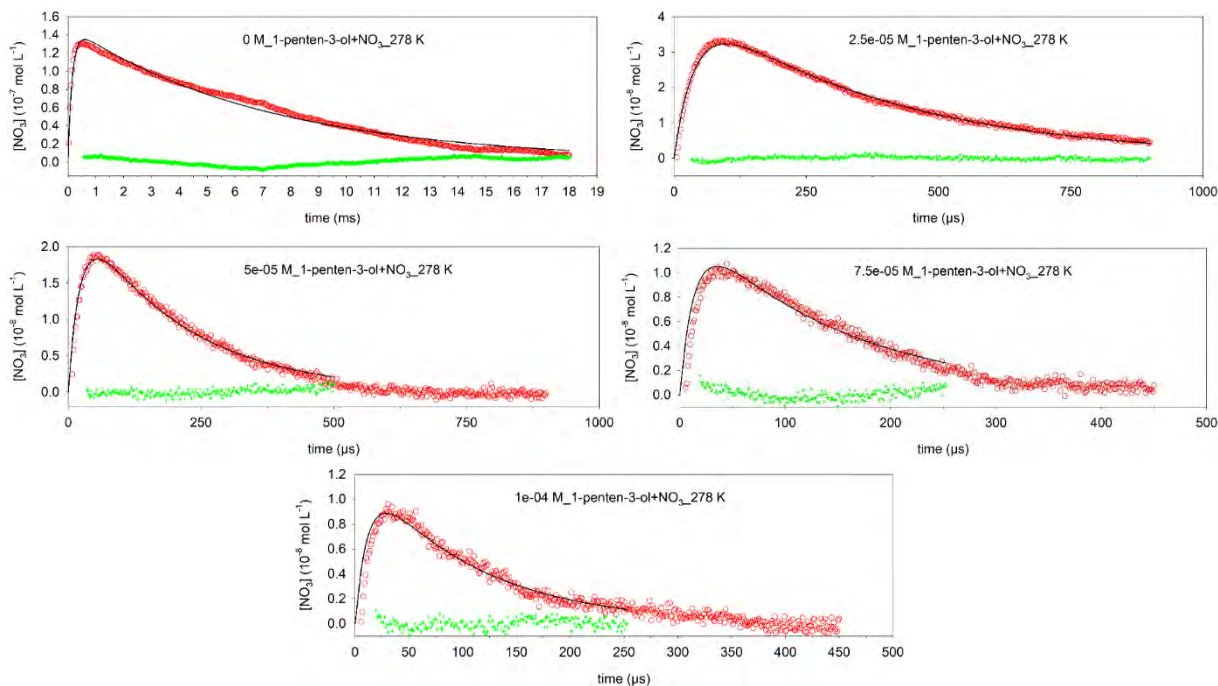


Figure 6.4. Concentration-time profiles of NO_3^\bullet in experiments at **278 K** and various initial concentrations of 1-penten-3-ol (specified in the legends). Experimental data points are red circles, simulations are black lines, and residuals are green crosses.

Chapter 6. Evaluating bias of the experimental rate constants determined for the aqueous-phase reactions of selected GLVs with NO_3^\bullet

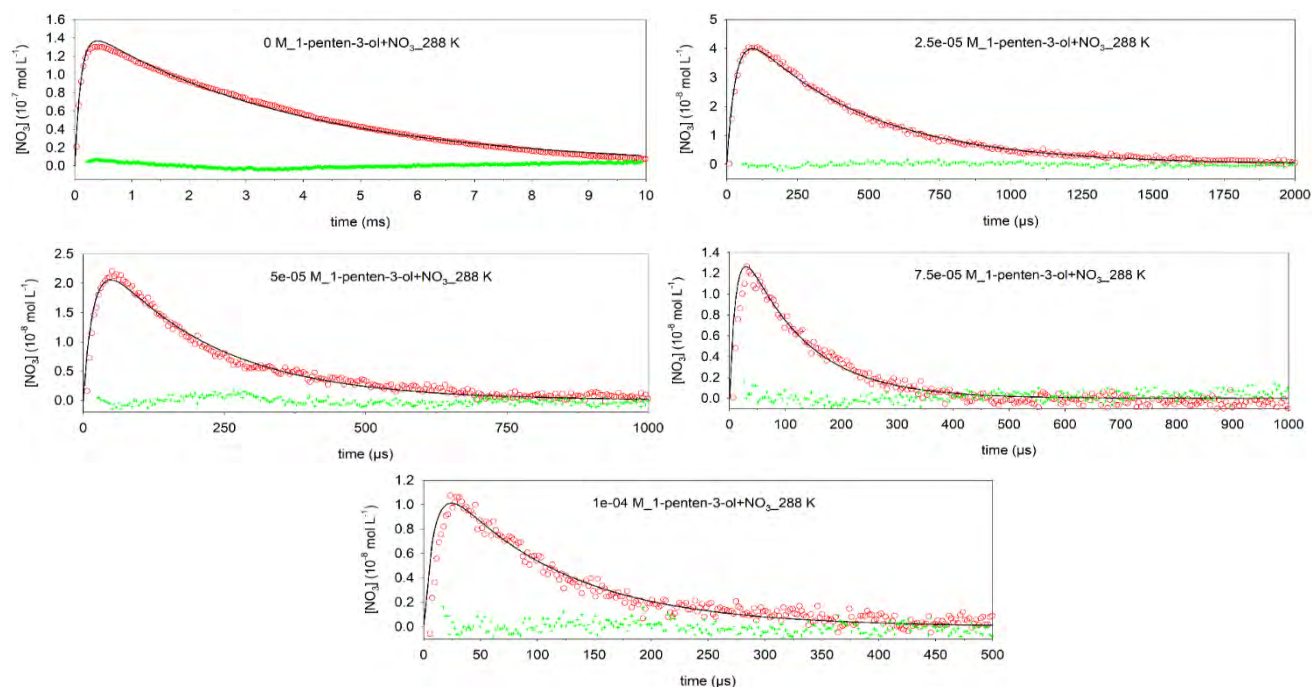


Figure 6.5. Concentration-time profiles of NO_3^\bullet in experiments at 288 K and various initial concentrations of 1-penten-3-ol (specified in the legends). Experimental data points are red circles, simulations are black lines, and residuals are green crosses.

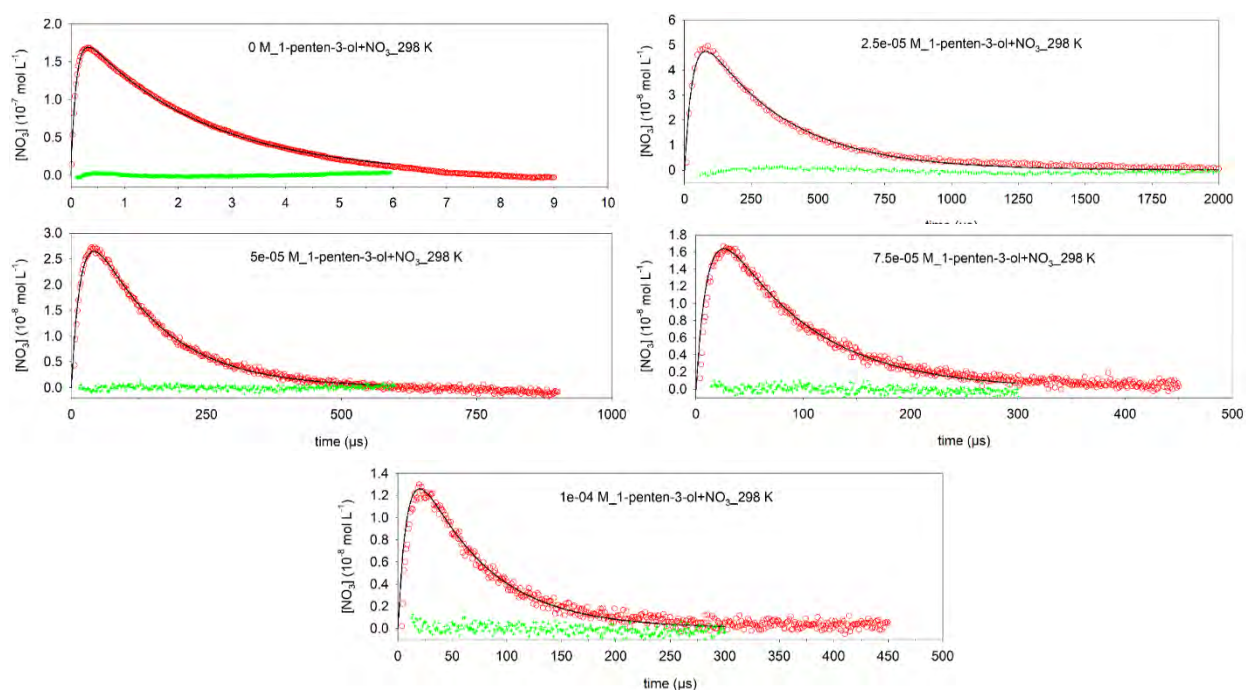


Figure 6.6. Concentration-time profiles of NO_3^\bullet in experiments at 298 K and various initial concentrations of 1-penten-3-ol (specified in the legends). Experimental data points are red circles, simulations are black lines, and residuals are green crosses.

Chapter 6. Evaluating bias of the experimental rate constants determined for the aqueous-phase reactions of selected GLVs with NO_3^\bullet

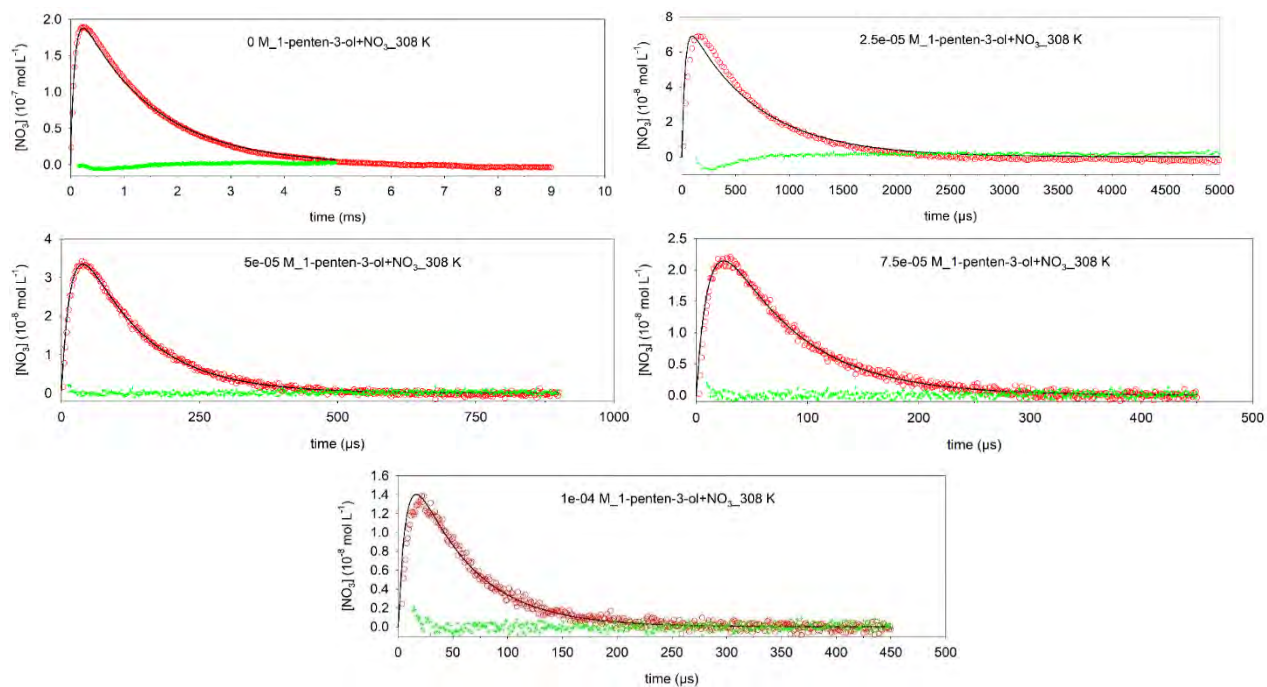


Figure 6.7. Concentration-time profiles of NO_3^\bullet in experiments at **308 K** and various initial concentrations of 1-penten-3-ol (specified in the legends). Experimental data points are red circles, simulations are black lines, and residuals are green crosses.

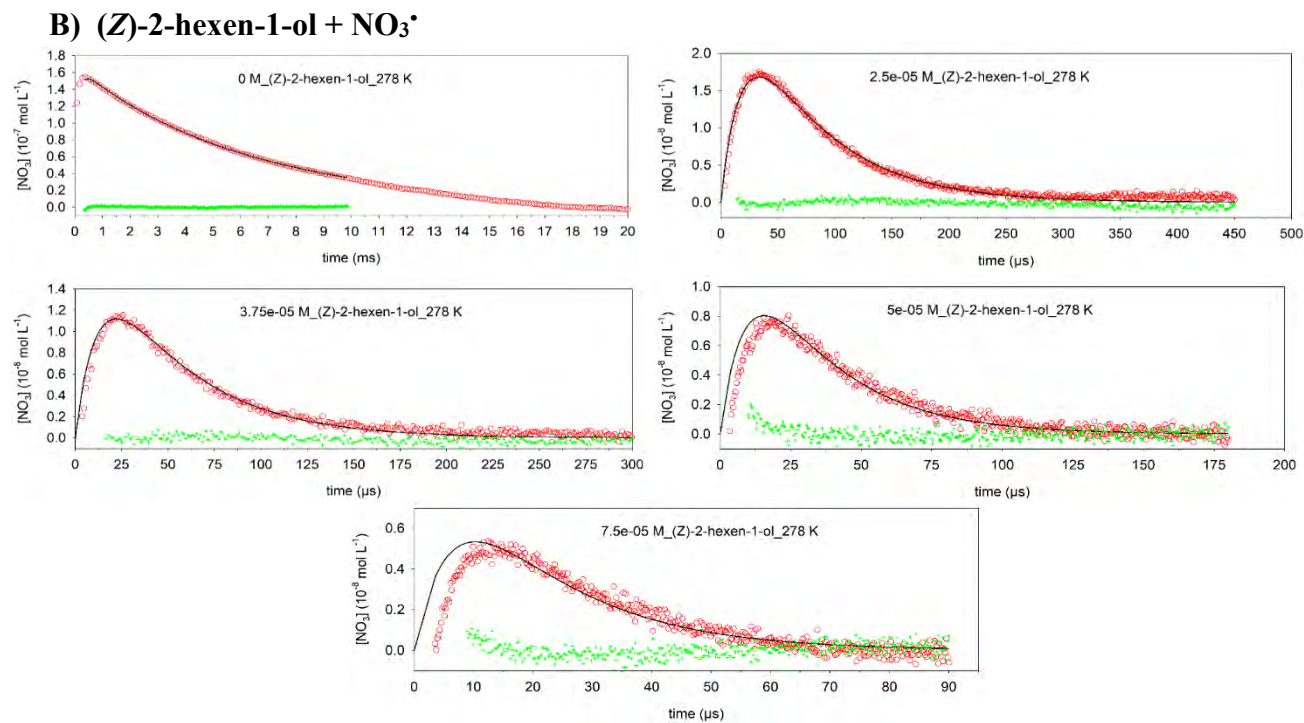


Figure 6.8. Concentration-time profiles of NO_3^\bullet in experiments at **278 K** and various initial concentrations of (Z)-2-hexen-1-ol (specified in the legends). Experimental data points are red circles, simulations are black lines, and residuals are green crosses.

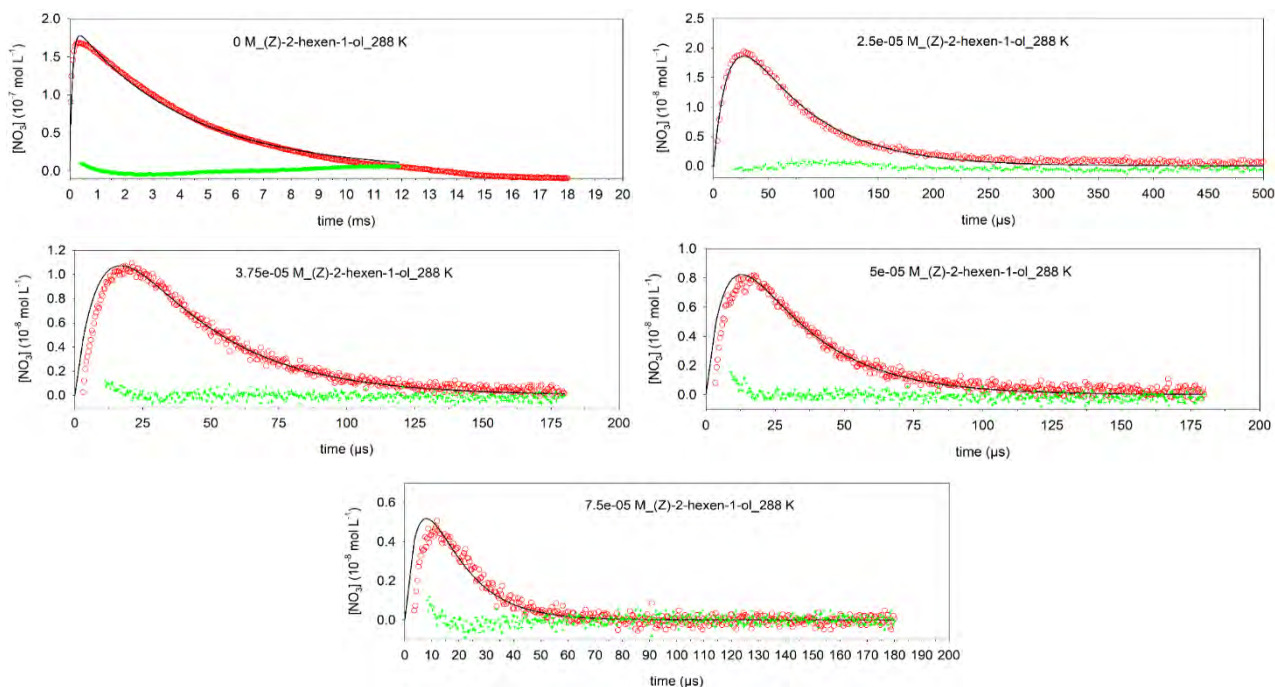


Figure 6.9. Concentration-time profiles of NO_3^\bullet in experiments at **288 K** and various initial concentrations of (Z)-2-hexen-1-ol (specified in the legends). Experimental data points are red circles, simulations are black lines, and residuals are green crosses.

Chapter 6. Evaluating bias of the experimental rate constants determined for the aqueous-phase reactions of selected GLVs with NO_3^\bullet

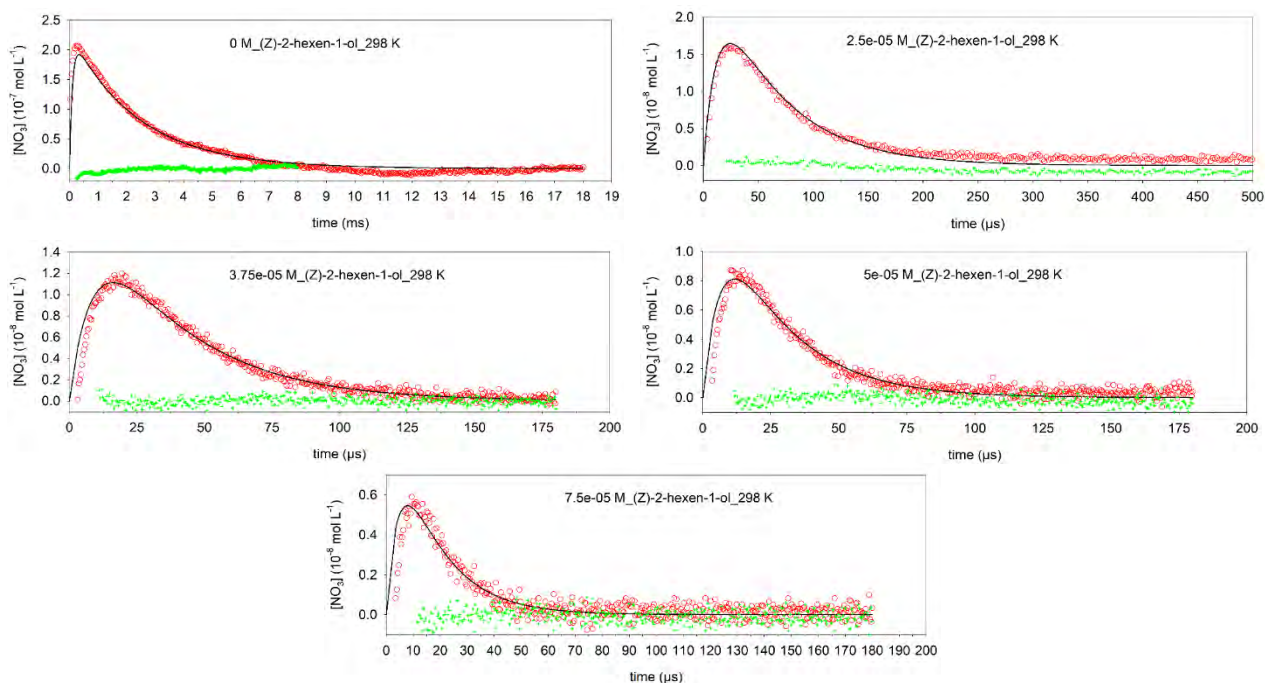


Figure 6.10. Concentration-time profiles of NO_3^\bullet in experiments at **298 K** and various initial concentrations of (Z)-2-hexen-1-ol (specified in the legends). Experimental data points are red circles, simulations are black lines, and residuals are green crosses.

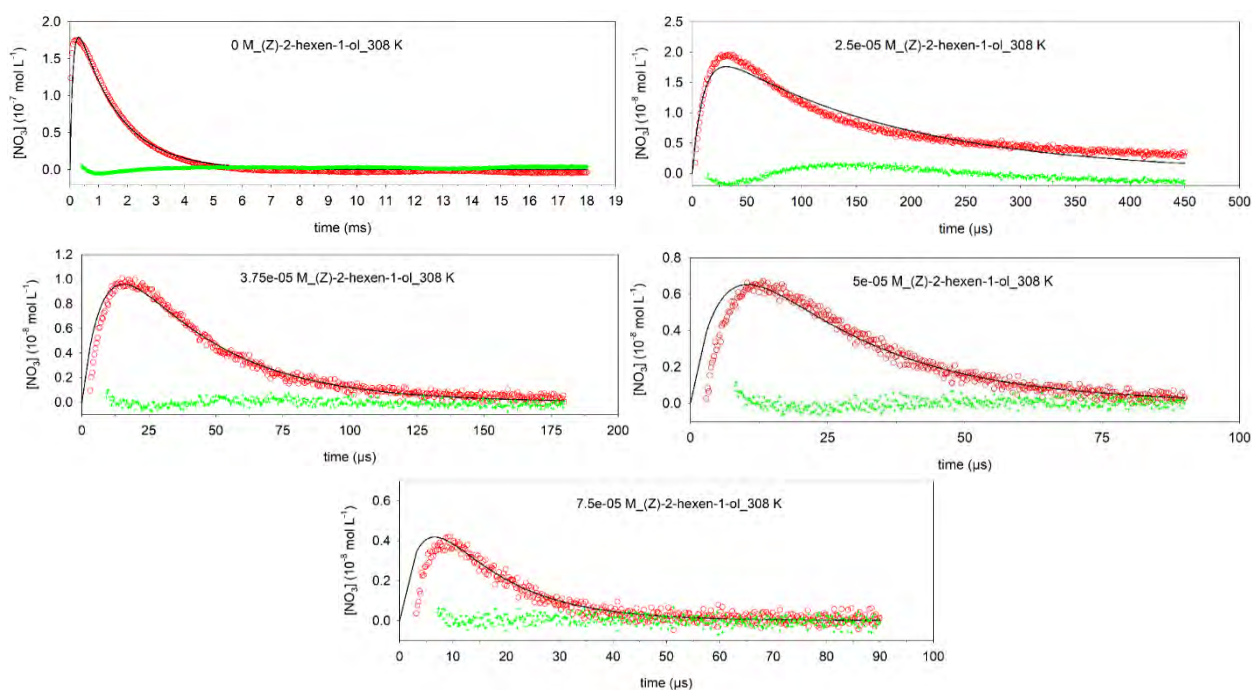


Figure 6.11. Concentration-time profiles of NO_3^\bullet in experiments at **308 K** and various initial concentrations of (Z)-2-hexen-1-ol (specified in the legends). Experimental data points are red circles, simulations are black lines, and residuals are green crosses.

C) (*E*)-2-hexen-1-al + NO_3^\bullet

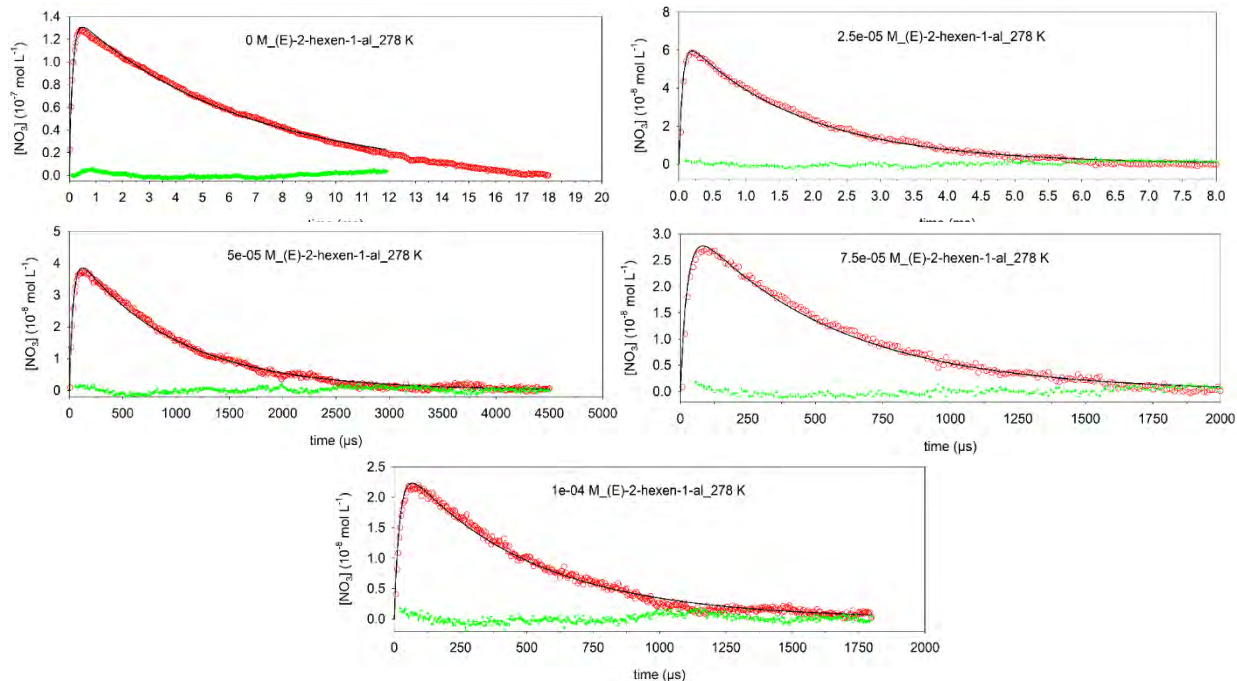


Figure 6.12. Concentration-time profiles of NO_3^\bullet in experiments at **278 K** and various initial concentrations of (*E*)-2-hexen-1-al (specified in the legends). Experimental data points are red circles, simulations are black lines, and residuals are green crosses.

Chapter 6. Evaluating bias of the experimental rate constants determined for the aqueous-phase reactions of selected GLVs with NO_3^\bullet

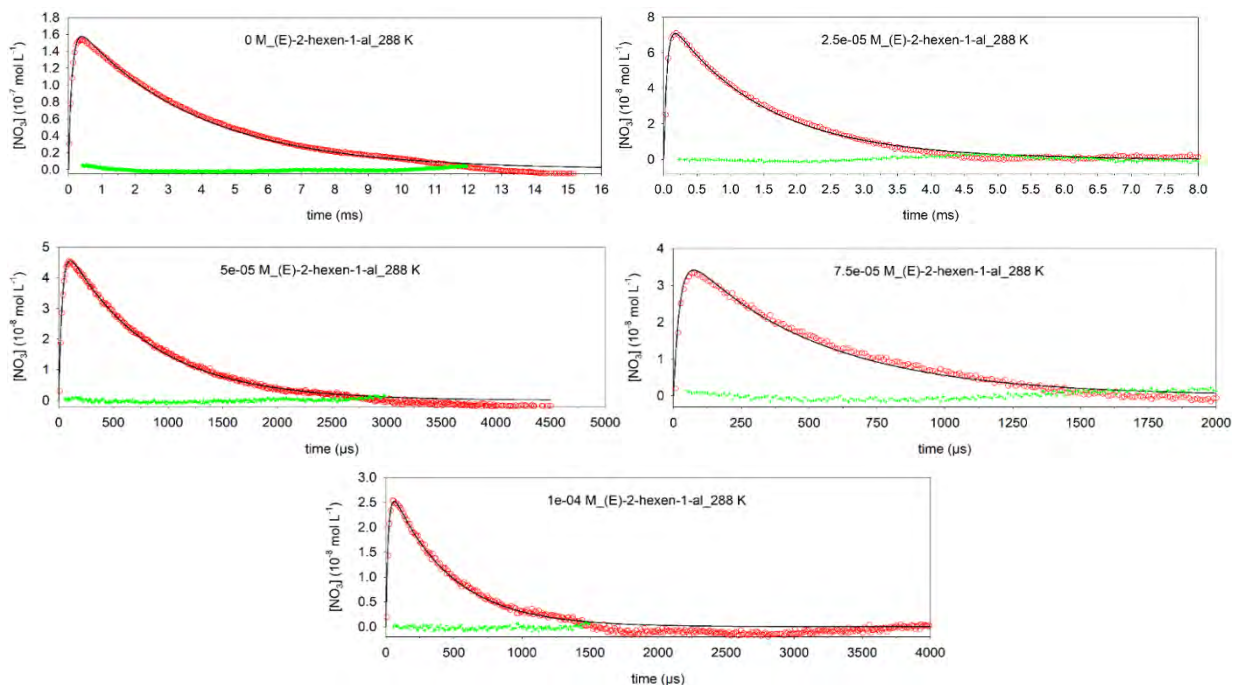


Figure 6.13. Concentration-time profiles of NO_3^\bullet in experiments at **288 K** and various initial concentrations of (E)-2-hexen-1-al (specified in the legends). Experimental data points are red circles, simulations are black lines, and residuals are green crosses.

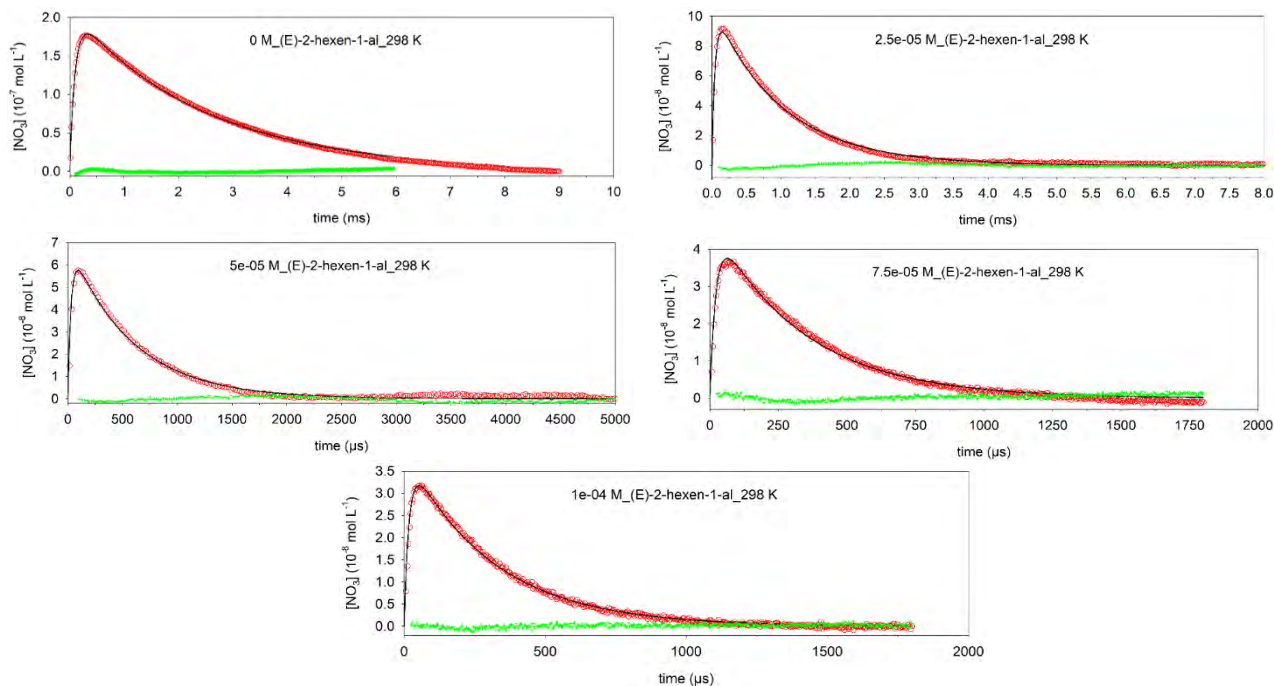


Figure 6.14. Concentration-time profiles of NO_3^\bullet in experiments at **298 K** and various initial concentrations of (E)-2-hexen-1-al (specified in the legends). Experimental data points are red circles, simulations are black lines, and residuals are green crosses.

Chapter 6. Evaluating bias of the experimental rate constants determined for the aqueous-phase reactions of selected GLVs with NO_3^\bullet

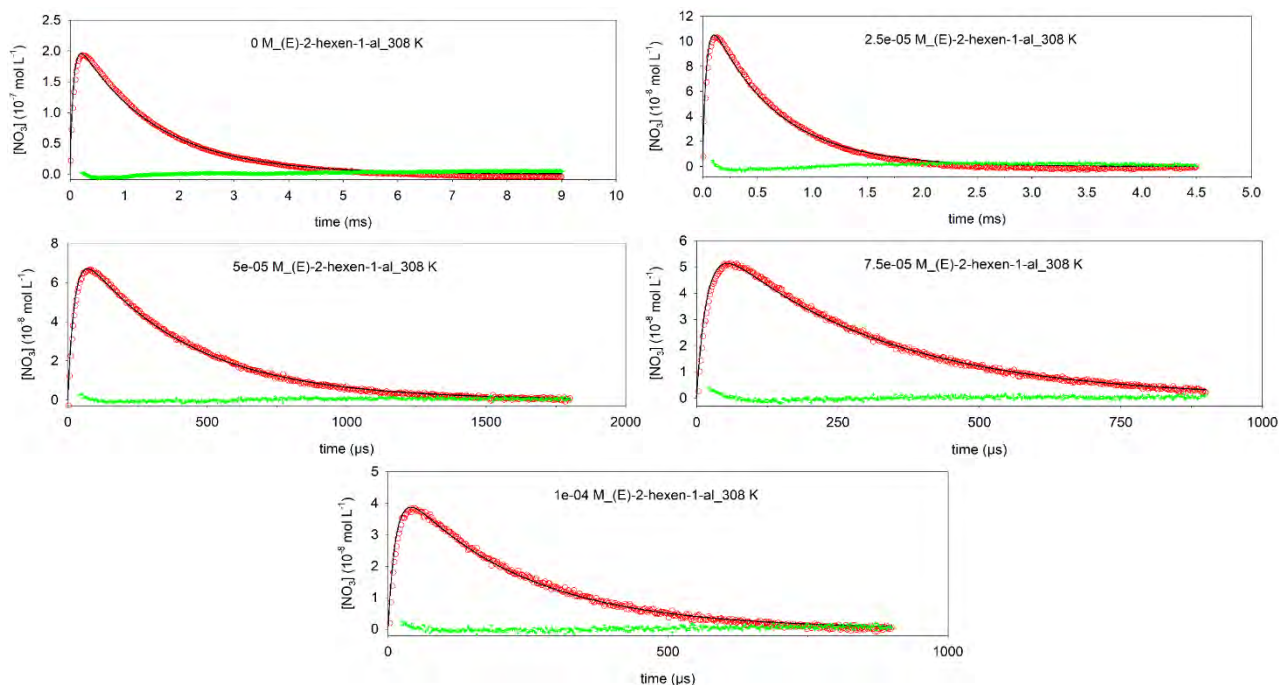


Figure 6.15. Concentration-time profiles of NO_3^\bullet in experiments at **308 K** and various initial concentrations of (*E*)-2-hexen-1-al (specified in the legends). Experimental data points are red circles, simulations are black lines, and residuals are green crosses.

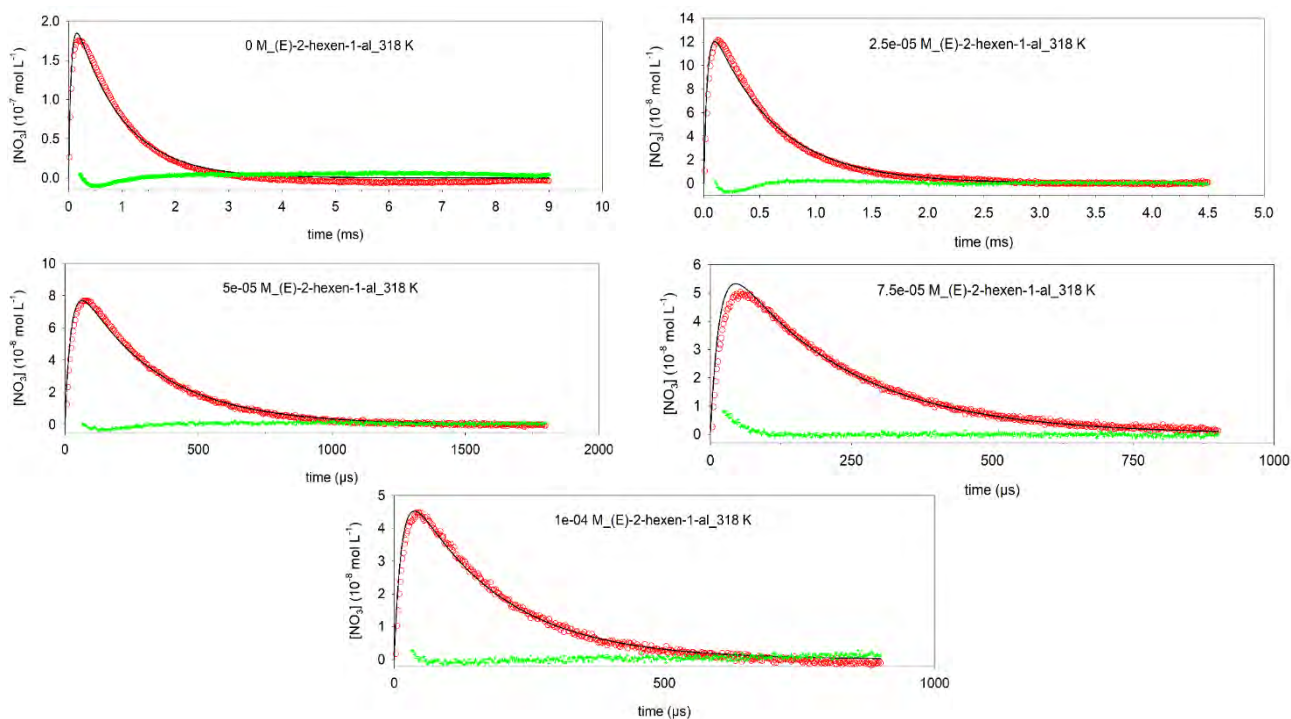


Figure 6.16. Concentration-time profiles of NO_3^\bullet in experiments at **318 K** and various initial concentrations of (*E*)-2-hexen-1-al (specified in the legends). Experimental data points are red circles, simulations are black lines, and residuals are green crosses.

6.4. Percentage bias of the experimentally determined GLV + NO₃[•] reaction rate constants vs. Model_1 estimations

Table 6.6. Experimental and model-estimated rate constants (L mol⁻¹ s⁻¹) for reactions between GLV and NO₃[•].

	278 K	288 K	298 K	308 K	318 K
PENTOL					
Model_1 (<i>k_{Model}</i>)	9.3×10 ⁷	9.3×10 ⁷	1.4×10 ⁸	1.7×10 ⁸	
Experimental (<i>k_{obs}</i>)	8.8×10 ⁷	1.1×10 ⁸	1.5×10 ⁸	2.0×10 ⁸	
Δ Model-Exp, %	+5	-13	-7	-14	
Experimental uncertainty, %	± 18	± 22	± 10	± 21	
HEXOL					
Model_1 (<i>k_{Model}</i>)	6.6×10 ⁸	7.8×10 ⁸	7.7×10 ⁸	8.5×10 ⁸	
Experimental (<i>k_{obs}</i>)	6.4×10 ⁸	7.9×10 ⁸	8.4×10 ⁸	9.8×10 ⁸	
Δ Model-Exp, %	+3	-1	-9	-15	
Experimental uncertainty, %	± 23	± 31	± 23	± 27	
HEXAL					
Model_1 (<i>k_{Model}</i>)	1.6×10 ⁷	1.7×10 ⁷	2.6×10 ⁷	3.5×10 ⁷	4.5×10 ⁷
Experimental (<i>k_{obs}</i>)	2.0×10 ⁷	2.1×10 ⁷	3.0×10 ⁷	3.7×10 ⁷	5.0×10 ⁷
Δ Model-Exp, %	-25	-24	-15	-6	-10
Experimental uncertainty, %	± 27	± 11	± 24	± 3	± 15

In Table 6.6 the rate constants for GLV reactions with NO₃[•] estimated using Model_1 and determined experimentally in LFP-LLPA experiments are compared. Equation 6.4 shows the percentage bias of the experimental rate constants due to the “neglected” sinks of NO₃[•].

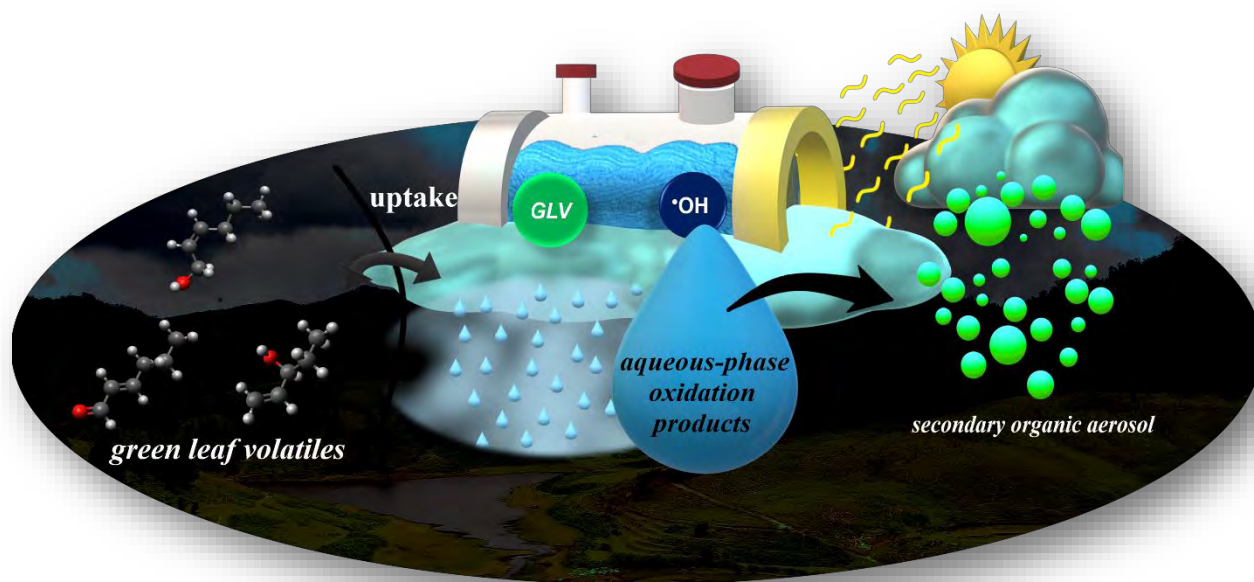
$$\Delta_{Model-Exp} = \frac{k_{Model} - k_{obs}}{k_{obs}} \times 100\% \quad (6.4)$$

(*E*)-2-hexen-1-al was the slowest reacting GLV with NO₃[•] among those studied and had the highest bias in the experimental rate constants, namely (6 – 25)% (Table 6.6). The bias decreased with temperature, probably due to the relative acceleration of the reaction between NO₃[•]

Chapter 6. *Evaluating bias of the experimental rate constants determined for the aqueous-phase reactions of selected GLVs with NO_3^\bullet*

and GLV. For 1-penten-3-ol and (*Z*)-2-hexen-1-ol, the rate constants bias were less than 15% at all temperatures. Interestingly, the intrinsic experimental uncertainty for the rate constants determined using LFP-LLPA procedure was significantly more considerable than the bias due to the “neglected” sink of NO_3^\bullet , including the $\text{NO}_3^\bullet +$ peroxy intermediate pathway. Exceptions to that rule occurred for (*E*)-2-hexen-1-al at 288 and 308 K. Thus, the experimental LFP-LLPA method appeared robust and applicable to NO_3^\bullet reactions.

Chapter 7. Product studies on the OH radical-mediated aqueous-phase GLV photooxidation



Results presented in the chapter have been submitted to Chemosphere

<http://rcin.org.pl>

Synopsis

The present chapter explores the aqueous-phase photooxidation pathways of selected GLVs (PENTOL, HEXOL, and HEXAL) with $\cdot\text{OH}$ radicals to investigate and determine their main oxidation products as a novel source of SOA. The analyses using gas and liquid chromatography were targeted to identify carbonyls, alcohols, and carboxylic acid. The carbonyl-targeted cGC-MS analysis confirmed short chain aliphatic aldehydes (i.e., propanal, butanal), and unsaturated ketone (i.e., 1-penten-3-one or ethyl vinyl ketone) as abundant reaction products. The alcohol-targeted cGC-MS analysis was done to quantify the GLVs (1-penten-3-ol, and (*Z*)-2-hexen-1-ol) in the reaction samples. Another major product with a molecular formula $\text{C}_6\text{H}_{10}\text{O}_2$ was confirmed using the reversed phase LC-MS analysis for both, (*Z*)-2-hexen-1-ol and (*E*)-2-hexen-1-al. The novel $\text{C}_6\text{H}_{10}\text{O}_2$ product was tentatively proposed to be the hydroxyhexenal or hydroxyhexenone; however, its unequivocal structural assignment could not be pursued due to the lack of authentic standards. The density functional theory (DFT), along with the group contribution method was used to assess and evaluate the relative importance of addition and hydrogen abstraction reaction channels for studied reactions. In conclusion, good agreement between experimental and theoretical findings was achieved, and suggested that the combination of mass spectrometric data with theoretical calculation showed a comprehensive method to unravel a complex chemical mechanism of studied processes.

7.1. Introduction

The oxidative degradation pathways of GLVs is considered complicated under atmospheric conditions, especially during warm seasons where high GLVs emission episodes from plants are reported.^{146, 478} To date, many studies have dealt with the oxidative degradation of GLVs in the atmospheric gas-phase,^{162, 167, 176, 184, 194, 204, 217, 220, 243, 269, 479, 480} and air-water interface^{241, 481-483} as an additional source of SOA; while only few studies report on aqueous-phase oxidation kinetics of GLVs and products formation.¹²⁸ As a preliminary research, Chapter 4 – 6 provided physical properties, aqueous-phase kinetics data for selected GLVs (PENTOL, HEXOL, and HEXAL), along with the atmospheric significance of their investigated atmospheric reactions with $\cdot\text{OH}$, $\text{SO}_4^{\cdot-}$, and NO_3^{\cdot} , respectively^{168, 298} This chapter reports on the chemical characterization of the

oxidation products obtained from the $\cdot\text{OH}$ radicals-driven photooxidation reactions of selected GLVs in aqueous droplets.

7.2. Experimental methods

The information on chemicals used are provided in Chapter 3. The details of the experimental set-up (Figure 3.7) and characterization techniques / method used (Section 3.3.2, and 3.4) are also highlighted in Chapter 3.

7.3. Results and Discussion

Product and mechanistic studies of $\cdot\text{OH}$ radicals-mediated reactions of PENTOL, HEXOL, and HEXAL

The aqueous-phase photooxidation of GLVs (PENTOL, HEXOL, and HEXAL) with $\cdot\text{OH}$ radicals were carried out at 298 K.. The 300 mL glass photoreactor was used to perform GLVs photooxidation product studies in the presence of $\cdot\text{OH}$ radicals. The O_3 free solar simulator Xe arc lamp was used to photolyze H_2O_2 and produce *in situ* $\cdot\text{OH}$ radicals. The light wavelengths below 290 nm was filtered off by the AM1.5 filter to mimic daylight conditions. The UV absorbance for PENTOL, and HEXOL above 290 nm is negligible (compare Figures 4.1, and 4.2 in Chapter 4). In agreement, no photodegradation was observed within the reaction sample during photolysis experiments for both PENTOL and HEXOL. In contrast, HEXAL (Figure 4.3) does absorb between 400 – 290 nm ($0.6 \text{ M}^{-1} \text{ cm}^{-1} < \epsilon > 51 \text{ M}^{-1} \text{ cm}^{-1}$, Table A4.5.a and $1.3 \text{ M}^{-1} \text{ cm}^{-1} < \epsilon > 62 \text{ M}^{-1} \text{ cm}^{-1}$, Table A4.5.b) and was observed to undergo considerable photodegradation in the form of photoisomerization (*E* to *Z* isomer), in photolysis (without $\cdot\text{OH}$) as well as in photooxidation experiments.

The pseudo first-order rate constants for the decay of GLVs were determined using the slope of a linear plot of $-\ln [\text{GLV}]_t / [\text{GLV}]_0$ vs time (hour). The standard errors were determined using regression analysis with a 95 % confidence interval. Overall, the rate of the GLV loss was calculated based on the equation 7.1, constituting the loss due to the reaction with $\cdot\text{OH}$ radicals ($k_{\text{OH}+\text{GLV}}[\text{OH}][\text{GLV}]$) and direct photolysis ($j_{\text{GLV}}[\text{GLV}]$ parts in eq. 7.1), and all other unknown pathways ($k_{\text{other}}[\text{GLV}]$):^{128, 129}

$$-\frac{d[GLV]}{dt} = k_{OH+GLV}[OH][GLV] + j_{GLV}[GLV] + k_{other}[GLV] \quad (7.1)$$

The steady-state $\cdot OH$ radical concentration determined using COPASI was found to be 1×10^{-13} M (Table 7.1).^{290, 382} Given that [$\cdot OH$] concentrations follow a steady-state pattern, the above equation can be simplified to equation 7.3 upon the combination of equation 7.1 and 7.2 followed by its integration.

$$k'_{GLV} = k_{OH+GLV}[OH] + j_{GLV} + k_{other} \quad (7.2)$$

$$\ln \frac{[GLV]_t}{[GLV]_0} = -k'_{GLV} \times t \quad (7.3)$$

According to equation 7.3, within the aqueous-phase photooxidation reaction with $\cdot OH$ radicals, the selected GLVs, i.e., PENTOL, HEXOL, and HEXAL follow a decay scenario with a pseudo first-order rate loss of (0.023 ± 0.003) , (0.025 ± 0.003) , and (0.050 ± 0.004) hr^{-1} , respectively, which correspond to the observed 12%, 20%, and 20% losses, respectively in the total reaction duration of 6 hours.

Table 7.1. The Initial concentrations and considered reactions used in the COPASI estimation model to determine steady state $\cdot OH$ concentrations.

No.	Reaction	k (298 K)	Ref.	Species	[Conc.] ₀ , M
1	$H_2O_2 \rightarrow OH + OH$	$2.8 \times 10^{-6} s^{-1}$	290	H_2O_2	5.0×10^{-3}
2	$OH + OH \rightarrow H_2O_2$	$3.6 \times 10^9 L mol^{-1} s^{-1}$	462	OH	0
3	$OH + H_2O_2 \rightarrow H_2O + HO_2$	$2.7 \times 10^7 L mol^{-1} s^{-1}$	463	H_2O	55.37
4	$OH + HO_2 \rightarrow H_2O + O_2$	$6.0 \times 10^9 L mol^{-1} s^{-1}$	462	HO_2	0
5	$OH + O_2^- \rightarrow OH^- + O_2$	$1.1 \times 10^{10} L mol^{-1} s^{-1}$	463	O_2	2.6×10^{-4}
6	$H_2O \rightleftharpoons H^+ + OH^-$	$\rightarrow 0.0014 s^{-1}$, $\leftarrow 1.4 \times 10^{11} L mol^{-1} s^{-1}$	459	O_2^-	0
7	$HO_2 \rightleftharpoons O_2^- + H^+$	$\rightarrow 1.4 \times 10^6 s^{-1}$, $\leftarrow 5.0 \times 10^{10} L mol^{-1} s^{-1}$	459	OH^-	1.0×10^{-7}

8	GLV + OH → Products		*this work	H ⁺	1.0 × 10 ⁻⁷
	a. 1-penten-3-ol;	a. 6.3 × 10 ⁹ L mol ⁻¹ s ⁻¹	Table 5.3		
	b. (Z)-2-hexen-1-ol;	b. 6.7 × 10 ⁹ L mol ⁻¹ s ⁻¹		GLV	1.0 × 10 ⁻⁴
	c. (E)-2-hexen-1-ol	c. 4.8 × 10 ⁹ L mol ⁻¹ s ⁻¹		*Products	0

*GLV-OH reaction products

7.3.1. Group contribution method (GCM) estimation (k_{2nd} GLV-OH)

The group contribution method (GCM) by Minakata et al.,⁴⁸⁴ was used for the estimation of k_{2nd} . GCM estimated second-order rate constant values for the aqueous-phase reactions between GLV and [•]OH are provided in Chapter 5. The determined reactivity rate values for all possible reaction pathways (i.e., addition vs. H-abstraction ones) are provided to evaluate their relative importance and compare with experimental ones as well as DFT-obtained (vide subsequent sections).

a. PENTOL

i) H-abstraction

$$\begin{aligned}
 k(5) &= 3k_{\text{prim}}^{\circ} \times X_{\text{-CH}_2} \\
 &= 3 \times (1.17580 \times 10^8) \times 1.174 \\
 &= 4.14 \times 10^8 \text{ L mol}^{-1} \text{ s}^{-1}
 \end{aligned}$$

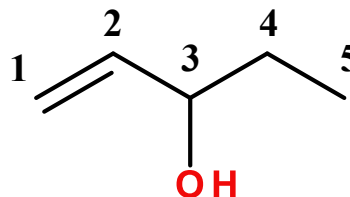
$$\begin{aligned}
 k(4) &= 2k_{\text{sec}}^{\circ} \times X_{\text{-CH}_3} \times X_{\text{-CHOH}} \\
 &= 2 \times (5.1097 \times 10^8) \times 1.12 \times 1.174 \\
 &= 1.34 \times 10^9 \text{ L mol}^{-1} \text{ s}^{-1}
 \end{aligned}$$

$$\begin{aligned}
 k(3) &= k_{\text{ter}}^{\circ} \times X_{\text{-OH}} \times X_{\text{-CH}_2} \times X_{\text{-CH}} \\
 &= (1.99026 \times 10^9) \times 0.578 \times 1.174 \times 1.174 \\
 &= 1.59 \times 10^9 \text{ L mol}^{-1} \text{ s}^{-1}
 \end{aligned}$$

$$\begin{aligned}
 k(\text{OH}) &= k_{\text{OH}} \\
 &= (1.0000 \times 10^8) \text{ L mol}^{-1} \text{ s}^{-1}
 \end{aligned}$$

$$k_{\text{overall}}(\text{H-abs}) = 3.44 \times 10^9 \text{ L mol}^{-1} \text{ s}^{-1}$$

ii) Double bond addition



Since Y (group contribution factor for CHOH is not available in Minakata et al.,⁴⁸⁴ and thus, I took a closest approximated group contribution of -CHO

$$\begin{aligned} k(2) &= g k^{\circ}_{\text{structure}} \times Y_{\text{-CHO}} \\ &= 1 \times (1.0102 \times 10^8) \times 0.6000 \\ &= 6.0612 \times 10^7 \text{ L mol}^{-1} \text{ s}^{-1} \end{aligned}$$

$$\begin{aligned} k(1) &= g k^{\circ}_{\text{structure}} \times Y_{\text{-CHO}} \\ &= 1 \times 9.9999 \times 10^9 \times 0.6000 \\ &= 5.99994 \times 10^9 \text{ L mol}^{-1} \text{ s}^{-1} \end{aligned}$$

$$k_{\text{overall}} (\text{addition-alkene}) = 6.06 \times 10^9 \text{ L mol}^{-1} \text{ s}^{-1}$$

$$\text{PENTOL-OH: } k_{\text{sum}} (\text{addition} + \text{H-abs}) = 9.50 \times 10^9 \text{ L mol}^{-1} \text{ s}^{-1}$$

b. HEXOL

i) H-abstraction

$$\begin{aligned} k(6) &= 3k^{\circ}_{\text{prim}} \times X_{\text{-CH}_2} \\ &= 3 \times (1.17580 \times 10^8) \times 1.174 \\ &= 4.14 \times 10^8 \text{ L mol}^{-1} \text{ s}^{-1} \end{aligned}$$

$$\begin{aligned} k(5) &= 2k^{\circ}_{\text{sec}} \times X_{\text{-CH}_3} \times X_{\text{-CH}_2} \\ &= 2 \times (5.1097 \times 10^8) \times 1.12 \times 1.174 \\ &= 1.34 \times 10^9 \text{ L mol}^{-1} \text{ s}^{-1} \end{aligned}$$

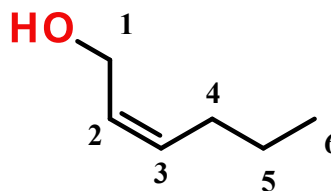
$$\begin{aligned} k(4) &= 2k^{\circ}_{\text{sec}} \times X_{\text{-CH}_2} \times X_{\text{-CH}} \\ &= 2 \times (5.1097 \times 10^8) \times 1.74 \times 1.174 \\ &= 1.40 \times 10^9 \text{ L mol}^{-1} \text{ s}^{-1} \end{aligned}$$

$$\begin{aligned} k(1) &= 2k^{\circ}_{\text{sec}} \times X_{\text{-CH}} \times X_{\text{-OH}} \\ &= 2 \times (5.1097 \times 10^8) \times 1.74 \times 0.578 \\ &= 6.93 \times 10^8 \text{ L mol}^{-1} \text{ s}^{-1} \end{aligned}$$

$$\begin{aligned} k(\text{OH}) &= k_{\text{OH}} \\ &= (1.0000 \times 10^8) \text{ L mol}^{-1} \text{ s}^{-1} \end{aligned}$$

$$k_{\text{overall}} (\text{H-abs}) = 3.96 \times 10^9 \text{ L mol}^{-1} \text{ s}^{-1}$$

ii) Double bond addition



$$\begin{aligned}
 k(2) &= g k^{\circ}_{\text{structure}} \times Y_{\text{-CH}_2} \times Y_{\text{-CH}_2} \\
 &= 1 \times (3.01 \times 10^{10}) \times 0.3880 \times 0.3880 \\
 &= 4.5313 \times 10^9 \text{ L mol}^{-1} \text{ s}^{-1}
 \end{aligned}$$

$$\begin{aligned}
 k(3) &= g k^{\circ}_{\text{structure}} \times Y_{\text{-CH}_2} \times Y_{\text{-CH}_2} \\
 &= 1 \times (3.01 \times 10^{10}) \times 0.3880 \times 0.3880 \\
 &= 4.5313 \times 10^9 \text{ L mol}^{-1} \text{ s}^{-1}
 \end{aligned}$$

$$k_{\text{overall}} (\text{addition-alkene}) = 9.07 \times 10^9 \text{ L mol}^{-1} \text{ s}^{-1}$$

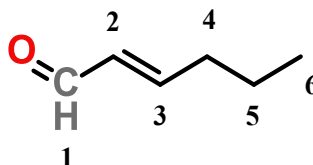
$$\text{HEXOL-OH: } k_{\text{sum}} (\text{addition} + \text{H-abs}) = 1.30 \times 10^{10} \text{ L mol}^{-1} \text{ s}^{-1}$$

c. HEXAL

The hydrogen atom abstraction from the aldehyde moiety cannot be directly predicted using the GCM method. Therefore, I assumed it as a secondary carbon to calculate the estimated rate.

i) H-abstraction

$$\begin{aligned}
 k(6) &= 3k^{\circ}_{\text{prim}} \times X_{\text{-CH}_2} \\
 &= 3 \times (1.17580 \times 10^8) \times 1.174 \\
 &= 4.14 \times 10^8 \text{ L mol}^{-1} \text{ s}^{-1}
 \end{aligned}$$



$$\begin{aligned}
 k(5) &= 2k^{\circ}_{\text{sec}} \times X_{\text{-CH}_3} \times X_{\text{-CH}_2} \\
 &= 2 \times (5.1097 \times 10^8) \times 1.12 \times 1.174 \\
 &= 1.34 \times 10^9 \text{ L mol}^{-1} \text{ s}^{-1}
 \end{aligned}$$

$$\begin{aligned}
 k(4) &= 2k^{\circ}_{\text{sec}} \times X_{\text{-CH}_2} \times X_{\text{-CH}} \\
 &= 2 \times (5.1097 \times 10^8) \times 1.74 \times 1.174 \\
 &= 1.40 \times 10^9 \text{ L mol}^{-1} \text{ s}^{-1}
 \end{aligned}$$

$$\begin{aligned}
 k(1) &= k^{\circ}_{\text{-CHO}} = k^{\circ}_{\text{sec}} \times X_{\text{-CH}} \times X_{\text{-O}} \\
 &= (5.1097 \times 10^8) \times 1.174 \times 0.36 \\
 &= 2.16 \times 10^8 \text{ L mol}^{-1} \text{ s}^{-1}
 \end{aligned}$$

$$k_{\text{overall}} (\text{H-abs}) = 3.3 \times 10^9 \text{ L mol}^{-1} \text{ s}^{-1}$$

ii) Double bond addition

$$\begin{aligned}
 k(2) &= g k^{\circ}_{\text{structure}} \times Y_{\text{-CH}_2} \times Y_{\text{-CHO}} \\
 &= 1 \times (5.21 \times 10^{10}) \times 0.6000 \times 0.3880 \\
 &= 1.2128 \times 10^{10} \text{ L mol}^{-1} \text{ s}^{-1}
 \end{aligned}$$

$$\begin{aligned}
 k(3) &= g k^{\circ}_{\text{structure}} \times Y_{\text{-CH}_2} \times Y_{\text{-CHO}} \\
 &= 1 \times (5.21 \times 10^{10}) \times 0.6000 \times 0.3880 \\
 &= 1.2128 \times 10^{10} \text{ L mol}^{-1} \text{ s}^{-1}
 \end{aligned}$$

$$k_{\text{overall}} (\text{addition-alkene}) = 2.43 \times 10^{10} \text{ L mol}^{-1} \text{ s}^{-1}$$

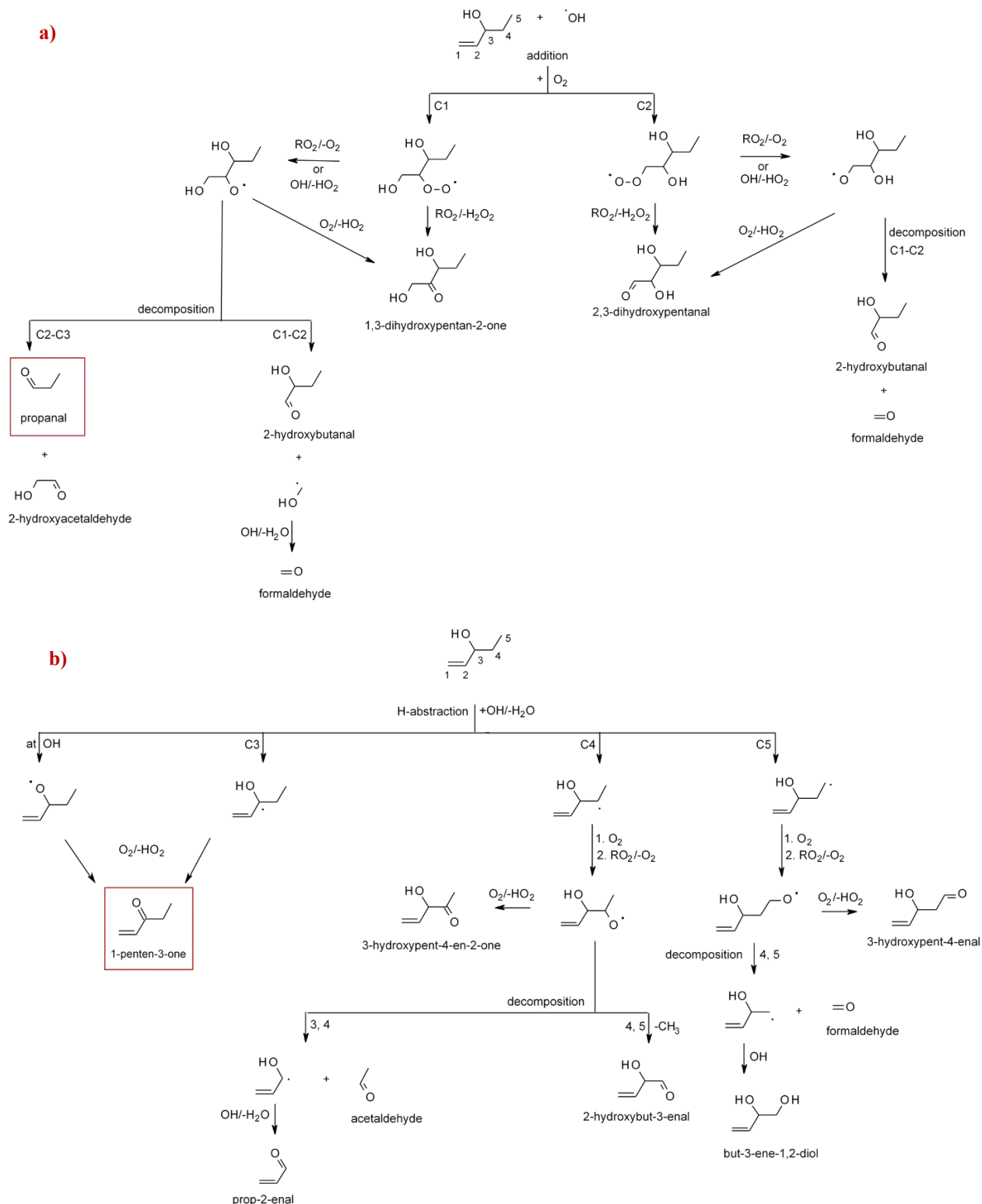
$$\text{HEXAL-OH: } k_{\text{sum}} (\text{addition+H-abs}) = 2.79 \times 10^{10} \text{ L mol}^{-1} \text{ s}^{-1}$$

Table 7.2. Type of analysis, retention times (RT, min), molar masses, and characteristic fragments.

Analyte	Type of Analysis	Retention time, min	Molar Mass, g mol ⁻¹	Characteristic fragment ion(s)
PENTOL	GC-MS (alcohol)	7.5	86.13	<i>m/z</i> 57
1-penten-3-one	GC-MS (oxime dvt. carbonyl)	11.35	84.12	<i>m/z</i> 279
propanal	GC-MS (oxime dvt. carbonyl)	9.46	58.08	<i>m/z</i> 236, <i>m/z</i> 253
2,2,6,6-cyclohexaone-d ₄ (Int. std.)	GC-MS (oxime dvt. carbonyl)	14.025	102.18	<i>m/z</i> 297
HEXOL	GC-MS (alcohol)	11.70	100.16	
HEXOL	LC-MS (PDA detector)	8.10	100.16	Abs. max. 218 nm
butanal		10.691	72.11	<i>m/z</i> 239, <i>m/z</i> 267
HEXAL	GC-MS (oxime dvt. carbonyl)	13.767, 13.925	98.14	<i>m/z</i> 293
HEXAL	LC-MS (PDA detector)	9.16	98.14	Abs. max. 222 nm
HEXAL	LC-MS (MS detector)	9.29, 9.31	98.14	<i>m/z</i> 99.080441 [M+H] ⁺
C ₆ H ₁₀ O ₂	LC-MS	6.6	114.14	<i>m/z</i> 113.06080 [M-H] ⁻

7.3.2. PENTOL with $\cdot\text{OH}$ radicals

Remaining 1-penten-3-ol and its carbonyl products in reaction samples were identified and quantified using carbonyl and alcohol targeted cGC-MS methods. Neither reactant traces nor products could be detected in reaction samples using the reversed-phase LC-MS analysis. Two carbonyls, i.e., propionaldehyde (propanal) and 1-penten-3-one were firmly identified as the key oxidation product of PENTOL, shown in red boxes in Scheme 7.1 below.



Scheme 7.1. Proposed mechanistic reaction pathways and the essential products formation (*shown in red boxes*) from the reaction of 1-penten-3-ol (PENTOL) and $\cdot\text{OH}$: a) addition channel, b) H-abstraction channel.

The radical addition of $\cdot\text{OH}$ at a PENTOL can occur at positions C1 or C2 (Scheme 7.1.a), to form alkyl radicals. The latter follow the subsequent O_2 uptake, thereby leading to peroxy radicals. These radicals can further recombine with other peroxy radical present and, *via* removal of either HO_2 or H_2O_2 produces alkoxy radicals. Finally, alkoxy radicals can either decompose or undergo O_2 -/ HO_2 pathway to give carbonyl products. The aqueous-phase reactions between PENTOL and $\cdot\text{OH}$ can also proceed *via* the hydrogen-abstraction pathway (Scheme 7.1.b). The $\cdot\text{OH}$ species can remove a hydrogen atom from either C3, C4, C5 or -OH sites in PENTOL. The alkyl radical formed adds O_2 to form corresponding peroxy radicals. Following a reaction similar to the addition one, alkoxy radicals can react with other peroxy radicals, eventually affording alkoxy radicals and finally carbonyls. In addition, peroxy radicals upon reaction with O_2 and HO_2 removal can also form carbonyls. Based on the proposed mechanistic scheme (Scheme 7.1), the experimentally observed propanal results from the addition reaction at a C1 position, while the 1-penten-3-one results from the $\cdot\text{OH}$ radicals driven hydrogen-abstraction at either a C3 site or at the hydroxyl group of PENTOL. The c-GC-MS total ion chromatogram (TIC) of the reaction samples (0 h and 6 h, respectively) with the labeled identified reactant or product peaks is provided in Figure 7.1.

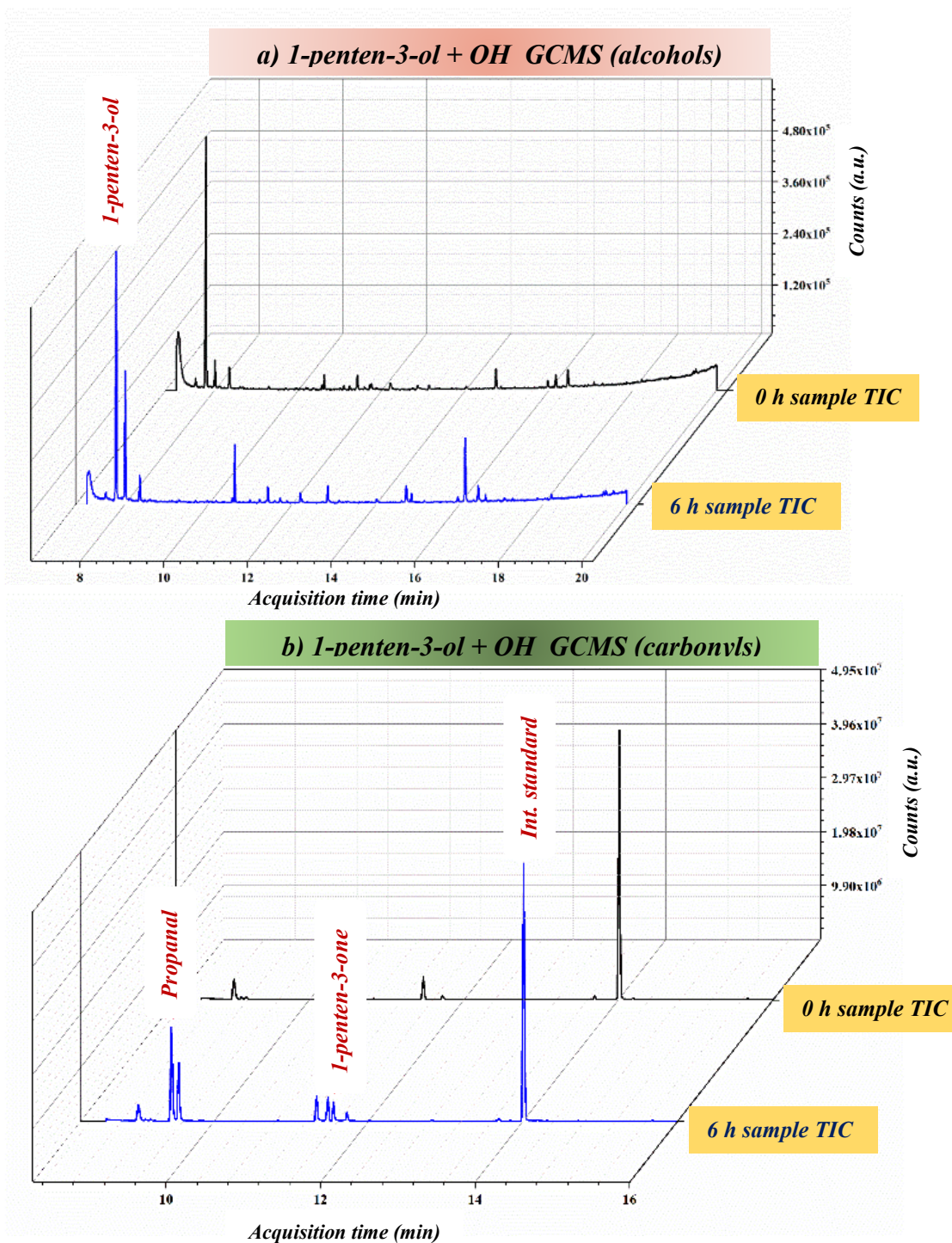
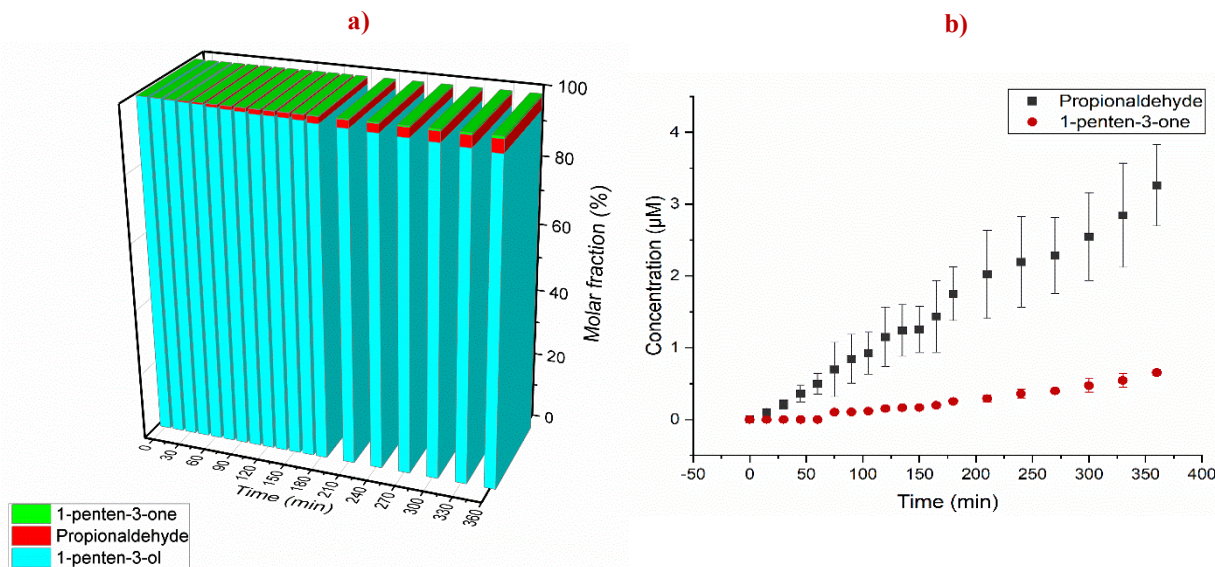


Figure 7.1. c-GC-MS Total Ion Chromatogram (TIC) obtained for the photooxidation reaction samples of 1-penten-3-ol (PENTOL) with $\cdot\text{OH}$ radicals at time: $t = 0$ h (**black**), and $t = 6$ h (**blue**). **a)** c-GC-MS TIC for PENTOL (RT = 7.5 min); **b)** c-GC-MS TIC of the carbonyl products. (See Table 7.2)

The photooxidation reaction between PENTOL and $\bullet\text{OH}$ radicals results in the formation of an average molar fraction ($3.5 \pm 0.6\%$) of propanal, and ($0.7 \pm 0.2\%$) of 1-penten-3-one with ($12 \pm 6\%$) molar fraction PENTOL decay till the end of 6 h (Figure 7.2). Figure 7.2.a provides the molar fraction vs. time plots for the PENTOL-OH photooxidation reaction, while Figure 7.2.b depicts the concentration-time profile for the photooxidation products, propanal and 1-penten-3-one, respectively. The molar fraction ratio of propanal and 1-penten-3-one is 3:1, which is in agreement with the reactivity rate predicted using GCM for addition at C1 ($k(1) = 6 \times 10^9 \text{ L mol}^{-1} \text{ s}^{-1}$) and H-abstraction at C3 ($k(1) = 2 \times 10^9 \text{ L mol}^{-1} \text{ s}^{-1}$), respectively (Section 7.3.1).⁴⁸⁴ The addition and H-abstraction pathways were further investigated using density functional theory (DFT) approach, and results are presented and discussed separately in Section 7.3.5. The gas-phase reaction products of PENTOL reported so far, include: formaldehyde ($35 \pm 4\%$), and glycolaldehyde ($47 \pm 6\%$) for a reaction with OH radicals;¹⁸⁴ formaldehyde (0.49 ± 0.02), 2-hydroxybutanal (0.46 ± 0.03) and propanal (0.15 ± 0.02) *via* ozonolysis,¹⁹⁴ propanal, and 2-hydroxybutanal *via* ozonolysis,^{195, 485} and propanal and 1-penten-3-one with Cl radicals.²⁰² Scheme 7.1 assumes products, such as formaldehyde, 2-hydroxybutanal, and acetaldehyde also reported within the above-mentioned gas-phase studies. However, none of these could be detected during my c-GC-MS or reversed-phase LC-MS analyses owing likely to their low concentrations achieved upon 6 h of the reaction run, which possibly also contribute towards the 2.4 – 13 % unaccountable loss of PENTOL reported.

Th results of the control experiments, the photolysis (i.e., the absence of $\bullet\text{OH}$ radical precursor, H_2O_2), and dark oxidation (in the absence of UV light), revealed no change in the PENTOL concentration over the period of 6 h (Figure 7.3.b). This observation is in good agreement with the results previously reported by Jimenez *et al.*¹⁶² according to which the PENTOL photolysis in the actinic region is of a little importance and its main sink in the tropospheric gas phase is $\bullet\text{OH}$ radicals, while O_3 and $\text{NO}_3\bullet$ are not significant.



Figures 7.2. *a)* Percentage of molar fraction of PENTOL and its $\cdot\text{OH}$ -driven oxidation products in aqueous-phase; *b)* Concentration-time profile of the products, propionaldehyde and 1-penten-3-one, during the photooxidation of 1-penten-3-ol with OH radicals ($n=2$).

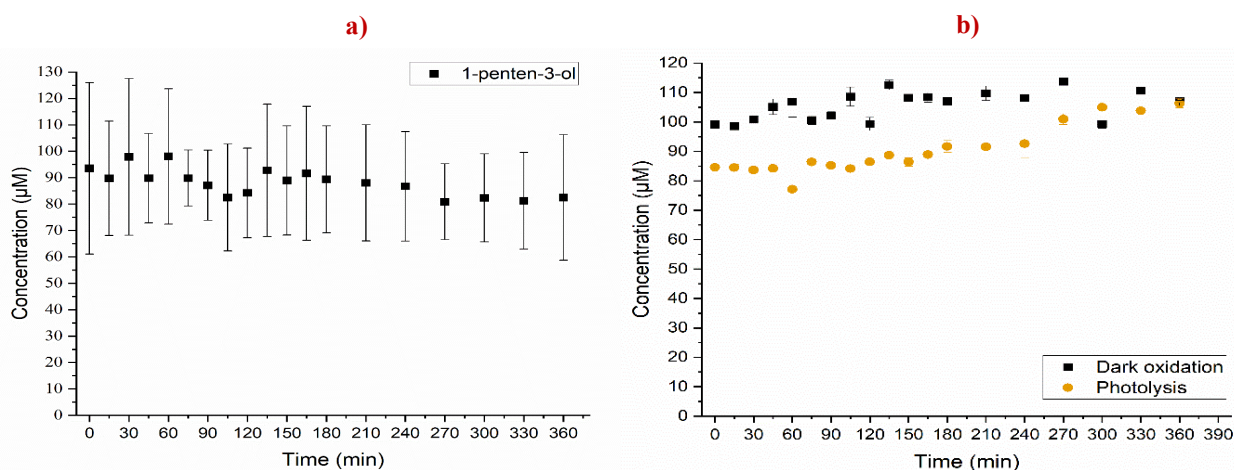
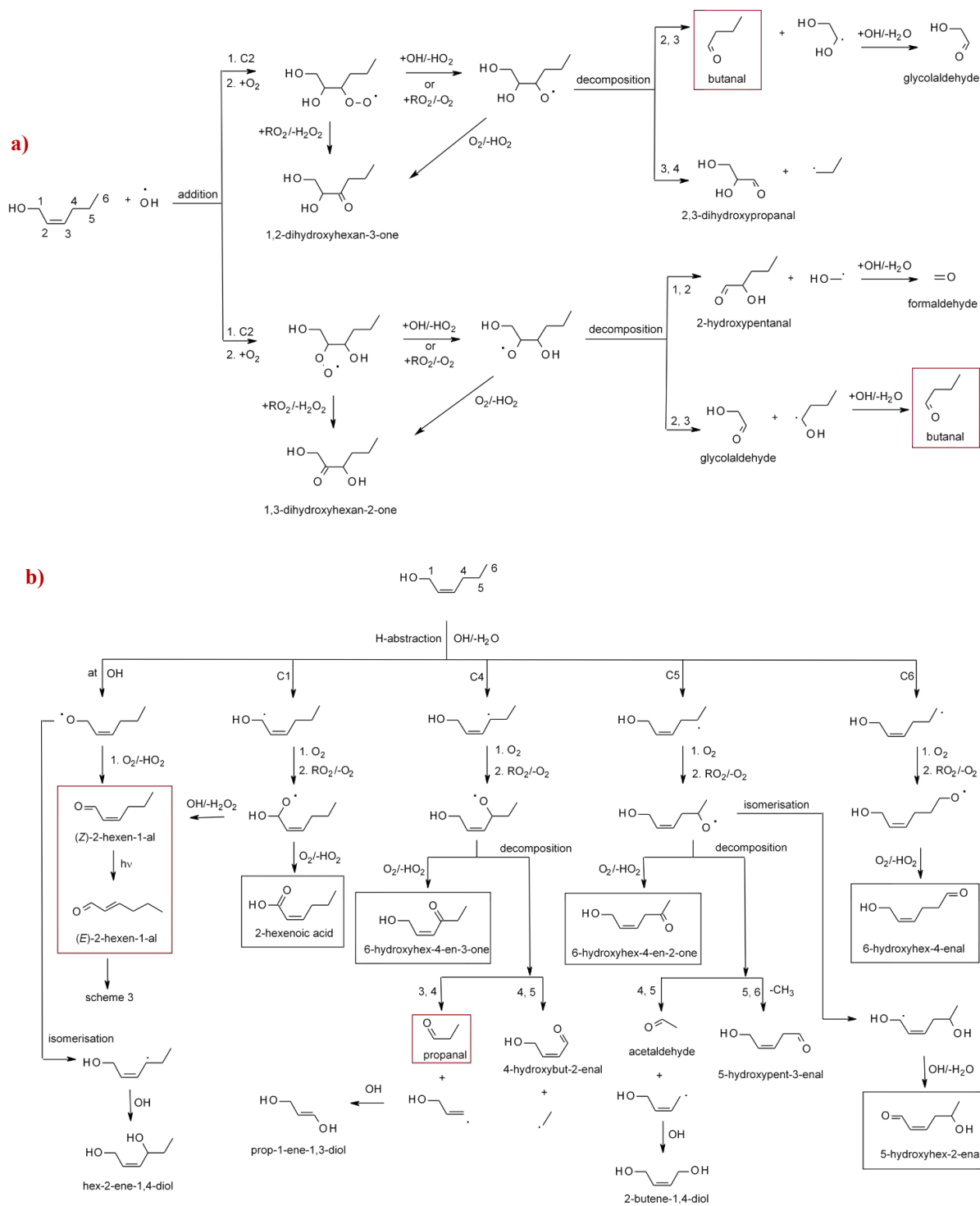


Figure 7.3. Concentration-time profile of PENTOL during: *a)* photo-oxidation experiments ($n=2$); *b)* photolysis ($n=1$) and dark oxidation ($n=1$) as control experiments.

7.3.3. HEXOL with $\cdot\text{OH}$ radicals

Details of the proposed mechanism for the aqueous-phase reaction between HEXOL and $\cdot\text{OH}$ radicals are shown in Scheme 7.2. The rationale for the reaction mechanism is similar to that of PENTOL-OH, as explained in the previous section (Section 7.3.2).



Scheme 7.2. Proposed reaction mechanistic pathways and the key product formation (*shown in red boxes*) from the reaction of (*Z*)-2-hexen-1-ol (HEXOL) and $\cdot\text{OH}$ radicals: a) addition channel, b) H-abstraction channel.

In contrast to PENTOL analysis, where only cGC-MS was useful, the rpLC-MS approach for post-reaction HEXOL samples revealed one oxidation product. The HEXOL traces were also detected, and quantified using the alcohol-targeted teUHPLC-UV/PDA-HESI/MS with a PDA detector and cGC-MS analysis.

The results from LC-MS were found to be more accurate and consistent as obtained from four injections from each set of the photooxidation experiments ($n = 2 \times 4 = 8$ injections) in comparison to two single injections from each set of experiments on cGC-MS. The latter could be improved with an addition of internal standards in future analyses. In Figure 7.7 molar fraction profiles of HEXOL and in Figure 7.6.a concentration-time profiles using the LC-MS data are presented. The cGC-MS total ion chromatogram (TIC) of reaction samples (at 0 h and 6 h, respectively) with the identified reactant and product peaks is depicted in Figure 7.4.

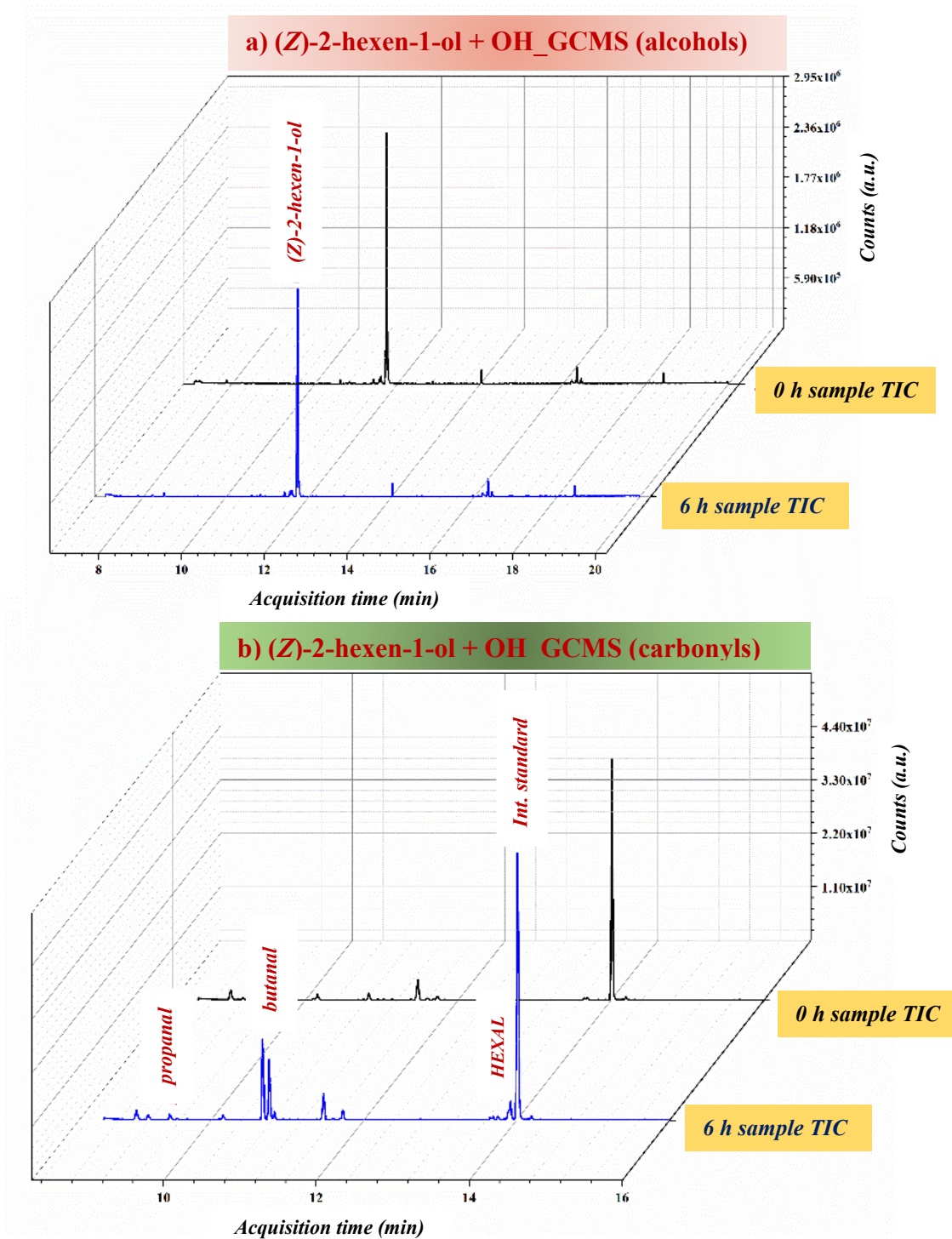


Figure 7.4. c-GC-MS Total Ion Chromatogram (TIC) obtained for the photooxidation reaction samples of (Z)-2-hexen-1-ol (HEXOL) with $\cdot\text{OH}$ radicals at time: $t = 0$ h (**black**), and $t = 6$ h (**blue**). **a)** c-GC-MS TIC for HEXOL (RT = 11.7 min); **b)** c-GC-MS TIC of carbonyl products. (See Table 7.2)

Figure 7.5 shows the total ion chromatogram (TIC) obtained for HEXOL using HPLC in PDA/UV mode.

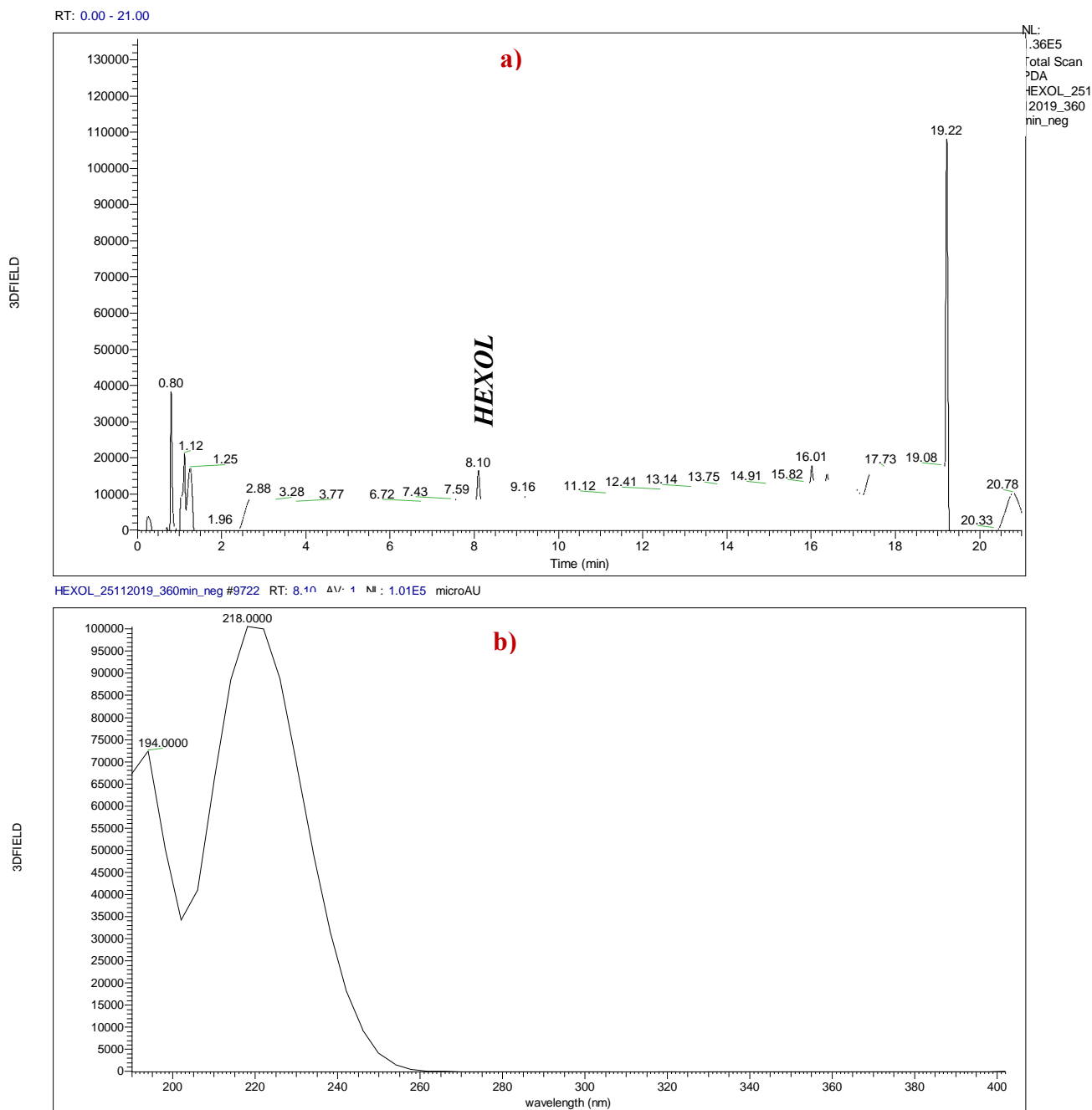
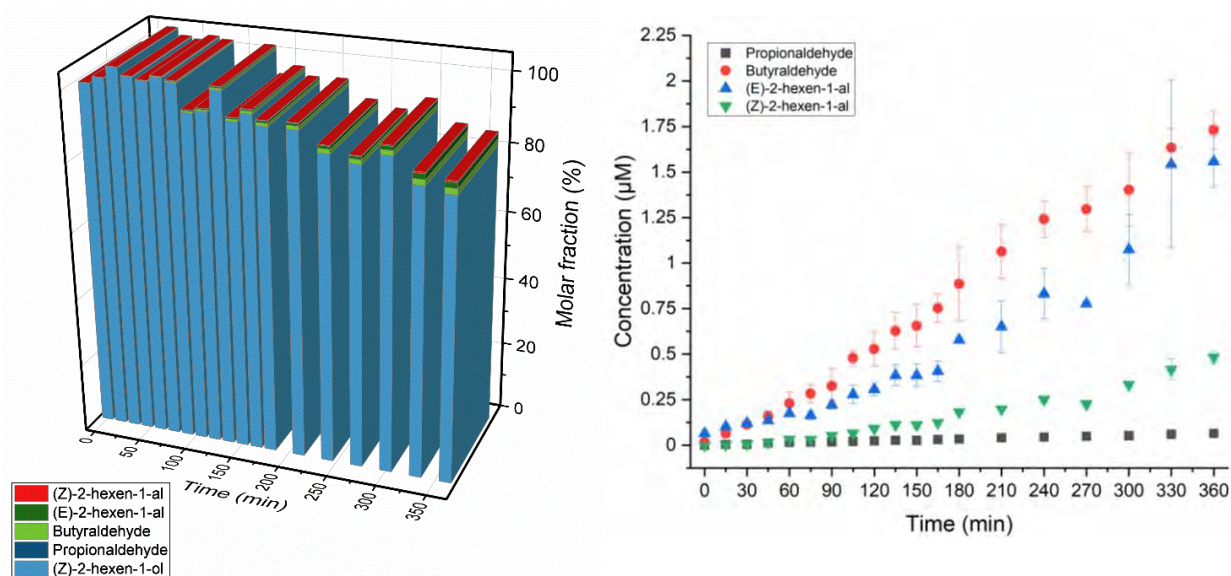


Figure 7.5. HPLC-PDA/UV data from the photooxidation experiment of HEXOL with $\cdot\text{OH}$ radicals at time, $t = 6$ h sample. **a)** Observed peak in the LC chromatogram for HEXOL the RT 8.1 min, confirmed using an authentic standard. **b)** PDA absorbance spectra (0 - 400 nm) of HEXOL, with the maximal absorbance at 218 nm (See Table 7.2).

As shown in Figure 7.6.a, after 6 h of the photooxidation up to $(20 \pm 3)\%$ of the molar fraction of HEXOL decays into its oxidation products. The carbonyl targeted c-GC-MS analysis confirmed the following molar fractions: propanal $(0.08 \pm 0.01)\%$, butanal $(2.04 \pm 0.12)\%$, (*E*)-2-hexen-1-al (HEXAL) $(1.8 \pm 0.2)\%$, and (*Z*)-2-hexen-1-al $(0.57 \pm 0.04)\%$, respectively (Figure 7.6.a).

According to the proposed mechanism (Scheme 7.2.a), the formation of butanal can be rationalized *via* the radical addition of $\bullet\text{OH}$ species to a C=C double bond (either C2 or C3 position) in HEXOL followed by the decomposition of corresponding HEXOL-based alkoxy radicals. The other two determined products, i.e., propanal and (*E/Z*)-2-hexen-1-al are proposed to be formed *via* a hydrogen-abstraction channel (Scheme 7.2.b). The HEXOL-based alkoxy radicals formed *via* the H-abstraction at a C4 site, decomposes to form propanal. While the H-abstraction at either a C1 site or the $-\text{OH}$ group can lead to (*E/Z*)-2-hexen-1-al. The GCM method predicts an addition reaction ($k = 9.07 \times 10^9 \text{ L mol}^{-1} \text{ s}^{-1}$, Section 7.3.1) resulting in the formation of butanal (as the major product), here to be at least two times faster than overall the H-abstraction (Section 7.3.1). It is followed by the subsequent H-abstraction at a C4 site ($k(4) = 1.40 \times 10^9 \text{ L mol}^{-1} \text{ s}^{-1}$, Section 7.3.1). Despite the GCM method predicts the H-abstraction at $-\text{OH}$ and a C1 site to a relatively much slower rate, I observed an unexpected higher yield of the (*E/Z*)-2-hexen-1-al as a reaction product during 6 h of the reaction. Thus, in contrast to PENTOL, GCM-predicted rate constants could not explain the ratio of the molar fraction of products formed. However, the DFT (discussed in Section 7.3.5) data reveals that the product resulting from the H-abstraction at a C1 site is the most thermodynamically stable, and thus likely to be formed as a novel HEXOL-originated SOA product.



Figures 7.6. *a*) Percentage of molar fraction of the HEXOL and its $\cdot\text{OH}$ -driven oxidation products in the aqueous phase; *b*) Concentration-time profiles of products, i.e., propionaldehyde, butyraldehyde, (*E*)-2-hexen-1-al, and (*Z*)-2-hexen-1-al during the photooxidation of HEXOL with $\cdot\text{OH}$ radicals ($n=2$).

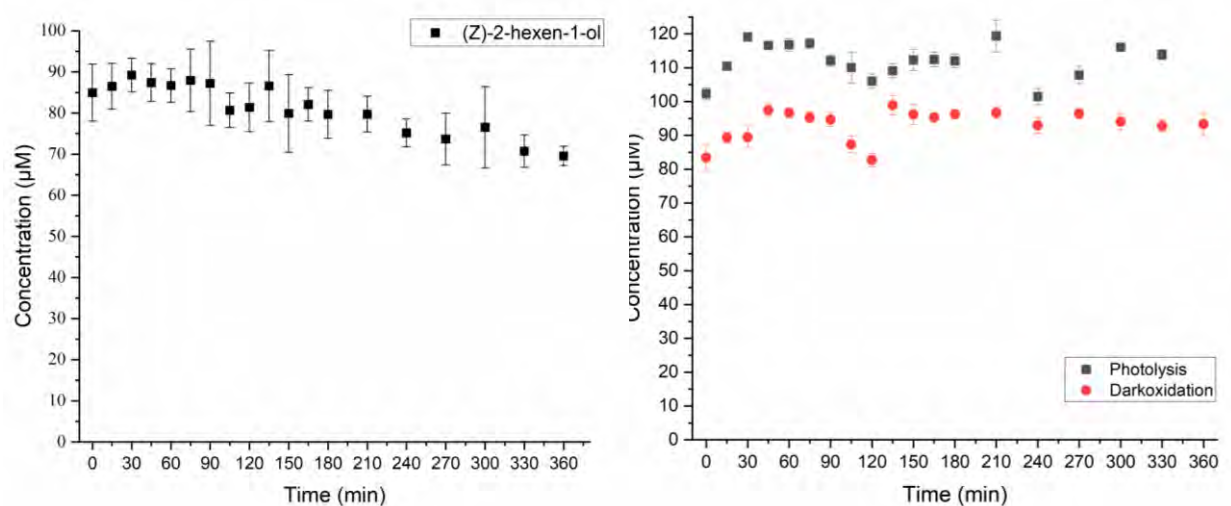


Figure 7.7. Concentration-time profiles of HEXOL during: *a*) photooxidation experiments ($n=2$); *b*) photolysis ($n=1$) and dark oxidation ($n=1$) as control experiments.

The LC-MS analyses recorded in the negative ion mode for the HEXOL- $\cdot\text{OH}$ reaction samples revealed the presence of the unknown detected as the m/z 113.06080 $[\text{M}-\text{H}]^-$ ion with a retention time of 6.6 min (Figure 7.8). The extracted ion chromatogram (EIC) of the ion shows its absence at $t=0$ h and its appearance later during the reaction run (Figure 7.8). Based on its accurate mass

data (Figure 7.9.a) and MS/MS profile (not shown here), the novel product of the formula $C_6H_{10}O_2$ could be tentatively assigned either to hydroxy hexenal, or hexenoic acid or hydroxy hexenone, respectively. These products can be explained either *via* a HEXAL pathway (explained later in section 7.3.4 and Scheme 7.3) or *via* the hydrogen abstraction at C4/C5 sites. While the H-abstraction at a C4 site appears to be proceeded faster due to the allylic radical formation (GCM, $k(4) = 1.4 \times 10^9 \text{ L mol}^{-1} \text{ s}^{-1}$), the isomerization through 1,5-hydrogen shift makes the H-abstraction at a C5 site comparatively stable (GCM, $k(5) = 1.34 \times 10^9 \text{ L mol}^{-1} \text{ s}^{-1}$), and may lead to 5-hydroxyhex-2-enal. The structure of 2-hexenoic acid assigned to the $[M-H]^-$ ion (m/z 113.06080) was ruled out with the aid of the authentic standard. Due to the unavailability of the authentic standards, the confirmation of the other two structures could not be completed, and thus, warrants further efforts. A $C_6H_{10}O_2$ signal intensity profile (Figure 7.9.b), points to continuous growth of the product in the mimicking photooxidation experiments.

The control experiments, i.e., photolysis and dark oxidation, confirmed no change in the initial concentration of HEXOL over the period of 6 h (Figure 7.7.b). The DFT findings supporting the mechanistic proposal will be discussed in details later in Section 7.3.5 within this chapter. Gibilisco *et al.*,¹⁷⁶ investigated the gas-phase products and mechanism of the reaction between 2-hexen-1-ol and $\cdot\text{OH}$ radical, and reported on butanal as the significant oxidation product. While for another isomeric hexenol, i.e., 3-hexen-1-ol, propanal was reported to be the major oxidation product. In the gas phase, for an isomer of HEXOL, i.e. (*E*)-2-hexen-1-ol the reaction proceeded *via* the addition of $\cdot\text{OH}$ radicals to the double bond, resulting in the formation of corresponding aldehyde and alcohol following a C2-C3 decomposition route.¹⁷⁶

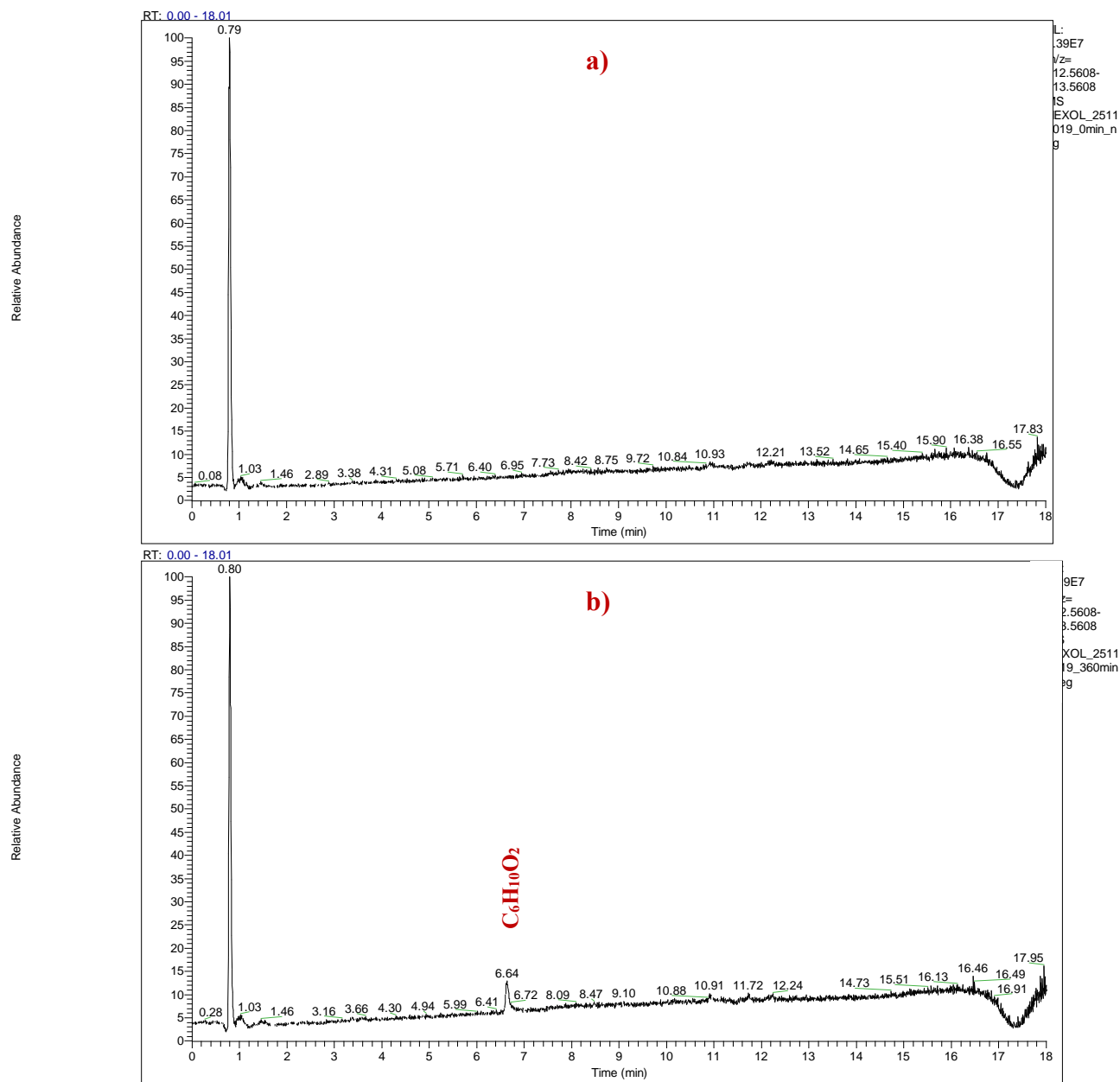


Figure 7.8. HPLC-ESI/MS Extracted Ion Chromatogram (EIC) acquired for of the m/z 113.06080 $[M-H]^-$ ion observed in the photooxidation samples containing 0.1 mM HEXOL with 5.0 mM H_2O_2 exposed to the UV light in a negative ion mode. a) at $t = 0$ h; b) at $t = 6$ h RT 6.6 min.

HEXOL_25112019_360min_neg #1454 RT: 6.65 AV: 1 NL: 9.83E5
T: FTMS - p ESI Full ms [50.0000-750.0000]

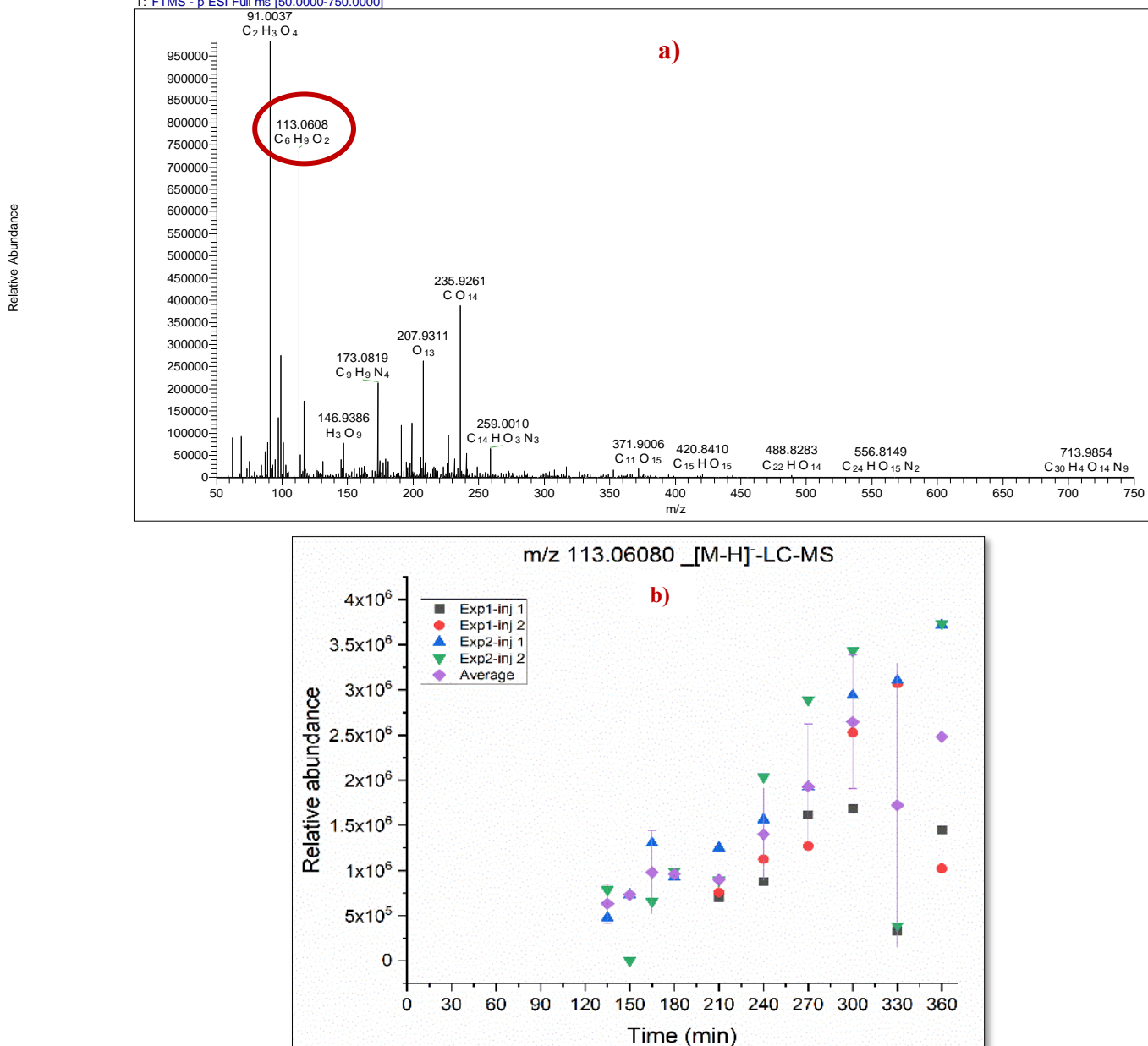


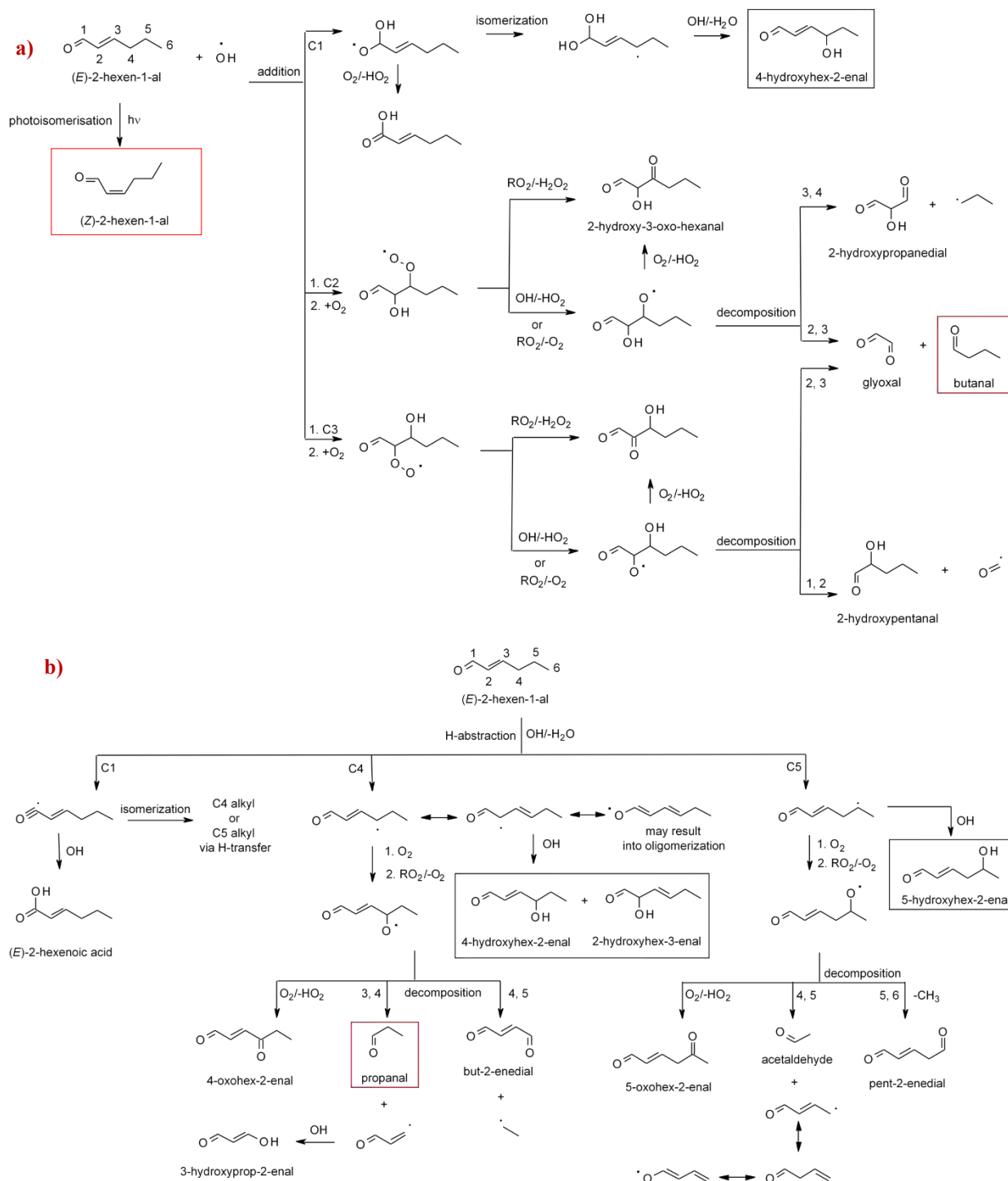
Figure 7.9. *a)* HPLC-ESI/MS mass data showing the m/z 113.06080 $[M-H]^-$ product with a formula of $C_6H_{10}O_2$ and detected at the RT 6.6 min (Figure 7.8), which arise from the photooxidation of (*Z*)-2-hexen-1-ol with $\cdot OH$ radicals at 6 h.; *b)* Signal intensity-time profile of the m/z 113.0608 ion during the $\cdot OH$ radicals-driven HEXOL photooxidation (0 – 360 min).

7.3.4. HEXAL with $\cdot OH$ radicals

In analogy to the product study discussed in previous sections, (*E*)-2-hexen-1-al (*E*-HEXAL) can also undergo aqueous-phase solar reactions *via* either addition or H-abstraction pathways. The formulated tentative mechanistic picture (Scheme 7.3) is similar to the that explained for

PENTOL-OH (Section 7.3.2). However, alkyl radicals produced *via* the H-abstraction at a C4 site may additionally undergo the oligomerization at later stages of the photooxidation. In my study, I could not identify any of these product(s) even after 6 h of the run. I could explain the outcome in two ways. First, the concentration of the higher MW products could be far below the method detection limit. Second, these products are later stage ones (i.e., aging products), and thus their formation could require far longer photooxidation times. In Scheme 7.3, identified products are marked in red boxes (i.e., butanal, propanal, and (*Z*)-2-hexen-1-al), while structurally-unassigned product with a formula C₆H₁₀O₂ in black boxes.

In contrast to the other two GLVs (PENTOL, and HEXOL), *E*-HEXAL shows considerable absorption (290 – 400 nm, Section 7.3 above), and therefore the 10 – 12% molar fraction of a photoisomerization product (i.e., (*Z*)-2-hexen-1-al) was observed in both photooxidation and control photolysis experiments at 6 h of the reaction time (Figure 7.13 and 7.10.b, respectively). Hitherto gas-phase studies,^{204, 486} reported on the \cdot OH radicals as the major oxidation source for *E*-HEXAL in the troposphere and upon photolysis undergoing photo-isomerisation to produce (*Z*)-2-hexen-1-al. Figure 7.10.b shows the concentration-time profile during the control photolysis experiment. No products were observed in the control dark experiment (Figure 7.10.a).



Scheme 7.3. Proposed mechanistic reaction pathways and the key product formation (*shown in red boxes*) during the photooxidation of (*E*)-2-hexen-1-al (*E*-HEXAL) and $\cdot\text{OH}$: a) addition channel, b) H-abstraction channel.

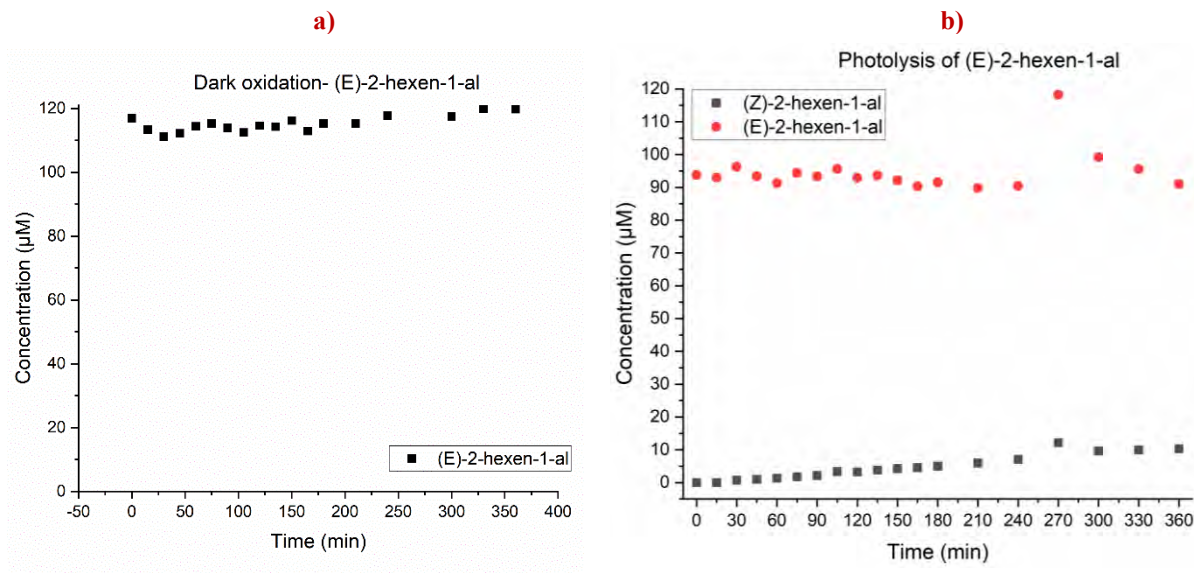


Figure 7.10. Concentration-time profile of reactant *E*-HEXAL during: **a)** dark-oxidation experiments ($n=1$); **b)** photolysis ($n=1$) as control experiments.

The c-GC-MS total ion chromatogram (TIC) for the reaction samples at 0 and 6 h (Figure 7.11.a), shows the unreacted reactant and product retention times 9.46, 10.69, 12.3, 13.76, 13.93, and 14.025 min, respectively. The TIC obtained using HPLC-PDA/UV for the reactant *E*-HEXAL is also provided (Figure 7.12). The similar data could be retrieved using a positive mode electrospray mass spectrometry (Table 7.2). The *E*-HEXAL quantification results from carbonyl targeted c-GC-MS were found to be consistent, too, owing to the usage of authentic standards during the analysis. Thus, the *E*-HEXAL molar fraction and concentration-time profile results presented in Figure 7.13.a, 7.11.b and 7.10.b were calculated based on c-GC-MS data.

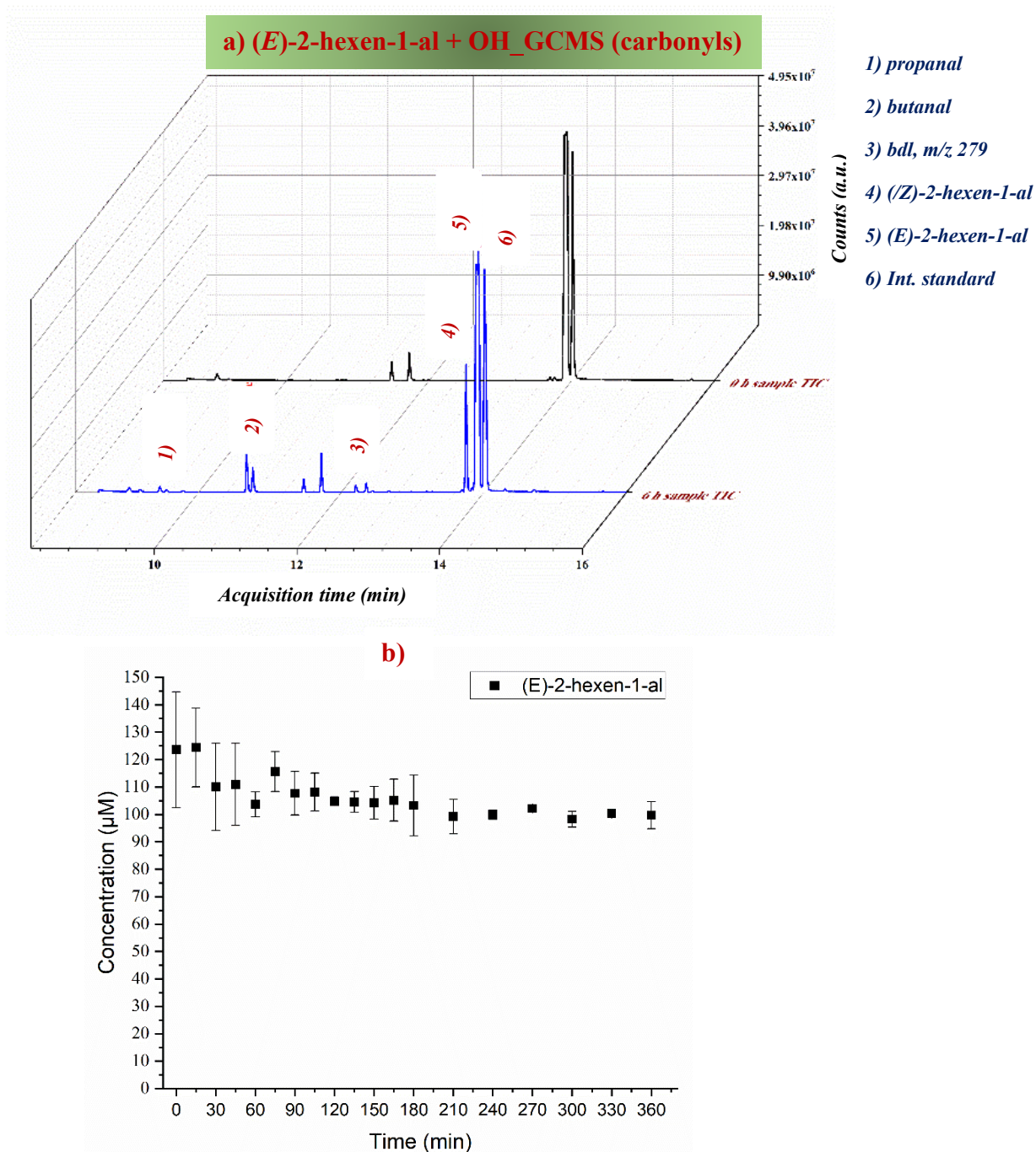


Figure 7.11. *a)* GC-MS Total Ion Chromatogram (TIC) obtained for the photooxidation reaction samples of (*E*)-2-hexen-1-al (E-HEXAL) with \cdot OH radicals at time: $t = 0$ h (**black**), and $t = 6$ h (**blue**) (See Table 7.2); *b)* Concentration-time profile of reactant *E*-HEXAL during photooxidation.

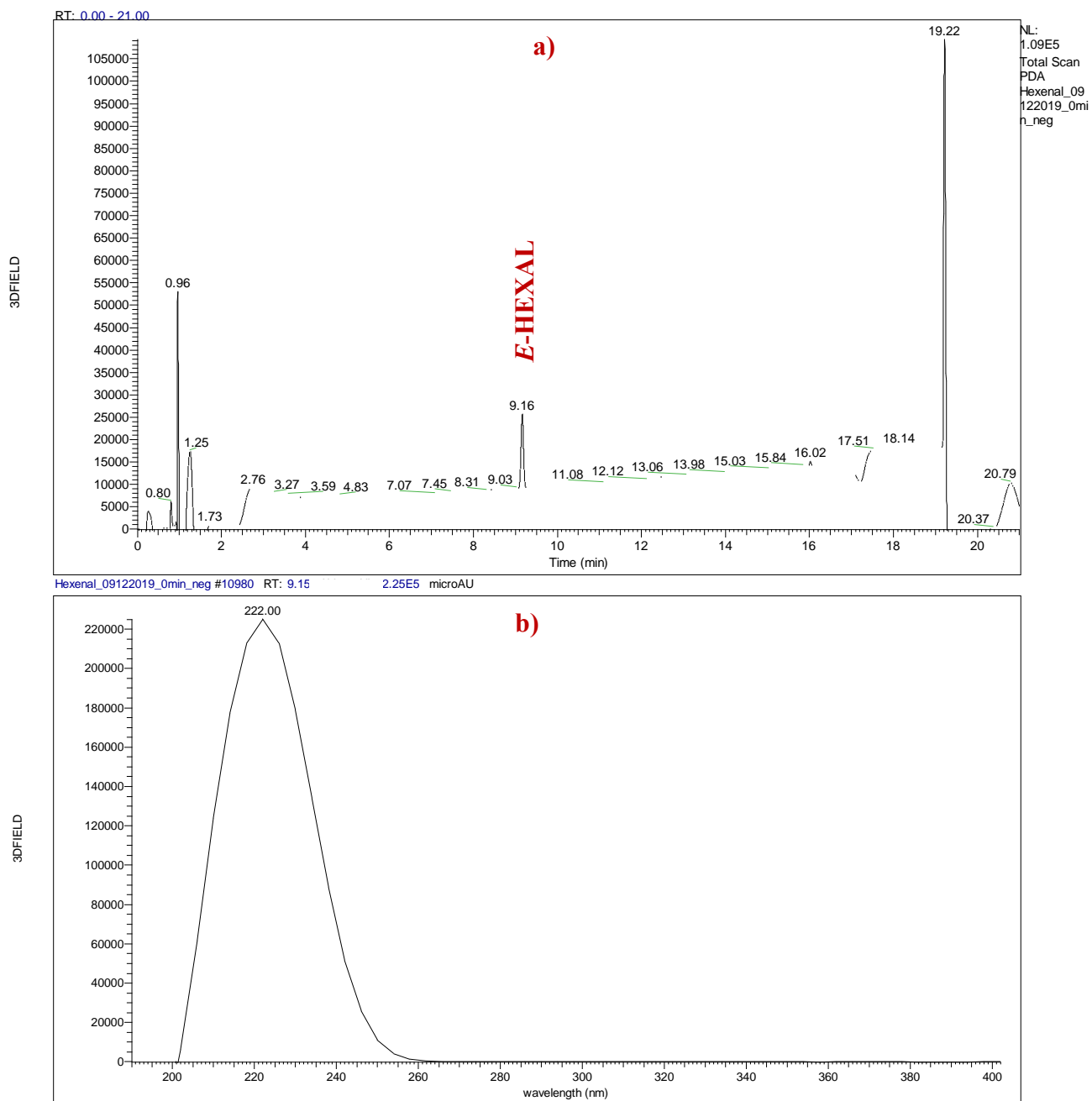
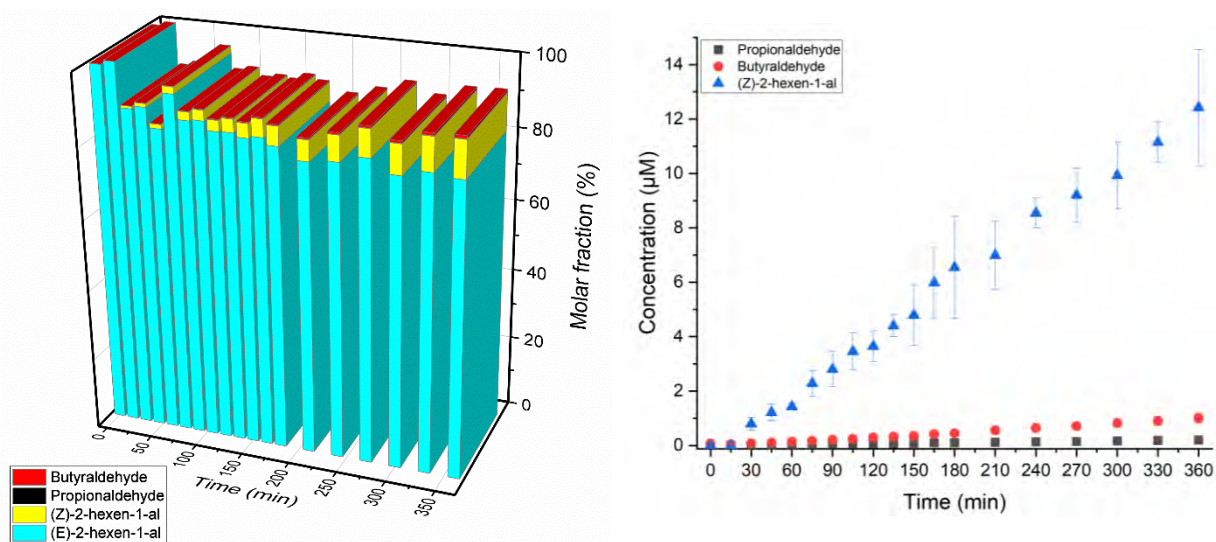


Figure 7.12. HPLC-PDA/UV data from the photooxidation experiment of *E*-HEXAL with $\cdot\text{OH}$ radicals at time, $t=6$ h sample. **a)** Observed peak in the LC chromatogram for *E*-HEXAL with the RT 9.16 min, confirmed using an authentic standard. **b)** PDA absorbance spectra (0 - 400 nm) of *E*-HEXAL with a characteristic absorbance maximum at 222 nm (See Table 7.2).

The gas-phase ozonolysis of HEXAL reported elsewhere¹⁹⁸ showed the formation of carbonyl products, including glyoxal (0.56 ± 0.04) and n-butanal (0.53 ± 0.06) yield, respectively. During

the aqueous-phase photooxidation, the $(18.5 \pm 9.9)\%$ molar fraction of the *E*-HEXAL was observed to decay at the expense of the fractions of butanal $(0.81 \pm 0.02)\%$ and propanal $(0.162 \pm 0.004)\%$, along with the photo-isomerization to *Z*-HEXAL $(10 \pm 0.01)\%$, respectively (Figure 7.13.a). Figure 7.13.b shows the concentration-time profile of the observed reaction products. According to the proposed mechanism (Scheme 7.3.a), the butanal formation can be explained *via* the $\cdot\text{OH}$ radicals addition to either C=C double bond position (i.e., C2 or C3) in HEXAL followed by the decomposition of corresponding HEXAL-based alkoxy radical. The other product, i.e., propanal is proposed to be formed *via* the hydrogen-abstraction channel (Scheme 7.3.b). The HEXAL-alkoxy radical formed *via* the H-abstraction at a C4 site, decomposes to form propanal. The GCM estimated rate constants (Section 7.3.1) suggests the addition process to be at least one magnitude faster than any H-abstraction routes, and thus favorable. The experimentally observed ratio of butanal to propanal is 5:1. However, it cannot be correlated to the ratio of the estimated reactivity rate from the GCM approach. Further mechanistic investigation using the DFT approach will be discussed later (Section 7.3.5).



Figures 7.13. *a*) Percentage of molar fraction of the *E*-HEXAL and its $\cdot\text{OH}$ radicals-driven oxidation products in the aqueous phase; *b*) Concentration-time profile of key products, propionaldehyde, butyraldehyde, (*Z*)-HEXAL during the photooxidation ($n = 2$).

Similar to HEXOL, the reversed-phase LC-MS analysis for reaction samples from the HEXAL-OH reaction system revealed the presence of the $\text{C}_6\text{H}_{10}\text{O}_2$ product(s) (m/z 113.06080 [M-H] $^-$) in *E*-HEXAL reaction samples as well (Figure 7.14 and 7.15). Correlating the results from the

reaction samples of two different substrates and their proposed mechanism schemes (Scheme 7.2 and Scheme 7.3), $C_6H_{10}O_2$ was more likely assigned to either hydroxy hexenal than hydroxy hexenone. In addition, its early formation (soon after $t=0$ h) and high relative abundance (at least two orders of magnitudes greater compared to HEXOL) were observed. The signal intensity-time profile of $C_6H_{10}O_2$ m/z 113.06080 $[M-H]^-$ are provided in Figure 7.15.b. These results further narrow the possible structures to 5-hydroxyhex-2-enal which could be explained *via* a HEXAL pathway in HEXOL (Schemes 7.2 and 7.3) and the H-abstraction at a C5 site. Thus, the major input to the unaccountable loss of up to 8% molar fraction of HEXAL may come from the formation of the unknown $C_6H_{10}O_2$.

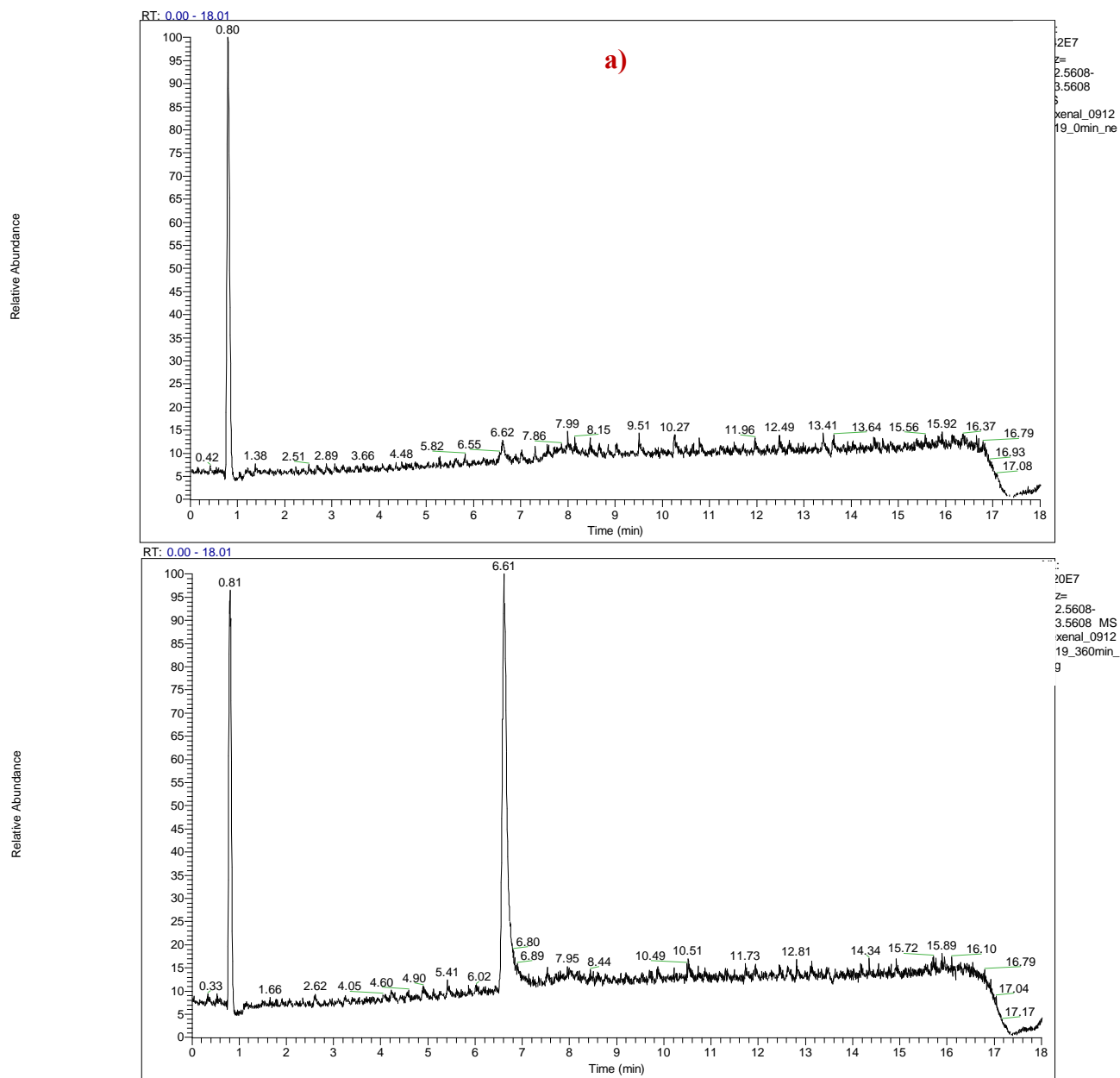


Figure 7.14. HPLC-ESI/MS EIC data of m/z 113.06080 $[M-H]^-$ product observed in photooxidation experiments with 0.1 mM *HEXAL* and 5.0 mM H_2O_2 exposed to the UV light in a negative ion mode. **a)** at $t=0$ h; **b)** at $t=6$ h, RT 6.6 min (See Table 7.2).

Hexenal_09122019_360min_neg #1462 RT: 6.61 AV: 1 NL: 9.46E6
 T: FTMS - p ESI Full ms [50.0000-750.0000]

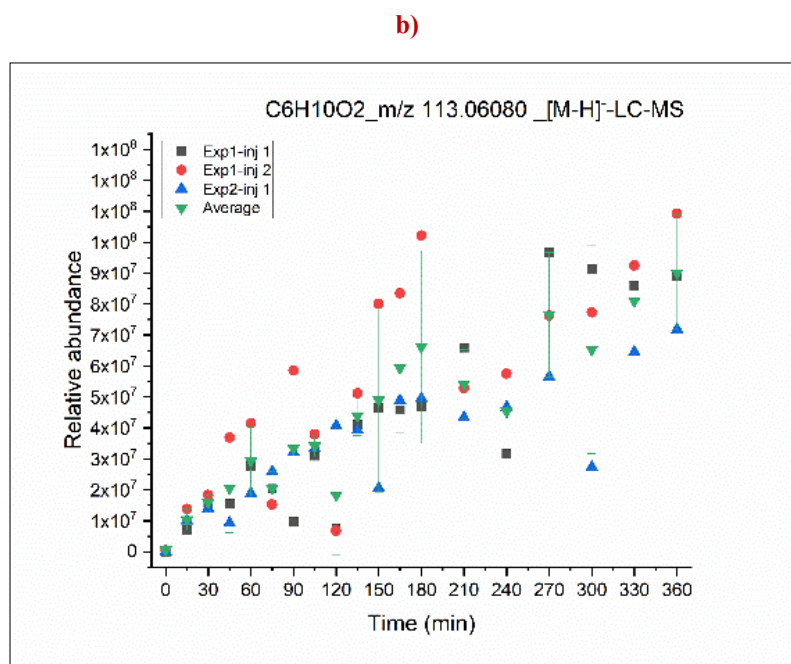
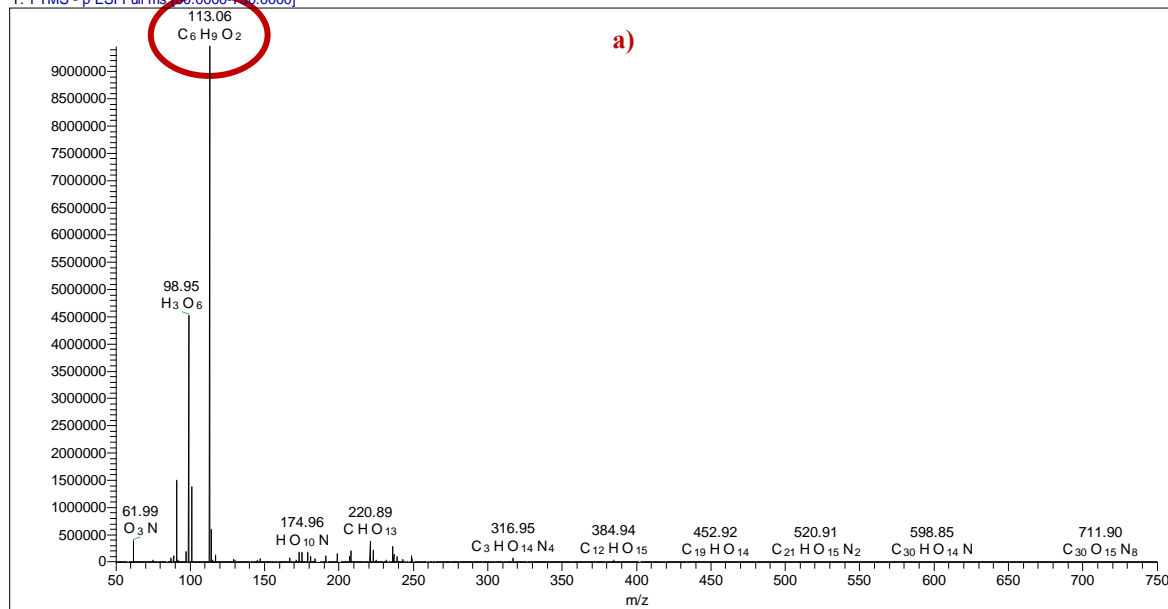


Figure 7.15. *a)* HPLC-ESI/MS mass spectrum of m/z 113.06080 $[M-H]^-$ product, corresponding to a $C_6H_{10}O_2$ formula at the RT 6.6 min observed during the photooxidation of *HEXAL* with $\cdot OH$ radicals over 6 h. (corresponding chromatogram is shown in Figure 7.14.b); *b)* Signal intensity-time profile of m/z 113.0608 during the $\cdot OH$ radicals-driven photooxidation of *HEXAL* (0 – 360 min).

7.3.5. DFT results

Details of the method are provided in Chapter 3 (Section 3.4.2). To summarise, the computational investigation with the density functional theory (DFT) was performed using an ORCA 5.0 programs.³⁹³ The calculations utilized hybrid B3LYP functional³⁹⁴⁻³⁹⁷ augmented with the Grimme's dispersion correction (D3BJ).^{398, 399} In all cases, def2-TZVP basis set⁴⁰⁰ was employed. A series of computer-assisted calculations for reaction processes discussed were carried out to provide a more comprehensive understanding of experimental results. Vacuum optimized 3D structures of GLVs are provided in Figure A1 (a – c), Appendix. All XYZ coordinates of the optimized structures and intermediates can be downloaded as a dataset zip folder from a repository website RepOD at <https://repod.icm.edu.pl/dataset.xhtml?persistentId=doi:10.18150/1J2I3C>. The potential energy scans (PES) were carried out to confirm the most stable conformers of the corresponding adducts arising from the addition reaction pathways for each GLVs with $\cdot\text{OH}$ radicals and are shown in Figures A2, A4, and A6 (Appendix).

In this section, I present and discuss the DFT results obtained for all three compounds with the aid of simple 2-D schemes (Scheme 7.4 – 7.9) showing relative energy (ΔE) for each intermediate i.e., reaction complex (RC), addition adducts (adducts), transition states (TS), and hydrogen abstraction products (P-H, or P-H-C).

The DFT calculations for the reaction between PENTOL, HEXOL, and HEXAL with $\cdot\text{OH}$ radicals revealed that addition pathways most probably do not involve any transition states, as we were unable to locate any of them. Here, it should be mentioned that such addition reactions proceed analogously to bond formation between two atoms in a vacuum, and as such, no electronic barrier is expected. This outcome agrees with our small experimental activation energies, E_A obtained 7 – 15 kJ mol⁻¹ (Chapter 5, Table 5.9), which is converted to 1.7 to 3.6 kcal mol⁻¹ (1 kcal = 4.184 kJ). In addition, the experimental activation entropy change (ΔS^\ddagger) value was also negative, suggesting the low energy reactive complex between GLV and $\cdot\text{OH}$ radicals is formed very quickly, paving the way for fast reactions (Chapter 5, Table 5.9). For a few cases, the hydrogen abstraction pathway is also observed to be dominant, and thus cannot be ruled out. The activation energy barrier, dE^\ddagger for the H-abstraction reaction indicated in Scheme 7.5, 7.7, and 7.9 was always calculated using the lowest energy RC state (See appendix for other possible RC and their ΔE value), and were found to be less than 6 kcal mol⁻¹ or even negative in few cases (discussed later in this section).

In all cases, the activation barriers went down in CPCM, indicating that reactions of such GLVs in atmospheric water should be accelerated. The largest influence was observed for the most polarized C-H bond in 1-penten-3-ol, where the transition state TS-3 has small negative activation barrier (Scheme 7.5, $dE^\ddagger = -0.37 \text{ kcal mol}^{-1}$). Such negative value is rather an artifact of a rather simplistic approach, but we expect the trends to be captured correctly. Further work should for relaxation effects occur due to the presence of a solvent or cover the hydrogen bond network alternation during the reaction. DFT observations are correlated to the experimentally identified product in later subsections.

The bond dissociation energy (BDE) calculation results provided in Table 7.3 below are later compared and discussed alongside DFT findings for H-abstraction of each GLV in this section later.

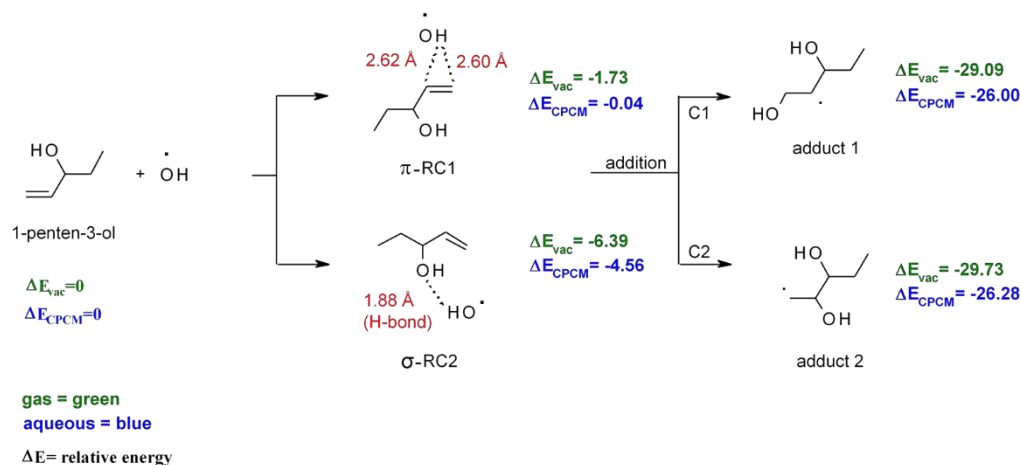
Table 7.3. Bond dissociation energies (BDEs) of C-H and O-H bond in PENTOL, HEXOL, and HEXAL calculated in vacuum and aqueous-phase compared to experimentally obtained typical bond enthalpies^{487*}, (kcal mol^{-1}) at 298 K.

GLV	position	O-H	C1-H	C3-H	C4-H	C5-H	C6-H	Reference
	Experimental	105 ^a	^b 88	^c 97 ^d 89	99 ^c	99 ^e	101 ^f	⁴⁸⁷
PENTOL	gas	98		73	94	96		this study
	aqueous	96		69	91	94		
HEXOL	gas	97	74		78	94	97	this study
	aqueous	97	73		78	93	97	
HEXAL	gas		87		77	94	98	this study
	aqueous		88		76	94	98	

*Experimental values for: ^a CH₃O-H; ^b aldehydic group (H-CHO); ^c 3° hydrogen H-C(CH₃)₃; ^d allylic hydrogen CH₂CHCH₂-H; ^e isopropyl hydrogen H-CH(CH₃)₂; ^f H-CH₂CH₃.

7.3.5.1. Reactivity of PENTOL with ·OH radical

Addition pathway. Scheme 7.4 below shows the DFT investigated pathway of the formation of GLV alkyl radicals *via* the addition of ·OH radicals to PENTOL. The obtained relative energies (ΔE , kcal mol^{-1}) with the zero point energy (ZPE) correction included is provided for each substrate in Scheme 7.4. Due to the presence of H-bond between H atom of ·OH radical and O atom of the -OH functional group in PENTOL, reaction complex σ -RC2 is observed to be more stable than reaction complex π -RC1 by at least 4 kcal mol^{-1} in the aqueous phase calculated with CPCM continuum model.

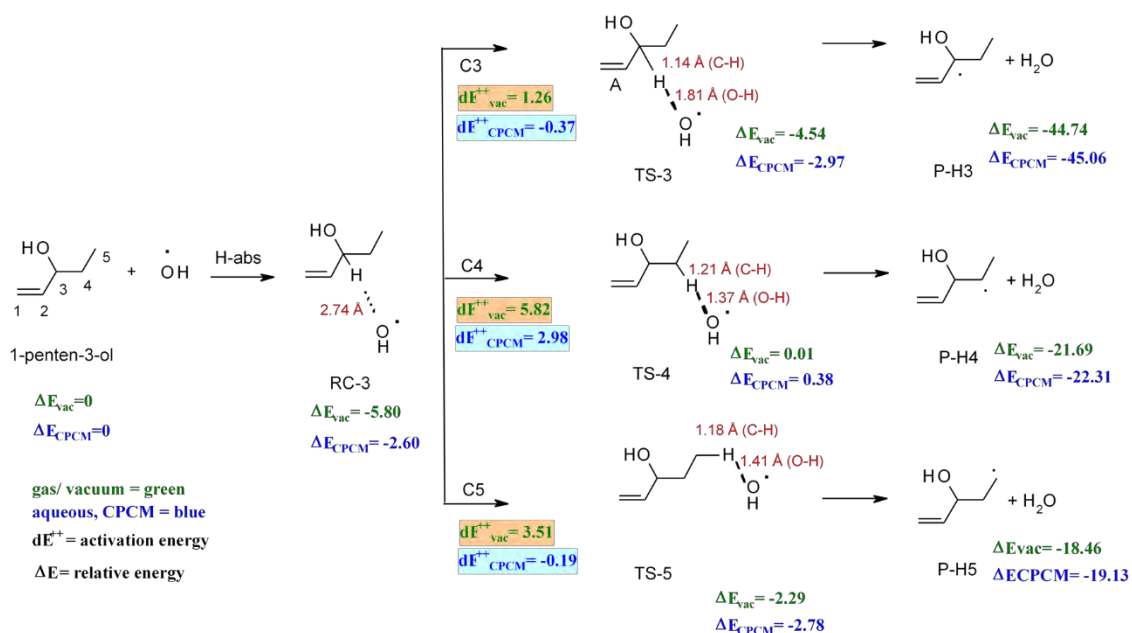


Scheme 7.4. 2-D scheme of the optimized geometries (B3LYP def2-tzvp) investigated for the addition reaction pathway from the reaction of 1-penten-3-ol (PENTOL) and $\cdot\text{OH}$ radicals in the aqueous phase, using CPCM continuum solvation model. ΔE is in kcal mol^{-1} .

The formation of both adduct 1 and 2 seems equally favorable in aqueous-phase (Scheme 7.4). However, the long-range interaction between the two intramolecular $-\text{OH}$ functional groups is a little higher in adduct 1 (2.08 \AA), than that for adduct 2 (2.25 \AA). Scheme 7.4 shows slightly higher stability based on DFT of adduct 2 (even though being a terminal radical) than adduct 1 by $0.03 \text{ kcal mol}^{-1}$ which may be accounted to the relative position of OH groups. Based on reactivity rate, GCM estimation (Section 7.3.1) suggested the addition at position C1 to be faster ($k(1) > k(2)$) by at least two orders of magnitude. Accounting for both kinetic (based on GCM) and thermodynamical (based on ΔE), factor formation of the experimentally observed product, i.e., propanal can be explained *via* addition at C1 as proposed in Scheme 7.1. The other products might be below the detection limit for a total reaction time of 6 h, and therefore, were not detected during GC-MS or LC-MS analysis.

H-abstraction pathway. The lowest $dE_{\text{CPCM}}^{\ddagger}$ barrier ($-0.37 \text{ kcal mol}^{-1}$) for TS-3 and ΔE values for P-H3 ($\Delta E_{\text{CPCM}} = -45.06 \text{ kcal mol}^{-1}$) in Scheme 7.5 shows the H-abstraction at C3 favours the formation of stable allylic radical product (P-H3). Product P-H3 (C3) is more stable by at least $22 - 25 \text{ kcal mol}^{-1}$ in comparison to the H-abstraction products P-H4 (C4), and P-H5 (C5). The BDE for hydrogen at C3 was found to be the lowest ($\text{C3} < \text{C4} < \text{C5}$, Table 7.3), and it is in agreement with the ΔE values (Scheme 7.5) as well as reactivity rate based on GCM ($k(3) > k(4) > k(5)$, Section 7.3.1).

Overall, the H-abstraction at a C3 site gives the most stable alkyl radical product ($\Delta E_{\text{CPCM}} = -45.06$ kcal mol⁻¹, Scheme 7.5), followed by the addition reaction at C1 and C2 ($\Delta E_{\text{CPCM}} = -26.00$, and -26.28 kcal mol⁻¹, Scheme 7.4). However, experimentally observed molar fraction of addition product (propanal) is more than H-abstraction (1-penten-3-one), i.e., 3:1, which is supported by the GCM estimated reactivity rate (Section 7.3.1). This contradictory observation was also found in the previously published DFT results for a reaction of PENTOL with Cl by Rodriguez *et al.*²⁰⁰ They found that although the barrier for the H-abstraction was a little higher in comparison to the addition, the product of the H-abstraction at a C3 was found to be more stable by at least 1.4 kcal/mol. We cannot exclude that the adapted theoretical model presented in this thesis cannot capture effects responsible for experimentally observed selectivity, such as H-bonds with solvent molecules or the dynamic behavior of the intermediates.

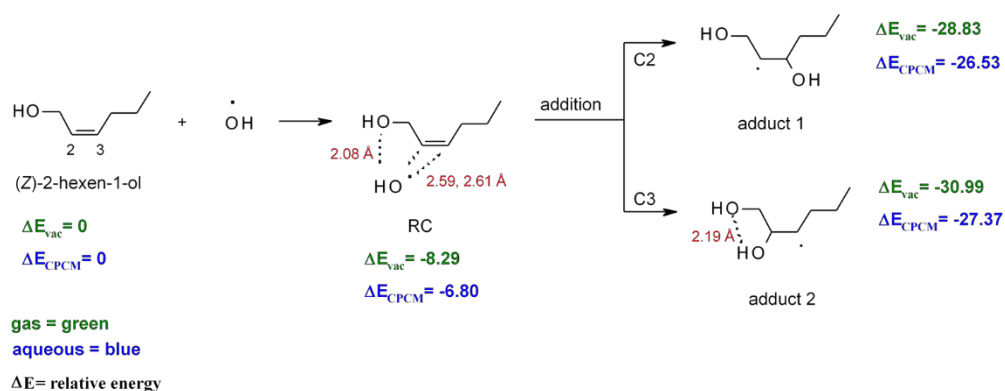


Scheme 7.5. 2-D scheme of the optimized geometries (B3LYP def2-tzvp) investigated for the H-abstraction reaction pathway from the reaction of 1-penten-3-ol and $\cdot\text{OH}$ radicals in the aqueous phase using CPCM continuum solvation model.

7.3.5.2. Reactivity of HEXOL with $\cdot\text{OH}$ radical

Addition pathway. Addition at a C3 site is at least 1 kcal/mol more stable than addition at a C2 position in the aqueous phase (Scheme 7.6). Adduct 1 is free from any steric hindrance.

However, in adduct 2 the intramolecular long range interaction between O and H atoms of the two adjacent hydroxyl groups ($d_{O...H} = 2.19 \text{ \AA}$, Scheme 6) increases its stability compared to adduct 1. Based on the DFT results as well as reactivity rate from GCM ($k(2) = k(3)$) (SI section 7.3.1), both adduct 1 and 2 can equally lead to the formation of experimentally observed butanal (Scheme 7.2a).

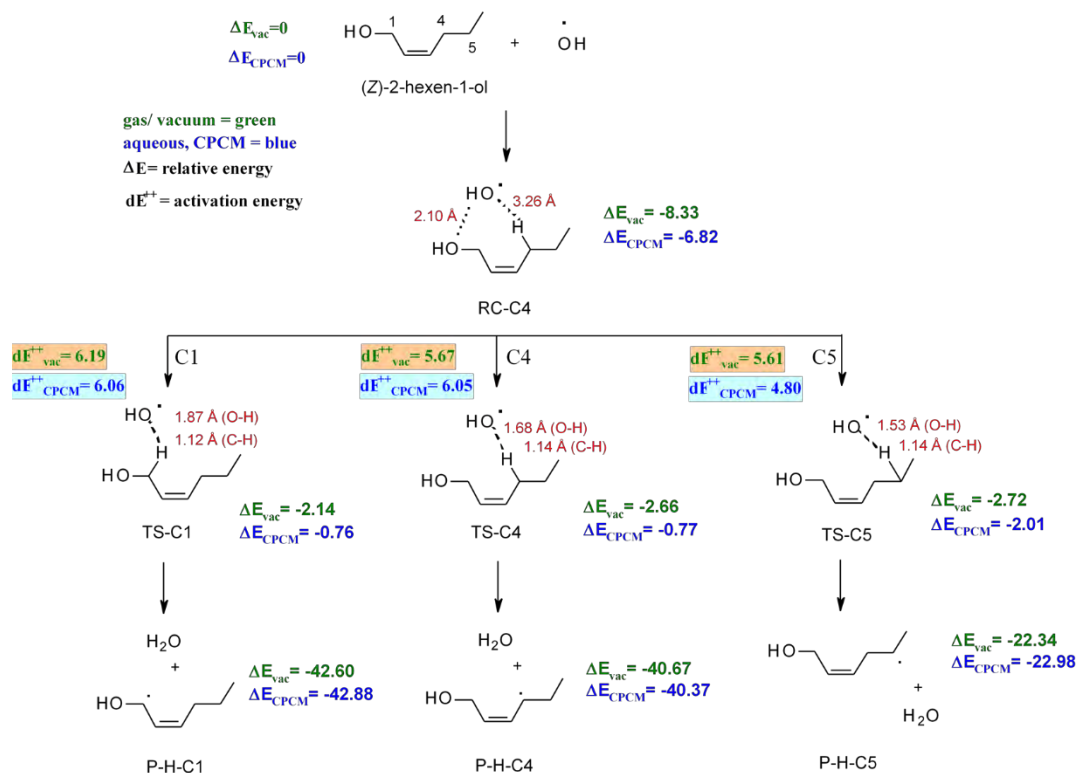


Scheme 7.6. 2-D scheme of the optimized geometries (B3LYP def2-tzvp) investigated for the addition reaction pathway from the reaction of (Z)-2-hexen-1-ol and $\cdot\text{OH}$ radicals in the aqueous phase using CPCM continuum solvation model.

H-abstraction pathway. The product of the H-abstraction at a C1 site (P-H-C1) is found to be most stable ($\Delta E_{\text{CPCM}}, -42.88 \text{ kcal mol}^{-1}$), followed by the P-H-C4 ($\Delta E_{\text{CPCM}}, -40.37 \text{ kcal mol}^{-1}$) in the aqueous phase. Such observation could be rationalized by the formation of a stable allylic radical product (P-H-C1, and P-H-C4, Scheme 7.7) and could confirm the formation of propanal and (E/Z)-2-hexenal (Scheme 7.2), both observed in photooxidation experiments. These results are also in good agreement with the BDE calculations ($C1 < C4 < C5$) (Table 7.3). However, the reaction barrier $dE_{\text{CPCM}}^\ddagger$ ($4.80 \text{ kcal mol}^{-1}$) is observed to be the lowest for RC-C4 to TS-C5 (Scheme 7.7), which could also provide theoretical evidence of the formation of experimentally observed unknown product(s) $\text{C}_6\text{H}_{10}\text{O}_2$ via the 1, 5- hydrogen-transfer or isomerization of HEXOL-alkoxy radical as proposed in Scheme 7.2.

Overall, DFT results show that the product of H-abstraction at C4 and C1 are more stable and favorable in comparison to that of addition adducts by at least 15 kcal mol^{-1} . Similarly, Gai *et al.*,²⁰⁸ explained the relevance of the H-abstraction channel in the gas-phase reaction of hexenols.

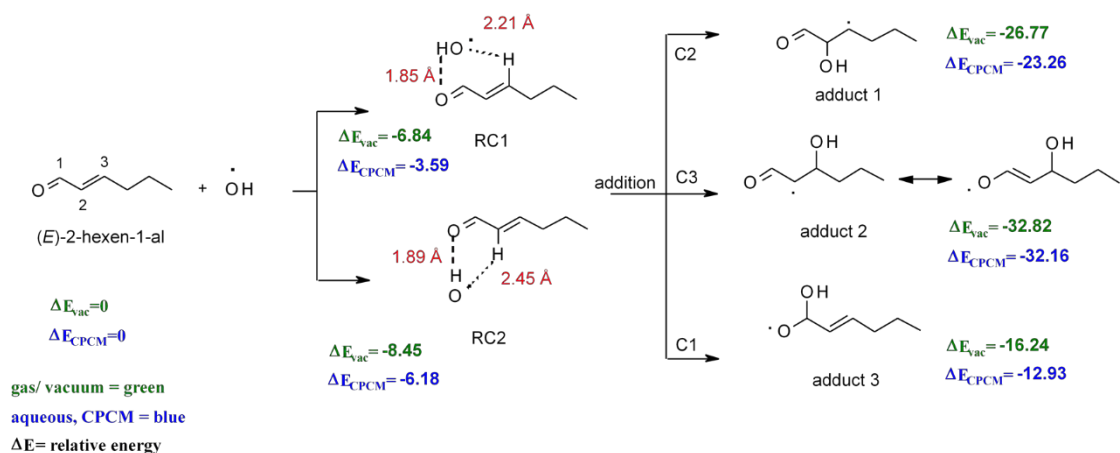
Nevertheless, addition reactions are also fast enough (GCM) and rather barrier less (DFT); hence, the major product observed is butanal.



Scheme 7.7. 2-D scheme of the optimized geometries (B3LYP def2-tzvp) investigated for the H-abstraction reaction pathway from the reaction of (Z)-2-hexen-1-ol and $\cdot\text{OH}$ in the aqueous phase using CPCM continuum solvation model.

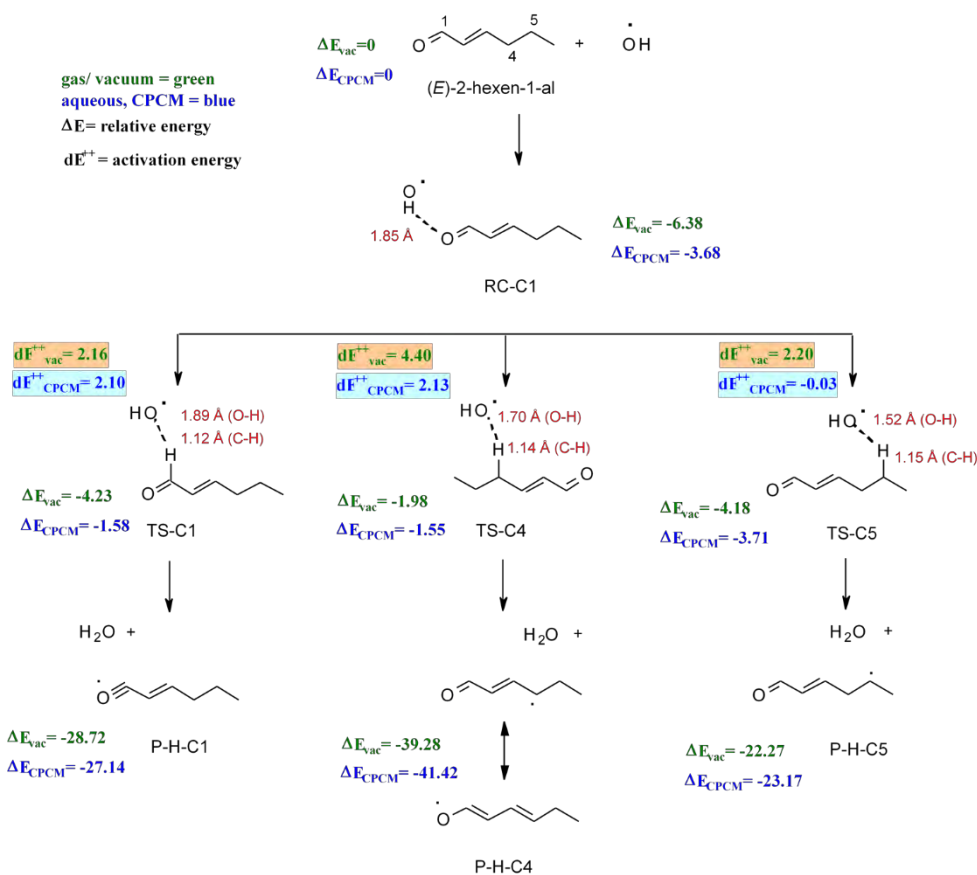
7.3.5.3. Reactivity of HEXAL with $\cdot\text{OH}$ radical

Addition pathway. Adduct 2 (addition product at C3) is at least 9 kcal mol⁻¹ more stable than adduct 1 (addition at C2) in the aqueous phase (Scheme 7.8), which also results in the formation of butanal experimentally. Both proposed reaction complexes (RC1 and RC2) are stabilized with a strong intermolecular hydrogen bonding (Scheme 7.8). The addition of $\cdot\text{OH}$ radicals at the carbonyl group (adduct 3) is least favorable, and thus highly unlikely to occur.



Scheme 7.8. 2-D scheme of the optimized geometries (B3LYP def2-tzvp) investigated for the addition reaction pathway from the reaction of (*E*)-2-hexen-1-al and $\cdot\text{OH}$ in the aqueous phase using CPCM continuum solvation model.

H-abstraction pathway. The hydrogen abstraction at a carbon position 4 produces the most stable radical product (ΔE_{CPCM} , -41.42 kcal mol $^{-1}$) by at least 12 – 15 kcal mol $^{-1}$, due to the formation of stable allylic radical in P-H-C4 (Scheme 7.9) with a low energy barrier ($dE_{\text{CPCM}}^{\ddagger} = 2.13$ kcal mol $^{-1}$). The H abstraction follows it at aldehydic hydrogen at a C1 site, based on the ΔE ($\Delta E_{\text{CPCM}} = -27.14$ kcal mol $^{-1}$) of P-H-C1. Results of BDE ($\text{C4} < \text{C1} < \text{C5}$) are in perfect agreement (Table 7.3), while reactivity rates (based on GCM) shows slightly different results ($k(4) > k(5) > k(1)$, Section 7.3.1). Activation energy barrier for TS-C1, $dE_{\text{CPCM}}^{\ddagger} = 2.10$ kcal mol $^{-1}$ is a little lower than that for a TS-C4, which suggests that the isomerization proposed in Scheme 7.3 due to hydrogen-transfer to C4 and C5 sites can certainly provide extra stability to the formation of P-H-C1 in comparison to P-H-C5 (least stable product in terms of ΔE).



Scheme 7.9. 2-D scheme of the optimized geometries (B3LYP def2-tzvp) investigated for the H-abstraction reaction pathway from the reaction of (E)-2-hexen-1-al (HEXAL) and $\cdot\text{OH}$ radicals in the aqueous phase deploying a CPCM continuum solvation model.

Overall, the H-abstraction at a C4 site in HEXAL, which can possibly result in the formation of propanal as well as product(s) with the molecular formula $\text{C}_6\text{H}_{10}\text{O}_2$ (Scheme 7.3), gives the most stable radical product P-H-C4 by at least 9 kcal mol⁻¹ in comparison to the addition adducts (1, 2, and 3). Alongside the lowest dE_{vac}^{\ddagger} for TS-C1 can also explain the formation of $\text{C}_6\text{H}_{10}\text{O}_2$ unknown product *via* formation of P-H-C1 (Scheme 7.3). The two distinct H-abstraction pathways (C4 and C1) leading to the formation of observed $\text{C}_6\text{H}_{10}\text{O}_2$ can account for more than 5% of the missing molar fraction of HEXAL decay in experiments. A more stable addition product at a C3 site proves the butanal formation during photooxidation experiments.

The GCM method by Minakata *et al.*⁴⁸⁴ must be used carefully for predicting the overall rate constants, as concluded with a comparison of experimental rate constants (Chapter 5). However, still, it is useful in predicting and comparing the importance of individual pathways of addition

and H-abstraction reactions. We note that most of these estimated rate constants or reactivity rates correspond well with the calculation results from DFT approach.

All calculated gas-phase activation energies are small but positive. Moreover, in most cases one GLV alkyl product characterized with the lowest ΔE value is well energetically separated from other products. For PENTOL, the $dE_{\text{CPCM}}^{\ddagger}$ ($-0.37 \text{ kcal mol}^{-1}$) is the lowest for a TS-3, and the lowest ΔE_{CPCM} ($-45.06 \text{ kcal mol}^{-1}$) for a P-H3 (Scheme 7.5). Thus, the determined kinetic ($dE_{\text{CPCM}}^{\ddagger}$) and thermodynamic (ΔE_{CPCM}) values agree and indicate that the reaction might be more thermodynamically controlled, depending upon the temperature. However, for the other two GLVs HEXOL and HEXAL, dE^{\ddagger} and ΔE values do not correlate. For HEXOL, the dE^{\ddagger} ($4.80 \text{ kcal mol}^{-1}$) is the lowest for a TS-C5, and the lowest ΔE ($-42 \text{ kcal mol}^{-1}$) for P-H-C1 (Scheme 7.7). For HEXAL, the dE^{\ddagger} ($-0.03 \text{ kcal mol}^{-1}$) is the lowest for a TS-C5, and the lowest ΔE ($-41.42 \text{ kcal mol}^{-1}$) for P-H-C1 (Scheme 7.7). In this case, the difference in selectivity directed by dE^{\ddagger} (kinetics) or by ΔE (thermodynamics) indicates a balance between the kinetic and thermodynamic control of the reaction for HEXOL and HEXAL.

The application of such simple DFT models in my Ph.D. study assisted: (i) to explain the mechanistic pathways of the formation of experimentally-observed reaction products; (ii) the confident construction of mechanistic pathway of formations of the unknown product(s) observed with molecular formula $\text{C}_6\text{H}_{12}\text{O}_2$; (iii) Although addition reactions appear to be faster and follow barrier more minor route, the hydrogen-abstraction still appears to be dominant for some instances and contributes significantly to the formation of products in the mimicing experiments of the selected GLVs (PENTOL, HEXOL, HEXAL) with $\cdot\text{OH}$ radicals.

7.4. Atmospheric Implications

7.4.1. GLVs and their oxidation products as a SOA precursor

Chapter 4 already describes all of the EPI suite 2012 from EPA⁴¹² estimated and experimentally available data based on physical properties of the parent GLV compounds, while here in addition, the same was collected and obtained for the oxidation products from PENTOL, HEXOL, and HEXAL (Table 7.4). Such data aid to get insights into the efficiency or tendency of the oxidation products to remain in the aqueous-phase and contribute towards aq-SOA formation after water evaporation. The estimated physical properties values can vary by several orders of

magnitude based on the type of method used for estimation.^{57, 128, 488, 489} The recent comparison of such data for GLVs methyl jasmonate (MeJa) and methyl salicylate (MeSa) by Hansel *et al.*,¹²⁸ suggested their wise evaluation only for relative comparison purposes. The EPI suite provides good values of HLC (i.e., bond estimation method) and vapor pressure mainly agrees with the experimental results reported for propanal, and butanal (Table 7.4).^{421, 490} The EPI suite estimated HLC for all oxidation products is relatively lower than the parent GLV compound, exception $C_6H_{10}O_2$ that has at least three orders of magnitude higher values. For simplicity, estimated values only for one of the hydroxy-hexenal is included in Table 7.4, as the EPI suite practically produces the same results for all hydroxy-hexenal or hydroxy hexenone. The estimated VP of the oxidation products (propanal, butanal, and 1-penten-3-one) is higher than the parent GLV compounds, exception $C_6H_{10}O_2$, (Scheme 7.2 and 7.3) due to the higher O:C ratio than parent GLV, and therefore can potentially contribute towards aq. SOA. Confirmation of the structure of $C_6H_{10}O_2$ (possibly hydroxy-hexenal or hydroxy-hexenone) can lead to an unidentified organo-sulfate fraction, and nitrate marker compounds within the ambient atmosphere originating from the C-6 GLVs. Due to the missing standards of $C_6H_{10}O_2$ product(s), their identification and quantification in the ambient aerosol samples is a challenge for the future work.

Table 7.4. Physical properties of GLVs and observed oxidation products at 298 K, experimental and estimated with EPI suite⁴¹² and $H_d = HRT$, where, R , atm L mol⁻¹ K⁻¹

Compounds	Molecular formula	Henry's Law Constant mol L ⁻¹ atm ⁻¹	Vapor pressure atm	Water solubility mg L ⁻¹	H_d
1-penten-3-ol	C ₅ H ₁₀ O	101.22 ^a	1.20×10 ⁻² , ^c	4.53×10 ⁴ ^d	2.4×10 ³
		43.75 ^b		9.01×10 ⁴ , ⁴²⁹	1.1×10 ³
(Z)-2-hexen-1-ol	C ₆ H ₁₂ O	64.52 ^a	1.19×10 ⁻³ , ^c	1.60×10 ⁴ ^d	1.6×10 ³
		133.26 ^b			3.3×10 ³
(E)-2-hexen-1-al	C ₆ H ₁₀ O	10.12 ^a	6.21×10 ⁻³ , ^c	5.26×10 ³ ^d	2.5×10 ²
		8.63 ^b			2.1×10 ²
1-penten-3-one	C ₅ H ₈ O	28.82 ^a 5.18 ^b	5.03×10 ⁻² , ^c	2.19×10 ⁴ ^d	
Propionaldehyde	C ₃ H ₆ O	11.10 ^a	4.17×10 ⁻¹ , ^c	5.108×10 ⁴ , ^d	
		1.77 ^b	4.17×10 ⁻¹ , 490	3.06×10 ⁵ , ⁴³⁹	
		13.62 ⁴²¹			
Butyraldehyde	C ₄ H ₈ O	8.33 ^a	1.42×10 ⁻¹ , ^c	3.018×10 ⁴ ^d	
		2.33 ^b	1.46×10 ⁻¹ , 490	7.1×10 ⁴ ^c	
		8.70 ⁴²¹			
hydroxy-hexenal	C ₆ H ₁₀ O ₂	2.77×10 ^{5a} 2.65×10 ^{4b}	1.03×10 ⁻⁴ , ^c	3.118×10 ⁵ ^d	

^a Bond estimation method; ^b via VP/WSol estimate; ^c Mean of Antoine & Grain methods; ^d EPI Suite WSKowwin v1.43 Estimate; ^e Cited as Union Carbide (1974) by EPA database

7.4.2. Atmospheric significance and impact of aqueous-phase GLVs conversion pathways

The short-chain carbonyls, such as propanal and butanal, identified in this study as products of GLV reactions, are ubiquitous and play a key role in the atmospheric photochemical processes.^{491, 492} These carbonyls are usually formed as the first oxidation products from atmospheric reactions between oxidants such as •OH radicals and primary emitted hydrocarbons.⁴⁹³ In addition, these carbonyls can be further photolyzed and act as a source of •OH radicals,⁴⁹⁴ or *via* photolysis, gas-, and aqueous-phase reactions can lead to products, such as peroxyacetyl nitrate, nitric acids, carboxylic acids, and other aerosol-bound components,⁴⁹⁵

eventually leading to the formation of photochemical smog.⁴⁹⁶⁻⁴⁹⁸ The ambient air concentration of propanal, and butanal reported by Grosjean et al., was 0.79 ± 0.54 , and 0.71 ± 0.32 ppb, respectively.⁴⁹⁹ Possanzini et. al., reported 0.6-3.0 ppb (propanal), and 0.7-2.4 ppb (butanal), respectively.⁵⁰⁰ The photolysis rate constants of propanal and butanal have been reported to be $32 \text{ J (s}^{-1}) \times 10^5$, and $27 \text{ J (s}^{-1}) \times 10^5$, respectively.⁴⁹⁶ In the present study, I firmly identified four low molecular weight carbonyls arising from aqueous oxidation of 1-penten-3-ol, (*Z*)-2-hexen-1-ol, and (*E*)-2-hexen-1-al, respectively. The identified products, especially propanal, butanal are of high importance because of the chemistry with OH, O₃, and other free radicals, which can lead to peroxy acyl nitrates and/or carboxylic acids. In regions, where GLV concentrations become higher in warm periods, they may influence local air quality, and human health. Thus, the atmospheric lifetimes of the GLVs with ·OH radical calculated here, and reported in the literature are compared in Table 7.6.

The atmospheric lifetimes(τ) shown in Table 7.5 were calculated using Equation 7.4.

$$\tau = \frac{1}{k_{2nd} \times [X]} \quad (7.4)$$

where, k_{2nd} is the second-order rate constant of the compound with the radical and $[X]$ is the concentration of radicals. See Table 5.8 (Chapter 5) for the aqueous-phase radical concentrations, and Table 7.5 for the gas phase concentrations used.

Table 7.5. Concentrations of the radicals within the tropospheric gas phase.

[X]	gas, molecule cm ⁻³	Ref.
·OH	1×10^6	382, 501
NO ₃ ·	5×10^7	502
O ₃	7×10^{11}	225

The decreased aqueous-phase lifetimes of oxidation products compared to the parent GLV compounds (Table 7.6) indicate their increased reactivity towards atmospheric radicals, such as ·OH in the aqueous- and gas-phase. Likely, the carbonyl products (especially C₆H₁₂O₂, hydroxy-hexenal, or hydroxy-hexenone) are the reactive starting points towards the aging of SOA formed from PENTOL, HEXOL, and HEXAL. Based on previously published studies,^{242, 297, 449} the identified unsaturated carbonyl products such as 1-penten-3-one (ethyl vinyl ketone), hydroxy hexenal, or hydroxy hexenone can contribute to the formation of organosulfates within the ambient

atmosphere and require attention. In addition, Monod et al.⁵⁰³ highlighted the importance of the aqueous droplets acting as a powerful reacting medium for removing such unsaturated compounds from the atmosphere.

Table 7.6. Atmospheric lifetimes of the GLVs and their carbonyl products determined in this study against the reaction with $\cdot\text{OH}$ radicals in the cloud droplets and deliquescent aerosols.

Compounds	Atmospheric lifetimes (with $\cdot\text{OH}$ (aq)) , τ			$k_{\text{OH},298}$	References, $k_{\text{OH},298}$
	Urban clouds	Remote clouds	Urban aerosols		
1-penten-3-ol	12.6 h	2.0 h	6.0 min	6.3×10^9	thesis work* ²⁹⁸
(Z)-2-hexen-1-ol	11.8 h	1.9 h	5.7 min	6.7×10^9	thesis work* ²⁹⁸
(E)-2-hexen-1-ol	16.5 h	2.6 h	7.9 min	4.8×10^9	thesis work* ²⁹⁸
1-penten-3-one	10.9 h	1.7 h	5.2 min	7.3×10^9	GCM estimated ⁴⁸⁴
propionaldehyde	28.3 h	4.5 h	13.5 min	2.8×10^9	²⁷³
butyraldehyde	20.4 h	3.2 h	9.7 min	3.9×10^9	²⁷³
6-hydroxy hex-4-enal	6.7 h	1.1 h	3.2 min	1.2×10^{10}	GCM estimated ⁴⁸⁴
5-hydroxy hex-2-enal	4.4 h	42.4 min	2.1 min	1.8×10^{10}	GCM estimated ⁴⁸⁴
6-hydroxy hex-4-en-2-one	7.2 h	1.1 h	3.4 min	1.1×10^{10}	GCM estimated ⁴⁸⁴

7.4.3. Flux analysis

The flux analysis was performed to assess the impact of the reaction between selected GLVs and $\cdot\text{OH}$ radicals within the aqueous phase. Table 7.7 describes the reactions considered as pathways for removal of PENTOL, HEXOL, and HEXAL from the tropospheric gas- and aqueous-phase. A similar analysis to evaluate the competing processes was discussed in Section 5.5, Chapter 5. Here the aqueous-phase reaction of the GLVs with $\cdot\text{OH}$ competes with the $\text{SO}_4^{\cdot-}$, and

NO₃[•] reactions in the aqueous phase, and [•]OH, NO₃[•], and O₃ reactions in the gas phase, along with photolysis loss of GLV in the gas phase, which is a minor removal pathway.

Table 7.7. Reactions and their rate constants considered for estimating the GLV flux removal independent of the GLV concentrations in the tropospheric aqueous and gas phases.

GLV	Pathway	k_g cm ³ molecule ⁻¹ s ⁻¹	Ref.	k_{aq} L mol ⁻¹ s ⁻¹	Ref.
1-penten-3-ol	[•] OH	6.2 × 10 ⁻¹¹	a	6.3 × 10 ⁹	a
	SO ₄ ^{•-}			9.4 × 10 ⁸	a
	NO ₃ [•]	1.4 × 10 ⁻¹⁴	a	1.5 × 10 ⁸	a
	O ₃	1.7 × 10 ⁻¹⁶	194		
	hv, s ⁻¹	2 × 10 ⁻⁶	162		
	(average value)				
(Z)-2-hexen-1-ol	[•] OH	6.2 × 10 ⁻¹¹	a	6.7 × 10 ⁹	a
	SO ₄ ^{•-}			2.5 × 10 ⁹	a
	NO ₃ [•]	1.6 × 10 ⁻¹³	a	8.4 × 10 ⁸	a
	O ₃	7.4 × 10 ⁻¹⁷	504		
	hv	negligible loss in actinic region	176		
(E)-2-hexen-1-ol	[•] OH	4.4 × 10 ⁻¹¹	a	4.8 × 10 ⁹	a
	SO ₄ ^{•-}			4.8 × 10 ⁸	a
	NO ₃ [•]	1.2 × 10 ⁻¹⁴	a	3.0 × 10 ⁸	a
	O ₃	1.5 × 10 ⁻¹⁸	196		
	hv, s ⁻¹	1.6 × 10 ⁻⁵	486		

^aaverage of the value provided in Chapter 5, Table 5.11

The removal of GLVs independent from GLV concentration is described by Equation 7.2 for the gas phase and Equation 7.3 for the aqueous phase:

$$\frac{d[GLV]_g}{[GLV]_g dt} = -k_{g,O_3}[O_3]_g - k_{g,OH}[OH]_g - k_{g,NO_3}[NO_3]_g - k_{hv,g} \quad (7.2)$$

$$\frac{d[GLV]_g}{[GLV]_g dt} = -k_{aq,OH}H_{a,GLV}\omega[OH]_{aq} - k_{aq,NO_3}H_{a,GLV}\omega[NO_3]_{aq} - k_{aq,SO_4}H_{a,GLV}\omega[SO_4^-]_{aq} \quad (7.3)$$

The percent flux contribution is evaluated in three scenarios, i.e., urban clouds, remote clouds, and urban aerosol. The constraining parameters and concentration of radicals in the scenarios are described in Tables 5.7, 5.8, 5.9 (Chapter 5), Table 7.6.

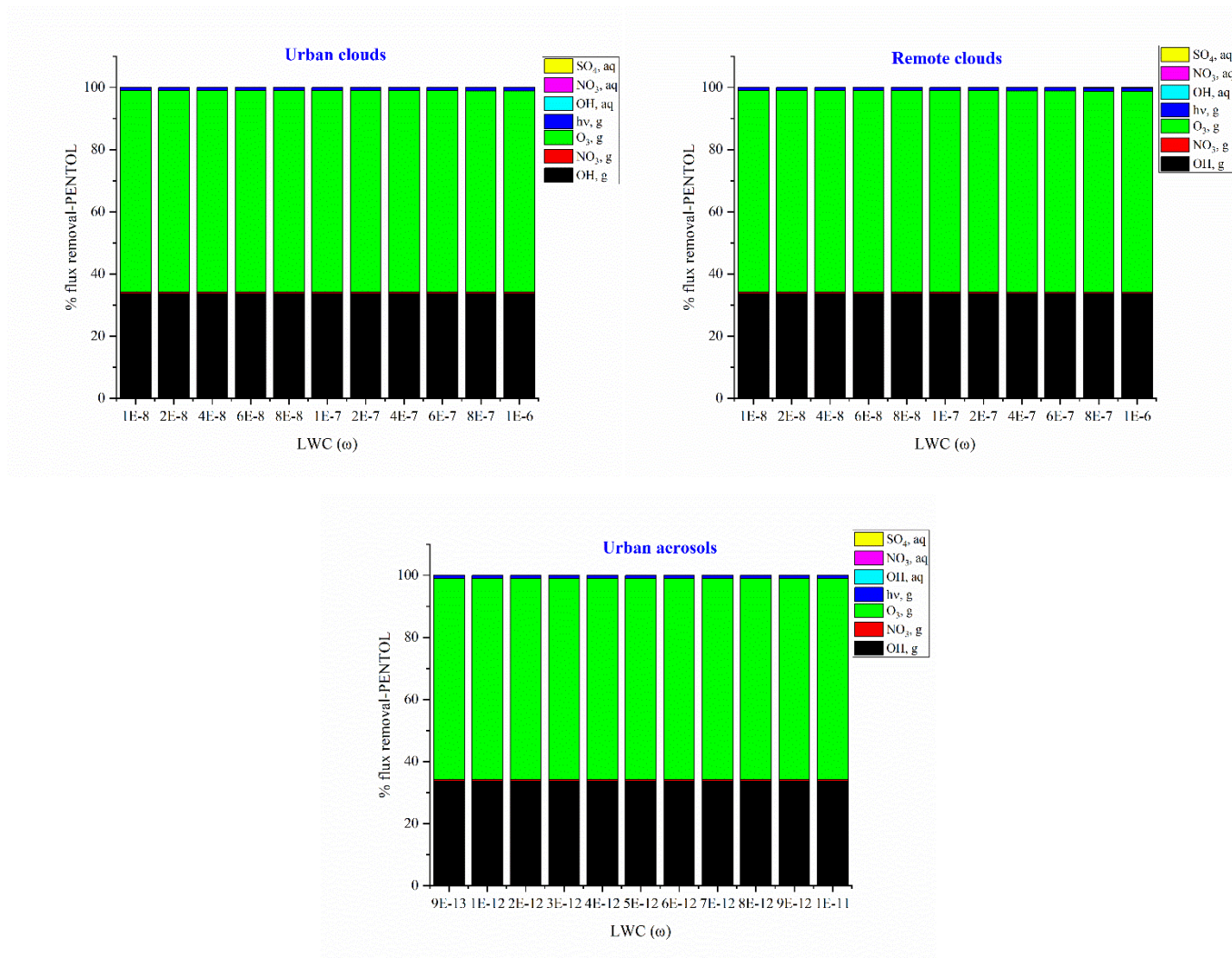


Figure 7.16. The GLV concentration-independent percentage fluxes of 1-penten-3-ol ($\% \frac{d[GLV]_g}{[GLV]_g dt}$) removed due to the individual reaction in the tropospheric gas and aqueous phases.

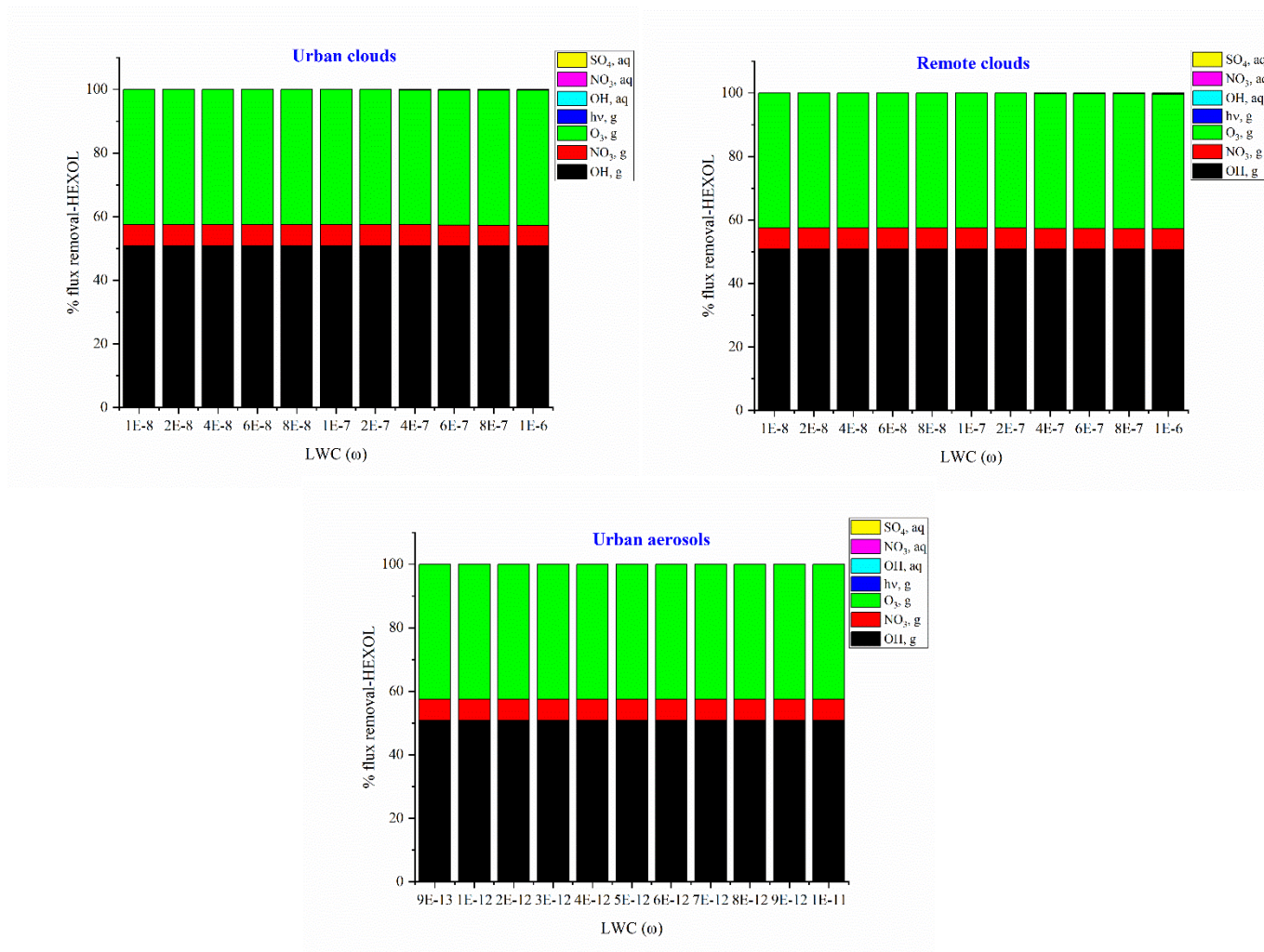


Figure 7.17. The GLV concentration-independent percentage fluxes of (*Z*)-2-hexen-1-ol ($\% \frac{d[GLV]_g}{[GLV]_g dt}$) removed due to the individual reaction pathways in the tropospheric gas and aqueous phases.

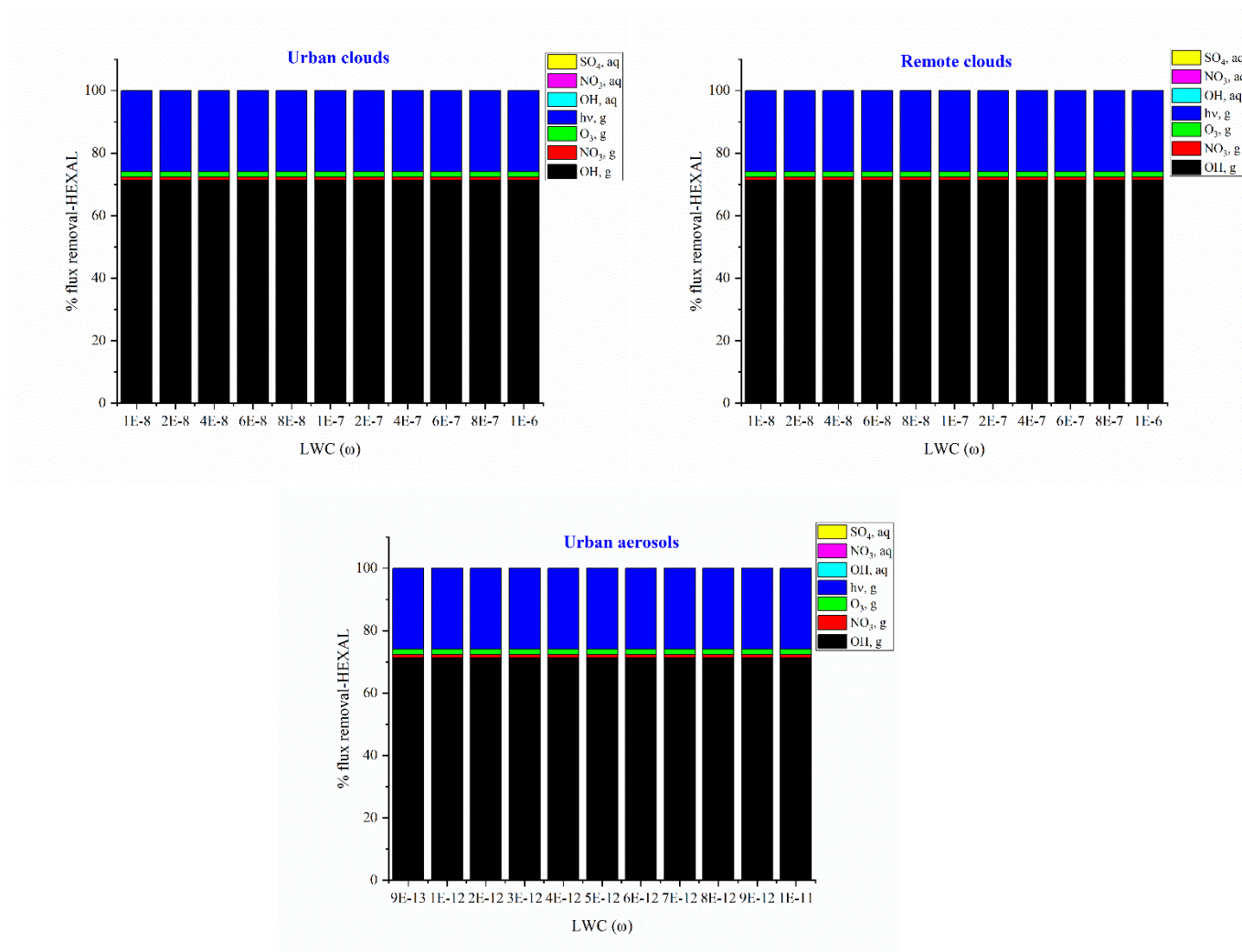


Figure 7.18. The GLV concentration-independent percentage fluxes of (*E*)-2-hexen-1-al ($\% \frac{d[GLV]_g}{[GLV]_g dt}$) removed due to the individual reaction pathways in the tropospheric gas and aqueous phases.

Figures 7.16 – 7.18 depict the percent fluxes of GLV removed over the entire range of liquid water content (LWC, ω) in urban clouds, remote clouds, and urban aerosols. Approximately 74%, 45%, and 67% removal of the PENTOL, HEXOL, and HEXAL, respectively occurs due to the aqueous-phase reactions with $\cdot\text{OH}$ radicals to that of total aqueous-phase reactions with $\cdot\text{OH}$, $\text{SO}_4^{\cdot-}$, and NO_3^{\cdot} combined. However, it is only 0.02% (PENTOL), 0.04% (HEXOL), and 0.005% (HEXAL) of the total flux removal by combined gas- and aqueous-phase reactions. The PENTOL and HEXOL removal due to photolysis in the gas phase is comparable to that from the aqueous phase, i.e., is minor or negligible. In contrast, around 26% of the tropospheric HEXAL is removed *via* photolysis (Figure 7.18).

Chapter 8. Summary and future perspective

The present Ph.D. thesis aimed to unravel the potential of GLVs as a source of secondary organic aerosol using the kinetic and chemical analysis of their aqueous-phase reactions. The present work was conducted using a combination of experimental, simulation, and theoretical techniques, and aimed to demonstrate the importance of the selected GLVs atmospheric chemistry in the aqueous phase. Several past studies have provided evidence of SOA originating from GLVs *via* gas- and aqueous-phase processes. GLVs emissions may appear minor globally compared to isoprene and monoterpenes; however, the influence of GLVs chemistry might become significant under local scenarios, such as harvesting, switchgrass cultivation, or lawn mowing, which result in high GLV emissions. The review article published within the framework of this work proves the substantial interest of atmospheric scientists in GLV chemistry.¹⁶⁸ A vast field of scientific research on GLVs is still pending, where the presented thesis research helps fill the gap. The significant outcomes are briefly discussed and presented below.

8.1. Kinetic studies of the aqueous-phase reaction of GLVs with sulfate, hydroxyl and nitrate radicals in the troposphere and its atmospheric implications

The present study provided the rate constants for GLVs reactions with $\cdot\text{OH}$, $\text{SO}_4^{\cdot-}$, and NO_3^{\cdot} radicals in the aqueous phase in the 288-318 K temperature range. The rate constants for $\text{SO}_4^{\cdot-}$, and NO_3^{\cdot} were obtained for the first time. The investigated GLVs (PENTOL, HEXOL, and HEXAL) differed in reactivity towards radicals in the order: $k_{\text{OH}} (10^9) > k_{\text{SO}_4} (10^8) > k_{\text{NO}_3} (10^7) \text{ L mol}^{-1} \text{ s}^{-1}$ at 298 K. Evaluation of the atmospheric significance of these reactions revealed, that they are negligible in deliquescent aerosol and haze water, but dominate in atmospheric systems with a high liquid water content, such as rains and storms, reducing the lifetime of GLVs from years to a few minutes. In systems with sufficient excess of $\text{SO}_4^{\cdot-}$ radicals, the aqueous-phase GLV- $\text{SO}_4^{\cdot-}$ reactions dominate over combined gas- and aqueous-phase reactions with $\cdot\text{OH}$ or NO_3^{\cdot} radicals. Thus, GLVs may effectively contribute to the formation of aqueous SOA and influence cloud properties.

In addition, kinetic simulations of complete models of GLV reactions with nitrate radicals using COMplex PATHway SIMulator (COPASI) software were used to evaluate the bias in experimental rate constants from the LFP-LLPA that arose due to the neglected reaction sinks of NO_3^{\cdot} including the $\text{NO}_3^{\cdot} + \text{peroxy}$ intermediate pathway. The results showed that the intrinsic LFP-

LLPA experimental uncertainty of the rate constants was considerably more significant than the bias due to the "neglected" reactions. This finding proved the LFP-LLPA method can be safely used for the determination of the rate constants for NO_3^\bullet reactions.

8.2. Product studies on the $\bullet\text{OH}$ radical-mediated aqueous-phase GLV photooxidation

The aqueous-phase photooxidation of selected GLVs (PENTOL, HEXOL, and HEXAL) in the presence of $\bullet\text{OH}$ radicals revealed several carbonyl products (i.e., propanal, butanal, 1-penten-3-one, (*E/Z*)-2-hexen-1-al, and $\text{C}_6\text{H}_{10}\text{O}_2$) as the first stage reaction products. Propanal and butanal are highly important, because they react with $\bullet\text{OH}$, O_3 , and other free radicals, leading to the formation of peroxy acyl nitrate or carboxylic acids, hurting air quality and human health under scenarios with high GLV emissions. Other identified carbonyl products ($\text{C}_6\text{H}_{10}\text{O}_2$ – possibly hydroxy-hexenal, or hydroxy-hexenone, and 1-penten-3-one) can serve as starting points towards SOA aging, including the formation of organosulfates in the ambient atmosphere, and requires attention. Henry's constant and vapor pressure of the product $\text{C}_6\text{H}_{10}\text{O}_2$ estimated with EPI suite were higher and lower than the parent compounds, respectively. Density functional theory calculations were carried out to support and explain each oxidation product formation and molar proportion. The application of a simple DFT model could explain: (i) mechanistic pathways of the formation of experimentally-observed reaction products; (ii) the formation pathways of the unknown product with the molecular formula $\text{C}_6\text{H}_{12}\text{O}_2$; (iii) despite the addition reaction appears to be faster and follows the barrierless route, hydrogen-abstraction still dominates for some instances and contributes significantly to the formation of oxidation products. The atmospheric removal flux calculations suggested that more than 65% of the GLVs (PENTOL, HEXOL, and HEXAL) was removed *via* aqueous-phase reaction with $\bullet\text{OH}$ radicals compared to combined aqueous-phase removal due to reactions with $\bullet\text{OH}$, $\text{SO}_4^{\bullet-}$, and NO_3^\bullet species. There was no significant removal *via* photolysis for PENTOL, and HEXOL, while around 26% HEXAL was lost due to the photolytic processes in the atmosphere. The total flux removal of GLVs due to aqueous-phase processes appears relatively low.

8.3. Formation of aqueous SOA

GLVs, except Methyl Jasmonate (MeJa) have Henry's constant lower than 100 M atm^{-1} , suggesting that they reside primarily in the gas phase and hardly partition to the aqueous phase.

However, they are highly reactive (Chapter 5) and give more soluble products like small aldehydes (Chapter 7) and, possibly, oligomers (like glyoxal) leading to aqueous SOA formation.

8.4. Future direction

The findings presented in the thesis provide deeper insights into the atmospheric aqueous-phase reactions concerning GLVs. Still, a number of questions is to be addressed in future research work.

1. Investigation of GLVs reactions at the air-water interface to obtain the overall picture of the contribution to the SOA formation.
2. Many fundamental GLVs physical properties need to be experimentally determined to model the multiphase processes better, such as Henry's constant, octanol-air, and octanol-water partition coefficients.
3. The SOA formation from GLVs has been proved, yet warrants further research. SOA yields from the gas phase and multiphase processes need to be analyzed under various conditions to estimate GLVs SOA formation in the atmosphere better.
4. So far, no data related to the health effects of GLVs and their atmospheric transformation products can be found, and warrants further research. This is of particular interest to social groups exposed to high GLV emissions, like farmers and residents of houses with grass yards.
5. Theoretical and simulation methods, which proved helpful in evaluating the GLVs reactivity in the present work, should be further developed to explain the results of experimental studies.

Appendix

1. Molar absorption coefficients for selected GLVs in the aqueous phase

Table A4.3. Molar absorption coefficients values, $\epsilon(\lambda)$ of 1-penten-3-ol in the aqueous phase at 298 K and pH =7, at wavelengths between 200 – 400 nm.⁴⁴⁴

1-penten-3-ol, Mean value for concentration range 500 – 31.25 mM (aqueous), TROPOS					
Wavelength	Average	σ , n=10	Wavelength	Average	σ , n=10
λ , nm	$\epsilon/ M^{-1} cm^{-1}$	$\Delta\epsilon/ M^{-1} cm^{-1}$	λ , nm	$\epsilon/ M^{-1} cm^{-1}$	$\Delta\epsilon/ M^{-1} cm^{-1}$
400	0.0247	0.0123	300	0.0798	0.0189
399	0.0235	0.0111	299	0.0818	0.0186
398	0.0234	0.0108	298	0.0832	0.0174
397	0.0245	0.0116	297	0.0862	0.0179
396	0.0264	0.0135	296	0.0897	0.0193
395	0.0231	0.0106	295	0.0920	0.0191
394	0.0236	0.0111	294	0.0944	0.0191
393	0.0238	0.0110	293	0.0989	0.0206
392	0.0250	0.0119	292	0.1010	0.0201
391	0.0239	0.0113	291	0.1023	0.0195
390	0.0248	0.0120	290	0.1050	0.0199
389	0.0249	0.0118	289	0.1076	0.0201
388	0.0238	0.0104	288	0.1111	0.0211
387	0.0246	0.0116	287	0.1137	0.0212
386	0.0241	0.0122	286	0.1167	0.0219
385	0.0238	0.0104	285	0.1193	0.0220
384	0.0265	0.0129	284	0.1204	0.0216
383	0.0247	0.0114	283	0.1222	0.0219
382	0.0243	0.0111	282	0.1261	0.0236
381	0.0248	0.0119	281	0.1288	0.0247
380	0.0254	0.0124	280	0.1306	0.0246
379	0.0260	0.0126	279	0.1316	0.0239
378	0.0211	0.0093	278	0.1332	0.0237
377	0.0259	0.0127	277	0.1359	0.0257
376	0.0256	0.0118	276	0.1375	0.0264
375	0.0243	0.0111	275	0.1388	0.0262
374	0.0245	0.0115	274	0.1395	0.0251
373	0.0238	0.0110	273	0.1423	0.0262
372	0.0237	0.0107	272	0.1440	0.0259
371	0.0253	0.0118	271	0.1461	0.0260
370	0.0259	0.0122	270	0.1498	0.0273

369	0.0269	0.0131	269	0.1546	0.0292
368	0.0255	0.0119	268	0.1595	0.0306
367	0.0254	0.0125	267	0.1629	0.0299
366	0.0260	0.0127	266	0.1675	0.0291
365	0.0245	0.0113	265	0.1751	0.0301
364	0.0258	0.0121	264	0.1819	0.0288
363	0.0259	0.0120	263	0.1914	0.0282
362	0.0283	0.0143	262	0.2062	0.0311
361	0.0281	0.0135	261	0.2181	0.0305
360	0.0281	0.0134	260	0.2303	0.0296
359	0.0292	0.0144	259	0.2434	0.0299
358	0.0278	0.0133	258	0.2570	0.0299
357	0.0259	0.0111	257	0.2736	0.0312
356	0.0271	0.0120	256	0.2918	0.0325
355	0.0284	0.0126	255	0.3107	0.0319
354	0.0277	0.0126	254	0.3325	0.0324
353	0.0280	0.0131	253	0.3549	0.0323
352	0.0291	0.0131	252	0.3798	0.0321
351	0.0292	0.0132	251	0.4065	0.0320
350	0.0288	0.0128	250	0.4372	0.0329
349	0.0287	0.0120	249	0.4711	0.0326
348	0.0299	0.0127	248	0.5087	0.0334
347	0.0309	0.0141	247	0.5465	0.0310
346	0.0323	0.0149	246	0.5902	0.0315
345	0.0309	0.0132	245	0.6369	0.0314
344	0.0331	0.0137	244	0.6848	0.0301
343	0.0329	0.0134	243	0.7371	0.0316
342	0.0328	0.0131	242	0.7928	0.0307
341	0.0348	0.0145	241	0.8528	0.0301
340	0.0321	0.0124	240	0.9170	0.0309
339	0.0324	0.0126	239	0.9831	0.0306
338	0.0355	0.0142	238	1.0544	0.0316
337	0.0362	0.0147	237	1.1280	0.0319
336	0.0363	0.0150	236	1.2031	0.0314
335	0.0339	0.0126	235	1.2817	0.0324
334	0.0356	0.0137	234	1.3634	0.0327
333	0.0374	0.0152	233	1.4542	0.0359
332	0.0394	0.0163	232	1.5511	0.0381
331	0.0390	0.0147	231	1.6552	0.0401
330	0.0408	0.0156	230	1.7659	0.0411
329	0.0405	0.0155	229	1.8840	0.0433
328	0.0408	0.0149	228	2.0121	0.0494
327	0.0403	0.0139	227	2.1454	0.0527
326	0.0409	0.0138	226	2.2867	0.0590

325	0.0439	0.0157	225	2.4310	0.0665
324	0.0432	0.0136	224	2.5738	0.0711
323	0.0420	0.0114	223	2.7216	0.0804
322	0.0452	0.0143	222	2.8706	0.0879
321	0.0462	0.0153	221	3.0179	0.0981
320	0.0460	0.0150	220	3.1652	0.1107
319	0.0467	0.0146	219	3.3045	0.1202
318	0.0473	0.0136	218	3.4431	0.1311
317	0.0497	0.0151	217	3.5879	0.1442
316	0.0501	0.0144	216	3.7425	0.1531
315	0.0527	0.0159	215	3.9281	0.1678
314	0.0538	0.0163	214	4.1780	0.1902
313	0.0543	0.0160	213	4.5294	0.2166
312	0.0563	0.0169	212	5.0488	0.2575
311	0.0584	0.0178	211	5.8289	0.3354
310	0.0593	0.0172	210	7.0250	0.4801
309	0.0604	0.0167	209	8.9334	0.6709
308	0.0627	0.0172	208	11.5892	1.1470
307	0.0639	0.0164	207	15.3776	1.8322
306	0.0647	0.0154	206	21.5754	2.0961
305	0.0675	0.0168	205	29.2559	3.5632
304	0.0715	0.0194	204	42.1436	3.7705
303	0.0733	0.0189	203	56.0993	6.1618
302	0.0749	0.0182	202	77.3882	5.6191
301	0.0772	0.0183	201	108.1686	2.2035

Table A4.4.a. Molar absorption coefficients values, ϵ (λ) of (Z)-2-hexen-1-ol in the aqueous phase at 298 K and pH =7, at wavelengths between 200 – 400 nm.⁴⁴⁴

(Z)-2-hexen-1-ol, mean value for concentration range 100 – 6.25 mM (aqueous), TROPOS					
Wavelength	Average	σ , n=10	Wavelength	Average	σ , n=10
λ , nm	ϵ / M ⁻¹ cm ⁻¹	$\Delta\epsilon$ / M ⁻¹ cm ⁻¹	λ , nm	ϵ / M ⁻¹ cm ⁻¹	$\Delta\epsilon$ / M ⁻¹ cm ⁻¹
400	0.5084	0.2294	300	1.6585	0.1469
399	0.5135	0.2276	299	1.6966	0.1452
398	0.5087	0.2293	298	1.7389	0.1442
397	0.5122	0.2291	297	1.7835	0.1429
396	0.5137	0.2285	296	1.8293	0.1423
395	0.5078	0.2305	295	1.8699	0.1417
394	0.5158	0.2275	294	1.9089	0.1414
393	0.5133	0.2282	293	1.9475	0.1409
392	0.5182	0.2267	292	1.9800	0.1401

391	0.5273	0.2236	291	2.0000	0.1369
390	0.5212	0.2260	290	2.0262	0.1355
389	0.5241	0.2246	289	2.0628	0.1382
388	0.5270	0.2242	288	2.0905	0.1397
387	0.5192	0.2270	287	2.1139	0.1416
386	0.5239	0.2253	286	2.1384	0.1454
385	0.5273	0.2246	285	2.1599	0.1473
384	0.5329	0.2233	284	2.1630	0.1431
383	0.5362	0.2221	283	2.1649	0.1396
382	0.5285	0.2245	282	2.1723	0.1400
381	0.5285	0.2252	281	2.1749	0.1394
380	0.5390	0.2225	280	2.1852	0.1421
379	0.5394	0.2225	279	2.1992	0.1478
378	0.5358	0.2227	278	2.2069	0.1505
377	0.5561	0.2161	277	2.2113	0.1516
376	0.5406	0.2223	276	2.2203	0.1511
375	0.5414	0.2223	275	2.2252	0.1459
374	0.5566	0.2179	274	2.2406	0.1437
373	0.5572	0.2187	273	2.2734	0.1478
372	0.5689	0.2164	272	2.3204	0.1516
371	0.5688	0.2177	271	2.3724	0.1510
370	0.5692	0.2175	270	2.4429	0.1521
369	0.5697	0.2178	269	2.5334	0.1522
368	0.5723	0.2182	268	2.6471	0.1543
367	0.5697	0.2199	267	2.7926	0.1598
366	0.5764	0.2195	266	2.9657	0.1644
365	0.5859	0.2182	265	3.1575	0.1636
364	0.5945	0.2164	264	3.3754	0.1636
363	0.6043	0.2149	263	3.6313	0.1667
362	0.6133	0.2136	262	3.9217	0.1694
361	0.6162	0.2146	261	4.2501	0.1786
360	0.6342	0.2112	260	4.6071	0.1863
359	0.6359	0.2135	259	4.9990	0.1976
358	0.6448	0.2124	258	5.4111	0.1993
357	0.6546	0.2096	257	5.8530	0.2026
356	0.6622	0.2098	256	6.3475	0.2204
355	0.6823	0.2057	255	6.8847	0.2423
354	0.7018	0.2030	254	7.4715	0.2598
353	0.7112	0.2031	253	8.1291	0.2719
352	0.7168	0.2028	252	8.8937	0.2904
351	0.7282	0.2026	251	9.7794	0.3148
350	0.7469	0.1997	250	10.7897	0.3335
349	0.7610	0.1978	249	11.9654	0.3658
348	0.7614	0.2003	248	13.3133	0.4153

347	0.7766	0.1992	247	14.8359	0.4582
346	0.7956	0.1963	246	16.5163	0.5007
345	0.8053	0.1965	245	18.3782	0.5570
344	0.8204	0.1945	244	20.4234	0.6164
343	0.8415	0.1924	243	22.6428	0.6634
342	0.8520	0.1913	242	25.0535	0.7188
341	0.8573	0.1920	241	27.6522	0.7654
340	0.8702	0.1929	240	30.3919	0.7767
339	0.8932	0.1906	239	33.2455	0.7501
338	0.9148	0.1878	238	36.2103	0.6992
337	0.9312	0.1863	237	39.4764	0.9595
336	0.9438	0.1856	236	42.6940	1.7672
335	0.9518	0.1861	235	44.8833	0.6122
334	0.9662	0.1858	234	47.4939	0.5901
333	0.9834	0.1855	233	49.9734	0.5593
332	1.0017	0.1840	232	52.3108	0.5296
331	1.0062	0.1852	231	54.4115	0.5549
330	1.0213	0.1831	230	56.2520	0.5874
329	1.0491	0.1796	229	57.8556	0.5366
328	1.0661	0.1795	228	59.2558	0.4274
327	1.0738	0.1796	227	60.3304	0.4276
326	1.0920	0.1793	226	61.0079	0.4462
325	1.1142	0.1767	225	61.3791	0.4627
324	1.1350	0.1738	224	61.4232	0.4732
323	1.1491	0.1733	223	61.2821	0.5108
322	1.1626	0.1733	222	61.2023	0.4605
321	1.1775	0.1722	221	61.0453	0.4622
320	1.1964	0.1714	220	60.9718	0.4529
319	1.2088	0.1695	219	61.1832	0.4361
318	1.2305	0.1677	218	62.1353	0.4312
317	1.2494	0.1668	217	64.2836	0.4422
316	1.2580	0.1666	216	68.5299	0.5172
315	1.2713	0.1657	215	76.3375	2.0641
314	1.2836	0.1653	214	86.0817	1.7196
313	1.3038	0.1635	213	102.1557	3.4171
312	1.3274	0.1609	212	126.0037	6.2183
311	1.3454	0.1607	211	162.4448	6.7187
310	1.3727	0.1586	210	213.9767	11.2055
309	1.3976	0.1570	209	280.0228	16.1929
308	1.4177	0.1567	208	383.5250	0.6160
307	1.4328	0.1548	207	500.3163	1.5796
306	1.4575	0.1550	206	702.8832	
305	1.4872	0.1534			
304	1.5181	0.1509			

303	1.5590	0.1511		
302	1.5936	0.1498		
301	1.6239	0.1485		

Table A4.4.b. Molar absorption coefficients values, ϵ (λ) of (Z)-2-hexen-1-ol in the aqueous phase at 295 K and pH =7, at wavelengths between 200 – 400 nm.¹⁷²

(Z)-2-hexen-1-ol, mean value for concentration 2 mM (aqueous), IPC PAS					
Wavelength	Average	σ , n=2	Wavelength	Average	σ , n=2
λ , nm	ϵ / M-1 cm-1	$\Delta\epsilon$ / M-1 cm-1	λ , nm	ϵ / M-1 cm-1	$\Delta\epsilon$ / M-1 cm-1
400	0.9775	0.0177	300.5	1.6675	0.3854
399.5	0.9425	0.0389	300	1.7400	0.4384
399	0.9850	0.0212	299.5	1.6225	0.4207
398.5	0.9675	0.0035	299	1.4625	0.4066
398	1.0700	0.0707	298.5	1.4525	0.4137
397.5	1.1225	0.1450	298	1.3450	0.3182
397	1.1125	0.1237	297.5	1.3550	0.2121
396.5	1.0600	0.1697	297	1.4400	0.2121
396	1.1150	0.1697	296.5	1.4925	0.2227
395.5	1.0975	0.2157	296	1.5200	0.1414
395	1.1400	0.2121	295.5	1.4150	0.0990
394.5	1.1350	0.1838	295	1.4350	0.0849
394	1.1275	0.2298	294.5	1.3000	0.0636
393.5	1.0825	0.2369	294	1.2925	0.0884
393	1.0375	0.2934	293.5	1.2625	0.0318
392.5	1.0275	0.3217	293	1.2775	0.1308
392	1.0025	0.3005	292.5	1.2200	0.1909
391.5	0.9900	0.2899	292	1.2350	0.2404
391	1.0200	0.3111	291.5	1.3600	0.2899
390.5	1.0350	0.2970	291	1.2925	0.2793
390	0.9500	0.3111	290.5	1.3525	0.2227
389.5	0.9175	0.3005	290	1.3375	0.3005
389	0.9150	0.3465	289.5	1.4550	0.2616
388.5	0.9175	0.3147	289	1.3825	0.2440
388	0.9250	0.3111	288.5	1.4600	0.2121
387.5	0.9625	0.3429	288	1.3750	0.1344
387	0.9700	0.3536	287.5	1.3775	0.0106
386.5	0.9625	0.2864	287	1.3775	0.0318
386	1.0225	0.2793	286.5	1.4600	0.0000
385.5	0.8875	0.2652	286	1.6425	0.0601
385	0.7800	0.1838	285.5	1.6750	0.1556
384.5	0.7500	0.1414	285	1.8125	0.1450

384	0.7425	0.0813	284.5	1.8525	0.0813
383.5	0.7450	0.0990	284	1.9050	0.1414
383	0.7300	0.0495	283.5	1.8175	0.1167
382.5	0.6675	0.0813	283	1.8925	0.1308
382	0.6550	0.0354	282.5	1.9200	0.2192
381.5	0.6600	0.0141	282	1.9875	0.2581
381	0.6575	0.0035	281.5	2.1375	0.3429
380.5	0.6450	0.0495	281	2.1450	0.3111
380	0.7400	0.0424	280.5	2.2100	0.3677
379.5	0.7625	0.1167	280	2.2275	0.4490
379	0.8550	0.0566	279.5	2.3100	0.3889
378.5	0.8975	0.0601	279	2.2950	0.3465
378	0.8400	0.0354	278.5	2.2700	0.3323
377.5	0.8200	0.0071	278	2.2900	0.3323
377	0.8900	0.0919	277.5	2.4600	0.3253
376.5	0.8925	0.0813	277	2.4550	0.3536
376	0.9500	0.0990	276.5	2.4500	0.3748
375.5	0.9400	0.1061	276	2.4225	0.3500
375	0.9525	0.1379	275.5	2.3700	0.3111
374.5	0.9550	0.1202	275	2.4275	0.2652
374	0.9750	0.0707	274.5	2.5400	0.2404
373.5	0.9650	0.1414	274	2.6550	0.2121
373	1.0650	0.2192	273.5	2.5975	0.2015
372.5	1.1250	0.2475	273	2.5800	0.1626
372	1.1800	0.3111	272.5	2.6175	0.1732
371.5	1.1125	0.3429	272	2.5375	0.1803
371	1.1275	0.3429	271.5	2.4925	0.1732
370.5	1.0500	0.3111	271	2.5550	0.2121
370	1.1100	0.2475	270.5	2.6100	0.2051
369.5	1.2100	0.2121	270	2.7100	0.2616
369	1.1550	0.1273	269.5	2.7175	0.2086
368.5	1.1600	0.0424	269	2.6350	0.1909
368	1.1050	0.0354	268.5	2.6875	0.0742
367.5	1.1275	0.0530	268	2.8175	0.1308
367	1.1125	0.0389	267.5	2.7850	0.0919
366.5	1.0150	0.1344	267	2.8200	0.0849
366	1.0675	0.2157	266.5	2.8575	0.1237
365.5	1.1800	0.1980	266	2.8075	0.0318
365	1.3350	0.1768	265.5	2.8600	0.0141
364.5	1.2275	0.2086	265	2.7850	0.0212
364	1.2400	0.3041	264.5	2.8625	0.1096
363.5	1.2250	0.2404	264	2.9050	0.0707
363	1.2050	0.2475	263.5	3.0800	0.0566
362.5	1.2025	0.2722	263	3.2650	0.0849

362	1.1200	0.2051	262.5	3.3300	0.1061
361.5	1.1525	0.2793	262	3.4900	0.0566
361	1.1050	0.3182	261.5	3.5250	0.1061
360.5	1.1100	0.2546	261	3.5525	0.0247
360	1.1450	0.3111	260.5	3.7950	0.0354
359.5	1.1125	0.3712	260	3.9550	0.0212
359	1.1450	0.3748	259.5	4.1050	0.0000
358.5	1.1550	0.4879	259	4.3875	0.0530
358	1.0950	0.5162	258.5	4.6250	0.0778
357.5	1.0525	0.4419	258	4.9450	0.0141
357	1.0300	0.4738	257.5	5.1500	0.0141
356.5	1.0725	0.4561	257	5.4275	0.0035
356	1.1150	0.4738	256.5	5.6975	0.0106
355.5	1.1250	0.3960	256	6.0900	0.0778
355	1.1150	0.2970	255.5	6.3525	0.0884
354.5	1.0950	0.2687	255	6.6550	0.1131
354	1.2000	0.1485	254.5	7.1025	0.1732
353.5	1.1150	0.1697	254	7.5325	0.1591
353	1.2425	0.1520	253.5	8.0975	0.1732
352.5	1.1675	0.1308	253	8.6375	0.2227
352	1.1275	0.1379	252.5	9.1375	0.2652
351.5	1.1375	0.1167	252	9.7275	0.2652
351	1.2175	0.0884	251.5	10.2175	0.2652
350.5	1.2625	0.0318	251	10.8725	0.2934
350	1.3150	0.0566	250.5	11.4400	0.2970
349.5	1.3375	0.0106	250	12.0975	0.3642
349	1.3625	0.0601	249.5	12.8825	0.3429
348.5	1.3350	0.0212	249	13.5725	0.3429
348	1.3500	0.0283	248.5	14.4175	0.3359
347.5	1.4300	0.0071	248	15.2125	0.3429
347	1.3975	0.0389	247.5	16.0975	0.3924
346.5	1.3625	0.0247	247	16.9825	0.3571
346	1.4100	0.0566	246.5	17.8000	0.4384
345.5	1.3350	0.1414	246	18.7350	0.4243
345	1.2450	0.1061	245.5	19.6050	0.4808
344.5	1.3200	0.0566	245	20.5375	0.4066
344	1.4150	0.0283	244.5	21.6025	0.4278
343.5	1.4025	0.0318	244	22.7125	0.4844
343	1.3625	0.0318	243.5	23.8925	0.4632
342.5	1.3875	0.0035	243	24.8900	0.3182
342	1.3725	0.0672	242.5	26.1050	0.3182
341.5	1.3475	0.1803	242	27.2500	0.3182
341	1.2850	0.1485	241.5	28.4150	0.2758
340.5	1.3400	0.0283	241	29.5475	0.3005

340	0.9950	0.2333	240.5	30.8025	0.2793
339.5	1.0800	0.2899	240	31.9500	0.2828
339	1.0725	0.2864	239.5	33.0825	0.2510
338.5	1.1400	0.2899	239	34.3675	0.2369
338	1.1375	0.2510	238.5	35.5650	0.2475
337.5	0.9750	0.3182	238	36.6250	0.2475
337	0.8750	0.3394	237.5	37.7425	0.2864
336.5	0.9200	0.4031	237	38.8475	0.2015
336	0.8775	0.3995	236.5	40.0650	0.2404
335.5	0.9225	0.3147	236	41.1925	0.3217
335	0.9725	0.3642	235.5	42.2725	0.2934
334.5	1.0500	0.5374	235	43.3900	0.2687
334	1.1200	0.4455	234.5	44.2950	0.1202
333.5	1.0550	0.4879	234	45.3500	0.1556
333	0.9675	0.4066	233.5	46.3300	0.1838
332.5	0.8675	0.4985	233	47.2325	0.1662
332	1.0225	0.4632	232.5	48.0700	0.1273
331.5	1.0250	0.4172	232	48.7450	0.1202
331	1.0600	0.4101	231.5	49.4575	0.0247
330.5	1.0875	0.3359	231	50.1175	0.0247
330	1.1275	0.3783	230.5	50.6275	0.0247
329.5	1.1375	0.3924	230	51.2150	0.1980
329	1.2350	0.3111	229.5	51.5875	0.0884
328.5	1.3050	0.1838	229	52.1325	0.0813
328	1.5700	0.2687	228.5	52.4800	0.1697
327.5	1.7275	0.2086	228	52.7200	0.0495
327	1.7475	0.0106	227.5	53.0350	0.1061
326.5	1.7975	0.0318	227	53.3925	0.1591
326	1.7125	0.0742	226.5	53.6750	0.1909
325.5	1.8650	0.1414	226	53.6725	0.2015
325	1.8525	0.2440	225.5	53.7225	0.2581
324.5	1.9275	0.2298	225	53.8975	0.2369
324	1.9975	0.2793	224.5	54.0625	0.3147
323.5	1.9825	0.2652	224	54.1900	0.3606
323	2.0775	0.3076	223.5	54.1275	0.2015
322.5	1.9300	0.3041	223	54.3000	0.1485
322	1.9100	0.4172	222.5	54.5750	0.2192
321.5	1.9250	0.5374	222	54.8075	0.3005
321	1.9800	0.6435	221.5	55.3375	0.3995
320.5	2.0225	0.7177	221	56.0700	0.3889
320	1.9275	0.5409	220.5	57.1150	0.3606
319.5	1.8600	0.6010	220	58.4200	0.2970
319	1.7300	0.6223	219.5	60.1700	0.2899
318.5	1.6825	0.5621	219	62.4100	0.2970

318	1.7000	0.5303	218.5	65.1100	0.2828
317.5	1.6350	0.5374	218	68.6325	0.3500
317	1.6400	0.5798	217.5	72.9475	0.3712
316.5	1.6750	0.6223	217	78.0775	0.3642
316	1.5500	0.6223	216.5	84.0725	0.4137
315.5	1.4075	0.6541	216	90.8750	0.4384
315	1.3900	0.6647	215.5	98.8400	0.5515
314.5	1.1350	0.6010	215	107.7350	0.7000
314	1.1600	0.5657	214.5	117.4325	0.6611
313.5	1.0925	0.5904	214	128.1125	0.6611
313	1.2650	0.6152	213.5	139.7950	0.5940
312.5	1.2200	0.5162	213	152.4875	0.6187
312	1.2850	0.3253	212.5	165.9850	0.6010
311.5	1.2625	0.3924	212	180.4875	0.5692
311	1.3150	0.3606	211.5	196.0425	0.6682
310.5	1.2875	0.4207	211	212.7750	0.7849
310	1.2875	0.4702	210.5	230.8825	0.9581
309.5	1.2250	0.4667	210	250.0100	1.0112
309	1.1475	0.4066	209.5	271.2850	1.0748
308.5	1.1525	0.2934	209	294.5475	1.1420
308	1.1125	0.1945	208.5	319.5775	1.0006
307.5	1.2450	0.2263	208	346.9900	0.9758
307	1.3550	0.3041	207.5	377.0350	1.1879
306.5	1.4750	0.4172	207	410.2875	1.7006
306	1.5300	0.4455	206.5	447.0275	1.8491
305.5	1.5750	0.6293	206	487.3925	1.9481
305	1.5525	0.6894	205.5	531.8100	2.1355
304.5	1.5975	0.7319	205	580.4475	2.6410
304	1.5925	0.7036	204.5	634.2250	2.7436
303.5	1.5050	0.6930	204	692.6475	3.3694
303	1.5125	0.6541	203.5	755.1550	4.5184
302.5	1.6000	0.5657	203	822.0475	5.9503
302	1.6900	0.6081	202.5	889.4700	5.1407
301.5	1.7675	0.5975	202	954.8650	7.7640
301	1.7275	0.4914	201.5	1013.0075	9.9667
			201	1057.8825	12.1799
			200.5	1087.1300	11.2006
			200	1099.7025	12.6961

Table A4.5.a. Molar absorption coefficients values, $\varepsilon(\lambda)$ of (*E*)-2-hexen-1-al in the aqueous phase at 298 K and pH =7, at wavelengths between 247 – 400 nm.⁴⁴⁴

(E)-2-hexen-1-al, mean value for concentration range 30 – 1.875 mM (aqueous), TROPOS

Wavelength	Average	σ , n=10	Wavelength	Average	σ , n=10
λ , nm	$\mathcal{E}/\text{M}^{-1}\text{cm}^{-1}$	$\Delta\mathcal{E}/\text{M}^{-1}\text{cm}^{-1}$	λ , nm	$\mathcal{E}/\text{M}^{-1}\text{cm}^{-1}$	$\Delta\mathcal{E}/\text{M}^{-1}\text{cm}^{-1}$
400	0.6135	0.3120	323	35.2416	1.8905
399	0.6204	0.3275	322	36.6259	1.9774
398	0.6276	0.3215	321	38.0196	2.0322
397	0.6525	0.3242	320	39.3548	2.1114
396	0.7069	0.3533	319	40.6765	2.1774
395	0.6242	0.3013	318	42.0133	2.2470
394	0.6543	0.3120	317	43.3711	2.3430
393	0.6455	0.2978	316	44.5141	2.4366
392	0.6886	0.3186	315	45.6150	2.4928
391	0.6927	0.3011	314	46.6694	2.5477
390	0.6531	0.2879	313	47.6655	2.6084
389	0.6888	0.2908	312	48.6171	2.6494
388	0.7251	0.2968	311	49.5347	2.6746
387	0.7275	0.3004	310	50.3631	2.7382
386	0.7405	0.3031	309	51.0873	2.7924
385	0.7638	0.3093	308	51.7708	2.8087
384	0.7913	0.3048	307	52.3744	2.8078
383	0.8595	0.3230	306	52.8488	2.8300
382	0.8171	0.2849	305	53.2496	2.8360
381	0.8282	0.2603	304	53.5823	2.8207
380	0.9199	0.3049	303	53.8144	2.8240
379	0.9390	0.2883	302	53.9586	2.8211
378	0.9745	0.2671	301	54.0320	2.7988
377	1.0958	0.3162	300	54.0538	2.7596
376	1.0901	0.2638	299	54.0095	2.6940
375	1.1353	0.2440	298	53.8891	2.6230
374	1.2436	0.2738	297	53.6995	2.5451
373	1.3046	0.2648	296	53.4566	2.4585
372	1.3744	0.2624	295	53.1482	2.3754
371	1.4636	0.2506	294	52.7845	2.2860
370	1.5417	0.2297	293	52.3835	2.1876
369	1.6444	0.2300	292	51.9670	2.0707
368	1.7516	0.2069	291	51.4948	1.9588
367	1.9040	0.2062	290	50.9605	1.8611
366	2.0405	0.1974	289	50.3856	1.7781
365	2.1927	0.1968	288	49.7717	1.7053
364	2.3268	0.1647	287	49.1557	1.6490
363	2.5082	0.1752	286	48.5179	1.6235
362	2.7297	0.2184	285	47.8535	1.6124
361	2.9659	0.2341	284	47.1983	1.5987

360	3.1799	0.2063	283	46.5305	1.5852
359	3.4470	0.2210	282	45.9215	1.6089
358	3.7257	0.2220	281	45.3697	1.6501
357	4.0062	0.2092	280	44.8458	1.6839
356	4.3472	0.2345	279	44.4113	1.7189
355	4.6814	0.2283	278	44.0911	1.7337
354	5.0326	0.2291	277	43.9625	1.7519
353	5.4263	0.2452	276	44.0627	1.7809
352	5.8843	0.2692	275	44.3884	1.7923
351	6.3901	0.2999	274	44.9840	1.7890
350	6.8975	0.3197	273	45.8713	1.7559
349	7.4335	0.3417	272	47.1528	1.7239
348	8.0097	0.3567	271	48.9648	1.6978
347	8.6510	0.3851	270	51.3595	1.6959
346	9.3401	0.4283	269	54.4018	1.7405
345	10.0126	0.4545	268	58.2606	1.8458
344	10.7621	0.4862	267	63.0981	2.0239
343	11.5525	0.5257	266	69.0300	2.3125
342	12.3779	0.5804	265	76.2555	2.7190
341	13.2883	0.6187	264	85.1801	3.2466
340	14.2241	0.6818	263	96.3635	3.8646
339	15.1800	0.7415	262	110.5734	4.6969
338	16.1935	0.8080	261	128.5989	5.7447
337	17.2635	0.8585	260	154.8044	6.6656
336	18.3574	0.9153	259	183.3975	7.7055
335	19.4955	0.9750	258	221.6790	9.0790
334	20.6482	1.0401	257	275.3103	12.4624
333	21.8207	1.1298	256	332.8382	14.3464
332	23.1161	1.1721	255	408.2574	17.0885
331	24.4131	1.2383	254	501.9188	20.4474
330	25.6954	1.3384	253	619.4017	27.5137
329	27.0330	1.4299	252	775.7439	24.4249
328	28.4055	1.5079	251	966.3459	38.0522
327	29.8019	1.5687	250	1190.3296	68.8856
326	31.1800	1.6438	249	1409.4997	0.7460
325	32.5157	1.7346	248	1722.1291	12.7769
324	33.8815	1.8041	247	2180.3736	95.5808

Table A4.5.b. Molar absorption coefficients values, $\epsilon(\lambda)$ of (*E*)-2-hexen-1-al in the aqueous phase at 295 K and pH =7, at wavelengths between 200 – 400 nm, measured for 1 mM and 0.1 mM concentrations, respectively.¹⁷²

<i>(E)</i> -2-hexen-1-al (IPC PAS), 1 mM aqueous			<i>(E)</i> -2-hexen-1-al (IPC PAS), 0.1 mM aqueous		
Wavelength	Average	σ , n=2	Wavelength	Average	σ , n=2
λ , nm	ϵ / M ⁻¹ cm ⁻¹	$\Delta\epsilon$ / M ⁻¹ cm ⁻¹	λ , nm	ϵ / M ⁻¹ cm ⁻¹	$\Delta\epsilon$ / M ⁻¹ cm ⁻¹
400	1.2700	0.3677	400	-0.850	0.636
399.5	1.2750	0.3041	399.5	-1.150	0.919
399	1.2350	0.3465	399	-1.550	1.768
398.5	1.1950	0.5162	398.5	-1.550	3.041
398	1.1650	0.4738	398	-2.700	4.101
397.5	1.1100	0.4950	397.5	-1.350	2.616
397	0.9750	0.4738	397	-1.500	0.566
396.5	0.9100	0.3960	396.5	-0.800	1.273
396	0.8450	0.4738	396	1.300	1.414
395.5	0.9650	0.5162	395.5	-0.200	1.273
395	1.0150	0.4879	395	-0.400	1.980
394.5	1.1000	0.4525	394.5	0.700	3.818
394	1.2350	0.3182	394	-0.450	5.020
393.5	1.1800	0.4667	393.5	-0.500	4.667
393	1.3950	0.5303	393	-0.400	4.384
392.5	1.3250	0.5728	392.5	0.300	4.384
392	1.2850	0.5020	392	2.800	4.384
391.5	1.2550	0.4596	391.5	3.300	5.091
391	1.3050	0.3748	391	2.700	4.667
390.5	1.3500	0.2970	390.5	2.100	3.818
390	1.3050	0.2051	390	3.000	2.828
389.5	1.2550	0.1344	389.5	4.150	2.333
389	1.1700	0.1556	389	3.700	2.404
388.5	1.1250	0.1626	388.5	4.700	2.404
388	1.0000	0.1273	388	4.050	2.475
387.5	1.1500	0.0707	387.5	4.750	3.465
387	1.0650	0.0354	387	6.200	4.243
386.5	1.2900	0.0283	386.5	6.600	5.091
386	1.3050	0.0212	386	7.950	4.313
385.5	1.4450	0.0495	385.5	9.400	3.677
385	1.3900	0.0000	385	8.900	3.536
384.5	1.4650	0.0212	384.5	9.600	5.091
384	1.5250	0.1202	384	8.150	5.445
383.5	1.7250	0.1768	383.5	7.650	5.728
383	1.7300	0.2263	383	7.300	6.364
382.5	1.7750	0.1485	382.5	8.650	5.869
382	1.8850	0.2758	382	9.450	6.152
381.5	1.8750	0.3041	381.5	10.900	4.808

381	1.8700	0.3394	381	10.650	4.879
380.5	1.8950	0.3323	380.5	11.400	5.515
380	1.7650	0.2333	380	11.600	3.818
379.5	1.5500	0.3818	379.5	11.350	4.455
379	1.4650	0.4738	379	11.650	3.465
378.5	1.5000	0.4808	378.5	12.050	3.465
378	1.6950	0.5162	378	11.800	4.525
377.5	1.8050	0.5303	377.5	13.000	3.677
377	1.8450	0.4879	377	11.700	4.950
376.5	2.0300	0.3536	376.5	10.050	4.879
376	2.0600	0.4667	376	11.100	4.384
375.5	2.2200	0.4667	375.5	12.300	3.677
375	2.3050	0.4455	375	11.100	3.394
374.5	2.2200	0.3960	374.5	11.550	2.475
374	2.3250	0.3041	374	9.850	3.041
373.5	2.3900	0.3677	373.5	8.600	2.546
373	2.2650	0.2475	373	6.700	1.980
372.5	2.3700	0.2263	372.5	5.550	1.344
372	2.5550	0.2758	372	5.450	2.333
371.5	2.5300	0.0849	371.5	6.000	2.121
371	2.5550	0.1344	371	7.000	1.131
370.5	2.6050	0.1768	370.5	6.350	0.354
370	2.5350	0.2616	370	6.600	3.818
369.5	2.5850	0.2333	369.5	5.650	4.031
369	2.7150	0.0778	369	4.150	4.031
368.5	2.9750	0.0778	368.5	4.150	4.172
368	3.1100	0.1131	368	5.600	2.828
367.5	3.1700	0.1273	367.5	6.450	1.768
367	3.1400	0.1414	367	5.750	3.465
366.5	3.3600	0.1838	366.5	7.550	4.172
366	3.3450	0.1768	366	8.750	2.051
365.5	3.3400	0.1131	365.5	8.700	1.131
365	3.4400	0.1556	365	11.400	1.273
364.5	3.4250	0.1909	364.5	7.350	0.636
364	3.4850	0.1909	364	6.100	0.566
363.5	3.7750	0.1768	363.5	7.000	2.546
363	4.1350	0.1626	363	7.400	0.000
362.5	4.1900	0.2828	362.5	9.000	0.141
362	4.3350	0.4313	362	6.250	1.202
361.5	4.5150	0.2475	361.5	7.250	1.061
361	4.6650	0.4031	361	10.050	0.354
360.5	4.9250	0.4596	360.5	10.050	0.071

360	5.3500	0.6223	360	11.300	1.131
359.5	5.5750	0.4172	359.5	10.200	1.697
359	5.8500	0.5374	359	8.800	4.384
358.5	5.9700	0.8202	358.5	9.000	5.515
358	6.2150	0.6435	358	9.900	6.788
357.5	6.4700	0.6081	357.5	9.900	7.495
357	6.6200	0.7071	357	10.250	7.425
356.5	6.8100	0.6505	356.5	11.750	7.000
356	6.9700	0.6223	356	12.750	7.283
355.5	7.0500	0.4808	355.5	12.900	7.495
355	7.1500	0.3960	355	13.950	7.283
354.5	7.7250	0.2899	354.5	14.900	7.354
354	7.9050	0.3041	354	14.350	8.132
353.5	8.0350	0.1485	353.5	13.800	9.051
353	8.3950	0.2899	353	12.600	3.960
352.5	8.3700	0.3536	352.5	12.000	3.677
352	8.7450	0.1909	352	13.400	4.808
351.5	9.1100	0.1273	351.5	17.300	5.374
351	9.4850	0.1202	351	20.150	5.303
350.5	9.5550	0.0354	350.5	20.700	6.364
350	9.8400	0.1273	350	20.900	4.525
349.5	10.1050	0.1202	349.5	22.350	4.031
349	10.4700	0.1131	349	21.800	6.081
348.5	11.0900	0.0424	348.5	20.750	5.162
348	11.5350	0.0354	348	19.450	3.748
347.5	11.9050	0.0919	347.5	18.850	3.748
347	12.0650	0.1485	347	19.250	4.596
346.5	12.3750	0.1909	346.5	20.050	3.182
346	12.8900	0.0283	346	22.200	0.990
345.5	13.1800	0.0707	345.5	24.650	1.202
345	13.5750	0.0778	345	24.750	1.061
344.5	14.1100	0.1556	344.5	26.350	0.778
344	14.7400	0.2263	344	29.250	0.495
343.5	15.0250	0.2616	343.5	27.450	1.626
343	15.5500	0.2546	343	26.650	3.041
342.5	15.8950	0.2475	342.5	27.650	1.626
342	16.2400	0.1414	342	26.900	1.697
341.5	16.5400	0.1131	341.5	29.350	1.344
341	17.0550	0.1061	341	29.150	2.051
340.5	17.5900	0.0566	340.5	30.200	2.404
340	21.8350	0.5162	340	25.900	13.294
339.5	22.4450	0.8697	339.5	26.200	14.142

339	22.8350	0.8556	339	24.400	15.839
338.5	23.2750	0.8697	338.5	23.650	13.647
338	23.9650	0.9263	338	27.450	12.233
337.5	24.4550	1.3223	337.5	27.050	12.233
337	24.7550	1.3647	337	27.250	13.506
336.5	24.9950	1.4637	336.5	31.250	14.354
336	25.5200	1.6546	336	31.000	12.304
335.5	25.7750	1.6334	335.5	30.700	9.192
335	26.5700	1.3576	335	33.750	10.677
334.5	26.9700	1.2728	334.5	37.300	9.192
334	27.4650	1.4496	334	41.200	8.910
333.5	27.7400	1.3294	333.5	43.000	7.637
333	28.4700	1.1314	333	43.250	5.162
332.5	29.0450	1.2657	332.5	43.650	4.879
332	29.7350	1.4213	332	41.650	2.192
331.5	30.3350	1.5203	331.5	42.200	0.424
331	31.4000	1.6405	331	43.450	3.606
330.5	32.3300	1.2728	330.5	46.100	4.243
330	32.7700	1.3576	330	50.500	1.980
329.5	33.2850	1.0960	329.5	56.050	3.323
329	33.9550	0.8980	329	56.650	5.020
328.5	34.6850	0.5586	328.5	59.900	4.808
328	35.1600	0.4808	328	60.650	6.152
327.5	36.1550	0.7849	327.5	57.100	3.536
327	36.5750	0.5586	327	57.900	3.394
326.5	37.3700	0.3960	326.5	58.600	4.101
326	38.1900	0.3253	326	62.050	3.748
325.5	38.8550	0.4031	325.5	62.200	2.828
325	39.1250	0.1909	325	60.250	3.606
324.5	39.5550	0.0495	324.5	60.050	3.465
324	40.5150	0.1061	324	59.900	2.687
323.5	41.5550	0.1344	323.5	60.900	2.970
323	42.2600	0.0141	323	57.750	4.313
322.5	42.7700	0.3536	322.5	58.600	6.081
322	43.1900	0.3253	322	56.650	4.596
321.5	43.9850	0.0212	321.5	54.500	4.101
321	44.7650	0.1626	321	55.150	3.606
320.5	45.5100	0.0566	320.5	53.350	3.323
320	46.3300	0.2546	320	53.600	5.374
319.5	47.1650	0.4172	319.5	56.650	4.313
319	47.6250	0.2899	319	57.600	6.223
318.5	48.2750	0.3606	318.5	59.700	6.505

318	48.9100	0.5374	318	60.050	5.303
317.5	49.5100	0.3394	317.5	59.000	5.374
317	50.3700	0.1556	317	60.450	6.718
316.5	50.7500	0.1131	316.5	57.700	6.081
316	51.0950	0.1909	316	59.300	3.818
315.5	51.7450	0.2333	315.5	58.350	5.020
315	52.0900	0.1697	315	58.750	5.303
314.5	52.7450	0.0495	314.5	58.450	4.738
314	53.5350	0.0636	314	59.550	3.748
313.5	53.5950	0.0778	313.5	58.500	3.111
313	54.2250	0.0354	313	58.100	5.374
312.5	54.7250	0.1344	312.5	57.950	4.738
312	55.0650	0.1626	312	58.150	4.455
311.5	55.6400	0.2546	311.5	57.250	5.303
311	56.0600	0.4101	311	59.650	2.192
310.5	56.2350	0.3182	310.5	58.350	1.061
310	56.8400	0.0990	310	60.850	1.202
309.5	57.3000	0.0707	309.5	59.800	1.414
309	57.6100	0.0000	309	60.050	0.071
308.5	57.6100	0.1980	308.5	55.700	2.970
308	57.9800	0.2828	308	56.700	1.556
307.5	58.1600	0.4243	307.5	59.650	2.192
307	58.3000	0.5091	307	59.550	1.485
306.5	58.2900	0.5374	306.5	58.250	1.626
306	58.3800	0.2263	306	59.850	0.919
305.5	58.4450	0.4879	305.5	60.600	0.707
305	58.3950	0.5869	305	61.550	1.626
304.5	58.5450	0.6859	304.5	61.250	1.202
304	58.7850	0.5586	304	59.500	0.000
303.5	58.9450	0.6152	303.5	60.650	0.071
303	59.0050	0.4455	303	63.100	0.141
302.5	59.0350	0.1061	302.5	64.150	1.768
302	59.1600	0.2970	302	63.650	1.202
301.5	58.6100	0.2828	301.5	65.000	2.546
301	58.7550	0.3182	301	65.950	2.616
300.5	58.5950	0.3748	300.5	67.400	4.243
300	58.2400	0.4525	300	67.500	4.667
299.5	58.0650	0.3041	299.5	67.350	3.465
299	57.8800	0.4101	299	67.450	3.041
298.5	57.4900	0.3253	298.5	68.400	3.818
298	57.0900	0.2121	298	65.950	3.889
297.5	57.0950	0.0778	297.5	65.900	4.667

297	56.8750	0.0212	297	64.400	8.202
296.5	56.4000	0.1838	296.5	64.250	8.273
296	56.2300	0.0849	296	65.900	7.354
295.5	55.9500	0.3253	295.5	69.100	8.768
295	55.5650	0.2899	295	68.200	10.324
294.5	55.1800	0.3960	294.5	67.550	9.122
294	54.9050	0.3606	294	67.400	10.182
293.5	54.6200	0.2546	293.5	67.250	9.546
293	54.1600	0.3253	293	68.700	7.920
292.5	53.7450	0.5869	292.5	64.850	8.839
292	53.5300	0.6364	292	62.850	9.546
291.5	52.9000	0.6930	291.5	64.250	9.263
291	52.3450	0.8132	291	64.100	9.617
290.5	51.7050	0.6859	290.5	63.050	7.990
290	51.1200	0.7778	290	62.200	7.637
289.5	50.3850	0.6152	289.5	61.000	6.788
289	50.0000	0.7354	289	61.050	7.849
288.5	49.5300	0.6788	288.5	62.400	7.495
288	48.8200	0.6647	288	60.500	7.495
287.5	48.5200	0.8344	287.5	59.650	7.990
287	47.8900	0.6930	287	58.400	7.920
286.5	47.3800	0.7212	286.5	59.400	8.910
286	46.9400	0.6788	286	55.950	7.566
285.5	46.4300	0.8344	285.5	55.550	7.142
285	45.9300	0.7637	285	56.300	6.788
284.5	45.0850	0.7990	284.5	57.800	7.212
284	44.2650	0.6435	284	57.700	5.657
283.5	44.0300	0.5798	283.5	58.500	5.657
283	43.2800	0.5940	283	58.550	5.728
282.5	42.9950	0.5586	282.5	57.500	6.223
282	42.6400	0.6081	282	58.250	5.869
281.5	42.2350	0.5869	281.5	57.650	6.576
281	41.8300	0.6223	281	57.050	6.010
280.5	41.2800	0.6505	280.5	60.050	6.152
280	40.9200	0.5798	280	57.550	7.142
279.5	40.7200	0.7354	279.5	58.100	6.505
279	40.4550	0.7142	279	57.200	5.515
278.5	40.3050	0.5303	278.5	56.400	4.667
278	40.4000	0.5091	278	57.350	3.748
277.5	40.2950	0.3465	277.5	57.600	5.233
277	40.4500	0.2970	277	57.150	3.041
276.5	40.5150	0.3041	276.5	56.500	3.536

276	40.5850	0.5020	276	54.050	3.182
275.5	41.0300	0.5940	275.5	53.650	2.192
275	41.3950	0.6859	275	54.300	1.131
274.5	41.9000	0.7212	274.5	54.250	0.495
274	42.6650	0.5869	274	56.350	0.071
273.5	43.1650	0.6859	273.5	56.250	1.061
273	43.9450	0.6859	273	58.300	1.838
272.5	44.9250	0.7425	272.5	60.900	1.838
272	45.7900	0.8768	272	62.000	1.697
271.5	47.1600	0.8061	271.5	63.750	0.636
271	48.7800	0.7071	271	66.050	0.212
270.5	50.6000	0.6081	270.5	67.600	0.990
270	52.4200	0.5374	270	67.850	1.626
269.5	54.1450	0.4738	269.5	69.500	1.131
269	56.3850	0.4313	269	70.050	2.333
268.5	58.9850	0.2899	268.5	74.200	2.121
268	62.0350	0.2758	268	76.750	3.323
267.5	65.5850	0.3748	267.5	80.300	3.960
267	69.4800	0.1697	267	86.150	4.172
266.5	73.8050	0.0354	266.5	88.900	4.525
266	78.8100	0.0424	266	95.200	2.404
265.5	84.4950	0.0354	265.5	101.900	1.697
265	90.5800	0.0424	265	108.000	2.404
264.5	97.6200	0.0424	264.5	115.700	1.838
264	105.2750	0.0778	264	126.250	0.636
263.5	113.9150	0.1485	263.5	137.650	2.192
263	123.5850	0.2758	263	148.250	2.192
262.5	134.2600	0.4101	262.5	162.800	2.121
262	146.2050	0.4172	262	176.150	3.323
261.5	159.5800	0.6081	261.5	192.050	3.182
261	174.3400	0.6930	261	210.800	2.828
260.5	190.7800	0.7354	260.5	231.150	3.606
260	208.7350	0.8556	260	257.550	3.323
259.5	228.3800	1.0182	259.5	283.250	0.778
259	249.5700	1.1738	259	313.950	0.495
258.5	272.7600	1.2021	258.5	347.500	0.707
258	297.4250	1.1809	258	384.500	0.141
257.5	324.0400	1.1172	257.5	426.750	0.636
257	352.8800	1.0748	257	474.500	0.424
256.5	383.6900	1.1172	256.5	528.500	1.697
256	416.5300	1.2304	256	588.800	4.384
255.5	451.6600	1.2304	255.5	655.050	2.616

255	488.8000	1.3152	255	727.550	4.313
254.5	528.6100	1.5556	254.5	808.550	5.303
254	571.1300	1.5839	254	898.850	5.869
253.5	616.4100	1.5274	253.5	995.450	5.728
253	664.9200	1.7678	253	1102.700	6.364
252.5	716.6650	2.0860	252.5	1216.650	6.152
252	772.3900	1.8809	252	1341.700	5.657
251.5	832.8850	2.1001	251.5	1476.150	4.596
251	897.9700	2.0223	251	1620.350	5.020
250.5	968.5700	2.2062	250.5	1775.250	6.293
250	1044.6400	1.9375	250	1943.850	5.303
249.5	1127.0700	2.5456	249.5	2122.950	7.142
249	1216.0100	2.5739	249	2311.800	9.899
248.5	1312.5350	3.0335	248.5	2515.900	8.910
248	1416.6300	3.5072	248	2731.500	9.758
247.5	1529.1200	2.6163	247.5	2958.750	9.405
247	1650.9450	3.5709	247	3200.050	8.556
246.5	1781.3400	4.6245	246.5	3455.850	10.819
246	1920.9550	2.5668	246	3725.900	12.728
245.5	2067.8050	3.0335	245.5	4007.250	13.789
245	2221.8100	3.2668	245	4304.500	14.991
244.5	2378.0250	1.7466	244.5	4615.300	14.425
244	2529.5350	1.2092	244	4942.000	14.566
243.5	2670.1200	5.5861	243.5	5284.050	15.486
243	2795.1350	9.7793	243	5640.450	14.071
242.5	2891.7500	3.9032	242.5	6006.800	16.263
242	2962.1800	3.1961	242	6389.400	16.829
241.5	3015.2300	6.2791	241.5	6784.950	11.102
241	3046.4450	12.0562	241	7196.350	11.526
240.5	3068.2300	9.9702	240.5	7618.100	11.455
240	3078.6950	13.4421	240	8056.600	7.354
239.5	3089.5350	6.4983	239.5	8501.250	10.394
239	3099.4000	10.5500	239	8959.500	8.485
238.5	3112.5350	13.3007	238.5	9425.500	8.910
238	3124.1850	14.2199	238	9900.550	11.384
237.5	3132.6050	16.6099	237.5	10383.600	11.314
237	3133.7250	16.5251	237	10865.850	15.768
236.5	3134.4850	19.1272	236.5	11347.400	10.748
236	3140.7700	13.4067	236	11829.650	3.889
235.5	3141.2850	11.9006	235.5	12305.400	6.788
235	3147.9850	14.5593	235	12779.850	8.697
234.5	3154.3250	22.5779	234.5	13243.000	10.465

234	3160.9150	26.9903	234	13696.550	11.667
233.5	3162.2950	29.2106	233.5	14135.150	4.031
233	3168.6300	36.0200	233	14556.350	1.061
232.5	3177.7050	42.7163	232.5	14961.400	6.788
232	3183.6550	49.7591	232	15342.050	20.577
231.5	3193.6000	51.2652	231.5	15700.350	20.435
231	3194.8700	57.7423	231	16029.400	12.021
230.5	3205.4400	64.9973	230.5	16328.950	3.041
230	3213.6950	67.2812	230	16602.100	11.172
229.5	3210.6850	58.4848	229.5	16842.050	4.172
229	3211.4000	57.6575	229	17034.400	10.889
228.5	3220.1850	58.3292	228.5	17193.600	9.899
228	3214.8200	67.3307	228	17321.250	9.263
227.5	3210.9600	65.5347	227.5	17393.150	11.809
227	3209.1700	78.5878	227	17442.850	16.900
226.5	3212.6450	78.0717	226.5	17444.150	11.243
226	3200.6750	68.8510	226	17415.300	24.183
225.5	3192.8100	69.9470	225.5	17347.300	37.335
225	3181.8150	73.3058	225	17242.850	37.406
224.5	3178.3100	71.5733	224.5	17100.250	27.931
224	3188.0400	80.8506	224	16924.450	23.971
223.5	3185.8450	82.0032	223.5	16719.200	21.355
223	3185.4500	89.5339	223	16484.250	8.415
222.5	3176.8100	96.8595	222.5	16220.550	1.344
222	3176.7500	98.8818	222	15945.400	2.828
221.5	3168.5950	91.6623	221.5	15645.250	6.152
221	3165.5000	84.5275	221	15326.700	12.445
220.5	3159.6550	73.4189	220.5	14985.950	14.920
220	3150.1300	72.0118	220	14627.250	13.223
219.5	3141.2400	78.8424	219.5	14263.650	12.233
219	3130.1200	71.7572	219	13887.450	5.020
218.5	3129.3100	61.1647	218.5	13501.100	7.778
218	3137.6150	63.6467	218	13110.450	8.556
217.5	3124.3350	59.1212	217.5	12715.050	9.970
217	3112.7000	63.0739	217	12315.700	0.566
216.5	3113.8250	64.8063	216.5	11920.800	2.263
216	3104.1250	50.5086	216	11522.000	5.374
215.5	3100.9900	57.1908	215.5	11122.950	6.293
215	3096.2400	46.3579	215	10727.150	1.485
214.5	3099.7350	45.1629	214.5	10336.450	10.536
214	3084.4850	43.1972	214	9945.750	5.728
213.5	3077.2000	38.5656	213.5	9564.800	6.930

213	3076.4200	38.5656	213	9189.450	5.020
212.5	3067.2650	22.6911	212.5	8816.150	6.435
212	3062.1900	25.8801	212	8454.650	10.960
211.5	3054.3550	11.1652	211.5	8102.150	11.667
211	3047.7650	20.2303	211	7752.300	11.597
210.5	3035.7450	28.2206	210.5	7417.750	5.586
210	3025.8900	31.6218	210	7093.100	0.424
209.5	3014.6450	20.9374	209.5	6772.150	1.202
209	2993.2650	12.4097	209	6462.850	6.293
208.5	2965.8300	20.7324	208.5	6166.650	6.010
208	2944.9600	2.3900	208	5872.550	6.859
207.5	2895.3900	5.6003	207.5	5590.500	6.647
207	2850.8000	5.4306	207	5320.550	7.566
206.5	2795.7450	1.6193	206.5	5060.250	7.566
206	2737.3600	7.0994	206	4810.600	7.212
205.5	2659.2200	1.5839	205.5	4571.250	6.576
205	2572.8000	2.7436	205	4344.500	4.808
204.5	2485.3550	9.1995	204.5	4131.000	4.525
204	2404.4550	10.3025	204	3919.500	2.546
203.5	2316.4550	3.7689	203.5	3723.150	4.455
203	2226.8800	2.7436	203	3532.250	5.869
202.5	2140.5600	2.2769	202.5	3355.850	9.405
202	2060.6600	4.5821	202	3187.300	11.031
201.5	1981.0400	3.3517	201.5	3030.150	7.283
201	1909.4400	3.8325	201	2878.400	6.223
200.5	1841.2200	3.6770	200.5	2731.700	5.233
200	1780.5300	8.5843	200	2594.000	4.101

Table A4.6. Molar absorption coefficients values, $\varepsilon(\lambda)$ of (*Z*)-3-hexenyl acetate in the aqueous phase at 295 K and pH =7, at wavelengths between 200 – 400 nm.¹⁷²

<i>(Z)</i> -3-hexenyl acetate, mean value for concentration 2 mM (aqueous), IPC PAS					
Wavelength	Average	σ , n=2	Wavelength	Average	σ , n=2
λ , nm	$\varepsilon/ \text{M}^{-1} \text{cm}^{-1}$	$\Delta\varepsilon/ \text{M}^{-1} \text{cm}^{-1}$	λ , nm	$\varepsilon/ \text{M}^{-1} \text{cm}^{-1}$	$\Delta\varepsilon/ \text{M}^{-1} \text{cm}^{-1}$
400	-0.0400	0.0849	300	0.9825	0.3642
399.5	-0.0475	0.0955	299.5	1.1075	0.4066
399	-0.0175	0.1450	299	1.0525	0.3359
398.5	-0.0125	0.1591	298.5	0.9525	0.2652
398	-0.0275	0.1237	298	0.9725	0.0955
397.5	-0.0525	0.1591	297.5	0.8725	0.1025
397	0.0225	0.1732	297	0.6925	0.0672

396.5	0.0975	0.1945	296.5	0.5425	0.1520
396	0.0850	0.2546	296	0.5200	0.2828
395.5	0.0450	0.2404	295.5	0.5300	0.2970
395	0.0450	0.1980	295	0.4600	0.3323
394.5	-0.0100	0.2192	294.5	0.4100	0.3182
394	0.0175	0.1520	294	0.4925	0.3147
393.5	0.0150	0.1414	293.5	0.5550	0.2758
393	0.0700	0.1131	293	0.6450	0.2263
392.5	0.0400	0.0990	292.5	0.6250	0.1556
392	0.0925	0.1096	292	0.6400	0.1768
391.5	0.0350	0.1556	291.5	0.8200	0.2121
391	0.0650	0.1626	291	0.9375	0.1874
390.5	0.1225	0.2227	290.5	0.8650	0.2758
390	0.2425	0.2793	290	0.8925	0.2722
389.5	0.2750	0.2828	289.5	0.9325	0.2652
389	0.2725	0.3147	289	1.0125	0.2652
388.5	0.2300	0.2758	288.5	1.1150	0.2404
388	0.2375	0.3076	288	1.0300	0.3182
387.5	0.3450	0.2758	287.5	1.1350	0.2475
387	0.3300	0.3041	287	1.1725	0.3147
386.5	0.2750	0.3182	286.5	1.2075	0.1945
386	0.2200	0.2687	286	1.3375	0.2864
385.5	0.2375	0.1945	285.5	1.2725	0.4066
385	0.3200	0.2192	285	1.3175	0.4490
384.5	0.3425	0.1945	284.5	1.2250	0.4525
384	0.3400	0.1768	284	1.3175	0.3642
383.5	0.3825	0.1732	283.5	1.3225	0.3500
383	0.3750	0.1131	283	1.3725	0.2864
382.5	0.4900	0.0990	282.5	1.5275	0.2015
382	0.5300	0.1626	282	1.5250	0.1202
381.5	0.5475	0.1803	281.5	1.5500	0.0424
381	0.5125	0.2369	281	1.5400	0.0495
380.5	0.4850	0.2333	280.5	1.5575	0.0106
380	0.5000	0.2828	280	1.6450	0.0495
379.5	0.4900	0.3253	279.5	1.5450	0.0849
379	0.4575	0.3500	279	1.6775	0.0813
378.5	0.4750	0.3323	278.5	1.6500	0.0849
378	0.4800	0.2758	278	1.6100	0.0283
377.5	0.3800	0.2333	277.5	1.7525	0.0813
377	0.4700	0.2404	277	1.7525	0.0672
376.5	0.4575	0.2298	276.5	1.7900	0.0707
376	0.4025	0.2157	276	1.8825	0.0530
375.5	0.4300	0.1909	275.5	1.9175	0.0601
375	0.4800	0.1838	275	2.0050	0.0636

374.5	0.4200	0.2687	274.5	2.0100	0.0071
374	0.4325	0.2652	274	2.1025	0.0318
373.5	0.5225	0.3147	273.5	2.1575	0.0247
373	0.5700	0.3677	273	2.2700	0.0000
372.5	0.4400	0.3536	272.5	2.4300	0.0283
372	0.4125	0.3571	272	2.5700	0.0071
371.5	0.5025	0.3995	271.5	2.7800	0.0141
371	0.4350	0.3818	271	2.9325	0.0247
370.5	0.4575	0.3924	270.5	3.1425	0.0106
370	0.2675	0.2864	270	3.1850	0.0071
369.5	0.3000	0.2616	269.5	3.3650	0.1061
369	0.2900	0.2687	269	3.4225	0.1732
368.5	0.2825	0.2722	268.5	3.5700	0.2475
368	0.2275	0.1874	268	3.7300	0.4101
367.5	0.2425	0.1662	267.5	3.8075	0.4349
367	0.2175	0.0884	267	3.9650	0.4384
366.5	0.2425	0.0530	266.5	4.0650	0.4596
366	0.2700	0.0141	266	4.2000	0.4950
365.5	0.3200	0.0071	265.5	4.3350	0.3748
365	0.2875	0.0177	265	4.4625	0.3642
364.5	0.1450	0.0212	264.5	4.6000	0.3748
364	0.1200	0.0566	264	4.6300	0.3960
363.5	0.1225	0.0530	263.5	4.7650	0.3677
363	0.1750	0.0849	263	4.8375	0.4137
362.5	0.1350	0.1131	262.5	4.9250	0.3889
362	0.0700	0.1273	262	5.1075	0.3571
361.5	0.0800	0.1414	261.5	5.2450	0.2828
361	0.0500	0.0849	261	5.4150	0.2546
360.5	0.0150	0.1131	260.5	5.5650	0.3253
360	0.0800	0.1556	260	5.6500	0.3394
359.5	0.1225	0.1096	259.5	5.7175	0.2722
359	-0.0075	0.1379	259	5.9125	0.2793
358.5	0.0025	0.1096	258.5	5.9900	0.3182
358	0.1250	0.1626	258	6.1525	0.3854
357.5	0.2175	0.1874	257.5	6.3250	0.4596
357	0.1925	0.2157	257	6.4550	0.4455
356.5	0.2750	0.2404	256.5	6.6525	0.5339
356	0.2850	0.2546	256	6.8950	0.4525
355.5	0.2500	0.2192	255.5	7.1625	0.3995
355	0.2575	0.2369	255	7.4650	0.2546
354.5	0.2700	0.2970	254.5	7.6950	0.2546
354	0.3425	0.2652	254	7.9925	0.3288
353.5	0.3200	0.2263	253.5	8.2575	0.2864
353	0.3200	0.2758	253	8.6050	0.3253

352.5	0.2950	0.2404	252.5	8.9750	0.3606
352	0.3825	0.3288	252	9.3000	0.3182
351.5	0.4300	0.2546	251.5	9.7425	0.2015
351	0.4725	0.2086	251	10.1700	0.1838
350.5	0.3450	0.2687	250.5	10.5525	0.2086
350	0.3775	0.1803	250	10.9625	0.1379
349.5	0.5650	0.2616	249.5	11.3700	0.1414
349	0.5675	0.2227	249	11.8450	0.1414
348.5	0.5525	0.2298	248.5	12.3825	0.2086
348	0.6300	0.2121	248	12.9150	0.2192
347.5	0.5650	0.2475	247.5	13.4125	0.1874
347	0.4275	0.1874	247	13.9775	0.1732
346.5	0.5100	0.1556	246.5	14.5150	0.1980
346	0.6400	0.0990	246	15.2275	0.0884
345.5	0.6875	0.0389	245.5	15.8700	0.0354
345	0.4975	0.0106	245	16.6025	0.0035
344.5	0.3325	0.0177	244.5	17.2600	0.0212
344	0.3775	0.0672	244	18.0150	0.0354
343.5	0.4000	0.0636	243.5	18.8075	0.0247
343	0.4600	0.1768	243	19.5750	0.0636
342.5	0.5475	0.2369	242.5	20.3100	0.1626
342	0.5050	0.2051	242	21.0950	0.1485
341.5	0.5825	0.2298	241.5	22.0550	0.1626
341	0.4700	0.1697	241	22.9225	0.0106
340.5	0.4075	0.1591	240.5	23.8175	0.0742
340	0.9425	0.2581	240	24.7775	0.0813
339.5	0.9300	0.1061	239.5	25.6575	0.0389
339	0.9175	0.0530	239	26.6575	0.1096
338.5	0.9275	0.0177	238.5	27.5825	0.1662
338	0.9500	0.0495	238	28.6325	0.1379
337.5	0.9400	0.0141	237.5	29.6925	0.1591
337	0.8175	0.1167	237	30.7450	0.1909
336.5	0.7200	0.2404	236.5	31.7875	0.1945
336	0.6925	0.3217	236	32.9200	0.1909
335.5	0.6150	0.3323	235.5	33.9925	0.1732
335	0.4925	0.2581	235	35.1100	0.1768
334.5	0.4900	0.2828	234.5	36.3400	0.2404
334	0.6125	0.3147	234	37.5075	0.2157
333.5	0.6000	0.4313	233.5	38.6700	0.2051
333	0.6250	0.4172	233	39.8050	0.2828
332.5	0.5175	0.3995	232.5	40.9050	0.2404
332	0.4425	0.5551	232	42.1625	0.1874
331.5	0.4925	0.5268	231.5	43.4500	0.1838
331	0.5550	0.5869	231	44.6650	0.1414

330.5	0.4650	0.5728	230.5	45.8575	0.1025
330	0.4475	0.6753	230	47.1125	0.1308
329.5	0.2850	0.5869	229.5	48.3850	0.1061
329	0.3900	0.4455	229	49.5575	0.0742
328.5	0.3025	0.3995	228.5	50.8200	0.0636
328	0.0950	0.4525	228	52.1925	0.0247
327.5	-0.0425	0.4702	227.5	53.4375	0.0106
327	0.0150	0.3465	227	54.9050	0.0141
326.5	0.0750	0.3889	226.5	56.3375	0.0460
326	0.0025	0.4773	226	57.8275	0.1237
325.5	0.0575	0.3288	225.5	59.2675	0.1096
325	0.1575	0.2864	225	60.7925	0.0742
324.5	0.2600	0.2828	224.5	62.3050	0.0990
324	0.4350	0.2192	224	64.0925	0.1379
323.5	0.3950	0.0990	223.5	65.9050	0.0495
323	0.4375	0.0318	223	67.7300	0.0424
322.5	0.5750	0.0778	222.5	69.8350	0.0424
322	0.6100	0.0283	222	71.9575	0.1167
321.5	0.6175	0.0106	221.5	74.5100	0.1980
321	0.4250	0.0566	221	77.2900	0.1273
320.5	0.3925	0.1662	220.5	80.2100	0.1626
320	0.3050	0.0990	220	83.5275	0.2440
319.5	0.4100	0.1202	219.5	87.1950	0.1980
319	0.2550	0.1838	219	91.4175	0.3147
318.5	0.1750	0.2192	218.5	96.0300	0.3041
318	0.1925	0.0955	218	101.3525	0.3995
317.5	0.3725	0.1308	217.5	107.2275	0.3854
317	0.3725	0.0955	217	113.6700	0.5303
316.5	0.2925	0.0813	216.5	121.0400	0.5586
316	0.3050	0.0354	216	129.0625	0.6116
315.5	0.4600	0.0071	215.5	137.8775	0.5763
315	0.4350	0.0071	215	147.5325	0.5975
314.5	0.3900	0.0495	214.5	158.1575	0.6470
314	0.3600	0.0919	214	169.5175	0.6824
313.5	0.3075	0.0177	213.5	181.8900	0.8556
313	0.2475	0.0177	213	195.1575	1.0076
312.5	0.1750	0.0141	212.5	209.3425	1.0571
312	0.1225	0.0177	212	224.6375	1.0854
311.5	0.0550	0.0495	211.5	240.8075	1.2551
311	0.0050	0.0495	211	258.1875	1.2834
310.5	0.2175	0.0742	210.5	276.8025	1.2693
310	0.3075	0.0884	210	296.6800	1.4425
309.5	0.2950	0.1273	209.5	317.9200	1.2233
309	0.3275	0.0389	209	340.6625	1.2410

308.5	0.3925	0.0106	208.5	365.1500	1.4920
308	0.5275	0.0318	208	391.4925	1.6440
307.5	0.6450	0.0778	207.5	420.0525	1.8420
307	0.6900	0.0354	207	450.8125	2.0541
306.5	0.6200	0.0778	206.5	484.1475	2.2309
306	0.6250	0.0990	206	519.7650	2.0435
305.5	0.6475	0.1945	205.5	558.6850	2.0011
305	0.5450	0.1980	205	600.8050	2.9416
304.5	0.5575	0.2722	204.5	645.3125	3.1077
304	0.5150	0.2687	204	692.4675	2.9168
303.5	0.5625	0.2793	203.5	743.2300	2.5314
303	0.5850	0.2051	203	796.6825	2.2026
302.5	0.5150	0.2616	202.5	851.3300	2.0930
302	0.5700	0.3889	202	905.2175	2.9734
301.5	0.6325	0.3217	201.5	958.1075	4.4512
301	0.7675	0.4207	201	1006.5275	5.2644
300.5	0.8750	0.4172	200.5	1044.9225	7.3221
			200	1072.4325	7.1100

Table A4.7. Molar absorption coefficients values, ε (λ) of MeSa in the aqueous phase at 295 K and pH =7, at wavelengths between 200 – 400 nm.¹⁷²

Methyl salicylate (MeSa), mean value for concentration 0.1 mM (aqueous), IPC PAS					
Wavelength	Average	σ , n=2	Wavelength	Average	σ , n=2
λ , nm	$\varepsilon/ M^{-1} cm^{-1}$	$\Delta\varepsilon/ M^{-1} cm^{-1}$	λ , nm	$\varepsilon/ M^{-1} cm^{-1}$	$\Delta\varepsilon/ M^{-1} cm^{-1}$
400	2.0500	6.4347	300	3609.4500	0.9192
399.5	4.0000	7.2125	299.5	3582.0000	1.8385
399	3.3500	7.1418	299	3552.5500	2.1920
398.5	3.7000	6.3640	298.5	3518.4000	1.5556
398	4.6500	7.5660	298	3480.8000	1.4142
397.5	4.2000	7.7782	297.5	3440.5000	1.6971
397	3.1000	7.3539	297	3397.4000	0.5657
396.5	4.2000	6.6468	296.5	3347.2000	0.4243
396	4.0000	6.3640	296	3297.4000	0.8485
395.5	2.8000	6.2225	295.5	3247.3500	2.1920
395	2.5500	6.1518	295	3193.8500	0.3536
394.5	3.2500	7.9903	294.5	3139.5000	0.2828
394	4.3500	8.2731	294	3086.1000	0.1414
393.5	4.1000	9.0510	293.5	3024.5500	1.2021
393	5.2500	8.8388	293	2965.3000	1.6971
392.5	5.6000	9.3338	292.5	2903.8000	3.1113
392	4.9000	9.1924	292	2838.8000	5.0912

391.5	3.6500	9.4045	291.5	2773.7000	3.5355
391	3.3500	9.6874	291	2706.3000	2.8284
390.5	3.6000	9.3338	290.5	2638.9000	2.1213
390	3.8500	8.9803	290	2572.5500	1.0607
389.5	2.7000	9.1924	289.5	2507.4500	1.4849
389	2.6500	9.5459	289	2439.8000	2.6870
388.5	4.4500	11.1016	288.5	2375.1500	4.4548
388	4.7000	10.7480	288	2310.3500	5.3033
387.5	3.6500	11.8087	287.5	2242.6000	4.9497
387	4.6500	10.8187	287	2176.9000	5.5154
386.5	4.0500	11.1016	286.5	2111.0500	5.3033
386	5.1500	11.1016	286	2047.0500	5.7276
385.5	5.1000	11.1723	285.5	1982.1000	6.3640
385	3.7500	9.9702	285	1918.0000	7.4953
384.5	2.2000	8.9095	284.5	1853.9500	6.1518
384	2.2000	8.9095	284	1792.2000	5.3740
383.5	2.4000	7.7782	283.5	1730.3000	8.2024
383	1.9500	8.6974	283	1670.2500	7.1418
382.5	3.0500	8.6974	282.5	1608.7500	5.8690
382	2.9500	8.5560	282	1550.7500	4.8790
381.5	2.8000	7.7782	281.5	1490.7000	5.9397
381	2.6000	6.0811	281	1434.9000	5.3740
380.5	2.1000	6.5054	280.5	1377.6500	2.7577
380	1.4500	4.7376	280	1325.1000	1.9799
379.5	0.9000	4.8083	279.5	1273.7000	1.9799
379	-0.1000	4.5255	279	1221.3500	2.4749
378.5	0.1000	4.6669	278.5	1172.1500	0.3536
378	1.0500	4.5962	278	1122.5500	0.7778
377.5	1.2000	2.9699	277.5	1074.6000	0.8485
377	0.7500	3.3234	277	1027.2000	1.8385
376.5	0.7000	1.9799	276.5	983.0500	1.4849
376	1.1000	1.4142	276	936.6500	4.0305
375.5	-1.0500	2.1920	275.5	893.9500	2.6163
375	-0.8000	2.4042	275	853.8500	2.7577
374.5	-0.6500	1.3435	274.5	816.0000	0.2828
374	-1.0500	0.7778	274	777.9500	0.3536
373.5	-0.9000	1.2728	273.5	742.6000	0.2828
373	-0.2000	1.2728	273	707.2500	0.4950
372.5	0.1000	1.6971	272.5	674.0000	1.4142
372	1.7500	1.4849	272	640.9500	1.2021
371.5	3.5500	1.3435	271.5	610.4500	2.3335
371	4.4000	1.9799	271	579.2500	3.6062
370.5	5.7500	2.3335	270.5	552.0500	4.7376
370	6.8000	1.1314	270	525.6500	5.4447

369.5	6.0000	1.9799	269.5	500.5500	3.6062
369	6.5000	0.8485	269	478.1500	3.6062
368.5	6.0000	2.9698	268.5	458.4000	3.2527
368	4.5500	3.6062	268	439.9000	3.5355
367.5	4.1000	5.6569	267.5	419.3000	1.5556
367	2.9000	5.0912	267	399.8500	1.3435
366.5	3.2500	6.2933	266.5	385.3500	1.7678
366	2.2500	5.5861	266	372.0000	2.4042
365.5	1.9500	6.7175	265.5	358.5500	3.4648
365	2.4000	7.0711	265	345.4500	3.4648
364.5	2.7500	7.0004	264.5	338.4000	4.2426
364	4.4500	7.4246	264	331.0000	6.2225
363.5	5.1000	8.3439	263.5	325.3000	6.0811
363	4.7000	7.9196	263	324.8000	5.7983
362.5	3.7000	6.6468	262.5	324.7000	6.9296
362	1.9000	7.7782	262	327.8500	7.4246
361.5	3.5500	9.4045	261.5	335.9500	7.4246
361	4.8000	8.7681	261	347.7000	8.9095
360.5	7.4500	7.0004	260.5	367.9000	9.1924
360	6.7500	7.4246	260	391.1000	8.2024
359.5	7.2500	8.4146	259.5	418.8000	8.2024
359	7.3000	5.5154	259	457.0500	6.2933
358.5	5.8500	6.2933	258.5	501.4000	4.9497
358	7.8000	6.5054	258	552.7000	3.8184
357.5	9.4000	6.5054	257.5	613.7000	3.5355
357	10.0000	7.0711	257	682.5500	2.7577
356.5	10.1500	7.9903	256.5	760.4500	2.3335
356	10.7000	7.2125	256	848.9500	3.3234
355.5	12.5500	6.2933	255.5	946.0000	4.1012
355	14.9000	5.6569	255	1056.4500	3.6062
354.5	16.3000	3.6770	254.5	1178.2000	3.9598
354	16.4000	5.9397	254	1311.0000	2.8284
353.5	14.7000	7.4953	253.5	1455.5000	2.1213
353	14.5000	6.3640	253	1610.7500	0.0707
352.5	15.8500	5.3033	252.5	1778.1500	1.4849
352	14.3000	6.6468	252	1955.3500	2.6163
351.5	15.1000	6.7882	251.5	2143.7500	5.3033
351	12.3000	5.5154	251	2348.5000	5.7983
350.5	10.3500	4.5962	250.5	2563.5500	5.7276
350	10.3500	5.1619	250	2792.5500	5.8690
349.5	11.3500	4.3134	249.5	3032.3500	6.2933
349	12.9500	2.7577	249	3285.2000	6.0811
348.5	12.1000	2.4042	248.5	3550.5000	5.6569
348	13.2500	3.0406	248	3823.8500	7.5660

347.5	13.0500	4.8790	247.5	4110.9500	5.8690
347	15.1500	5.0205	247	4409.7000	4.3841
346.5	12.8500	7.2832	246.5	4715.7500	4.1719
346	16.1000	8.0610	246	5030.0500	0.3536
345.5	17.7500	6.8589	245.5	5348.4500	0.4950
345	18.8500	7.4246	245	5669.6500	2.0506
344.5	20.1500	6.2933	244.5	5988.5500	0.3536
344	21.6500	5.7276	244	6302.9000	0.9899
343.5	23.2000	4.8083	243.5	6615.2000	1.2728
343	26.9500	3.7477	243	6913.0500	0.0707
342.5	29.0500	5.0205	242.5	7194.5000	0.7071
342	31.5000	3.8184	242	7454.8000	2.8284
341.5	33.3500	6.8589	241.5	7699.1000	0.9899
341	35.4000	5.3740	241	7911.7500	0.7778
340.5	39.4500	5.5861	240.5	8098.7000	0.4243
340	78.9000	2.2627	240	8255.3500	6.5761
339.5	84.9000	1.1314	239.5	8378.6000	4.8083
339	89.0500	0.4950	239	8473.8500	6.2933
338.5	96.3000	0.9899	238.5	8536.5000	6.6468
338	103.9500	0.6364	238	8568.4000	7.7782
337.5	112.5000	0.5657	237.5	8570.6000	5.5154
337	120.5500	0.6364	237	8543.4500	7.8489
336.5	129.9000	0.5657	236.5	8495.5500	5.5861
336	143.6500	0.0707	236	8422.1500	7.9903
335.5	156.6000	0.7071	235.5	8329.5000	5.7983
335	169.4000	0.4243	235	8217.6500	9.1217
334.5	185.1000	3.1113	234.5	8095.4500	6.1518
334	202.9000	3.9598	234	7957.9500	4.7376
333.5	221.3000	2.2627	233.5	7809.1500	1.7678
333	243.5000	2.1213	233	7653.6500	0.9192
332.5	270.8000	2.1213	232.5	7490.9000	2.8284
332	298.3000	3.2527	232	7326.0000	3.3941
331.5	329.4500	1.9092	231.5	7159.2000	4.1012
331	363.2000	1.1314	231	6991.5000	3.3941
330.5	396.5500	2.4749	230.5	6822.0000	1.2728
330	428.7500	3.8891	230	6659.6000	2.6870
329.5	468.3000	2.6870	229.5	6502.0000	4.8083
329	510.2000	1.1314	229	6344.4500	5.3033
328.5	556.1500	0.6364	228.5	6193.1500	3.8891
328	602.3500	1.9092	228	6047.7000	4.9497
327.5	650.8500	0.6364	227.5	5906.3500	3.8891
327	700.8000	1.4142	227	5772.5500	4.5962
326.5	752.8500	1.2021	226.5	5647.6500	3.6062
326	809.2000	2.6870	226	5533.8000	2.9698

325.5	866.5000	3.1113	225.5	5429.6000	3.5355
325	928.6000	3.3941	225	5337.3500	3.4648
324.5	992.4500	3.0406	224.5	5258.8500	1.9092
324	1063.0500	3.8891	224	5196.7500	1.2021
323.5	1133.6000	3.3941	223.5	5149.6500	2.1920
323	1203.9500	6.5761	223	5119.6000	1.1314
322.5	1278.8500	7.4246	222.5	5115.7500	2.0506
322	1352.6500	8.9803	222	5128.9000	0.4243
321.5	1428.9500	9.9702	221.5	5167.7000	0.7071
321	1508.0000	7.6368	221	5231.8000	0.5657
320.5	1589.4500	7.9903	220.5	5322.7500	1.4849
320	1671.9000	5.5154	220	5439.0000	1.5556
319.5	1753.7500	7.4246	219.5	5578.6500	1.0607
319	1835.7000	6.7882	219	5737.9000	2.4042
318.5	1919.3000	5.5154	218.5	5918.4500	3.6062
318	2005.7500	3.4648	218	6118.0500	3.6062
317.5	2090.8500	4.8790	217.5	6335.8000	4.1012
317	2179.3500	5.4447	217	6573.0500	5.0205
316.5	2264.4500	4.5962	216.5	6831.7500	6.0104
316	2347.5000	2.4042	216	7113.8500	5.4447
315.5	2431.4000	1.5556	215.5	7421.9000	5.7983
315	2513.4000	4.6669	215	7760.3000	6.9296
314.5	2596.1000	6.3640	214.5	8126.7500	10.1116
314	2677.2000	5.0912	214	8533.4000	14.4250
313.5	2757.7500	3.0406	213.5	8978.9000	9.0510
313	2837.6500	1.9092	213	9469.3000	12.1622
312.5	2911.5500	0.4950	212.5	10012.4500	13.0815
312	2985.0500	2.1920	212	10609.6500	9.9702
311.5	3053.6500	2.0506	211.5	11276.3000	14.4250
311	3116.7500	2.7577	211	12014.1500	23.6881
310.5	3181.1500	2.1920	210.5	12847.2500	30.4763
310	3241.4500	0.6364	210	13779.5000	29.8399
309.5	3299.3500	3.0406	209.5	14797.5000	27.2943
309	3358.0000	4.1012	209	15926.7500	20.2940
308.5	3408.7000	0.4243	208.5	17144.1000	15.1321
308	3453.7000	0.7071	208	18403.1000	27.2943
307.5	3497.4500	0.2121	207.5	19706.8500	52.1138
307	3532.8500	1.2021	207	20969.0500	55.9321
306.5	3567.4500	1.4849	206.5	22063.8500	67.3873
306	3594.2000	1.9799	206	22957.3500	60.5991
305.5	3615.9500	2.6163	205.5	23626.4500	84.7821
305	3637.7500	4.0305	205	24017.5000	86.4084
304.5	3653.3000	5.3740	204.5	24241.9000	3.8184
304	3668.3000	5.3740	204	24255.9000	44.1235

<i>303.5</i>	3678.6000	4.1012	<i>203.5</i>	24104.3000	31.6784
<i>303</i>	3683.0500	3.8891	<i>203</i>	23843.7000	0.1414
<i>302.5</i>	3681.1000	2.4042	<i>202.5</i>	23494.9500	41.3657
<i>302</i>	3673.4000	1.6971	<i>202</i>	23005.3000	9.4752
<i>301.5</i>	3663.0000	2.8284	<i>201.5</i>	22497.4500	7.9903
<i>301</i>	3649.4000	0.8485	<i>201</i>	21885.2500	68.2358
<i>300.5</i>	3633.5000	0.1414	<i>200.5</i>	21252.8500	95.3887
			<i>200</i>	20616.3500	33.1633

Table A4.8. Molar absorption coefficients values, $\varepsilon(\lambda)$ of MBO in the aqueous phase at 295 K and pH =7, at wavelengths between 200 – 400 nm.¹⁷²

MBO, mean value for concentration 20 mM (aqueous), IPC PAS					
Wavelength	Average	σ , n=2	Wavelength	Average	σ , n=2
λ , nm	$\varepsilon/ M^{-1} cm^{-1}$	$\Delta\varepsilon/ M^{-1} cm^{-1}$	λ , nm	$\varepsilon/ M^{-1} cm^{-1}$	$\Delta\varepsilon/ M^{-1} cm^{-1}$
<i>400</i>	0.0978	0.0018	<i>300</i>	0.1740	0.0438
<i>399.5</i>	0.0943	0.0039	<i>299.5</i>	0.1623	0.0421
<i>399</i>	0.0985	0.0021	<i>299</i>	0.1463	0.0407
<i>398.5</i>	0.0968	0.0004	<i>298.5</i>	0.1453	0.0414
<i>398</i>	0.1070	0.0071	<i>298</i>	0.1345	0.0318
<i>397.5</i>	0.1123	0.0145	<i>297.5</i>	0.1355	0.0212
<i>397</i>	0.1113	0.0124	<i>297</i>	0.1440	0.0212
<i>396.5</i>	0.1060	0.0170	<i>296.5</i>	0.1493	0.0223
<i>396</i>	0.1115	0.0170	<i>296</i>	0.1520	0.0141
<i>395.5</i>	0.1098	0.0216	<i>295.5</i>	0.1415	0.0099
<i>395</i>	0.1140	0.0212	<i>295</i>	0.1435	0.0085
<i>394.5</i>	0.1135	0.0184	<i>294.5</i>	0.1300	0.0064
<i>394</i>	0.1128	0.0230	<i>294</i>	0.1293	0.0088
<i>393.5</i>	0.1083	0.0237	<i>293.5</i>	0.1263	0.0032
<i>393</i>	0.1038	0.0293	<i>293</i>	0.1278	0.0131
<i>392.5</i>	0.1028	0.0322	<i>292.5</i>	0.1220	0.0191
<i>392</i>	0.1003	0.0301	<i>292</i>	0.1235	0.0240
<i>391.5</i>	0.0990	0.0290	<i>291.5</i>	0.1360	0.0290
<i>391</i>	0.1020	0.0311	<i>291</i>	0.1293	0.0279
<i>390.5</i>	0.1035	0.0297	<i>290.5</i>	0.1353	0.0223
<i>390</i>	0.0950	0.0311	<i>290</i>	0.1338	0.0301
<i>389.5</i>	0.0918	0.0301	<i>289.5</i>	0.1455	0.0262
<i>389</i>	0.0915	0.0346	<i>289</i>	0.1383	0.0244
<i>388.5</i>	0.0918	0.0315	<i>288.5</i>	0.1460	0.0212
<i>388</i>	0.0925	0.0311	<i>288</i>	0.1375	0.0134
<i>387.5</i>	0.0963	0.0343	<i>287.5</i>	0.1378	0.0011
<i>387</i>	0.0970	0.0354	<i>287</i>	0.1378	0.0032

386.5	0.0963	0.0286	286.5	0.1460	0.0000
386	0.1023	0.0279	286	0.1643	0.0060
385.5	0.0888	0.0265	285.5	0.1675	0.0156
385	0.0780	0.0184	285	0.1813	0.0145
384.5	0.0750	0.0141	284.5	0.1853	0.0081
384	0.0743	0.0081	284	0.1905	0.0141
383.5	0.0745	0.0099	283.5	0.1818	0.0117
383	0.0730	0.0049	283	0.1893	0.0131
382.5	0.0668	0.0081	282.5	0.1920	0.0219
382	0.0655	0.0035	282	0.1988	0.0258
381.5	0.0660	0.0014	281.5	0.2138	0.0343
381	0.0658	0.0004	281	0.2145	0.0311
380.5	0.0645	0.0049	280.5	0.2210	0.0368
380	0.0740	0.0042	280	0.2228	0.0449
379.5	0.0763	0.0117	279.5	0.2310	0.0389
379	0.0855	0.0057	279	0.2295	0.0346
378.5	0.0898	0.0060	278.5	0.2270	0.0332
378	0.0840	0.0035	278	0.2290	0.0332
377.5	0.0820	0.0007	277.5	0.2460	0.0325
377	0.0890	0.0092	277	0.2455	0.0354
376.5	0.0893	0.0081	276.5	0.2450	0.0375
376	0.0950	0.0099	276	0.2423	0.0350
375.5	0.0940	0.0106	275.5	0.2370	0.0311
375	0.0953	0.0138	275	0.2428	0.0265
374.5	0.0955	0.0120	274.5	0.2540	0.0240
374	0.0975	0.0071	274	0.2655	0.0212
373.5	0.0965	0.0141	273.5	0.2598	0.0202
373	0.1065	0.0219	273	0.2580	0.0163
372.5	0.1125	0.0247	272.5	0.2618	0.0173
372	0.1180	0.0311	272	0.2538	0.0180
371.5	0.1113	0.0343	271.5	0.2493	0.0173
371	0.1128	0.0343	271	0.2555	0.0212
370.5	0.1050	0.0311	270.5	0.2610	0.0205
370	0.1110	0.0247	270	0.2710	0.0262
369.5	0.1210	0.0212	269.5	0.2718	0.0209
369	0.1155	0.0127	269	0.2635	0.0191
368.5	0.1160	0.0042	268.5	0.2688	0.0074
368	0.1105	0.0035	268	0.2818	0.0131
367.5	0.1128	0.0053	267.5	0.2785	0.0092
367	0.1113	0.0039	267	0.2820	0.0085
366.5	0.1015	0.0134	266.5	0.2858	0.0124
366	0.1068	0.0216	266	0.2808	0.0032
365.5	0.1180	0.0198	265.5	0.2860	0.0014
365	0.1335	0.0177	265	0.2785	0.0021

364.5	0.1228	0.0209	264.5	0.2863	0.0110
364	0.1240	0.0304	264	0.2905	0.0071
363.5	0.1225	0.0240	263.5	0.3080	0.0057
363	0.1205	0.0247	263	0.3265	0.0085
362.5	0.1203	0.0272	262.5	0.3330	0.0106
362	0.1120	0.0205	262	0.3490	0.0057
361.5	0.1153	0.0279	261.5	0.3525	0.0106
361	0.1105	0.0318	261	0.3553	0.0025
360.5	0.1110	0.0255	260.5	0.3795	0.0035
360	0.1145	0.0311	260	0.3955	0.0021
359.5	0.1113	0.0371	259.5	0.4105	0.0000
359	0.1145	0.0375	259	0.4388	0.0053
358.5	0.1155	0.0488	258.5	0.4625	0.0078
358	0.1095	0.0516	258	0.4945	0.0014
357.5	0.1053	0.0442	257.5	0.5150	0.0014
357	0.1030	0.0474	257	0.5428	0.0004
356.5	0.1073	0.0456	256.5	0.5698	0.0011
356	0.1115	0.0474	256	0.6090	0.0078
355.5	0.1125	0.0396	255.5	0.6353	0.0088
355	0.1115	0.0297	255	0.6655	0.0113
354.5	0.1095	0.0269	254.5	0.7103	0.0173
354	0.1200	0.0148	254	0.7533	0.0159
353.5	0.1115	0.0170	253.5	0.8098	0.0173
353	0.1243	0.0152	253	0.8638	0.0223
352.5	0.1168	0.0131	252.5	0.9138	0.0265
352	0.1128	0.0138	252	0.9728	0.0265
351.5	0.1138	0.0117	251.5	1.0218	0.0265
351	0.1218	0.0088	251	1.0873	0.0293
350.5	0.1263	0.0032	250.5	1.1440	0.0297
350	0.1315	0.0057	250	1.2098	0.0364
349.5	0.1338	0.0011	249.5	1.2883	0.0343
349	0.1363	0.0060	249	1.3573	0.0343
348.5	0.1335	0.0021	248.5	1.4418	0.0336
348	0.1350	0.0028	248	1.5213	0.0343
347.5	0.1430	0.0007	247.5	1.6098	0.0392
347	0.1398	0.0039	247	1.6983	0.0357
346.5	0.1363	0.0025	246.5	1.7800	0.0438
346	0.1410	0.0057	246	1.8735	0.0424
345.5	0.1335	0.0141	245.5	1.9605	0.0481
345	0.1245	0.0106	245	2.0538	0.0407
344.5	0.1320	0.0057	244.5	2.1603	0.0428
344	0.1415	0.0028	244	2.2713	0.0484
343.5	0.1403	0.0032	243.5	2.3893	0.0463
343	0.1363	0.0032	243	2.4890	0.0318

342.5	0.1388	0.0004	242.5	2.6105	0.0318
342	0.1373	0.0067	242	2.7250	0.0318
341.5	0.1348	0.0180	241.5	2.8415	0.0276
341	0.1285	0.0148	241	2.9548	0.0301
340.5	0.1340	0.0028	240.5	3.0803	0.0279
340	0.0995	0.0233	240	3.1950	0.0283
339.5	0.1080	0.0290	239.5	3.3083	0.0251
339	0.1073	0.0286	239	3.4368	0.0237
338.5	0.1140	0.0290	238.5	3.5565	0.0247
338	0.1138	0.0251	238	3.6625	0.0247
337.5	0.0975	0.0318	237.5	3.7743	0.0286
337	0.0875	0.0339	237	3.8848	0.0202
336.5	0.0920	0.0403	236.5	4.0065	0.0240
336	0.0878	0.0400	236	4.1193	0.0322
335.5	0.0923	0.0315	235.5	4.2273	0.0293
335	0.0973	0.0364	235	4.3390	0.0269
334.5	0.1050	0.0537	234.5	4.4295	0.0120
334	0.1120	0.0445	234	4.5350	0.0156
333.5	0.1055	0.0488	233.5	4.6330	0.0184
333	0.0968	0.0407	233	4.7233	0.0166
332.5	0.0868	0.0499	232.5	4.8070	0.0127
332	0.1023	0.0463	232	4.8745	0.0120
331.5	0.1025	0.0417	231.5	4.9458	0.0025
331	0.1060	0.0410	231	5.0118	0.0025
330.5	0.1088	0.0336	230.5	5.0628	0.0025
330	0.1128	0.0378	230	5.1215	0.0198
329.5	0.1138	0.0392	229.5	5.1588	0.0088
329	0.1235	0.0311	229	5.2133	0.0081
328.5	0.1305	0.0184	228.5	5.2480	0.0170
328	0.1570	0.0269	228	5.2720	0.0049
327.5	0.1728	0.0209	227.5	5.3035	0.0106
327	0.1748	0.0011	227	5.3393	0.0159
326.5	0.1798	0.0032	226.5	5.3675	0.0191
326	0.1713	0.0074	226	5.3673	0.0202
325.5	0.1865	0.0141	225.5	5.3723	0.0258
325	0.1853	0.0244	225	5.3898	0.0237
324.5	0.1928	0.0230	224.5	5.4063	0.0315
324	0.1998	0.0279	224	5.4190	0.0361
323.5	0.1983	0.0265	223.5	5.4128	0.0202
323	0.2078	0.0308	223	5.4300	0.0148
322.5	0.1930	0.0304	222.5	5.4575	0.0219
322	0.1910	0.0417	222	5.4808	0.0301
321.5	0.1925	0.0537	221.5	5.5338	0.0400
321	0.1980	0.0643	221	5.6070	0.0389

320.5	0.2023	0.0718	220.5	5.7115	0.0361
320	0.1928	0.0541	220	5.8420	0.0297
319.5	0.1860	0.0601	219.5	6.0170	0.0290
319	0.1730	0.0622	219	6.2410	0.0297
318.5	0.1683	0.0562	218.5	6.5110	0.0283
318	0.1700	0.0530	218	6.8633	0.0350
317.5	0.1635	0.0537	217.5	7.2948	0.0371
317	0.1640	0.0580	217	7.8078	0.0364
316.5	0.1675	0.0622	216.5	8.4073	0.0414
316	0.1550	0.0622	216	9.0875	0.0438
315.5	0.1408	0.0654	215.5	9.8840	0.0552
315	0.1390	0.0665	215	10.7735	0.0700
314.5	0.1135	0.0601	214.5	11.7433	0.0661
314	0.1160	0.0566	214	12.8113	0.0661
313.5	0.1093	0.0590	213.5	13.9795	0.0594
313	0.1265	0.0615	213	15.2488	0.0619
312.5	0.1220	0.0516	212.5	16.5985	0.0601
312	0.1285	0.0325	212	18.0488	0.0569
311.5	0.1263	0.0392	211.5	19.6043	0.0668
311	0.1315	0.0361	211	21.2775	0.0785
310.5	0.1288	0.0421	210.5	23.0883	0.0958
310	0.1288	0.0470	210	25.0010	0.1011
309.5	0.1225	0.0467	209.5	27.1285	0.1075
309	0.1148	0.0407	209	29.4548	0.1142
308.5	0.1153	0.0293	208.5	31.9578	0.1001
308	0.1113	0.0194	208	34.6990	0.0976
307.5	0.1245	0.0226	207.5	37.7035	0.1188
307	0.1355	0.0304	207	41.0288	0.1701
306.5	0.1475	0.0417	206.5	44.7028	0.1849
306	0.1530	0.0445	206	48.7393	0.1948
305.5	0.1575	0.0629	205.5	53.1810	0.2135
305	0.1553	0.0689	205	58.0448	0.2641
304.5	0.1598	0.0732	204.5	63.4225	0.2744
304	0.1593	0.0704	204	69.2648	0.3369
303.5	0.1505	0.0693	203.5	75.5155	0.4518
303	0.1513	0.0654	203	82.2048	0.5950
302.5	0.1600	0.0566	202.5	88.9470	0.5141
302	0.1690	0.0608	202	95.4865	0.7764
301.5	0.1768	0.0598	201.5	101.3008	0.9967
301	0.1728	0.0491	201	105.7883	1.2180
300.5	0.1668	0.0385	200.5	108.7130	1.1201
			200	109.9703	1.2696

2. Density functional theory (DFT)

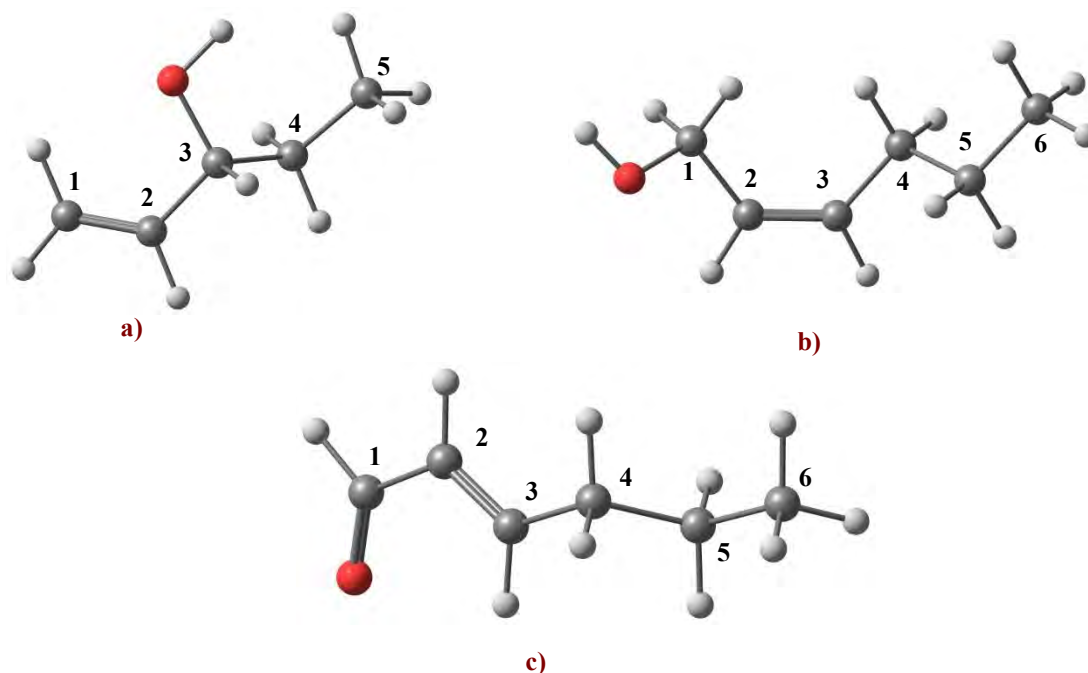


Figure A1. Vacuum optimized geometries of green leaf volatile compounds (GLVs) at B3LYP functional and def2-TZVP basis set: **a)** 1-penten-3-ol; **b)** (*Z*)-2-hexen-1-ol; **c)** (*E*)-2-hexen-1-ol (with atom numbers) where, **C:** grey, **H:** white, and **O:** red. (C=C 1.33 Å , C-C 1.50 Å ,C-H 1.50 Å, C-O 1.42 Å , O-H 0.96 Å)

Table A7.1. XYZ coordinates of vacuum optimized structures of selected GLVs

1-penten-3-ol, C₅H₁₀O

C	0.397115000	1.209445000	-0.077502000
C	-0.237127000	1.420045000	1.066822000
H	0.983220000	1.989428000	-0.544132000
H	0.342882000	0.251290000	-0.578177000
H	-0.823628000	0.625847000	1.519824000
C	-0.216055000	2.697551000	1.849736000
C	0.308400000	2.463068000	3.273346000
H	-0.294535000	1.674616000	3.733562000
H	1.330509000	2.082590000	3.198550000
C	0.269471000	3.712937000	4.148441000

H	-0.742493000	4.123122000	4.209831000
H	0.597931000	3.490195000	5.164768000
H	0.931214000	4.494177000	3.766151000
O	0.568858000	3.657733000	1.148914000
H	0.484922000	4.503901000	1.598658000
H	-1.253370000	3.062785000	1.928178000

(Z)-2-hexen-1-ol, C₆H₁₂O

C	0.508859000	-0.851735000	-2.837206000
H	0.975582000	-0.738384000	-1.861418000
C	0.192429000	-2.085997000	-3.220791000
H	0.408461000	-2.913032000	-2.551289000
C	-0.443111000	-2.498242000	-4.507666000
H	-0.751877000	-1.630888000	-5.098445000
H	0.284050000	-3.066201000	-5.104832000
C	-0.776220000	2.749244000	-3.492900000
H	-1.257263000	2.610780000	-4.464452000
H	-1.398165000	3.429769000	-2.908302000
C	-0.588552000	1.414306000	-2.778124000
H	-1.561192000	0.949936000	-2.592419000
H	-0.136606000	1.581626000	-1.795258000
H	0.184131000	3.241343000	-3.667103000
C	0.283004000	0.433328000	-3.573428000
H	1.252065000	0.908124000	-3.770851000
H	-0.173123000	0.254625000	-4.549037000
O	-1.571146000	-3.324356000	-4.197477000
H	-1.889348000	-3.724846000	-5.013329000

(E)-2-hexen-1-ol, C₆H₁₂O

C	0.347932000	0.694641000	-2.310386000
H	-0.163834000	1.332869000	-1.561139000
C	0.363898000	-0.743740000	-1.989449000
H	-0.104579000	-1.041306000	-1.056214000
C	0.922111000	-1.651146000	-2.795097000
H	1.375473000	-1.291383000	-3.715904000

C	1.000468000	-3.114019000	-2.527588000
H	0.478782000	-3.650208000	-3.330147000
H	0.483923000	-3.355421000	-1.594604000
C	2.449675000	-3.622539000	-2.468738000
H	2.983955000	-3.080532000	-1.683522000
H	2.953525000	-3.378620000	-3.408667000
C	2.530253000	-5.124089000	-2.210472000
H	2.023041000	-5.687617000	-2.997339000
H	3.567204000	-5.462264000	-2.172781000
H	2.059879000	-5.385032000	-1.259391000
O	0.840888000	1.195739000	-3.296256000

For XYZ coordinates of the vacuum optimized structures of all other intermediates investigated can be downloaded from the ICM based repository website for the dataset

<https://repod.icm.edu.pl/dataset.xhtml?persistentId=doi:10.18150/1J2I3C>

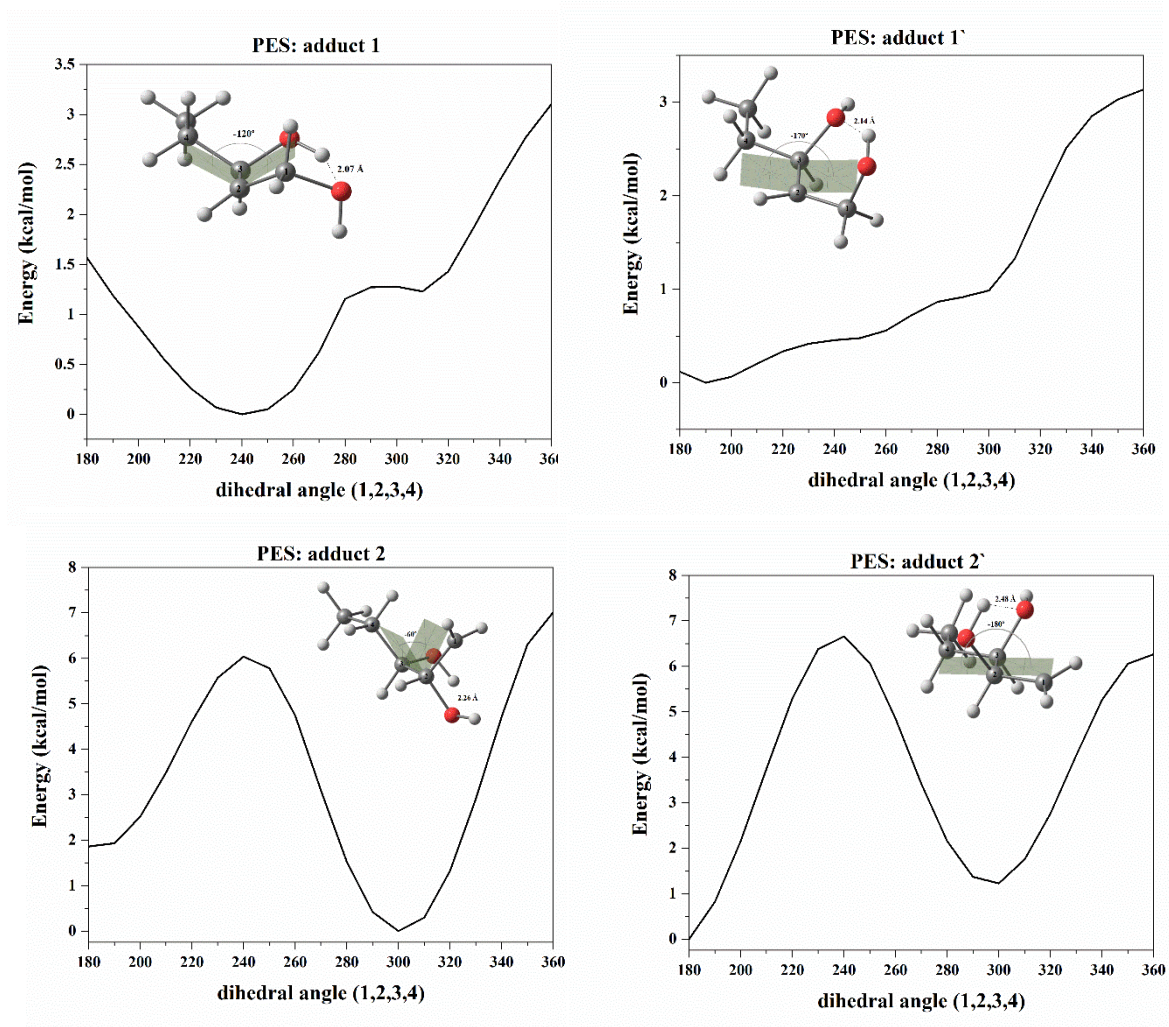
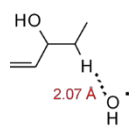
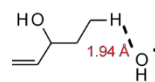
a) 1-penten-3-ol with $\cdot\text{OH}$ 

Figure A2. Potential energy scans (PES) for the dihedral angle between C(1,2,3,4) for the adduct 1 & 1', and 2 & 2' resulting from the addition of $\cdot\text{OH}$ at C1 and C2 of 1-penten-3-ol, respectively.



$$\Delta E_{\text{vac}} = -4.46$$

$$\Delta E_{\text{CPCM}} = -2.45$$



$$\Delta E_{\text{vac}} = -1.35$$

$$\Delta E_{\text{CPCM}} = -1.14$$

Figure A3. Other possible higher energy reaction complexes for a hydrogen-abstraction pathway of reaction between 1-penten-3-ol and $\cdot\text{OH}$ radicals and their respective relative energy, ΔE shown in vacuum and aqueous phase.

b) (Z)-2-hexen-1-ol with $\cdot\text{OH}$

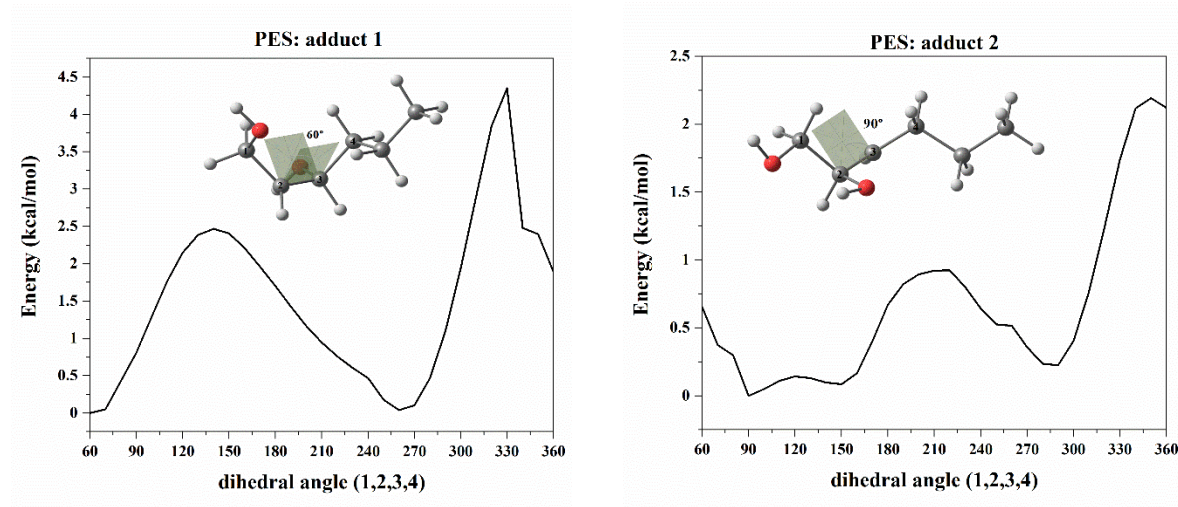


Figure A4. Potential energy scans (PES) for the dihedral angle between C1, 2, 3, 4 for the adduct 1 and adduct 2 resulting from the addition of $\cdot\text{OH}$ at C3 (adduct1) and C2 (adduct2) of (Z)-2-hexen-1-ol.

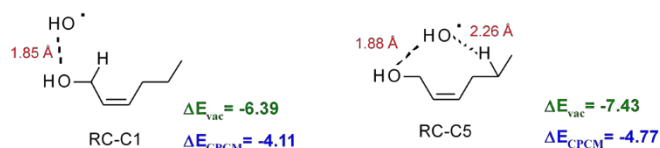


Figure A5. Other possible higher energy reaction complexes for a hydrogen-abstraction pathway of reaction between (Z)-2-hexen-1-ol and $\cdot\text{OH}$ radicals and their respective relative energy, ΔE shown in vacuum and aqueous phase.

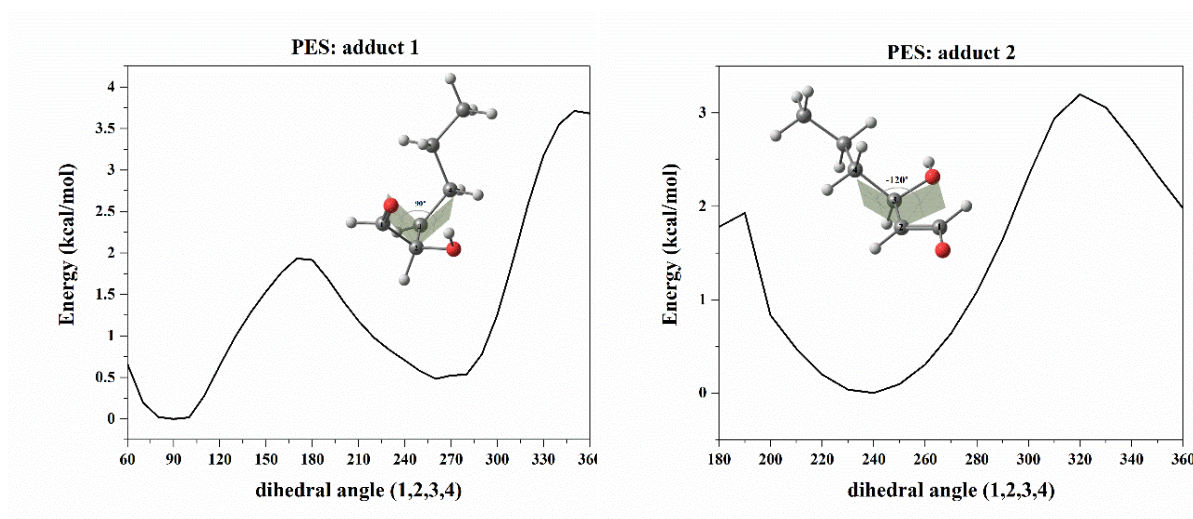
c) (*E*)-2-hexen-1-al with $\bullet\text{OH}$ 

Figure A6. Potential energy scans (PES) for the dihedral angle between C1, 2, 3, 4 for the adduct 1, and adduct 2 resulting from the addition of $\bullet\text{OH}$ at C3 (adduct1) and C2 (adduct2) of (*E*)-2-hexen-1-al.

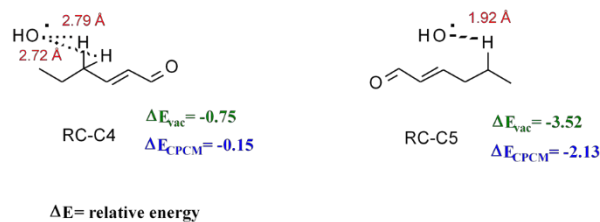


Figure A7. Other possible higher energy reaction complexes for a hydrogen-abstraction pathway of reaction between (*E*)-2-hexen-1-al and $\bullet\text{OH}$ radicals and their respective relative energy, ΔE shown in vacuum and aqueous phase.

■ References

1. Robert Whytlaw-Gray, J. B. S. a. J. H. P. C., Smokes: Part I.—A study of their behaviour and a method of determining the number of particles they contain. *Proceedings of the Royal Society of London* **1923**, *102*, (718), 600-615.
2. A, S., Die chemie des nebls der wolken und des regens. *Die Unschau* **1920**, *24*, 61–63.
3. Manahan, S. E., *Environmental Chemistry*. CRC Press: Boca Raton, 2000, seventh edition.
4. Seinfeld, J. H.; Pandis, S. N., *Atmospheric chemistry and physics : from air pollution to climate change*. 3rd Edition. John Wiley & Sons: New York, USA, 2016.
5. Lagzi, I.; Mészáros, R.; Gelybó, G.; Leelddoto, Á., *Atmospheric Chemistry*. 2013.
6. Shalamzari, M. S. Molecular characterization of polar organosulfates in secondary organic aerosol from isoprene and unsaturated aldehydes using liquid chromatography/(-)electrospray ionization mass spectrometry. Ph.D. thesis, University of Antwerp, Ghent University, Antwerp, 2015.
7. Schraufnagel, D. E., The health effects of ultrafine particles. *Exp. Mol. Med.* **2020**, *52*, (3), 311-317.
8. Hussein, T.; Juwhari, H.; Al Kuisi, M.; Alkattan, H.; Lahlouh, B.; Al-Hunaiti, A., Accumulation and coarse mode aerosol concentrations and carbonaceous contents in the urban background atmosphere in Amman, Jordan. *Arab. J. Geosci.* **2018**, *11*, (20), 11.
9. Kumar, P.; Rivas, I.; Singh, A. P.; Ganesh, V. J.; Ananya, M.; Frey, H. C., Dynamics of coarse and fine particle exposure in transport microenvironments. *Npj Climate and Atmospheric Science* **2018**, *1*, 12.
10. Tomasi, C.; Lupi, A., Primary and Secondary Sources of Atmospheric Aerosol. In *Atmospheric Aerosols*, 2017; pp 1-86.
11. Noziere, B.; Kaberer, M.; Claeys, M.; Allan, J.; D'Anna, B.; Decesari, S.; Finessi, E.; Glasius, M.; Grgic, I.; Hamilton, J. F.; Hoffmann, T.; Iinuma, Y.; Jaoui, M.; Kahno, A.; Kampf, C. J.; Kourtchev, I.; Maenhaut, W.; Marsden, N.; Saarikoski, S.; Schnelle-Kreis, J.; Surratt, J. D.; Szidat, S.; Szmigielski, R.; Wisthaler, A., The Molecular Identification of Organic Compounds in the Atmosphere: State of the Art and Challenges. *Chem. Rev.* **2015**, *115*, (10), 3919-3983.
12. Hallquist, M.; Wenger, J. C.; Baltensperger, U.; Rudich, Y.; Simpson, D.; Claeys, M.; Dommen, J.; Donahue, N. M.; George, C.; Goldstein, A. H.; Hamilton, J. F.; Herrmann, H.; Hoffmann, T.; Iinuma, Y.; Jang, M.; Jenkin, M. E.; Jimenez, J. L.; Kiendler-Scharr, A.; Maenhaut, W.; McFiggans, G.; Mentel, T. F.; Monod, A.; Prevot, A. S. H.; Seinfeld, J. H.; Surratt, J. D.; Szmigielski, R.; Wildt, J., The formation, properties and impact of secondary organic aerosol: current and emerging issues. *Atmos. Chem. Phys.* **2009**, *9*, (14), 5155-5236.
13. Jaoui, M.; Szmigielski, R.; Nestorowicz, K.; Kolodziejczyk, A.; Sarang, K.; Rudzinski, K. J.; Konopka, A.; Bulska, E.; Lewandowski, M.; Kleindienst, T. E., Organic Hydroxy Acids as Highly Oxygenated Molecular (HOM) Tracers for Aged Isoprene Aerosol. *Environ. Sci. Technol.* **2019**, *53*, (24), 14516-14527.
14. Rudzinski, K. J.; Szmigielski, R.; Kuznietsova, I.; Wach, P.; Staszek, D., Aqueous-phase story of isoprene - A mini-review and reaction with HONO. *Atmos. Environ.* **2016**, *130*, 163-171.
15. Wach, P.; Spolnik, G.; Surratt, J. D.; Blaziak, K.; Rudzinski, K. J.; Lin, Y. H.; Maenhaut, W.; Danikiewicz, W.; Claeys, M.; Szmigielski, R., Structural Characterization of Lactone-Containing MW 212 Organosulfates Originating from Isoprene Oxidation in Ambient Fine Aerosol. *Environ. Sci. Technol.* **2020**, *54*, (3), 1415-1424.

16. Kolodziejczyk, A.; Pyrcz, P.; Blaziak, K.; Pobudkowska, A.; Sarang, K.; Szmigielski, R., Physicochemical Properties of Terebic Acid, MBTCA, Diaterpenylic Acid Acetate, and Pinanediol as Relevant alpha-Pinene Oxidation Products. *ACS Omega* **2020**, *5*, (14), 7919-7927.
17. Szmigielski, R., Chemistry of Organic Sulfates and Nitrates in the Urban Atmosphere. *NATO Sci. Peace Secur. Ser. C- Environ. Secur.* **2013**, 211-226.
18. Szmigielski, R.; Surratt, J. D.; Gomez-Gonzalez, Y.; Van der Veken, P.; Kourtchev, I.; Vermeylen, R.; Blockhuys, F.; Jaoui, M.; Kleindienst, T. E.; Lewandowski, M.; Offenberg, J. H.; Edney, E. O.; Seinfeld, J. H.; Maenhaut, W.; Claeys, M., 3-methyl-1,2,3-butanetricarboxylic acid: An atmospheric tracer for terpene secondary organic aerosol. *Geophys. Res. Lett.* **2007**, *34*, (24), 6.
19. Nestorowicz, K.; Jaoui, M.; Rudzinski, K. J.; Lewandowski, M.; Kleindienst, T. E.; Spolnik, G.; Danikiewicz, W.; Szmigielski, R., Chemical composition of isoprene SOA under acidic and non-acidic conditions: effect of relative humidity. *Atmos. Chem. Phys.* **2018**, *18*, (24), 18101-18121.
20. Sun, J. M.; Ariya, P. A., Atmospheric organic and bio-aerosols as cloud condensation nuclei (CCN): A review. *Atmos. Environ.* **2006**, *40*, (5), 795-820.
21. Poschl, U., Atmospheric aerosols: Composition, transformation, climate and health effects. *Angew. Chem.-Int. Edit.* **2005**, *44*, (46), 7520-7540.
22. Wallace, J. M.; Hobbs, P. V., Chapter 5 - Atmospheric Chemistry. In *Atmospheric Science (Second Edition)*, Academic Press: San Diego, 2006; pp 153-207.
23. McDonald, B. C.; de Gouw, J. A.; Gilman, J. B.; Jathar, S. H.; Akherati, A.; Cappa, C. D.; Jimenez, J. L.; Lee-Taylor, J.; Hayes, P. L.; McKeen, S. A.; Cui, Y. Y.; Kim, S. W.; Gentner, D. R.; Isaacman-VanWertz, G.; Goldstein, A. H.; Harley, R. A.; Frost, G. J.; Roberts, J. M.; Ryerson, T. B.; Trainer, M., Volatile chemical products emerging as largest petrochemical source of urban organic emissions. *Science* **2018**, *359*, (6377), 760-764.
24. Goldstein, A. H.; Galbally, I. E., Known and unexplored organic constituents in the earth's atmosphere. *Environ. Sci. Technol.* **2007**, *41*, (5), 1514-1521.
25. Guenther, A.; Hewitt, C. N.; Erickson, D.; Fall, R.; Geron, C.; Graedel, T.; Harley, P.; Klinger, L.; Lerdau, M.; McKay, W. A.; Pierce, T.; Scholes, B.; Steinbrecher, R.; Tallamraju, R.; Taylor, J.; Zimmerman, P., A global-model of natural volatile organic-compound emissions. *J. Geophys. Res.-Atmos.* **1995**, *100*, (D5), 8873-8892.
26. Guenther, A.; Karl, T.; Harley, P.; Wiedinmyer, C.; Palmer, P. I.; Geron, C., Estimates of global terrestrial isoprene emissions using MEGAN (Model of Emissions of Gases and Aerosols from Nature). *Atmos. Chem. Phys.* **2006**, *6*, 3181-3210.
27. Kanakidou, M.; Seinfeld, J. H.; Pandis, S. N.; Barnes, I.; Dentener, F. J.; Facchini, M. C.; Van Dingenen, R.; Ervens, B.; Nenes, A.; Nielsen, C. J.; Swietlicki, E.; Putaud, J. P.; Balkanski, Y.; Fuzzi, S.; Horth, J.; Moortgat, G. K.; Winterhalter, R.; Myhre, C. E. L.; Tsigaridis, K.; Vignati, E.; Stephanou, E. G.; Wilson, J., Organic aerosol and global climate modelling: a review. *Atmos. Chem. Phys.* **2005**, *5*, 1053-1123.
28. Andreae, M. O.; Hegg, D. A.; Baltensperger, U., Sources and Nature of Atmospheric Aerosols. In *Aerosol Pollution Impact on Precipitation: A Scientific Review*, Levin, Z.; Cotton, W. R., Eds. Springer Netherlands: Dordrecht, 2009; pp 45-89.
29. Szidat, S.; Jenk, T. M.; Synal, H. A.; Kalberer, M.; Wacker, L.; Hajdas, I.; Kasper-Giebl, A.; Baltensperger, U., Contributions of fossil fuel, biomass-burning, and biogenic emissions to carbonaceous aerosols in Zurich as traced by C-14. *J. Geophys. Res.-Atmos.* **2006**, *111*, (D7), 12.

30. Lanz, V. A.; Alfarra, M. R.; Baltensperger, U.; Buchmann, B.; Hueglin, C.; Prevot, A. S. H., Source apportionment of submicron organic aerosols at an urban site by factor analytical modelling of aerosol mass spectra. *Atmos. Chem. Phys.* **2007**, *7*, (6), 1503-1522.
31. Simpson, D.; Yttri, K. E.; Klimont, Z.; Kupiainen, K.; Caseiro, A.; Gelencser, A.; Pio, C.; Puxbaum, H.; Legrand, M., Modeling carbonaceous aerosol over Europe: Analysis of the CARBOSOL and EMEP EC/OC campaigns. *J. Geophys. Res.-Atmos.* **2007**, *112*, (D23), 26.
32. Schichtel, B. A.; Malm, W. C.; Bench, G.; Fallon, S.; McDade, C. E.; Chow, J. C.; Watson, J. G., Fossil and contemporary fine particulate carbon fractions at 12 rural and urban sites in the United States. *J. Geophys. Res.-Atmos.* **2008**, *113*, (D2), 20.
33. Colbeck, I.; Lazaridis, M., Aerosols and environmental pollution. *Naturwissenschaften* **2010**, *97*, (2), 117-131.
34. Pachauri, R. K.; Qin, D. H.; Stocker, T. F., Climate Change 2013 The Physical Science Basis Working Group I Contribution to the Fifth Assessment Report of the Intergovernmental Panel on Climate Change Preface. In *Climate Change 2013: the Physical Science Basis*, Stocker, T. F.; Qin, D.; Plattner, G. K.; Tignor, M. M. B.; Allen, S. K.; Boschung, J.; Nauels, A.; Xia, Y.; Bex, V.; Midgley, P. M., Eds. Cambridge Univ Press: Cambridge, 2014; pp VII-IX.
35. Kalaiarasan, M.; Balasubramanian, R.; Cheong, K. W. D.; Tham, K. W., Traffic-generated airborne particles in naturally ventilated multi-storey residential buildings of Singapore: Vertical distribution and potential health risks. *Build. Environ.* **2009**, *44*, (7), 1493-1500.
36. Zhao, B.; Wang, S. X.; Donahue, N. M.; Jathar, S. H.; Huang, X. F.; Wu, W. J.; Hao, J. M.; Robinson, A. L., Quantifying the effect of organic aerosol aging and intermediate-volatility emissions on regional-scale aerosol pollution in China. *Sci Rep* **2016**, *6*, 10.
37. Nel, A., Air pollution-related illness: Effects of particles. *Science* **2005**, *308*, (5723), 804-806.
38. Wilson, W. E.; Suh, H. H., Fine particles and coarse particles: Concentration relationships relevant to epidemiologic studies. *J. Air Waste Manage. Assoc.* **1997**, *47*, (12), 1238-1249.
39. Wyzga, R. E.; Folinsbee, L. J., Health effects of acid aerosols. *Water Air Soil Pollut.* **1995**, *85*, (1), 177-188.
40. Kennedy, I. M., The health effects of combustion-generated aerosols. *Proc. Combust. Inst.* **2007**, *31*, 2757-2770.
41. Mauderly, J. L.; Chow, J. C., Health effects of organic aerosols. *Inhal. Toxicol.* **2008**, *20*, (3), 257-288.
42. Khan, F. Chemical Profiling and Toxicological Assessment of Atmospheric Aerosol Using Human Lung Cells. Ph.D. thesis, Institute of Physical Chemistry, Polish Academy of Sciences, 2022.
43. Chameides, W. L.; Lindsay, R. W.; Richardson, J.; Kiang, C. S., The role of biogenic hydrocarbons in urban photochemical smog - Atlanta as a case study. *Science* **1988**, *241*, (4872), 1473-1475.
44. Shilling, J. E.; Zaveri, R. A.; Fast, J. D.; Kleinman, L.; Alexander, M. L.; Canagaratna, M. R.; Fortner, E.; Hubbe, J. M.; Jayne, J. T.; Sedlacek, A.; Setyan, A.; Springston, S.; Worsnop, D. R.; Zhang, Q., Enhanced SOA formation from mixed anthropogenic and biogenic emissions during the CARES campaign. *Atmos. Chem. Phys.* **2013**, *13*, (4), 2091-2113.
45. Guenther, A. B.; Jiang, X.; Heald, C. L.; Sakulyanontvittaya, T.; Duhl, T.; Emmons, L. K.; Wang, X., The Model of Emissions of Gases and Aerosols from Nature version 2.1 (MEGAN2.1): an extended and updated framework for modeling biogenic emissions. *Geosci. Model Dev.* **2012**, *5*, (6), 1471-1492.
46. Claeys, M.; Graham, B.; Vas, G.; Wang, W.; Vermeylen, R.; Pashynska, V.; Cafmeyer, J.; Guyon, P.; Andreae, M. O.; Artaxo, P.; Maenhaut, W., Formation of secondary organic aerosols through photooxidation of isoprene. *Science* **2004**, *303*, (5661), 1173-1176.

47. Carlton, A. G.; Wiedinmyer, C.; Kroll, J. H., A review of Secondary Organic Aerosol (SOA) formation from isoprene. *Atmos. Chem. Phys.* **2009**, *9*, (14), 4987-5005.
48. Khan, M. A. H.; Jenkin, M. E.; Foulds, A.; Derwent, R. G.; Percival, C. J.; Shallcross, D. E., A modeling study of secondary organic aerosol formation from sesquiterpenes using the STOCHEM global chemistry and transport model. *J. Geophys. Res.-Atmos.* **2017**, *122*, (8), 4426-4439.
49. Tsigaridis, K.; Daskalakis, N.; Kanakidou, M.; Adams, P. J.; Artaxo, P.; Bahadur, R.; Balkanski, Y.; Bauer, S. E.; Bellouin, N.; Benedetti, A.; Bergman, T.; Berntsen, T. K.; Beukes, J. P.; Bian, H.; Carslaw, K. S.; Chin, M.; Curci, G.; Diehl, T.; Easter, R. C.; Ghan, S. J.; Gong, S. L.; Hodzic, A.; Hoyle, C. R.; Iversen, T.; Jathar, S.; Jimenez, J. L.; Kaiser, J. W.; Kirkevag, A.; Koch, D.; Kokkola, H.; Lee, Y. H.; Lin, G.; Liu, X.; Luo, G.; Ma, X.; Mann, G. W.; Mihalopoulos, N.; Morcrette, J. J.; Muller, J. F.; Myhre, G.; Myriokefalitakis, S.; Ng, N. L.; O'Donnell, D.; Penner, J. E.; Pozzoli, L.; Pringle, K. J.; Russell, L. M.; Schulz, M.; Sciare, J.; Seland, O.; Shindell, D. T.; Sillman, S.; Skeie, R. B.; Spracklen, D.; Stavrou, T.; Steenrod, S. D.; Takemura, T.; Tiitta, P.; Tilmes, S.; Tost, H.; van Noije, T.; van Zyl, P. G.; von Salzen, K.; Yu, F.; Wang, Z.; Zaveri, R. A.; Zhang, H.; Zhang, K.; Zhang, Q.; Zhang, X., The AeroCom evaluation and intercomparison of organic aerosol in global models. *Atmos. Chem. Phys.* **2014**, *14*, (19), 10845-10895.
50. Finlayson-Pitts, B. J., *Chemistry of the upper and lower atmosphere : theory, experiments, and applications*. San Diego : Academic Press: San Diego, 2000.
51. Finlayson-Pitts, B. J.; Pitts, J. N., CHAPTER 5 - Kinetics and Atmospheric Chemistry. In *Chemistry of the Upper and Lower Atmosphere*, Finlayson-Pitts, B. J.; Pitts, J. N., Eds. Academic Press: San Diego, 2000; pp 130-178.
52. Paula, P. A. a. J. d., *Physical Chemistry: Thermodynamics, Structure, and Change*. Tenth Edition ed.; Great Britain by Oxford University Press, 2014.
53. Terrie K. Boguski, P. E., Understanding Units of Measurement. *Center for Hazardous Substance Research, Environmental Science and Technology Briefs for Citizens* **2006**, (2), 2.
54. Monson, R. K., Reactions of Biogenic Volatile Organic Compounds in the Atmosphere. In *The Chemistry and Biology of Volatiles*, 2010; pp 363-388.
55. Atkinson, R.; Arey, J., Gas-phase tropospheric chemistry of biogenic volatile organic compounds: a review. *Atmos. Environ.* **2003**, *37*, S197-S219.
56. Kroll, J. H.; Seinfeld, J. H., Chemistry of secondary organic aerosol: Formation and evolution of low-volatility organics in the atmosphere. *Atmos. Environ.* **2008**, *42*, (16), 3593-3624.
57. Pankow, J. F.; Asher, W. E., SIMPOL.1: a simple group contribution method for predicting vapor pressures and enthalpies of vaporization of multifunctional organic compounds. *Atmos. Chem. Phys.* **2008**, *8*, (10), 2773-2796.
58. Atkinson, R., Atmospheric chemistry of VOCs and NOx. *Atmos. Environ.* **2000**, *34*, (12-14), 2063-2101.
59. Levy, H., Normal atmosphere - large radical and formaldehyde concentrations predicted. *Science* **1971**, *173*, (3992), 141-&.
60. Perner, D.; Platt, U.; Trainer, M.; Hubler, G.; Drummond, J.; Junkermann, W.; Rudolph, J.; Schubert, B.; Volz, A.; Ehhalt, D. H.; Rumpel, K. J.; Helas, G., Measurements of tropospheric OH concentrations - a comparison of field data with model predictions. *J. Atmos. Chem.* **1987**, *5*, (2), 185-216.
61. Griffith, S. M.; Hansen, R. F.; Dusanter, S.; Michoud, V.; Gilman, J. B.; Kuster, W. C.; Veres, P. R.; Graus, M.; de Gouw, J. A.; Roberts, J.; Young, C.; Washenfelder, R.; Brown, S. S.; Thalman, R.; Waxman, E.; Volkamer, R.; Tsai, C.; Stutz, J.; Flynn, J. H.; Grossberg, N.; Lefer, B.; Alvarez, S. L.;

- Rappenglueck, B.; Mielke, L. H.; Osthoff, H. D.; Stevens, P. S., Measurements of hydroxyl and hydroperoxy radicals during CalNex-LA: Model comparisons and radical budgets. *J. Geophys. Res.-Atmos.* **2016**, *121*, (8), 4211-4232.
62. Pattantyus, A. K.; Businger, S.; Howell, S. G., Review of sulfur dioxide to sulfate aerosol chemistry at Kilauea Volcano, Hawai'i. *Atmos. Environ.* **2018**, *185*, 262-271.
63. Eatough, D. J.; Caka, F. M.; Farber, R. J., The conversion of SO₂ to sulfate in the atmosphere. *Isr. J. Chem.* **1994**, *34*, (3-4), 301-314.
64. Seigneur, C.; Saxena, P., A theoretical investigation of sulfate formation in clouds. *Atmos. Environ.* **1988**, *22*, (1), 101-115.
65. Liao, H.; Adams, P. J.; Chung, S. H.; Seinfeld, J. H.; Mickley, L. J.; Jacob, D. J., Interactions between tropospheric chemistry and aerosols in a unified general circulation model. *J. Geophys. Res.-Atmos.* **2003**, *108*, (D1), 23.
66. Brandt, C.; Vaneldik, R., Transition-metal-catalyzed oxidation of sulfur(IV) oxides - atmospheric-relevant processes and mechanisms. *Chem. Rev.* **1995**, *95*, (1), 119-190.
67. Warneck, P., Chemical-reactions in clouds. *Fresenius J. Anal. Chem.* **1991**, *340*, (9), 585-590.
68. Grgic, I.; Bercic, G., A simple kinetic model for autoxidation of S(IV) oxides catalyzed by iron and/or manganese ions. *J. Atmos. Chem.* **2001**, *39*, (2), 155-170.
69. Pandis, S. N.; Seinfeld, J. H.; Pilinis, C., Heterogeneous sulfate production in an urban fog. *Atmospheric Environment Part a-General Topics* **1992**, *26*, (14), 2509-2522.
70. Ibusuki, T.; Takeuchi, K., Sulfur-dioxide oxidation by oxygen catalyzed by mixtures of manganese(II) and iron(III) in aqueous-solutions at environmental reaction conditions. *Atmos. Environ.* **1987**, *21*, (7), 1555-1560.
71. Martin, L. R.; Hill, M. W.; Tai, A. F.; Good, T. W., The iron catalyzed oxidation of sulfur(IV) in aqueous-solution - differing effects of organics at high and low pH. *J. Geophys. Res.-Atmos.* **1991**, *96*, (D2), 3085-3097.
72. Grgic, I.; Hudnik, V.; Bizjak, M.; Levec, J., Aqueous S(IV) oxidation .2. synergistic effects of some metal-ions. *Atmospheric Environment Part a-General Topics* **1992**, *26*, (4), 571-577.
73. Ziajka, J.; Rudzinski, K. J., Autoxidation of S-IV inhibited by chlorophenols reacting with sulfate radicals. *Environ. Chem.* **2007**, *4*, (5), 355-363.
74. Ziajka, J.; Pasiuk-Bronikowska, W., Autoxidation of sulphur dioxide in the presence of alcohols under conditions related to the tropospheric aqueous phase. *Atmos. Environ.* **2003**, *37*, (28), 3913-3922.
75. Ziajka, J.; Pasiuk-Bronikowska, W., Rate constants for atmospheric trace organics scavenging SO₄ center dot- in the Fe-catalysed autoxidation of S(IV). *Atmos. Environ.* **2005**, *39*, (8), 1431-1438.
76. Grgic, I.; Hudnik, V.; Bizjak, M.; Levec, J., Aqueous S(IV) oxidation .1. catalytic effects of some metal-ions. *Atmospheric Environment Part a-General Topics* **1991**, *25*, (8), 1591-1597.
77. Podkrajsek, B.; Grgic, I.; Tursic, J., Determination of sulfur oxides formed during the S(IV) oxidation in the presence of iron. *Chemosphere* **2002**, *49*, (3), 271-277.
78. Rudzinski, K. J., Degradation of isoprene in the presence of sulphony radical anions. *J. Atmos. Chem.* **2004**, *48*, (2), 191-216.
79. Rudzinski, K. J.; Gmachowski, L.; Kuznietsova, I., Reactions of isoprene and sulphony radical-anions - a possible source of atmospheric organosulphites and organosulphates. *Atmos. Chem. Phys.* **2009**, *9*, (6), 2129-2140.
80. Rafal Szmigielski, K. J. R., Addition of bisulfite ions to methyl vinyl ketone and methacrolein relevant to atmospheric processes. *Ecological Chemistry and Engineering. A* **2013**, *20*, (9), 935-949.

81. Rudzinski, K. J.; Szmigielski, R., Aqueous Reactions of Sulfate Radical-Anions with Nitrophenols in Atmospheric Context. *Atmosphere* **2019**, *10*, (12), 14.
82. Huss, A.; Lim, P. K.; Eckert, C. A., Oxidation of aqueous sulfur-dioxide .1. homogeneous manganese(II) and iron(II) catalysts at low pH. *J. Phys. Chem.* **1982**, *86*, (21), 4224-4228.
83. Podkrajsek, B.; Bercic, G.; Tursic, J.; Grgic, I., Aqueous oxidation of sulfur(IV) catalyzed by Manganese(II): A generalized simple kinetic model. *J. Atmos. Chem.* **2004**, *47*, (3), 287-303.
84. Podkrajsek, B.; Grgic, I.; Tursic, J.; Bercic, G., Influence of atmospheric carboxylic acids on catalytic oxidation of sulfur(IV). *J. Atmos. Chem.* **2006**, *54*, (2), 103-120.
85. Grgic, I.; Podkrajsek, B.; Barzaghi, P.; Herrmann, H., Scavenging of SO₄⁻ radical anions by mono- and dicarboxylic acids in the Mn(II)-catalyzed S(IV) oxidation in aqueous solution. *Atmos. Environ.* **2007**, *41*, (39), 9187-9194.
86. Tursic, J.; Grgic, I.; Podkrajsek, B., Influence of ionic strength on aqueous oxidation of SO₂ catalyzed by manganese. *Atmos. Environ.* **2003**, *37*, (19), 2589-2595.
87. Farman, J. C.; Gardiner, B. G.; Shanklin, J. D., Large losses of total ozone in antarctica reveal seasonal ClO_x/NO_x interaction. *Nature* **1985**, *315*, (6016), 207-210.
88. Butchart, N.; Scaife, A. A., Removal of chlorofluorocarbons by increased mass exchange between the stratosphere and troposphere in a changing climate. *Nature* **2001**, *410*, (6830), 799-802.
89. Solomon, S., Stratospheric ozone depletion: A review of concepts and history. *Rev. Geophys.* **1999**, *37*, (3), 275-316.
90. Wang, L.; Arey, J.; Atkinson, R., Reactions of chlorine atoms with a series of aromatic hydrocarbons. *Environ. Sci. Technol.* **2005**, *39*, (14), 5302-5310.
91. Hossaini, R.; Chipperfield, M. P.; Saiz-Lopez, A.; Fernandez, R.; Monks, S.; Feng, W. H.; Brauer, P.; von Glasow, R., A global model of tropospheric chlorine chemistry: Organic versus inorganic sources and impact on methane oxidation. *J. Geophys. Res.-Atmos.* **2016**, *121*, (23), 14271-14297.
92. Ravishankara, A. R., Are chlorine atoms significant tropospheric free radicals? *Proc. Natl. Acad. Sci. U. S. A.* **2009**, *106*, (33), 13639-13640.
93. Gunthe, S. S.; Liu, P. F.; Panda, U.; Raj, S. S.; Sharma, A.; Darbyshire, E.; Reyes-Villegas, E.; Allan, J.; Chen, Y.; Wang, X.; Song, S. J.; Pohlker, M. L.; Shi, L. H.; Wang, Y.; Kommula, S. M.; Liu, T. J.; Ravikrishna, R.; McFiggans, G.; Mickley, L. J.; Martin, S. T.; Poschl, U.; Andreae, M. O.; Coe, H., Enhanced aerosol particle growth sustained by high continental chlorine emission in India. *Nat. Geosci.* **2021**, *14*, (2), 20.
94. Qiu, X. H.; Ying, Q.; Wang, S.; Duan, L.; Wang, Y. H.; Lu, K. D.; Wang, P.; Xing, J.; Zheng, M.; Zhao, M. J.; Zheng, H. T.; Zhang, Y. H.; Hao, J. M., Significant impact of heterogeneous reactions of reactive chlorine species on summertime atmospheric ozone and free-radical formation in north China. *Sci. Total Environ.* **2019**, *693*, 11.
95. Faxon, C. B.; Allen, D. T., Chlorine chemistry in urban atmospheres: a review. *Environ. Chem.* **2013**, *10*, (3), 221-233.
96. Ezell, M. J.; Wang, W. H.; Ezell, A. A.; Soskin, G.; Finlayson-Pitts, B. J., Kinetics of reactions of chlorine atoms with a series of alkenes at 1 atm and 298 K: structure and reactivity. *Phys. Chem. Chem. Phys.* **2002**, *4*, (23), 5813-5820.
97. Cicerone, R. J., Halogens in the atmosphere. *Rev. Geophys.* **1981**, *19*, (1), 123-139.
98. Simpson, W. R.; Brown, S. S.; Saiz-Lopez, A.; Thornton, J. A.; von Glasow, R., Tropospheric Halogen Chemistry: Sources, Cycling, and Impacts. *Chem. Rev.* **2015**, *115*, (10), 4035-4062.

99. World Health Organization. Regional Office for, E., *Air quality guidelines for Europe: second edition*. World Health Organization. Regional Office for Europe: Copenhagen, 2000.
100. VanLoon, G. W.; Duffy, S. J., Environmental chemistry : a global perspective. **2005**.
101. Report, E. *Air quality in Europe*; European Environment Agency: 2020.
102. Oberdorster, G.; Utell, M. J., Ultrafine particles in the urban air: To the respiratory tract - And beyond? *Environ. Health Perspect.* **2002**, *110*, (8), A440-A441.
103. Breslow, L.; Goldsmith, J., Health-effects of air-pollution. *American Journal of Public Health and the Nations Health* **1958**, *48*, (7), 913-917.
104. Gauderman, W. J.; Avol, E.; Gilliland, F.; Vora, H.; Thomas, D.; Berhane, K.; McConnell, R.; Kuenzli, N.; Lurmann, F.; Rappaport, E.; Margolis, H.; Bates, D.; Peters, J., The effect of air pollution on lung development from 10 to 18 years of age. *N. Engl. J. Med.* **2004**, *351*, (11), 1057-1067.
105. Samet, J.; Wassel, R.; Holmes, K. J.; Abt, E.; Bakshi, K., Research priorities for airborne particulate matter in the United States. *Environ. Sci. Technol.* **2005**, *39*, (14), 299A-304A.
106. Boucher, O., D. Randall, P. Artaxo, C. Bretherton, G. Feingold, P. Forster, V.-M. Kerminen, Y. Kondo, H. Liao, U. Lohmann, P. Rasch, S.K. Satheesh, S. Sherwood, B. Stevens and X.Y. Zhang *Clouds and Aerosols. In: Climate Change 2013: The Physical Science Basis. Contribution of Working Group I to the Fifth Assessment Report of the Intergovernmental Panel on Climate Change* Cambridge, United Kingdom and New York, NY, USA: Cambridge University Press, 2013.
107. Matsui, K.; Koeduka, T., Green leaf volatiles in plant signaling and response. In *Lipids in Plant and Algae Development*, Nakamura, Y.; LiBeisson, Y., Eds. Springer: New York, 2016; Vol. 86, pp 427-443.
108. Dong, F.; Fu, X. M.; Watanabe, N.; Su, X. G.; Yang, Z. Y., Recent Advances in the Emission and Functions of Plant Vegetative Volatiles. *Molecules* **2016**, *21*, (2), 10.
109. Holopainen, J. K., Can forest trees compensate for stress-generated growth losses by induced production of volatile compounds? *Tree Physiol.* **2011**, *31*, (12), 1356-1377.
110. Baldwin, I. T.; Halitschke, R.; Paschold, A.; von Dahl, C. C.; Preston, C. A., Volatile Signaling in Plant-Plant Interactions: "Talking Trees" in the Genomics Era. *Science* **2006**, *311*, (5762), 812-815.
111. Arimura, G.; Pearse, I. S., Chapter One - From the Lab Bench to the Forest: Ecology and Defence Mechanisms of Volatile-Mediated 'Talking Trees'. In *Advances in Botanical Research*, Becard, G., Ed. Academic Press: 2017; Vol. 82, pp 3-17.
112. Farmer, E. E., Surface-to-air signals. *Nature* **2001**, *411*, (6839), 854-856.
113. Shulaev, V.; Silverman, P.; Raskin, I., Airborne signalling by methyl salicylate in plant pathogen resistance. *Nature* **1997**, *385*, (6618), 718-721.
114. Loreto, F.; Schnitzler, J.-P., Abiotic stresses and induced BVOCs. *Trends in Plant Science* **2010**, *15*, (3), 154-166.
115. Shen, J. Y.; Tieman, D.; Jones, J. B.; Taylor, M. G.; Schmelz, E.; Huffaker, A.; Bies, D.; Chen, K. S.; Klee, H. J., A 13-lipoxygenase, TomloxC, is essential for synthesis of C5 flavour volatiles in tomato. *J. Exp. Bot.* **2014**, *65*, (2), 419-428.
116. Hatanaka, A., The biogenesis of green odor by green leaves. *Phytochemistry* **1993**, *34*, (5), 1201-1218.
117. Matsui, K.; Sugimoto, K.; Mano, J.; Ozawa, R.; Takabayashi, J., Differential Metabolisms of Green Leaf Volatiles in Injured and Intact Parts of a Wounded Leaf Meet Distinct Ecophysiological Requirements. *PLoS One* **2012**, *7*, (4), 10.

118. Maffei, M. E., Sites of synthesis, biochemistry and functional role of plant volatiles. *S. Afr. J. Bot.* **2010**, *76*, (4), 612-631.
119. Fisher, A. J.; Baker, B. M.; Greenberg, J. P.; Fall, R., Enzymatic Synthesis of Methylbutenol from Dimethylallyl Diphosphate in Needles of *Pinus sabiniana*. *Archives of Biochemistry and Biophysics* **2000**, *383*, (1), 128-134.
120. Brilli, F.; Ruuskanen, T. M.; Schnitzhofer, R.; Muller, M.; Breitenlechner, M.; Bittner, V.; Wohlfahrt, G.; Loreto, F.; Hansel, A., Detection of Plant Volatiles after Leaf Wounding and Darkening by Proton Transfer Reaction "Time-of-Flight" Mass Spectrometry (PTR-TOF). *PLoS One* **2011**, *6*, (5), 12.
121. de Gouw, J. A.; Howard, C. J.; Custer, T. G.; Fall, R., Emissions of volatile organic compounds from cut grass and clover are enhanced during the drying process. *Geophys. Res. Lett.* **1999**, *26*, (7), 811-814.
122. Jardine, K.; Barron-Gafford, G. A.; Norman, J. P.; Abrell, L.; Monson, R. K.; Meyers, K. T.; Pavao-Zuckerman, M.; Dontsova, K.; Kleist, E.; Werner, C.; Huxman, T. E., Green leaf volatiles and oxygenated metabolite emission bursts from mesquite branches following light-dark transitions. *Photosynth. Res.* **2012**, *113*, (1-3), 321-333.
123. Jardine, K. J.; Chambers, J. Q.; Holm, J.; Jardine, A. B.; Fontes, C. G.; Zorzanelli, R. F.; Meyers, K. T.; de Souza, V. F.; Garcia, S.; Gimenez, B. O.; Piva, L. R. d. O.; Higuchi, N.; Artaxo, P.; Martin, S.; Manzi, A. O., Green leaf volatile emissions during high temperature and drought stress in a Central Amazon rainforest. *Plants* **2015**, (Plants 2015, 4), 678-690.
124. Karl, T.; Harren, F.; Warneke, C.; de Gouw, J.; Grayless, C.; Fall, R., Senescing grass crops as regional sources of reactive volatile organic compounds. *J. Geophys. Res.-Atmos.* **2005**, *110*, (D15), 12.
125. Kirstine, W.; Galbally, I.; Ye, Y. R.; Hooper, M., Emissions of volatile organic compounds (primarily oxygenated species) from pasture. *J. Geophys. Res.-Atmos.* **1998**, *103*, (D9), 10605-10619.
126. Kirstine, W. V.; Galbally, I. E., A simple model for estimating emissions of volatile organic compounds from grass and cut grass in urban airsheds and its application to two Australian cities. *J. Air Waste Manage. Assoc.* **2004**, *54*, (10), 1299-1311.
127. Scala, A.; Allmann, S.; Mirabella, R.; Haring, M.; Schuurink, R., Green Leaf Volatiles: A Plant's Multifunctional Weapon against Herbivores and Pathogens. *International Journal of Molecular Sciences* **2013**, *14*, (9), 17781.
128. Hansel, A. K.; Ehrenhauser, F. S.; Richards-Henderson, N. K.; Anastasio, C.; Valsaraj, K. T., Aqueous-phase oxidation of green leaf volatiles by hydroxyl radical as a source of SOA: Product identification from methyl jasmonate and methyl salicylate oxidation. *Atmos. Environ.* **2015**, *102*, 43-51.
129. Richards-Henderson, N. K.; Hansel, A. K.; Valsaraj, K. T.; Anastasio, C., Aqueous oxidation of green leaf volatiles by hydroxyl radical as a source of SOA: Kinetics and SOA yields. *Atmos. Environ.* **2014**, *95*, 105-112.
130. Loreto, F.; Barta, C.; Brilli, F.; Nogues, I., On the induction of volatile organic compound emissions by plants as consequence of wounding or fluctuations of light and temperature. *Plant Cell Environ.* **2006**, *29*, (9), 1820-1828.
131. Mochizuki, S.; Sugimoto, K.; Koeduka, T.; Matsui, K., Arabidopsis lipoxygenase 2 is essential for formation of green leaf volatiles and five-carbon volatiles. *FEBS Lett.* **2016**, *590*, (7), 1017-1027.
132. Fisher, A. J.; Grimes, H. D.; Fall, R., The biochemical origin of pentenol emissions from wounded leaves. *Phytochemistry* **2003**, *62*, (2), 159-163.

133. Mayland, H. F.; Flath, R. A.; Shewmaker, G. E., Volatiles from Fresh and Air-Dried Vegetative Tissues of Tall Fescue (*Festuca arundinacea* Schreb.): Relationship to Cattle Preference. *Journal of Agricultural and Food Chemistry* **1997**, *45*, (6), 2204-2210.
134. Fall, R.; Karl, T.; Jordon, A.; Lindinger, W., Biogenic C5 VOCs release from leaves after freeze-thaw wounding and occurrence in air at a high mountain observatory. *Atmos. Environ.* **2001**, *35*, (22), 3905-3916.
135. López-Gresa, M. P.; Lisón, P.; Campos, L.; Rodrigo, I.; Rambla, J. L.; Granell, A.; Conejero, V.; Bellés, J. M., A Non-targeted Metabolomics Approach Unravels the VOCs Associated with the Tomato Immune Response against *Pseudomonas syringae*. *Frontiers in Plant Science* **2017**, *8*, (1188).
136. Connor, E. C.; Rott, A. S.; Zeder, M.; Juttner, F.; Dorn, S., (¹³C)-labelling patterns of green leaf volatiles indicating different dynamics of precursors in Brassica leaves. *Phytochemistry* **2008**, *69*, (6), 1304-1312.
137. Matsui, K., Green leaf volatiles: hydroperoxide lyase pathway of oxylipin metabolism. *Curr. Opin. Plant Biol.* **2006**, *9*, (3), 274-280.
138. Fall, R.; Karl, T.; Hansel, A.; Jordan, A.; Lindinger, W., Volatile organic compounds emitted after leaf wounding: On-line analysis by proton-transfer-reaction mass spectrometry. *Journal of Geophysical Research: Atmospheres* **1999**, *104*, (D13), 15963-15974.
139. Engelberth, J.; Alborn, H. T.; Schmelz, E. A.; Tumlinson, J. H., Airborne signals prime plants against insect herbivore attack. *Proc. Natl. Acad. Sci. U. S. A.* **2004**, *101*, (6), 1781-1785.
140. Croft, K. P. C.; Juttner, F.; Slusarenko, A. J., Volatile products of the lipoxygenase pathway evolved from *Phaseolus-vulgaris* (L.) leaves inoculated with *Pseudomonas syringae* pv *phaseolicola*. *Plant Physiology* **1993**, *101*, (1), 13-24.
141. Fukui, Y.; Doskey, P. V., Identification of nonmethane organic compound emissions from grassland vegetation. *Atmospheric Environment* **2000**, *34*, (18), 2947-2956.
142. Rose, U.; Manukian, A.; Heath, R. R.; Tumlinson, J. H., Volatile Semiochemicals Released from Undamaged Cotton Leaves (A Systemic Response of Living Plants to Caterpillar Damage). *Plant Physiology* **1996**, *111*, (2), 487-495.
143. Matsui, K.; Minami, A.; Hornung, E.; Shibata, H.; Kishimoto, K.; Ahnert, V.; Kindl, H.; Kajiwara, T.; Feussner, I., Biosynthesis of fatty acid derived aldehydes is induced upon mechanical wounding and its products show fungicidal activities in cucumber. *Phytochemistry* **2006**, *67*, (7), 649-657.
144. Matsui, K.; Kurishita, S.; Hisamitsu, A.; Kajiwara, T., A lipid-hydrolysing activity involved in hexenal formation. *Biochem. Soc. Trans.* **2000**, *28*, 857-860.
145. Peterson, D. L.; Böröczky, K.; Tumlinson, J.; Cipollini, D., Ecological fitting: Chemical profiles of plant hosts provide insights on selection cues and preferences for a major buprestid pest. *Phytochemistry* **2020**, *176*, 112397.
146. Zhang, Q. H.; Birgersson, G.; Zhu, J. W.; Lofstedt, C.; Lofqvist, J.; Schlyter, F., Leaf volatiles from nonhost deciduous trees: Variation by tree species, season and temperature, and electrophysiological activity in *Ips typographus*. *J. Chem. Ecol.* **1999**, *25*, (8), 1923-1943.
147. Gaquerel, E.; Weinhold, A.; Baldwin, I. T., Molecular Interactions between the Specialist Herbivore *Manduca sexta* (Lepidoptera, Sphingidae) and Its Natural Host *Nicotiana attenuata*. VIII. An Unbiased GCxGC-ToFMS Analysis of the Plant's Elicited Volatile Emissions. *Plant Physiology* **2009**, *149*, (3), 1408-1423.
148. Kessler, A.; Baldwin, I. T., Defensive function of herbivore-induced plant volatile emissions in nature. *Science* **2001**, *291*, (5511), 2141-2144.

149. Blande, J. D.; Korjus, M.; Holopainen, J. K., Foliar methyl salicylate emissions indicate prolonged aphid infestation on silver birch and black alder. *Tree Physiology* **2010**, *30*, (3), 404-416.
150. Wiedinmyer, C.; Guenther, A.; Harley, P.; Hewitt, N.; Geron, C.; Artaxo, P.; Steinbrecher, R.; Rasmussen, R., Global organic emissions from vegetation. In *Emissions of atmospheric trace compound*, Granier, C.; Artaxo, P.; Reeves, C. E., Eds. Springer: Dordrecht, 2004; pp 115-170.
151. Karl, T. G.; Spirig, C.; Rinne, J.; Stroud, C.; Prevost, P.; Greenberg, J.; Fall, R.; Guenther, A., Virtual disjunct eddy covariance measurements of organic compound fluxes from a subalpine forest using proton transfer reaction mass spectrometry. *Atmos. Chem. Phys.* **2002**, *2*, (4), 279-291.
152. Geron, C. D.; Daly, R. W.; Arnts, R. R.; Guenther, A. B.; Mowry, F. L., Canopy level emissions of 2-methyl-3-buten-2-ol, monoterpenes, and sesquiterpenes from an experimental Pinus taeda plantation. *Science of The Total Environment* **2016**, *565*, 730-741.
153. Fischer, K. B.; Gold, C. S.; Harvey, R. M.; Petrucci, A. N.; Petrucci, G. A., Ozonolysis Chemistry and Phase Behavior of 1-Octen-3-ol-Derived Secondary Organic Aerosol. *ACS Earth and Space Chemistry* **2020**, *4*, (8), 1298-1308.
154. Creelman, R. A.; Mullet, J. E., Biosynthesis and action of jasmonates in plants. *Annu. Rev. Plant Physiol. Plant Molec. Biol.* **1997**, *48*, 355-381.
155. Sindelarova, K.; Granier, C.; Bouarar, I.; Guenther, A.; Tilmes, S.; Stavrakou, T.; Müller, J. F.; Kuhn, U.; Stefani, P.; Knorr, W., Global data set of biogenic VOC emissions calculated by the MEGAN model over the last 30 years. *Atmos. Chem. Phys.* **2014**, *14*, (17), 9317-9341.
156. Guenther, A.; Geron, C.; Pierce, T.; Lamb, B.; Harley, P.; Fall, R., Natural emissions of non-methane volatile organic compounds; carbon monoxide, and oxides of nitrogen from North America. *Atmos. Environ.* **2000**, *34*, (12-14), 2205-2230.
157. Su, Q.; Yang, F.; Zhang, Q.; Tong, H.; Hu, Y.; Zhang, X.; Xie, W.; Wang, S.; Wu, Q.; Zhang, Y., Defence priming in tomato by the green leaf volatile (Z)-3-hexenol reduces whitefly transmission of a plant virus. *Plant, Cell & Environment* **2020**, *43*, (11), 2797-2811.
158. Guo, R.-Z.; Yan, H.-Y.; Li, X.-X.; Zou, X.-X.; Zhang, X.-J.; Yu, X.-N.; Ci, D.-W.; Wang, Y.-F.; Si, T., Green leaf volatile (Z)-3-hexenyl-1-yl acetate reduces salt stress in peanut by affecting photosynthesis and cellular redox homeostasis. *Physiologia Plantarum* **2020**, *170*, (1), 75-92.
159. Wakai, J.; Kusama, S.; Nakajima, K.; Kawai, S.; Okumura, Y.; Shiojiri, K., Effects of trans-2-hexenal and cis-3-hexenal on post-harvest strawberry. *Scientific Reports* **2019**, *9*, (1), 10112.
160. Cofer, T. M.; Engelberth, M.; Engelberth, J., Green leaf volatiles protect maize (*Zea mays*) seedlings against damage from cold stress. *Plant, Cell & Environment* **2018**, *41*, (7), 1673-1682.
161. Payá, C.; López-Gresa, M. P.; Intrigliolo, D. S.; Rodrigo, I.; Bellés, J. M.; Lisón, P., (Z)-3-Hexenyl Butyrate Induces Stomata Closure and Ripening in *Vitis vinifera*. *Agronomy* **2020**, *10*, (8), 1122.
162. Jimenez, E.; Lanza, B.; Antinolo, M.; Albaladejo, J., Photooxidation of Leaf-Wound Oxygenated Compounds, 1-Penten-3-ol, (Z)-3-Hexen-1-ol, and 1-Penten-3-one, Initiated by OH Radicals and Sunlight. *Environ. Sci. Technol.* **2009**, *43*, (6), 1831-1837.
163. Yli-Pirilä, P.; Copolovici, L.; Kännaste, A.; Noe, S.; Blande, J. D.; Mikkonen, S.; Klemola, T.; Pulkkinen, J.; Virtanen, A.; Laaksonen, A.; Joutsensaari, J.; Niinemets, Ü.; Holopainen, J. K., Herbivory by an Outbreaking Moth Increases Emissions of Biogenic Volatiles and Leads to Enhanced Secondary Organic Aerosol Formation Capacity. *Environmental Science & Technology* **2016**, *50*, (21), 11501-11510.

164. Hodzic, A.; Kasibhatla, P. S.; Jo, D. S.; Cappa, C. D.; Jimenez, J. L.; Madronich, S.; Park, R. J., Rethinking the global secondary organic aerosol (SOA) budget: stronger production, faster removal, shorter lifetime. *Atmos. Chem. Phys.* **2016**, *16*, (12), 7917-7941.
165. Lin, G.; Penner, J. E.; Zhou, C., How will SOA change in the future? *Geophysical Research Letters* **2016**, *43*, (4), 1718-1726.
166. Lim, H.-J.; Carlton, A. G.; Turpin, B. J., Isoprene Forms Secondary Organic Aerosol through Cloud Processing: Model Simulations. *Environmental Science & Technology* **2005**, *39*, (12), 4441-4446.
167. Hamilton, J. F.; Lewis, A. C.; Carey, T. J.; Wenger, J. C.; Garcia, E. B. I.; Munoz, A., Reactive oxidation products promote secondary organic aerosol formation from green leaf volatiles. *Atmos. Chem. Phys.* **2009**, *9*, (11), 3815-3823.
168. Sarang, K.; Rudziński, K. J. J.; Szmigielski, R., Green Leaf Volatiles in the Atmosphere- Properties, Transformation, and Significance. *Atmosphere* **2021**, *12*, (12), 1655.
169. Atkinson, R.; Arey, J., Atmospheric Degradation of Volatile Organic Compounds. *Chemical Reviews* **2003**, *103*, (12), 4605-4638.
170. Atkinson, R., Atmospheric chemistry of VOCs and NOx. *Atmospheric Environment* **2000**, *34*, (12), 2063-2101.
171. Davis, M. E.; Gilles, M. K.; Ravishankara, A. R.; Burkholder, J. B., Rate coefficients for the reaction of OH with (E)-2-pentenal, (E)-2-hexenal, and (E)-2-heptenal. *Physical Chemistry Chemical Physics* **2007**, *9*, (18), 2240-2248.
172. Sarang, K.; Rudziński, K. J. J.; Szmigielski, R., Green Leaf Volatiles in the Atmosphere-Properties, Transformation, and Significance. *Atmosphere* **2021**, *12*, (12), 1655.
173. Arey, J.; Winer, A. M.; Atkinson, R.; Aschmann, S. M.; Long, W. D.; Lynn Morrison, C., The emission of (Z)-3-hexen-1-ol, (Z)-3-hexenylacetate and other oxygenated hydrocarbons from agricultural plant species. *Atmospheric Environment. Part A. General Topics* **1991**, *25*, (5), 1063-1075.
174. Atkinson, R.; Arey, J.; Aschmann, S. M.; Corchnoy, S. B.; Shu, Y., Rate constants for the gas-phase reactions of cis-3-Hexen-1-ol, cis-3-Hexenylacetate, trans-2-Hexenal, and Linalool with OH and NO₃ radicals and O₃ at 296 ± 2 K, and OH radical formation yields from the O₃ reactions. *International Journal of Chemical Kinetics* **1995**, *27*, (10), 941-955.
175. Gibilisco, R. G.; Blanco, M. a. B.; Bejan, I.; Barnes, I.; Wiesen, P.; Teruel, M. A., Atmospheric Sink of (E)-3-Hexen-1-ol, (Z)-3-Hepten-1-ol, and (Z)-3-Octen-1-ol: Rate Coefficients and Mechanisms of the OH-Radical Initiated Degradation. *Environmental Science & Technology* **2015**, *49*, (13), 7717-7725.
176. Gibilisco, R. G.; Santiago, A. N.; Teruel, M. A., OH-initiated degradation of a series of hexenols in the troposphere. Rate coefficients at 298 K and 1 atm. *Atmos. Environ.* **2013**, *77*, 358-364.
177. Alvarado, A.; Tuazon, E. C.; M. Aschmann, S.; Arey, J.; Atkinson, R., Products and mechanisms of the gas-phase reactions of OH radicals and O₃ with 2-methyl-3-buten-2-ol. *Atmospheric Environment* **1999**, *33*, (18), 2893-2905.
178. Carrasco, N.; Doussin, J. F.; O'Connor, M.; Wenger, J. C.; Picquet-Varrault, B.; Durand-Jolibois, R.; Carlier, P., Simulation Chamber Studies of the Atmospheric Oxidation of 2-Methyl-3-Buten-2-ol: Reaction with Hydroxyl Radicals and Ozone Under a Variety of Conditions. *Journal of Atmospheric Chemistry* **2007**, *56*, (1), 33-55.
179. Ferronato, C.; Orlando, J. J.; Tyndall, G. S., Rate and mechanism of the reactions of OH and Cl with 2-methyl-3-buten-2-ol. *Journal of Geophysical Research: Atmospheres* **1998**, *103*, (D19), 25579-25586.

180. Reisen, F.; Aschmann, S. M.; Atkinson, R.; Arey, J., Hydroxyaldehyde Products from Hydroxyl Radical Reactions of Z-3-Hexen-1-ol and 2-Methyl-3-buten-2-ol Quantified by SPME and API-MS. *Environmental Science & Technology* **2003**, *37*, (20), 4664-4671.
181. Orlando, J. J.; Tyndall, G. S., Laboratory studies of organic peroxy radical chemistry: an overview with emphasis on recent issues of atmospheric significance. *Chemical Society Reviews* **2012**, *41*, (19), 6294-6317.
182. Fantechi, G.; Jensen, N. R.; Hjorth, J.; Peeters, J., Mechanistic studies of the atmospheric oxidation of methyl butenol by OH radicals, ozone and NO₃ radicals. *Atmospheric Environment* **1998**, *32*, (20), 3547-3556.
183. Aschmann, S. M.; Shu, Y.; Arey, J.; Atkinson, R., Products of the gas-phase reactions of cis-3-hexen-1-ol with OH radicals and O₃. *Atmospheric Environment* **1997**, *31*, (21), 3551-3560.
184. Orlando, J. J.; Tyndall, G. S.; Ceazan, N., Rate coefficients and product yields from reaction of OH with 1-penten-3-ol, (Z)-2-penten-1-ol, and allyl alcohol (2-propen-1-ol). *Journal of Physical Chemistry A* **2001**, *105*, (14), 3564-3569.
185. Noda, J.; Hallquist, M.; Langer, S.; Ljungström, E., Products from the gas-phase reaction of some unsaturated alcohols with nitrate radicals. *Physical Chemistry Chemical Physics* **2000**, *2*, (11), 2555-2564.
186. Pfrang, C.; Romero, M. T. B.; Cabanas, B.; Canosa-Mas, C. E.; Villanueva, F.; Wayne, R. P., Night-time tropospheric chemistry of the unsaturated alcohols (Z)-pent-2-en-1-ol and pent-1-en-3-ol: Kinetic studies of reactions of NO₃ and N₂O₅ with stress-induced plant emissions. *Atmos. Environ.* **2007**, *41*, (8), 1652-1662.
187. Kerdouci, J.; Picquet-Varrault, B.; Durand-Jolibois, R.; Gaimoz, C.; Doussin, J. F., An Experimental Study of the Gas-Phase Reactions of NO₃ Radicals with a Series of Unsaturated Aldehydes: trans-2-Hexenal, trans-2-Heptenal, and trans-2-Octenal. *J. Phys. Chem. A* **2012**, *116*, (41), 10135-10142.
188. Horie, O.; Moortgat, G. K., Gas-Phase Ozonolysis of Alkenes. Recent Advances in Mechanistic Investigations. *Accounts of Chemical Research* **1998**, *31*, (7), 387-396.
189. Johnson, D.; Marston, G., The gas-phase ozonolysis of unsaturated volatile organic compounds in the troposphere. *Chemical Society Reviews* **2008**, *37*, (4), 699-716.
190. Li, J.; Sun, Y.; Cao, H.; Han, D.; He, M., Mechanisms and kinetics of the ozonolysis reaction of cis-3-hexenyl acetate and trans-2-hexenyl acetate in atmosphere: a theoretical study. *Structural Chemistry* **2014**, *25*, (1), 71-83.
191. Li, J. J., Criegee mechanism of ozonolysis. In *Name Reactions: A Collection of Detailed Mechanisms and Synthetic Applications*, Springer Berlin Heidelberg: Berlin, Heidelberg, 2009; pp 161-161.
192. Harvey, R. M.; Zahardis, J.; Petrucci, G. A., Establishing the contribution of lawn mowing to atmospheric aerosol levels in American suburbs. *Atmos. Chem. Phys.* **2014**, *14*, (2), 797-812.
193. Jain, S.; Zahardis, J.; Petrucci, G. A., Soft Ionization Chemical Analysis of Secondary Organic Aerosol from Green Leaf Volatiles Emitted by Turf Grass. *Environmental Science & Technology* **2014**, *48*, (9), 4835-4843.
194. O'Dwyer, M. A.; Carey, T. J.; Healy, R. M.; Wenger, J. C.; Picquet-Varrault, B.; Doussin, J. F., The gas-phase ozonolysis of 1-penten-3-ol, (z)-2-penten-1-ol and 1-penten-3-one: kinetics, products and secondary organic aerosol formation. *Z. Phys. Chemie-Int. J. Res. Phys. Chem. Chem. Phys.* **2010**, *224*, (7-8), 1059-1080.

195. Grosjean, E.; Grosjean, D., The Gas Phase Reaction of Unsaturated Oxygenates with Ozone: Carbonyl Products and Comparison with the Alkene-Ozone Reaction. *Journal of Atmospheric Chemistry* **1997**, *27*, (3), 271-289.
196. Grosjean, D.; Grosjean, E., Carbonyl products of the ozone-unsaturated alcohol reaction. *J. Geophys. Res.-Atmos.* **1995**, *100*, (D11), 22815-22820.
197. Uchida, R.; Sato, K.; Imamura, T., Gas-phase Ozone Reactions with Z-3-Hexenal and Z-3-Hexen-1-ol: Formation Yields of OH Radical, Propanal, and Ethane. *Chem. Lett.* **2015**, *44*, (4), 457-458.
198. Grosjean, E.; Grosjean, D.; Seinfeld, J. H., Gas-phase reaction of ozone with trans-2-hexenal, trans-2-hexenyl acetate, ethylvinyl ketone, and 6-methyl-5-hepten-2-one. *Int. J. Chem. Kinet.* **1996**, *28*, (5), 373-382.
199. Fantechi, G.; Jensen, N. R.; Saastad, O.; Hjorth, J.; Peeters, J., Reactions of Cl Atoms with Selected VOCs: Kinetics, Products and Mechanisms. *Journal of Atmospheric Chemistry* **1998**, *31*, (3), 247-267.
200. Rodríguez, A.; Rodríguez, D.; Garzón, A.; Soto, A.; Aranda, A.; Notario, A., Kinetics and mechanism of the atmospheric reactions of atomic chlorine with 1-penten-3-ol and (Z)-2-penten-1-ol: an experimental and theoretical study. *Phys. Chem. Chem. Phys.* **2010**, *12*, (38), 12245-12258.
201. Zhang, W. C.; Zhang, D. J., Theoretical investigation of the oxidation pathways of the Cl-initiated reaction of 2-methyl-3-buten-2-ol. *Molecular Physics* **2012**, *110*, (23), 2901-2917.
202. Rodríguez, A.; Rodríguez, D.; Garzón, A.; Soto, A.; Aranda, A.; Notario, A., Kinetics and mechanism of the atmospheric reactions of atomic chlorine with 1-penten-3-ol and (Z)-2-penten-1-ol: an experimental and theoretical study. *Physical Chemistry Chemical Physics* **2010**, *12*, (38), 12245-12258.
203. Gaona-Colman, E.; Blanco, M. B.; Teruel, M. A., Kinetics and product identification of the reactions of (E)-2-hexenyl acetate and 4-methyl-3-penten-2-one with OH radicals and Cl atoms at 298 K and atmospheric pressure. *Atmos. Environ.* **2017**, *161*, 155-166.
204. O'Connor, M. P.; Wenger, J. C.; Mellouki, A.; Wirtz, K.; Munoz, A., The atmospheric photolysis of E-2-hexenal, Z-3-hexenal and E,E-2,4-hexadienal. *Physical Chemistry Chemical Physics* **2006**, *8*, (44), 5236-5246.
205. Tang, Y.; Zhu, L., Wavelength-Dependent Photolysis of n-Hexanal and n-Heptanal in the 280–330-nm Region. *The Journal of Physical Chemistry A* **2004**, *108*, (40), 8307-8316.
206. Imamura, T.; Iida, Y.; Obi, K.; Nagatani, I.; Nakagawa, K.; Patroescu-Klotz, I.; Hatakeyama, S., Rate coefficients for the gas-phase reactions of OH radicals with methylbutenols at 298 K. *International Journal of Chemical Kinetics* **2004**, *36*, (7), 379-385.
207. Priya, A. M.; Senthilkumar, L., Reaction of OH radical and ozone with methyl salicylate – a DFT study. *Journal of Physical Organic Chemistry* **2015**, *28*, (8), 542-553.
208. Gai, Y. B.; Lin, X. X.; Ma, Q.; Hu, C. J.; Gu, X. J.; Zhao, W. X.; Fang, B.; Zhang, W. J.; Long, B.; Long, Z. W., Experimental and Theoretical Study of Reactions of OH Radicals with Hexenols: An Evaluation of the Relative Importance of the H-Abstraction Reaction Channel. *Environ. Sci. Technol.* **2015**, *49*, (17), 10380-10388.
209. Albaladejo, J.; Ballesteros, B.; Jiménez, E.; Martín, P.; Martínez, E., A PLP-LIF kinetic study of the atmospheric reactivity of a series of C4–C7 saturated and unsaturated aliphatic aldehydes with OH. *Atmospheric Environment* **2002**, *36*, (20), 3231-3239.
210. Grosjean, D.; Williams, E. L., Environmental persistence of organic compounds estimated from structure-reactivity and linear free-energy relationships. Unsaturated aliphatics. *Atmospheric Environment. Part A. General Topics* **1992**, *26*, (8), 1395-1405.

211. Aschmann, S. M.; Atkinson, R., Kinetics of the gas-phase reactions of the OH radical with selected glycol ethers, glycols, and alcohols. *Int. J. Chem. Kinet.* **1998**, *30*, (8), 533-540.
212. Peirone, S. A.; Barrera, J. A.; Taccone, R. A.; Cometto, P. M.; Lane, S. I., Relative rate coefficient measurements of OH radical reactions with (Z)-2-hexen-1-ol and (E)-3-hexen-1-ol under simulated atmospheric conditions. *Atmospheric Environment* **2014**, *85*, 92-98.
213. Gai, Y.; Lin, X.; Ma, Q.; Hu, C.; Gu, X.; Zhao, W.; Fang, B.; Zhang, W.; Long, B.; Long, Z., Experimental and Theoretical Study of Reactions of OH Radicals with Hexenols: An Evaluation of the Relative Importance of the H-Abstraction Reaction Channel. *Environmental Science & Technology* **2015**, *49*, (17), 10380-10388.
214. Gibilisco, R. G.; Santiago, A. N.; Teruel, M. A., OH-initiated degradation of a series of hexenols in the troposphere. Rate coefficients at 298 K and 1 atm. *Atmospheric Environment* **2013**, *77*, 358-364.
215. Gao, T. T.; Andino, J. M.; Rivera, C. C.; Marquez, M. F., Rate Constants of the Gas-Phase Reactions of OH Radicals with trans-2-Hexenal, trans-2-Octenal, and trans-2-Nonenal. *Int. J. Chem. Kinet.* **2009**, *41*, (7), 483-489.
216. Xing, J.-H.; Ono, M.; Kuroda, A.; Obi, K.; Sato, K.; Imamura, T., Kinetic Study of the Daytime Atmospheric Fate of (Z)-3-Hexenal. *The Journal of Physical Chemistry A* **2012**, *116*, (33), 8523-8529.
217. Davis, M. E.; Burkholder, J. B., Rate coefficients for the gas-phase reaction of OH with (Z)-3-hexen-1-ol, 1-penten-3-ol, (E)-2-penten-1-ol, and (E)-2-hexen-1-ol between 243 and 404 K. *Atmos. Chem. Phys.* **2011**, *11*, (7), 3347-3358.
218. Jiménez, E.; Lanza, B.; Antiñolo, M.; Albaladejo, J., Photooxidation of leaf-wound oxygenated compounds, 1-penten-3-ol, (Z)-3-hexen-1-ol, and 1-penten-3-one, initiated by OH radicals and sunlight. *Environmental Science & Technology* **2009**, *43*, (6), 1831-1837.
219. Jiménez, E.; Lanza, B.; Martínez, E.; Albaladejo, J., Daytime tropospheric loss of hexanal and <I>trans</I>-2-hexenal: OH kinetics and UV photolysis. *Atmos. Chem. Phys.* **2007**, *7*, (6), 1565-1574.
220. Zhao, Z. J.; Husainy, S.; Smith, G. D., Kinetics studies of the gas-phase reactions of NO₃ radicals with series of 1-alkenes, dienes, cycloalkenes, alkenols, and alkenals. *J. Phys. Chem. A* **2011**, *115*, (44), 12161-12172.
221. Pfrang, C.; Martin, R.; Canosa-Mas, C.; Wayne, R., Gas-phase reactions of NO₃ and N₂O₅ with (Z)-hex-4-en-1-ol, (Z)-hex-3-en-1-ol ('leaf alcohol'), (E)-hex-3-en-1-ol, (Z)-hex-2-en-1-ol and (E)-hex-2-en-1-ol. *Physical chemistry chemical physics : PCCP* **2006**, *8*, 354-63.
222. Cabañas, B.; Salgado, S.; Martín, P.; Baeza, M. T.; Martínez, E., Night-time Atmospheric Loss Process for Unsaturated Aldehydes: Reaction with NO₃ Radicals. *The Journal of Physical Chemistry A* **2001**, *105*, (18), 4440-4445.
223. Grosjean, E.; Grosjean, D., Rate constants for the gas-phase reactions of ozone with unsaturated aliphatic-alcohols. *International Journal of Chemical Kinetics* **1994**, *26*, (12), 1185-1191.
224. Lin, X.; Ma, Q.; Yang, C.; Tang, X.; Zhao, W.; Hu, C.; Gu, X.; Fang, B.; Gai, Y.; Zhang, W., Kinetics and mechanisms of gas phase reactions of hexenols with ozone. *RSC Advances* **2016**, *6*, (87), 83573-83580.
225. Gibilisco, R. G.; Bejan, I.; Barnes, I.; Wiesen, P.; Teruel, M. A., FTIR gas kinetic study of the reactions of ozone with a series of hexenols at atmospheric pressure and 298 K. *Chem. Phys. Lett.* **2015**, *618*, 114-118.
226. Kalalian, C.; El Dib, G.; Singh, H. J.; Rao, P. K.; Roth, E.; Chakir, A., Temperature dependent kinetic study of the gas phase reaction of ozone with 1-penten-3-ol, cis-2-penten-1-ol and trans-3-hexen-1-ol: Experimental and theoretical data. *Atmospheric Environment* **2020**, *223*, 117306.

227. Kalalian, C.; Roth, E.; Chakir, A., Rate Coefficients for the Gas-Phase Reaction of Ozone with C5 and C6 Unsaturated Aldehydes. *Int. J. Chem. Kinet.* **2018**, *50*, (1), 47-56.
228. Grira, A.; Amarandei, C.; Romanias, M. N.; El Dib, G.; Canosa, A.; Arsene, C.; Bejan, I. G.; Olariu, R. I.; Coddeville, P.; Tomas, A., Kinetic Measurements of Cl Atom Reactions with C5–C8 Unsaturated Alcohols. *Atmosphere* **2020**, *11*, (3), 256.
229. Rodriguez, D.; Rodriguez, A.; Notario, A.; Aranda, A.; Diaz-de-Mera, Y.; Martinez, E., Kinetic study of the gas-phase reaction of atomic chlorine with a series of aldehydes. *Atmos. Chem. Phys.* **2005**, *5*, 3433-3440.
230. Teruel, M. A.; Achad, M.; Blanco, M. B., Kinetic study of the reactions of Cl atoms with alpha,beta-unsaturated carbonyl compounds at atmospheric pressure and structure activity relations (SARs). *Chem. Phys. Lett.* **2009**, *479*, (1-3), 25-29.
231. Kaiser, E. W.; Wallington, T. J.; Hurley, M. D., Products and Mechanism of the Reaction of Chlorine Atoms with 3-Pentanone in 700-950 Torr of N-2/O-2 Diluent at 297-515 K. *J. Phys. Chem. A* **2010**, *114*, (1), 343-354.
232. Gibilisco, R. G.; Bejan, I.; Barnes, I.; Wiesen, P.; Teruel, M. A., Rate coefficients at 298 K and 1 atm for the tropospheric degradation of a series of C6, C7 and C8 biogenic unsaturated alcohols initiated by Cl atoms. *Atmospheric Environment* **2014**, *94*, 564-572.
233. Cuevas, C. A.; Notario, A.; Martinez, E.; Albaladejo, J., Temperature-dependence study of the gas-phase reactions of atmospheric Cl atoms with a series of aliphatic aldehydes. *Atmos. Environ.* **2006**, *40*, (21), 3845-3854.
234. Rodríguez, A.; Rodríguez, D.; Soto, A.; Notario, A.; Aranda, A.; Díaz-de-Mera, Y.; Bravo, I., Relative rate measurements of reactions of unsaturated alcohols with atomic chlorine as a function of temperature. *Atmospheric Environment* **2007**, *41*, (22), 4693-4702.
235. Priya, A. M.; Senthilkumar, L., Degradation of methyl salicylate through Cl initiated atmospheric oxidation – a theoretical study. *RSC Advances* **2014**, *4*, (45), 23464-23475.
236. Rudich, Y.; Talukdar, R.; Burkholder, J. B.; Ravishankara, A. R., Reaction of Methylbutenol with the OH Radical: Mechanism and Atmospheric Implications. *The Journal of Physical Chemistry* **1995**, *99*, (32), 12188-12194.
237. Ren, Y. G.; McGillen, M. R.; Daele, V.; Casas, J.; Mellouk, A., The fate of methyl salicylate in the environment and its role as signal in multitrophic interactions. *Sci. Total Environ.* **2020**, *749*.
238. Kalalian, C.; Samir, B.; Roth, E.; Chakir, A., UV absorption spectra of trans-2-pentenal, trans-2-hexenal and 2-methyl-2-pentenal. *Chem. Phys. Lett.* **2019**, *718*, 22-26.
239. Richards-Henderson, N. K.; Pham, A. T.; Kirk, B. B.; Anastasio, C., Secondary organic aerosol from aqueous reactions of green leaf volatiles with organic triplet excited states and singlet molecular oxygen. *Environmental Science & Technology* **2015**, *49*, (1), 268-276.
240. Heath, A.; Valsaraj, K. T., An experimental study of the atmospheric oxidation of a biogenic organic compound (methyl jasmonate) in a thin water film as in fog or aerosols. *Open Journal of Air Pollution* **2017**, *6*, 44-51.
241. Liyana-Arachchi, T. P.; Stevens, C.; Hansel, A. K.; Ehrenhauser, F. S.; Valsaraj, K. T.; Hung, F. R., Molecular simulations of green leaf volatiles and atmospheric oxidants on air/water interfaces. *Physical Chemistry Chemical Physics* **2013**, *15*, (10), 3583-3592.
242. Wach, P.; Spolnik, G.; Rudzinski, K. J.; Skotak, K.; Claeys, M.; Danikiewicz, W.; Szmigielski, R., Radical oxidation of methyl vinyl ketone and methacrolein in aqueous droplets: Characterization of organosulfates and atmospheric implications. *Chemosphere* **2019**, *214*, 1-9.

243. Shalamzari, M. S.; Vermeylen, R.; Blockhuys, F.; Kleindienst, T. E.; Lewandowski, M.; Szmigielski, R.; Rudzinski, K. J.; Spolnik, G.; Danikiewicz, W.; Maenhaut, W.; Claeys, M., Characterization of polar organosulfates in secondary organic aerosol from the unsaturated aldehydes 2-E-pentenal, 2-E-hexenal, and 3-Z-hexenal. *Atmos. Chem. Phys.* **2016**, *16*, (11), 7135-7148.
244. Ren, H.; Sedlak, J. A.; Elrod, M. J., General Mechanism for Sulfate Radical Addition to Olefinic Volatile Organic Compounds in Secondary Organic Aerosol. *Environmental Science & Technology* **2021**, *55*, (3), 1456-1465.
245. Hansel, A. K. Reaction of green leaf volatiles as a source of secondary organic aerosols in fog droplets. LSU Master's Theses. 497, 2013.
246. Barbosa, T. S.; Riva, M.; Chen, Y. Z.; da Silva, C. M.; Ameida, J. C. S.; Zhang, Z.; Gold, A.; Arbilla, G.; Bauerfeldt, G. F.; Surratt, J. D., Chemical characterization of organosulfates from the hydroxyl radical-initiated oxidation and ozonolysis of cis-3-hexen-1-ol. *Atmos. Environ.* **2017**, *162*, 141-151.
247. Hamilton, J. F.; Lewis, A. C.; Carey, T. J.; Wenger, J. C., Characterization of polar compounds and oligomers in secondary organic aerosol using liquid chromatography coupled to mass spectrometry. *Anal. Chem.* **2008**, *80*, (2), 474-480.
248. Novelli, A.; Kaminski, M.; Rolletter, M.; Acir, I. H.; Bohn, B.; Dorn, H. P.; Li, X.; Lutz, A.; Nehr, S.; Rohrer, F.; Tillmann, R.; Wegener, R.; Holland, F.; Hofzumahaus, A.; Kiendler-Scharr, A.; Wahner, A.; Fuchs, H., Evaluation of OH and HO₂ concentrations and their budgets during photooxidation of 2-methyl-3-butene-2-ol (MBO) in the atmospheric simulation chamber SAPHIR. *Atmos. Chem. Phys.* **2018**, *18*, (15), 11409-11422.
249. Jaoui, M.; Kleindienst, T. E.; Offenberg, J. H.; Lewandowski, M.; Lonneman, W. A., SOA formation from the atmospheric oxidation of 2-methyl-3-buten-2-ol and its implications for PM_{2.5}. *Atmos. Chem. Phys.* **2012**, *12*, (4), 2173-2188.
250. Chan, A. W. H.; Galloway, M. M.; Kwan, A. J.; Chhabra, P. S.; Keutsch, F. N.; Wennberg, P. O.; Flagan, R. C.; Seinfeld, J. H., Photooxidation of 2-Methyl-3-Buten-2-ol (MBO) as a Potential Source of Secondary Organic Aerosol. *Environmental Science & Technology* **2009**, *43*, (13), 4647-4652.
251. Mael, L. E.; Jacobs, M. I.; Elrod, M. J., Organosulfate and Nitrate Formation and Reactivity from Epoxides Derived from 2-Methyl-3-buten-2-ol. *J Phys Chem A* **2015**, *119*, (19), 4464-72.
252. Lewandowski, M.; Piletic, I. R.; Kleindienst, T. E.; Offenberg, J. H.; Beaver, M. R.; Jaoui, M.; Docherty, K. S.; Edney, E. O., Secondary organic aerosol characterisation at field sites across the United States during the spring–summer period. *International Journal of Environmental Analytical Chemistry* **2013**, *93*, (10), 1084-1103.
253. Edney, E. O.; Kleindienst, T. E.; Conner, T. S.; McIver, C. D.; Corse, E. W.; Weathers, W. S., Polar organic oxygenates in PM_{2.5} at a southeastern site in the United States. *Atmospheric Environment* **2003**, *37*, (28), 3947-3965.
254. Hettiyadura, A. P. S.; Al-Naiema, I. M.; Hughes, D. D.; Fang, T.; Stone, E. A., Organosulfates in Atlanta, Georgia: anthropogenic influences on biogenic secondary organic aerosol formation. *Atmos. Chem. Phys.* **2019**, *19*, (5), 3191-3206.
255. Hansen, A. M. K.; Kristensen, K.; Nguyen, Q. T.; Zare, A.; Cozzi, F.; Nøjgaard, J. K.; Skov, H.; Brandt, J.; Christensen, J. H.; Ström, J.; Tunved, P.; Krejci, R.; Glasius, M., Organosulfates and organic acids in Arctic aerosols: speciation, annual variation and concentration levels. *Atmos. Chem. Phys.* **2014**, *14*, (15), 7807-7823.
256. Nguyen, Q. T.; Christensen, M. K.; Cozzi, F.; Zare, A.; Hansen, A. M. K.; Kristensen, K.; Tulinius, T. E.; Madsen, H. H.; Christensen, J. H.; Brandt, J.; Massling, A.; Nøjgaard, J. K.; Glasius, M.,

- Understanding the anthropogenic influence on formation of biogenic secondary organic aerosols in Denmark via analysis of organosulfates and related oxidation products. *Atmos. Chem. Phys.* **2014**, *14*, (17), 8961-8981.
257. Kristensen, K.; Bilde, M.; Aalto, P. P.; Petaja, T.; Glasius, M., Denuder/filter sampling of organic acids and organosulfates at urban and boreal forest sites: Gas/particle distribution and possible sampling artifacts. *Atmospheric Environment* **2016**, *130*, 36-53.
258. Hettiyadura, A. P. S.; Stone, E. A.; Kundu, S.; Baker, Z.; Geddes, E.; Richards, K.; Humphry, T., Determination of atmospheric organosulfates using HILIC chromatography with MS detection. *Atmos. Meas. Tech.* **2015**, *8*, (6), 2347-2358.
259. Hettiyadura, A. P. S.; Jayarathne, T.; Baumann, K.; Goldstein, A. H.; de Gouw, J. A.; Koss, A.; Keutsch, F. N.; Skog, K.; Stone, E. A., Qualitative and quantitative analysis of atmospheric organosulfates in Centreville, Alabama. *Atmospheric Chemistry and Physics* **2017**, *17*, (2), 1343-1359.
260. Wang, Y.; Hu, M.; Guo, S.; Wang, Y.; Zheng, J.; Yang, Y.; Zhu, W.; Tang, R.; Li, X.; Liu, Y.; Le Breton, M.; Du, Z.; Shang, D.; Wu, Y.; Wu, Z.; Song, Y.; Lou, S.; Hallquist, M.; Yu, J., The secondary formation of organosulfates under interactions between biogenic emissions and anthropogenic pollutants in summer in Beijing. *Atmos. Chem. Phys.* **2018**, *18*, (14), 10693-10713.
261. Huang, R. J.; Cao, J.; Chen, Y.; Yang, L.; Shen, J.; You, Q.; Wang, K.; Lin, C.; Xu, W.; Gao, B.; Li, Y.; Chen, Q.; Hoffmann, T.; O'Dowd, C. D.; Bilde, M.; Glasius, M., Organosulfates in atmospheric aerosol: synthesis and quantitative analysis of PM_{2.5} from Xi'an, northwestern China. *Atmos. Meas. Tech.* **2018**, *11*, (6), 3447-3456.
262. Le Breton, M.; Wang, Y.; Hallquist, Å. M.; Pathak, R. K.; Zheng, J.; Yang, Y.; Shang, D.; Glasius, M.; Bannan, T. J.; Liu, Q.; Chan, C. K.; Percival, C. J.; Zhu, W.; Lou, S.; Topping, D.; Wang, Y.; Yu, J.; Lu, K.; Guo, S.; Hu, M.; Hallquist, M., Online gas- and particle-phase measurements of organosulfates, organosulfonates and nitrooxy organosulfates in Beijing utilizing a FIGAERO ToF-CIMS. *Atmos. Chem. Phys.* **2018**, *18*, (14), 10355-10371.
263. Olson, C. N.; Galloway, M. M.; Yu, G.; Hedman, C. J.; Lockett, M. R.; Yoon, T.; Stone, E. A.; Smith, L. M.; Keutsch, F. N., Hydroxycarboxylic Acid-Derived Organosulfates: Synthesis, Stability, and Quantification in Ambient Aerosol. *Environmental Science & Technology* **2011**, *45*, (15), 6468-6474.
264. Hughes, D. D.; Christiansen, M. B.; Milani, A.; Vermeuel, M. P.; Novak, G. A.; Alwe, H. D.; Dickens, A. F.; Pierce, R. B.; Millet, D. B.; Bertram, T. H.; Stanier, C. O.; Stone, E. A., PM_{2.5} chemistry, organosulfates, and secondary organic aerosol during the 2017 Lake Michigan Ozone Study. *Atmospheric Environment* **2021**, *244*, 117939.
265. Safi Shalamzari, M.; Ryabtsova, O.; Kahnt, A.; Vermeylen, R.; Hérent, M.-F.; Quetin-Leclercq, J.; Van der Veken, P.; Maenhaut, W.; Claeys, M., Mass spectrometric characterization of organosulfates related to secondary organic aerosol from isoprene. *Rapid Communications in Mass Spectrometry* **2013**, *27*, (7), 784-794.
266. Brüggemann, M.; Xu, R.; Tilgner, A.; Kwong, K. C.; Mutzel, A.; Poon, H. Y.; Otto, T.; Schaefer, T.; Poulain, L.; Chan, M. N.; Herrmann, H., Organosulfates in Ambient Aerosol: State of Knowledge and Future Research Directions on Formation, Abundance, Fate, and Importance. *Environmental Science & Technology* **2020**, *54*, (7), 3767-3782.
267. Tolocka, M. P.; Turpin, B., Contribution of Organosulfur Compounds to Organic Aerosol Mass. *Environ. Sci. Technol.* **2012**, *46*, (15), 7978-7983.
268. Zhang, H.; Worton, D. R.; Lewandowski, M.; Ortega, J.; Rubitschun, C. L.; Park, J.-H.; Kristensen, K.; Campuzano-Jost, P.; Day, D. A.; Jimenez, J. L.; Jaoui, M.; Offenberg, J. H.; Kleindienst, T. E.;

- Gilman, J.; Kuster, W. C.; de Gouw, J.; Park, C.; Schade, G. W.; Frossard, A. A.; Russell, L.; Kaser, L.; Jud, W.; Hansel, A.; Cappellin, L.; Karl, T.; Glasius, M.; Guenther, A.; Goldstein, A. H.; Seinfeld, J. H.; Gold, A.; Kamens, R. M.; Surratt, J. D., Organosulfates as Tracers for Secondary Organic Aerosol (SOA) Formation from 2-Methyl-3-Buten-2-ol (MBO) in the Atmosphere. *Environmental Science & Technology* **2012**, *46*, (17), 9437-9446.
269. Shalamzari, M. S.; Kahnt, A.; Vermeylen, R.; Kleindienst, T. E.; Lewandowski, M.; Cuyckens, F.; Maenhaut, W.; Claeys, M., Characterization of polar organosulfates in secondary organic aerosol from the green leaf volatile 3-Z-hexenal. *Environ. Sci. Technol.* **2014**, *48*, (21), 12671-12678.
270. Eller, A. S. D.; Sekimoto, K.; Gilman, J. B.; Kuster, W. C.; de Gouw, J. A.; Monson, R. K.; Graus, M.; Crespo, E.; Warneke, C.; Fall, R., Volatile organic compound emissions from switchgrass cultivars used as biofuel crops. *Atmos. Environ.* **2011**, *45*, (19), 3333-3337.
271. White, R. P.; Murray, S.; Rohweder, M., Grassland Ecosystems. In World Research Institute: 2000.
272. Kang, S.; Nair, S. S.; Kline, K. L.; Nichols, J. A.; Wang, D.; Post, W. M.; Brandt, C. C.; Wullschlegel, S. D.; Singh, N.; Wei, Y., Global simulation of bioenergy crop productivity: analytical framework and case study for switchgrass. *GCB Bioenergy* **2014**, *6*, (1), 14-25.
273. Herrmann, H., Kinetics of aqueous phase reactions relevant for atmospheric chemistry. *Chem. Rev.* **2003**, *103*, (12), 4691-4716.
274. Herrmann, H., On the photolysis of simple anions and neutral molecules as sources of O-/OH, SO_x- and Cl in aqueous solution. *Phys. Chem. Chem. Phys.* **2007**, *9*, (30), 3935-3964.
275. Orzel, L.; Janczyk, A.; Brindell, M.; Stopa, G.; Stochel, G., New trends in the application of laser flash photolysis - case studies. *J. Coord. Chem.* **2010**, *63*, (14-16), 2695-2714.
276. C. Knowles, A. K., *Practical Absorption Spectrometry*. 1 ed.; Springer, Dordrecht: p XXII, 234.
277. Geiger, C. A.; Beran, A.; Libowitzky, E., An introduction to spectroscopic methods in the mineral sciences and geochemistry. In *Spectroscopic methods in mineralogy*, Mineralogical Society of Great Britain and Ireland: 2004; Vol. 6, p 0.
278. Pietrzyk, D. J.; Frank, C. W., Chapter Eighteen - Qualitative Analysis: Ultraviolet, Visible, and Infrared. In *Anal. Chem.*, Pietrzyk, D. J.; Frank, C. W., Eds. Academic Press: 1979; pp 410-424.
279. Owen, T., *Fundamentals of modern UV-visible spectroscopy Primer*. Agilent Technologies
280. Jones, W. J., LASERS. *Quarterly Reviews* **1969**, *23*, (1), 73-+.
281. Kovalenko, L. J.; Leone, S. R., Innovative laser techniques in chemical-kinetics - a pedagogical survey. *J. Chem. Educ.* **1988**, *65*, (8), 681-687.
282. Shields, D. J.; Chakraborty, M.; Abdelaziz, N.; Duley, A.; Gudmundsdottir, A. D., Review of laser flash photolysis of organic molecules (2015-2018). In *Photochemistry, Vol 47*, Albini, A.; Protti, S., Eds. Royal Soc Chemistry: Cambridge, 2020; Vol. 47, pp 70-121.
283. Porter, G., Flash photolysis and spectroscopy a new method for the study of free radical reactions *Proceedings of the Royal Society of London Series a-Mathematical and Physical Sciences* **1950**, *200*, (1061), 284-&.
284. Zewail, A. H., Laser femtochemistry. *Science* **1988**, *242*, (4886), 1645-1653.
285. Hutchinson, M. H. R., Excimer Lasers. In *Tunable Lasers*, Mollenauer, L. F.; White, J. C., Eds. Springer Berlin Heidelberg: Berlin, Heidelberg, 1987; pp 19-56.
286. Nakamura, S., InGaN-based laser diodes. *Annu. Rev. Mater. Sci.* **1998**, *28*, 125-152.
287. Nasim, H.; Jamil, Y., Recent advancements in spectroscopy using tunable diode lasers. *Laser Phys. Lett.* **2013**, *10*, (4), 14.

288. Kravtsov, N. V., Basic trends in the development of diode-pumped solid-state lasers. *Quantum Electron.* **2001**, *31*, (8), 661-677.
289. Woodruff, W. H., Lasers, laser spectroscopy, and laser chemistry. *ACS Symp. Ser.* **1983**, *211*, 473-508.
290. Otto, T.; Stieger, B.; Mettke, P.; Herrmann, H., Tropospheric aqueous-phase oxidation of isoprene-derived dihydroxycarbonyl compounds. *J. Phys. Chem. A* **2017**, *121*, (34), 6460-6470.
291. Schaefer, T.; Schindelka, J.; Hoffmann, D.; Herrmann, H., Laboratory Kinetic and Mechanistic Studies on the OH-Initiated Oxidation of Acetone in Aqueous Solution. *J. Phys. Chem. A* **2012**, *116*, (24), 6317-6326.
292. Ervens, B.; Gligorovski, S.; Herrmann, H., Temperature-dependent rate constants for hydroxyl radical reactions with organic compounds in aqueous solutions. *Phys. Chem. Chem. Phys.* **2003**, *5*, (9), 1811-1824.
293. Hoffmann, D.; Weigert, B.; Barzaghi, P.; Herrmann, H., Reactivity of poly-alcohols towards OH, NO₃ and SO₄⁻ in aqueous solution. *Phys. Chem. Chem. Phys.* **2009**, *11*, (41), 9351-9363.
294. Schaefer, T.; van Pinxteren, D.; Herrmann, H., Multiphase Chemistry of Glyoxal: Revised Kinetics of the Alkyl Radical Reaction with Molecular Oxygen and the Reaction of Glyoxal with OH, NO₃, and SO₄⁻ in Aqueous Solution. *Environ. Sci. Technol.* **2015**, *49*, (1), 343-350.
295. Schaefer, T.; Herrmann, H., Competition kinetics of OH radical reactions with oxygenated organic compounds in aqueous solution: rate constants and internal optical absorption effects. *Phys. Chem. Chem. Phys.* **2018**, *20*, (16), 10939-10948.
296. Otto, T.; Schaefer, T.; Herrmann, H., Aqueous-Phase Oxidation of Terpene-Derived Acids by Atmospherically Relevant Radicals. *J. Phys. Chem. A* **2018**, *122*, (47), 9233-9241.
297. Schone, L.; Schindelka, J.; Szeremeta, E.; Schaefer, T.; Hoffmann, D.; Rudzinski, K. J.; Szmigielski, R.; Herrmann, H., Atmospheric aqueous phase radical chemistry of the isoprene oxidation products methacrolein, methyl vinyl ketone, methacrylic acid and acrylic acid - kinetics and product studies. *Phys. Chem. Chem. Phys.* **2014**, *16*, (13), 6257-6272.
298. Sarang, K.; Otto, T.; Rudzinski, K.; Schaefer, T.; Grgic, I.; Nestorowicz, K.; Herrmann, H.; Szmigielski, R., Reaction Kinetics of Green Leaf Volatiles with Sulfate, Hydroxyl, and Nitrate Radicals in Tropospheric Aqueous Phase. *Environ. Sci. Technol.* **2021**, *55*, (20), 13666-13676.
299. Pacot, G. M. M.; Lee, L. M.; Chin, S. T.; Marriott, P. J., Introducing Students to Gas Chromatography-Mass Spectrometry Analysis and Determination of Kerosene Components in a Complex Mixture. *J. Chem. Educ.* **2016**, *93*, (4), 742-746.
300. Stauffer, E., Gas Chromatography-Mass Spectrometry. In *Materials Analysis in Forensic Science*, Houck, M. M., Ed. Elsevier Academic Press Inc: San Diego, 2016; pp 115-122.
301. Leemans, F. A. J.; McCloske, J., Combination gas chromatography-mass spectrometry. *J. Am. Oil Chem. Soc.* **1967**, *44*, (1), 11-&.
302. Jaoui, M.; Corse, E.; Kleindienst, T. E.; Offenber, J. H.; Lewandowski, M.; Edney, E. O., Analysis of secondary organic aerosol compounds from the photooxidation of d-limonene in the presence of NO_x and their detection in ambient PM_{2.5}. *Environ. Sci. Technol.* **2006**, *40*, (12), 3819-3828.
303. Halket, J. M.; Zaikin, V. G., Derivatization in mass spectrometry - 1. Silylation. *European Journal of Mass Spectrometry* **2003**, *9*, (1), 1-21.
304. Blau, K.; Halket, J. M. In *Handbook of derivatives for chromatography*, 1978; 1978.
305. Marriott, P. J.; Carpenter, P. D., Capillary gas chromatography injection - An exercise for students of instrumental analysis. *J. Chem. Educ.* **1996**, *73*, (1), 96-99.

306. Gross, J. H., Practical Aspects of Electron Ionization. In *Mass Spectrometry: A Textbook*, Springer International Publishing: Cham, 2017; pp 293-324.
307. Gross, J. H., Chemical Ionization. In *Mass Spectrometry: A Textbook*, Springer International Publishing: Cham, 2017; pp 439-496.
308. Pratt, K. A.; Prather, K. A., Mass spectrometry of atmospheric aerosols—Recent developments and applications. Part I: Off-line mass spectrometry techniques. *Mass Spectrometry Reviews* **2012**, *31*, (1), 1-16.
309. Hübschmann, H.-J., *Handbook of GC-MS: Fundamentals and Applications*. 3rd ed.; John Wiley and Sons: 2015.
310. Gross, J. H., *Mass Spectrometry*. 3 ed.; Springer, Cham: Springer International Publishing AG, 2017; p XXV, 968.
311. Ardrey, R., *Liquid Chromatography - Mass Spectrometry: An Introduction*. 2003.
312. Vestal, M. L., High-performance liquid-chromatography mass-spectrometry. *Science* **1984**, *226*, (4672), 275-281.
313. Gross, J. H., Hyphenated Methods. In *Mass Spectrometry: A Textbook*, Springer International Publishing: Cham, 2017; pp 831-887.
314. Games, D. E., Combined high-performance liquid-chromatography mass-spectrometry. *Biomedical Mass Spectrometry* **1981**, *8*, (9), 454-462.
315. Ishii, D.; Takeuchi, T., New interfacing techniques for capillary high-performance liquid-chromatography mass-spectrometry *Trac-Trends Anal. Chem.* **1989**, *8*, (1), 25-29.
316. Karger, B. L.; Vouros, P., A chromatography perspective of high-performance liquid-chromatography mass spectrometry. *Journal of Chromatography* **1985**, *323*, (1), 13-32.
317. Fenn, J. B.; Mann, M.; Meng, C. K.; Wong, S. F.; Whitehouse, C. M., ELECTROSPRAY IONIZATION FOR MASS-SPECTROMETRY OF LARGE BIOMOLECULES. *Science* **1989**, *246*, (4926), 64-71.
318. Pitt, J. J., Principles and applications of liquid chromatography-mass spectrometry in clinical biochemistry. *Clin Biochem Rev* **2009**, *30*, (1), 19-34.
319. Tanaka, K.; Waki, H.; Ido, Y.; Akita, S.; Yoshida, Y.; Yoshida, T.; Matsuo, T., Protein and polymer analyses up to m/z 100 000 by laser ionization time-of-flight mass spectrometry. *Rapid Commun. Mass Spectrom.* **1988**, *2*, (8), 151-153.
320. Kebarle, P., A brief overview of the present status of the mechanisms involved in electrospray mass spectrometry. *J. Mass Spectrom.* **2000**, *35*, (7), 804-817.
321. Herderich, M.; Richling, E.; Roscher, R.; Schneider, C.; Schwab, W.; Humpf, H. U.; Schreier, P., Application of atmospheric pressure ionization HPLC-MS-MS for the analysis of natural products. *Chromatographia* **1997**, *45*, 127-132.
322. Byrdwell, W. C., Atmospheric pressure chemical ionization mass spectrometry for analysis of lipids. *Lipids* **2001**, *36*, (4), 327-346.
323. Rosenberg, E., The potential of organic (electrospray- and atmospheric pressure chemical ionisation) mass spectrometric techniques coupled to liquid-phase separation for speciation analysis. *J. Chromatogr. A* **2003**, *1000*, (1-2), 841-889.
324. Robb, D. B.; Covey, T. R.; Bruins, A. P., Atmospheric pressure photoionisation: An ionization method for liquid chromatography-mass spectrometry. *Anal. Chem.* **2000**, *72*, (15), 3653-3659.
325. Hanold, K. A.; Fischer, S. M.; Cormia, P. H.; Miller, C. E.; Syage, J. A., Atmospheric pressure photoionization. 1. General properties for LC/MS. *Anal. Chem.* **2004**, *76*, (10), 2842-2851.

326. Raffaelli, A.; Saba, A., Atmospheric pressure photoionization mass spectrometry. *Mass Spectrometry Reviews* **2003**, *22*, (5), 318-331.
327. Gross, J. H., Instrumentation. In *Mass Spectrometry: A Textbook*, Springer International Publishing: Cham, 2017; pp 151-292.
328. Hoffmann, E. d. S. V., *Mass spectrometry : principles and applications*. J. Wiley: Chichester, West Sussex, England; Hoboken, NJ, 2007.
329. Brunnee, C., New instrumentation in mass-spectrometry *Int. J. Mass Spectrom. Ion Process.* **1982**, *45*, (DEC), 51-86.
330. Chapman, J. R.; Errock, G. A.; Race, J. A., Science and technology in Manchester: The nurture of mass spectrometry. *Rapid Commun. Mass Spectrom.* **1997**, *11*, (14), 1575-1586.
331. Stephens, W. E., A pulsed mass spectrometer with time dispersion. *Physical Review* **1946**, *69*, (11-1), 691-691.
332. Wolff, M. M.; Stephens, W. E., A pulsed mass spectrometer with time dispersion. *Rev. Sci. Instrum.* **1953**, *24*, (8), 616-617.
333. Wiley, W. C.; McLaren, I. H., Time-of-flight mass spectrometer with improved resolution. *Rev. Sci. Instrum.* **1955**, *26*, (12), 1150-1157.
334. Cameron, A. E.; Eggers, D. F., An ion velocitron *Rev. Sci. Instrum.* **1948**, *19*, (9), 605-607.
335. Bristow, A. W. T., Accurate mass measurement for the determination of elemental formula - A tutorial. *Mass Spectrometry Reviews* **2006**, *25*, (1), 99-111.
336. Paul, W., Electromagnetic traps for charged and neutral particles. *Angewandte Chemie-International Edition in English* **1990**, *29*, (7), 739-748.
337. Paul, W.; Steinwedel, H., *Ein neues massenspektrometer ohne magnetfeld *Z. Naturfors. Sect. A-J. Phys. Sci.* **1953**, *8*, (7), 448-450.
338. Paul, W.; Raether, M., Das elektrische massenfilter. *Zeitschrift Fur Physik* **1955**, *140*, (3), 262-273.
339. Kingdon, K. H., A Method for the Neutralization of Electron Space Charge by Positive Ionization at Very Low Gas Pressures. *Physical Review* **1923**, *21*, (4), 408-418.
340. Hu, Q. Z.; Noll, R. J.; Li, H. Y.; Makarov, A.; Hardman, M.; Cooks, R. G., The Orbitrap: a new mass spectrometer. *J. Mass Spectrom.* **2005**, *40*, (4), 430-443.
341. Makarov, A., Electrostatic axially harmonic orbital trapping: A high-performance technique of mass analysis. *Anal. Chem.* **2000**, *72*, (6), 1156-1162.
342. Scigelova, M.; Makarov, A., Orbitrap mass analyzer - Overview and applications in proteomics. *Proteomics* **2006**, 16-21.
343. Eliuk, S.; Makarov, A., Evolution of Orbitrap Mass Spectrometry Instrumentation. In *Annual Review of Analytical Chemistry, Vol 8*, Cooks, R. G.; Pemberton, J. E., Eds. Annual Reviews: Palo Alto, 2015; Vol. 8, pp 61-80.
344. McLafferty, F. W., A Century of Progress in Molecular Mass Spectrometry. In *Annual Review of Analytical Chemistry, Vol 4*, Cooks, R. G.; Yeung, E. S., Eds. Annual Reviews: Palo Alto, 2011; Vol. 4, pp 1-22.
345. Johnston, M. V.; Kerecman, D. E., Molecular Characterization of Atmospheric Organic Aerosol by Mass Spectrometry. In *Annual Review of Analytical Chemistry, Vol 12*, Bohn, P. W.; Pemberton, J. E., Eds. Annual Reviews: Palo Alto, 2019; Vol. 12, pp 247-274.
346. Hamilton, J. F., Using Comprehensive Two-Dimensional Gas Chromatography to Study the Atmosphere. *J. Chromatogr. Sci.* **2010**, *48*, (4), 274+.

347. Welthagen, W.; Schnelle-Kreis, J.; Zimmermann, R., Search criteria and rules for comprehensive two-dimensional gas chromatography-time-of-flight mass spectrometry analysis of airborne particulate matter. *J. Chromatogr. A* **2003**, *1019*, (1-2), 233-249.
348. Kallio, M.; Hyotylainen, T.; Lehtonen, M.; Jussila, M.; Hartonen, K.; Shimmo, M.; Riekkola, M. L., Comprehensive two-dimensional gas chromatography in the analysis of urban aerosols. *J. Chromatogr. A* **2003**, *1019*, (1-2), 251-260.
349. Hamilton, J. F.; Webb, P. J.; Lewis, A. C.; Hopkins, J. R.; Smith, S.; Davy, P., Partially oxidised organic components in urban aerosol using GCXGC-TOF/MS. *Atmos. Chem. Phys.* **2004**, *4*, 1279-1290.
350. Ho, S. S. H.; Yu, J. Z.; Chow, J. C.; Zielinska, B.; Watson, J. G.; Sit, E. H. L.; Schauer, J. J., Evaluation of an in-injection port thermal desorption-gas chromatography/mass spectrometry method for analysis of non-polar organic compounds in ambient aerosol samples. *J. Chromatogr. A* **2008**, *1200*, (2), 217-227.
351. Goldstein, A. H.; Worton, D. R.; Williams, B. J.; Hering, S. V.; Kreisberg, N. M.; Panic, O.; Gorecki, T., Thermal desorption comprehensive two-dimensional gas chromatography for in-situ measurements of organic aerosols. *J. Chromatogr. A* **2008**, *1186*, (1-2), 340-347.
352. Gao, S.; Surratt, J. D.; Knipping, E. M.; Edgerton, E. S.; Shahgholi, M.; Seinfeld, J. H., Characterization of polar organic components in fine aerosols in the southeastern United States: Identity, origin, and evolution. *J. Geophys. Res.-Atmos.* **2006**, *111*, (D14), 27.
353. Surratt, J. D.; Kroll, J. H.; Kleindienst, T. E.; Edney, E. O.; Claeys, M.; Sorooshian, A.; Ng, N. L.; Offenberg, J. H.; Lewandowski, M.; Jaoui, M.; Flagan, R. C.; Seinfeld, J. H., Evidence for organosulfates in secondary organic aerosol. *Environ. Sci. Technol.* **2007**, *41*, (2), 517-527.
354. Lukacs, H.; Gelencser, A.; Hoffer, A.; Kiss, G.; Horvath, K.; Hartyani, Z., Quantitative assessment of organosulfates in size-segregated rural fine aerosol. *Atmos. Chem. Phys.* **2009**, *9*, (1), 231-238.
355. Spolnik, G.; Wach, P.; Rudzinski, K. J.; Skotak, K.; Danikiewicz, W.; Szmigielski, R., Improved UHPLC-MS/MS Methods for Analysis of Isoprene-Derived Organosulfates. *Anal. Chem.* **2018**, *90*, (5), 3416-3423.
356. Kitanovski, Z.; Grgic, I.; Yasmeeen, F.; Claeys, M.; Cusak, A., Development of a liquid chromatographic method based on ultraviolet-visible and electrospray ionization mass spectrometric detection for the identification of nitrocatechols and related tracers in biomass burning atmospheric organic aerosol. *Rapid Commun. Mass Spectrom.* **2012**, *26*, (7), 793-804.
357. Claeys, M.; Vermeylen, R.; Yasmeeen, F.; Gomez-Gonzalez, Y.; Chi, X. G.; Maenhaut, W.; Meszaros, T.; Salma, I., Chemical characterisation of humic-like substances from urban, rural and tropical biomass burning environments using liquid chromatography with UV/vis photodiode array detection and electrospray ionisation mass spectrometry. *Environ. Chem.* **2012**, *9*, (3), 273-284.
358. Roach, P. J.; Laskin, J.; Laskin, A., Nanospray desorption electrospray ionization: an ambient method for liquid-extraction surface sampling in mass spectrometry. *Analyst* **2010**, *135*, (9), 2233-2236.
359. Laskin, J.; Laskin, A.; Roach, P. J.; Slysz, G. W.; Anderson, G. A.; Nizkorodov, S. A.; Bones, D. L.; Nguyen, L. Q., High-Resolution Desorption Electrospray Ionization Mass Spectrometry for Chemical Characterization of Organic Aerosols. *Anal. Chem.* **2010**, *82*, (5), 2048-2058.
360. Roach, P. J.; Laskin, J.; Laskin, A., Molecular Characterization of Organic Aerosols Using Nanospray-Desorption/Electrospray Ionization-Mass Spectrometry. *Anal. Chem.* **2010**, *82*, (19), 7979-7986.
361. Takats, Z.; Wiseman, J. M.; Gologan, B.; Cooks, R. G., Mass spectrometry sampling under ambient conditions with desorption electrospray ionization. *Science* **2004**, *306*, (5695), 471-473.

362. Kind, T.; Fiehn, O., Seven Golden Rules for heuristic filtering of molecular formulas obtained by accurate mass spectrometry. *BMC Bioinformatics* **2007**, *8*, 20.
363. Laskin, J.; Laskin, A.; Nizkorodov, S. A., Mass Spectrometry Analysis in Atmospheric Chemistry. *Anal. Chem.* **2018**, *90*, (1), 166-189.
364. Pratt, K. A.; Prather, K. A., Mass spectrometry of atmospheric aerosols—Recent developments and applications. Part II: On-line mass spectrometry techniques. *Mass Spectrometry Reviews* **2012**, *31*, (1), 17-48.
365. McMurry, P. H., A review of atmospheric aerosol measurements. *Atmos. Environ.* **2000**, *34*, (12-14), 1959-1999.
366. Rudich, Y.; Donahue, N. M.; Mentel, T. F., Aging of organic aerosol: Bridging the gap between laboratory and field studies. In *Annu. Rev. Phys. Chem.*, Annual Reviews: Palo Alto, 2007; Vol. 58, pp 321-352.
367. Herrmann, H.; Hoffmann, D.; Schaefer, T.; Brauer, P.; Tilgner, A., Tropospheric Aqueous-Phase Free-Radical Chemistry: Radical Sources, Spectra, Reaction Kinetics and Prediction Tools. *ChemPhysChem* **2010**, *11*, (18), 3796-3822.
368. Chin, M.; Wine, P. H., A temperature-dependent kinetics study of the aqueous phase reactions $\text{OH} + \text{SCN}^- \rightarrow \text{SCNOH}^-$ and $\text{SCN} + \text{SCN}^- \rightleftharpoons (\text{SCN})_2^-$. *J. Photochem. Photobiol. A-Chem.* **1992**, *69*, (1), 17-25.
369. Nielsen, S. O.; Michael, B. D.; Hart, E. J., Ultraviolet-absorption spectra of e_{aq}^- , H, OH, D, and OD from pulse-radiolysis of aqueous-solutions. *J. Phys. Chem.* **1976**, *80*, (22), 2482-2488.
370. Behar, D.; Bevan, P. L. T.; Scholes, G., Pulse radiolysis of aqueous thiocyanate solutions. Nature of the intermediate transient species. *The Journal of Physical Chemistry* **1972**, *76*, (11), 1537-1542.
371. Zhu, L.; Nicovich, J. M.; Wine, P. H., Temperature-dependent kinetics studies of aqueous phase reactions of hydroxyl radicals with dimethylsulfoxide, dimethylsulfone, and methanesulfonate. *Aquat. Sci.* **2003**, *65*, (4), 425-435.
372. de Semainville, P. G.; Hoffmann, D.; George, C.; Herrmann, H., Study of nitrate radical (NO_3) reactions with carbonyls and acids in aqueous solution as a function of temperature. *Phys. Chem. Chem. Phys.* **2007**, *9*, (8), 958-968.
373. Herrmann, H. Photochemische Bildung, Spektroskopie und Kinetik freier Radikale in wässriger Lösung. University of Essen, 1998.
374. Elliot, A. J.; McCracken, D. R.; Buxton, G. V.; Wood, N. D., Estimation of rate constants for near-diffusion-controlled reactions in water at high-temperatures. *J. Chem. Soc.-Faraday Trans.* **1990**, *86*, (9), 1539-1547.
375. Smoluchowski, M. V., Versuch einer mathematischen Theorie der Koagulationskinetik kolloider Lösungen. *Z. Phys. Chem* **1918**, *XCII*, (92), 129-168.
376. Wilke, C. R.; Chang, P., Correlation of diffusion coefficients in dilute solutions. *Aiche J.* **1955**, *1*, (2), 264-270.
377. Kojima, H.; Bard, A. J., Determination of rate constants for electroreduction of aromatic-compounds and their correlation with homogeneous electron-transfer rates. *J. Am. Chem. Soc.* **1975**, *97*, (22), 6317-6324.
378. Buxton, G. V.; Greenstock, C. L.; Helman, W. P.; Ross, A. B., Critical-review of rate constants for reactions of hydrated electrons, hydrogen-atoms and hydroxyl radicals ($\cdot\text{OH}/\text{O}^-$) in aqueous-solution *J. Phys. Chem. Ref. Data* **1988**, *17*, (2), 513-886.

379. Nightingale, E. R., Phenomenological theory of ion solvation-effective radii of hydrated ions. *J. Phys. Chem.* **1959**, *63*, (9), 1381-1387.
380. Bruce, E. P.; John, M. P.; John, P. O. C., *Properties of Gases and Liquids, Fifth Edition*. McGraw-Hill Education: New York, 2001.
381. Joback, K. G.; Reid, R. C., Estimation of pure-component properties from group-contributions. *Chem. Eng. Commun.* **1987**, *57*, (1-6), 233-243.
382. Otto, T.; Schaefer, T.; Herrmann, H., Aqueous-Phase Oxidation of cis-beta-Isoprene Epoxydiol by Hydroxyl Radicals and Its Impact on Atmospheric Isoprene Processing. *J. Phys. Chem. A* **2019**, *123*, (49), 10599-10608.
383. Rodigast, M.; Mutzel, A.; Iinuma, Y.; Haferkorn, S.; Herrmann, H., Characterisation and optimisation of a sample preparation method for the detection and quantification of atmospherically relevant carbonyl compounds in aqueous medium. *Atmos. Meas. Tech.* **2015**, *8*, (6), 2409-2416.
384. Hoops, S.; Sahle, S.; Gauges, R.; Lee, C.; Pahle, J.; Simus, N.; Singhal, M.; Xu, L.; Mendes, P.; Kummer, U., COPASI- A COMplex PATHway SIMulator. *Bioinformatics* **2006**, *22*, (24), 3067-3074.
385. Mendes, P.; Hoops, S.; Sahle, S.; Gauges, R.; Dada, J.; Kummer, U., Computational Modeling of Biochemical Networks Using COPASI. In *Systems Biology*, Maly, I. V., Ed. Humana Press: Totowa, NJ, 2009; pp 17-59.
386. Mendes, P.; Messiha, H.; Malys, N.; Hoops, S., Enzyme kinetics and computational modeling for systems biology In *Methods in Enzymology: Computer Methods, Part B*, Johnson, M. L.; Brand, L., Eds. Elsevier Academic Press Inc: San Diego, 2009; Vol. 467, pp 583-599.
387. Sahle, S.; Gauges, R.; Pahle, J.; Simus, N.; Kummer, U.; Hoops, S.; Lee, C.; Singhal, M.; Xu, L.; Mendes, P.; Ieee, Simulation of biochemical networks using COPASI - A complex pathway simulator. *Proceedings of the 2006 Winter Simulation Conference, Vols 1-5* **2006**, 1698-+.
388. Gillespie, D. T., General method for numerically simulating stochastic time evolution of coupled chemical-reactions. *J. Comput. Phys.* **1976**, *22*, (4), 403-434.
389. Gillespie, D. T., Exact stochastic simulation of coupled chemical-reactions *Abstr. Pap. Am. Chem. Soc.* **1977**, *173*, (MAR20), 128-128.
390. Gillespie, D. T., Stochastic simulation of chemical kinetics. In *Annu. Rev. Phys. Chem.*, Annual Reviews: Palo Alto, 2007; Vol. 58, pp 35-55.
391. Petzold, L., Automatic Selection of Methods for Solving Stiff and Nonstiff Systems of Ordinary Differential Equations. *SIAM Journal on Scientific and Statistical Computing* **1983**, *4*, (1), 136-148.
392. Hindmarsh, A. C., ODEPACK, A Systematized Collection of ODE Solvers. *Scientific Computing* **1983**, *1*, 55-64.
393. Neese, F.; Wennmohs, F.; Becker, U.; Riplinger, C., The ORCA quantum chemistry program package. *J. Chem. Phys.* **2020**, *152*, (22), 18.
394. Becke, A. D., Density-functional thermochemistry .3. the role of exact exchange. *J. Chem. Phys.* **1993**, *98*, (7), 5648-5652.
395. Lee, C. T.; Yang, W. T.; Parr, R. G., Development of the colle-salvetti correlation-energy formula into a functional of the electron-density. *Phys. Rev. B* **1988**, *37*, (2), 785-789.
396. Vosko, S. H.; Wilk, L.; Nusair, M., Accurate spin-dependent electron liquid correlation energies for local spin-density calculations - a critical analysis *Can. J. Phys.* **1980**, *58*, (8), 1200-1211.
397. Stephens, P. J.; Devlin, F. J.; Chabalowski, C. F.; Frisch, M. J., Ab initio calculation of vibrational absorption and circular-dichroism spectra using density-functional force-fields. *J. Phys. Chem.* **1994**, *98*, (45), 11623-11627.

398. Grimme, S.; Antony, J.; Ehrlich, S.; Krieg, H., A consistent and accurate ab initio parametrization of density functional dispersion correction (DFT-D) for the 94 elements H-Pu. *J. Chem. Phys.* **2010**, *132*, (15), 19.
399. Grimme, S.; Ehrlich, S.; Goerigk, L., Effect of the Damping Function in Dispersion Corrected Density Functional Theory. *J. Comput. Chem.* **2011**, *32*, (7), 1456-1465.
400. Weigend, F.; Ahlrichs, R., Balanced basis sets of split valence, triple zeta valence and quadruple zeta valence quality for H to Rn: Design and assessment of accuracy. *Phys. Chem. Chem. Phys.* **2005**, *7*, (18), 3297-3305.
401. Eichkorn, K.; Weigend, F.; Treutler, O.; Ahlrichs, R., Auxiliary basis sets for main row atoms and transition metals and their use to approximate Coulomb potentials. *Theor. Chem. Acc.* **1997**, *97*, (1-4), 119-124.
402. Eichkorn, K.; Treutler, O.; Ohm, H.; Haser, M.; Ahlrichs, R., Auxiliary basis-sets to approximate coulomb potentials. *Chem. Phys. Lett.* **1995**, *242*, (6), 652-660.
403. Izsak, R.; Neese, F., An overlap fitted chain of spheres exchange method. *J. Chem. Phys.* **2011**, *135*, (14), 11.
404. Weigend, F., Accurate Coulomb-fitting basis sets for H to Rn. *Phys. Chem. Chem. Phys.* **2006**, *8*, (9), 1057-1065.
405. Barone, V.; Cossi, M., Quantum calculation of molecular energies and energy gradients in solution by a conductor solvent model. *J. Phys. Chem. A* **1998**, *102*, (11), 1995-2001.
406. Ho, J. M.; Klamt, A.; Coote, M. L., Comment on the Correct Use of Continuum Solvent Models. *J. Phys. Chem. A* **2010**, *114*, (51), 13442-13444.
407. He, L.; Schaefer, T.; Otto, T.; Kroflic, A.; Herrmann, H., Kinetic and Theoretical Study of the Atmospheric Aqueous-Phase Reactions of OH Radicals with Methoxyphenolic Compounds. *J. Phys. Chem. A* **2019**, *123*, (36), 7828-7838.
408. Sander, R., Compilation of Henry's law constants (version 4.0) for water as solvent. *Atmos. Chem. Phys.* **2015**, *15*, (8), 4399-4981.
409. Staudinger, J.; Roberts, P. V., A critical review of Henry's law constants for environmental applications. *Critical Reviews in Environmental Science and Technology* **1996**, *26*, (3), 205-297.
410. Sangster, J., Octanol-water partition coefficients of simple organic compounds. *Journal of Physical and Chemical Reference Data* **1989**, *18*, (3), 1111-1229.
411. Meylan, W. M.; Howard, P. H., Estimating octanol-air partition coefficients with octanol-water partition coefficients and Henry's law constants. *Chemosphere* **2005**, *61*, (5), 640-644.
412. US_EPA, Estimation Programs Interface Suite™ for Microsoft® Windows, v 4.11. United States Environmental Protection Agency, Washington, DC, USA. In 2012.
413. Hine, J.; Mookerjee, P. K., Structural effects on rates and equilibria. XIX. Intrinsic hydrophilic character of organic compounds. Correlations in terms of structural contributions. *The Journal of Organic Chemistry* **1975**, *40*, (3), 292-298.
414. Altschuh, J.; Bruggemann, R.; Santl, H.; Eichinger, G.; Piringer, O. G., Henry's law constants for a diverse set of organic chemicals: Experimental determination and comparison of estimation methods. *Chemosphere* **1999**, *39*, (11), 1871-1887.
415. Butler, J. A. V.; Ramchandani, C. N.; Thomson, D. W., 58. The solubility of non-electrolytes. Part I. The free energy of hydration of some aliphatic alcohols. *Journal of the Chemical Society (Resumed)* **1935**, (0), 280-285.

416. Hwang, Y. L.; Olson, J. D.; Keller, G. E., Steam stripping for removal of organic pollutants from water .2. vapor-liquid-equilibrium data. *Ind. Eng. Chem. Res.* **1992**, *31*, (7), 1759-1768.
417. Li, J. J.; Carr, P. W., Measurement of water-hexadecane partition-coefficients by headspace gas-chromatography and calculation of limiting activity-coefficients in water *Anal. Chem.* **1993**, *65*, (10), 1443-1450.
418. Mackay, D., Shiu, W.-Y., Shiu, W.-Y., & Lee, S.C. , *Handbook of Physical-Chemical Properties and Environmental Fate for Organic Chemicals*. 2nd edition ed.; CRC Press: 2006.
419. Mackay, D.; Yeun, A. T. K., Mass-transfer correlations for volatilization of organic solutes from water. *Environ. Sci. Technol.* **1983**, *17*, (4), 211-217.
420. Rytting, J. H.; Huston, L. P.; Higuchi, T., Thermodynamic group contributions for hydroxyl, amino, and methylene groups *J. Pharm. Sci.* **1978**, *67*, (5), 615-618.
421. Buttery, R. G.; Ling, L. C.; Guadagni, D. G., Food volatilities- Volatilities of aldehydes ketones and esters in dilute water solution. *J. Agric. Food Chem.* **1969**, *17*, (2), 385-389.
422. Amoore, J. E.; Buttery, R. G., Partition-coefficients and comparative olfactometry *Chemical Senses & Flavour* **1978**, *3*, (1), 57-71.
423. Buttery, R. G.; Guadagni, D. G.; Okano, S., Air-water partition coefficients of some aldehydes *J. Sci. Food Agric.* **1965**, *16*, (11), 691-&.
424. Sieg, K.; Fries, E.; Puttmann, W., Analysis of benzene, toluene, ethylbenzene, xylenes and n-aldehydes in melted snow water via solid-phase dynamic extraction combined with gas chromatography/mass spectrometry. *J. Chromatogr. A* **2008**, *1178*, (1-2), 178-186.
425. Zhou, X.; Mopper, K., Apparent partition coefficients of 15 carbonyl compounds between air and seawater and between air and freshwater; implications for air-sea exchange. *Environmental Science & Technology* **1990**, *24*, (12), 1864-1869.
426. Abraham, M. H.; Le, J.; Acree, W. E.; Carr, P. W.; Dallas, A. J., The solubility of gases and vapours in dry octan-1-ol at 298 K. *Chemosphere* **2001**, *44*, (4), 855-863.
427. Shunthirasingham, C.; Cao, X. S.; Lei, Y. D.; Wania, F., Large Bubbles Reduce the Surface Sorption Artifact of the Inert Gas Stripping Method. *J. Chem. Eng. Data* **2013**, *58*, (3), 792-797.
428. Hansch, C.; Quinlan, J. E.; Lawrence, G. L., Linear free-energy relationship between partition coefficients and aqueous solubility of organic liquids. *J. Org. Chem.* **1968**, *33*, (1), 347-+.
429. Suzuki, T., Development of an automatic estimation system for both the partition-coefficient and aqueous-solubility *Journal of Computer-Aided Molecular Design* **1991**, *5*, (2), 149-166.
430. Karl, T.; Yeretzyan, C.; Jordan, A.; Lindinger, W., Dynamic measurements of partition coefficients using proton-transfer-reaction mass spectrometry (PTR-MS). *International Journal of Mass Spectrometry* **2003**, *223-224*, 383-395.
431. Sander, R. *Compilation of Henry's law constants for inorganic and organic species of potential importance in environmental chemistry*; Max-Planck Institute of Chemistry: Mainz, 1999; p 107.
432. Vempati, H.; Vaitilingom, M.; Zhang, Z. H.; Liyana-Arachchi, T. P.; Stevens, C. S.; Hung, F. R.; Valsararj, K. T., Physico-chemical properties of green leaf volatiles (GLV) for ascertaining atmospheric fate and transport in fog. *Ad. Environ. Res.* **2018**, *7*, (2), 139-159.
433. Buttery, R. G.; Bomben, J. L.; Guadagni, D. G.; Ling, L. C., Volatilities of organic flavor compounds in foods. *Journal of Agricultural and Food Chemistry* **1971**, *19*, (6), 1045-1048.
434. Nozière, B.; Voisin, D.; Longfellow, C. A.; Friedli, H.; Henry, B. E.; Hanson, D. R., The Uptake of Methyl Vinyl Ketone, Methacrolein, and 2-Methyl-3-butene-2-ol onto Sulfuric Acid Solutions. *The Journal of Physical Chemistry A* **2006**, *110*, (7), 2387-2395.

435. Iraci, L. T.; Baker, B. M.; Tyndall, G. S.; Orlando, J. J., Measurements of the Henry's Law Coefficients of 2-Methyl-3-buten-2-ol, Methacrolein, and Methylvinyl Ketone. *Journal of Atmospheric Chemistry* **1999**, *33*, (3), 321-330.
436. Roberts, D. D.; Pollien, P., Analysis of aroma release during microwave heating. *J. Agric. Food Chem.* **1997**, *45*, (11), 4388-4392.
437. Karl, T.; Guenther, A.; Turnipseed, A.; Patton, E. G.; Jardine, K., Chemical sensing of plant stress at the ecosystem scale. *Biogeosciences* **2008**, *5*, (5), 1287-1294.
438. Yalkowsky, S. H.; Valvani, S. C., Solubility and partitioning .1. solubility of non-electrolytes in water *J. Pharm. Sci.* **1980**, *69*, (8), 912-922.
439. Riddick, J. A.; Bunger, W. B.; Sakano, T. K., *Organic solvents: physical properties and methods of purification. Fourth edition.* John Wiley and Sons, New York, NY: United States, 1986.
440. Daubert, T. E.; Danner, R. P., *Physical and thermodynamic properties of pure chemicals: Data compilation.* Taylor & Francis: Washington, DC, 1989.
441. Yalkowsky, S. H.; Dannenfelser, R., Aquasol database of aqueous solubility, Version 5. *Tucson, Arizona: University of Arizona, College of Pharmacy* **1992**.
442. Yaws, C. L., *Handbook of vapor pressure.* Gulf Pub. Co.: Houston, 1994.
443. Kerr, J. B.; Fioletov, V. E., Surface ultraviolet radiation. *Atmosphere-Ocean* **2008**, *46*, (1), 159-184.
444. Sarang, K.; Otto, T.; Rudzinski, K.; Schaefer, T.; Grgić, I.; Nestorowicz, K.; Herrmann, H.; Szmigielski, R., Reaction Kinetics of Green Leaf Volatiles with Sulfate, Hydroxyl, and Nitrate Radicals in Tropospheric Aqueous Phase. *Environmental Science & Technology* **2021**, *55*, (20), 13666-13676.
445. Lin, G.; Sillman, S.; Penner, J. E.; Ito, A., Global modeling of SOA: the use of different mechanisms for aqueous-phase formation. *Atmos. Chem. Phys.* **2014**, *14*, (11), 5451-5475.
446. McNeill, V. F., Aqueous Organic Chemistry in the Atmosphere: Sources and Chemical Processing of Organic Aerosols. *Environ. Sci. Technol.* **2015**, *49*, (3), 1237-1244.
447. Herrmann, H.; Schaefer, T.; Tilgner, A.; Styler, S. A.; Weller, C.; Teich, M.; Otto, T., Tropospheric Aqueous-Phase Chemistry: Kinetics, Mechanisms, and Its Coupling to a Changing Gas Phase. *Chem. Rev.* **2015**, *115*, (10), 4259-4334.
448. Kampf, C. J.; Waxman, E. M.; Slowik, J. G.; Dommen, J.; Pfaffenberger, L.; Praplan, A. P.; Prevot, A. S. H.; Baltensperger, U.; Hoffmann, T.; Volkamer, R., Effective Henry's Law Partitioning and the Salting Constant of Glyoxal in Aerosols Containing Sulfate. *Environ. Sci. Technol.* **2013**, *47*, (9), 4236-4244.
449. Sareen, N.; Carlton, A. G.; Surratt, J. D.; Gold, A.; Lee, B.; Lopez-Hilfiker, F. D.; Mohr, C.; Thornton, J. A.; Zhang, Z. F.; Lim, Y. B.; Turpin, B. J., Identifying precursors and aqueous organic aerosol formation pathways during the SOAS campaign. *Atmos. Chem. Phys.* **2016**, *16*, (22), 14409-14420.
450. Herrmann, H.; Ervens, B.; Jacobi, H. W.; Wolke, R.; Nowacki, P.; Zellner, R., CAPRAM2.3: A chemical aqueous phase radical mechanism for tropospheric chemistry. *J. Atmos. Chem.* **2000**, *36*, (3), 231-284.
451. Ervens, B.; Herrmann, H., Mechanism development for tropospheric multiphase chemistry with CAPRAM. *Air Pollution Modelling and Simulation, Proceedings* **2002**, 413-421.
452. Herrmann, H.; Tilgner, A.; Barzagli, P.; Majdik, Z.; Gligorovski, S.; Poulain, L.; Monod, A., Towards a more detailed description of tropospheric aqueous phase organic chemistry: CAPRAM 3.0. *Atmos. Environ.* **2005**, *39*, (23-24), 4351-4363.

453. Cox, R. A., Chemical kinetics and atmospheric chemistry: Role of data evaluation. *Chem. Rev.* **2003**, *103*, (12), 4533-4548.
454. Long, B.; Bao, J. L.; Truhlar, D. G., Kinetics of the Strongly Correlated CH₃O + O₂ Reaction: The Importance of Quadruple Excitations in Atmospheric and Combustion Chemistry. *J. Am. Chem. Soc.* **2019**, *141*, (1), 611-617.
455. Kalalian, C.; El Dib, G.; Singh, H. J.; Rao, P. K.; Roth, E.; Chakir, A., Temperature dependent kinetic study of the gas phase reaction of ozone with 1-penten-3-ol, cis-2-penten-1-ol and trans-3-hexen-1-ol: Experimental and theoretical data. *Atmos. Environ.* **2020**, *223*, 11.
456. Richards, N. K.; Anastasio, C., Oxidation of green leaf volatiles in fog water, part 2: Reaction kinetics. *Abstr. Pap. Am. Chem. Soc.* **2013**, *245*, 1.
457. Hansel, A. K.; Ehrenhauser, F. S.; Kaur, R.; Anastasio, C.; Valsaraj, K. T., Oxidation of green leaf volatiles in fog water: Part 1-SOA formation. *Abstr. Pap. Am. Chem. Soc.* **2013**, *245*, 1.
458. Neta, P.; Huie, R. E.; Ross, A. B., Rate constants for reactions of inorganic radicals in aqueous-solution. *J. Phys. Chem. Ref. Data* **1988**, *17*, (3), 1027-1284.
459. Pastina, B.; LaVerne, J. A., Effect of molecular hydrogen on hydrogen peroxide in water radiolysis. *J. Phys. Chem. A* **2001**, *105*, (40), 9316-9322.
460. Elliot, A. J. *Rate constants and g-values for the simulation of the radiolysis of light water over the range 0-300 deg C*; Canada, 1994; p 69.
461. Graedel, T. E.; Weschler, C. J., Chemistry within aqueous atmospheric aerosols and raindrops. *Rev. Geophys.* **1981**, *19*, (4), 505-539.
462. Elliot, A. J.; Buxton, G. V., Temperature-dependence of the reactions OH + O²⁻ AND OH + HO₂ in water upto 200-degrees-C. *J. Chem. Soc.-Faraday Trans.* **1992**, *88*, (17), 2465-2470.
463. Christensen, H.; Sehested, K.; Corfitzen, H., Reactions of hydroxyl radicals with hydrogen-peroxide at ambient and elevated-temperatures. *J. Phys. Chem.* **1982**, *86*, (9), 1588-1590.
464. Tang, Y.; Thorn, R. P.; Mauldin, R. L.; Wine, P. H., Kinetics and spectroscopy of the SO₄⁻ radical in aqueous-solution. *J. Photochem. Photobiol. A-Chem.* **1988**, *44*, (3), 243-258.
465. Bao, Z. C.; Barker, J. R., Temperature and ionic strength effects on some reactions involving sulfate radical SO₄⁻(aq). *J. Phys. Chem.* **1996**, *100*, (23), 9780-9787.
466. Neta, P.; Huie, R. E., Rate constants for reaction of NO₃ radicals in aqueous-solutions. *J. Phys. Chem.* **1986**, *90*, (19), 4644-4648.
467. Exner, M.; Herrmann, H.; Zellner, R., Laser-based studies of reactions of the nitrate radical in aqueous-solution. *Ber. Bunsen-Ges. Phys. Chem. Chem. Phys.* **1992**, *96*, (3), 470-477.
468. Jiang, P. Y.; Katsumura, Y.; Nagaishi, R.; Domae, M.; Ishikawa, K.; Ishigure, K.; Yoshida, Y., Pulse-radiolysis study of concentrated sulfuric-acid-solutions-formation mechanism, yield and reactivity of sulfate radicals. *J. Chem. Soc.-Faraday Trans.* **1992**, *88*, (12), 1653-1658.
469. Klaning, U. K.; Sehested, K.; Appelman, E. H., Laser flash-photolysis and pulse-radiolysis of aqueous-solutions of the fluoroxysulfate ion, SO₄F. *Inorg. Chem.* **1991**, *30*, (18), 3582-3584.
470. Maruthamuthu, P.; Neta, P., Radiolytic chain decomposition of peroxomonophosphoric and peroxomonosulfuric acids. *J. Phys. Chem.* **1977**, *81*, (10), 937-940.
471. Herrmann, H.; Reese, A.; Zellner, R., Time-resolved UV/Vis diode-array absorption-spectroscopy of SO_X⁻(X=3, 4, 5) radical-anions in aqueous-solution. *J. Mol. Struct.* **1995**, *348*, 183-186.
472. Wine, P. H.; Mauldin, R. L.; Thorn, R. P., Kinetics and spectroscopy of the NO₃ radical in aqueous ceric nitrate nitric-acid solutions. *J. Phys. Chem.* **1988**, *92*, (5), 1156-1162.

473. Neta, P.; Huie, R. E.; Ross, A. B., Rate constants for reactions of peroxy radicals in fluid solutions. *J. Phys. Chem. Ref. Data* **1990**, *19*, (2), 413-513.
474. *Peroxy radicals / edited by Zeev B. Alfassi*. Wiley: Chichester ;, 1997.
475. Tyndall, G. S.; Cox, R. A.; Granier, C.; Lesclaux, R.; Moortgat, G. K.; Pilling, M. J.; Ravishankara, A. R.; Wallington, T. J., Atmospheric chemistry of small organic peroxy radicals. *J. Geophys. Res.-Atmos.* **2001**, *106*, (D11), 12157-12182.
476. Assaf, E.; Song, B.; Tomas, A.; Schoemaeker, C.; Fittschen, C., Rate Constant of the Reaction between CH₃O₂ Radicals and OH Radicals Revisited. *J. Phys. Chem. A* **2016**, *120*, (45), 8923-8932.
477. Vaughan, S.; Canosa-Mas, C. E.; Pfrang, C.; Shallcross, D. E.; Watson, L.; Wayne, R. P., Kinetic studies of reactions of the nitrate radical (NO₃) with peroxy radicals (RO₂): an indirect source of OH at night? *Phys. Chem. Chem. Phys.* **2006**, *8*, (32), 3749-3760.
478. Gentner, D. R.; Ormeno, E.; Fares, S.; Ford, T. B.; Weber, R.; Park, J. H.; Brioude, J.; Angevine, W. M.; Karlik, J. F.; Goldstein, A. H., Emissions of terpenoids, benzenoids, and other biogenic gas-phase organic compounds from agricultural crops and their potential implications for air quality. *Atmos. Chem. Phys.* **2014**, *14*, (11), 5393-5413.
479. Mentel, T. F.; Kleist, E.; Andres, S.; Dal Maso, M.; Hohaus, T.; Kiendler-Scharr, A.; Rudich, Y.; Springer, M.; Tillmann, R.; Uerlings, R.; Wahner, A.; Wildt, J., Secondary aerosol formation from stress-induced biogenic emissions and possible climate feedbacks. *Atmos. Chem. Phys.* **2013**, *13*, (17), 8755-8770.
480. M. A. O'Dwyer¹, T. J. C., R. M. Healy¹, J. C. Wenger^{1,*}, B. Picquet-Varrault², and J. F. Doussin², The Gas-phase Ozonolysis of 1-Penten-3-ol, (Z)-2-Penten-1-ol and 1-Penten-3-one: Kinetics Products and Secondary Organic Aerosol Formation.
481. Liyana-Arachchi, T. P.; Hansel, A. K.; Stevens, C.; Ehrenhauser, F. S.; Valsaraj, K. T.; Hung, F. R., Molecular Modeling of the Green Leaf Volatile Methyl Salicylate on Atmospheric Air/Water Interfaces. *J. Phys. Chem. A* **2013**, *117*, (21), 4436-4443.
482. Liyana-Arachchi, T. P.; Valsaraj, K. T.; Hung, F. R., Molecular dynamics simulations of green leaf volatiles and OH radicals on atmospheric air/water interfaces. *Abstracts of Papers of the American Chemical Society* **2013**, *245*, 1.
483. Liyana-Arachchi, T. P.; Zhang, Z. H.; Vempati, H.; Hansel, A. K.; Stevens, C.; Pham, A. T.; Ehrenhauser, F. S.; Valsaraj, K. T.; Hung, F. R., Green Leaf Volatiles on Atmospheric Air/Water Interfaces: A Combined Experimental and Molecular Simulation Study. *J. Chem. Eng. Data* **2014**, *59*, (10), 3025-3035.
484. Minakata, D.; Li, K.; Westerhoff, P.; Crittenden, J., Development of a Group Contribution Method To Predict Aqueous Phase Hydroxyl Radical (HO center dot) Reaction Rate Constants. *Environ. Sci. Technol.* **2009**, *43*, (16), 6220-6227.
485. Grosjean, D.; Grosjean, E., Carbonyl products of the ozone-unsaturated alcohol reaction. *Journal of Geophysical Research: Atmospheres* **1995**, *100*, (D11), 22815-22820.
486. Jimenez, E.; Lanza, B.; Martinez, E.; Albaladejo, J., Daytime tropospheric loss of hexanal and trans-2-hexenal: OH kinetics and UV photolysis. *Atmos. Chem. Phys.* **2007**, *7*, (6), 1565-1574.
487. Blanksby, S. J.; Ellison, G. B., Bond dissociation energies of organic molecules. *Accounts Chem. Res.* **2003**, *36*, (4), 255-263.
488. Boethling, R. S.; Howard, P. H.; Meylan, W. M., Finding and estimating chemical property data for environmental assessment. *Environ. Toxicol. Chem.* **2004**, *23*, (10), 2290-2308.

489. Meylan, W. M.; Howard, P. H., Bond contribution method for estimating Henry's law constants *Environ. Toxicol. Chem.* **1991**, *10*, (10), 1283-1293.
490. Daubert, T. E.; Danner, R. P.; Design Institute for Physical Property, D.; American Institute of Chemical, E., *Data compilation tables of properties of pure compounds*. Design Institute for Physical Property Data, American Institute of Chemical Engineers: New York, N.Y. (345 E. 47th St., New York 10017), 1985.
491. Grosjean, E.; Williams, E. L.; Grosjean, D., Ambient levels of formaldehyde and acetaldehyde in Atlanta, Georgia. *J. Air Waste Manage. Assoc.* **1993**, *43*, (4), 469-474.
492. Baez, A.; Padilla, H.; Garcia, R.; Torres, M. D.; Rosas, I.; Belmont, R., Carbonyl levels in indoor and outdoor air in Mexico City and Xalapa, Mexico. *Sci. Total Environ.* **2003**, *302*, (1-3), 211-226.
493. Granby, K.; Christensen, C. S.; Lohse, C., Urban and semi-rural observations of carboxylic acids and carbonyls. *Atmos. Environ.* **1997**, *31*, (10), 1403-1415.
494. National Research Council . Committee on, A., *Formaldehyde and other aldehydes / Committee on Aldehydes, Board on Toxicology and Environmental Health Hazards, Assembly of Life Sciences, National Research Council*. National Academy Press: Washington, D.C, 1981.
495. Veyret, B.; Lesclaux, R.; Rayez, M. T.; Rayez, J. C.; Cox, R. A.; Moortgat, G. K., Kinetics and mechanism of the photo-oxidation of formaldehyde. 1. Flash photolysis study. *The Journal of Physical Chemistry* **1989**, *93*, (6), 2368-2374.
496. Carlier, P.; Hannachi, H.; Mouvier, G., The chemistry of carbonyl-compounds in the atmosphere - a review *Atmos. Environ.* **1986**, *20*, (11), 2079-2099.
497. Bakeas, E. B.; Argyris, D. I.; Siskos, P. A., Carbonyl compounds in the urban environment of Athens, Greece. *Chemosphere* **2003**, *52*, (5), 805-813.
498. Grosjean, D., Aldehydes, carboxylic-acids and inorganic nitrate during NSMCS *Atmos. Environ.* **1988**, *22*, (8), 1637-1648.
499. Grosjean, E.; Grosjean, D.; Fraser, M. P.; Cass, G. R., Air quality model evaluation data for organics .2. C-1-C-14 carbonyls in Los Angeles air. *Environ. Sci. Technol.* **1996**, *30*, (9), 2687-2703.
500. Possanzini, M.; Dipalo, V.; Petricca, M.; Fratarcangeli, R.; Brocco, D., Measurements of lower carbonyls in Rome ambient air. *Atmos. Environ.* **1996**, *30*, (22), 3757-3764.
501. Li, M. Z.; Karu, E.; Brenninkmeijer, C.; Fischer, H.; Lelieveld, J.; Williams, J., Tropospheric OH and stratospheric OH and Cl concentrations determined from CH₄, CH₃Cl, and SF₆ measurements. *Npj Climate and Atmospheric Science* **2018**, *1*.
502. Atkinson, R.; Arey, J.; Aschmann, S. M.; Corchnoy, S. B.; Shu, Y. H., Rate constants for the gas-phase reactions of cis-3-hexen-1-ol, cis-3-hexenylacetate, trans-2-hexenal, and linalool with OH and NO₃ radicals and O⁻³ at 296±2 K, and OH radical formation yields from the O⁻³ reactions. *Int. J. Chem. Kinet.* **1995**, *27*, (10), 941-955.
503. Monod, A.; Poulain, L.; Grubert, S.; Voisin, D.; Wortham, H., Kinetics of OH-initiated oxidation of oxygenated organic compounds in the aqueous phase: new rate constants, structure-activity relationships and atmospheric implications. *Atmos. Environ.* **2005**, *39*, (40), 7667-7688.
504. Lin, X. X.; Ma, Q.; Yang, C. Q.; Tang, X. F.; Zhao, W. X.; Hu, C. J.; Gu, X. J.; Fang, B.; Gai, Y. B.; Zhang, W. J., Kinetics and mechanisms of gas phase reactions of hexenols with ozone. *RSC Adv.* **2016**, *6*, (87), 83573-83580.





Atmospheric aerosol is a suspension of liquid or solid particles with complex chemical composition and sizes far below 100 μm . It includes primary organic aerosol (POA) emitted directly from various sources, e.g., volcano eruptions, and secondary organic aerosol (SOA), which forms through chemical reactions of organic trace gases combined with physical processes, such as nucleation and condensation.

With increasing emission of anthropogenic pollutants, frequently changing weather patterns, and climate change, Earth's natural vegetation such as forests is permanently exposed to extreme stress conditions altering their emission patterns of volatile organic compounds (VOCs) which are the main precursors of secondary organic aerosol (SOA) in the Earth's atmosphere. In the presence of various oxidants such as ozone (O_3), hydroxyl ($\bullet\text{OH}$) and nitrate ($\text{NO}_3\bullet$) radicals, VOCs undergo the gas-phase or aqueous-phase oxidation followed by gas to particle transfer leading to the formation and growth of SOA. The limited knowledge of the SOA formation processes leads to significant underestimation of global SOA budget and its impact on climate change and health.

The present Ph.D. thesis by Kumar Sarang titled "Atmospheric Secondary Organic Aerosol: Kinetic and Chemical Studies of in-Cloud Reactions of Selected Plant Volatiles" investigates the aqueous-phase reactions of selected plant volatiles with atmospheric oxidants at the molecular level leading to secondary organic aerosol (SOA) through kinetic analysis and product identification using high-resolution tandem mass spectrometry.

**IChF**

Institute of Physical Chemistry PAS

Cover illustration from original photos taken by thesis author Kumar Sarang

Cover design by Kumar Sarang

<http://rcin.org.pl>